



Michigan Technological University
Create the Future Digital Commons @ Michigan Tech

Dissertations, Master's Theses and Master's
Reports - Open

Dissertations, Master's Theses and Master's
Reports

2012

Investigation into the enhancement of polycarbonate with conductive nanomaterials

Michael D. Via Jr.
Michigan Technological University

Follow this and additional works at: <https://digitalcommons.mtu.edu/etds>


 Part of the [Chemical Engineering Commons](#)

Copyright 2012 Michael D. Via Jr.

Recommended Citation

Via Jr., Michael D., "Investigation into the enhancement of polycarbonate with conductive nanomaterials",
Dissertation, Michigan Technological University, 2012.
<https://doi.org/10.37099/mtu.dc.etds/10>

Follow this and additional works at: <https://digitalcommons.mtu.edu/etds>

 Part of the [Chemical Engineering Commons](#)

INVESTIGATION INTO THE ENHANCEMENT OF POLYCARBONATE WITH
CONDUCTIVE NANOMATERIALS

By

Michael D. Via Jr.

A DISSERTATION

Submitted in partial fulfillment of the requirements for the degree of

DOCTOR OF PHILOSOPHY

(Chemical Engineering)

MICHIGAN TECHNOLOGICAL UNIVERSITY

2012

© 2012 Michael D. Via Jr.

This dissertation, "Investigation into the Enhancement of Polycarbonate with Conductive Nanomaterials," is hereby approved in partial fulfillment of the requirements for the Degree of DOCTOR OF PHILOSOPHY IN CHEMICAL ENGINEERING.

Department of Chemical Engineering

Signatures:

Dissertation Advisor

Dr. Julia A. King

Department Chair

Dr. Tony N. Rogers

Date

Table of Contents

TABLE OF CONTENTS.....	i
LIST OF FIGURES.....	vii
LIST OF TABLES.....	xix
ACKNOWLEDGEMENTS.....	xlili
NOMENCLATURE	xliv
ABSTRACT	xlvi
CHAPTER 1: INTRODUCTION	1
1.1: INTRODUCTION	1
1.2: MOTIVATION	3
1.3: OBJECTIVES.....	4
CHAPTER 2: BACKGROUND.....	5
2.1: ELECTRICAL CONDUCTIVITY	5
2.2: THERMAL CONDUCTIVITY	8
2.3: TENSILE MODULUS	10
CHAPTER 3: MATERIALS.....	14
3.1: MATERIALS	14
3.2: MATRIX MATERIAL	14
3.3: FILLERS	15
3.3.1: <i>Hyperion Catalysis International’s FIBRIL Multiwalled Carbon Nanotubes</i>	15
3.3.2: <i>Ketjenblack EC-600 JD Carbon Black</i>	17
3.3.3: <i>XG Sciences xGnP™ Graphene Nanoplatelets</i>	19
3.4: FORMULATION NAMING CONVENTION	21
CHAPTER 4: FABRICATION AND EXPERIMENTAL METHODS.....	23
4.1: FABRICATION METHODS	23
4.1.1: <i>Drying</i>	23
4.1.2: <i>Extrusion</i>	24
4.1.3: <i>Injection Molding</i>	28
4.2: EXPERIMENTAL TEST METHODS.....	30
4.2.1: <i>Density: ASTM D792-98 Test Method</i>	30
4.2.2: <i>Melt-Flow Indexing (MFI) Test Method</i>	31
4.2.3: <i>Differential Scanning Calorimetry (DSC) Test Method</i>	32
4.2.4: <i>Capillary Rheology Test Method</i>	33

4.2.5: <i>Small Amplitude Oscillatory Shear Rheology Test Method</i>	37
4.2.6: <i>Through-Plane Electrical Resistivity Test Method</i>	39
4.2.7: <i>In-Plane Electrical Resistivity Test Method</i>	40
4.2.8: <i>Thermal Conductivity: Guarded Heat Flow Meter Test Method</i>	42
4.2.9: <i>Mechanical Tensile Property Test Method</i>	43
4.2.10: <i>Mechanical Flexural Property Test Method</i>	44
4.2.11: <i>Optical Polishing Method</i>	45
4.2.12: <i>Field Emission Scanning Electron Microscope (FESEM) Test Method</i>	49
4.2.13: <i>Transmission Electron Microscope (TEM) Test Method</i>	51
4.2.14: <i>Environmental Scanning Electron Microscope (ESEM) Test Method</i>	53
CHAPTER 5: MISCELLANEOUS RESULTS	55
5.1: DENSITY RESULTS	55
5.2: MELT FLOW INDEX (MFI) RESULTS	57
5.3: DIFFERENTIAL SCANNING CALORIMETRY (DSC) RESULTS	60
5.4: IN-PLANE ELECTRICAL RESISTIVITY OF EXTRUDED RODS	64
CHAPTER 6: ELECTRICAL RESISTIVITY, THERMAL CONDUCTIVITY AND TENSILE AND FLEXURAL PROPERTIES OF CARBON NANOTUBE/POLYCARBONATE COMPOSITES	67
6.1: FIELD EMISSION SCANNING ELECTRON MICROSCOPE (FESEM) AND TRANSMISSION ELECTRON MICROSCOPY RESULTS	67
6.2: ELECTRICAL RESISTIVITY RESULTS	68
6.3: THERMAL CONDUCTIVITY RESULTS	70
6.4: TENSILE TEST RESULTS	71
6.5: FLEXURAL TEST RESULTS	74
6.6: CONCLUSIONS	76
CHAPTER 7: ELECTRICAL RESISTIVITY, THERMAL CONDUCTIVITY AND TENSILE AND FLEXURAL PROPERTIES OF CARBON BLACK/POLYCARBONATE COMPOSITES AND COMPARISON WITH CARBON NANOTUBE/POLYCARBONATE COMPOSITES	77
7.1: FIELD EMISSION SCANNING ELECTRON MICROSCOPE (FESEM) RESULTS	77
7.2: ELECTRICAL RESISTIVITY RESULTS	78
7.3: THERMAL CONDUCTIVITY RESULTS	82
7.4: TENSILE TEST RESULTS	84
7.5: FLEXURAL TEST RESULTS	87
7.6: CONCLUSIONS	89

CHAPTER 8: RHEOLOGICAL PROPERTIES OF CARBON NANOTUBE/POLYCARBONATE COMPOSITES AND CARBON BLACK/POLYCARBONATE COMPOSITES.....	91
8.1: TRANSMISSION ELECTRON MICROSCOPE (TEM) RESULTS.....	91
8.2: SMALL-AMPLITUDE OSCILLATOR SHEAR (SAOS) RESULTS	91
8.3: CAPILLARY RHEOMETER RESULTS: CNT/PC	95
8.4: CAPILLARY RHEOMETER RESULTS AND DISCUSSION: CB/PC	102
8.5: CONCLUSIONS	105
CHAPTER 9: ELECTRICAL RESISTIVITY, THERMAL CONDUCTIVITY, AND TENSILE, FLEXURAL, AND RHEOLOGICAL PROPERTIES OF EXFOLIATED GRAPHITE NANOPLATELET/POLYCARBONATE COMPOSITES.....	107
9.1: ENVIRONMENTAL SCANNING ELECTRON MICROSCOPE (ESEM) RESULTS.....	107
9.2: ELECTRICAL RESISTIVITY RESULTS.....	108
9.3: THERMAL CONDUCTIVITY RESULTS.....	110
9.4: TENSILE TEST RESULTS.....	112
9.5: FLEXURAL TEST RESULTS	114
9.6: CAPILLARY RHEOMETER RESULTS	117
9.7: CONCLUSIONS	120
CHAPTER 10: MODELING THE ELECTRICAL CONDUCTIVITY OF CARBON BLACK/POLYCARBONATE, CARBON NANOTUBE/POLYCARBONATE, AND EXFOLIATED GRAPHITE NANOPLATELET/POLYCARBONATE COMPOSITES.....	122
10.1: ELECTRICAL CONDUCTIVITY (EC) RESULTS	122
10.2: ELECTRICAL CONDUCTIVITY MODELS	127
10.3: CONCLUSIONS	132
CHAPTER 11: TENSILE MODULUS MODELING OF CARBON BLACK/POLYCARBONATE, CARBON NANOTUBE/POLYCARBONATE, AND EXFOLIATED GRAPHITE NANOPLATELET/POLYCARBONATE COMPOSITES.....	134
11.1: ELECTRICAL CONDUCTIVITY AND PERCOLATION MODELS	134
11.2: TENSILE MODULUS MODELS	137
11.3: CONCLUSIONS	144
CHAPTER 12: EFFECTS OF MULTIPLE FILLERS ON THE ELECTRICAL RESISTIVITY, THERMAL CONDUCTIVITY AND	

TENSILE AND FLEXURAL PROPERTIES OF POLYCARBONATE BASED COMPOSITES.....	146
12.1: TRANSMISSION ELECTRON MICROSCOPE (TEM) RESULTS.....	146
12.2: ELECTRICAL RESISTIVITY (ER) RESULTS	148
12.3: THERMAL CONDUCTIVITY (TC) RESULTS	157
12.4: TENSILE MODULUS RESULTS	162
12.5: FLEXURAL MODULUS RESULTS.....	170
12.6: CONCLUSIONS	178
CHAPTER 13: EFFECTS OF MULTIPLE FILLERS ON THE RHEOLOGY OF POLYCARBONATE BASED RESINS.....	180
13.1: CAPILLARY RHEOMETER RESULTS	180
13.2: CONCLUSIONS	190
CHAPTER 14: CONCLUSIONS AND FUTURE WORK.....	192
14.1: CONCLUSIONS	192
14.1.1: <i>Electrical Resistivity (ER)</i>	192
14.1.2: <i>Thermal Conductivity (TC)</i>	193
14.1.3: <i>Tensile Properties</i>	194
14.1.4: <i>Flexural Properties</i>	196
14.1.5: <i>Rheological Properties</i>	197
14.1.6: <i>Electrical Conductivity and Tensile Modulus Modeling</i>	199
14.2: RECOMMENDATIONS FOR FUTURE WORK.....	200
CHAPTER 15: REFERENCES	205
 APPENDIX A: SCREW DESIGN AND EXTRUSION RUN CONDITIONS	 216
APPENDIX A.1: POLYCARBONATE WITH CARBON NANOTUBES	216
APPENDIX A.2: POLYCARBONATE WITH CARBON BLACK	221
APPENDIX A.3: POLYCARBONATE WITH GRAPHITE NANOPATELETS	226
APPENDIX A.4: POLYCARBONATE WITH MULTIPLE FILLERS	231
APPENDIX B: INJECTION MOLDING RUN CONDITIONS.....	241
APPENDIX B.1: POLYCARBONATE WITH CARBON NANOTUBES	241
APPENDIX B.2: POLYCARBONATE WITH CARBON BLACK	243
APPENDIX B.3: POLYCARBONATE WITH GRAPHITE NANOPATELETS	247
APPENDIX B.4: POLYCARBONATE WITH MULTIPLE FILLERS	251
APPENDIX C: DENSITY DATA.....	271
APPENDIX C.1: POLYCARBONATE WITH CARBON NANOTUBES	271

APPENDIX C.2: POLYCARBONATE WITH CARBON BLACK	275
APPENDIX C.3: POLYCARBONATE WITH GRAPHENE NANOPATELETS	280
APPENDIX C.4: POLYCARBONATE WITH MULTIPLE FILLERS	285
APPENDIX D: MELT FLOW INDEXING RESULTS	294
APPENDIX D.1: POLYCARBONATE WITH CARBON NANOTUBES	294
APPENDIX D.2: POLYCARBONATE WITH CARBON BLACK	298
APPENDIX D.3: POLYCARBONATE WITH GRAPHENE NANOPATELETS	300
APPENDIX D.4: POLYCARBONATE WITH MULTIPLE FILLERS	303
APPENDIX E: SAMPLE DIFFERENTIAL SCANNING CALORIMETRY (DSC) RESULTS.....	309
APPENDIX E.1: POLYCARBONATE WITH CARBON NANOTUBES	309
APPENDIX E.2: POLYCARBONATE WITH CARBON BLACK.....	316
APPENDIX E.3: POLYCARBONATE WITH GRAPHENE NANOPATELETS	321
APPENDIX E.4: POLYCARBONATE WITH MULTIPLE FILLERS	326
APPENDIX F: IN-PLANE ELECTRICAL RESISTIVITY (TWO-PROBE) RESULTS ON EXTRUDED RODS.....	356
APPENDIX F.1: POLYCARBONATE WITH CARBON BLACK	356
APPENDIX F.2: POLYCARBONATE WITH GRAPHENE NANOPATELETS	363
APPENDIX F.3: POLYCARBONATE WITH MULTIPLE FILLERS	366
APPENDIX G: THROUGH PLANE ELECTRICAL RESISTIVITY (ASTM D257) RESULTS	380
APPENDIX G.1: POLYCARBONATE WITH CARBON NANOTUBES	380
APPENDIX G.2: POLYCARBONATE WITH CARBON BLACK	382
APPENDIX G.3: POLYCARBONATE WITH GRAPHITE NANOPARTICLES	385
APPENDIX G.4: POLYCARBONATE WITH MULTIPLE FILLERS	389
APPENDIX H: IN-PLANE ELECTRICAL RESISTIVITY (TWO-PROBE) RESULTS	394
APPENDIX H.1: POLYCARBONATE WITH CARBON NANOTUBES	394
APPENDIX H.2: POLYCARBONATE WITH CARBON BLACK	398
APPENDIX H.3: POLYCARBONATE WITH GRAPHITE NANOPARTICLES	405
APPENDIX H.4: POLYCARBONATE WITH MULTIPLE FILLERS	407
APPENDIX I: THROUGH-PLANE THERMAL CONDUCTIVITY (ASTM F433) TEST RESULTS	424
APPENDIX I.1: POLYCARBONATE WITH CARBON NANOTUBES	424
APPENDIX I.2: POLYCARBONATE WITH CARBON BLACK	428

APPENDIX I.3: POLYCARBONATE WITH GRAPHITE NANOPARTICLES	432
APPENDIX I.4: POLYCARBONATE WITH MULTIPLE FILLERS.....	437
APPENDIX J: MECHANICAL TENSILE PROPERTY RESULTS	448
APPENDIX J.1: POLYCARBONATE WITH CARBON NANOTUBES	448
APPENDIX J.2: POLYCARBONATE WITH CARBON BLACK.....	464
APPENDIX J.3: POLYCARBONATE WITH GRAPHITE NANOPARTICLES	482
APPENDIX J.4: POLYCARBONATE WITH MULTIPLE FILLERS	500
APPENDIX K: MECHANICAL FLEXURAL PROPERTY RESULTS	576
APPENDIX K.1: POLYCARBONATE WITH CARBON NANOTUBES	576
APPENDIX K.2: POLYCARBONATE WITH CARBON BLACK	592
APPENDIX K.3: POLYCARBONATE WITH GRAPHITE NANOPARTICLES	610
APPENDIX K.4: POLYCARBONATE WITH MULTIPLE FILLERS	628
APPENDIX L: SMALL AMPLITUDE OSCILLATORY SHEAR RHEOLOGY RESULTS.....	706
APPENDIX L.1: POLYCARBONATE WITH CARBON NANOTUBES	706
APPENDIX F.2: POLYCARBONATE WITH CARBON BLACK	719
APPENDIX L.3: POLYCARBONATE WITH GRAPHENE NANOPATELETS	731
APPENDIX M: CAPILLARY RHEOLOGY RESULTS.....	749
APPENDIX M.1: POLYCARBONATE WITH CARBON NANOTUBES	749
APPENDIX M.2: POLYCARBONATE WITH CARBON BLACK.....	752
APPENDIX M.3: POLYCARBONATE WITH GRAPHENE NANOPATELETS	754
APPENDIX M.4: POLYCARBONATE WITH MULTIPLE FILLERS	756

List of Figures

Figure 2.1: Effect of increasing filler loading on electrical conductivity	6
Figure 2.2: Bond percolation theory with channels	7
Figure 2.3: Two dimensional ball and spring model crystal lattice of sodium chloride	9
Figure 2.4: Generic ductile material tensile stress vs. tensile strain graph	11
Figure 3.1: Lexan HF1130-111 Polycarbonate Structure	15
Figure 3.2: Diagram of carbon nanotube	16
Figure 3.3: Diagram of Ketjenblack EC-600 JD carbon black structure	18
Figure 3.4: Diagram of graphene structure	20
Figure 3.5: ASTM Type I Tensile Bar, 2.5” diameter thermal conductivity disk, ASTM D790 Flex Bar	22
Figure 4.1: Bry Air RD-20 Dryer	23
Figure 4.2: American Leistritz Extruder Corporation Model ZSE 27 twin screw extruder	24
Figure 4.3: Side Stuffers seen disengaged from extruder	25
Figure 4.4: Zone 1 Feeder (Feeder 3) used to feed PC and Masterbatch pellets	25
Figure 4.5: Zone 5 Feeder (Feeder 4) used to add CB to extruder	26
Figure 4.6: Water bath	27
Figure 4.7: Conair Pelletizer and pre-pelletizer air-dryer	27
Figure 4.8: Niigata model NE85UA ₄ injection molding machine	29
Figure 4.9: 4-cavity mold showing ASTM type I Tensile, 2.5” disk, ASTM type V Tensile and ASTM D790 Flex Bar	29
Figure 4.10: Olsen Plastometer MP 987/WL 987 Melt Indexer	32
Figure 4.11: Mettler Toledo 823E DSC	33
Figure 4.12: Goettfert Rheo-Tester 1000 capillary rheometer	34
Figure 4.13: 30/1 capillary die and die nut, drive piston, 1400 bar pressure transducer, 200 bar pressure transducer	35
Figure 4.14: Bohlin C-VOR rotational rheometer with installed 25mm parallel plates	38
Figure 4.15: ASTM D257 apparatus comprised of Keithley 6517A Electrometer/High Resistance Meter and Keithley 8009 Resistivity Test fixture	40
Figure 4.16: Holometrix TCA-300 Thermal Conductivity Analyzer with constant temperature ethylene glycol/water circulator	42
Figure 4.17: Instru-Met Sintech mechanical testing machine with tensile apparatus installed	44

Figure 4.18: Instru-Met Sintech mechanical testing machine with flex apparatus installed	45
Figure 4.19: Diamond Pacific rotating lap with water drip apparatus	47
Figure 4.21: Buehler Vibromet I vibratory polisher	48
Figure 4.22: Olympus BX-60 System microscope with Optixcam Summit 1.3 camera on top	49
Figure 4.23: Hitachi S-4700 FESEM with energy dispersive x-ray spectrometer seen on left	50
Figure 4.24: Leica EM UC6 ultramicrotome shown without cryo chamber	52
Figure 4.25: JEOL JEM-4000FX transmission electron microscope	52
Figure 4.26: FEI/Phillips XL40 ESEM.....	54
Figure 6.1: FESEM image of 6 wt% CNT in PC fracture surface.....	67
Figure 6.2: TEM images of 3 wt% CNT in PC (a) and 6 wt% CNT in PC (b)	68
Figure 6.3: Log(electrical resistivity) versus filler volume for CNT/PC composites.....	69
Figure 6.4: Thermal conductivity versus filler volume for CNT/PC composites.....	71
Figure 6.5: Tensile modulus of CNT/PC composites	72
Figure 6.6: Ultimate tensile strength and strain at ultimate tensile strength for CNT/PC composites.....	73
Figure 6.7: Typical stress-strain curves for CNT/PC composites	73
Figure 6.8: Flexural modulus of CNT/PC composites.....	75
Figure 6.9: Ultimate flexural strength and strain at ultimate flexural strength for CNT/PC composites.....	75
Figure 7.1: FESEM image of 6 wt% CB in PC	77
Figure 7.2: Electrical resistivity (ER) versus filler volume for CB/PC and CNT/PC composites.....	79
Figure 7.3: Thermal conductivity (TC) versus filler volume for CB/PC and CNT/PC composites.....	84
Figure 7.4: Tensile modulus of CB/PC and CNT/PC composites.....	86
Figure 7.5: Ultimate tensile strength and strain at ultimate tensile strength for CB/PC and CNT/PC composites	86
Figure 7.6: Typical stress-strain curves for CB/PC composites	87
Figure 7.7: Flexural modulus of CB/PC and CNT/PC composites	88
Figure 7.8: Ultimate flexural strength and strain at ultimate flexural strength for CB/PC and CNT/PC composites	89
Figure 8.1: a. TEM image of 2 wt% CNT in PC b. TEM image of 8 wt% CNT in PC.....	91

Figure 8.2: Time-temperature shifted complex viscosity as a function of shifted frequency for CNT/PC studied at 270°C	92
Figure 8.3: Time-temperature shift factors a_T for both steady and oscillatory rheological data of CNT/PC as a function of inverse temperature	93
Figure 8.4: Time-temperature shifted complex viscosity as a function of shifted frequency CB/PC studied at 270°C	93
Figure 8.5: Time-temperature shift factors a_T for both steady and oscillatory rheological data of CB/PC as a function of inverse temperature	94
Figure 8.6: Time-temperature shifted steady-shear viscosity as a function of shifted shear rate for CNT/PC studied at 270°C. Compositions range from pure polycarbonate (0 wt % CNT) to 4 wt% CNT.	96
Figure 8.7: Time-temperature shifted steady-shear viscosity as a function of shifted shear rate for CNT/PC studied at 270°C. Compositions range from 4 wt% CNT to 8 wt% CNT	97
Figure 8.8: Schematic of a possible mechanism for viscosity reduction effect observed at high shear rates.	101
Figure 8.9: Time-temperature shifted steady-shear viscosity as a function of shifted shear rate for CB/PC studied at 270°C. Compositions range from pure polycarbonate (0 wt % CB) to 4 wt% CB	102
Figure 8.10: Time-temperature shifted steady-shear viscosity as a function of shifted shear rate for CB/PC studied at 270°C. Compositions range from 4 wt% CB to 8 wt%	103
Figure 9.1: ESEM micrograph of 5 wt% GNP in PC composite	107
Figure 9.2: Electrical resistivity of GNP/PC, CB/PC, and CNT/PC composites	109
Figure 9.3: Thermal conductivity of GNP/PC, CB/PC, and CNT/PC composites	111
Figure 9.4: Tensile modulus of GNP/PC, CB/PC, and CNT/PC composites	112
Figure 9.5: Ultimate tensile strength and strain at ultimate tensile strength for GNP/PC composites	113
Figure 9.6: Tensile stress-strain curves for GNP/PC composites	114
Figure 9.7: Flexural modulus for GNP/PC, CB/PC and CNT/PC composites	115
Figure 9.8: Ultimate flexural strength and strain at ultimate flexural strength for GNP/PC composites	116
Figure 9.9: Time-temperature shifted steady-shear viscosity as a function of steady rate for GNP/PC composites studied at 270°C	118
Figure 9.10: Reduced viscosity versus volume fraction, ϕ , GNP at a shear stress of 10^5 Pa for GNP/PC composites: experimental data along with Maron-Pierce models for various filler shapes and a Kitano-modified Maron-Pierce model ($A=0.3$)	120

Figure 10.1: CB/PC electrical resistivity results along with Mamunya, additive and GEM models.	124
Figure 10.2: CNT/PC electrical resistivity results along with Mamunya, additive and GEM models.	125
Figure 10.3: GNP/PC electrical resistivity results along with Mamunya, additive and GEM models.	126
Figure 11.1: Tensile Modulus Results Along With Halpin-Tsai 2D and 3D Randomly Oriented Fiber and Nielsen Models for CB/PC Composites.....	141
Figure 11.2: Tensile Modulus Results Along With Halpin-Tsai 2D and 3D Randomly Oriented Fiber and Nielsen Models for CNT/PC Composites.....	143
Figure 11.3: Tensile Modulus Results Along With Halpin-Tsai 2D and 3D Randomly Oriented Fiber and Nielsen Models for GNP/PC Composites.....	144
Figure 12.1: TEM Micrograph of Composite Containing 5 wt% CB and 5 wt% CNT in PC.....	147
Figure 12.2: TEM Micrograph of Composite Containing 5 wt% CB and 5 wt% GNP in PC a) Bright Field Image b) Dark Field Image	147
Figure 12.3: TEM Micrograph of Composite Containing 5 wt% CNT and 5 wt% GNP in PC a) Bright Field Image b) Dark Field Image	148
Figure 12.4: Contour Plot of Log (Log Electrical Resistivity, ohm-cm) for CB/CNT Composites	154
Figure 12.5: Contour Plot of Log (Log Electrical Resistivity, ohm-cm) for CNT/GNP Composites.....	156
Figure 12.6: Contour Plot of Tensile Modulus (MPa) for CB/CNT Composites.....	168
Figure 12.7: Contour Plot of Tensile Modulus (MPa) for CB/GNP Composites.....	169
Figure 12.8: Contour Plot of Flexural Modulus (MPa) for CB/CNT Composites	176
Figure 12.9: Contour Plot of Flexural Modulus (MPa) for CB/GNP Composites	177
Figure 13.1: Viscosity versus Shear Rate for CB/PC Composites at 270°C	180
Figure 13.2: Viscosity versus Shear Rate for GNP/PC Composites at 270°C.....	181
Figure 13.3: Viscosity versus Shear Rate for CNT/PC Composites at 270°C.....	181
Figure 13.4: Viscosity versus Shear Rate for PC Composites with CB and GNP at 270°C.....	186
Figure 13.5: Viscosity versus Shear Rate PC Composites with CB and CNT at 270°C.....	187
Figure 13.6: Viscosity versus Shear Rate for PC Composites with CNT and GNP at 270°C.....	188
Figure 13.7: Viscosity versus Shear-Rate PC Composites with CB and CNT at 270°C.....	190

Figure A.1: 2-9-2009 Extruder Screw Design	216
Figure A.2: Extruder Screw Design 2-9-09 used on 5-6-09 and 5-7-09.....	217
Figure A.3: Extruder Screw Design 10-30-09 used on 11-5-09 and 11-11-09.....	221
Figure A.4: Twin Screw Extruder Screw named 10-30-09	222
Figure A.5: Extruder Screw Design 2-9-09 used on 5-26-10 and 5-27-10.....	226
Figure A.6: Twin Screw Extruder Screw named 2-9-09	227
Figure A.7: Extruder Screw Design 2-9-09	231
Figure A.8: Twin Screw Extruder Screw named 2-9-09	232
Figure E.1: DSC for Lexan HF1130-111 (BL) Run 1 vs. Time	310
Figure E.2: DSC for Lexan HF1130-111 (BL) Run 2 vs. Time	311
Figure E.3: DSC for BQ2L Run 1 vs. Time	312
Figure E.4: DSC for BQ2L Run 2 vs. Time	313
Figure E.5: DSC for BQ5L Run 1 vs. Time	314
Figure E.6: DSC for BQ5L Run 2 vs. Time	315
Figure E.7: DSC for BA2L Run 1 vs. Time	317
Figure E.8: DSC for BA2L Run 2 vs. Time	318
Figure E.9: DSC for BA5L Run 1 vs. Time	319
Figure E.10: DSC for BA5L Run 2 vs. Time	320
Figure E.11: DSC for BG2L Run 1 vs. Time	322
Figure E.12: DSC for BG2L Run 2 vs. Time	323
Figure E.13: DSC for BG5L Run 1 vs. Time	324
Figure E.14: DSC for BG5L Run 2 vs. Time	325
Figure E.15: DSC for BA2LR Run 1 vs. Time.....	326
Figure E.16: DSC for BA2LR Run 2 vs. Time.....	327
Figure E.17: DSC for BA5LR Run 1 vs. Time.....	328
Figure E.18: DSC for BA5LR Run 2 vs. Time.....	329
Figure E.19: DSC for BQ1L Run 1 vs. Time	330
Figure E.20: DSC for BQ1L Run 2 vs. Time	331
Figure E.21: DSC for BA2Q1L Run 1 vs. Time.....	332
Figure E.22: DSC for BA2Q1L Run 2 vs. Time.....	333
Figure E.23: DSC for BA2Q5L Run 1 vs. Time.....	334
Figure E.24: DSC for BA2Q5L Run 2 vs. Time.....	335
Figure E.25: DSC for BA5Q1L Run 1 vs. Time.....	336
Figure E.26: DSC for BA5Q1L Run 2 vs. Time.....	337
Figure E.27: DSC for BA5Q5L Run 1 vs. Time.....	338
Figure E.28: DSC for BA5Q5L Run 2 vs. Time.....	339
Figure E.29: DSC for BA2G2L Run 1 vs. Time.....	340
Figure E.30: DSC for BA2G2L Run 2 vs. Time.....	341

Figure E.31: DSC for BA2G5L Run 1 vs. Time.....	342
Figure E.32: DSC for BA2G5L Run 2 vs. Time.....	343
Figure E.33: DSC for BA5G2L Run 1 vs. Time.....	344
Figure E.34: DSC for BA5G2L Run 2 vs. Time.....	345
Figure E.35: DSC for BA5G5L Run 1 vs. Time.....	346
Figure E.36: DSC for BA5G5L Run 2 vs. Time.....	347
Figure E.37: DSC for BQ1G2L Run 1 vs. Time.....	348
Figure E.38: DSC for BQ1G2L Run 2 vs. Time.....	349
Figure E.39: DSC for BQ1G5L Run 1 vs. Time.....	350
Figure E.40: DSC for BQ1G5L Run 2 vs. Time.....	351
Figure E.41: DSC for BQ5G2L Run 1 vs. Time.....	352
Figure E.42: DSC for BQ5G2L Run 2 vs. Time.....	353
Figure E.43: DSC for BQ5G5L Run 1 vs. Time.....	354
Figure E.44: DSC for BQ5G5L Run 2 vs. Time.....	355
Figure J.1: Tensile Results for BL: Lexan HF1130-111: Injection Molded 5-26-09	448
Figure J.2: Tensile Results for BLE: Extruded Lexan HF1130-111: Injection Molded 5-26-09	450
Figure J.3: Tensile Results for BQ2L: 2 wt% fibrils (carbon nanotubes) in Lexan HF1130-111: Injection Molded 5-26-09.....	452
Figure J.4: Tensile Results for BQ3L: 3 wt% fibrils (carbon nanotubes) in Lexan HF1130-111: Injection Molded 5-26-09.....	454
Figure J.5: Tensile Results for BQ4L: 4 wt% fibrils (carbon nanotubes) in Lexan HF1130-111: Injection Molded 5-26-09.....	456
Figure J.6: Tensile Results for BQ5L: 5 wt% fibrils (carbon nanotubes) in Lexan HF1130-111: Injection Molded 5-26-09.....	458
Figure J.7: Tensile Results for BQ6L: 6 wt% fibrils (carbon nanotubes) in Lexan HF1130-111: Injection Molded 5-26-09.....	460
Figure J.8: Tensile Results for BQ8L: 8 wt% fibrils (carbon nanotubes) in Lexan HF1130-111: Injection Molded 5-26-09.....	462
Figure J.9: Tensile Results for BL2: Lexan HF1130-111: Injection Molded 12-4- 09.....	464
Figure J.10: Tensile Results for BLE2: Extruded Lexan HF1130-111: Extruded 11-5-09, Injection Molded 12-4-09.....	466
Figure J.11: Tensile Results for BA2L: 2 wt% Ketjenblack EC-600 JD (carbon black) in Lexan HF1130-111: Injection Molded 12-4-09.....	468
Figure J.12: Tensile Results for BA3L: 3 wt% Ketjenblack EC-600 JD (carbon black) in Lexan HF1130-111: Injection Molded 12-4-09.....	470
Figure J.13: Tensile Results for BA4L: 4 wt% Ketjenblack EC-600 JD (carbon black) in Lexan HF1130-111: Injection Molded 12-4-09.....	472

Figure J.14: Tensile Results for BA5L: 5 wt% Ketjenblack EC-600 JD (carbon black) in Lexan HF1130-111: Injection Molded 12-4-09.....	474
Figure J.15: Tensile Results for BA6L: 6 wt% Ketjenblack EC-600 JD (carbon black) in Lexan HF1130-111: Injection Molded 12-4-09.....	476
Figure J.16: Tensile Results for BA8L: 8 wt% Ketjenblack EC-600 JD (carbon black) in Lexan HF1130-111: Injection Molded 12-4-09.....	478
Figure J.17: Tensile Results for BA10L: 10 wt% Ketjenblack EC-600 JD (carbon black) in Lexan HF1130-111: Injection Molded 12-4-09.....	480
Figure J.18: Tensile Results for BL3: Lexan HF1130-111: Injection Molded 6-3-10.....	482
Figure J.19: Tensile Results for BLE3: Extruded Lexan HF1130-111: Extruded 5-26-10, Injection Molded 6-3-10.....	484
Figure J.20: Tensile Results for BG2L: 2 wt% xGnP in Lexan HF1130-111: Injection Molded 6-3-10, Extruded 5-26-10.....	486
Figure J.21: Tensile Results for BG3L: 3 wt% xGnP in Lexan HF1130-111: Injection Molded 6-3-10, Extruded 5-26-10.....	488
Figure J.22: Tensile Results for BG4L: 4 wt% xGnP in Lexan HF1130-111: Injection Molded 6-3-10, Extruded 5-26-10.....	490
Figure J.23: Tensile Results for BG5L: 5 wt% xGnP in Lexan HF1130-111: Injection Molded 6-3-10, Extruded 5-26-10.....	492
Figure J.24: Tensile Results for BG6L: 6 wt% xGnP in Lexan HF1130-111: Injection Molded 6-8-10, Extruded 5-27-10.....	494
Figure J.25: Tensile Results for BG8L: 8 wt% xGnP in Lexan HF1130-111: Injection Molded 6-8-10, Extruded 5-27-10.....	496
Figure J.26: Tensile Results for BG10L: 10 wt% xGnP in Lexan HF1130-111: Injection Molded 6-8-10, Extruded 5-27-10.....	498
Figure J.27: Tensile Results for BA2LR Set 1: Extruded 7-8-10, Injection Molded 7-26-10.....	500
Figure J.28: Tensile Results for BA2LR Set 2: Extruded 7-8-10, Injection Molded 7-26-10.....	502
Figure J.29: Tensile Results for BA5LR Set 1: Extruded 7-8-10, Injection Molded 7-26-10.....	504
Figure J.30: Tensile Results for BA5LR Set 2: Extruded 7-8-10, Injection Molded 7-26-10.....	506
Figure J.31: Tensile Results for BQ1L Set 1: Extruded 6-30-10, Injection Molded 7-26-10.....	508
Figure J.32: Tensile Results for BQ1L Set 2: Extruded 6-30-10, Injection Molded 7-26-10.....	510
Figure J.33: Tensile Results for BQ5L Set 1: Extruded May 2009, Injection Molded 5-26-09	512

Figure J.34: Tensile Results for BQ5L Set 2: Extruded May 2009, Injection Molded 5-26-09	514
Figure J.35: Tensile Results for BG2L set 1: 2 wt% xGnP in Lexan HF1130-111: Injection Molded 6-3-10, Extruded 5-26-10	516
Figure J.36: Tensile Results for BG2L set 2: 2 wt% xGnP in Lexan HF1130-111: Injection Molded 9-9-10, Extruded 5-26-10	518
Figure J.37: Tensile Results for BG5L Set 1: 5 wt% xGnP in Lexan HF1130-111: Injection Molded 6-3-10, Extruded 5-26-10	520
Figure J.38: Tensile Results for BG5L set 2: 2 wt% xGnP in Lexan HF1130-111: Extruded 5-26-10	522
Figure J.39: Tensile Results for BG12L: 12 wt% xGnP in Lexan HF1130-111: Injection Molded 8-18-10, Extruded 7-8-10	524
Figure J.40: Tensile Results for BG15L: 15 wt% xGnP in Lexan HF1130-111: Injection Molded 8-18-10, Extruded 7-8-10	526
Figure J.41: Tensile Results for BA2Q1L set 1: Injection Molded 7-26-10, Extruded 7-7-10	528
Figure J.42: Tensile Results for BA2Q1L set 2: Injection Molded 7-26-10, Extruded 7-7-10	530
Figure J.43: Tensile Results for BA2Q5L set 1: Injection Molded 8-25-10, Extruded 7-7-10	532
Figure J.44: Tensile Results for BA2Q5L set 2: Injection Molded 8-25-10, Extruded 7-7-10	534
Figure J.45: Tensile Results for BA5Q1L set 1: Injection Molded 8-6-10, Extruded 7-7-10	536
Figure J.46: Tensile Results for BA5Q1L set 2: Injection Molded 8-25-10, Extruded 7-7-10	538
Figure J.47: Tensile Results for BA5Q5L set 1: Injection Molded 8-25-10, Extruded 7-7-10	540
Figure J.48: Tensile Results for BA5Q5L set 2: Injection Molded 8-25-10, Extruded 7-7-10	542
Figure J.49: Tensile Results for BA2G2L set 1: Injection Molded 8-18-10, Extruded 7-6-10	544
Figure J.50: Tensile Results for BA2G2L set 2: Injection Molded 8-18-10, Extruded 7-6-10	546
Figure J.51: Tensile Results for BA2G5L set1: Injection Molded 8-18-10, Extruded 7-6-10	548
Figure J.52: Tensile Results for BA2G5L set 2: Injection Molded 8-18-10, Extruded 7-6-10	550
Figure J.53: Tensile Results for BA5G2L set 1: Injection Molded 8-18-10, Extruded 7-6-10	552

Figure J.54: Tensile Results for BA5G2L set 2: Injection Molded 8-18-10, Extruded 7-6-10	554
Figure J.55: Tensile Results for BA5G5L set 1: Injection Molded 8-6-10, Extruded 7-6-10	556
Figure J.56: Tensile Results for BA5G5L set 2: Injection Molded 8-6-10, Extruded 7-6-10	558
Figure J.57: Tensile Results for BQ1G2L set 1: Injection Molded 8-18-10, Extruded 7-1-10	560
Figure J.58: Tensile Results for BQ1G2L set 2: Injection Molded 8-18-10, Extruded 7-1-10	562
Figure J.59: Tensile Results for BQ1G5L set 1: Injection Molded 8-18-10, Extruded 7-1-10	564
Figure J.60: Tensile Results for BQ1G5L set 2: Injection Molded 8-6-10, Extruded 7-1-10	566
Figure J.61: Tensile Results for BQ5G2L set 1: Injection Molded 9-9-10, Extruded 7-1-10	568
Figure J.62: Tensile Results for BQ5G2L set 2: Injection Molded 9-9-10, Extruded 7-1-10	570
Figure J.63: Tensile Results for BQ5G5L set 1: Injection Molded 9-9-10, Extruded 7-1-10	572
Figure J.64: Tensile Results for BQ5G5L set 2: Injection Molded 9-9-10, Extruded 7-1-10	574
Figure K.1: Flexural Results for BL Lexan HF1130-111: Injection molded 5-26- 09.....	576
Figure K.2: Flexural Results for BL E Extruded Lexan HF1130-111: Injection molded 5-26-09.....	578
Figure K.3: Flexural Results for BQ2L: 2 wt% fibrils (carbon nanotubes) in Lexan HF1130-111: Injection Molded 5-26-09.....	580
Figure K.4: Flexural Results for BQ3L: 3 wt% fibrils (carbon nanotubes) in Lexan HF1130-111: Injection Molded 5-26-09.....	582
Figure K.5: Flexural Results for BQ4L: 4 wt% fibrils (carbon nanotubes) in Lexan HF1130-111: Injection Molded 5-26-09.....	584
Figure K.6: Flexural Results for BQ5L: 5 wt% fibrils (carbon nanotubes) in Lexan HF1130-111: Injection Molded 5-26-09.....	586
Figure K.7: Flexural Results for BQ6L: 6 wt% fibrils (carbon nanotubes) in Lexan HF1130-111: Injection Molded 5-26-09.....	588
Figure K.8: Flexural Results for BQ8L: 8 wt% fibrils (carbon nanotubes) in Lexan HF1130-111: Injection Molded 5-26-09.....	590

Figure K.9: Flexural Results for BL2 Lexan HF1130-111: Injection molded 12-4-09.....	592
Figure K.10: Flexural Results for BLE2 Extruded Lexan HF1130-111: Extruded 11-5-09, Injection molded 12-4-09.....	594
Figure K.11: Flexural Results for BA2L: 2 wt% Ketjenblack EC-600 JD (carbon black) in Lexan HF1130-111: Injection Molded 12-4-09.....	596
Figure K.12: Flexural Results for BA3L: 3 wt% Ketjenblack EC-600 JD (carbon black) in Lexan HF1130-111: Injection Molded 12-4-09.....	598
Figure K.13: Flexural Results for BA4L: 4 wt% Ketjenblack EC-600 JD (carbon black) in Lexan HF1130-111: Injection Molded 12-4-09.....	600
Figure K.14: Flexural Results for BA5L: 5 wt% Ketjenblack EC-600 JD (carbon black) in Lexan HF1130-111: Injection Molded 12-4-09.....	602
Figure K.15: Flexural Results for BA6L: 6 wt% Ketjenblack EC-600 JD (carbon black) in Lexan HF1130-111: Injection Molded 12-4-09.....	604
Figure K.16: Flexural Results for BA8L: 8 wt% Ketjenblack EC-600 JD (carbon black) in Lexan HF1130-111: Injection Molded 12-4-09.....	606
Figure K.17: Flexural Results for BA10L: 10 wt% Ketjenblack EC-600 JD (carbon black) in Lexan HF1130-111: Injection Molded 12-4-09	608
Figure K.18: Flexural Results for BL3 Lexan HF1130-111: Injection molded 6-3-10.....	610
Figure K.19: Flexural Results for BLE3 Extruded Lexan HF1130-111: Extruded 5-26-10, Injection molded 6-3-10	612
Figure K.20: Flexural Results for BG2L: 2 wt% xGnP in Lexan HF1130-111: Injection Molded 6-3-10	614
Figure K.21: Flexural Results for BG3L: 3 wt% xGnP in Lexan HF1130-111: Injection Molded 6-3-10	616
Figure K.22: Flexural Results for BG4L: 4 wt% xGnP (carbon black) in Lexan HF1130-111: Injection Molded 6-3-10.....	618
Figure K.23: Flexural Results for BG5L: 5 wt% xGnP in Lexan HF1130-111: Injection Molded 6-3-10	620
Figure K.24: Flexural Results for BG6L: 6 wt% xGnP in Lexan HF1130-111: Injection Molded 6-8-10	622
Figure K.25: Flexural Results for BG8L: 8 wt% xGnP in Lexan HF1130-111: Injection Molded 6-8-10	624
Figure K.26: Flexural Results for BG10L: 10 wt% xGnP in Lexan HF1130-111: Injection Molded 6-8-10	626
Figure K.27: Flexural Results for BL4 Lexan HF1130-111: Injection molded 7-26-10	628
Figure K.28: Flexural Results for BA2LR Set 1: Extruded 7-8-10, Injection molded 7-26-10.....	630

Figure K.29: Flexural Results for BA2LR Set 2: Extruded 7-8-10, Injection molded 7-26-10	632
Figure K.30: Flexural Results for BA5LR Set 1: Extruded 7-8-10, Injection molded 7-26-10	634
Figure K.31: Flexural Results for BA5LR Set 2: Extruded 7-8-10, Injection molded 7-26-10	636
Figure K.32: Flexural Results for BQ1L Set 1: Extruded 6-30-10, Injection molded 7-26-10	638
Figure K.33: Flexural Results for BQ1L Set 2: Extruded 6-30-10, Injection molded 7-26-10	640
Figure K.34: Flexural Results for BQ5LR Set 1: Extruded 6-30-10, Injection molded 8-25-10	642
Figure K.35: Flexural Results for BQ5LR Set 2: Extruded 6-30-10, Injection molded 8-25-10	644
Figure K.36: Flexural Results for BG2L Set 1: Extruded May 2010, Injection molded 9-9-10	646
Figure K.37: Flexural Results for BG2L Set 2: Extruded May 2010, Injection molded 9-9-10	648
Figure K.38: Flexural Results for BG5L Set 1: Extruded May 2010, Injection molded 9-9-10	650
Figure K.39: Flexural Results for BG5L Set 2: Extruded May 2010, Injection molded 9-9-10	652
Figure K.40: Flexural Results for BG12L: Extruded 7-8-10, Injection molded 8- 18-10	654
Figure K.41: Flexural Results for BG15L: Extruded 7-8-10, Injection molded 8- 18-10	656
Figure K.42: Flexural Results for BA2Q1L Set 1: Extruded 7-7-10, Injection molded 7-26-10	658
Figure K.43: Flexural Results for BA2Q1L Set 2: Extruded 7-7-10, Injection molded 7-26-10	660
Figure K.44: Flexural Results for BA2Q5L Set 1: Extruded 7-7-10, Injection molded 8-25-10	662
Figure K.45: Flexural Results for BA2Q5L Set 2: Extruded 7-7-10, Injection molded 8-25-10	664
Figure K.46: Flexural Results for BA5Q1L Set 1: Extruded 7-7-10, Injection molded 7-26-10	666
Figure K.47: Flexural Results for BA5Q1L Set 2: Extruded 7-7-10, Injection molded 7-26-10	668
Figure K.48: Flexural Results for BA5Q5L Set 1: Extruded 7-7-10, Injection molded 8-25-10	670

Figure K.49: Flexural Results for BA5Q5L Set 2: Extruded 7-7-10, Injection molded 8-25-10	672
Figure K.50: Flexural Results for BA2G2L Set 1: Extruded 7-6-10, Injection molded 8-18-10	674
Figure K.51: Flexural Results for BA2G2L Set 2: Extruded 7-6-10, Injection molded 8-18-10	676
Figure K.52: Flexural Results for BA2G5L Set 1: Extruded 7-6-10, Injection molded 8-18-10	678
Figure K.53: Flexural Results for BA2G5L Set 2: Extruded 7-6-10, Injection molded 8-18-10	680
Figure K.54: Flexural Results for BA5G2L Set 1: Extruded 7-6-10, Injection molded 8-18-10	682
Figure K.55: Flexural Results for BA5G2L Set 2: Extruded 7-6-10, Injection molded 8-18-10	684
Figure K.56: Flexural Results for BA5G5L Set 1: Extruded 7-6-10, Injection molded 8-18-10	686
Figure K.57: Flexural Results for BA5G5L Set 2: Extruded 7-6-10, Injection molded 8-18-10	688
Figure K.58: Flexural Results for BQ1G2L Set 1: Extruded 7-1-10, Injection molded 8-18-10	690
Figure K.59: Flexural Results for BQ1G2L Set 2: Extruded 7-1-10, Injection molded 8-18-10	692
Figure K.60: Flexural Results for BQ1G5L Set 1: Extruded 7-1-10, Injection molded 8-18-10	694
Figure K.61: Flexural Results for BQ1G5L Set 2: Extruded 7-1-10, Injection molded 8-18-10	696
Figure K.62: Flexural Results for BQ5G2L Set 1: Extruded 7-1-10, Injection molded 9-9-10	698
Figure K.63: Flexural Results for BQ5G2L Set 2: Extruded 7-1-10, Injection molded 9-9-10	700
Figure K.64: Flexural Results for BQ5G5L Set 1: Extruded 7-1-10, Injection molded 9-9-10	702
Figure K.65: Flexural Results for BQ5G5L Set 2: Extruded 7-1-10, Injection molded 9-9-10	704

List of Tables

Table 1.1: Electrical conductivity of polymer, metals and carbon	2
Table 1.2: Thermal conductivity of polymer, metals, ceramics and carbon	2
Table 1.3: Tensile modulus of polycarbonate and common reinforcing materials.....	3
Table 3.1: Properties of Sabic's Polycarbonate Lexan HF 1130	15
Table 3.2: Properties of FIBRIL™ Carbon Nanotubes	17
Table 3.3: Properties of Akzo Nobel Ketjenblack EC-600 JD Carbon Black	19
Table 4.1: Niigata model NE85UA ₄ injection molding machine specifications	28
Table 5.1: Individual Component Theoretical Densities	55
Table 5.2: CNT/PC Composite Density Results	55
Table 5.3: CB/PC Composite Density Results	56
Table 5.4: GNP/PC Composite Density Results	56
Table 5.5: CB/CNT, CB/GNP and CNT/GNP Density Results	56
Table 5.6: CNT/PC MFI Results	58
Table 5.7: CB/PC MFI Results	58
Table 5.8: GNP/PC MFI Results	58
Table 5.9: CB/CNT, CB/GNP and CNT/GNP Composites MFI Results	59
Table 5.10: PC and CNT/PC DSC Midpoint T _g Values	60
Table 5.11: CB/PC DSC Midpoint T _g Values	61
Table 5.12: GNP/PC DSC Midpoint T _g Values	62
Table 5.13: CB/CNT, CB/GNP and CNT/GNP DSC Midpoint T _g Values	63
Table 5.14: Average In-Plane Volume Electrical Resistivity of CB/PC Extruded Rods	64
Table 5.15: Average In-Plane Volume Electrical Resistivity of GNP/PC Extruded Rods	65
Table 5.16: Average In-Plane Volume Electrical Resistivity of CB/CNT, CB/GNP and GNP/CNT Extruded Rods.....	66
Table 6.1: Electrical resistivity results for CNT/PC composites	69
Table 6.2: Thermal conductivity results for CNT/PC composites.....	70
Table 7.1: Electrical resistivity results for CB/PC and CNT/PC composites	78
Table 7.2: Thermal conductivity results for CB/PC and CNT/PC composites.....	83
Table 8.1: CNT/PC properties: ER, yield stress, matrix-zero-shear-viscosity and infinite-shear viscosity parameters	99

Table 8.2: Composite properties: ER, yield stress, matrix-zero-shear-viscosity and infinite-shear viscosity parameters	104
Table 9.1: GNP/PC Electrical Resistivity Results	108
Table 9.2: GNP/PC Thermal Conductivity Results	111
Table 10.1: CB/PC, CNT/PC and GNP/PC Electrical Resistivity Results	123
Table 12.1: ER Results for Factorial Design Formulations Containing CB and CNT	149
Table 12.2: ER Results for Factorial Design Formulations Containing CB and GNP	150
Table 12.3: ER Results for Factorial Design Formulations Containing CNT and GNP	151
Table 12.4: 3 ² Regression Results for Log (Log Electrical Resistivity, ohm-cm)	152
Table 12.5: TC Results for Factorial Design Formulations Containing CB and CNT	158
Table 12.6: TC Results for Factorial Design Formulations Containing CB and GNP	159
Table 12.7: TC Results for Factorial Design Formulations Containing CNT and GNP	160
Table 12.8: 3 ² Regression Results for Thermal Conductivity (W/m·K)	161
Table 12.10: Tensile Modulus Results for Factorial Design Formulations Containing CB and GNP	164
Table 12.11: Tensile Modulus Results for Factorial Design Formulations Containing CNT and GNP	165
Table 12.12: 3 ² Regression Results for 3 ² Regression Results for Tensile Modulus (MPa)	166
Table 12.13: Flexural Modulus Results for Factorial Design Formulations Containing CB and CNT	171
Table 12.14: Flexural Modulus Results for Factorial Design Formulations Containing CB and GNP	172
Table 12.16: 3 ² Regression Results for 3 ² Regression Results for Flexural Modulus (MPa)	174
Table 13.1: Newtonian Zero-Shear Plateau Results for Factorial Design Formulations Containing CB and GNP	182
Table 13.2: Electrical Resistivity and Zero-Shear Viscosity Results for Factorial Design Formulations Containing CB and CNT	183

Table 13.3: Electrical Resistivity and Zero-Shear Viscosity Results for Factorial Design Formulations Containing CNT and GNP	184
Table A.1: Extrusion Conditions: Lexan HF1130-111 with Hyperion Fibrils MB6015-00	218
Table A.2: Extrusion Conditions: Lexan HF1130-111 with Ketjenblack EC-600 JD	223
Table A.3: Extrusion Conditions: Lexan HF1130-111 with GNP	228
Table A.4: Extrusion Conditions: Lexan HF1130-111 with 8 wt% Ketjenblack EC-600 JD in Lexan HF1130-111 Masterbatch (extruder screw used = 10-30-09).....	233
Table A.5: Extrusion Conditions: Lexan HF1130-111 Carbon Fillers for Factorial Design (extruder screw used = 2-9-09).....	235
Table B.1: Injection Molding Conditions for CNT/PC Composites.....	241
Table B.2: Injection Molding Conditions for CB/PC Composites	243
Table B.3: Injection Molding conditions for GNP/PC composites	247
Table B.4: Injection Molding Conditions for Combinations in PC	251
Table C.1: Density Results for Lexan HF1130-111:BL: Injection Molded May 26, 2009.....	271
Table C.2: Density Results for Extruded Lexan HF1130-111:BLE: Injection Molded May 26, 2009.....	271
Table C.3: Density Results for 2 wt% fibrils in Lexan HF1130-111: BQ2L: Injection Molded May 26, 2009.....	272
Table C.4: Density Results for 3 wt% fibrils in Lexan HF1130-111: BQ3L: Injection Molded May 26, 2009.....	272
Table C.5: Density Results for 4 wt% fibrils in Lexan HF1130-111: BQ4L: Injection Molded May 26, 2009.....	273
Table C.6: Density Results for 5 wt% fibrils in Lexan HF1130-111: BQ5L: Injection Molded May 26, 2009.....	273
Table C.7: Density Results for 6 wt% fibrils in Lexan HF1130-111: BQ6L: Injection Molded May 26, 2009.....	274
Table C.8: Density Results for 8 wt% fibrils in Lexan HF1130-111: BQ8L: Injection Molded May 26, 2009.....	274
Table C.9: Density Results for Lexan HF1130-111:BL2: Injection Molded December 4, 2009	275
Table C.10: Density Results for Extruded Lexan HF1130-111:BLE2: Extruded Nov 5, 2009; Injection Molded December 4, 2009	275

Table C.11: Density Results for 2 wt% Ketjenblack EC-600 JD in Lexan HF1130-111: BA2L: Extruded November 5, 2009; Injection Molded December 4, 2009.....	276
Table C.12: Density Results for 3 wt% Ketjenblack EC-600 JD in Lexan HF1130-111: BA3L: Extruded November 5, 2009; Injection Molded December 4, 2009.....	276
Table C.13: Density Results for 4 wt% Ketjenblack EC-600 JD in Lexan HF1130-111: BA4L: Extruded November 5, 2009; Injection Molded December 4, 2009.....	277
Table C.15: Density Results for 5 wt% Ketjenblack EC-600 JD in Lexan HF1130-111: BA5L: Extruded November 11, 2009; Injection Molded December 4, 2009.....	277
Table C.14: Density Results for 6 wt% Ketjenblack EC-600 JD in Lexan HF1130-111: BA6L: Extruded November 11, 2009; Injection Molded December 4, 2009.....	278
Table C.16: Density Results for 8 wt% Ketjenblack EC-600 JD in Lexan HF1130-111: BA8L: Extruded November 11, 2009; Injection Molded December 4, 2009.....	278
Table C.17: Density Results for 10 wt% Ketjenblack EC-600 JD in Lexan HF1130-111: BA10L: Extruded November 11, 2009; Injection Molded December 4, 2009	279
Table C.18: Density Results for Lexan HF1130-111:BL3: Injection Molded June 3, 2010.....	280
Table C.19: Density Results for Extruded Lexan HF1130-111:BLE3: Extruded May 26, 2010; Injection Molded June 3, 2010	280
Table C.20: Density Results for 2 wt% xGnP in Lexan HF1130-111: BG2L: Extruded May 26, 2010; Injection Molded June 3, 2010	281
Table C.21: Density Results for 3 wt% xGnP in Lexan HF1130-111: BG3L: Extruded May 26, 2010; Injection Molded June 3, 2010	281
Table C.22: Density Results for 4 wt% xGnP in Lexan HF1130-111: BG4L: Extruded May 26, 2010; Injection Molded June 3, 2010	282
Table C.23: Density Results for 5 wt% xGnP in Lexan HF1130-111: BG5L: Extruded May 26, 2010; Injection Molded June 3, 2010	282
Table C.24: Density Results for 6 wt% xGnP in Lexan HF1130-111: BG5L: Extruded May 27, 2010; Injection Molded June 8, 2010	283
Table C.25: Density Results for 8 wt% xGnP in Lexan HF1130-111: BG5L: Extruded May 27, 2010; Injection Molded June 8, 2010	283
Table C.26: Density Results for 10 wt% xGnP in Lexan HF1130-111: BG5L: Extruded May 27, 2010; Injection Molded June 8, 2010	284

Table C.27: Density Results for Lexan HF1130-111:BL4: Injection Molded July 26, 2010.....	285
Table C.28: Density Results for BA2LR: Extruded 7-8-10; Injection Molded 7-26-10	285
Table C.29: Density Results for BA5LR: Extruded 7-8-10; Injection Molded 7-26-10.....	286
Table C.30: Density Results for BG12L: Extruded 7-8-10; Injection Molded 8-18-10	286
Table C.31: Density Results for BG15L: Extruded 7-8-10; Injection Molded 8-18-10	287
Table C.32: Density Results for BA2Q1L: Extruded 7-7-10; Injection Molded June 26, 2010	287
Table C.33: Density Results for BA2Q5L: Extruded 7-7-10; Injection Molded 8-25-10	288
Table C.34: Density Results for BA5Q1L: Extruded 7-7-10; Injection Molded 7-26-10	288
Table C.35: Density Results for BA5Q5L: Extruded 7-7-10; Injection Molded 8-25-10	289
Table C.36: Density Results for BA2G2L: Extruded 7-6-10; Injection Molded 8-18-10	289
Table C.37: Density Results for BA2G5L: Extruded 7-6-10; Injection Molded 8-18-10	290
Table C.38: Density Results for BA5G2L: Extruded 7-6-10; Injection Molded 8-18-10	290
Table C.39: Density Results for BA5G5L: Extruded 7-6-10; Injection Molded 8-18-10	291
Table C.40: Density Results for BQ1G2L: Extruded 7-1-10; Injection Molded 8-18-10	291
Table C.41: Density Results for BQ1G5L: Extruded 7-1-10; Injection Molded 8-18-10	292
Table C.42: Density Results for BQ5G2L: Extruded 7-1-10; Injection Molded 8-18-10	292
Table C.43: Density Results for BQ5G5L: Extruded 7-1-10; Injection Molded 8-18-10	293
Table D.1: MFI Results for BL.....	294
Table D.2: MFI Results for BLE	294
Table D.3: MFI Results for BQ2L.....	295
Table D.4: MFI Results for BQ3L.....	295
Table D.5: MFI Results for BQ4L.....	296

Table D.6: MFI Results for BQ5L	296
Table D.7: MFI Results for BQ6L	297
Table D.9: MFI Results for BA3L	298
Table D.10: MFI Results for BA4L	299
Table D.11: MFI Results for BA5L	299
Table D.12: MFI Results for BA6L	299
Table D.13: MFI Results for BLE3	300
Table D.14: MFI Results for BG2L	300
Table D.15: MFI Results for BG3L	301
Table D.16: MFI Results for BG4L	301
Table D.17: MFI Results for BG5L	301
Table D.18: MFI Results for BG6L	302
Table D.19: MFI Results for BG8L	302
Table D.20: MFI Results for BG10L	302
Table D.21: MFI Results for BA2LR	303
Table D.22: MFI Results for BA5LR	303
Table D.23: MFI Results for BQ0.5L	303
Table D.24: MFI Results for BQ1L	304
Table D.25: MFI Results for BG12L	304
Table D.26: MFI Results for BG15L	304
Table D.27: MFI Results for BA2Q1L	305
Table D.28: MFI Results for BA2Q5L	305
Table D.29: MFI Results for BA5Q1L	305
Table D.30: MFI Results for BA2G2L	306
Table D.31: MFI Results for BA2G5L	306
Table D.32: MFI Results for BA5G2L	306
Table D.34: MFI Results for BQ1G2L	307
Table D.35: MFI Results for BQ1G5L	307
Table D.36: MFI Results for BQ5G2L	308
Table D.37: MFI Results for BQ5G5L	308
Table F.1: Two Point Two Probe In-Plane Electrical Resistivity Results for BA2L: 2 wt% Ketjenblack EC-600 JD in Lexan HF1130-111: Extruded Rods: Extruded Nov 5, 2009	356
Table F.2: Two Point Two Probe In-Plane Electrical Resistivity Results for BA3L: 3 wt% Ketjenblack EC-600 JD in Lexan HF1130-111: Extruded Rods: Extruded Nov 5, 2009	357
Table F.3: Two Point Two Probe In-Plane Electrical Resistivity Results for BA4L: 4 wt% Ketjenblack EC-600 JD in Lexan HF1130-111: Extruded Rods: Extruded Nov 5, 2009	358

Table F.4: Two Point Two Probe In-Plane Electrical Resistivity Results for BA5L: 5 wt% Ketjenblack EC-600 JD in Lexan HF1130-111: Extruded Rods: Extruded Nov 11, 2009.....	359
Table F.5: Two Point Two Probe In-Plane Electrical Resistivity Results for BA6L: 6 wt% Ketjenblack EC-600 JD in Lexan HF1130-111: Extruded Rods: Extruded Nov 11, 2009.....	360
Table F.6: Two Point Two Probe In-Plane Electrical Resistivity Results for BA8L: 8 wt% Ketjenblack EC-600 JD in Lexan HF1130-111: Extruded Rods: Extruded Nov 11, 2009.....	361
Table F.7: Two Point Two Probe In-Plane Electrical Resistivity Results for BA10L: 10 wt% Ketjenblack EC-600 JD in Lexan HF1130-111: Extruded Rods: Extruded Nov 11, 2009.....	362
Table F.8: Two Point Two Probe In-Plane Electrical Resistivity Results for Ovation Polymers Extima GP MB PC 1515B As- Received Pellets: 15 wt% xGnP in Lexan HF1130-111.....	363
Table F.9: Two Point Two Probe In-Plane Electrical Resistivity Results for BG8L: 8 wt% xGnP in Lexan HF1130-111: Extruded Rods: Extruded May 27, 2010	364
Table F.10: Two Point Two Probe In-Plane Electrical Resistivity Results for BG10L: 10 wt% xGnP in Lexan HF1130-111: Extruded Rods: Extruded May 27, 2010	365
Table F.11: Two Point Two Probe In-Plane Electrical Resistivity Results for BA5LR Extruded Rods: Extruded on 7-8-10.....	366
Table F.12: Two Point Two Probe In-Plane Electrical Resistivity Results for BA8LR Extruded Rods: Extruded on 4-14-10 Masterbatch.....	367
Table F.13: Two Point Two Probe In-Plane Electrical Resistivity Results for BG12L Extruded Rods: Extruded on 7-8-10	368
Table F.14: Two Point Two Probe In-Plane Electrical Resistivity Results for BG15L Extruded Rods: Extruded on 7-8-10	369
Table F.15: Two Point Two Probe In-Plane Electrical Resistivity Results for Ovation Polymers Extima GP MB PC 1515B As- Received Pellets: 15 wt% xGnP in Lexan HF1130-111.....	370
Table F.16: Two Point Two Probe In-Plane Electrical Resistivity Results for BA2Q1L: Extruded Rods: Extruded 7-7-10	370
Table F.17: Two Point Two Probe In-Plane Electrical Resistivity Results for BA2Q5L: Extruded Rods: Extruded 7-7-10	371
Table F.18: Two Point Two Probe In-Plane Electrical Resistivity Results for BA5Q1L: Extruded Rods: Extruded 7-7-10	372
Table F.19: Two Point Two Probe In-Plane Electrical Resistivity Results for BA5Q5L: Extruded Rods: Extruded 7-7-10	373

Table F.20: Two Point Two Probe In-Plane Electrical Resistivity Results for BA2G5L: Extruded Rods: Extruded 7-6-10	374
Table F.21: Two Point Two Probe In-Plane Electrical Resistivity Results for BA5G2L: Extruded Rods: Extruded 7-6-10	375
Table F.22: Two Point Two Probe In-Plane Electrical Resistivity Results for BA5G5L: Extruded Rods: Extruded 7-6-10	376
Table F.23: Two Point Two Probe In-Plane Electrical Resistivity Results for BQ1G5L: Extruded Rods: Extruded 7-1-10	377
Table F.24: Two Point Two Probe In-Plane Electrical Resistivity Results for BQ5G2L: Extruded Rods: Extruded 7-1-10	378
Table F.25: Two Point Two Probe In-Plane Electrical Resistivity Results for BQ5G5L: Extruded Rods: Extruded 7-1-10	379
Table G.1: ASTM D257 Through Plane Electrical Resistivity Results for BL: Lexan HF1130-111: Injection Molded May 26, 2009	380
Table G.2: ASTM D257 Through Plane Electrical Resistivity Results for BLE: Extruded Lexan HF1130-111: Injection Molded May 26, 2009	381
Table G.3: ASTM D257 Through Plane Electrical Resistivity Results for BL2: Lexan HF1130-111: Injection Molded December 4, 2009	382
Table G.4: ASTM D257 Through Plane Electrical Resistivity Results for BLE2: Extruded Lexan HF1130-111: Extruded Nov 5, 2009; Injection Molded December 4, 2009	383
Table G.5: ASTM D257 Through Plane Electrical Resistivity Results for BA2L: 2 wt% Ketjenblack EC-600 JD in Lexan HF1130-111: Injection Molded December 4, 2009	383
Table G.6: ASTM D257 Through Plane Electrical Resistivity Results for BA3L: 3 wt% Ketjenblack EC-600 JD in Lexan HF1130-111: Injection Molded December 4, 2009	384
Table G.7: ASTM D257 Through Plane Electrical Resistivity Results for BL3: Lexan HF1130-111: Injection Molded 6-3-10.....	385
Table G.8: ASTM D257 Through Plane Electrical Resistivity Results for BLE3: Extruded Lexan HF1130-111: Extruded 5-26-10; Injection Molded 6-3-10.....	386
Table G.9: ASTM D257 Through Plane Electrical Resistivity Results for BG2L: 2 wt% xGnP in Lexan HF1130-111: Injection Molded 6-3-10	386
Table G.10: ASTM D257 Through Plane Electrical Resistivity Results for BG3L: 3 wt% xGnP in Lexan HF1130-111: Injection Molded 6-3-10	387
Table G.11: ASTM D257 Through Plane Electrical Resistivity Results for BG4L: 4 wt% xGnP in Lexan HF1130-111: Injection Molded 6-3-10	387
Table G.12: ASTM D257 Through Plane Electrical Resistivity Results for BG5L: 5 wt% xGnP in Lexan HF1130-111: Injection Molded 6-3-10	388

Table G.13: ASTM D257 Through Plane Electrical Resistivity Results for BG6L: 6 wt% xGnP in Lexan HF1130-111: Injection Molded 6-8-10	388
Table G.14: ASTM D257 Through Plane Electrical Resistivity Results for BA2LR: Extruded 7-8-10, Injection Molded 7-26-10	389
Table G.15: ASTM D257 Through Plane Electrical Resistivity Results for BQ0.5L: Extruded 6-30-10, Injection Molded 7-26-10	389
Table G.16: ASTM D257 Through Plane Electrical Resistivity Results for BQ1L Set 1: Extruded 6-30-10, Injection Molded 7-26-10	390
Table G.17: ASTM D257 Through Plane Electrical Resistivity Results for BQ1L Set 2: Extruded 6-30-10, Injection Molded 7-26-10	390
Table G.18: ASTM D257 Through Plane Electrical Resistivity Results for BG2L Set 2: Extruded 5-26-10, Injection Molded 6-3-10	391
Table G.19: ASTM D257 Through Plane Electrical Resistivity Results for BG5L Set 2: Extruded 5-26-10, Injection Molded 6-3-10	391
Table G.20: ASTM D257 Through Plane Electrical Resistivity Results for BA2G2L set 1: Extruded 7-6-10, Injection Molded 8-18-10	392
Table G.21: ASTM D257 Through Plane Electrical Resistivity Results for BA2G2L set 2: Extruded 7-6-10, Injection Molded 8-18-10	392
Table G.22: ASTM D257 Through Plane Electrical Resistivity Results for BQ1G2L set 1: Extruded 7-1-10, Injection Molded 8-18-10	393
Table G.23: ASTM D257 Through Plane Electrical Resistivity Results for BQ1G2L set 2: Extruded 7-1-10, Injection Molded 8-18-10	393
Table H.1: Two Point Two Probe In-Plane Electrical Resistivity Results for BQ2L: 2 wt% fibrils in Lexan HF1130-111: Injection Molded May 26, 2009	394
Table H.2: Two Point Two Probe In-Plane Electrical Resistivity Results for BQ3L: 3 wt% fibrils in Lexan HF1130-111: Injection Molded May 26, 2009	395
Table H.3: Two Point Two Probe In-Plane Electrical Resistivity Results for BQ4L: 4 wt% fibrils in Lexan HF1130-111: Injection Molded May 26, 2009	395
Table H.4: Two Point Two Probe In-Plane Electrical Resistivity Results for BQ5L: 5 wt% fibrils in Lexan HF1130-111: Injection Molded May 26, 2009	396
Table H.5: Two Point Two Probe In-Plane Electrical Resistivity Results for BQ6L: 6 wt% fibrils in Lexan HF1130-111: Injection Molded May 26, 2009	396

Table H.6: Two Point Two Probe In-Plane Electrical Resistivity Results for BQ8L: 8 wt% fibrils in Lexan HF1130-111: Injection Molded May 26, 2009.....	397
Table H.7: Two Point Two Probe In-Plane Electrical Resistivity (ER) Results for BA2L: 2 wt% Ketjenblack EC-600 JD in Lexan HF1130-111: Tensile Bars: Injection Molded Dec 4, 2009	398
Table H.8: Two Point Two Probe In-Plane Electrical Resistivity Results for BA3L: 3 wt% Ketjenblack EC-600 JD in Lexan HF1130-111: Tensile Bars: Injection Molded Dec 4, 2009	399
Table H.9: Two Point Two Probe In-Plane Electrical Resistivity Results for BA4L: 4 wt% Ketjenblack EC-600 JD in Lexan HF1130-111: Tensile Bars: Injection Molded Dec 4, 2009	400
Table H.10: Two Point Two Probe In-Plane Electrical Resistivity Results for BA5L: 5 wt% Ketjenblack EC-600 JD in Lexan HF1130-111: Tensile Bars: Injection Molded Dec 4, 2009	401
Table H.11: Two Point Two Probe In-Plane Electrical Resistivity Results for BA6L: 6 wt% Ketjenblack EC-600 JD in Lexan HF1130-111: Tensile Bars: Injection Molded Dec 4, 2009	402
Table H.12: Two Point Two Probe In-Plane Electrical Resistivity Results for BA8L: 8 wt% Ketjenblack EC-600 JD in Lexan HF1130-111: Tensile Bars: Injection Molded Dec 4, 2009	403
Table H.13: Two Point Two Probe In-Plane Electrical Resistivity Results for BA10L: 10 wt% Ketjenblack EC-600 JD in Lexan HF1130-111: Tensile Bars: Injection Molded Dec 4, 2009	404
Table H.14: Two Point Two Probe In-Plane Electrical Resistivity (ER) Results for BG8L: 8 wt% xGnP in Lexan HF1130-111: Tensile Bars: Injection Molded June 8, 2010.....	405
Table H.15: Two Point Two Probe In-Plane Electrical Resistivity (ER) Results for BG10L: 10 wt% xGnP in Lexan HF1130-111: Tensile Bars: Injection Molded June 8, 2010.....	406
Table H.16: Two Point Two Probe In-Plane Electrical Resistivity (ER) Results for BA5LR set 1: 5 wt% Ketjenblack EC-600 JD in Lexan HF1130-111: Tensile Bars: Injection Molded July 26, 2010; Extruded 7-8-10; 2-9-09 extruder screw	407
Table H.17: Two Point Two Probe In-Plane Electrical Resistivity (ER) Results for BA5LR set 2: 5 wt% Ketjenblack EC-600 JD in Lexan HF1130-111: Tensile Bars: Injection Molded July 26, 2010; Extruded 7-8-10; 2-9-09 extruder screw	408

Table H.18: Two Point Two Probe In-Plane Electrical Resistivity (ER) Results for BQ5LR set 1: Tensile Bars: Injection Molded 8-25-10; Extruded 7-8-10; 2-9-09 extruder screw	409
Table H.19: Two Point Two Probe In-Plane Electrical Resistivity (ER) Results for BQ5LR set 2: Tensile Bars: Injection Molded 8-25-10; Extruded 7-8-10; 2-9-09 extruder screw	409
Table H.20: Two Point Two Probe In-Plane Electrical Resistivity (ER) Results for BG12L: 12 wt% xGnP in Lexan HF1130-111: Tensile Bars: Injection Molded 8-18-10; Extruded 7-8-10; 2-9-09 extruder screw.....	410
Table H.21: Two Point Two Probe In-Plane Electrical Resistivity (ER) Results for BG15L: 15 wt% xGnP in Lexan HF1130-111: Tensile Bars: Injection Molded 8-18-10; Extruded 7-8-10; 2-9-09 extruder screw.....	411
Table H.22: Two Point Two Probe In-Plane Electrical Resistivity (ER) Results for BA2Q1L Set 1: Tensile Bars: Injection Molded 7-26-10	412
Table H.23: Two Point Two Probe In-Plane Electrical Resistivity (ER) Results for BA2Q1L Set 2: Tensile Bars: Injection Molded 7-26-10	413
Table H.24: Two Point Two Probe In-Plane Electrical Resistivity (ER) Results for BA2Q5L Set 1: Tensile Bars: Injection Molded 8-6-10	414
Table H.25: Two Point Two Probe In-Plane Electrical Resistivity (ER) Results for BA2Q5L Set 2: Tensile Bars: Injection Molded 8-6-10	414
Table H.26: Two Point Two Probe In-Plane Electrical Resistivity (ER) Results for BA5Q1L Set 1: Tensile Bars: Injection Molded 8-25-10	415
Table H.27: Two Point Two Probe In-Plane Electrical Resistivity (ER) Results for BA5Q1L Set 2: Tensile Bars: Injection Molded 8-25-10	415
Table H.28: Two Point Two Probe In-Plane Electrical Resistivity (ER) Results for BA5Q5L Set 1: Tensile Bars: Injection Molded 8-6-10	416
Table H.29: Two Point Two Probe In-Plane Electrical Resistivity (ER) Results for BA5Q5L Set 2: Tensile Bars: Injection Molded 8-26-10	417
Table H.30 Two Point Two Probe In-Plane Electrical Resistivity (ER) Results for BA2G5L Set 1: Tensile Bars: Injection Molded 8-18-10	417
Table H.31: Two Point Two Probe In-Plane Electrical Resistivity (ER) Results for BA2G5L Set 2: Tensile Bars: Injection Molded 8-18-10	418
Table H.32: Two Point Two Probe In-Plane Electrical Resistivity (ER) Results for BA5G2L Set 1: Tensile Bars: Injection Molded 8-18-10	418
Table H.33: Two Point Two Probe In-Plane Electrical Resistivity (ER) Results for BA5G2L Set 2: Tensile Bars: Injection Molded 8-18-10	419
Table H.34: Two Point Two Probe In-Plane Electrical Resistivity (ER) Results for BA5G5L Set 1: Tensile Bars: Injection Molded 8-18-10	419
Table H.35: Two Point Two Probe In-Plane Electrical Resistivity (ER) Results for BA5G5L Set 2: Tensile Bars: Injection Molded 8-18-10	420

Table H.36: Two Point Two Probe In-Plane Electrical Resistivity (ER) Results for BQ1G5L Set 1: Tensile Bars: Injection Molded 8-18-10	420
Table H.37: Two Point Two Probe In-Plane Electrical Resistivity (ER) Results for BQ1G5L Set 2: Tensile Bars: Injection Molded 8-18-10	421
Table H.38: Two Point Two Probe In-Plane Electrical Resistivity (ER) Results for BQ5G2L Set 1: Tensile Bars: Injection Molded 8-18-10	421
Table H.39: Two Point Two Probe In-Plane Electrical Resistivity (ER) Results for BQ5G2L Set 2: Tensile Bars: Injection Molded 8-18-10	422
Table H.40: Two Point Two Probe In-Plane Electrical Resistivity (ER) Results for BQ5G5L Set 1: Tensile Bars: Injection Molded 9-9-10	422
Table H.41: Two Point Two Probe In-Plane Electrical Resistivity (ER) Results for BQ5G5L Set 2: Tensile Bars: Injection Molded 9-9-10	423
Table I.1: Through-Plane Thermal Conductivity at 55°C using Holometrix TCA- 300 Guarded Heat Flow Meter Method for Lexan HF1130-111 (BL): Injection Molded May 26, 2009	424
Table I.2: Through-Plane Thermal Conductivity at 55°C using Holometrix TCA- 300 Guarded Heat Flow Meter Method for Extruded Lexan HF1130-111 (BLE): Injection Molded May 26, 2009	424
Table I.3: Through-Plane Thermal Conductivity at 55°C using Holometrix TCA- 300 Guarded Heat Flow Meter Method for 2 wt% Hyperion Fibrils in Lexan HF1130-111 (BQ2L): Injection Molded May 26, 2009	425
Table I.4: Through-Plane Thermal Conductivity at 55°C using Holometrix TCA- 300 Guarded Heat Flow Meter Method for 3 wt% Hyperion Fibrils in Lexan HF1130-111 (BQ3L): Injection Molded May 26, 2009	425
Table I.5: Through-Plane Thermal Conductivity at 55°C using Holometrix TCA- 300 Guarded Heat Flow Meter Method for 4 wt% Hyperion Fibrils in Lexan HF1130-111 (BQ4L): Injection Molded May 26, 2009	426
Table I.6: Through-Plane Thermal Conductivity at 55°C using Holometrix TCA- 300 Guarded Heat Flow Meter Method for 5 wt% Hyperion Fibrils in Lexan HF1130-111 (BQ5L): Injection Molded May 26, 2009	426
Table I.7: Through-Plane Thermal Conductivity at 55°C using Holometrix TCA- 300 Guarded Heat Flow Meter Method for 6 wt% Hyperion Fibrils in Lexan HF1130-111 (BQ6L): Injection Molded May 26, 2009	427
Table I.8: Through-Plane Thermal Conductivity at 55°C using Holometrix TCA- 300 Guarded Heat Flow Meter Method for 8 wt% Hyperion Fibrils in Lexan HF1130-111 (BQ8L): Injection Molded May 26, 2009	427
Table I.9: Through-Plane Thermal Conductivity at 55°C using Holometrix TCA- 300 Guarded Heat Flow Meter Method for Lexan HF1130-111 (BL2): Injection Molded December 4, 2009	428

Table I.10: Through-Plane Thermal Conductivity at 55°C using Holometrix TCA-300 Guarded Heat Flow Meter Method for Extruded Lexan HF1130-111 (BLE2): Injection Molded Dec 4, 2009	428
Table I.11: Through-Plane Thermal Conductivity at 55°C using Holometrix TCA-300 Guarded Heat Flow Meter Method for 2 wt% Ketjenblack EC-600 JD in Lexan HF1130-111 (BA2L): Injection Molded Dec 4, 2009	429
Table I.12: Through-Plane Thermal Conductivity at 55°C using Holometrix TCA-300 Guarded Heat Flow Meter Method for 3 wt% Ketjenblack EC-600 JD in Lexan HF1130-111 (BA3L): Injection Molded Dec 4, 2009	429
Table I.13: Through-Plane Thermal Conductivity at 55°C using Holometrix TCA-300 Guarded Heat Flow Meter Method for 4 wt% Ketjenblack EC-600 JD in Lexan HF1130-111 (BA4L): Injection Molded Dec 4, 2009	429
Table I.14: Through-Plane Thermal Conductivity at 55°C using Holometrix TCA-300 Guarded Heat Flow Meter Method for 5 wt% Ketjenblack EC-600 JD in Lexan HF1130-111 (BA5L): Injection Molded Dec 4, 2009	430
Table I.15: Through-Plane Thermal Conductivity at 55°C using Holometrix TCA-300 Guarded Heat Flow Meter Method for 6 wt% Ketjenblack EC-600 JD in Lexan HF1130-111 (BA6L): Injection Molded Dec 4, 2009	430
Table I.16: Through-Plane Thermal Conductivity at 55°C using Holometrix TCA-300 Guarded Heat Flow Meter Method for 8 wt% Ketjenblack EC-600 JD in Lexan HF1130-111 (BA8L): Injection Molded Dec 4, 2009	430
Table I.17: Through-Plane Thermal Conductivity at 55°C using Holometrix TCA-300 Guarded Heat Flow Meter Method for 10 wt% Ketjenblack EC-600 JD in Lexan HF1130-111 (BA10L): Injection Molded Dec 4, 2009.....	431
Table I.18: Through-Plane Thermal Conductivity at 55°C using Holometrix TCA-300 Guarded Heat Flow Meter Method for Lexan HF1130-111 (BL3): Injection Molded June 3, 2010.....	432
Table I.19: Through-Plane Thermal Conductivity at 55°C using Holometrix TCA-300 Guarded Heat Flow Meter Method for Extruded Lexan HF1130-111 (BLE3): Injection Molded June 3, 2010	432
Table I.20: Through-Plane Thermal Conductivity at 55°C using Holometrix TCA-300 Guarded Heat Flow Meter Method for 2 wt% xGnP in Lexan HF1130-111 (BG2L): Injection Molded June 3, 2010	433
Table I.21: Through-Plane Thermal Conductivity at 55°C using Holometrix TCA-300 Guarded Heat Flow Meter Method for 3 wt% xGnP in Lexan HF1130-111 (BG3L): Injection Molded June 3, 2010	433
Table I.22: Through-Plane Thermal Conductivity at 55°C using Holometrix TCA-300 Guarded Heat Flow Meter Method for 4 wt% xGnP in Lexan HF1130-111 (BG4L): Injection Molded June 3, 2010	434

Table I.23: Through-Plane Thermal Conductivity at 55°C using Holometrix TCA-300 Guarded Heat Flow Meter Method 5 wt% xGnP in Lexan HF1130-111 (BG5L): Injection Molded June 3, 2010.....	434
Table I.24: Through-Plane Thermal Conductivity at 55°C using Holometrix TCA-300 Guarded Heat Flow Meter Method for 6 wt% xGnP in Lexan HF1130-111 (BG6L): Injection Molded June 8, 2010	435
Table I.25: Through-Plane Thermal Conductivity at 55°C using Holometrix TCA-300 Guarded Heat Flow Meter Method for for 8 wt% xGnP in Lexan HF1130-111 (BG8L): Injection Molded June 8, 2010	435
Table I.26: Through-Plane Thermal Conductivity at 55°C using Holometrix TCA-300 Guarded Heat Flow Meter Method for 10 wt% xGnP in Lexan HF1130-111 (BG10L): Injection Molded June 8, 2010	436
Table I.27: Through-Plane Thermal Conductivity at 55°C using Holometrix TCA-300 Guarded Heat Flow Meter Method for BQ0.5L: Injection Molded 7-26-10	437
Table I.28: Through-Plane Thermal Conductivity at 55°C using Holometrix TCA-300 Guarded Heat Flow Meter Method for BQ1L Set 1: Injection Molded 7-26-10.....	437
Table I.29: Through-Plane Thermal Conductivity at 55°C using Holometrix TCA-300 Guarded Heat Flow Meter Method for BQ1L Set 2: Injection Molded 7-26-10.....	437
Table I.30: Through-Plane Thermal Conductivity at 55°C using Holometrix TCA-300 Guarded Heat Flow Meter Method for BQ5L Set 2	438
Table I.31: Through-Plane Thermal Conductivity at 55°C using Holometrix TCA-300 Guarded Heat Flow Meter Method for BG2L Set 2: Injection Molded 6-3-10.....	438
Table I.32: Through-Plane Thermal Conductivity at 55°C using Holometrix TCA-300 Guarded Heat Flow Meter Method for BG5L Set 2: Injection Molded 6-3-10.....	438
Table I.33: Through-Plane Thermal Conductivity at 55°C using Holometrix TCA-300 Guarded Heat Flow Meter Method for BG12L: Injection Molded 8-18-10	439
Table I.34: Through-Plane Thermal Conductivity at 55°C using Holometrix TCA-300 Guarded Heat Flow Meter Method for BG15L: Injection Molded 8-18-10	439
Table I.35: Through-Plane Thermal Conductivity at 55°C using Holometrix TCA-300 Guarded Heat Flow Meter Method for BA2Q1L set 1: Injection Molded 7-26-10	439

Table I.36: Through-Plane Thermal Conductivity at 55°C using Holometrix TCA-300 Guarded Heat Flow Meter Method for BA2Q1L set 2: Injection Molded 7-26-10	440
Table I.37: Through-Plane Thermal Conductivity at 55°C using Holometrix TCA-300 Guarded Heat Flow Meter Method for BA2Q5L set 1: Injection Molded 8-25-10	440
Table I.38: Through-Plane Thermal Conductivity at 55°C using Holometrix TCA-300 Guarded Heat Flow Meter Method for BA2Q5L set 2: Injection Molded 8-25-10	440
Table I.4-39: Through-Plane Thermal Conductivity at 55°C using Holometrix TCA-300 Guarded Heat Flow Meter Method for BA5Q1L set 1: Injection Molded 7-26-10	441
Table I.4-40: Through-Plane Thermal Conductivity at 55°C using Holometrix TCA-300 Guarded Heat Flow Meter Method for BA5Q1L set 2: Injection Molded 7-26-10	441
Table I.41: Through-Plane Thermal Conductivity at 55°C using Holometrix TCA-300 Guarded Heat Flow Meter Method for BA5Q5L set 1: Injection Molded 8-25-10	441
Table I.42: Through-Plane Thermal Conductivity at 55°C using Holometrix TCA-300 Guarded Heat Flow Meter Method for BA5Q5L set 2: Injection Molded 8-25-10	442
Table I.43: Through-Plane Thermal Conductivity at 55°C using Holometrix TCA-300 Guarded Heat Flow Meter Method for BA2G2L set 1: Injection Molded 8-18-10	442
Table I.44: Through-Plane Thermal Conductivity at 55°C using Holometrix TCA-300 Guarded Heat Flow Meter Method for BA2G2L set 2: Injection Molded 8-18-10	442
Table I.45: Through-Plane Thermal Conductivity at 55°C using Holometrix TCA-300 Guarded Heat Flow Meter Method for BA2G5L set 1: Injection Molded 8-18-10	443
Table I.46: Through-Plane Thermal Conductivity at 55°C using Holometrix TCA-300 Guarded Heat Flow Meter Method for BA2G5L set 2: Injection Molded 8-18-10	443
Table I.47: Through-Plane Thermal Conductivity at 55°C using Holometrix TCA-300 Guarded Heat Flow Meter Method for BA5G2L set 1: Injection Molded 8-18-10	443
Table I.48: Through-Plane Thermal Conductivity at 55°C using Holometrix TCA-300 Guarded Heat Flow Meter Method for BA5G2L set 2: Injection Molded 8-18-10	444

Table I.49: Through-Plane Thermal Conductivity at 55°C using Holometrix TCA-300 Guarded Heat Flow Meter Method for BA5G5L set 1: Injection Molded 8-18-10	444
Table I.50: Through-Plane Thermal Conductivity at 55°C using Holometrix TCA-300 Guarded Heat Flow Meter Method for BA5G5L set 2: Injection Molded 8-18-10	444
Table I.51: Through-Plane Thermal Conductivity at 55°C using Holometrix TCA-300 Guarded Heat Flow Meter Method for BQ1G2L set 1: Injection Molded 8-18-10	445
Table I.52: Through-Plane Thermal Conductivity at 55°C using Holometrix TCA-300 Guarded Heat Flow Meter Method for BQ1G2L set 2: Injection Molded 8-18-10	445
Table I.53: Through-Plane Thermal Conductivity at 55°C using Holometrix TCA-300 Guarded Heat Flow Meter Method for BQ1G5L set 1: Injection Molded 8-18-10	445
Table I.54: Through-Plane Thermal Conductivity at 55°C using Holometrix TCA-300 Guarded Heat Flow Meter Method for BQ1G5L set 2: Injection Molded 8-18-10	446
Table I.55: Through-Plane Thermal Conductivity at 55°C using Holometrix TCA-300 Guarded Heat Flow Meter Method for BQ5G2L set 1: Injection Molded 8-18-10	446
Table I.56: Through-Plane Thermal Conductivity at 55°C using Holometrix TCA-300 Guarded Heat Flow Meter Method for BQ5G2L set 2: Injection Molded 8-18-10	446
Table I.57: Through-Plane Thermal Conductivity at 55°C using Holometrix TCA-300 Guarded Heat Flow Meter Method for BQ5G5L set 1: Injection Molded 8-18-10	447
Table I.58: Through-Plane Thermal Conductivity at 55°C using Holometrix TCA-300 Guarded Heat Flow Meter Method for BQ5G5L set 2: Injection Molded 8-18-10	447
Table J.1: Tensile Results for BL: Lexan HF1130-111: Injection Molded 5-26-09	449
Table J.2: Tensile Results for BLE: Extruded Lexan HF1130-111: Injection Molded 5-26-09	451
Table J.3: Tensile Results for BQ2L: 2 wt% fibrils (carbon nanotubes) in Lexan HF1130-111: Injection Molded 5-26-09	453
Table J.4: Tensile Results for BQ3L: 3 wt% fibrils (carbon nanotubes) in Lexan HF1130-111: Injection Molded 5-26-09	455
Table J.5: Tensile Results for BQ4L: 4 wt% fibrils (carbon nanotubes) in Lexan HF1130-111: Injection Molded 5-26-09	457

Table J.6: Tensile Results for BQ5L: 5 wt% fibrils (carbon nanotubes) in Lexan HF1130-111: Injection Molded 5-26-09.....	459
Table J.7: Tensile Results for BQ6L: 6 wt% fibrils (carbon nanotubes) in Lexan HF1130-111: Injection Molded 5-26-09.....	461
Table J.8: Tensile Results for BQ8L: 8 wt% fibrils (carbon nanotubes) in Lexan HF1130-111: Injection Molded 5-26-09 (all these samples broke in the grips)	463
Table J.9: Tensile Results for BL2: Lexan HF1130-111: Injection Molded 12-4-09.....	465
Table J.10: Tensile Results for BLE2: Extruded Lexan HF1130-111: Extruded 11-5-09, Injection Molded 12-4-09	467
Table J.11: Tensile Results for BA2L: 2 wt% Ketjenblack EC-600 JD (carbon black) in Lexan HF1130-111: Injection Molded 12-4-09.....	469
Table J.12: Tensile Results for BA3L: 3 wt% Ketjenblack EC-600 JD (carbon black) in Lexan HF1130-111: Injection Molded 12-4-09.....	471
Table J.13: Tensile Results for BA4L: 4 wt% Ketjenblack EC-600 JD (carbon black) in Lexan HF1130-111: Injection Molded 12-4-09.....	473
Table J.14: Tensile Results for BA5L: 5 wt% Ketjenblack EC-600 JD (carbon black) in Lexan HF1130-111: Injection Molded 12-4-09.....	475
Table J.15: Tensile Results for BA6L: 6 wt% Ketjenblack EC-600 JD (carbon black) in Lexan HF1130-111: Injection Molded 12-4-09.....	477
Table J.16: Tensile Results for BA8L: 8 wt% Ketjenblack EC-600 JD (carbon black) in Lexan HF1130-111: Injection Molded 12-4-09.....	479
Table J.17: Tensile Results for BA10L: 10 wt% Ketjenblack EC-600 JD (carbon black) in Lexan HF1130-111: Injection Molded 12-4-09.....	481
Table J.18: Tensile Results for BL3: Lexan HF1130-111: Injection Molded 6-3-10.....	483
Table J.19: Tensile Results for BLE3: Extruded Lexan HF1130-111: Extruded 5-26-10, Injection Molded 6-3-10.....	485
Table J.20: Tensile Results for BG2L: 2 wt% xGnP in Lexan HF1130-111: Injection Molded 6-3-10, Extruded 5-26-10	487
Table J.21: Tensile Results for BG3L: 3 wt% xGnP in Lexan HF1130-111: Injection Molded 6-3-10, Extruded 5-26-10	489
Table J.22: Tensile Results for BG4L: 4 wt% xGnP in Lexan HF1130-111: Injection Molded 6-3-10, Extruded 5-26-10	491
Table J.23: Tensile Results for BG5L: 5 wt% xGnP in Lexan HF1130-111: Injection Molded 6-3-10, Extruded 5-26-10	493
Table J.24: Tensile Results for BG6L: 6 wt% xGnP in Lexan HF1130-111: Injection Molded 6-8-10, Extruded 5-27-10	495

Table J.25: Tensile Results for BG8L: 8 wt% xGnP in Lexan HF1130-111: Injection Molded 6-8-10, Extruded 5-27-10	497
Table J.26: Tensile Results for BG10L: 10 wt% xGnP in Lexan HF1130-111: Injection Molded 6-8-10, Extruded 5-27-10	499
Table J.27: Tensile Results for BA2LR Set 1: Extruded 7-8-10, Injection Molded 7-26-10	501
Table J.28: Tensile Results for BA2LR Set 2: Extruded 7-8-10, Injection Molded 7-26-10	503
Table J.29: Tensile Results for BA5LR Set 1: Extruded 7-8-10, Injection Molded 7-26-10	505
Table J.30: Tensile Results for BA5LR Set 2: Extruded 7-8-10, Injection Molded 7-26-10	507
Table J.31: Tensile Results for BQ1L Set 1: Extruded 6-30-10, Injection Molded 7-26-10	509
Table J.32: Tensile Results for BQ1L Set 2: Extruded 6-30-10, Injection Molded 7-26-10	511
Table J.33: Tensile Results for BQ5L Set 1: Extruded May 2009, Injection Molded 5-26-09	513
Table J.34: Tensile Results for BQ5L Set 2: Extruded May 2009, Injection Molded 5-26-09	515
Table J.35: Tensile Results for BG2L set 1: 2 wt% xGnP in Lexan HF1130-111: Injection Molded 6-3-10, Extruded 5-26-10	517
Table J.36: Tensile Results for BG2L set 2: 2 wt% xGnP in Lexan HF1130-111: Injection Molded 9-9-10, Extruded 5-26-10	519
Table J.37: Tensile Results for BG5L set 1: 5 wt% xGnP in Lexan HF1130-111: Injection Molded 6-3-10, Extruded 5-26-10	521
Table J.38: Tensile Results for BG5L set 2: 2 wt% xGnP in Lexan HF1130-111: Extruded 5-26-10	523
Table J.39: Tensile Results for BG12L: 12 wt% xGnP in Lexan HF1130-111: Injection Molded 8-18-10, Extruded 7-8-10	525
Table J.40: Tensile Results for BG15L: 15 wt% xGnP in Lexan HF1130-111: Injection Molded 8-18-10, Extruded 7-8-10	527
Table J.41: Tensile Results for BA2Q1L set 1: Injection Molded 7-26-10, Extruded 7-7-10	529
Table J.42: Tensile Results for BA2Q1L set 2: Injection Molded 7-26-10, Extruded 7-7-10	531
Table J.43: Tensile Results for BA2Q5L set 1: Injection Molded 8-25-10, Extruded 7-7-10	533
Table J.44: Tensile Results for BA2Q5L set 2: Injection Molded 8-25-10, Extruded 7-7-10	535

Table J.45: Tensile Results for BA5Q1L set 1: Injection Molded 8-6-10, Extruded 7-7-10	537
Table J.46: Tensile Results for BA5Q1L set 2: Injection Molded 8-25-10, Extruded 7-7-10	539
Table J.47: Tensile Results for BA5Q5L set 1: Injection Molded 8-25-10, Extruded 7-7-10	541
Table J.48: Tensile Results for BA5Q5L set 2: Injection Molded 8-25-10, Extruded 7-7-10	543
Table J.49: Tensile Results for BA2G2L set 1: Injection Molded 8-18-10, Extruded 7-6-10	545
Table J.50: Tensile Results for BA2G2L set 2: Injection Molded 8-18-10, Extruded 7-6-10	547
Table J.51: Tensile Results for BA2G5L set 1: Injection Molded 8-18-10, Extruded 7-6-10	549
Table J.52: Tensile Results for BA2G5L set 2: Injection Molded 8-18-10, Extruded 7-6-10	551
Table J.53: Tensile Results for BA5G2L set 1: Injection Molded 8-18-10, Extruded 7-6-10	553
Table J.54: Tensile Results for BA5G2L set 2: Injection Molded 8-18-10, Extruded 7-6-10	555
Table J.55: Tensile Results for BA5G5L set 1: Injection Molded 8-6-10, Extruded 7-6-10	557
Table J.56: Tensile Results for BA5G5L set 2: Injection Molded 8-6-10, Extruded 7-6-10	559
Table J.57: Tensile Results for BQ1G2L set 1: Injection Molded 8-18-10, Extruded 7-1-10	561
Table J.58: Tensile Results for BQ1G2L set 2: Injection Molded 8-18-10, Extruded 7-1-10	563
Table J.59: Tensile Results for BQ1G5L set 1: Injection Molded 8-18-10, Extruded 7-1-10	565
Table J.60: Tensile Results for BQ1G5L set 2: Injection Molded 8-6-10, Extruded 7-1-10	567
Table J.61: Tensile Results for BQ5G2L set 1: Injection Molded 9-9-10, Extruded 7-1-10	569
Table J.62: Tensile Results for BQ5G2L set 2: Injection Molded 9-9-10, Extruded 7-1-10	571
Table J.63: Tensile Results for BQ5G5L set 1: Injection Molded 9-9-10, Extruded 7-1-10	573
Table J.64: Tensile Results for BQ5G5L set 2: Injection Molded 9-9-10, Extruded 7-1-10	575

Table K.1: Flexural Results for BL Lexan HF1130-111: Injection molded 5-26-09	577
Table K.2: Flexural Results for BLE Extruded Lexan HF1130-111: Injection molded 5-26-09	579
Table K.3: Flexural Results for BQ2L: 2 wt% fibrils (carbon nanotubes) in Lexan HF1130-111: Injection Molded 5-26-09	581
Table K.4: Flexural Results for BQ3L: 3 wt% fibrils (carbon nanotubes) in Lexan HF1130-111: Injection Molded 5-26-09	583
Table K.5: Flexural Results for BQ4L: 4 wt% fibrils (carbon nanotubes) in Lexan HF1130-111: Injection Molded 5-26-09	585
Table K.6: Flexural Results for BQ5L: 5 wt% fibrils (carbon nanotubes) in Lexan HF1130-111: Injection Molded 5-26-09	587
Table K.7: Flexural Results for BQ6L: 6 wt% fibrils (carbon nanotubes) in Lexan HF1130-111: Injection Molded 5-26-09	589
Table K.8: Flexural Results for BQ8L: 8 wt% fibrils (carbon nanotubes) in Lexan HF1130-111: Injection Molded 5-26-09	591
Table K.9: Flexural Results for BL2 Lexan HF1130-111: Injection molded 12-4- 09	593
Table K.10: Flexural Results for BLE2 Extruded Lexan HF1130-111: Extruded 11-5-09, Injection molded 12-4-09	595
Table K.11: Flexural Results for BA2L: 2 wt% Ketjenblack EC-600 JD (carbon black) in Lexan HF1130-111: Injection Molded 12-4-09	597
Table K.12: Flexural Results for BA3L: 3 wt% Ketjenblack EC-600 JD (carbon black) in Lexan HF1130-111: Injection Molded 12-4-09	599
Table K.13: Flexural Results for BA4L: 4 wt% Ketjenblack EC-600 JD (carbon black) in Lexan HF1130-111: Injection Molded 12-4-09	601
Table K.14: Flexural Results for BA5L: 5 wt% Ketjenblack EC-600 JD (carbon black) in Lexan HF1130-111: Injection Molded 12-4-09	603
Table K.15: Flexural Results for BA6L: 6 wt% Ketjenblack EC-600 JD (carbon black) in Lexan HF1130-111: Injection Molded 12-4-09	605
Table K.16: Flexural Results for BA8L: 8 wt% Ketjenblack EC-600 JD (carbon black) in Lexan HF1130-111: Injection Molded 12-4-09	607
Table K.17: Flexural Results for BA10L: 10 wt% Ketjenblack EC-600 JD (carbon black) in Lexan HF1130-111: Injection Molded 12-4-09: All samples fractured	609
Table K.18: Flexural Results for BL3 Lexan HF1130-111: Injection molded 6-3- 10	611
Table K.19: Flexural Results for BLE3 Extruded Lexan HF1130-111: Extruded 5- 26-10, Injection molded 6-3-10	613
Table K.20: Flexural Results for BG2L: 2 wt% xGnP in Lexan HF1130-111: Injection Molded 6-3-10	615

Table K.21: Flexural Results for BG3L: 3 wt% xGnP in Lexan HF1130-111: Injection Molded 6-3-10	617
Table K.22: Flexural Results for BG4L: 4 wt% xGnP (carbon black) in Lexan HF1130-111: Injection Molded 6-3-10.....	619
Table K.23: Flexural Results for BG5L: 5 wt% xGnP in Lexan HF1130-111: Injection Molded 6-3-10	621
Table K.24: Flexural Results for BG6L: 6 wt% xGnP in Lexan HF1130-111: Injection Molded 6-8-10: All samples fractured.....	623
Table K.25: Flexural Results for BG8L: 8 wt% xGnP in Lexan HF1130-111: Injection Molded 6-8-10 : All samples fractured. Flexural Maximum and Fracture Stress and Strain are identical.....	625
Table K.26: Flexural Results for BG10L: 10 wt% xGnP in Lexan HF1130-111: Injection Molded 6-8-10: All samples fractured. Flexural Maximum and Fracture Stress and Strain are identical.....	627
Table K.27: Flexural Results for BL4 Lexan HF1130-111: Injection molded 7-26- 10.....	629
Table K.28: Flexural Results for BA2LR Set 1: Extruded 7-8-10, Injection molded 7-26-10.....	631
Table K.29: Flexural Results for BA2LR Set 2: Extruded 7-8-10, Injection molded 7-26-10.....	633
Table K.30: Flexural Results for BA5LR Set 1: Extruded 7-8-10, Injection molded 7-26-10.....	635
Table K.31: Flexural Results for BA5LR Set 2: Extruded 7-8-10, Injection molded 7-26-10.....	637
Table K.32: Flexural Results for BQ1L Set 1: Extruded 6-30-10, Injection molded 7-26-10.....	639
Table K.33: Flexural Results for BQ1L Set 2: Extruded 6-30-10, Injection molded 7-26-10.....	641
Table K.34: Flexural Results for BQ5LR Set 1: Extruded 6-30-10, Injection molded 8-25-10.....	643
Table K.35: Flexural Results for BQ5LR Set 2: Extruded 6-30-10, Injection molded 8-25-10.....	645
Table K.36: Flexural Results for BG2L Set 1: Extruded May 2010, Injection molded 9-9-10.....	647
Table K.37: Flexural Results for BG2L Set 2: Extruded May 2010, Injection molded 9-9-10.....	649
Table K.38: Flexural Results for BG5L Set 1: Extruded May 2010, Injection molded 9-9-10.....	651
Table K.39: Flexural Results for BG5L Set 2: Extruded May 2010, Injection molded 9-9-10.....	653

Table K.40: Flexural Results for BG12L: Extruded 7-8-10, Injection molded 8-18-10	655
Table K.41: Flexural Results for BG15L: Extruded 7-8-10, Injection molded 8-18-10	657
Table K.42: Flexural Results for BA2Q1L Set 1: Extruded 7-7-10, Injection molded 7-26-10	659
Table K.43: Flexural Results for BA2Q1L Set 2: Extruded 7-7-10, Injection molded 7-26-10	661
Table K.44: Flexural Results for BA2Q5L Set 1: Extruded 7-7-10, Injection molded 8-25-10	663
Table K.45: Flexural Results for BA2Q5L Set 2: Extruded 7-7-10, Injection molded 8-25-10	665
Table K.46: Flexural Results for BA5Q1L Set 1: Extruded 7-7-10, Injection molded 7-26-10	667
Table K.47: Flexural Results for BA5Q1L Set 2: Extruded 7-7-10, Injection molded 7-26-10	669
Table K.48: Flexural Results for BA5Q5L Set 1: Extruded 7-7-10, Injection molded 8-25-10	671
Table K.49: Flexural Results for BA5Q5L Set 2: Extruded 7-7-10, Injection molded 8-25-10	673
Table K.50: Flexural Results for BA2G2L Set 1: Extruded 7-6-10, Injection molded 8-18-10	675
Table K.51: Flexural Results for BA2G2L Set 2: Extruded 7-6-10, Injection molded 8-18-10	677
Table K.52: Flexural Results for BA2G5L Set 1: Extruded 7-6-10, Injection molded 8-18-10	679
Table K.53: Flexural Results for BA2G5L Set 2: Extruded 7-6-10, Injection molded 8-18-10	681
Table K.54: Flexural Results for BA5G2L Set 1: Extruded 7-6-10, Injection molded 8-18-10	683
Table K.55: Flexural Results for BA5G2L Set 2: Extruded 7-6-10, Injection molded 8-18-10	685
Table K.56: Flexural Results for BA5G5L Set 1: Extruded 7-6-10, Injection molded 8-18-10	687
Table K.57: Flexural Results for BA5G5L Set 2: Extruded 7-6-10, Injection molded 8-18-10	689
Table K.58: Flexural Results for BQ1G2L Set 1: Extruded 7-1-10, Injection molded 8-18-10	691
Table K.59: Flexural Results for BQ1G2L Set 2: Extruded 7-1-10, Injection molded 8-18-10	693

Table K.60: Flexural Results for BQ1G5L Set 1: Extruded 7-1-10, Injection molded 8-18-10	695
Table K.61: Flexural Results for BQ1G5L Set 2: Extruded 7-1-10, Injection molded 8-18-10	697
Table K.62: Flexural Results for BQ5G2L Set 1: Extruded 7-1-10, Injection molded 9-9-10	699
Table K.63: Flexural Results for BQ5G2L Set 2: Extruded 7-1-10, Injection molded 9-9-10	701
Table K.64: Flexural Results for BQ5G5L Set 1: Extruded 7-1-10, Injection molded 9-9-10	703
Table K.65: Flexural Results for BQ5G5L Set 2: Extruded 7-1-10, Injection molded 9-9-10	705
Table L.1: SAOS Results for BL: Lexan HF1130-111 at various temperatures	706
Table L.2: SAOS Results for BQ2L: 2 wt% Hyperion Fibrils (CNT) in Lexan HF1130-111 at various temperatures	707
Table L.3: SAOS Results for BQ3L: 3 wt% Hyperion Fibrils (CNT) in Lexan HF1130-111 at various temperatures	709
Table L.4: SAOS Results for BQ4L: 4 wt% Hyperion Fibrils (CNT) in Lexan HF1130-111 at various temperatures	711
Table L.5: SAOS Results for BQ5L: 5 wt% Hyperion Fibrils (CNT) in Lexan HF1130-111 at various temperatures	713
Table L.6: SAOS Results for BQ6L: 6 wt% Hyperion Fibrils (CNT) in Lexan HF1130-111 at various temperatures	715
Table L.7: SAOS Results for BQ8L: 8 wt% Hyperion Fibrils (CNT) in Lexan HF1130-111 at various temperatures	717
Table L.8: SAOS Results for BA2L: 2 wt% Carbon Black (CB) in Lexan HF1130-111 at various temperatures	719
Table L.9: SAOS Results for BA3L: 3 wt% Carbon Black (CB) in Lexan HF1130-111 at various temperatures	721
Formulation BA3L	722
Table L.10: SAOS Results for BA4L: 4 wt% Carbon Black (CB) in Lexan HF1130-111 at various temperatures	723
Table L.10: SAOS Results for BA4L: 4 wt% Carbon Black (CB) in Lexan HF1130-111 at various temperatures continued	724
Table L.11: SAOS Results for BA5L: 5 wt% Carbon Black (CB) in Lexan HF1130-111 at various temperatures	725
Table L.12: SAOS Results for BA6L: 6 wt% Carbon Black (CB) in Lexan HF1130-111 at various temperatures	727

Table L.13: SAOS Results for BA8L: 8 wt% Carbon Black (CB) in Lexan HF1130-111 at various temperatures.....	729
Table L.14: SAOS Results for BG2L: 2 wt% Graphene Nanoplatelets (GNP) in Lexan HF1130-111 at various temperatures.....	731
Table L.15: SAOS Results for BG3L: 3 wt% Graphene Nanoplatelets (GNP) in Lexan HF1130-111 at various temperatures.....	733
Table L.16: SAOS Results for BG4L: 4 wt% Graphene Nanoplatelets (GNP) in Lexan HF1130-111 at various temperatures.....	735
Table L.17: SAOS Results for BG5L: 5 wt% Graphene Nanoplatelets (GNP) in Lexan HF1130-111 at various temperatures.....	737
Table L.18: SAOS Results for BG6L: 6 wt% Graphene Nanoplatelets (GNP) in Lexan HF1130-111 at various temperatures.....	739
Table L.19: SAOS Results for BG8L: 8 wt% Graphene Nanoplatelets (GNP) in Lexan HF1130-111 at various temperatures.....	741
Table L.20: SAOS Results for BG10L: 10 wt% Graphene Nanoplatelets (GNP) in Lexan HF1130-111 at various temperatures.....	743
Table L.21: SAOS Results for BG12L: 12 wt% Graphene Nanoplatelets (GNP) in Lexan HF1130-111 at various temperatures.....	745
Table L.22: SAOS Results for BG15L: 15 wt% Graphene Nanoplatelets (GNP) in Lexan HF1130-111 at various temperatures.....	747
Table M.1: Capillary Rheometer Results at 270°C.....	749
Table M.2: Capillary Rheometer Results at 300°C.....	750
Table M.3: Capillary Rheometer Results at 320°C.....	751
Table M.4: Capillary Rheometer Results at 270°C.....	752
Table M.5: Capillary Rheometer Results at 300°C.....	753
Table M.6: Capillary Rheometer Results at 270°C.....	754
Table M.7: Capillary Rheometer Results at 300°C.....	755
Table M.8: Capillary Rheometer Results at 270°C.....	756

Acknowledgements

I would like to thank Dr. Julia King for being my Ph.D. advisor. She has been an invaluable asset in the pursuit of my degree. She has assisted in the procedural aspects of obtaining my degree as well as assisting in the experimental and theoretical work. Without her it would have been much more difficult for me to obtain this degree and it certainly would have taken much longer.

I would also like to thank my committee members Drs. Ibrahim Miskioglu, Tamara Olson, Warren Perger and Tony Rogers for taking the time out of their busy schedules to be on my committee.

My undergraduate research assistants have greatly assisted me over these past 4 years. There have been well over 2 dozen undergrads that have helped at various points in this project. I would particularly like to thank Jeffery Caspary, Daniel Alpers, Edsel Beach, Mark Cieslinski and Kyle Weise. I could always count on these 5 students to return for multiple semesters and perform tedious tasks or experiments without complaint and I cannot thank them enough for their time and effort.

Possibly most importantly, I would like to thank my family. Their support was critical to my entire education. They were always there to talk when things were tough and assist when it was needed.

Lastly, I would like to thank Beth Johnson, the previous graduate student working for Dr. King. She was a great mentor and has been very supportive and helpful ever since.

Nomenclature

A	Adjustable parameter in Kitano-modified Maron-Pierce model
a	Exponential parameter
a_T	Shift factor
ASTM	American Society for Testing and Materials
c	Volumetric heat capacity ($\text{J}/\text{m}^3 \cdot \text{K}$)
CB	Carbon black
CNT	Carbon nanotubes
CNF	Carbon nanofibers
CVD	Chemical vapor deposition
CY	Carreau-Yasuda model
d	Diameter (cm or nm)
D	Diameter of capillary (mm)
DSC	Differential scanning calorimetry
E	Tensile modulus (MPa)
E	Adjustable parameter for additive model
E_C	Composite tensile modulus (MPa)
E_f	Tensile modulus of filler (MPa)
E_L	Longitudinal composite tensile modulus (MPa)
E_m	Tensile modulus of matrix (MPa)
E_T	Transverse composite tensile modulus (MPa)
EC	Electrical Conductivity (S/cm)
ER	Electrical Resistivity (ohm-cm)
ESEM	Environmental scanning electron microscopy
F	Maximum filler volume fraction
FESEM	Field-emission scanning electron microscopy
G	Adjustable parameter for additive model
$G'(\omega)$	Linear-viscoelastic elastic modulus (Pa)
$G'(T)$	Linear-viscoelastic elastic modulus at the test temperature (Pa)
$G''(\omega)$	Loss modulus (Pa)
$G''(T)$	Loss modulus at the test temperature (Pa)
GEM	General effective media model
GNP	Graphene nanoplatelets
H	Adjustable parameter for additive model
i	Electrical current (A)
IPD	Electron hopping distance (nm)
K	Adjustable parameter for Mamunya model
k	Thermal conductivity ($\text{W}/\text{m} \cdot \text{K}$)
K_E	Einstein coefficient

L	Length (cm or nm)
L	Demagnification coefficient of dispersion
L/d	Aspect ratio of filler
LVDT	Linear variable displacement transformer
m_{dry}	Dry mass (g)
m_{wet}	Submerged mass (g)
MFI	Melt flow index
MTU	Michigan Technological University
N	Proportionality constant
n	Power-law index
n	Adjustable parameter for Mamunya model
n	Adjustable parameter for additive model
ΔP	Pressure drop over the capillary (bar)
p	Mean free path of phonons (m)
PC	Polycarbonate
PP	Polypropylene
Q	Volumetric flow rate (m ³ /s)
q	Heat flux (W/m ²)
R	Radius of the capillary (mm)
R_0	Sum of all contact thermal resistances (m ² ·K/W)
R_S	Specimen thermal resistance (m ² ·K/W)
SAOS	Small-amplitude oscillatory shear
SiC	Silicon carbide
T	Temperature (K)
t	Thickness (cm or nm)
T_g	Glass-transition temperature (K)
T_L	Lower surface temperature
T_{ref}	Reference temperature (K)
T_U	Upper surface temperature (K)
TC	Thermal conductivity (W/m·K)
TEM	Transmission electron microscopy
u	Velocity of phonons (m/s)
UFS	Ultimate flexural strength (MPa)
UTS	Ultimate tensile strength (MPa)
ΔV	Voltage drop over sample (V)
V_f	Volume fraction of filler
vol%	Volume percent of filler
w	Sample width (cm)
w _{CB}	Weight percentage carbon black

w_{CNT}	Weight percentage carbon nanotubes
w_{GNP}	Weight percentage graphene nanoplatelets
$w\%$	Weight percent of filler
$\dot{\gamma}$	Shear rate (1/s)
$\dot{\gamma}_a$	Apparent shear rate in the capillary (1/s)
$\dot{\gamma}_R$	True shear rate at the wall (1/s)
$\frac{\partial T}{\partial x}$	Temperature gradient in the x-direction (K/m)
ε	Tensile strain (%)
ε	Total error
η	Steady-shear viscosity (Pa·s)
$\eta(T)$	Viscosity at the test temperature (Pa·s)
$\eta^*(\omega)$	Complex viscosity (Pa·s)
η_0	Newtonian zero-shear viscosity (Pa·s)
$\langle \cos^2 \theta \rangle$	Average of the squared cosine of orientation angle of filler
λ	Relaxation time (s)
μ_0	Viscosity parameter
ρ	Specimen density (g/cm ³)
ρ_i	Density of each individual component (g/cm ³)
ρ_{ref}	Sample density at the reference temperature (g/cm ³)
ρ_{water}	Density of test water (g/cm ³)
σ	Tensile stress (MPa)
σ	Electrical conductivity (S/cm)
σ_{calc}	Electrical conductivity predicted by model (S/cm)
σ_f	Electrical conductivity of composite at F (S/cm)
σ_h	Electrical conductivity of conductive filler (S/cm)
σ_m	Electrical conductivity of composite (S/cm)
σ_{measured}	Electrical conductivity measured from sample (S/cm)
σ_p	Electrical conductivity of polymer (S/cm)
τ_R	Shear stress at the wall (Pa)
τ_0	Yield stress (Pa)
τ_{21}	Shear stress (Pa)
ϕ	Filler volume fraction
ϕ_c	Percolation threshold
ϕ_i	Weight fraction of each individual component

ϕ_m	Maximum packing fraction
ω	Shear rate (rad/s)

Abstract

“Investigation into the Enhancement of Polycarbonate with Conductive Nanomaterials”

Polymers are typically electrically and thermally insulating materials. The electrical and thermal conductivities of polymers can be increased by the addition of conductive fillers such as carbons. Once the polymer composites have been made electrically and thermally conductive, they can be used in applications where these conductivities are desired such as electromagnetic shielding and static dissipation.

In this project, three carbon nanomaterials are added to polycarbonate to enhance the electrical and thermal conductivity of the resulting composite. Hyperion Catalysis FIBRILs carbon nanotubes were added to a maximum loading of 8 wt%. Ketjenblack EC-600 JD carbon black was added to a maximum loading of 10 wt%. XG Sciences xGnP™ graphene nanoplatelets were added to a maximum loading of 15 wt%. These three materials have drastically different morphologies and will have varying effects on the various properties of polycarbonate composites.

It was determined that carbon nanotubes have the largest effect on electrical conductivity with an 8 wt% carbon nanotube in polycarbonate composite having an electrical conductivity of 0.128 S/cm (from a pure polycarbonate value of 10^{-17} S/cm). Carbon black has the next largest effect with an 8 wt% carbon black in polycarbonate composite having an electrical conductivity of 0.008 S/cm. Graphene nanoplatelets have the least effect with an 8 wt% graphene nanoplatelet in polycarbonate having an electrical conductivity of 2.53×10^{-8} S/cm.

Graphene nanoplatelets show a significantly higher effect on increasing thermal conductivity than either carbon nanotubes or carbon black. Mechanically, all three materials have similar effects with graphene nanoplatelets being somewhat more effective at increasing the tensile modulus of the composite than the other fillers.

Carbon black and graphene nanoplatelets show standard carbon-filler rheology where the addition of filler increases the viscosity of the resulting composite. Carbon nanotubes, on the other hand, show an unexpected rheology. As carbon nanotubes are added to polycarbonate the viscosity of the composite is reduced below that of the original polycarbonate. It was seen that the addition of carbon nanotubes offsets the increased viscosity from a second filler, such as carbon black or graphene nanoplatelets.

Chapter 1: Introduction

1.1: Introduction

Most polymers are electrical and thermal insulators. Traditionally applications that required some electrical or thermal conductivity were restricted to metals if both properties are required, or ceramics for thermal conductivity only. Increasing the electrical and thermal conductivity of polymers allows them to be used in these other applications. Thermoplastic polymers are resistant to corrosion, have high impact resistance and are lighter than metals (1). These properties have led to polymers being used to replace metal components in a variety of applications (2). Thermoplastic components can have properties tailored to the application by changing the type of polymer used as well as the additives that are added to the polymer.

It can be seen from Table 1.1 that the electrical conductivity of typical insulating polymers is dramatically lower than that of metals and carbon (upwards of 22 orders of magnitude). Table 1.2 shows some typical values for the thermal conductivity of polymer compared to metals, ceramics and carbon. Again polymers are seen to be much less conductive than metals. One of the ways to increase the conductivities of polymers is to add conductive fillers. Ceramics (i.e. aluminum nitride and boron nitride), metals (i.e. copper, steel and aluminum) and carbons (i.e. carbon black, carbon fibers, carbon nanotubes and graphite) are added to polymers to increase both thermal and electrical conductivity (1-16). When the electrical conductivity of the polymer composite has been increased to the 10^{-10} to 10^{-3} S/cm range, they can be used in electrostatic dissipative applications such as electronic component handling trays and grounding straps for

workers. Polymer composites that have electrical conductivities in the range of 10^{-2} or 10^{-1} S/cm can be used for semiconductive applications such as fuel gages.

Table 1.1: Electrical conductivity of polymer, metals and carbon (1,10,17)

Material	Electrical Conductivity (S/cm)
Polymers	10^{-7} to 10^{-17}
Copper	5.9×10^5
Silver	6.3×10^5
Aluminum	3.6×10^5
Nickel	1.5×10^5
Carbon (amorphous)	300

Table 1.2: Thermal conductivity of polymer, metals, ceramics and carbon (2,10,18)

Material	Thermal Conductivity (W/m·K)
Polymer	0.2 to 0.3
Copper	400
Aluminum (extruded / cast)	225 / 60
Steel	45
Aluminum Nitride	140 to 180
Boron Nitride (cubic / hexagonal)	1700 / 33
Carbon (graphitic / amorphous)	600 / 1.7

While the conductivities of the polymers are increased, it is also often important to increase the tensile modulus of the polymer to better match the properties of the materials they are replacing. Table 1.3 shows the tensile modulus of polycarbonate as well as metals, glasses and graphites that are typically used as reinforcements. The addition of these reinforcements to polymers helps to increase the modulus of polymers to levels that are required to replace metal components.

Table 1.3: Tensile modulus of polycarbonate and common reinforcing materials (19,20)

Material	Tensile Modulus (GPa)
Polycarbonate	2.2
Boron	386
Steel	407
E-glass	72.4
S-glass	85.5
High-modulus graphite fiber	483 to 517
High-strength graphite fiber	234 to 255

1.2: Motivation

One emerging market for electrically conductive resins is aerospace components. With the introduction of the Boeing 787 Dreamliner™ (a new highly efficient twin aisle commercial aircraft that will carry 230 passengers on routes of 8,000 nautical miles), new demands are being placed on the performance of polymer based composite materials (21). The 787 uses a significant amount (50% by weight) of composites on its primary structure. Composite materials are chosen because of their increased fatigue life and resistance to corrosion, which reduces maintenance costs (21). Composites are also lighter weight versus metals, which increases aircraft fuel efficiency; and therefore, reduces the amount of greenhouse gases (primarily water and carbon dioxide) produced from burning fossil fuels. Fuel consumption is an important issue in today's society. Greenhouse gases could contribute to global climate change. With this increase in composite primary structure, there is an increase in the use of polymer materials for internal hardware and components such as brackets, shelves, ducts, interior support structure, and enclosures. Traditionally, these components would have used aluminum, but with the possibility of galvanic corrosion when aluminum is in contact with carbon fiber reinforced polymer composites, these components are now being designed with

polymer composites, which raises a new issue. Aluminum is inherently electrically conductive and provides a level of electromagnetic interference (EMI) shielding and radio frequency interference (RFI) shielding that the polymer based composite does not provide. Therefore, it is necessary to use polymer compounds that have been modified to provide the necessary electrical conductivity. These conductive materials must also have moderate mechanical properties. The addition of conductive fillers such as carbon black and synthetic graphite particles to polymers often degrades tensile and impact strength. Hence, the challenge is to produce a cost effective composite that meets the electrical conductivity and mechanical property needs.

1.3: Objectives

The goals of this Ph.D. project are listed below:

- The electrical resistivity, thermal conductivity, as well as tensile, flexural and rheological properties of polycarbonate-based composites containing various amounts of different carbon-based conductive fillers will be determined.
- The synergistic effects of combinations of different carbon-based conductive fillers on the electrical resistivity, thermal conductivity and mechanical and rheological properties of polycarbonate-based composites will be determined.
- Electrical conductivity, tensile modulus, and rheological models will be applied to the composite systems tested herein and modified if required to suitably fit the behavior noted.

Chapter 2: Background

2.1: Electrical Conductivity

Electrical conductivity of a composite describes the composite's ability to transmit electrons along its surface (surface electrical conductivity) or through its volume (volume electrical resistivity). Electrical conductivity is given in units of S/cm and it the reciprocal of electrical resistivity (given in units of ohm-cm). Electrical resistance is the directly measureable property of the material that is then converted to electrical resistivity by multiplying by the cross-sectional area of the conducting volume and dividing by the length over which the measurement is being made. Electrical conductivity is then found by simply taking the reciprocal of this electrical resistivity.

When discussing electrical conductivity in relation to conductive-filler filled polymer composites, the composite can be in one of 3 stages based upon the type and amount of filler added as seen in Figure 2.1. At low filler concentrations, the electrical conductivity of the composite will be similar to that of the original polymer. Many polymers are highly electrically resistive with electrical conductivities on the order of 10^{-14} to 10^{-17} S/cm (polycarbonate has a resistivity of about 10^{-17} S/cm). As more filler is added, the composite will reach a filler loading level at which the electrical conductivity rapidly increases by several orders of magnitude, known as the percolation threshold. After passing the percolation threshold, the electrical conductivity will flatten out and approach the electrical conductivity of the conductive filler as more filler is added. This percolation threshold is the point at which networks of conductive fillers begin to form

creating continuous pathways for electricity to flow through. This is known as percolation theory (22,23).

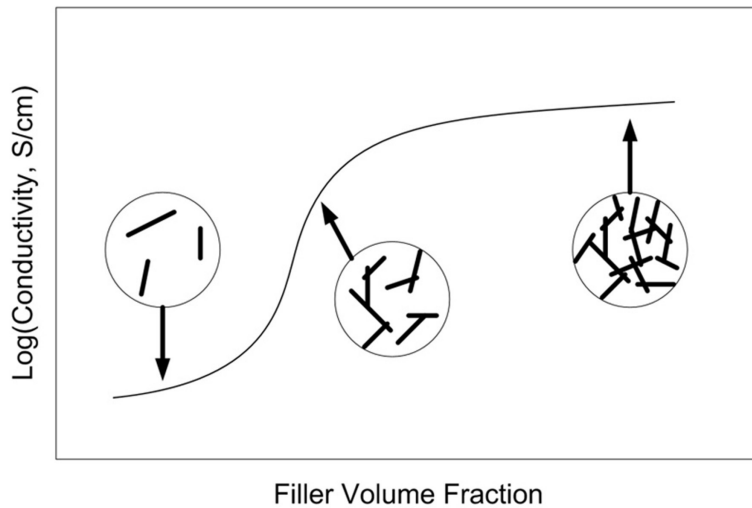


Figure 2.1: Effect of increasing filler loading on electrical conductivity

Percolation theory was introduced by Hammersley and Broadbent in 1957 (24). The theory was developed to describe how fluid flow would be affected by the random properties of the medium the fluid was flowing through. In this description, fluid and medium are used only in the broadest sense. The theory can describe liquid situations like solute flowing through a solvent, or it can describe other situations such as electrons flowing through the atomic lattice of a metal or, as suggested by Stauffer in 1985 (25), the spread of a fire through a forest. Hammersley and Broadbent suggested an example where water was flowing through a system of channels as illustrated in Figure 2.2. Each of the channels splits into two new channels. Each channel has a certain probability of being dammed. The flow of the water through the channels is then dependent upon the random set of dams. This system is known as bond percolation as each channel can be considered a bond through which the fluid flows. When enough of the channels are left

not dammed (as illustrated in Figure 2.2) the system is percolated and water is able to flow (24). This system is analogous to electrical percolation in polymers. Conductive fillers, such as nanotubes, act as the channels that electrons can flow through. The polymer matrix acts as a dam through which electrons essentially cannot pass. If enough conductive filler is present, probability dictates that a continuous network will be formed across the sample and the electrons will be able to flow continuously from filler particle to filler particle drastically increasing the electrical conductivity of the sample.

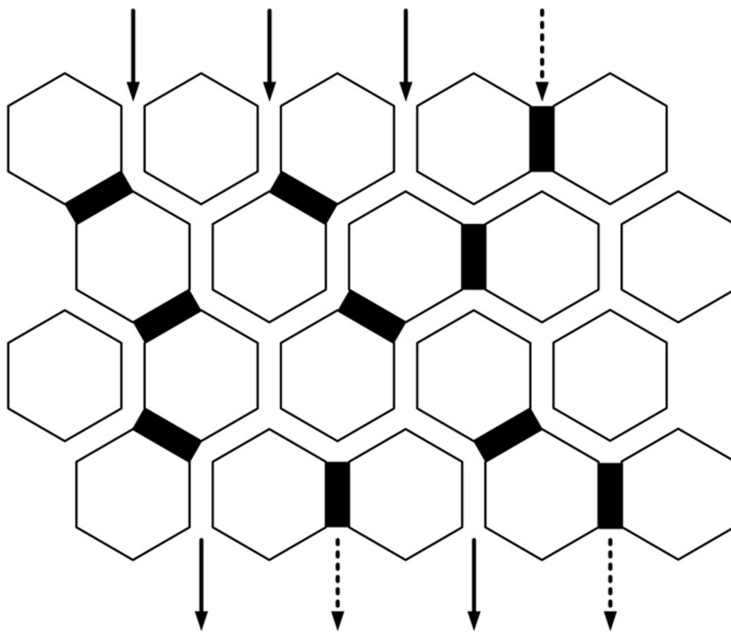


Figure 2.2: Bond percolation theory with channels

Conductive fillers that are added to polymers can vary greatly in properties. For example, multiwalled carbon nanotubes are hollow tubes that are nominally 10,000 nm long and 10 nm wide. Carbon black is a roughly spherical particle about 50 nm wide. Graphite nanoplatelets are flakes that are about 5000 nm wide and about 7 nm thick. These three fillers have very different geometries and will percolate differently. Fillers with high aspect ratios will align themselves with the direction of flow when melt

processing. Samples made in this manner will exhibit increased electrical conductivity in the direction of the flow (26). Additionally, filler/matrix adhesion can have a significant effect on the percolation threshold. If there is poor bonding between the polymer matrix and the filler, the filler particles will not distribute evenly throughout the polymer instead forming clusters of filler (27).

2.2: Thermal Conductivity

Heat is the energy that is transferred between two bodies, or between regions of a single body, that are different temperatures. This energy can be transferred in three ways; convection, radiation and conduction. Convection is the transfer of heat caused by the flow of molecules in a fluid. Radiation is the transfer of heat as electromagnetic radiation (primarily through infrared radiation). Conduction is the primary form of heat transfer in solids, including polymer composites. Conduction in solids is described by Fourier's Law shown in Equation 2.1 below:

$$q = -k \frac{\partial T}{\partial x} \quad (2.1)$$

where q is the heat flux (typically given in W/m^2), k is the thermal conductivity (typically given in $\text{W/m}\cdot\text{K}$) and $\frac{\partial T}{\partial x}$ is the temperature differential in the direction of heat transfer (typically in K/m) (28). It should be noted that heat always flows from areas of high temperature to areas of low temperature, thus the negative sign in Equation 2.1 (29). This heat is transferred through solids through phonons or, when available, free electrons. Free electrons are the primary energy carrier in metallic lattice solids. In non-metallic

materials, including polymers, heat is transferred using phonons. Phonon transport theory characterizes collective waves of vibrational energy within a solid such as thermal energy. A phonon itself is described as a quanta of vibrational energy. These phonons transport themselves by interacting with the subatomic particles within the solid (30). This can be simply illustrated in two dimensional representation of a crystal lattice where atoms are shown as balls and springs represent the bonds between the atoms as shown in Figure 2.3. As can be seen in this representation, when a vibration, such as a thermal vibration, is applied to one side of the lattice, the heat will transmit through the springs across the lattice to the other side (31).

The efficiency of phonon transport is dependent upon the material through which it is moving. When irregularities in the lattice structure occur, the collective wave of vibrational energy is scattered in the directions of the irregular bonds. When the phonons are scattered, the heat transfer is impeded and thus the thermal conductivity of the material is lower than a material where the phonons are not scattered (30). The Debye model, below as Equation 2.2, describes how phonons transmit heat through a solid.

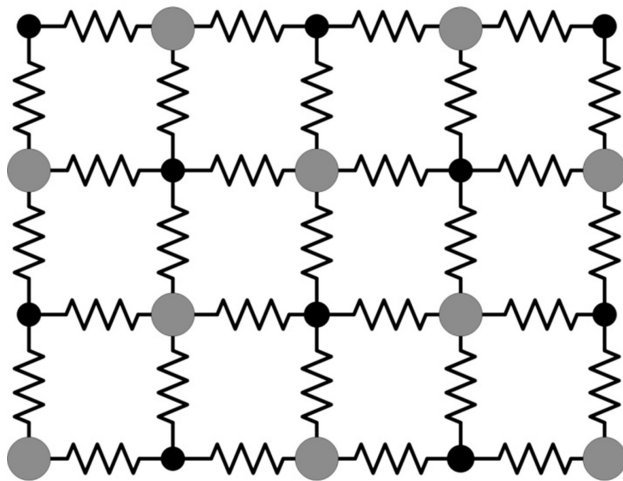


Figure 2.3: Two dimensional ball and spring model crystal lattice of sodium chloride

$$k = \frac{c \cdot u \cdot p}{3} \quad (2.2)$$

In Equation 2.2, k is thermal conductivity (typically in W/m-K), c is the volumetric heat capacity (typically in J/m³·K), u is the velocity of the phonons (approximately the speed of sound through the material, typically in m/s), and p is the mean free path (typically given in m) or the average distance the vibrational wave can travel before scattering attenuates the wave intensity to 1/e (about 0.3679) of its original value (32). The heat conduction within polymers and carbon fillers, even ones with crystalline lattices with disassociated electrons like carbon nanotubes, is dominated by phonon transport (32,33).

Thermal conductivity does not have a percolation threshold where it changes several orders of magnitudes with a small filler loading as electrical conductivity does (30). Previous work with carbon filled polymer systems has shown that thermal conductivity continually increases with increased filler loading as opposed to asymptotically tapering off at some value (34,35). This observation indicates that thermal conductivity is not dependent upon the presence or absence of filler networks within the polymer (4,36).

2.3: Tensile Modulus

Tensile modulus is a modulus of elasticity also known as Young's modulus. In general, modulus of elasticity is defined using Hooke's Law for an axially loaded member shown in Equation 2.3 below:

$$E = \frac{\sigma}{\epsilon} \quad (2.3)$$

where E is the tensile modulus, σ is tensile stress, and ε is tensile strain (20). This relationship allows the tensile modulus of a material to be found as the initial linear slope of a tensile stress vs. tensile strain curve. The initial linear portion of the curve must be used as Hooke's Law assumes Hookean behavior and by definition, any ductile material is non-Hookean and exhibits non-linear behavior as stress is applied (20). As seen in Figure 2.4 a generalized ductile material can exhibit up to 4 different behaviors as tensile stress is applied prior to failure.

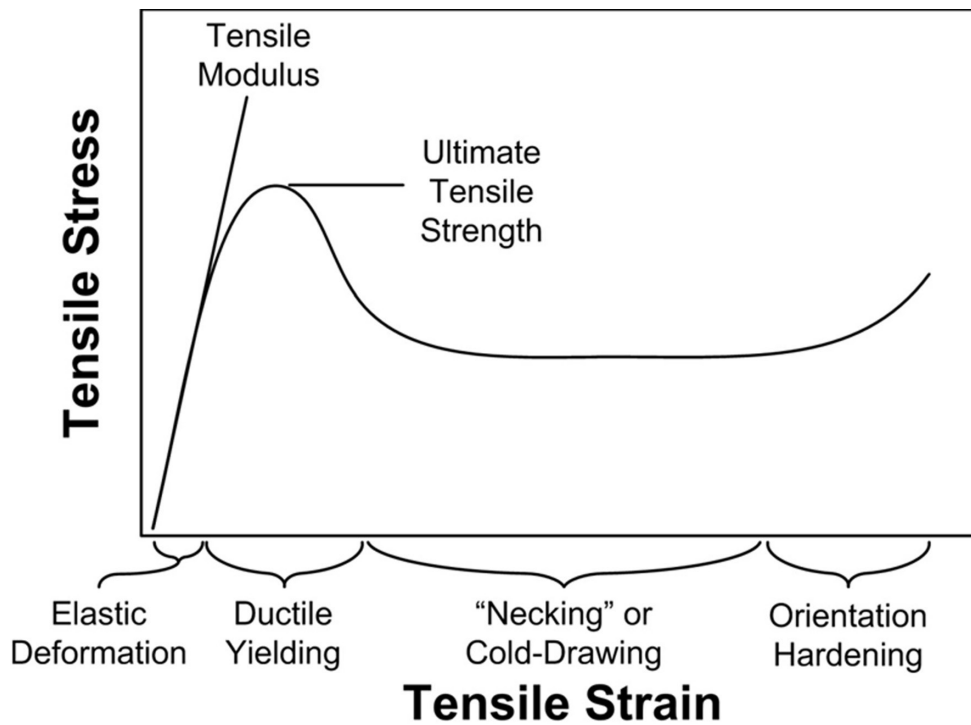


Figure 2.4: Generic ductile material tensile stress vs. tensile strain graph

Elastic deformation is the initial linear portion of the stress-strain curve where the material follows Hookean behavior and tensile modulus can be determined. Ductile yielding is the part following the initial linear portion of the stress strain curve. Ductile yielding is when plastic deformation begins to occur within the sample. Stress in the polymer will continue to increase to the ultimate tensile strength, then the composite will

undergo strain softening where the stress will decrease as strain increases and “necking” forms (20). Following ductile yielding materials may begin “necking” or cold-drawing where they decrease in cross-sectional area while greatly expanding in the tensile direction. This necking behavior can propagate throughout the constant width area of the tensile bar and often appears as a line of constant stress over a large strain. After necking, it is possible that materials may orientation harden. Orientation hardening occurs when polymer chains within the “neck” become oriented in the tensile direction by the strain and then the individual bonds within the chains begin to be stretched by the strain. This often appears as a second increase in stress with increasing strain (20).

The tensile modulus of a filled polymer is dependent upon the properties of the polymer and the filler being added. The tensile modulus of the polymer itself (typically 0.5 to 4 GPa) acts as a baseline value. The carbon fillers then modify the tensile modulus from that point. Carbon fillers often have very high tensile moduli compared to the polymer. For example, carbon black has a tensile modulus of about 827 GPa, graphite and carbon nanotubes can have tensile moduli of over 1000 GPa in the direction of their graphitic bonds, even in the c-axis, graphite has a tensile modulus of 37 GPa (37,38).

By virtue of their high tensile moduli, carbon fillers will increase the tensile modulus of the resulting composite to a value between the original polymer tensile modulus and the filler tensile modulus. When tensile stress is applied to a composite, the stress begins to deform the composite according to Hooke’s Law. When the polymer and higher tensile modulus fillers have good adhesion, the stress is transferred to those fillers. By having a higher tensile modulus, the fillers resist deformation more strongly than the polymer. In

order for the composite to continue to deform, the fillers must deform thus bringing the higher tensile modulus of the filler to bear. As was mentioned, the level of adhesion between the polymer and the filler is another important factor. In order to transfer the tensile stress to the high modulus filler, the polymer must bond well to the filler surface. If poor adhesion is evident between the filler and the polymer, the filler will simply pull or separate from the polymer as the polymer is stretched away.

Filler orientation and aspect ratio are also important factors for tensile modulus. Increased filler orientation has been shown to increase the tensile modulus of the resultant composite (39,40). Higher aspect ratios have also been shown to have a complex relationship with tensile modulus (as discussed in Chapter 11). Generally speaking, it has been shown that an increase in filler aspect ratio increases the tensile modulus of the resultant composite (41). A filler with a higher aspect ratio has the added benefit of increasing the orientation of the fillers in the direction of flow during sample creation. Many models of the tensile modulus, such as the Halpin-Tsai models, take the aspect ratio and orientation into account (37).

Chapter 3: Materials

3.1: Materials

For this study, three different carbon fillers and one polymer matrix were used. The polymer matrix studied was SABIC Innovative Plastic Lexan HF1130-111 polycarbonate. The carbon fillers studied were Hyperion Catalysis International Fibril multi-walled carbon nanotubes, Ketjenblack EC-600JD carbon black, and XG Sciences graphene nanoplatelets. The following sections will discuss the materials in more detail.

3.2: Matrix Material

The polymer matrix used in this study was SABIC Innovative Plastics Lexan HF1130-111 polycarbonate (PC). The chemical structure of polycarbonate is shown in Figure 3.1. Polycarbonate is a thermoplastic resin that can be re-melted and reshaped multiple times. Polycarbonate is primarily created through condensation polymerization of bisphenol-A and phosgene with a byproduct of hydrogen chloride or through condensation polymerization of the sodium salt of bisphenol-A and phosgene with sodium chloride as a byproduct (20). Polycarbonates are used in a variety of fields where durability or optical transparency is desired. Polycarbonate's very high impact strength and high optical transmittance along with high use temperature, tensile properties and flexural properties make it a very popular commercial and research plastic. It has been the focus of several other studies involving reinforcement with carbon fillers (42). This particular polycarbonate was chosen because it has high flow properties that are helpful for injection molding and allow for fillers to be added to the matrix. Table 3.1 shows properties of this material.

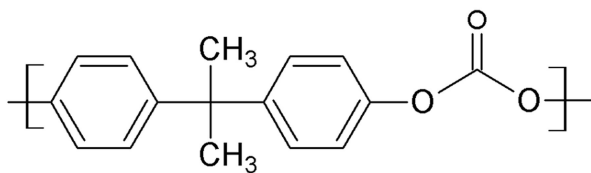


Figure 3.1: Lexan HF1130-111 Polycarbonate Structure

Table 3.1: Properties of Sabic's Polycarbonate Lexan HF 1130 (42).

Melt Flow Rate (300C/1.2kg)	25 g/10 min
Density	1.2 g/cc
Electrical Resistivity	1×10^{17} ohm-cm
Thermal Conductivity	0.19 W/m K

3.3: Fillers

3.3.1: Hyperion Catalysis International's FIBRIL Multiwalled Carbon Nanotubes

Carbon nanotubes are hollow cylinders formed from sheets of graphene. They can be single walled, being formed from a single sheet of graphene, or multiwalled, having several sheets of graphene forming coaxial cylinders. For this project Hyperion Catalysis International FIBRIL multiwalled carbon nanotubes (CNT) was used. A diagram of these nanotubes is shown in Figure 3.2. These particular nanotubes are ideally 8-walled tubes wrapped around a hollow 5 nm core forming a tube 10 nm in diameter and 1000 microns in length creating a high aspect ratio of 1000 (43). This aspect ratio allows low loading of nanotubes to have significant effects on electrical conductivity as well as mechanical properties.

FIBRIL multiwalled nanotubes are produced using a chemical vapor deposition (CVD) process (43). The CVD process produces very high yields of carbon nanotubes, but the purity is lower than other methods (e.g. arc discharge or laser ablation). CVD has been used to produce carbon fibers since 1959. By passing a hydrocarbon vapor, such as

benzene, over a catalyst at elevated temperatures (e.g. 1100°C) fibers of carbon can be formed. By changing the vapor, catalyst type, catalyst particle size and temperature different fibers, including nanotubes, can be formed. Typical industrial production CVD methods occur in fluidized bed reactors. When the hydrocarbon vapor comes in contact with the catalyst, it is decomposed into carbon and hydrogen. The carbon adheres to the catalyst and further carbon attaches to this carbon forming the nanotubes. As the nanotubes grow, the catalyst is disintegrated and distributes with the carbon nanotube agglomerate that leaves the reactor as a product. Typical carbon nanotube agglomerates will have over 95% carbon content and high bulk density making material handling easier.

For this project, CNT was provided by Hyperion Catalysis International as a 15 wt% masterbatch in polycarbonate, MB6015-00. Table 3.2 shows the properties of these nanotubes.

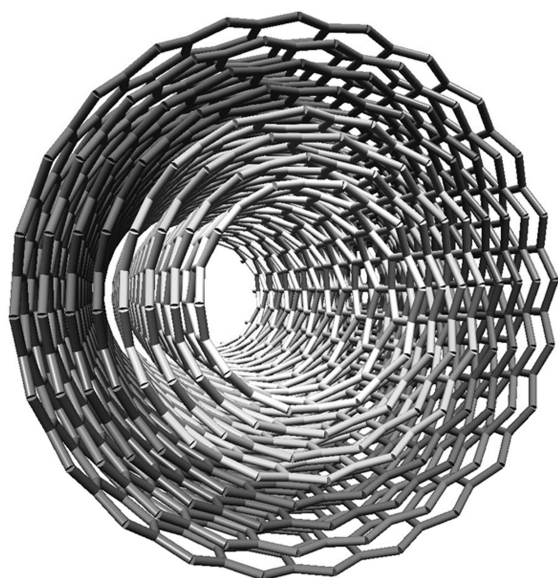


Figure 3.2: Diagram of carbon nanotube

Table 3.2: Properties of FIBRIL™ Carbon Nanotubes (43).

Composition	carbon with trace residual of metal oxide catalyst
Diameter	0.01 μm
Length	10 μm
Morphology	8 graphitic sheets wrapped around a hollow 0.005 μm core
Density	2.0 g/cc for the nanotube wall 1.75 g/cc for the hollow nanotube

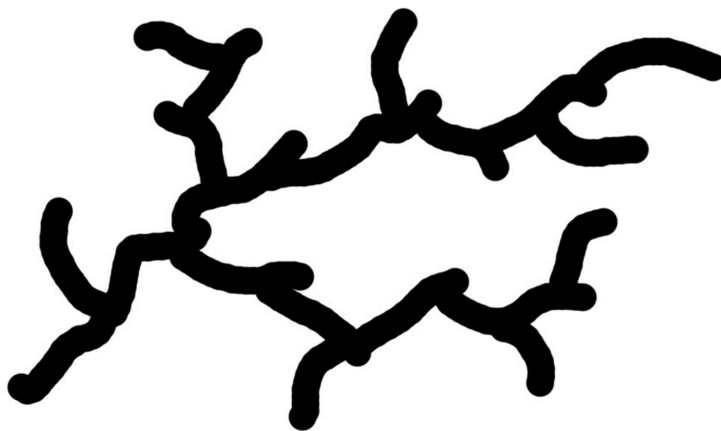
3.3.2: Ketjenblack EC-600 JD Carbon Black

Carbon black is a powdered form of amorphous carbon that is created from the incomplete combustion of heavy hydrocarbons and as a side-product in thermal cracking (14). It is used as a UV stabilizer, pigment, and sometimes thermal and electrical property enhancer in plastics and rubbers, as well as a colorant in inks and printer toner.

The primary production method of carbon black is the furnace process. The furnace process begins by taking a feedstock, typically aromatic hydrocarbons, and preheats them to 200°C to 250°C (44). The feedstock is then injected into the hot-flame zone of a gas-fired furnace (14). In the hot-flame zone, the feedstock is thermally decomposed into carbon and water vapor. Additional water is added to the furnace to quench the decomposition reaction. The reacted gas stream is then sent to filters where the carbon is separated from the unreacted feedstock and un-burnt furnace fuel. To increase the bulk-density of the carbon to easily handled and shipped levels, the carbon is typically mixed in a pin machine or pelletized with additional water in pelletizing drums and then dried in a rotary kiln drier (14,45). Carbon blacks can have different sizes and structures that are a function of the synthesis conditions of the carbon black. The type and concentration of

the feedstock chemicals, reactor temperature, and the time spent in the hot-flame zone of the reactor can have a significant effect on the properties of the carbon black (44). Carbon black with small aggregate size, high structure (high surface area), and low concentrations of un-reacted feedstock are optimal for increasing the electrical conductivity of polymer composites (44).

Ketjenblack EC-600 JD carbon black (CB) is produced using a proprietary process and is designed to have high electrical conductivity when added to polymers, even in small amounts. This was the reason it was selected for this project. Ketjenblack EC-600 JD has a large specific surface area and highly-branched morphology that allows it to interact with a large amount of the polymer matrix, as seen in Figure 3.3. As received, Ketjenblack EC-600 JD is in the form of pellets ranging from 100 microns to 2 millimeters in diameter. When subjected to high shear forces, like those found in a twin-screw extruder, the pellets separate out into primary aggregates of 30 to 100 nanometers. Table 3.3 lists the properties of this carbon black.



Primary Aggregate

Figure 3.3: Diagram of Ketjenblack EC-600 JD carbon black structure

Table 3.3: Properties of Akzo Nobel Ketjenblack EC-600 JD Carbon Black (46)

Electrical Resistivity of Carbon Black	0.01 to 0.1 ohm-cm
Product Form	Pellet in size from 100 microns to a few mm
Size of Carbon Black Aggregates	30-100 nm
Specific Gravity	1.8 g/cc
Bulk Density	100-120 kg/m ³
Ash, max	0.1 wt%
Moisture, max	0.5 wt%
BET (N ₂) Surface Area	1250 m ² /g
Pore Volume (DBP-absorption)	480-510 cm ³ /100 g

3.3.3: XG Sciences xGnP™ Graphene Nanoplatelets

Graphite is made up of many layers of hexagonal carbon sheets. Individual hexagonal carbon sheets are known as graphene as seen in Figure 3.4. Several of these sheets (~20) stacked together form what is called a graphene nanoplatelet. Exfoliated graphene nanoplatelets are primarily produced through high-yield, low purity, exfoliation of graphite particles. Exfoliated graphene particles will have properties dependent upon their production method and the graphite from which they are produced. Other methods produce graphene without the graphite intermediary. Epitaxial growth on silicon carbide involves heating silicon carbide substrates above 1100°C reducing the silicon carbide to graphene. Graphene is also created through chemical vapor deposition on to metal substrates. Different metals used as substrates impart different electrical properties to the resulting graphene sheet.

Often graphite particles are intercalated using sulfuric acid. This intercalation process introduces guest molecules into the van der Waals gap between the individual sheets. The graphite is then exposed to a proprietary microwave treatment that rapidly raises the

temperature of the graphite plates. This increase in temperature in the graphite causes the intercalated molecules to vaporize. The vaporization of the intercalated materials results in a separation of the individual sheets of graphite and expansion of around 500 times of the original graphite particle. The resultant particle is an accordion shaped expanded structure that can be broken down into individual nanoplatelets using ultrasonication. Following the ultrasonication the nanoplatelets are approximately 15 microns in diameter and nominally 5 nanometers in thickness. Further processing in a vibratory mill reduces the diameter of the nanoplatelets to 5 microns and maintains the nominal thickness (47). The graphene nanoparticles used in this project were made by XG Sciences. These particles are compounded into a 15 weight percent masterbatch with polycarbonate by Ovation Polymers Inc. as Extima GP MB PC 1515A which was then used for this project (48).

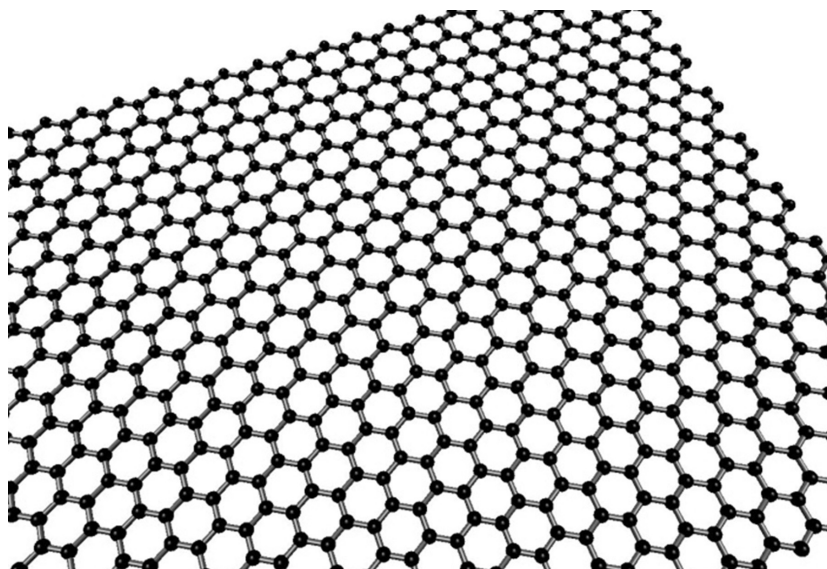


Figure 3.4: Diagram of graphene structure.

3.4: Formulation Naming Convention

In an effort to make labeling and subsequent identification of samples simple and efficient, each sample will have a unique name and number. Many of the samples in this project will look similar, thus it is important to have a consistent and meaningful naming system. The labels will be applied to the samples immediately following injection molding and will describe the filler or fillers present in the sample, and to what weight percent they are present. The naming system will be as follows:

B w x L y – z – #

Where:

B = project description (Boeing project)

w = filler type (A = carbon black, G = graphene, Q = carbon nanotubes)

x = weight percent of conductive filler in composite

L = polymer matrix (L = Lexan HF1130-111 polycarbonate)

y = replicate number (none for original, R for first replicate)

z = specimen type (F = flex bar, T = tensile bar, TC = thermal conductivity disks
(examples can be seen in Figure 3.5)

= specimen number (same as order it was injection molded)

An example of the naming system would be BQ4L-T-15. This would represent the 15th injection molded tensile bar containing 4 weight percent carbon nanotubes in polycarbonate. When samples contain multiple fillers a second filler type and weight percent pair will follow the first pair. For example, BA2G5L-F-5 would represent the 5th injection molded flex bar containing 2 weight percent carbon black, and 5 weight percent graphite nanoplatelets in polycarbonate.

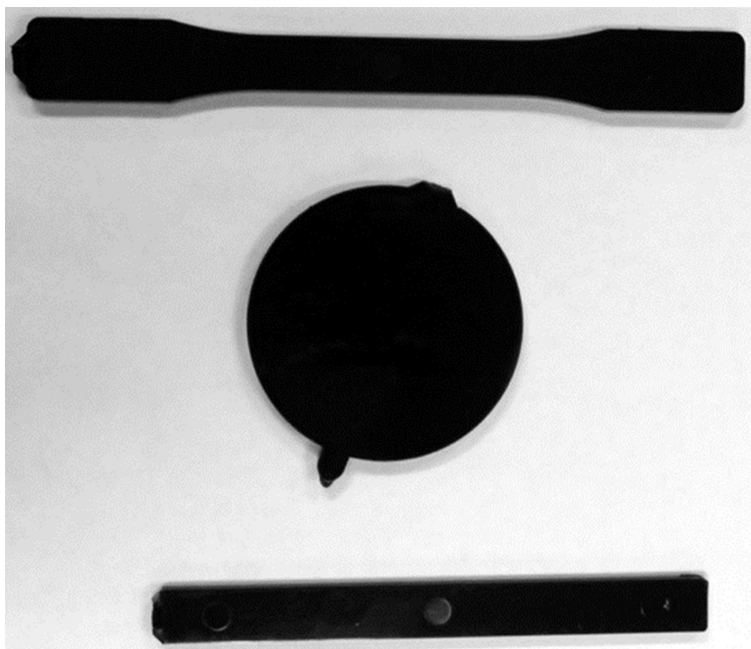


Figure 3.5: (Top to bottom) ASTM Type I Tensile Bar (T), 2.5" diameter thermal conductivity disk (TC), ASTM D790 Flex Bar (F)

Chapter 4: Fabrication and Experimental Methods

4.1: Fabrication Methods

This section will describe the details of fabrication for the test specimens. Specific information on the screw designs, extruding conditions, and the injection molding conditions can be found in the Appendices.

4.1.1: Drying

Prior to extrusion the Lexan HF1130-111, Hyperion Catalysis MB6015-00 CNT masterbatch, and Ovation Extima GP MB PC 1515B GNP masterbatch composites were dried in a Bry Air RD-20 indirect-heated dehumidifying drying oven at 121°C for 12 hours as seen in Figure 4.1. Following drying, the materials are stored in moisture barrier bags until extrusion. Following extrusion and pelletization, the PC and filled PC composites are dried in the Bry Air RD-20 indirect-heated dehumidifying drying oven at 121°C for 12 hours. Following drying, the materials are again stored in moisture barrier bags until injection molding.



Figure 4.1: Bry Air RD-20 Dryer

4.1.2: Extrusion

An American Leistritz Extruder Corporation Model ZSE 27 twin screw co-rotating extruder was used for this project and is shown in Figure 4.2. The extruder has a 27 mm co-rotating intermeshing twin screw, 10 independent heating zones, two side stuffers and a length to diameter ratio of 40. The screw designs, shown in Appendix A, were selected to minimize filler degradation while providing good dispersion of the fillers throughout the polymer.

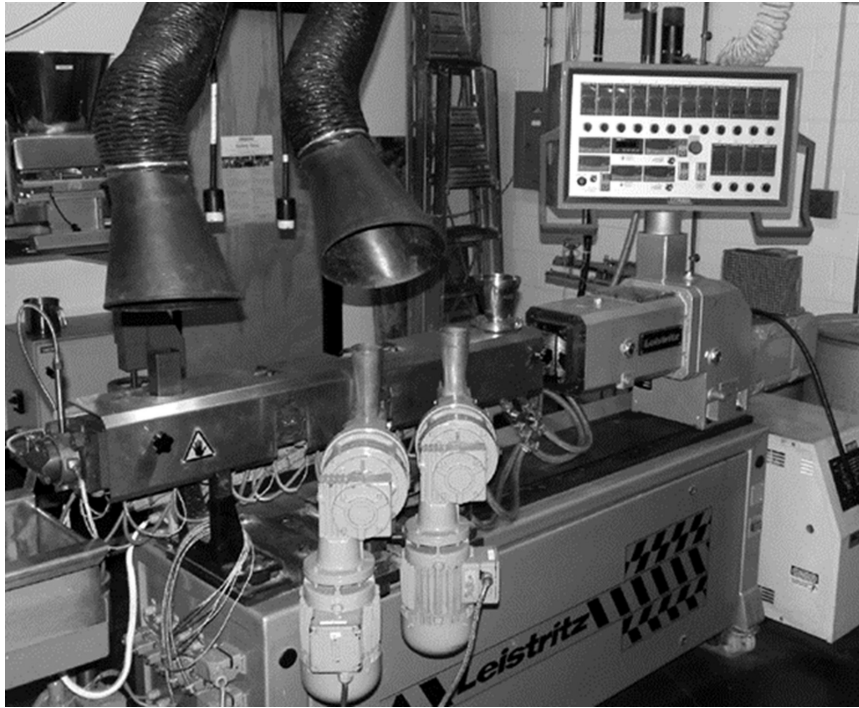


Figure 4.2: American Leistritz Extruder Corporation Model ZSE 27 twin screw extruder

The dried, pure polycarbonate pellets, dried CNT masterbatch and dried GNP masterbatch were introduced as received in the water-cooled Zone 1. For single filler systems, as received CB was introduced as received in Zone 5 by use of a side stuffer seen in Figure 4.2 and emphasized in Figure 4.3. Both Zones 1 and 5 were fed using

Schenck AccuRate Flexwall gravimetric feeders seen in Figures 4.4 and 4.5. Detailed parameters for the extrusion conditions for all formulations is given in Appendix A.

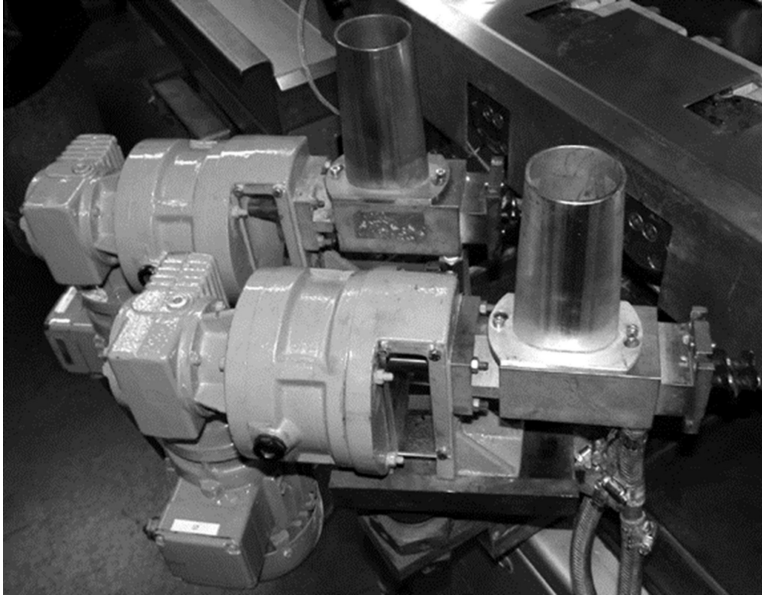


Figure 4.3: Side Stuffers seen disengaged from extruder



Figure 4.4: Zone 1 Feeder (Feeder 3) used to feed PC and Masterbatch pellets



Figure 4.5: Zone 5 Feeder (Feeder 4) used to add CB to extruder (shown without feed pipe)

After being extruded the 3 mm polymer strands are cooled in a water bath, seen in Figure 4.6, then passed to a Conair Model 20402HP-14A pelletizer (Figure 4.7) that produces 3 mm long pellets.

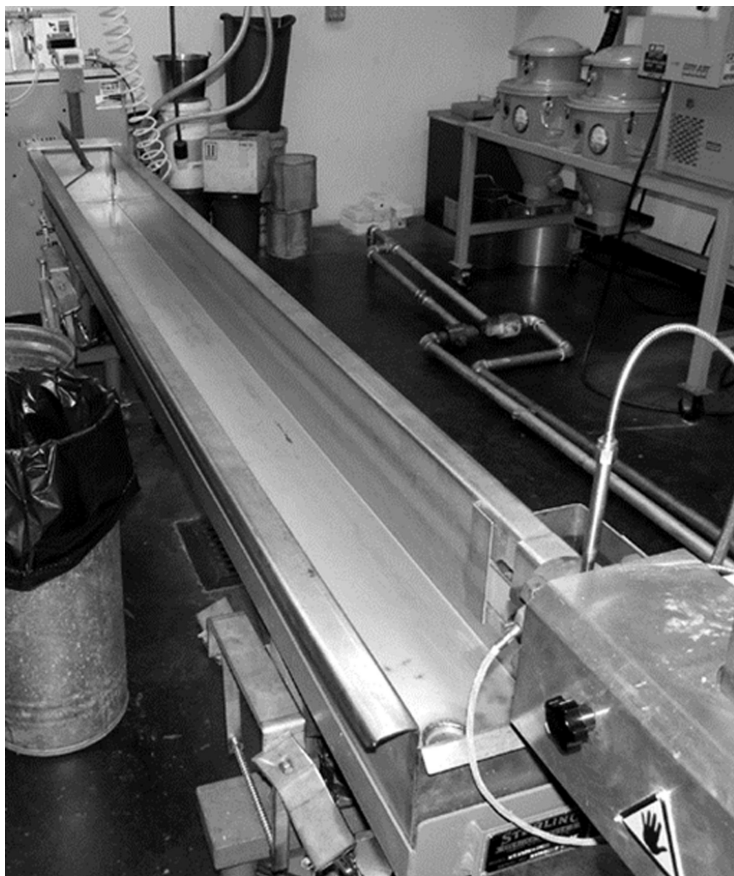


Figure 4.6: Water bath (here shown empty)

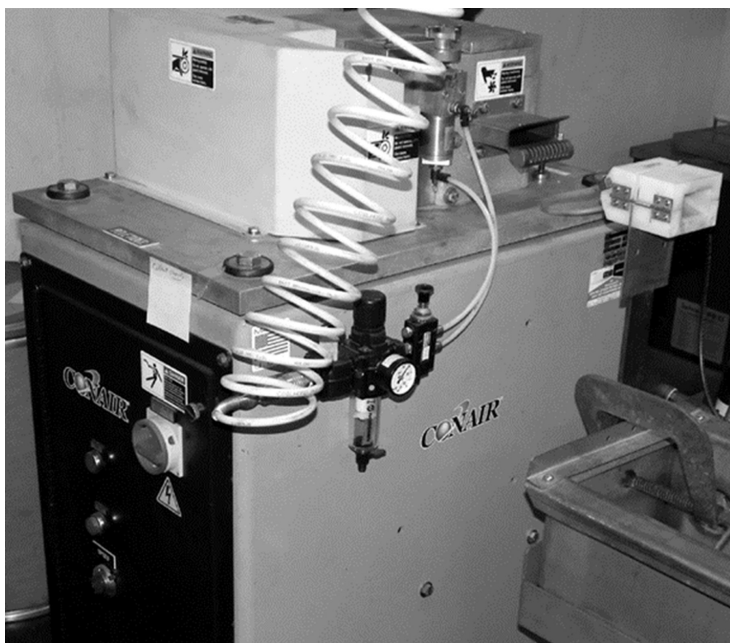


Figure 4.7: Conair Pelletizer and pre-pelletizer air-dryer

For the multiple filler systems containing CB, a masterbatch of 8 wt% CB in PC was created using the extruder. This masterbatch was then cooled in the water bath and pelletized. After drying, this masterbatch was introduced in Zone 1 along with the pure PC and other fillers.

4.1.3: Injection Molding

A Niigata model NE85UA₄ injection molding machine (shown in Figure 4.8) was used to produce test specimens. The injection molder has a 40 mm single screw with a length to diameter ratio of 18. The specifications of the machine are shown in Table 4.1. A four-cavity mold (Figure 4.9) was used to produce the test specimens. Detailed parameters for injection molding of all formulations are given in Appendix B.

Table 4.1: Niigata model NE85UA₄ injection molding machine specifications

NE85UA ₄ Specifications		
Maximum Injection Pressure		22,610 psi
Maximum Screw Speed		320 rpm
Maximum Clamping Force		82.50 US tons
Length of Screw Section	Feed	396 mm
	Compression	180 mm
	Metering	144 mm



Figure 4.8: Niigata model NE85UA₄ injection molding machine

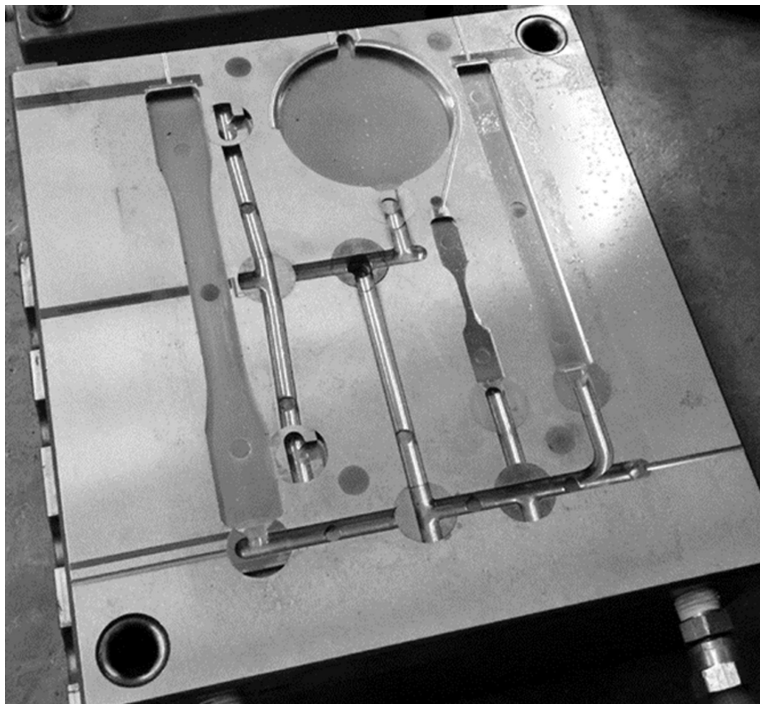


Figure 4.9: 4-cavity mold showing (left to right) ASTM type I Tensile, 2.5" disk, ASTM type V Tensile (not used) and ASTM D790 Flex Bar

4.2: Experimental Test Methods

This section will describe the details of test methods for the test specimens. Results of these tests will be discussed in Chapters 5-12 and detailed results are available in the appendices.

4.2.1: Density: ASTM D792-98 Test Method

The density of the composite materials was found using the ASTM D792-98 test method, Specific Gravity and Density of Plastics by Displacement (49). For this test, 6.4 cm diameter injection molded disks are used. The dry mass of the samples is measured first. The samples are then submerged in water that has been allowed to sit overnight exposed to the atmosphere to equilibrate dissolved gases and temperature and the mass is measured in this state. Composite density can then be calculated using Equation 4.1,

$$\rho = \frac{m_{dry}}{m_{dry} + m_{wet}} \cdot \rho_{water} \quad (4.1)$$

Where ρ is the specimen density, m_{dry} is the dry mass, m_{wet} is the submerged mass and ρ_{water} is the density of the test water. The density can then be compared to a theoretical density for the composite given by Equation 4.2,

$$\rho_{theo} = \frac{1}{\sum_i \frac{\phi_i}{\rho_i}} \quad (4.2)$$

Where ρ_{theo} is the theoretical specimen density, ϕ_i is the weight fraction of each individual component and ρ_i is the density of the individual component.

4.2.2: Melt-Flow Indexing (MFI) Test Method

The Melt Flow Index (MFI) was determined using a Tinius Olsen Plastometer Melt Indexer (MP 987/WL 987) shown in Figure 4.10. For the as received Lexan HF1130-111 and the extruded Lexan HF1130-111 a weight of 1.25 kg, temperature of 300°C, and a dwell time of 360 s, and a collection time of 15 s was used. For the filled composite samples the test was run at 320°C with a 5 kg weight and a dwell time of 360 s. A higher temperature and weight was needed to allow the extrudate to exit the apparatus with the filled polymer as compared to the neat polymer. The amount of time needed to empty the barrel was measured since the test happened very ‘quickly’. A test could not be conducted on the pure Lexan as the material emptied the barrel too quickly to be reliably timed. The 8 wt% carbon nanotubes in Lexan, 8 wt% carbon black in Lexan and 10 wt% carbon black in Lexan would not exit the barrel and were also not tested.



Figure 4.10: Olsen Plastometer MP 987/WL 987 Melt Indexer

4.2.3: Differential Scanning Calorimetry (DSC) Test Method

A Mettler Toledo 823E DSC (shown in Figure 4.11) was used to measure the glass transition temperature (T_g) of every composite. Approximately 10 mg of each extruded pellet was placed in a sealed aluminum pan with a 'vent hole' in the lid. Nitrogen purge gas was used. The following heating cycle was used and T_g was determined on the second heating cycle. T_g was determined by a change in heat flow (i.e. heat capacity). The heating method is shown below.

- 1) Heat 40°C to 350°C at 10°C/min
- 2) Cool 350°C to 40°C at 10°C/min
- 3) Hold 40°C and hold for 5 min
- 4) Heat 40°C to 350°C at 10°C/min



Figure 4.11: Mettler Toledo 823E DSC

4.2.4: Capillary Rheology Test Method

Capillary rheology testing is performed according to ASTM D3835-96 using a Goettfert Rheo-Tester 1000 capillary rheometer seen in Figure 4.12 (50). The capillary rheometer is heated to a test temperature of 270°C, 300°C or 320°C. A 1mm diameter, 30 mm long capillary die was used for this project. A 200 bar pressure transducer was used for low viscosity formulations. A 1400 bar pressure transducer was used for high viscosity formulations. Figure 4.13 shows the various components of the rheometer. At least 4

measurements were taken at 50, 100, 200, 500, 1000 and 2000 1/s shear rates. Prior to testing samples were dried in a vacuum oven at 30" Hg vacuum and 100°C for 6 hours. CNT/PC composites were tested at 270°C, 300°C and 320°C. 320°C began to degrade the pure PC so CB/PC samples were tested at 270°C and 300°C. The 300°C data was found to be unnecessary thus GNP/PC samples and multiple filler samples were only tested at 270°C.



Figure 4.12: Goettfert Rheo-Tester 1000 capillary rheometer



Figure 4.13: (Top to bottom) 30/1 capillary die and die nut, drive piston, 1400 bar pressure transducer, 200 bar pressure transducer

The apparent shear rate in the capillary, $\dot{\gamma}_a$, was calculated Equation 4.3 below

$$\dot{\gamma}_a = \frac{4Q}{\pi R^3} \quad (4.3)$$

where Q is the volumetric flow rate, and R is the radius of the capillary (51). Shear stress at the wall, τ_R , in a capillary is given by:

$$\tau_R = \frac{R\Delta P}{2L} \quad (4.4)$$

where ΔP is the pressure drop over the capillary, R is the radius of the capillary and L is the length of the capillary. The relationship between the apparent shear rate and the true shear rate at the wall for any fluid, $\dot{\gamma}_R$, is given by Equation 4.5 (51).

$$\dot{\gamma}_R = \dot{\gamma}_a \left[\frac{1}{4} \left(3 + \frac{d \ln \dot{\gamma}_a}{d \ln \tau_R} \right) \right] \quad (4.5)$$

The Weissenberg-Rabinowitsch correction, seen in Equation 4.5 as the quantity within the square brackets, corrects for the effects of a non-Newtonian flow. When the fluid is Newtonian, the wall stress changes linearly with the shear rate. This causes the Weissenberg-Rabinowitsch correction to be 1 (51).

To determine the value of the derivative in the Weissenberg-Rabinowitsch correction, a quadratic equation was fit to the $\ln(\dot{\gamma}_a)$ vs. $\ln(\tau_R)$ data. A quadratic fit provides good agreement with all data collected ($R^2 > 0.995$). The derivative of the quadratic equation can be simply determined. This allows calculation of a true shear rate that then allows the calculation of a steady-shear viscosity using Equation 4.6 (51).

$$\eta = \frac{\tau_R}{\dot{\gamma}_R} \quad (4.6)$$

Where steady-shear viscosity data is available at multiple test temperatures (CNT/PC and CB/PC) the data is time-temperature superpositioned to create a single master curve of shifted viscosity, η_r , versus shear rates at 270°C according to Equation 4.7 below,

$$\eta_r(a_T \dot{\gamma}) \equiv \frac{\eta(T) T_{ref} \rho_{ref}}{a_T T \rho} \quad (4.7)$$

where a_T is the shift factor, $\dot{\gamma}$ is the shear rate, $\eta(T)$ is the viscosity at the test temperature, T_{ref} is the reference temperature (270°C), ρ_{ref} is the sample density at the

reference temperature, T is the test temperature and ρ is the sample density at the test temperature (51).

4.2.5: Small Amplitude Oscillatory Shear Rheology Test Method

Small-amplitude oscillatory shear (SAOS) complex viscosity was determined using a Bohlin C-VOR rotational rheometer (shown in Figure 4.14). For these materials 25 mm diameter parallel plates (seen installed in Figure 4.14) with a 3mm nominal gap was used and testing was performed according to ISO 6721-99 (52). Two 25 mm diameter disks were cut from an injection-molded 6.4 cm diameter disk. Five 25 mm disks were tested from each formulation. The 25 mm disks were vacuum dried for 6 hours at 30 inches of mercury vacuum. CNT/PC samples were tested at 210°C, 230°C, 250°C, 270°C, 290°C, 310°C, 330°C and 350°C. Following this testing it was determined that 210°C, 230°C and 350°C testing did not provide helpful data thus CB/PC samples were tested at 250°C, 270°C, 290°C, 310°C and 330°C. Testing started with an amplitude sweep varying from 0.1% to 10% strain to determine the limits of the linear-viscoelastic regime in which SAOS analysis is valid. Frequency sweeps varying logarithmically from 0.1 to 100 rad/s at an amplitude of 1% strain were taken in a “ramp-up then ramp-down” fashion to determine the rheological properties of the samples.



Figure 4.14: Bohlin C-VOR rotational rheometer with installed 25mm parallel plates

Time-temperature superpositioning was performed using the linear-viscoelastic storage modulus, $G'(\omega)$, and the loss modulus, $G''(\omega)$. The data was shifted by a shift factor (a_T), according to Equations 4.8 and 4.9 below, to create master curves of $G'(\omega)$ and $G''(\omega)$ with a reference temperature of 270°C (51).

$$G'_r(a_T \omega) \equiv \frac{G'(T) T_{ref} \rho_{ref}}{T \rho} \quad (4.8)$$

$$G''_r(a_T \omega) \equiv \frac{G''(T) T_{ref} \rho_{ref}}{T \rho} \quad (4.9)$$

where ω is the oscillation frequency in radians/s, a_T is the shift factor, $G'(T)$ is the storage modulus at the test temperature, $G''(T)$ is the loss modulus at the test temperature, T_{ref} is the reference temperature for the superpositioning (270°C), ρ_{ref} is the density of the material at the reference temperature, T is the test temperature, and ρ is the sample density at the test temperature. The shift factors were chosen to optimize the fit of the

shifted data to a single master curve. Complex viscosity, $\eta^*(\omega)$ can then be calculated from the elastic and viscous moduli using Equation 4.10 (51).

$$\eta^*(\omega) \equiv \frac{\sqrt{G'(\omega)^2 + G''(\omega)^2}}{\omega} \quad (4.10)$$

When the steady-shear viscosity and SAOS complex viscosity are compared at $\omega = \dot{\gamma}$, many linear polymers show the same values. This is known as the Cox-Merz rule (51,53). The Cox-Merz rule will be tested for CNT/PC and CB/PC in this project.

While the Bohlin C-VOR is capable of steady-shear testing, the high stiffness of these filled systems prevents the rheometer from attaining the shear rates that are of interest to this project, thus only capillary steady-shear testing will be performed.

4.2.6: Through-Plane Electrical Resistivity Test Method

Injection molded specimens that had high electrical resistivity, greater than 10^4 ohm-cm, were tested for electrical resistivity using the through-plane, volumetric electrical resistivity test method. Following ASTM D257, this test uses a Keithley 6517A Electrometer/High Resistance Meter equipped with an 8009 Resistivity Test Fixture to apply a constant voltage (typically 100V) to the as-molded 6.4 cm diameter, 3.2 mm thick disk (54). The testing is automated using Keithley 6524 High Resistance Measurement software. A minimum of six specimens were tested for each formulation. The testing apparatus is shown in Figure 4.15.



Figure 4.15: ASTM D257 apparatus comprised of Keithley 6517A Electrometer/High Resistance Meter (left) and Keithley 8009 Resistivity Test fixture (right)

4.2.7: In-Plane Electrical Resistivity Test Method

Injection molded samples that had low electrical resistivity, less than 104 ohm-cm, were tested for electrical resistivity using the in-plane, volumetric electrical resistivity test method. The in-plane volumetric electrical resistivity of the center 60 mm long, 3.3 mm thick, 12.6 mm wide tensile bars (rectangular necked area) injection molded tensile bars was determined according to ASTM D 4496 at 23°C (55). This test was conducted with 2 probes. In the two probe method, the tensile bar is scratched (1mm depth if possible) with a razor blade, placed in liquid nitrogen, and then broken by hand (using pliers) at the desired location. Hence, a fracture surface is created on both ends of the in plane sample. Then the 3.3 mm thick by 12.6 mm wide ends are coated with conductive silver paint (one coat) and allowed to dry for 1 hr. One probe is placed on each silver painted fracture surface and a constant voltage is placed across the sample using a Keithley 2400 Source Meter. The resulting current is also measured on this same Keithley 2400. The volume electrical resistivity is calculated from Equation 4.11.

$$ER = \frac{(\Delta V)(w)(t)}{(i)(L)} \quad (4.11)$$

Where ER is the volume electrical resistivity, ΔV is the voltage drop over length of sample, w is the sample width, t is the sample thickness, i is the current, and L is the length over which ΔV is measured.

The in-plane volumetric electrical resistivity of 60 mm long, typically 3 mm diameter extruded rods were also tested according to ASTM D 4496 at 23°C (55). In the two probe method, fracture surface is created on both ends of the rod by scoring lines 60 mm apart on the rod and then, if necessary submersing the sample in liquid nitrogen for 2 minutes. The sample is retrieved from the liquid nitrogen, if used, and broken along the score lines. The ends of the 3 mm diameter rod are then coated with conductive silver paint (one coat) and allowed to dry for 1 hr. One probe is placed on each silver painted fracture surface and a constant voltage is placed across the sample using a Keithley 2400 Source Meter. The resulting current is also measured on this same Keithley 2400. The volume electrical resistivity (ER) is calculated from Equation 4.12 where R is radius of the rod and the other symbols retain their meaning from Equation 4.11.

$$ER = \frac{(\Delta V)(\pi R^2)}{(i)(L)} \quad (4.12)$$

4.2.8: Thermal Conductivity: Guarded Heat Flow Meter Test Method

Thermal conductivity testing of the specimens followed the ASTM F433 Guarded Heat Flow Meter method as seen in Figure 4.16 (56). To comply with this ASTM, a Holometrix (now Netzsch) Model TCA-300 Thermal Conductivity Analyzer was used to analyze 5 cm diameter 3.2 mm thick disks at 55°C. The 5 cm diameter disks were cut from injection molded 6.4 cm diameter disks with a hole saw. The 55°C test temperature was selected to allow the machine to maintain a temperature gradient across the sample. For each formulation at least 5 specimens were tested with TCA-300 calibration “locon13”.

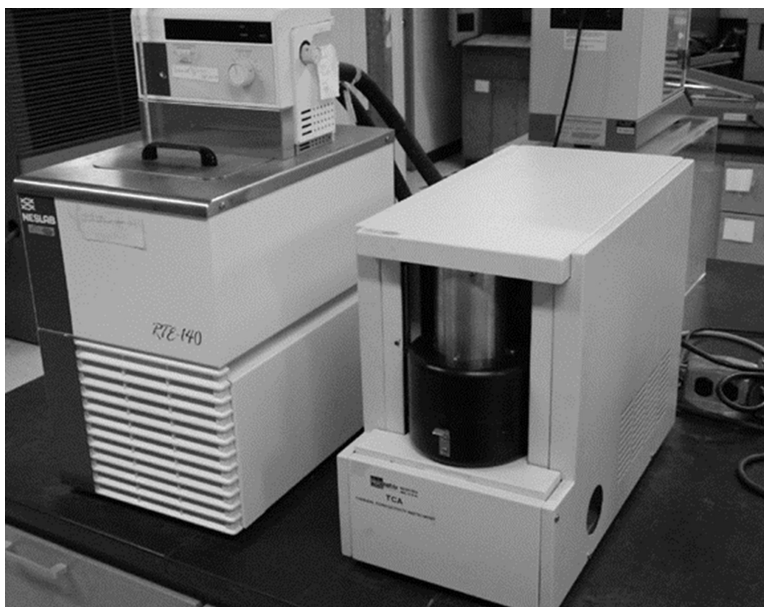


Figure 4.16: Holometrix TCA-300 Thermal Conductivity Analyzer (right) with constant temperature ethylene glycol/water circulator (left)

The TCA-300 controls the energy to the upper heater in an effort to maintain average temperature of the sample at the test temperature of 55°C. Heat flows from the upper heater to the specimen through a layer of heat-sink compound (applied to ensure good thermal contact). Heat passes through the sample and into the lower surface (again using

heat-sink compound to ensure thermal contact). In the lower surface the heat passes through a heat-flow meter. The lower surface also has a heater that helps maintain the average sample temperature at 55°C. There are thermocouples that monitor the temperature at the upper and lower surface of the specimen. Using these temperatures and the heat-flow the machine calculates thermal conductivity using Equation 4.13 below:

$$R_s = N \left(\frac{T_U - T_L}{q} \right) - R_0 \quad (4.13)$$

where R_s is the specimen thermal resistance, T_U is the upper surface temperature, T_L is the lower surface temperature, q is the heat flow, N is a proportionality constant and R_0 is the sum of all contact thermal resistances. N and R_0 are calibrated for the machine using reference specimens of known thermal conductivity (57). The specimen thermal conductivity is then calculated using Equation 4.14 below:

$$R_s = \frac{t}{k} \quad (4.14)$$

where t is the sample thickness and k is the thermal conductivity (57).

4.2.9: Mechanical Tensile Property Test Method

Tensile properties of the composites were obtained at ambient conditions using 16.5 cm long 3.3 mm thick injection molded ASTM Type 1 tensile bars. These samples are tested according to ASTM D638 with a crosshead rate of 5mm/min for reinforced plastics (58). Testing was performed on an Instru-Met Sintech screw driven mechanical testing machine as shown in Figure 4.17. Tensile modulus was calculated from the slope of the

initial linear portion of the tensile stress versus tensile strain curve. At least 5 samples of each composite were tested. These samples were preconditioned at 23°C and 50% relative humidity for 2 days.

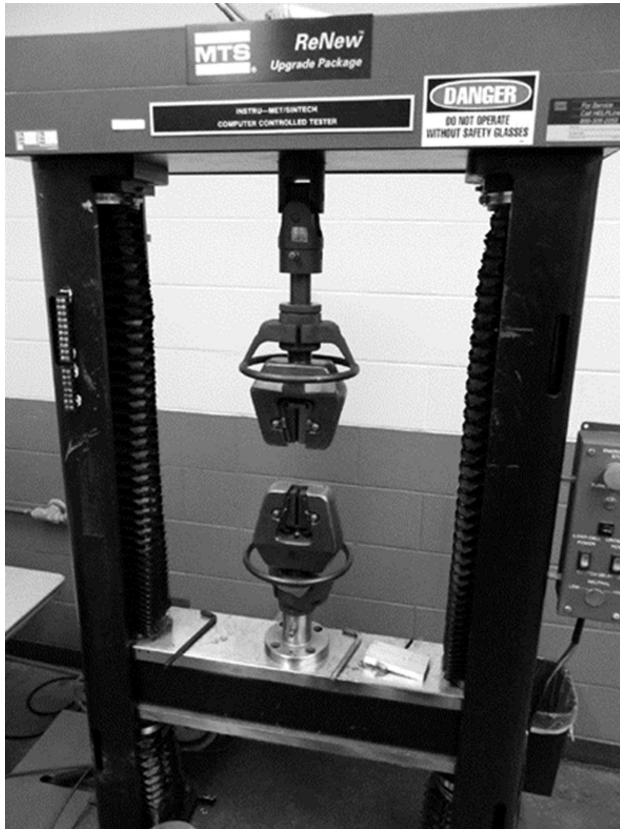


Figure 4.17: Instru-Met Sintech mechanical testing machine with tensile apparatus installed

4.2.10: Mechanical Flexural Property Test Method

Flexural properties of the composites were obtained at ambient conditions using 3.1 mm thick, 12.7 mm wide and 127 mm long flexural bars. The samples are tested using a three-point loading method in accordance with ASTM D790 with a crosshead rate of 5.3 mm/min (59). At least 8 samples from each specimen is tested with a span to thickness ratio of 16:1 on a Instru-Met Sintech screw driven mechanical testing machine as shown in Figure 4.18. Deflection of the flex bar was measured using a linear variable

displacement transformer (LVDT). The flexural moduli of the samples were calculated from the slope of the initial linear portion of the flexural stress versus flexural strain curve. These samples were preconditioned at 23°C and 50% relative humidity for 2 days.



Figure 4.18: Instru-Met Sintech mechanical testing machine with flex apparatus installed

4.2.11: Optical Polishing Method

Optical imaging samples are created from flex bars. Approximately 1cm squares were cut from the center of the flex bars using a scroll saw. Labeled 1.25 inch diameter reusable epoxy molds were prepared by first spraying the cylinders with mold release. Aluminum foil was placed over the removable bottoms. The bottoms were pressed onto the cylinder and the excess aluminum foil was trimmed off. The bottoms were again removed and double-sided tape was applied to the aluminum foil. The bottoms were pressed into the cylinder again and the excess tape was trimmed off. Disposable plastic

sample clips were then applied to the 1 cm square specimens. The specimens were then pressed, cut side down, onto the tape. Two-part optical epoxy was then poured over the sample to a depth of about 2-cm, any air trapped under the tape was pressed out and the epoxy was allowed to cure creating pucks.

Following curing of the epoxy, the sample pucks are removed from the mold and labeled on the anti-sample side with an indelible marker. The aluminum foil and tape were removed as much as possible. The sample pucks were then hand ground on a Diamond Pacific rotating lap (Figure 4.19) with 320 grit SiC paper with water lubrication until the sample is exposed, the surface is plane and the remaining tape has been removed. The anti-sample side of the sample pucks was also ground until plane and parallel to the sample side to facilitate optical imaging. The sample pucks were re-labeled on the anti-sample side after grinding. At this time the edge on the anti-sample side was ground down to better facilitate handheld grinding. The sample pucks were subsequently placed in an ultrasonic bath for 5-minutes to remove loose grit then hand ground on the rotating lap with 600 grit SiC paper with water lubrication until the grind marks from the 320 grit paper were removed. The sample pucks were then placed in an ultrasonic bath for 5 minutes to remove loose grit then hand ground on the rotating lap with 1200 grit SiC paper with water lubrication until the grind marks from the 600 grit paper were removed. The sample pucks were again placed in an ultrasonic bath for 5 minutes to remove loose grit.

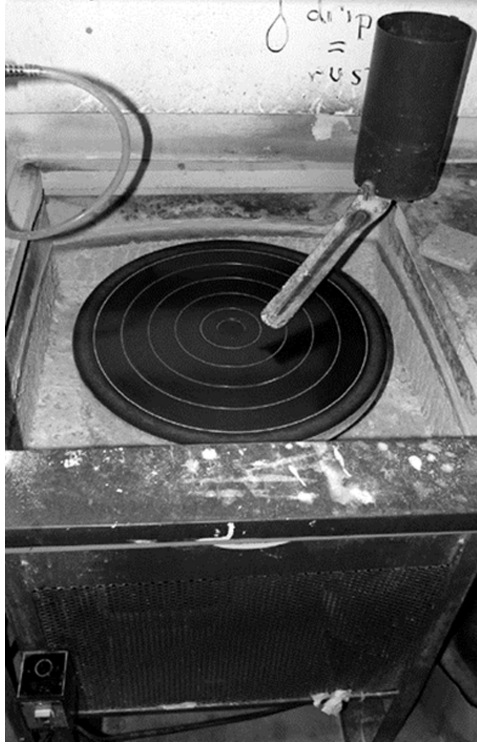


Figure 4.19: Diamond Pacific rotating lap with water drip apparatus

The cleaned sample pucks were then hand polished on a Buehler Ecomet (Figure 4.20) rotary polisher using a 9 micron diamond suspension until the grind marks from the 1200 grit SiC paper are removed. The sample pucks were cleaned after this and all following steps using an ultrasonicator with a ½” tip for 2 minutes after polishing except after the final step when they were cleaned for 4 minutes. The sample pucks were then hand polished on the rotary polished with a 3 micron diamond suspension until the grind marks from the 9 micron diamond suspension are removed as seen through a simple optical microscope. The sample pucks were then hand polished with a 1 micron deagglomerated alumina suspension until the grind marks from the 3 micron diamond suspension are removed as seen through a simple optical microscope. The sample pucks were then placed in a weighted vibratory polishing puck and placed on a Buehler Vibromet I vibratory polisher (seen in Figure 4.21) with 0.05 micron alumina suspension and

polished for 2 hours to obtain a satisfactory surface. Optical imaging is done on an Olympus BX-60 System Microscope shown in Figure 4.22. Images are captured using an Optixcam Summit 1.3 camera seen in the top of Figure 4.22.



Figure 4.20: Buehler Ecomet rotary polisher with Automet 2 automated polishing head



Figure 4.21: Buehler Vibromet I vibratory polisher



Figure 4.22: Olympus BX-60 System microscope with Optixcam Summit 1.3 camera on top

4.2.12: Field Emission Scanning Electron Microscope (FESEM) Test Method

CNT containing samples used for FESEM analysis were 2 mm by 2 mm sticks about 25 mm long cut from the center 6 cm section of tensile bars using a scroll saw. The sticks were placed in liquid nitrogen and then broken using two pairs of pliers. This created a cryogenic fracture surface that was the target of the imaging. The samples were mounted, with the cryogenic fracture surface facing upwards, to FESEM sample holders with hot-melt glue. Conductive carbon paint was applied from to sample over the hot-melt glue to the sample holder to ensure conductivity from the sample to the sample holder. The samples were then placed in the Hitachi S-4700 FESEM shown in Figure

4.23. Imaging was done at 2 kV accelerating voltage with a working distance of 1.9 mm. Images were collected using the upper secondary electron detector.

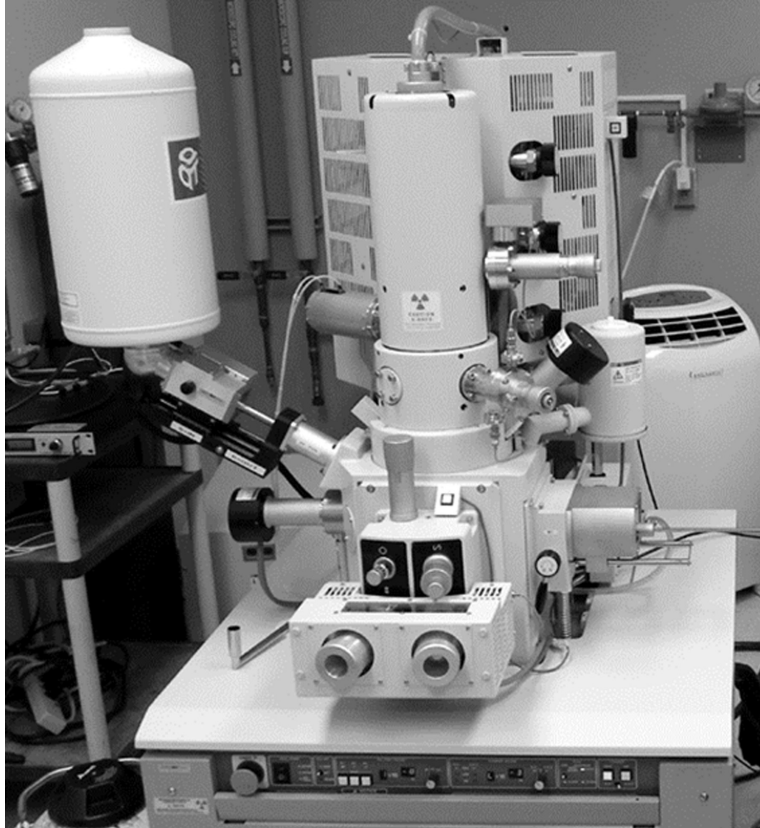


Figure 4.23: Hitachi S-4700 FESEM with energy dispersive x-ray spectrometer seen on left

CB containing samples used for FESEM analysis were sections taken from 3.2 mm thick by 12.7 mm wide flex bars. The sample sections were then cast into epoxy pucks similarly to the optical samples. The surface of the resultant pucks were then polished on a rotary lap with #4000 SiC grit. They were then polished on the same lap with a 1-micron alumina/water slurry. Following the polishing on the lap, the sample pucks were polished on a Buhler Vibromet vibratory polisher with 0.05 micron alumina/water slurry for 2 hours. The composite surface was then etched with O₂ plasma at 23°C and 0.28 torr for 1 hour. The etched surface was then sputter coated with gold to a thickness of

about 10 nm. The coated samples were then imaged in a JEOL Ltd. JSM-7500F FESEM at 15kV accelerating voltage, 6 mm working distance with images captured with the upper secondary electron detector.

4.2.13: Transmission Electron Microscope (TEM) Test Method

TEM samples were taken from 2 mm by 2 mm by about 15mm long sections the center 6 cm of a tensile bar with a scroll saw. The samples were then clamped and trimmed using a wire saw to get them down to less than 0.5 mm by 0.5 mm by about 5 mm. These sections are then placed in a parallel jaw sample holder. The holder is placed into a Leica EM UC6 ultramicrotome (shown in Figure 4.24) equipped with an EM FC7 cryo chamber. The ultramicrotome is cooled to -140°C and then the samples are cut until parallel with the diamond knives using a Diatome cryo-sectioning knife. Then the edges of the samples are sectioned about 30 microns deep leaving a mesa, approximately 50 microns wide by 50 microns tall, on the samples. The samples are then cut to approximately 70 nm thick slices. These slices are picked up and placed onto carbon coated, nickel TEM grids. The samples are then imaged in a JEOL Ltd. JEM-4000FX TEM shown in Figure 4.25. Composites containing GNP were imaged using bright field and dark field techniques. Bright field imaging allowed for the identification of CB or CNT if present and allowed the GNP particles to be seen in a true representation. Dark field imaging allowed for the positive identification of GNP particles (as opposed to torn TEM grid coating) by isolating the electrons that are diffracted by the crystalline structure of the GNP, following Bragg's Law, causing the GNP particles to brightly light up in the image. Dark field imaging was accomplished by positioning the objective

aperture slightly off-center. Images were obtained from the TEM using a Gatan Orius camera. Imaging was performed at 15000X.



Figure 4.24: Leica EM UC6 ultramicrotome shown without cryo chamber



Figure 4.25: JEOL JEM-4000FX transmission electron microscope

4.2.14: Environmental Scanning Electron Microscope (ESEM) Test Method

The samples for ESEM imaging were the previously polished optical imaging samples. The polished sample pucks were stored using a plastic end cap to maintain a clean, scratch-free surface following optical imaging. The sample pucks were then sputter-coated with gold/palladium alloy to a thickness of 5 nm on the sample side. Following coating, conductive carbon tape was placed on the edge of the sample surface of the pucks, not obscuring the sample, run down the side of the pucks, across the anti-sample side, up the other side of the pucks and back onto the sample side, again not obscuring the sample. This tape was then used to adhere the sample pucks to sample holders to be used in the ESEM. The sample was then placed into the ESEM chamber for imaging.

ESEM imaging was done on a FEI/Phillips XL40 Environmental Scanning Electron Microscope (shown in Figure 4.26) with a 15kV accelerating voltage at high vacuum and a working distance around 15 mm. The images were captured using the secondary electron detector.



Figure 4.26: FEI/Phillips XL40 ESEM

Chapter 5: Miscellaneous Results

5.1: Density Results

The density of each formulation was measured according to the procedure described in section 4.2.1. These measured values were then compared to theoretical density values.

Theoretical density values, ρ_{Theo} , are determined using Equation 5.1 below:

$$\rho_{\text{Theo}} = \frac{1}{\sum_i \frac{\Phi_i}{\rho_i}} \quad (5.1)$$

where ρ_i is the density of the individual components (PC, CNT, CB or GNP) and Φ_i is the weight fraction of individual component. This comparison verifies that each formulation has the target value of filler present. For this analysis it is assumed that the theoretical densities of the individual components are as given in Table 5.1.

Table 5.1: Individual Component Theoretical Densities

Component	Theoretical Density (g/cm ³)
Lexan HF1130-111 (PC)	1.20
Ketjenblack EC-600JD (CB)	1.80
FIBRILs MWCNT (CNT)	1.75
xGnP™ Graphite Nanoplatelets (GNP)	2.00

Tables 5.2 to 5.4 show the theoretical and average experimental densities (along with the standard deviation) for CNT/PC, CB/PC, GNP/PC composites respectively. Results of the individual specimens for each formulation can be found in Appendix C. These tables indicate that the samples were created with the target amount of filler.

Table 5.2: CNT/PC Composite Density Results

Formulation	Theoretical Density	Average Experimental
-------------	---------------------	----------------------

	(g/cm ³)	Density (g/cm ³)
BL	1.200	1.9123 ± 0.0016 n = 5
BQ2L	1.210	1.2015 ± 0.0005 n = 8
BQ3L	1.215	1.2052 ± 0.0010 n = 6
BQ4L	1.220	1.2123 ± 0.0013 n = 5
BQ5L	1.224	1.2168 ± 0.0004 n = 5
BQ6L	1.230	1.2214 ± 0.0004 n = 5
BQ8L	1.240	1.2313 ± 0.0005 n = 5

Table 5.3: CB/PC Composite Density Results

Formulation	Theoretical Density (g/cm ³)	Average Experimental Density (g/cm ³)
BA2L	1.208	1.2032 ± 0.0004 n = 7
BA3L	1.212	1.2080 ± 0.0001 n = 6
BA4L	1.216	1.2119 ± 0.0007 n = 6
BA5L	1.220	1.2153 ± 0.0001 n = 6
BA6L	1.224	1.2189 ± 0.0004 n = 5
BA8L	1.233	1.2268 ± 0.0002 n = 5
BA10L	1.241	1.2373 ± 0.0003 n = 5

Table 5.4: GNP/PC Composite Density Results

Formulation	Theoretical Density (g/cm ³)	Average Experimental Density (g/cm ³)
BG2L	1.2097	1.2027 ± 0.0009 n = 5
BG3L	1.2146	1.2062 ± 0.0007 n = 6
BG4L	1.2195	1.2104 ± 0.0019 n = 6
BG5L	1.2245	1.2154 ± 0.0005 n = 5
BG6L	1.2295	1.2229 ± 0.0006 n = 5
BG8L	1.2397	1.2306 ± 0.0005 n = 5
BG10L	1.2500	1.2402 ± 0.0008 n = 5
BG12L	1.2537	1.2521 ± 0.0002 n = 5
BG15L	1.2699	1.2683 ± 0.0003 n = 6

Table 5.5 shows the theoretical and average experimental densities for CB/CNT, CB/GNP, and CNT/GNP two filler composites. Results of the individual specimens for each formulation can be found in Appendix C. This table indicates that the samples were created with the target amount of fillers and the low standard deviations indicate the samples are made with significant reproducibility.

Table 5.5: CB/CNT, CB/GNP and CNT/GNP Density Results

Formulation	Theoretical Density (g/cm ³)	Average Experimental Density (g/cm ³)
BA2Q1L	1.2050	1.2074 ± 0.0004 n = 7
BA2Q5L	1.2207	1.2252 ± 0.0020 n = 6
BA5Q1L	1.2174	1.2192 ± 0.0002 n = 6
BA5Q5L	1.2334	1.2379 ± 0.0015 n = 5
BA2G2L	1.2109	1.2096 ± 0.0004 n = 6
BA2G5L	1.2260	1.2252 ± 0.0008 n = 5
BA5G2L	1.2235	1.2241 ± 0.0010 n = 6
BA5G5L	1.2389	1.2382 ± 0.0005 n = 4
BQ1G2L	1.2066	1.2053 ± 0.0004 n = 4
BQ1G5L	1.2215	1.2194 ± 0.0002 n = 4
BQ5G2L	1.2223	1.2229 ± 0.0006 n = 4
BQ5G5L	1.2377	1.2376 ± 0.0005 n = 4

5.2: Melt Flow Index (MFI) Results

Melt flow indexing was performed according to the procedure listed in section 4.2.2. Typical filled system behavior indicates that as filler loading to a polymer is increased, MFI decreases. Tables 5.6 to 5.8 show the average MFIs of CB/PC, CNT/PC and GNP/PC composites, respectively. Results of the individual specimens for each formulation can be found in Appendix D. As a general note, results in the appendices for factorial design formulations and supplemental formulations (BQ0.5L, BQ1L, BQ5LR, etc.) are given in the “Polycarbonate with Multiple Fillers” sections of the respective appendices.

Table 5.6: CNT/PC MFI Results

Formulation	MFI (g/10 min)
BQ0.5L	326 \pm 23 n = 5
BQ1L	320 \pm 29 n = 5
BQ2L	292 \pm 31 n = 5
BQ3L	246 \pm 14 n = 7
BQ4L	173 \pm 13 n = 7
BQ5L	114 \pm 8 n = 9
BQ6L	55 \pm 7 n = 7

Table 5.7: CB/PC MFI Results

Formulation	MFI (g/10 min)
BA2L	148.1 \pm 4.6 n = 5
BA3L	111.9 \pm 5.9 n = 6
BA4L	87.6 \pm 2.3 n = 6
BA5L	63.6 \pm 2.0 n = 6
BA6L	37.1 \pm 2.0 n = 6

Table 5.8: GNP/PC MFI Results

Formulation	MFI (g/10 min)
BG2L	155.1 \pm 7.9 n = 5
BG3L	142.9 \pm 2.9 n = 4
BG4L	127.7 \pm 3.0 n = 5
BG5L	116.6 \pm 3.1 n = 5
BG6L	106.8 \pm 2.9 n = 5
BG8L	83.7 \pm 3.8 n = 5
BG10L	70.5 \pm 1.3 n = 5
BG12L	55.9 \pm 0.8 n = 5
BG15L	31.8 \pm 2.0 n = 5

It can be seen from these results that all 3 systems act in a typical fashion, increased filler loading leads to decreased MFI. We can also see from these results that CB has the

largest effect on decreasing the MFI at equal wt% filler loadings and CNT has the smallest effect on decreasing the MFI at equal wt% filler loadings. GNP has similar effect to CB at low filler loadings, but has much less effect at high filler loadings.

Table 5.9 shows the average MFIs of CB/CNT, CB/GNP and CNT/GNP composites. Results of the individual specimens for each formulation can be found in Appendix C.

Table 5.9: CB/CNT, CB/GNP and CNT/GNP Composites MFI Results

Formulation	MFI (g/10 min)
BA2Q1L	292.8 \pm 6.1 n = 5
BA2Q5L	69.6 \pm 6.0 n = 5
BA5Q1L	119.0 \pm 5.1 n = 5
BA5Q5L	Will not run- too viscous
BA2G2L	109.7 \pm 4.6 n = 5
BA2G5L	80.7 \pm 1.9 n = 5
BA5G2L	49.6 \pm 2.2 n = 5
BA5G5L	22.0 \pm 2.5 n = 5
BQ1G2L	218.9 \pm 14.4 n = 5
BQ1G5L	160.5 \pm 3.1 n = 5
BQ5G2L	143.9 \pm 7.8 n = 5
BQ5G5L	59.4 \pm 3.2 n = 5

These results show that all binary filler systems behave in a typical fashion with MFI decreasing with increased filler loading. We again see that CB has a greater effect on decreasing the MFI than GNP when we compare the BA2G5L and the BA5G2L. These two composites both contain 7 wt% carbon filler, but when the majority is CB (BA5G2L), the MFI is 39% lower than when the majority is GNP (BA2G5L).

5.3: Differential Scanning Calorimetry (DSC) Results

Differential scanning calorimetry was performed according to the procedure given in section 4.2.3. The midpoint value of the glass transition temperature was chosen as the point to compare the different formulations. Table 5.10 shows the midpoint glass transition temperature (T_g) of each run of pure PC and CNT/PC composites.

Table 5.10: PC and CNT/PC DSC Midpoint T_g Values

Formulation:	T_g Midpont ($^{\circ}\text{C}$)
Lexan HF1130-111 (BL) run 1	143.40
Lexan HF1130-111 (BL) run 2	141.96
BQ0.5L run 1	141.06
BQ0.5L run 2	140.87
BQ1L run 1	140.85
BQ1L run 2	140.2
BQ2L run 1	140.52
BQ2L run 2	140.93
BQ3L run 1	140.78
BQ3L run 2	141.40
BQ4L run 1	141.45
BQ4L run 2	141.20
BQ5L run 1	141.02
BQ5L run 2	140.88
BQ6L run 1	139.15
BQ6L run 2	138.84
BQ8L run 1	139.14
BQ8L run 2	137.80

These results show very little change of the glass transition temperature with increased filler loading indicating that CNT does not restrict polymer chain movement unlike many filled systems.

Tables 5.11 and 5.12 show the midpoint glass transition temperature of the CB/PC and GNP/PC composites respectively.

Table 5.11: CB/PC DSC Midpoint T_g Values

Formulation:	T_g Midpont ($^{\circ}\text{C}$)
BA2L run 1	143.36
BA2L run 2	143.26
BA2LR run 1	142.84
BA2LR run 2	142.26
BA3L run 1	143.79
BA3L run 2	144.48
BA4L run 1	143.29
BA4L run 2	143.87
BA5L run 1	144.63
BA5L run 2	143.84
BA5LR run 1	144.30
BA5LR run 2	144.35
BA6L run 1	143.88
BA6L run 2	143.91
BA8L run 1	144.96
BA8L run 2	143.04
BA10L run 1	145.92
BA10L run 2	145.68

Table 5.12: GNP/PC DSC Midpoint T_g Values

Formulation:	T_g Midpont ($^{\circ}\text{C}$)
BG2L run 1	144.40
BG2L run 2	141.89
BG3L run 1	142.53
BG3L run 2	143.46
BG4L run 1	143.95
BG4L run 2	142.89
BG5L run 1	143.91
BG5L run 2	143.24
BG6L run 1	143.55
BG6L run 2	142.44
BG8L run 1	144.31
BG8L run 2	143.96
BG10L run 1	144.49
BG10L run 2	144.60
BG12L run 1	144.18
BG12L run 2	144.38
BG15L run 1	145.00
BG15L run 2	145.42

This data indicates that neither CB nor GNP have any significant effect on the T_g of the composites. This indicates that none of the fillers restrict polymer chain motion. The midpoint glass transition temperature for the multiple filler formulations is shown in Table 5.13.

Table 5.13: CB/CNT, CB/GNP and CNT/GNP DSC Midpoint T_g Values

Formulation:	T_g midpont (°C)
BA2Q1L run 1	141.79
BA2Q1L run 2	141.05
BA2Q5L run 1	140.42
BA2Q5L run 2	139.25
BA5Q1L run 1	141.86
BA5Q1L run 2	142.15
BA5Q5L run 1	141.36
BA5Q5L run 2	140.63
BA2G2L run 1	143.11
BA2G2L run 2	143.52
BA2G5L run 1	144.37
BA2G5L run 2	143.72
BA5G2L run 1	144.61
BA5G2L run 2	143.97
BA5G5L run 1	144.19
BA5G5L run 2	144.51
BQ1G2L run 1	141.23
BQ1G2L run 2	141.60
BQ1G5L run 1	142.70
BQ1G5L run 2	142.52
BQ5G2L run 1	139.96
BQ5G2L run 2	139.55
BQ5G5L run 1	140.52
BQ5G5L run 2	140.29

This data again indicates that none of the fillers have a significant effect on polymer chain mobility. It is interesting to note that for 10 wt% carbon filler formulations, the CNT containing composites (BA5Q5L and BQ5G5L) have T_g's that are about 4°C lower than the CB/GNP composite (BA5G5L). This may indicate (as discussed later in Chapters 8 and 13) that CNT increases polymer chain mobility. The graphs of the heat-flow versus time for all formulations are shown in Appendix E.

5.4: In-Plane Electrical Resistivity of Extruded Rods

Extruded rods of each formulation were measured according to the procedure given in section 4.2.7. The average volume electrical resistivity of the extruded rods for the CB/PC composites are given in Table 5.14. This table indicates the difference between the 2-9-09 screw design used for the majority of the formulations and the 10-30-09 screw design that was optimized for dispersion of the CB into PC. It also provides a baseline for the CB masterbatch material created at MTU for multiple filler formulations. Results for the individual samples are given in Appendix F.

Table 5.14: Average In-Plane Volume Electrical Resistivity of CB/PC Extruded Rods

Formulation	Average Volume Electrical Resistivity (ohm-cm)
BA2L (10-30-09 screw)	> 4E7
BA2LR (2-9-09 screw)	> 4E7
BA3L (10-30-09 screw)	608 ± 291
BA4L(10-30-09 screw)	99.3± 18.7
BA5L(10-30-09 screw)	26.8 ± 3.3
BA5LR (2-9-09 screw)	63.0 ± 7.1
BA6L (10-30-09 screw)	14.1 ± 1.7
BA8L (10-30-09 screw)	6.0 ± 0.2
BA8LR (April 14, 2010 masterbatch made at MTU, 10-30-09 screw)	6.1 ± 0.2
BA10L (10-30-09 screw)	3.3 ± 0.1

It can be seen that for the 5 wt% CB filled samples, the 10-30-09 screw design offered a 57% decrease in volume ER versus the formulation made with the 2-9-09 screw design. The further decrease in volume ER is due to better dispersion of the CB agglomerates provided by the optimized 10-30-09 screw design. This good dispersion allows the 8

wt% CB masterbatch to be mixed with the pure PC and other fillers using the 2-9-09 screw design while maintaining sufficient CB dispersion. The data also shows that the CB/PC composites percolate between 2 and 3 wt% filler.

Table 5.15 shows the average volume electrical resistivity of the extruded rods for the GNP/PC formulations as well as a baseline for the as-received GNP masterbatch to determine the effect of further extrusion on the volume electrical resistivity of the material. Results for the individual samples are again given in Appendix F.

Table 5.15: Average In-Plane Volume Electrical Resistivity of GNP/PC Extruded Rods

Formulation	Average Volume Electrical Resistivity (ohm-cm)
BG2L	$> 8E7$
BG3L	$> 8E7$
BG4L	$> 8E7$
BG5L	$> 8E7$
BG6L	$> 8E7$
BG8L	$5.7E4 \pm 6.5E3$
BG10L	$3.1E3 \pm 2.2E2$
BG12L	610.0 ± 56.9
BG15L	194.5 ± 15.3
PC1515B Ovation as received pellets	149.5 ± 47.8

This data shows that the further extrusion of the GNP masterbatch increases the volume electrical resistivity by 30%. This is likely due to the degradation of the flake-like GNP particles. It can also be seen that the GNP/PC composites percolate between 6 and 8 wt%, significantly higher than the CB/PC composites.

The average in-plane volume electrical resistivity of the multiple filler formulations is given in Table 5.16. Results for the individual samples are given in Appendix F.

Table 5.16: Average In-Plane Volume Electrical Resistivity of CB/CNT, CB/GNP and GNP/CNT Extruded Rods

Formulation	Volume Electrical Resistivity (ohm-cm)
BA2Q1L	300 ± 60 n = 5
BA2Q5L	4.79 ± 0.13 n = 10
BA5Q1L	18.23 ± 0.93 n=10
BA5Q5L	2.91 ± 0.11 n=10
BA2G2L	>E7 n = 6
BA2G5L	692 ± 114 n = 8
BA5G2L	22.1 ± 2.0 n = 8
BA5G5L	11.2 ± 0.4 n = 10
BQ1G2L	>E7 n=6
BQ1G5L	1009 ± 235.6 n = 6
BQ5G2L	4.91 ± 0.18 n = 10
BQ5G5L	2.57 ± 0.86 n = 9

It can be seen from this data that CNT has the largest effect on decreasing the volume electrical resistivity. When comparing 5 wt% CNT with 2 wt% GNP (BQ5G2L) and 5 wt% CB and 2 wt% GNP (BA5G2L) it can be seen that the formulation containing CNT as opposed to CB has a 78% lower volume ER. When comparing the BQ5G5L and BA5G5L, we see that the CNT containing formulation has a 77% lower volume ER than the CB containing formulation. It can also be seen that GNP has the least effect on lowering the composite volume ER. When comparing two formulations with 7 wt% carbon filler (BA5G2L and BA2G5L), we see when the majority filler is CB (BA5G2L), the volume ER is 97% lower than when the majority filler is GNP (BA2G5L).

Chapter 6: Electrical Resistivity, Thermal Conductivity and Tensile and Flexural Properties of Carbon Nanotube/Polycarbonate Composites

6.1: Field Emission Scanning Electron Microscope (FESEM) and Transmission Electron Microscopy Results

An FESEM image of a BQ6L fracture surface is shown as Figure 6.1. CNT can be seen as white fibers. The distributed, interconnecting structure of CNT indicates that conductive networks are being formed, enhancing electrical conductivity. TEM images of BQ3L (a) and BQ6L (b) are shown in Figure 6.2. This figure shows the dispersion of the CNT within the PC matrix. It can be seen that the 6 wt% composite has significant conductive networking present.

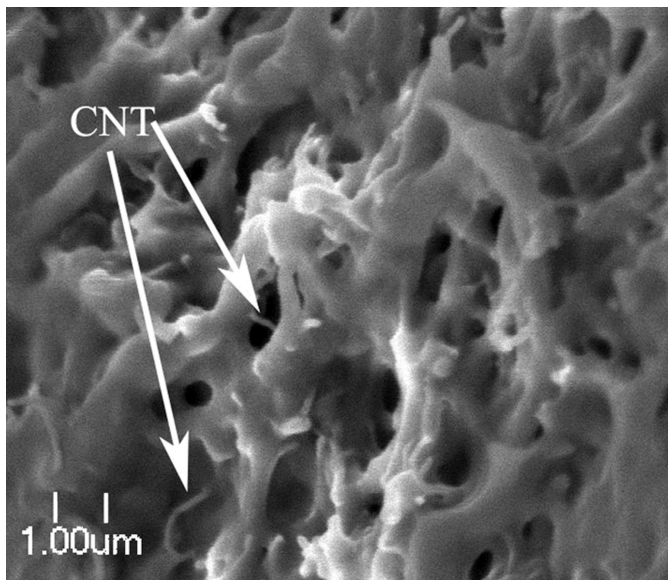


Figure 6.1: FESEM image of 6 wt% CNT in PC fracture surface

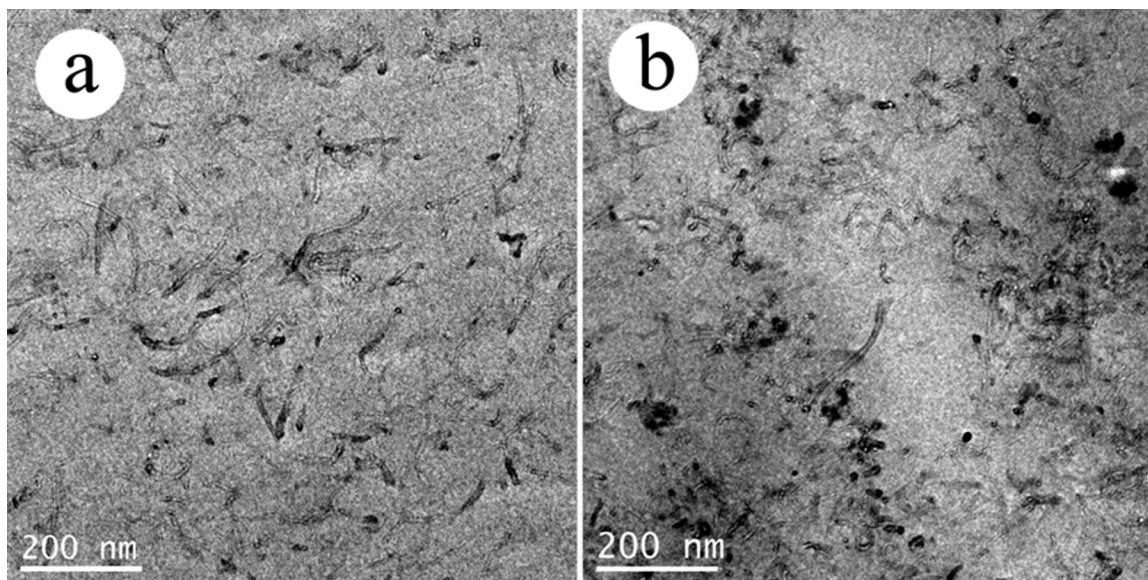


Figure 6.2: TEM images of 3 wt% CNT in PC (a) and 6 wt% CNT in PC (b)

6.2: Electrical Resistivity Results

Table 6.1 shows the mean electrical resistivity, standard deviation of the electrical resistivity and number of samples that were tested for each formulation. This data is plotted in Figure 6.3. This data is also given in Appendices G and H. We see a typical electrical resistivity curve in this figure. At low conductive filler loadings, the electrical resistivity of the composite will be similar to that of the pure polymer. As the loading of the conductive filler increases, there is a point at which conductive networks begin to form and the resistivity decreases dramatically over a very small range of filler loading. This point is known as the percolation threshold. After percolation occurs, the electrical resistivity of the composite levels out as additional conductive filler is added (7,60).

Table 6.1: Electrical resistivity results for CNT/PC composites

Formulation	Filler Wt %	Filler Vol %	Electrical Resistivity (ohm-cm)
PC	0	0.0	$1.06 \times 10^{17} \pm 7.96 \times 10^{16}$ n = 7
2CNT	2	1.38	4610 ± 1120 n = 6
3CNT	3	2.08	216 ± 44 n = 6
4CNT	4	2.78	73 ± 10 n = 6
5CNT	5	3.48	43 ± 7 n = 6
6CNT	6	4.19	18 ± 2 n = 6
8CNT	8	5.63	7.8 ± 0.4 n = 6

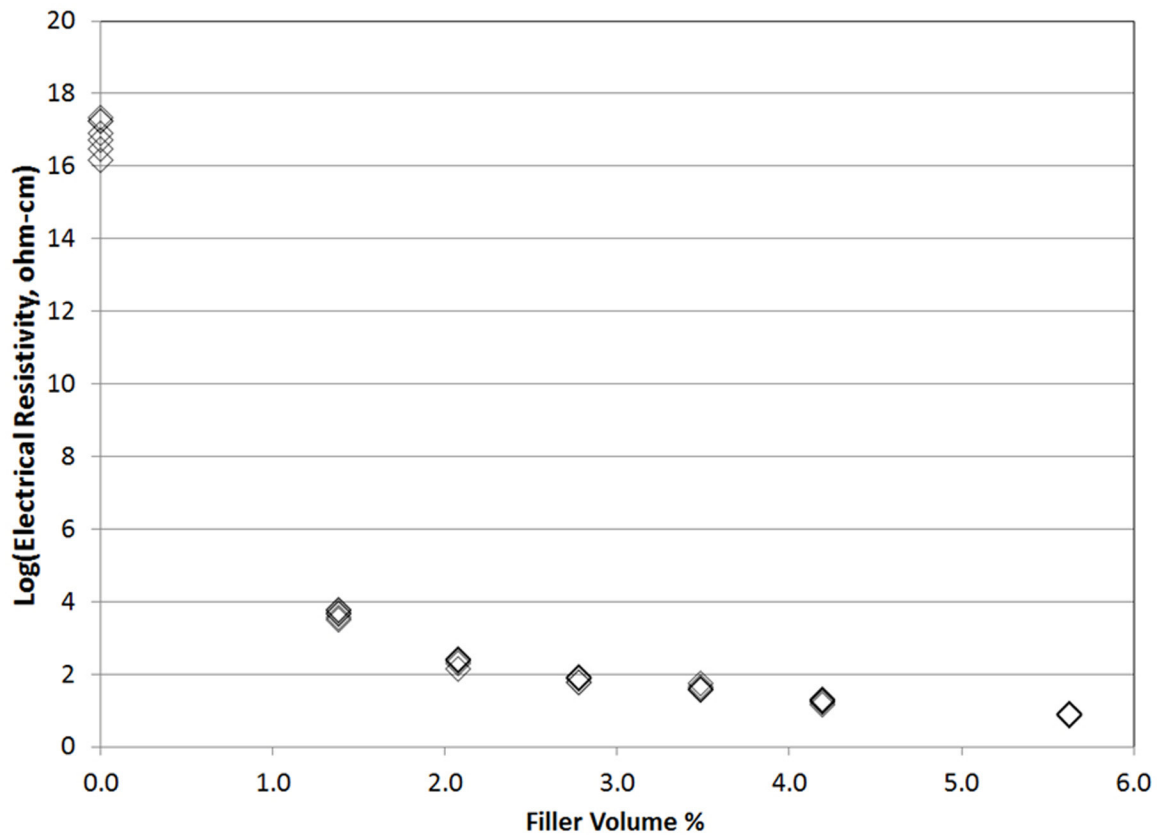


Figure 6.3: Log(electrical resistivity) versus filler volume for CNT/PC composites

It can be seen from Figure 6.3 that CNT is effective at decreasing the electrical resistivity of composites, even at low filler loadings. The pure polymer begins at a electrical resistivity of 1.1×10^{17} ohm-cm, a value that coincides with data provided by the vendor. The percolation threshold occurs somewhere below 1.4 vol% CNT for this system as the

2 wt% (1.4 vol%) formulation is already percolated. At the highest filler loading studied, 8 wt% (5.6 vol%) CNT, the electrical resistivity had dropped all the way down to 8 ohm-cm. A low percolation threshold is found in this system likely due to the extreme geometry of the CNT. Low percolation thresholds have often been found for CNT-based polycarbonate systems, both single-walled and multi-walled (61-64).

6.3: Thermal Conductivity Results

The results of through-plane thermal conductivity testing on the CNT composites are shown in Figure 6.4 and listed in Table 6.2. More detailed results are contained in Appendix I. We see that CNT does increase the through-plane thermal conductivity of the composite from 0.22 W/m·K for pure PC to 0.31 W/m·K for 8 wt% CNT composites. This increase is similar to that reported by King et al. for CNT in polypropylene (17) but are lower than those reported by Lee et al. for a vulcanized silicone filled with CNT (65).

Table 6.2: Thermal conductivity results for CNT/PC composites

Formulation	Filler Wt %	Thermal Conductivity (W/m·K)
PC	0	0.218 ± 0.002 n =5
2CNT	2	0.232 ± 0.002 n =5
3CNT	3	0.241 ± 0.003 n =5
4CNT	4	0.255 ± 0.001 n =5
5CNT	5	0.266 ± 0.003 n =5
6CNT	6	0.275 ± 0.003 n =5
8CNT	8	0.306 ± 0.003 n =5

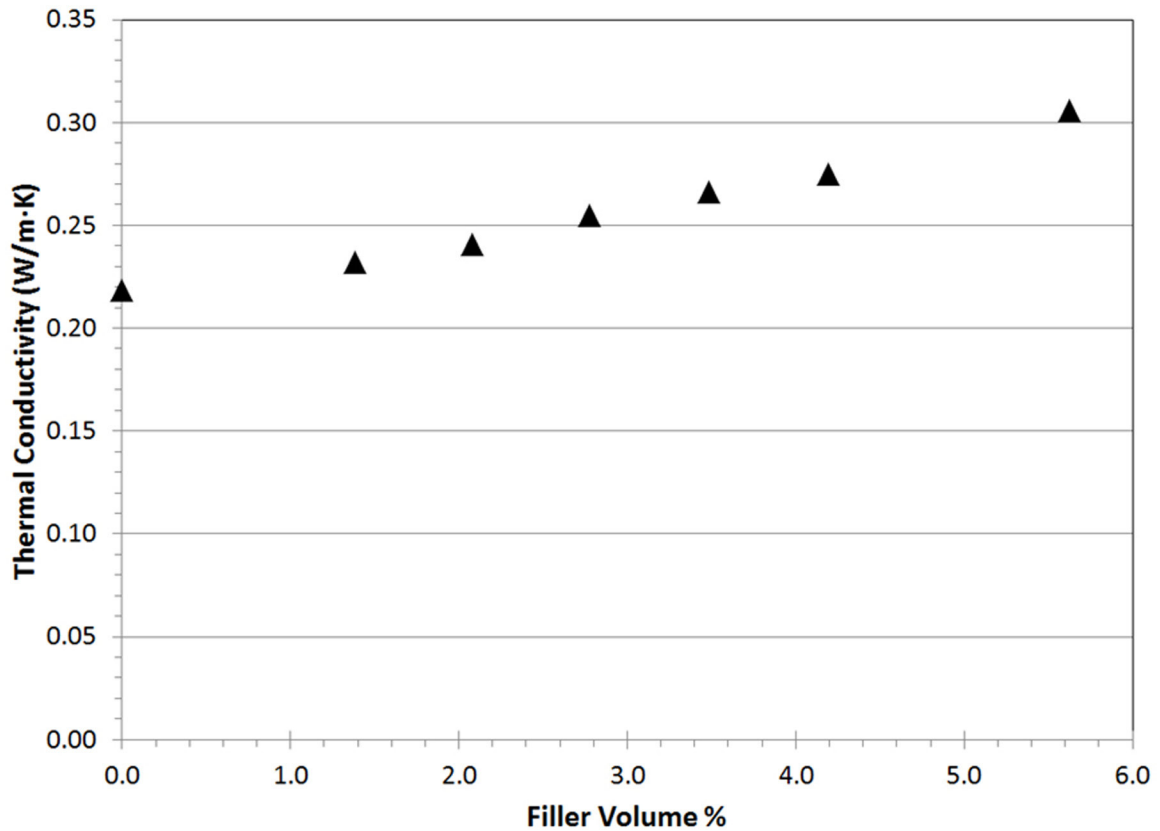


Figure 6.4: Thermal conductivity versus filler volume for CNT/PC composites

6.4: Tensile Test Results

The tensile modulus of the CNT based composites is shown in Figure 6.5. The associated ultimate tensile strengths (UTS) and the strains at the ultimate tensile strength are shown in Figure 6.6. Both of these figures display the mean value along with error bars representing one standard deviation. In cases where the error bars are smaller than the marker size, they have been omitted. It is shown in Figure 6.5 that the addition of 8 wt% (5.6 vol%) CNT increased the tensile modulus of the composite from 2.2 GPa for neat PC to 2.9 GPa. Figure 6.6 has omitted the results for the 8 wt% CNT composite as this composite broke prematurely. It is likely that the 8 wt% CNT composites were not injection molded optimally as the resin is very viscous and difficult to melt-process at this

filler loading. For the samples with ≤ 6 wt% CNT, we see that the UTS tends to remain constant at around 60 MPa, meanwhile strain at UTS generally decreases with increased CNT loading. This trend agrees with previously reported trends for single-walled and multi-walled CNT in various polymer systems (61,66,67). Figure 6.7 shows typical tensile stress-strain curves for the formulations created in this study with up to 6 wt% CNT including neat PC. As the stress increases, we initially see a linear Hookean response that can be used to calculate a tensile modulus. Following this initial linear response, all of the composites illustrated demonstrate a deviation below this line that indicates ductile yielding behavior. Detailed results for this data are listed in Appendix J.

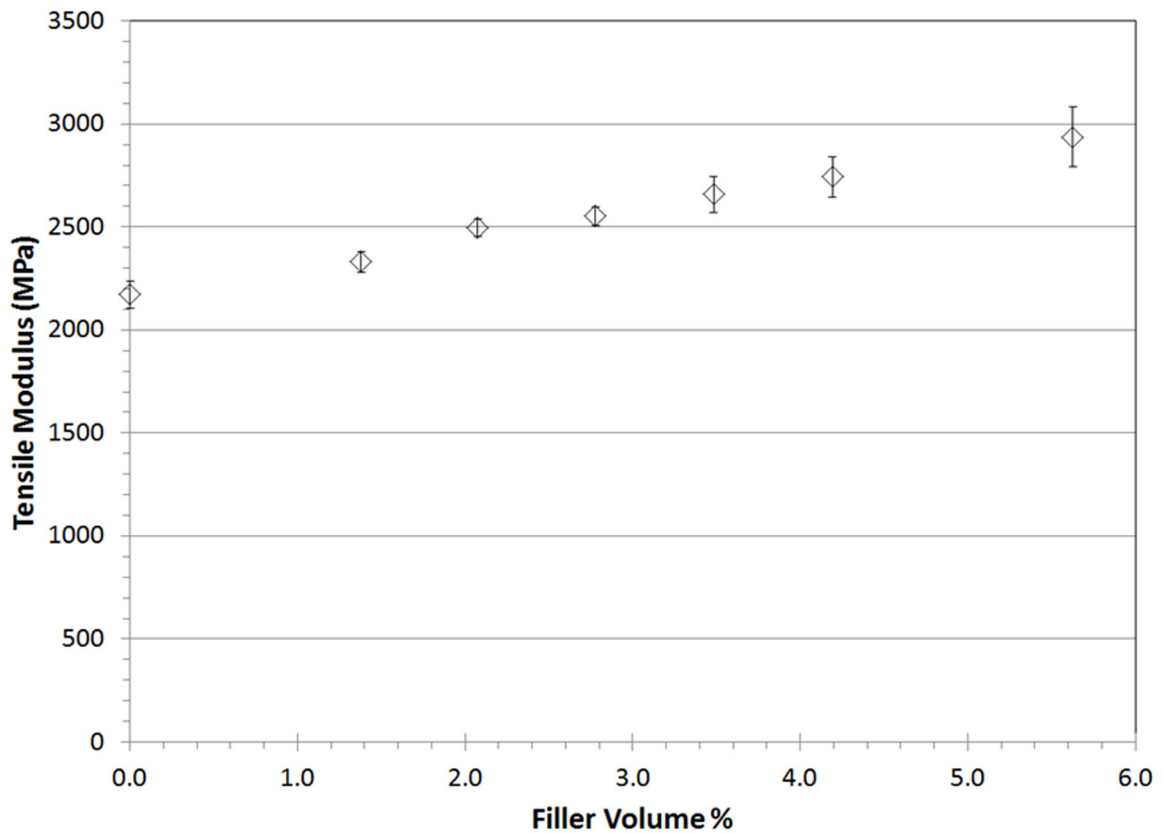


Figure 6.5: Tensile modulus of CNT/PC composites

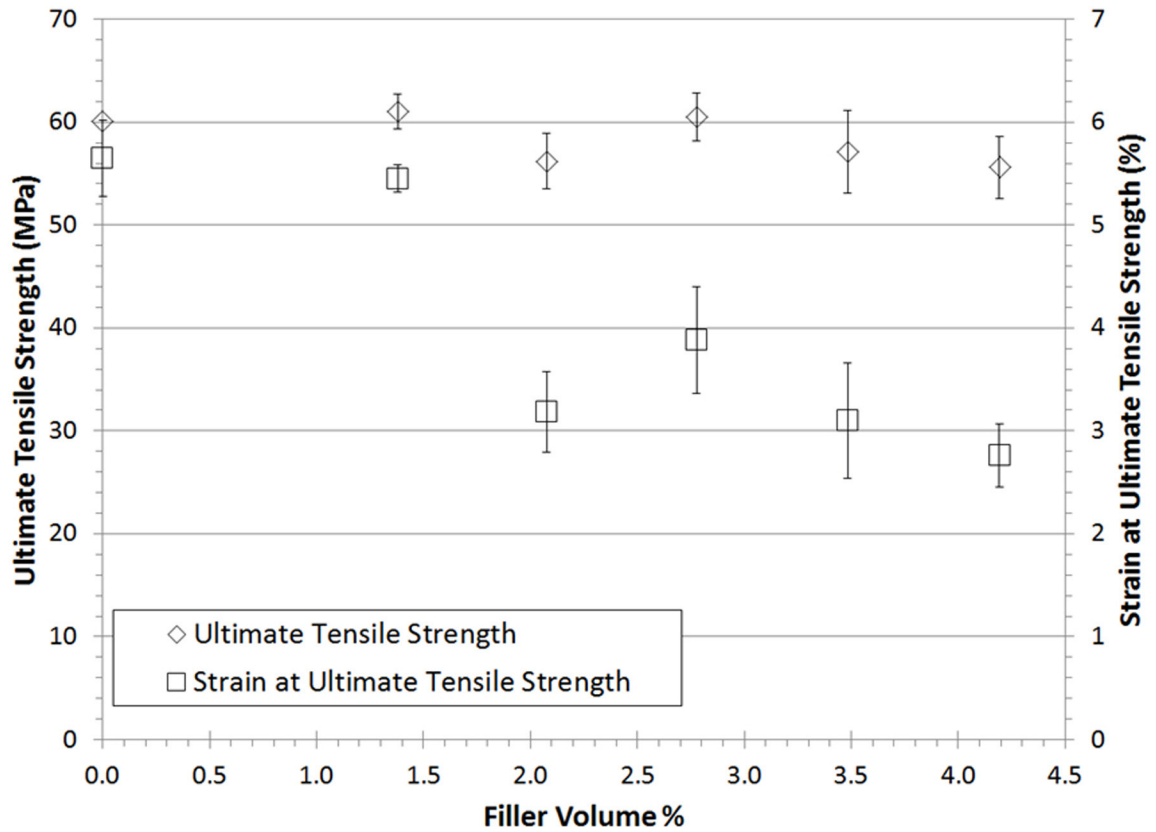


Figure 6.6: Ultimate tensile strength and strain at ultimate tensile strength for CNT/PC composites

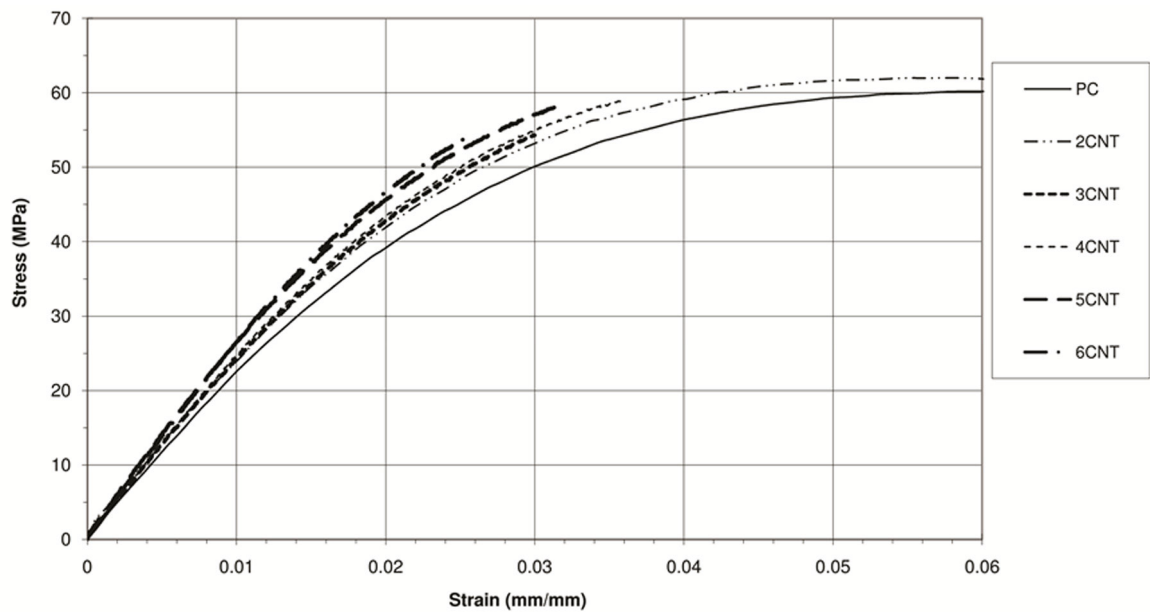


Figure 6.7: Typical stress-strain curves for CNT/PC composites

6.5: Flexural Test Results

The flexural modulus of the CNT based composites is shown in Figure 6.8. The associated ultimate flexural strengths (UFS) and the strains at the ultimate flexural strength are shown in Figure 6.9. Both of these figures display the mean value along with error bars representing one standard deviation. In cases where the error bars are smaller than the marker size, they have been omitted. Similarly to the tensile modulus, the flexural modulus increases with increased CNT loading. From a pure PC value of 3.0 GPa, the flexural modulus is increased to 3.6 GPa for the 8 wt% (5.6 vol%) CNT composite. In Figure 6.9 that we have again omitted the values for 8 wt% CNT composites for the same reasons as discussed for tensile results. In this figure we do see a difference from the tensile results however. The addition of CNT increased the UFS from a value of 115 MPa for the pure PC to 125 MPa for a 6 wt% (4.2 vol%) CNT composite. The strain at which this UFS was reached was approximately the same for all loading levels. Detailed results for this data are listed in Appendix K.

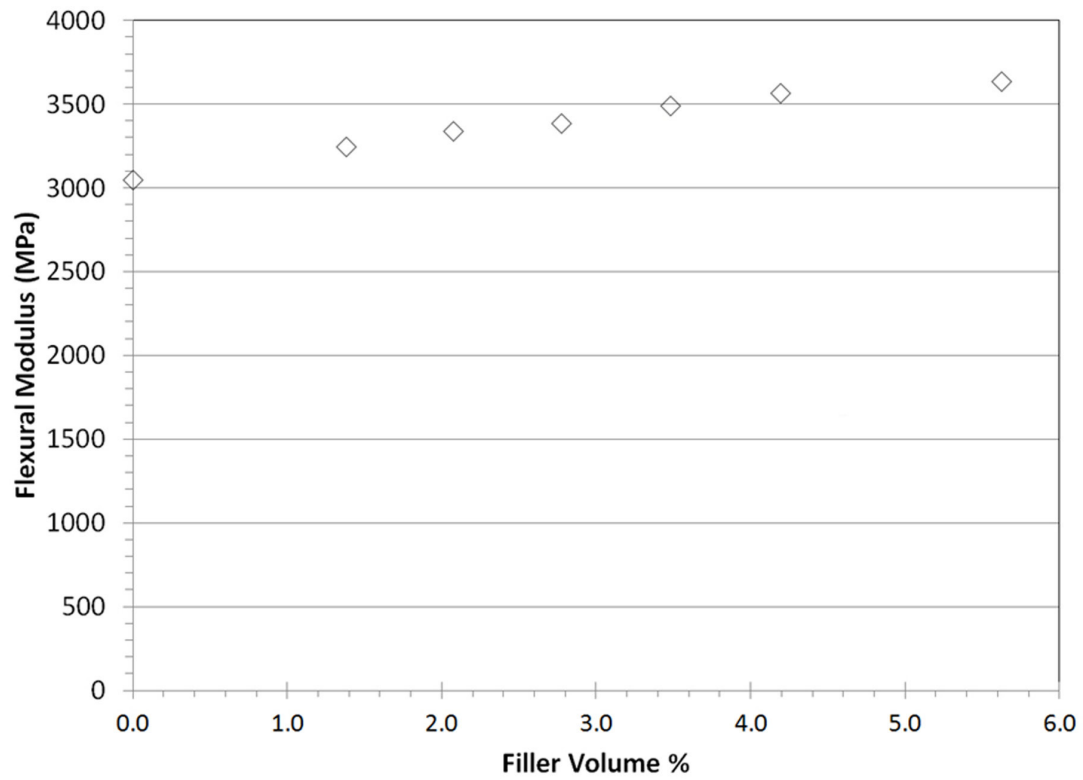


Figure 6.8: Flexural modulus of CNT/PC composites

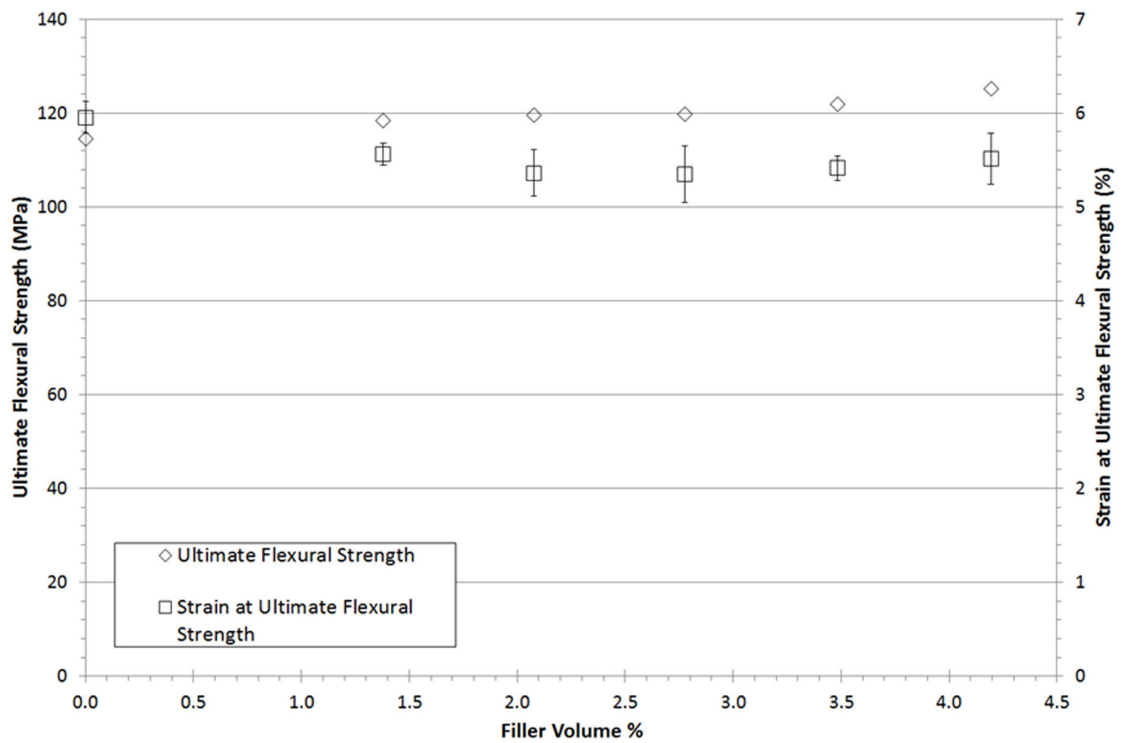


Figure 6.9: Ultimate flexural strength and strain at ultimate flexural strength for CNT/PC composites

6.6: Conclusions

The purpose of this section of the project was to determine the effects of CNT on the electrical, thermal and mechanical properties of PC. Electrically, CNT exhibits a percolation threshold in PC somewhere below 1.4 vol% CNT. This low percolation threshold is due to the high aspect ratio of the CNT. The addition of 5.6 vol% (8 wt%) CNT to PC reduced the ER of the composite from 1.1×10^{17} ohm-cm (ER of neat PC) to 8 ohm-cm. Thermally, the addition of 5.6 vol% CNT increased the TC from 0.22 W/m·K for neat PC to 0.31 W/m·K.

Mechanically, the addition of 5.6 vol% (8 wt%) CNT to PC increased the tensile modulus from 2.2 GPa for neat PC to 2.9 GPa. The ultimate tensile strength (UTS) was largely unchanged ranging from 56 to 62 MPa for all filler loadings. The strain at UTS decreased with increased CNT loadings. The CNT/PC composites retained ductile behavior for all formulations with up to 6 wt% CNT. The addition of 5.6 vol% (8 wt%) CNT to PC increased the flexural modulus from 3.0 GPa for neat PC to 3.6 GPa. The ultimate flexural strength (UFS) increased with increased CNT loading changing from 115 MPa for neat PC to 125 MPa for 6 wt% (4.2 vol%) CNT. The strain at UTS stayed roughly the same for all CNT loadings around 5.7 %.

Chapter 7: Electrical Resisitivity, Thermal Conductivity and Tensile and Flexural Properties of Carbon Black/Polycarbonate Composites and Comparison with Carbon Nanotube/Polycarbonate Composites

7.1: Field Emission Scanning Electron Microscope (FESEM) Results

An FESEM image of a 6 wt% CB composite is shown in Figure 7.1. In this figure CB can be seen as white spheres that form an extended network, this is an expected result due to the high structure of CB and the proximity of the CB particles to each other (14). The FESEM image for CNT has been discussed in Chapter 6.

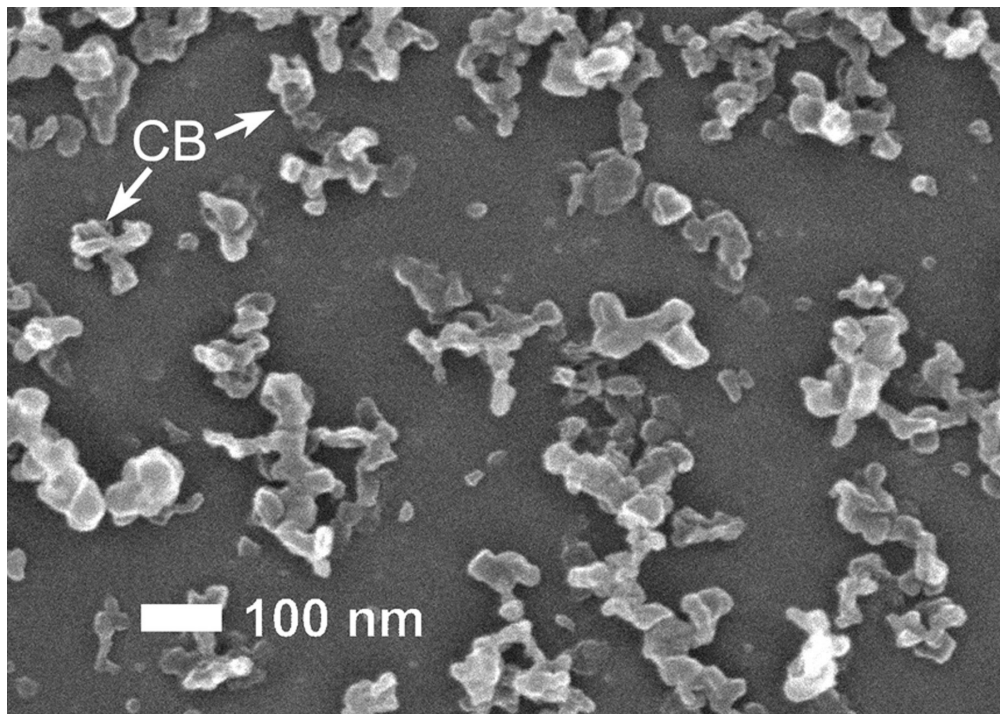


Figure 7.1: FESEM image of 6 wt% CB in PC

7.2: Electrical Resistivity Results

Table 7.1 shows the mean electrical resistivity, standard deviation of the electrical resistivity and number of samples that were tested for each CB-based formulation. Results for the individual values are found in Appendices G and H. This data is plotted in Figure 7.2 along with the CNT data from Chapter 6 for comparison. The CNT data shown has additional 0.5 wt% and 1 wt% CNT loadings. These loadings were added to better locate the percolation threshold of CNT (about 1.0 vol%). In Figure 7.2 we again see a typical electrical resistivity curve similar to that of CNT.

Table 7.1: Electrical resistivity results for CB/PC and CNT/PC composites

Formulation	Filler Wt %	Filler Vol %	Electrical Resistivity (ohm-cm)
PC	0	0.0	$1.26 \times 10^{17} \pm 3.35 \times 10^{16}$ n = 6
2CB	2	1.34	$4.05 \times 10^{16} \pm 2.66 \times 10^{16}$ n = 6
3CB	3	2.01	$2.85 \times 10^{15} \pm 4.58 \times 10^{14}$ n = 6
4CB	4	2.69	$1.17 \times 10^5 \pm 7.77 \times 10^4$ n = 8
5CB	5	3.38	2474 ± 646 n = 8
6CB	6	4.07	649 ± 18 n = 8
8CB	8	5.46	122 ± 4 n = 8
10CB	10	6.88	19.5 ± 0.5 n = 8
0.5CNT	0.5	0.34	$6.19 \times 10^{16} \pm 1.21 \times 10^{16}$ n = 6
1CNT	1	0.69	$2.02 \times 10^{16} \pm 6.62 \times 10^{15}$ n = 6
2CNT	2	1.38	4610 ± 1120 n = 6
3CNT	3	2.08	216 ± 44 n = 6
4CNT	4	2.78	73 ± 10 n = 6
5CNT	5	3.48	43 ± 7 n = 6
6CNT	6	4.19	18 ± 2 n = 6
8CNT	8	5.63	7.8 ± 0.4 n = 6

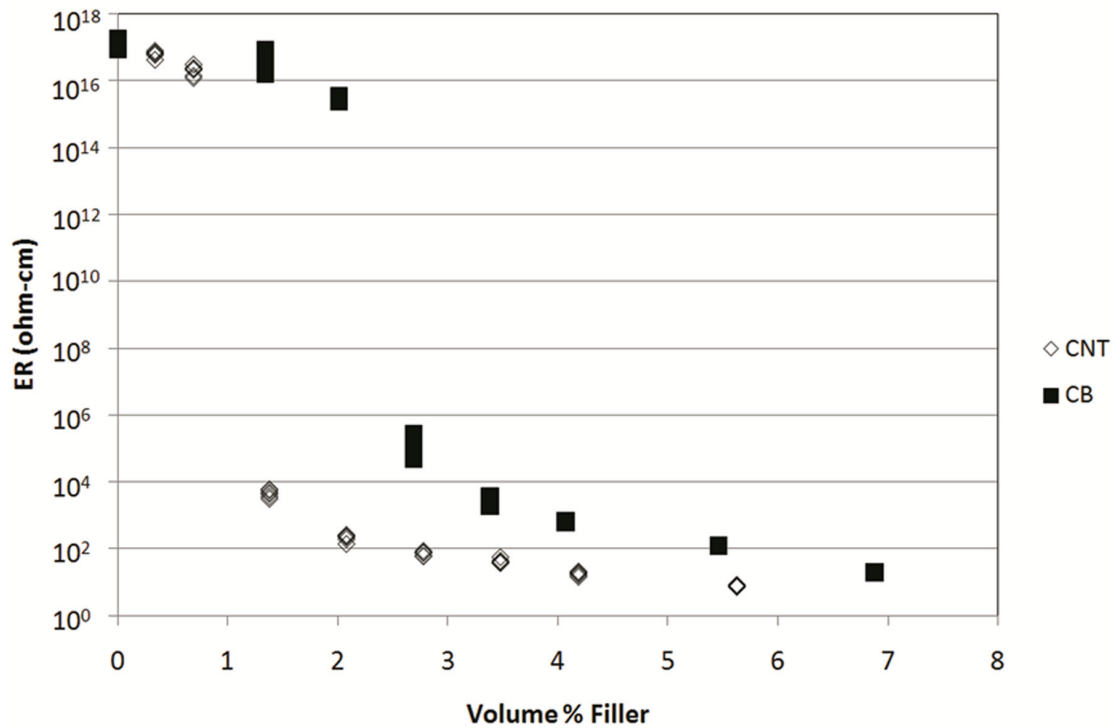


Figure 7.2: Electrical resistivity (ER) versus filler volume for CB/PC and CNT/PC composites

We note that CB is also effective at decreasing electrical resistivity at low filler loadings. The percolation threshold lies at approximately 2.3 vol%. At the highest concentration made, 10 wt% (6.9 vol%), the composite has an electrical resistivity of 20 ohm-cm. If we compare these results with the CNT results from Chapter 6, we see that the percolation threshold for CB is above that of CNT (~2.3 vol% versus 1.0 vol%). We also see that CNT typically shows a lower electrical resistivity than CB at equal volume loadings of filler. For example, at 5.6 vol% CNT, the electrical resistivity is 8 ohm-cm. At 5.5 vol% CB, the electrical resistivity is 122 ohm-cm. The lower percolation threshold for CNT likely is a result of its high aspect ratio of 1000 compared to the spherical CB particles. This higher aspect ratio is also the likely cause of CNT's lower electrical resistivity at equivalent volume filler loadings.

CB is a commonly studied filler for PC systems (7,68-72). At similar volume filler loadings, the CB/PC composite we made are more conductive than Tchoudakov et al., Ezquerro et al, Narkis et al., Lee et al., and Potschke et al. for CB in PC (7,68-71). One primary difference that may account for the difference in electrical conductivity is the processing method. This project used a small commercial scale twin-screw extruder and commercial scale injection molder. The use of these devices allow for an easy scale-up to a large-scale production facility as twin-screw extruders and injection molders are more cost effective and commercially viable than their alternatives. The use of injection molding also encourages orientation of any agglomerates of CB in the flow direction, decreasing ER in that direction. These other studies will be described here in more detail.

Potschke et al. studied a Mitsubishi Engineering Plastics polycarbonate filled with Cabot Corporation Vulcan XC-72 electrically conductive carbon black. The project used a small scale conical co-rotating twin-screw extruder with a 4.5 cm³ capacity and used a compression molder to create 0.35 mm thick test samples (69). For 10 wt% CB composites, Potschke's research group obtained a value of 10⁸ ohm-cm. In our project, we obtained 20 ohm-cm for a 10 wt% CB in PC composite.

Lee et al. studied SAMYANG Co. TRIREX 3022 polycarbonate filled with Korea Carbon Black co. Hiblack 30 electrically conductive carbon black. This project created 25 mm diameter disks with 1.5 mm thickness in a compression molding process (68). At 10 wt% CB, Lee's team found an ER of 10¹⁵ ohm-cm. Again at 10 wt% CB, our project found an ER value of 20 ohm-cm.

Ezquerria et al. studied a Bayer polycarbonate filled with Philips Petroleum XE2 electrically conductive carbon black. This project compounded the composite in a small scale mechanical mixer at 50 rpm for 10 minutes (71). This composite was then compression molded into test specimens. Ezquerria's group found an ER of 10^4 ohm-cm for 6.4 vol% CB. Our project found an ER of 20 ohm-cm for 6.9 vol% CB in PC.

Tchoudakov et al. studied GE Plastics (now SABIC Innovative Plastics) Lexan 103 polycarbonate filled with Akzo Ketjenblack EC carbon black. This project used a small scale mechanical mixer and compression molder to create test samples (70). Tchoudakov's group obtained an ER of 10^7 ohm-cm for an 8 wt% CB composite compared to our value of 122 ohm-cm for the same loading.

Narkis et al. studied a SABIC Innovative Plastics Lexan filled with Kejenblack EC-600 JD carbon black, the same CB studied in our project. Narkis et al. used a twin-screw extruder and injection molder to obtain test specimens (7). Narkis's team obtained an ER value of 10^8 ohm-cm for 6 wt% CB compared to our result of 650 ohm-cm for the same CB loading.

Electrical resistivity of composites is very sensitive to processing conditions and filler/matrix interactions. Based upon comparison with similar systems, our combination of Lexan HF1130-111 and Ketjenblack EC-600 JD along with larger scale twin-screw extruding and injection molding provides very good electrical resistivity results and indicate that commercial applications may be more viable than what is suggested by small scale fabrication.

7.3: Thermal Conductivity Results

Figure 7.2 shows mean through-plane thermal conductivity results for CNT/PC and CB/PC. These results correspond to the values listed in Tables 6.2 and 7.2. Detailed results for this test are given in Appendix I.

We see in Figure 7.3 that CB increases the thermal conductivity of the PC composite from 0.21 W/m·K for pure PC to 0.29 W/m·K for 10 wt% (6.9 vol%) CB in PC. This result compares well to previous studies of this CB in polypropylene and Vectra A950RX liquid crystal polymer performed by this research group (73,74). When compared to CNT values, we see that on an equal vol% filler basis that CNT increases thermal conductivity slightly more than CB for this system.

Table 7.2: Thermal conductivity results for CB/PC and CNT/PC composites

Formulation	Filler Wt %	Thermal Conductivity (W/m·K)
PC	0	0.214 ± 0.001 n =5
2CB	2	0.228 ± 0.001 n =5
3CB	3	0.234 ± 0.002 n =4
4CB	4	0.245 ± 0.001 n =4
5CB	5	0.254 ± 0.001 n =4
6CB	6	0.260 ± 0.001 n =4
8CB	8	0.275 ± 0.003 n =4
10CB	10	0.291 ± 0.003 n =4
0.5CNT	0.5	0.218 ± 0.002 n =4
1CNT	1	0.225 ± 0.005 n =4
2CNT	2	0.232 ± 0.002 n =5
3CNT	3	0.241 ± 0.003 n =5
4CNT	4	0.255 ± 0.001 n =5
5CNT	5	0.266 ± 0.003 n =5
6CNT	6	0.275 ± 0.003 n =5
8CNT	8	0.306 ± 0.003 n =5

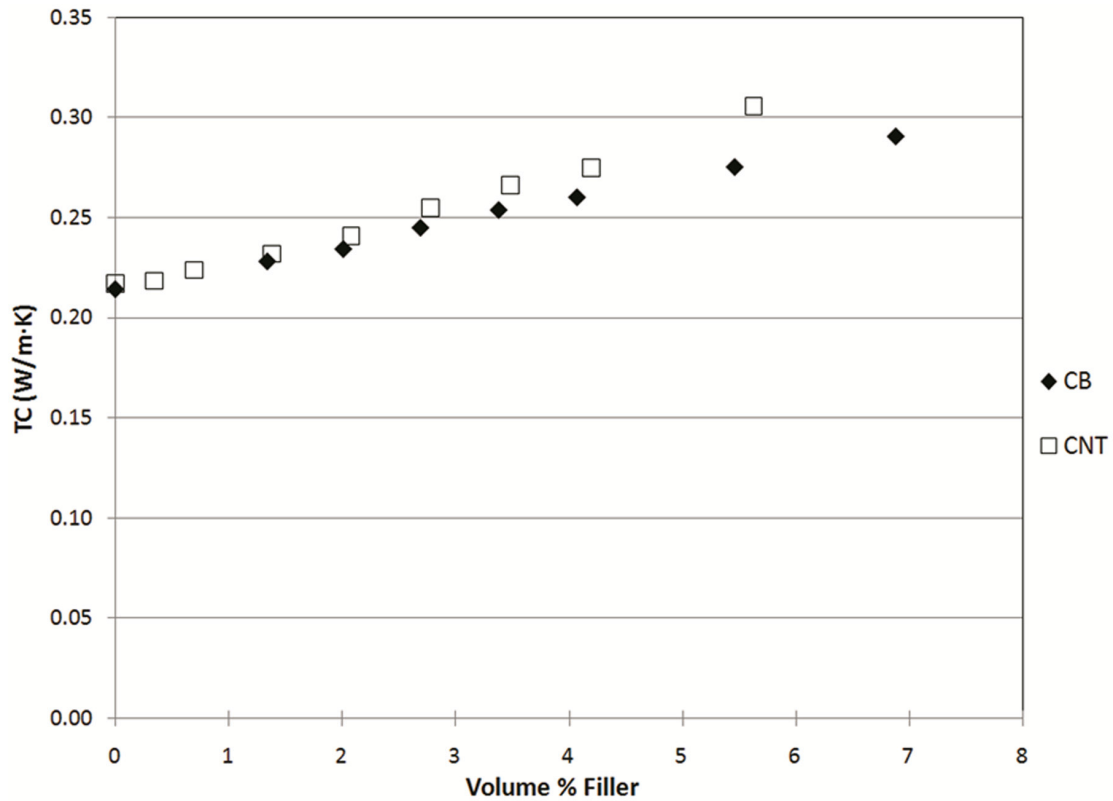


Figure 7.3: Thermal conductivity (TC) versus filler volume for CB/PC and CNT/PC composites

7.4: Tensile Test Results

The tensile moduli of the CB based and CNT based composites are shown in Figure 7.4. The associated ultimate tensile strengths (UTS) and the strains at the ultimate tensile strength are shown in Figure 7.4-2. Both of these figures display the mean value along with error bars representing one standard deviation. In cases where the error bars are smaller than the marker size, they have been omitted. It is shown in Figure 7.4-1 that the addition of 8 wt% (5.5 vol%) CB increased the tensile modulus of the composite from 2.2 GPa for neat PC to 2.8 GPa. The increasing the filler loading to 10 wt% (6.9 vol %) increased the tensile modulus to 3.0 GPa. By comparing with the results from Section

6.4 we see that CB and CNT have similar effects on the tensile modulus for similar volume loadings.

For Figure 7.5 we have omitted the 6.9 vol% CB composite as the high viscosity of the composite made it very difficult to successfully injection mold. We can see from the figure that the UTS for CB composites stays roughly constant at 60 to 63 MPa for all composites up to 8 wt% CB while, similarly to CNT, the strain at UTS tends to decrease with increased CB loading. It is worth noting that in this study, CB provided a higher UTS than CNT for similar filler loadings. Detailed results for this data are listed in Appendix J.

Huang et al. found similar results while studying Miles Inc. Makrolon 2608 polycarbonate filled with Vulcan XR 72R carbon black (75). They utilized a 19 mm single screw extruder and 20 ton injection molding machine to fabricate specimens. Huang's group reported tensile strength increase from 59.3 MPa for a neat PC to 63.4 for a 5 wt% CB composite. They also reported a 10% increase in tensile modulus over pure PC at 5 wt% CB.

Figure 7.6 illustrates a typical tensile stress-strain curve for CB systems up to 10 wt% CB. Similarly to the CNT system, CB shows ductile behavior for all the formulations shown as illustrated by the deviation of the data below the initial linear fit that represents the tensile modulus.

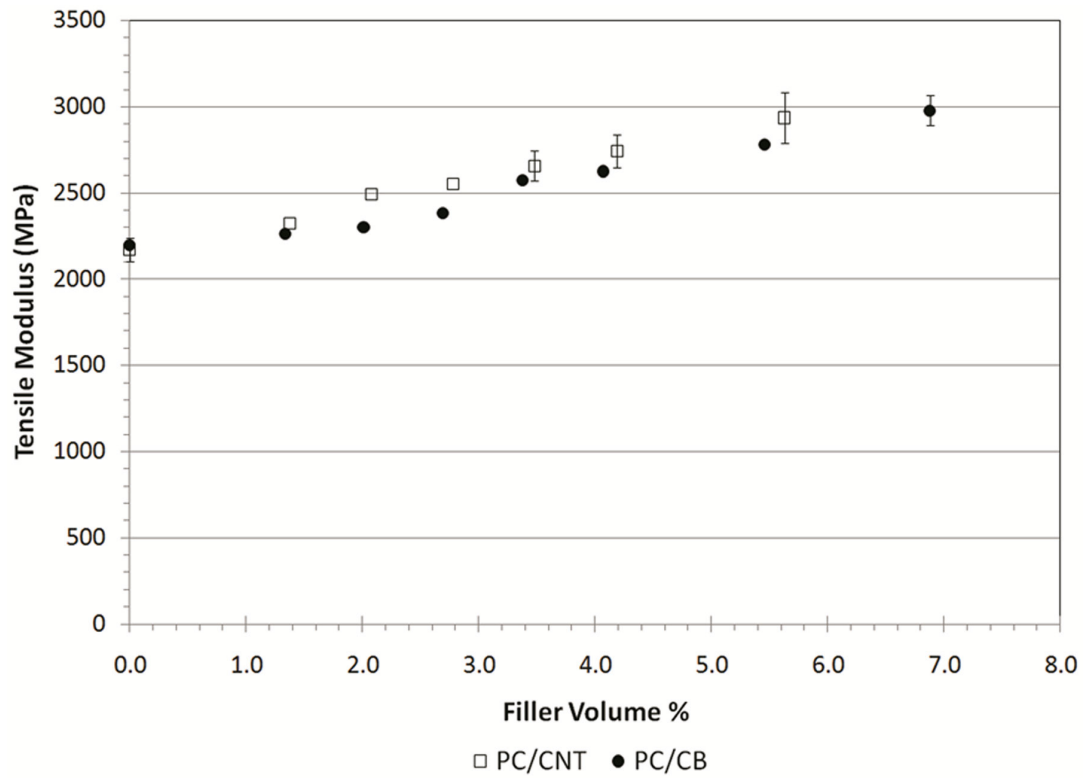


Figure 7.4: Tensile modulus of CB/PC and CNT/PC composites

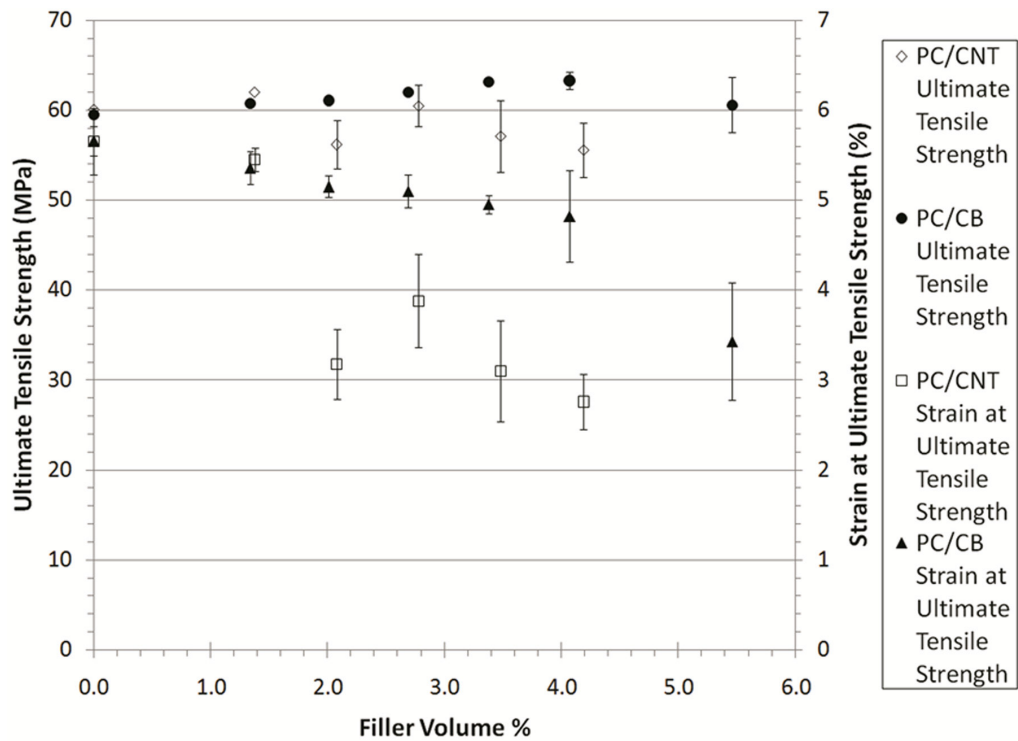


Figure 7.5: Ultimate tensile strength and strain at ultimate tensile strength for CB/PC and CNT/PC composites

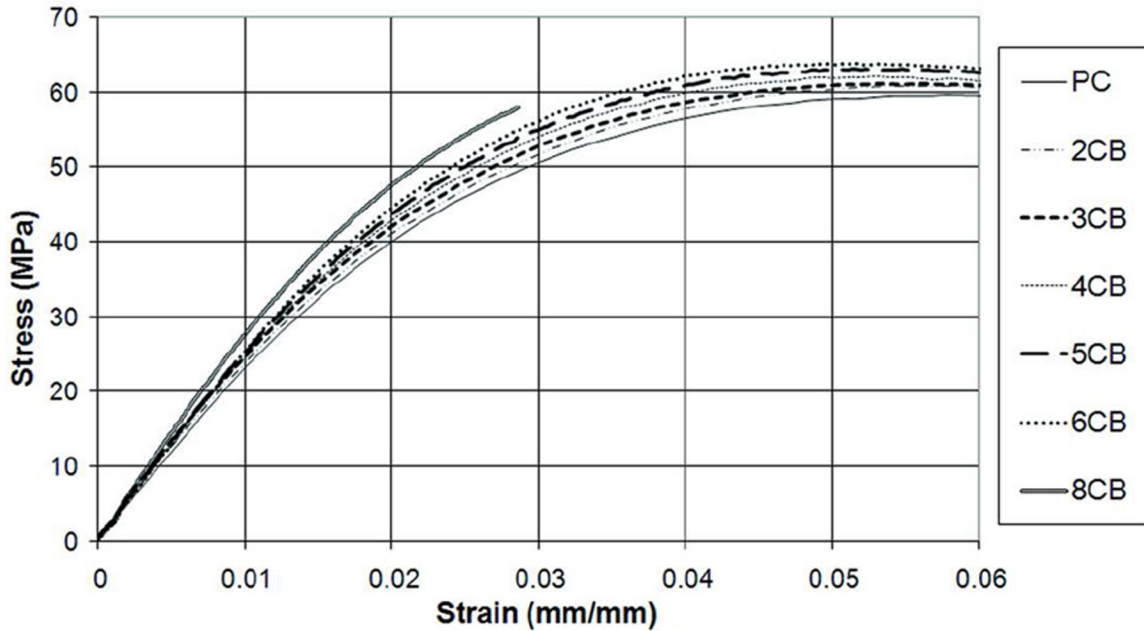


Figure 7.6: Typical stress-strain curves for CB/PC composites

7.5: Flexural Test Results

The flexural modulus of the CB based composites is shown in Figure 7.7. The associated ultimate flexural strengths (UFS) and the strains at the ultimate flexural strength are shown in Figure 7.5-2. Both of these figures display the mean value along with error bars representing one standard deviation. In cases where the error bars are smaller than the marker size, they have been omitted. Similarly to the tensile modulus, the flexural modulus increases with increased CB loading. The flexural modulus increases from 2.6 GPa for the pure PC to 3.4 GPa for the 8 wt% CB. These values are very similar to the results obtained for CNT as can be seen in Figure 7.7.

Figure 7.8 omits the results for 10 wt% CB as the sample broke prematurely. Looking at the other data in the figure, similarly to CNT, the addition on CB increases the UFS of the composites. The UFS increases from 108 MPa for pure PC to 116 MPa for 8 wt% (5.5 vol%) CB. The strain at UFS was fairly constant for all loading levels of CB around

6.2%. Detailed results for this data are given in Appendix K. It appears that the high structure and surface area of the CB allows it to form significant networks that allow for electrical conductivity and increase mechanical strengths. This trend has been seen before for CB in PC (75).

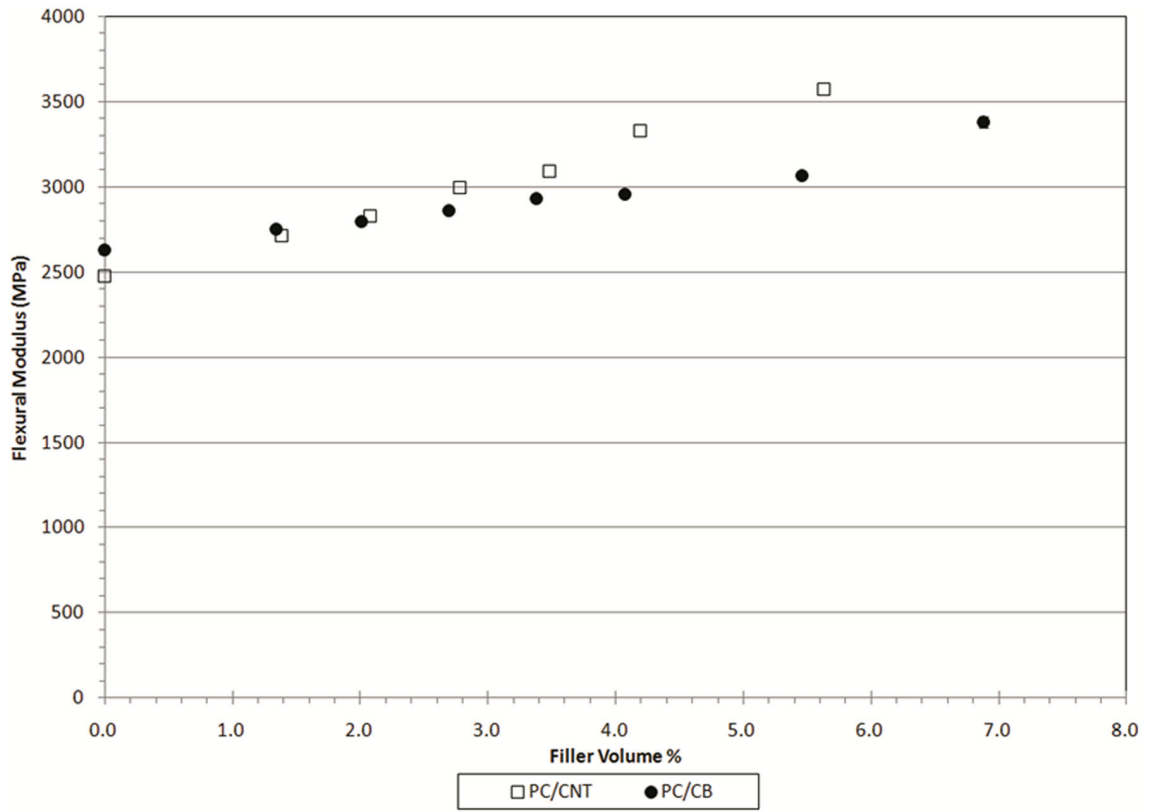


Figure 7.7: Flexural modulus of CB/PC and CNT/PC composites

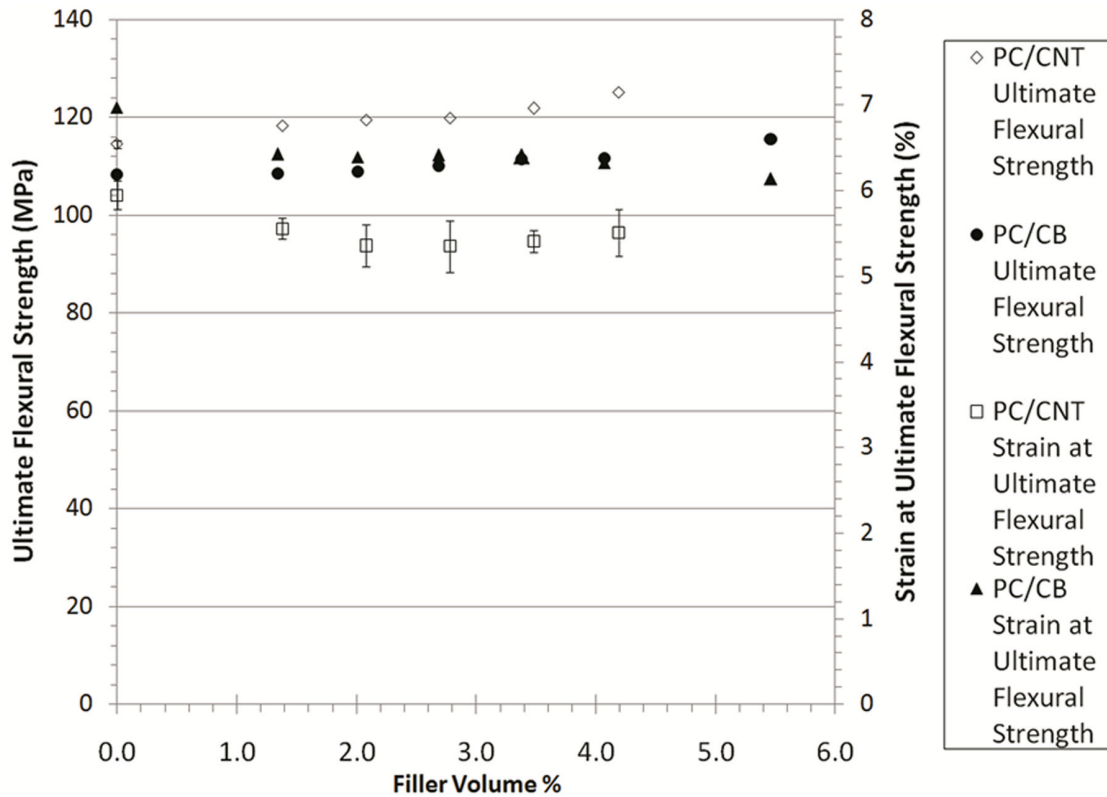


Figure 7.8: Ultimate flexural strength and strain at ultimate flexural strength for CB/PC and CNT/PC composites

7.6: Conclusions

The object of this section of the project was to measure the effects of carbon black on polycarbonate and compare these effects with those of carbon nanotubes as studied in Chapter 6. Electrically, we found the percolation threshold of CB in PC to be about 2.3 vol% compared to a percolation threshold of about 1 vol % for CNT in PC. CB decreased the electrical resistivity of PC from 1.3×10^{17} ohm-cm for the neat PC to 20 ohm-cm for 10 wt% (6.9 vol%) CB in PC. We see that CNT has a stronger effect on decreasing electrical resistivity in PC, CNT percolates at a lower filler volume (1.0 vol% versus 2.3 vol%) and has a lower resistivity when compared on an equal volume filler basis with CB (18 ohm-cm versus 649 ohm-cm for ~4 vol%). For similar loading levels,

these composites displayed a lower electrical conductivity than reported by others for CB/PC composites (7,19,34,37,42,75). The addition of 10 wt% CB increased the thermal conductivity of PC from 0.21 W/m·K for pure PC to 0.29 W/m·K, this is similar to the results for CNT/PC composites.

Mechanically, the addition of 10 wt% (6.9 vol%) CB increased the tensile modulus of PC from 2.2 GPa for neat PC to 3.0 GPa. The ultimate tensile strength for all CB composites up to 8 wt% was approximately the same, 60 to 63 MPa. The strain at ultimate tensile strength decreased with increasing CB loading. Up to 8 wt% CB, all composites showed ductile behavior. The addition of 10 wt% (6.9 vol%) CB increased the flexural modulus from 2.6 GPa for pure PC to 3.4 GPa. The ultimate flexural strength increased from 108 MPa for pure PC to 116 MPa for 8 wt% (5.5 vol%) CB. The strain at ultimate flexural strength remained fairly constant (6.1 to 7%) for all composites. All of these results are similar to those found for CNT. It is noteworthy that strain at ultimate tensile strength and ultimate flexural strength was higher in CB/PC versus CNT/PC.

Chapter 8: Rheological Properties of Carbon Nanotube/Polycarbonate Composites and Carbon Black/Polycarbonate Composites

8.1: Transmission Electron Microscope (TEM) Results

TEM images of CNT/PC composites were performed to get a better understanding of the morphology of the CNTs themselves and the conductive networks of CNTs as seen in the polymer matrix. Figure 8.1 shows the morphology of the CNTs within the PC matrix, it illustrates good dispersion of the CNT in 2 wt% and 8 wt% CNT composites. Conductive networks of CNT are seen in the 8 wt% CNT sample.

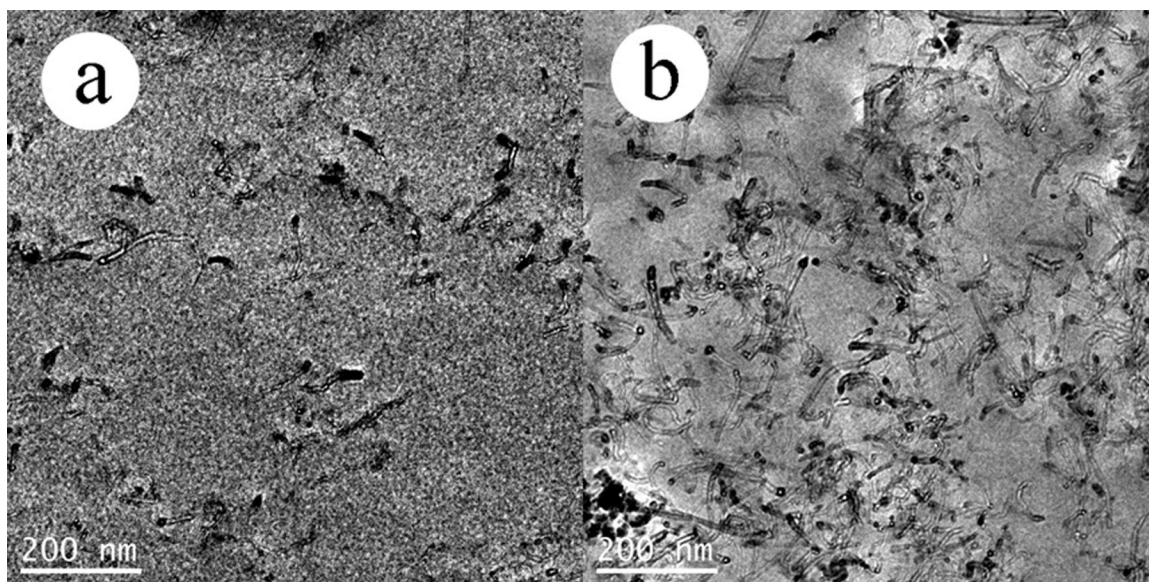


Figure 8.1: a. TEM image of 2 wt% CNT in PC b. TEM image of 8 wt% CNT in PC

8.2: Small-Amplitude Oscillator Shear (SAOS) Results

Figure 8.2 shows the SAOS master curves for the CNT/PC composites with the corresponding shift factors shown in Figure 8.3. The SAOS master curves and associated shift factors for the CB/PC composites are shown in Figure 8.4 and Figure 8.5

respectively. It can quickly be seen that in Figures 8.2 and 8.4 that the plots of the $\log \eta^*$ versus the \log frequency show a slope of -1 for the filled systems. This behavior indicates the presence of a rheological yield stress (51). Detailed results for this data are given in Appendix L.

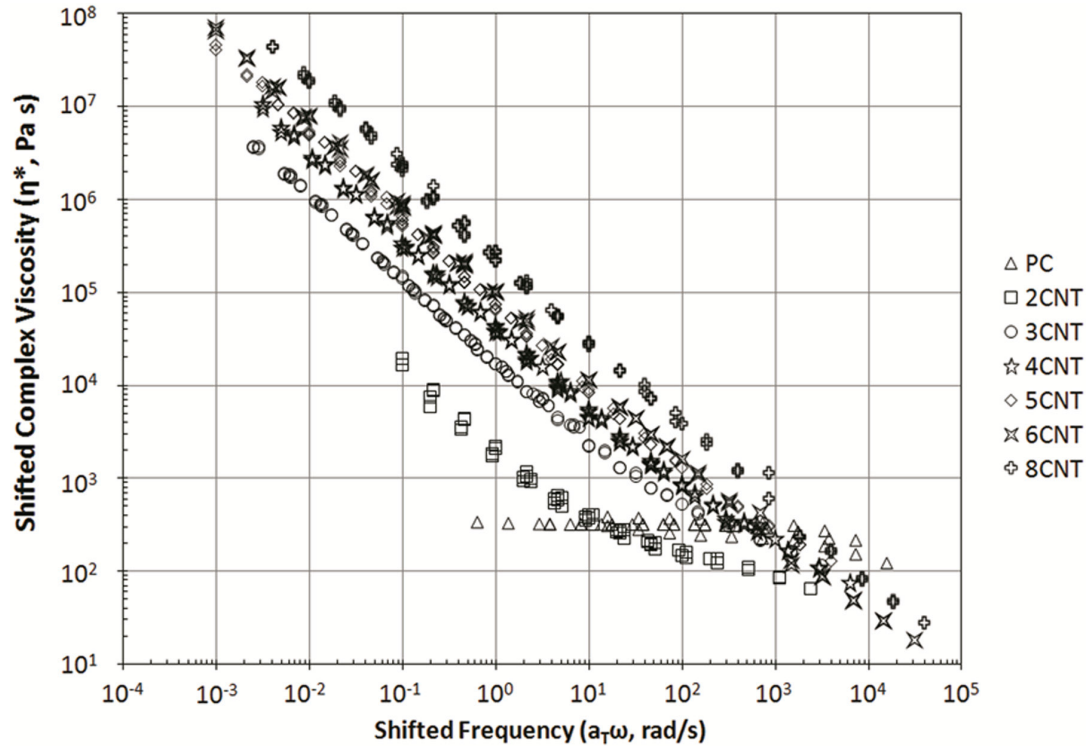


Figure 8.2: Time-temperature shifted complex viscosity as a function of shifted frequency for CNT/PC studied at 270°C

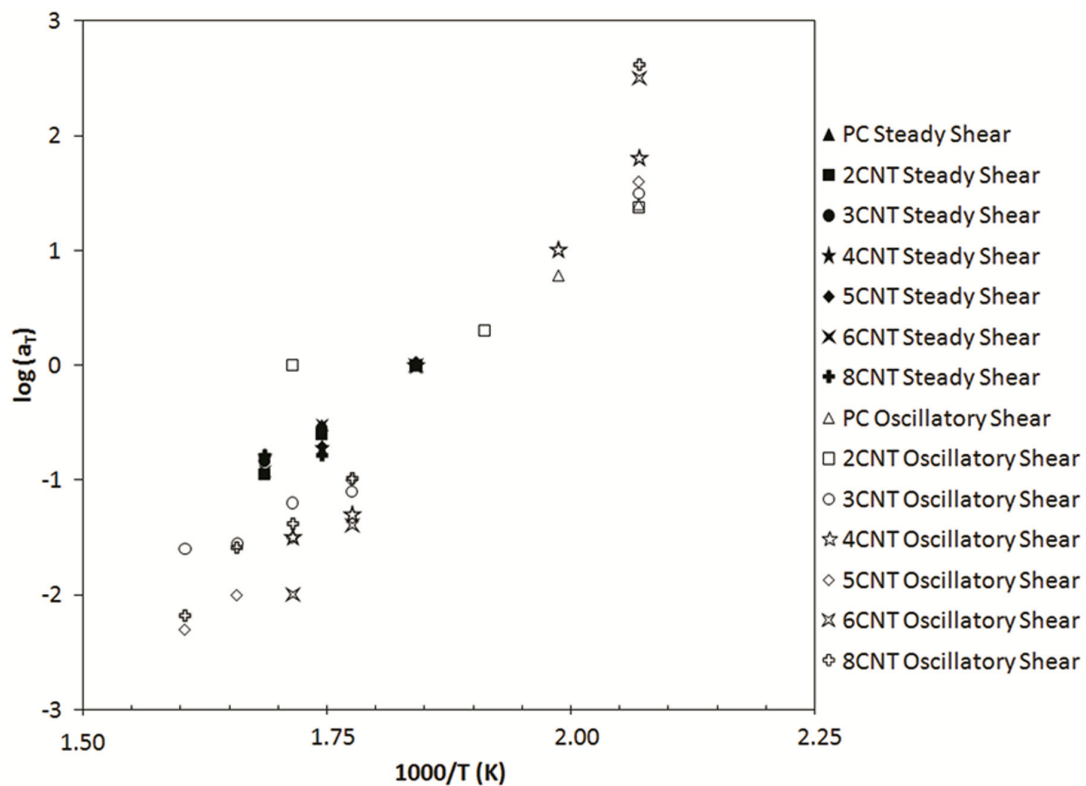


Figure 8.3: Time-temperature shift factors a_T for both steady and oscillatory rheological data of CNT/PC as a function of inverse temperature

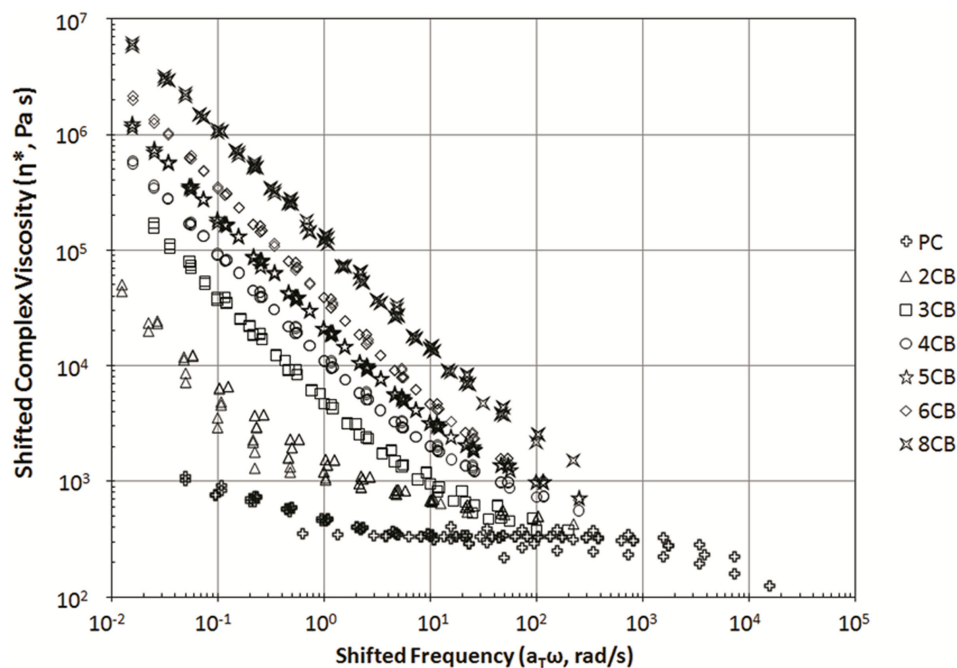


Figure 8.4: Time-temperature shifted complex viscosity as a function of shifted frequency CB/PC studied at 270°C

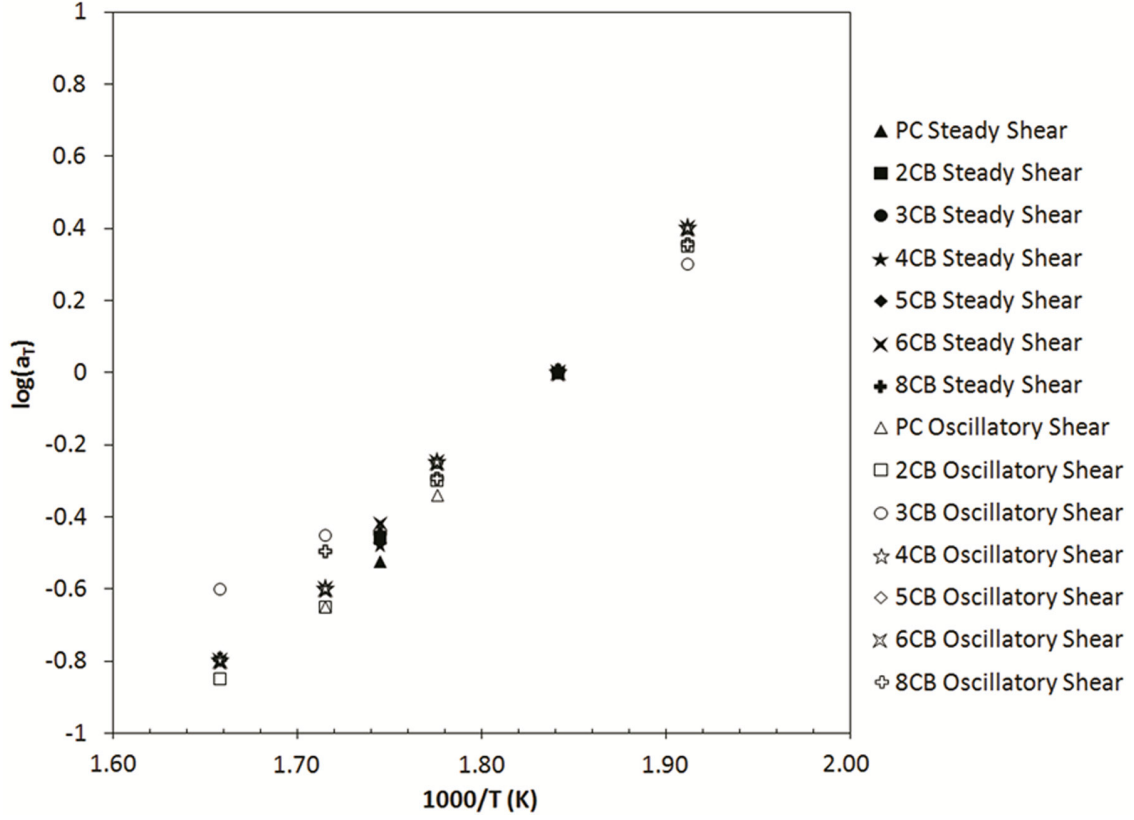


Figure 8.5: Time-temperature shift factors a_T for both steady and oscillatory rheological data of CB/PC as a function of inverse temperature

Bingham plastics are constant-viscosity fluids that have a yield-stress. The shear stress of these materials is given by Equation 8.1.

$$\tau_{21} = \mu_0 \dot{\gamma} + \tau_0 \quad (8.1)$$

In this equation, τ_{21} is the shear stress, $\dot{\gamma}$ is the shear rate, μ_0 is the viscosity parameter of the model and τ_0 is the yield stress (51). We can put this in terms of viscosity, η , by using the definition of viscosity, $\eta \equiv \tau_{21}/\dot{\gamma}$. When this is applied to Equation 8.1 we obtain Equation 8.2 known as the Bingham model.

$$\eta = \mu_0 + \frac{\tau_0}{\dot{\gamma}} \quad (8.2)$$

By taking the logarithm of both sides of the equation then applying the limit as shear rate goes to zero, we can see the slope of -1 develop as shown in Equations 8.3 and 8.4.

$$\log \eta = \log \left(\mu_0 + \frac{\tau_0}{\dot{\gamma}} \right) \quad (8.3)$$

$$\lim_{\dot{\gamma} \rightarrow 0} \left[\log \left(\mu_0 + \frac{\tau_0}{\dot{\gamma}} \right) \right] = \log \tau_0 - \log \dot{\gamma} \quad (8.4)$$

This derivation allows us to estimate the yield stress of a system by measuring the viscosity at a shear rate of 1 rad^{-1} as long as the systems exhibits a -1 slope on a plot of the $\log \eta^*$ versus the \log frequency. The yield stresses for CNT/PC and CB/PC as measured using this method are given in Table 8.1 and Table 8.2 respectively.

8.3: Capillary Rheometer Results: CNT/PC

Figure 8.6 and Figure 8.7 shows the steady-shear master curves for the CNT/PC composites. Detailed results for this data are listed in Appendix M. The corresponding shift factors are shown in Figure 8.3. Figures 8.6 and 8.7 also include model fits (CY) that are discussed later in this section.

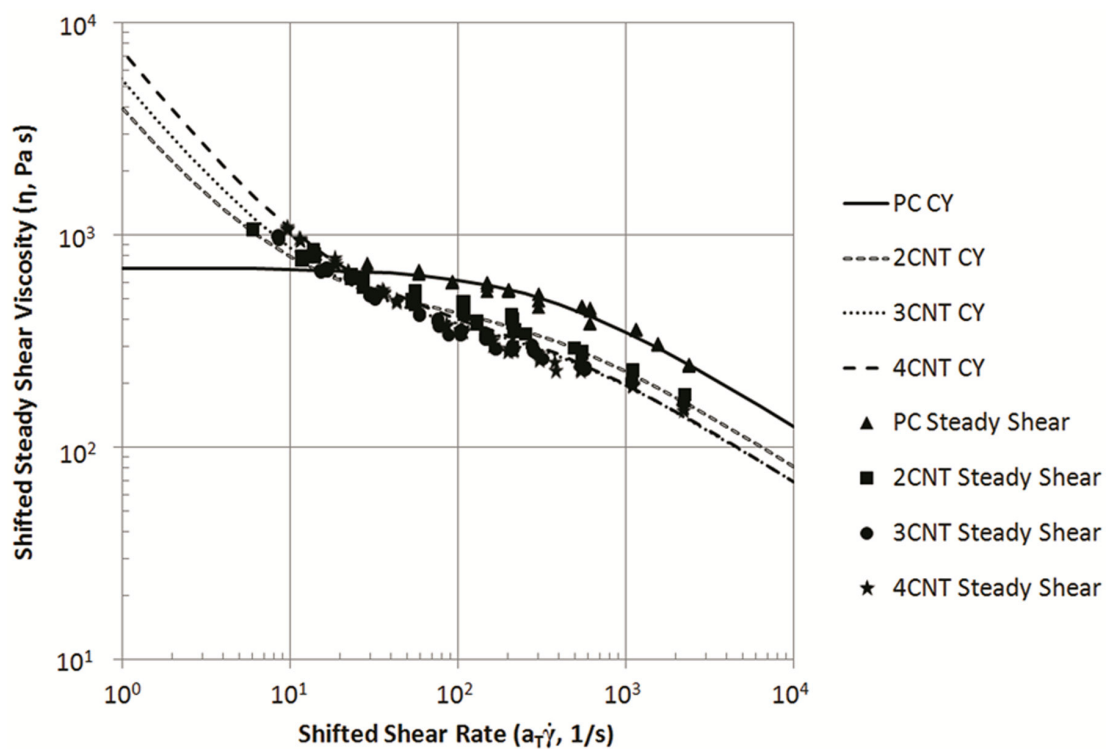


Figure 8.6: Time-temperature shifted steady-shear viscosity as a function of shifted shear rate for CNT/PC studied at 270°C. Compositions range from pure polycarbonate (0 wt % CNT) to 4 wt% CNT. Lines in the figure represent the modified Carreau-Yassuda (CY) model discussed in the text.

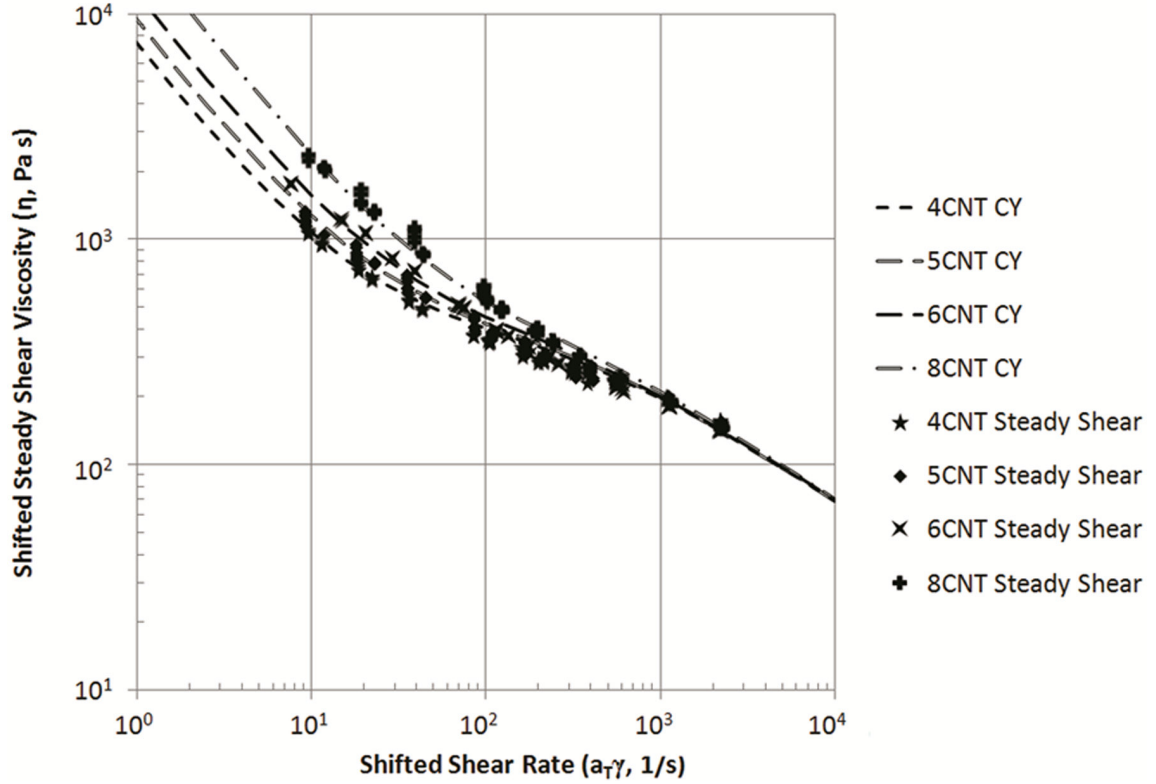


Figure 8.7: Time-temperature shifted steady-shear viscosity as a function of shifted shear rate for CNT/PC studied at 270°C. Compositions range from 4 wt% CNT to 8 wt% CNT. Lines in the figure represent the modified Carreau-Yassuda (CY) model discussed in the text.

The pure PC curve in Figure 8.6 shows a typical polymeric flow curve. It displays a Newtonian zero-shear plateau, η_0 , at about 700 Pa-s which is present at low shear rates. As the shear rate increases, the viscosity decreases, a condition known as shear-thinning. The addition of up to 4 wt% CNT results in a decrease in the viscosity by up to a factor two. This is unusual behavior as the addition of most carbons to most thermoplastic systems results in an increase in viscosity. Addition of CNT past 4 wt% is seen to increase the viscosity of the system at low shear rates while maintaining the reduction in viscosity shown with 4 wt% CNT loading at high shear rate.

This reduction in viscosity, while unusual, has also been seen by other researchers in CNT/PC systems (68). In trying to determining the cause for this behavior, it was found that the Cox-Merz rule does not hold for this system (51,53). The Cox-Merz rule states that, for many systems, when $\dot{\gamma} = \omega$, complex viscosity as obtained by SAOS, η^* , can be compared to steady shear viscosity, η , on a one-to-one basis. Even for pure PC, it was found that this rule did not hold, even at low shear rates ($\eta_0^* = 320 Pa-s$, $\eta_0 = 700 Pa-s$). It was still inferred from the SAOS data (Tables 8.1 and 8.2) that a yield stress was present, and should be included in any attempt to model steady-shear viscosity.

Using this information, it was postulated that the yield stress increases with increasing CNT loading and the increased CNT loading caused a decrease in the Newtonian zero-shear plateau, η_0 , of the composite. This postulation was tested using a modified Carreau-Yasuda model ((51), (76)) to fit our steady shear viscosity data. This model is shown as Equation 8.5. The model parameters used to fit the data are given in Table 8.1.

$$\eta(\dot{\gamma}) = \frac{\tau_0}{\dot{\gamma}} + \eta_0 \left(1 + (\dot{\gamma}\lambda)^a \right)^{\frac{n-1}{a}} \quad (8.5)$$

In this equation, τ_0 is the yield stress, $\dot{\gamma}$ is the shear rate, η_0 is the Newtonian zero-shear viscosity, λ is the relaxation time, n is the power-law index, and a is an exponential parameter. This fits given by this model using the parameters listed in Table 8.1 are shown in Figures 8.6 and 8.7.

Table 8.1: CNT/PC properties: ER, yield stress from the SAOS data; yield stress, matrix-zero-shear-viscosity and infinite-shear viscosity parameters used in modeling discussed in text. For all fits $\lambda = 0.003$, $a = 1$, and $n = 0.5$.

Formulation	Filler Wt %	Electrical Resistivity ($\Omega\text{-cm}$)	Yield stress from SAOS (Pa)	Yield stress in CY model (Pa)	η_0 (Pa s)
PC	0.0	$1.06 \times 10^{17} \pm 7.96 \times 10^{16}$ n=7	0	0	700
2CNT	2.0	4605 ± 1115 n=6	2500	3500	450
3CNT	3.0	216 ± 44 n=6	17,000	5000	380
4CNT	4.0	73 ± 10 n=6	43,000	7000	380
5CNT	5.0	43 ± 7 n=6	75,000	9000	380
6CNT	6.0	18 ± 2 n=6	87,000	12,000	380
8CNT	8.0	7.8 ± 0.4 n=6	220,000	20,000	380

This modified model has two primary parts, a Newtonian zero-shear viscosity with shear-thinning and a yield stress. The yield stress causes the model to have a slope of -1 at low shear rates. The Newtonian zero-shear viscosity with shear-thinning portion of the model dominates the model at high shear rates. We see that using the parameters listed in Table 8.1, our model generates crossover behavior of the viscosity, much as is seen in the experimental data.

An inspection of the parameters used in the fits can give us insight into the behavior of the CNT/PC composites. SAOS experimentation indicated that there was a yield stress and it increased with increasing filler loading. The steady-shear modeling shows the same behavior, the values, however, are not the same, this is expected as the Cox-Merz rule does not hold for this system. We also see from this data that the Newtonian zero-shear plateau decreases from 700 Pa-s for pure PC to 380 Pa-s as CNT loading is

increased to 3 wt%. The decrease in the zero-shear plateau saturates at this point and additional CNT loading, up to 8 wt% total CNT maintains the same level (380 Pa-s). The relaxation time, λ , is kept constant at 0.003 and the power-law index, n , is kept constant at 0.5 for all samples.

The increase in the yield strength as filler loading is increased (3.5 kPa for 2 wt% CNT to 20kPa for 8 wt% CNT) is consistent with the idea of a conductive network being formed amongst the carbon nanotubes within the PC. The electrical percolation threshold for CNT/PC is below the lowest loaded filler tested (2 wt%) thus it makes sense that all of the filled systems tested exhibit a yield stress as an electrically conductive network is likely a stress-bearing network (19).

The most notable parameter to look at when it comes to the unusual behavior seen in the CNT/PC composites is the Newtonian zero-shear plateau. The decrease in the value for the plateau indicates a lubrication effect that is happening at high shear-rate. The high shear-rate data in the pure PC represents the entangled nature of the PC molecules. At high shear-rates, the individual PC molecules are disentangling and thus shear-thinning. Our model suggests that the presence of CNT in PC acts to laminarize, or layer, the flow of the PC molecules, enhancing the disentanglement. It is postulated that the cause of this laminarization is the high aspect-ratio CNT particles getting forced (by the flow of the PC) to align either in the flow direction or perpendicular to the flow direction where it would take on a log-rolling behavior as illustrated in Figure 8.8. This alignment thus allows for the PC layers to have a greater degree of relative motion, creating an overall decrease in friction, thus lower viscosity. This kind of behavior is similar to that believed

to occur in drag reduction of turbulent flow (76). In turbulent flow drag reduction, polymers in a dilute solution are stretched out into the direction of the flow and to a degree straighten out the flow, this decreases overall friction.

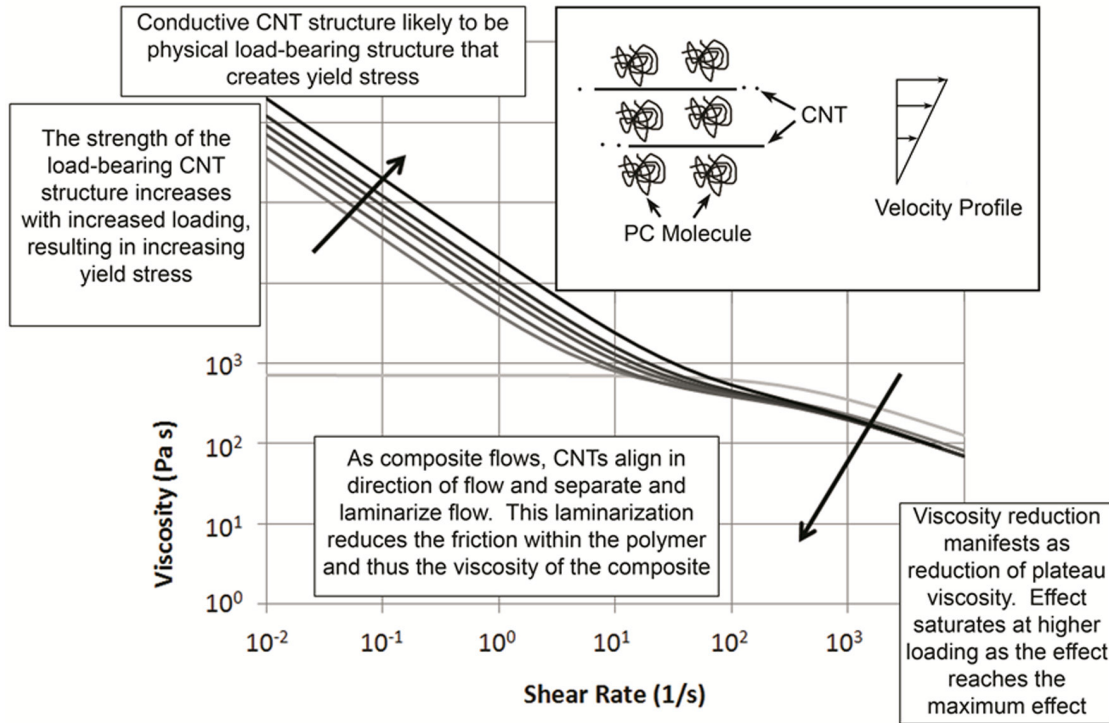


Figure 8.8: Schematic of a possible mechanism for viscosity reduction effect observed at high shear rates.

8.4: Capillary Rheometer Results and Discussion: CB/PC

Figure 8.9 and Figure 8.10 shows the steady-shear master curves for the CB/PC composites. The corresponding shift factors are shown in Figure 8.5. Figures 8.9 and 8.10 also include model fits (CY) that were discussed in section 8.3. The parameters used for this model, is included in Table 8.2.

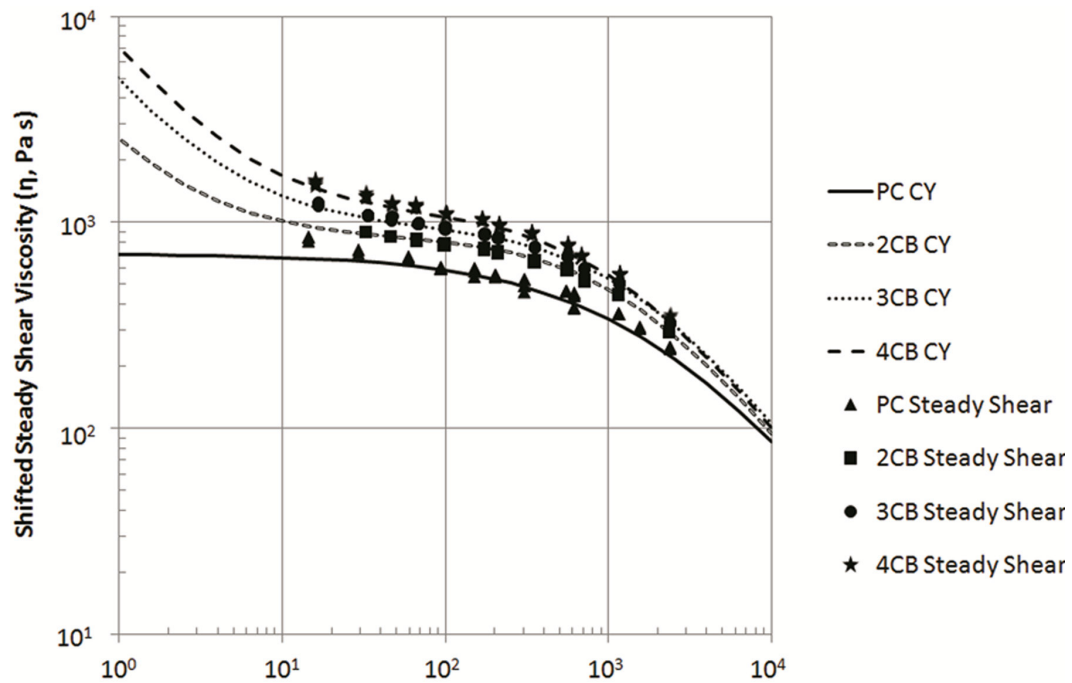


Figure 8.9: Time-temperature shifted steady-shear viscosity as a function of shifted shear rate for CB/PC studied at 270°C. Compositions range from pure polycarbonate (0 wt % CB) to 4 wt% CB. Lines in the figure represent the modified Carreau-Yassuda (CY) model discussed in the text.

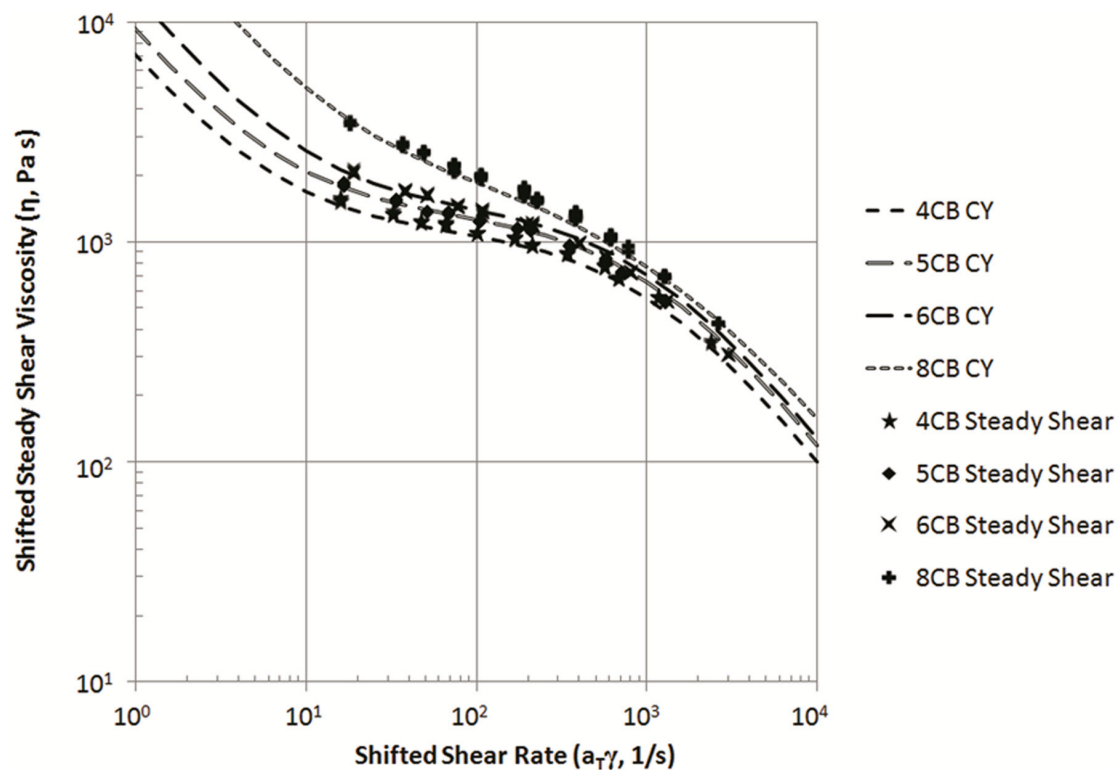


Figure 8.10: Time-temperature shifted steady-shear viscosity as a function of shifted shear rate for CB/PC studied at 270°C. Compositions range from 4 wt% CB to 8 wt% CB. Lines in the figure represent the modified Carreau-Yassuda (CY) model discussed in the text.

Table 8.2: Composite properties: ER showing percolation between 3 and 4 wt%; yield stress from the SAOS data; yield stress, matrix-zero-shear-viscosity and infinite-shear viscosity parameters used in modeling discussed in text. The parameters in the last three columns were used to fit steady shear data to the function given in Equation 12. For all fits $n=0$. Different yield stresses were obtained in SAOS and steady shear since the Cox-Merz rule was not observed to hold.

Formulation	Filler Wt %	Electrical Resistivity (ohm-cm)	Yield stress from SAOS (Pa)	Yield stress in CY model (Pa)	η_0 (Pa s)	a	λ
PC	0	$1.26 \times 10^{17} \pm 3.35 \times 10^{16}$ $n = 6$	0	0	700	0.7	0.0006
2CB	2	$4.05 \times 10^{16} \pm 2.66 \times 10^{16}$ $n = 6$	1200	1200	850	1	0.0008
3CB	3	$2.85 \times 10^{15} \pm 4.58 \times 10^{14}$ $n = 6$	5000	4000	950	1	0.0008
4CB	4	$1.17 \times 10^5 \pm 7.77 \times 10^4$ $n = 8$	11,000	6000	1100	1	0.001
5CB	5	2474 ± 646.2 $n = 8$	21,000	9000	1300	1	0.001
6CB	6	649.2 ± 17.6 $n = 8$	37,000	12,000	1400	1	0.001
8CB	8	122.2 ± 4.0 $n = 8$	120,000	29,000	2000	0.7	0.001

In Figures 8.9 and 8.10 along with the parameters used to obtain the models from Table 8.2, we see that the addition of CB to PC has the effect of increasing the Newtonian zero-shear plateau from 700 Pa-s for pure PC to 2000 Pa-s for an 8 wt% CB composite. Again we see that the Cox-Merz rule does not hold for PC, thus we do not expect it to hold for any of the CB/PC composite. For all shear rates, increasing the CB loading increases the

viscosity. This increase in viscosity is substantial at low shear rates and high filler loadings. This is the common behavior for carbon filled thermoplastic systems (77-82). No cross-over or lubrication effects are seen in these composites. The filled CB/PC composites also show a yield stress which increases with increased filler loading, this is expected for CB/PC for the same reasons that it was expected for CNT/PC as discussed in section 8.3. The growth in yield stress from 1.2kPa for neat PC to 29 kPa for 8 wt% CB is consistent with the building of a network of CB agglomerates within the PC matrix. For the CB/PC composites, the power-law parameter, n , was maintained at 0.

8.5: Conclusions

The object of this section of the project was to study the effect of CNT and CB on the viscosity of PC based composites. SAOS studies of CNT/PC and CB/PC composites showed that both CNT and CB created a yield-stress when added to PC. These yield-stresses were seen to increase monotonically with increasing filler loading for both systems. This yield-stress growth is postulated to be due to the creation of a stress-bearing system that is consistent with electrical percolation for each system as seen in Chapters 6 and 7. Steady-shear rheometry testing on the CB/PC system showed a classic increase in viscosity at all shear-rates with increased filler loading. Steady-shear rheometry testing on the CNT/PC system showed a decrease in the Newtonian zero-shear plateau with increase CNT loading to about 3 wt% CNT. Further addition of CNT past 3 wt% increased the yield stress of the composite thus increasing the low shear-rate viscosity. This is not the common behavior seen in carbon-filled thermoplastics. The reduction in viscosity is consistent with a lubrication effect that would be caused by CNT

within the matrix. The CNT are believed to laminarize the flow of PC molecules by either aligning in the flow direction, or aligning perpendicular to the flow direction and log-rolling. It is believed that this process saturates at 3 wt% CNT thus the addition of further CNT past this amount does not further decrease viscosity. The unusual behavior seen in the CNT/PC system is captured in a viscosity model based on a modification of the Carreau-Yasuda equation. The Cox-Merz rule was not found to hold for PC or either of the filled systems.

Chapter 9: Electrical Resistivity, Thermal Conductivity, and Tensile, Flexural, and Rheological Properties of Exfoliated Graphite Nanoplatelet/Polycarbonate Composites

9.1: Environmental Scanning Electron Microscope (ESEM) Results

An ESEM image of 5 wt% GNP in PC is shown in Figure 9.1. In this figure, the nanoplatelets appear as white elongated elements on the grey PC background. It is evident in this image that the GNP has a high aspect ratio.

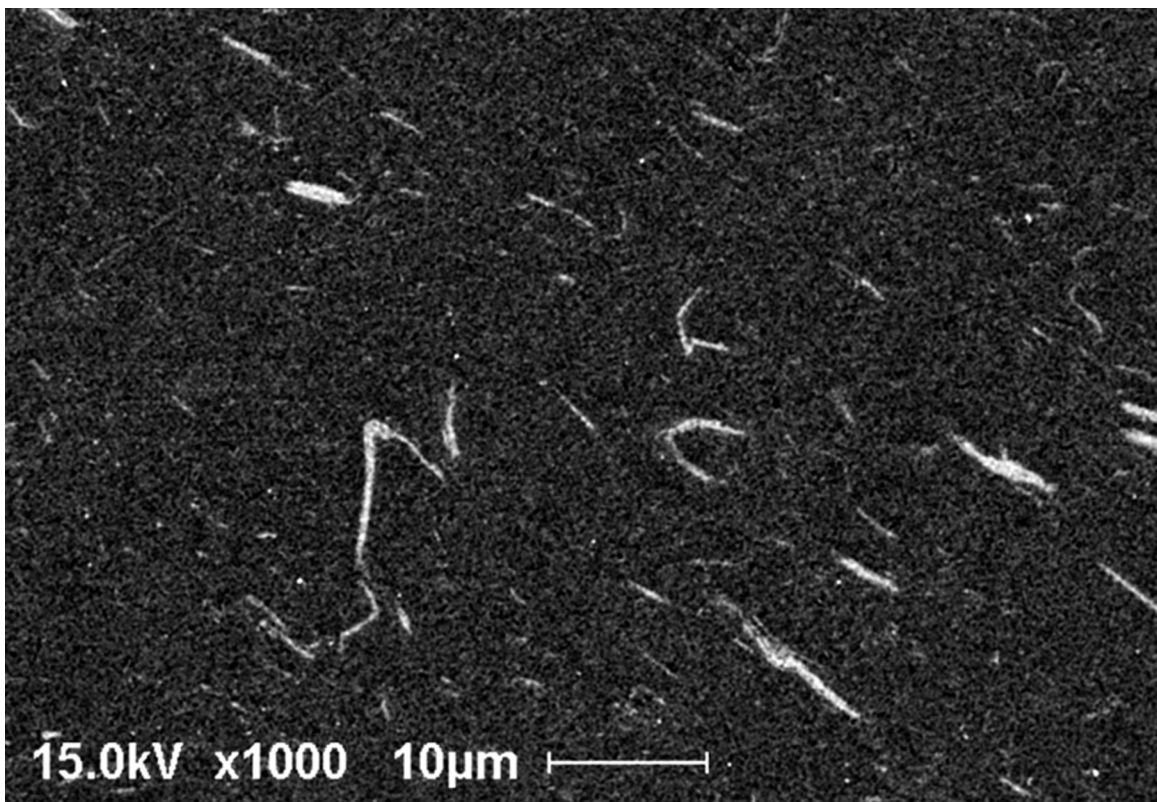


Figure 9.1: ESEM micrograph of 5 wt% GNP in PC composite

9.2: Electrical Resistivity Results

Table 9.1 shows the mean electrical resistivity, standard deviation of the electrical resistivity and number of samples that were tested for each formulation. This data is plotted in Figure 9.2. Results for the individual samples are given in Appendices G and H. We see a typical electrical resistivity curve in this figure. At low conductive filler loadings, the electrical resistivity of the composite will be similar to that of the pure polymer. As the loading of the conductive filler increases, there is a point at which conductive networks begin to form and the resistivity decreases dramatically over a very small range of filler loading. This point is known as the percolation threshold. After percolation occurs, the electrical resistivity of the composite levels out as additional conductive filler is added (7,60).

Table 9.1: GNP/PC Electrical Resistivity Results

Formulation	Filler Wt %	Filler Vol %	Electrical Resistivity (ohm-cm)
PC	0	0.0	$9.37 \times 10^{16} \pm 2.00 \times 10^{16}$ n = 6
2GNP	2	1.21	$5.46 \times 10^{16} \pm 4.89 \times 10^{15}$ n = 6
3GNP	3	1.82	$3.23 \times 10^{16} \pm 7.22 \times 10^{15}$ n = 8
4GNP	4	2.44	$1.20 \times 10^{16} \pm 3.54 \times 10^{14}$ n = 6
5GNP	5	3.06	$3.76 \times 10^{15} \pm 2.83 \times 10^{14}$ n = 6
6GNP	6	3.69	$2.01 \times 10^{14} \pm 4.99 \times 10^{12}$ n = 6
8GNP	8	4.96	$3.95 \times 10^7 \pm 1.53 \times 10^7$ n = 8
10GNP	10	6.25	$1.74 \times 10^6 \pm 2.65 \times 10^5$ n = 8
12GNP	12	7.56	$3.07 \times 10^5 \pm 9.50 \times 10^3$ n = 5
15GNP	15	9.57	$2.79 \times 10^4 \pm 8.31 \times 10^3$ n = 8

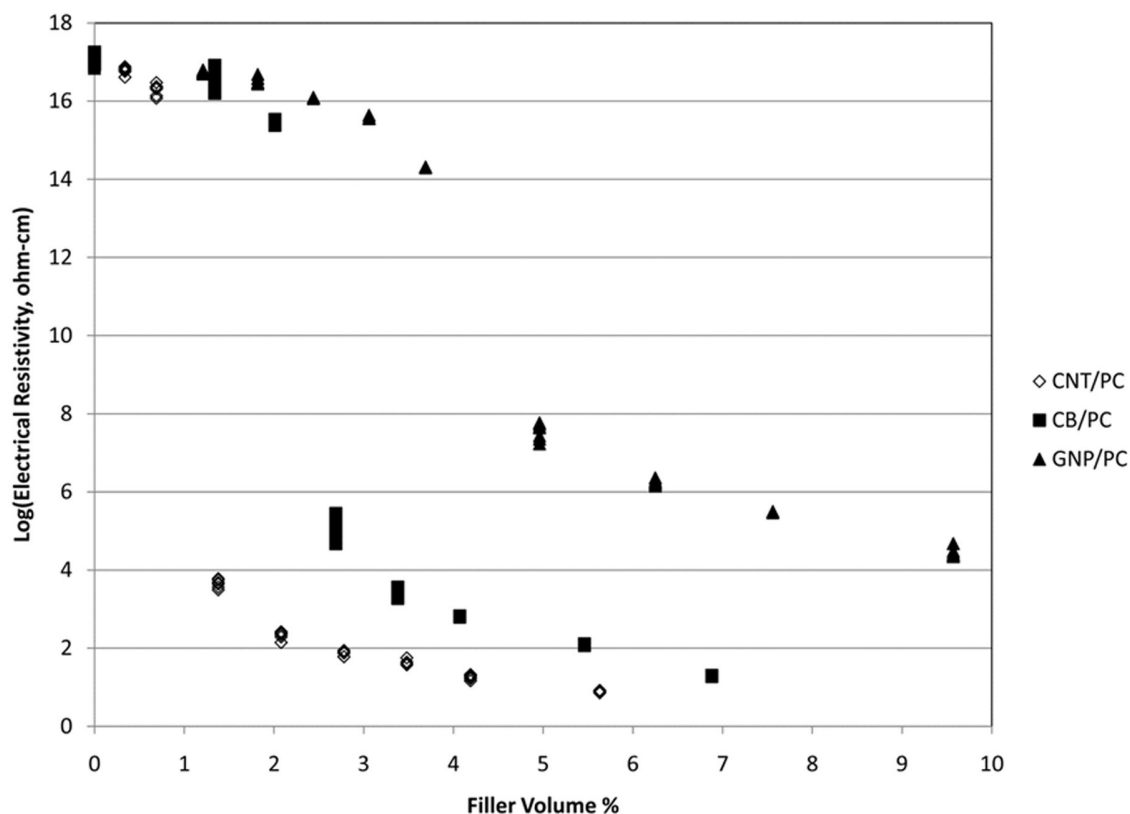


Figure 9.2: Electrical resistivity of GNP/PC, CB/PC, and CNT/PC composites

Figure 9.2 shows that GNP/PC does not percolate until over 6 wt% GNP. The ER of the composite drops from about 10^{17} ohm-cm for neat PC down to 2.8×10^4 ohm-cm for 15 wt% GNP (9.6 vol%). The percolation threshold for GNP/PC occurs at approximately 4.0 vol% (about 6.5 wt%) GNP. This is significantly higher than either the CNT or CB previously studied for this project (1 vol% and 2.3 vol% respectively). Additionally, the high end filler loadings of GNP had a much higher resistivity than the high end loadings of either the CNT or CB, despite the vol% of either of the other fillers being much lower. 15 wt% GNP (9.6 vol%) in PC had a resistivity of 2.8×10^4 ohm-cm compared to 8 ohm-cm for 8 wt% CNT (5.6 vol%) and 20 ohm-cm for 10 wt% CB (6.9 vol%).

The relatively flat shape of the ER curve indicates that GNP/PC composites would be suitable for electrostatic dissipative applications (10^{10} to 10^3 ohm-cm) in formulations of 8 to 15 wt% GNP in PC. The high value for the percolation threshold and electrical resistivity for GNP in PC is consistent with studies done by Kalaitzidou et al. (83). In his research, Kalaitzidou found that the percolation threshold of GNP in polypropylene was around 6 vol%. Additionally Kalaitzidou found that at 10 vol% the ER of GNP in polypropylene was about 10^5 ohm-cm. Both of these findings fit well with our results for GNP in PC.

9.3: Thermal Conductivity Results

The thermal conductivity test results for GNP/PC composites have been shown in Figure 9.3. The results from the previous systems, CNT/PC and CB/PC, have also been included for comparison. The results for the GNP/PC system have also been listed in Table 9.2. Detailed results for this data are given in Appendix I.

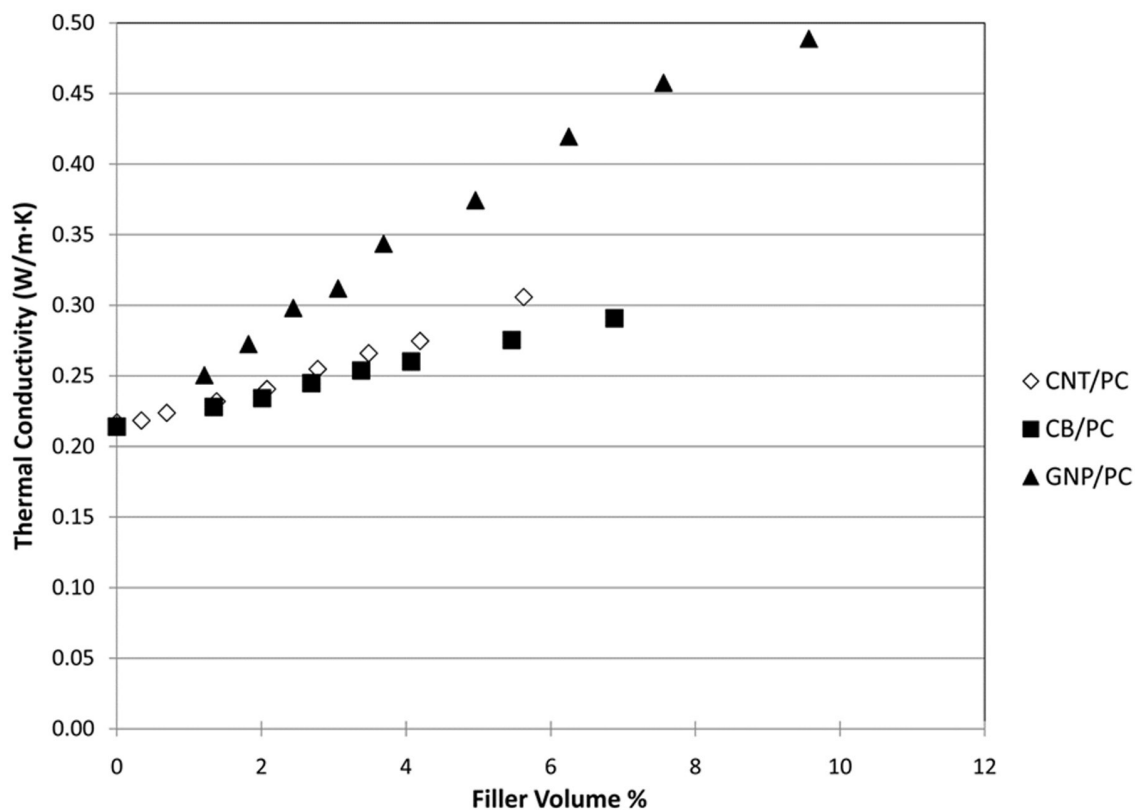


Figure 9.3: Thermal conductivity of GNP/PC, CB/PC, and CNT/PC composites

Table 9.2: GNP/PC Thermal Conductivity Results

Formulation	Filler Wt %	Thermal Conductivity (W/m·K)
PC	0	0.215 ± 0.002 n=4
2GNP	2	0.251 ± 0.003 n=5
3GNP	3	0.273 ± 0.005 n=5
4GNP	4	0.298 ± 0.003 n=4
5GNP	5	0.319 ± 0.001 n=5
6GNP	6	0.344 ± 0.002 n=4
8GNP	8	0.374 ± 0.007 n=5
10GNP	10	0.420 ± 0.002 n=5
12GNP	12	0.458 ± 0.016 n=4
15GNP	15	0.489 ± 0.016 n=4

We can see in this figure that the addition of 15 wt% GNP (9.6 vol%) increases the thermal conductivity of the composite from 0.21 W/m·K for neat PC to 0.49 W/m·K. We

can also see from the graph that GNP has a significantly higher thermal conductivity than CNT or CB for similar filler loadings. Our results for GNP/PC conform well to research done before by Fukushima et al. who studied GNP in high-density polyethylene (84).

9.4: Tensile Test Results

The tensile modulus of the GNP based composites is shown in Figure 9.4 along with the results for the previously tested systems for comparison. The ultimate tensile strengths (UTS) and the strains at the ultimate tensile strength for GNP/PC are shown in Figure 9.5. Both of these figures display the mean value along with error bars representing one standard deviation. In cases where the error bars are smaller than the marker size, they have been omitted. Detailed results for this data are given in Appendix J.

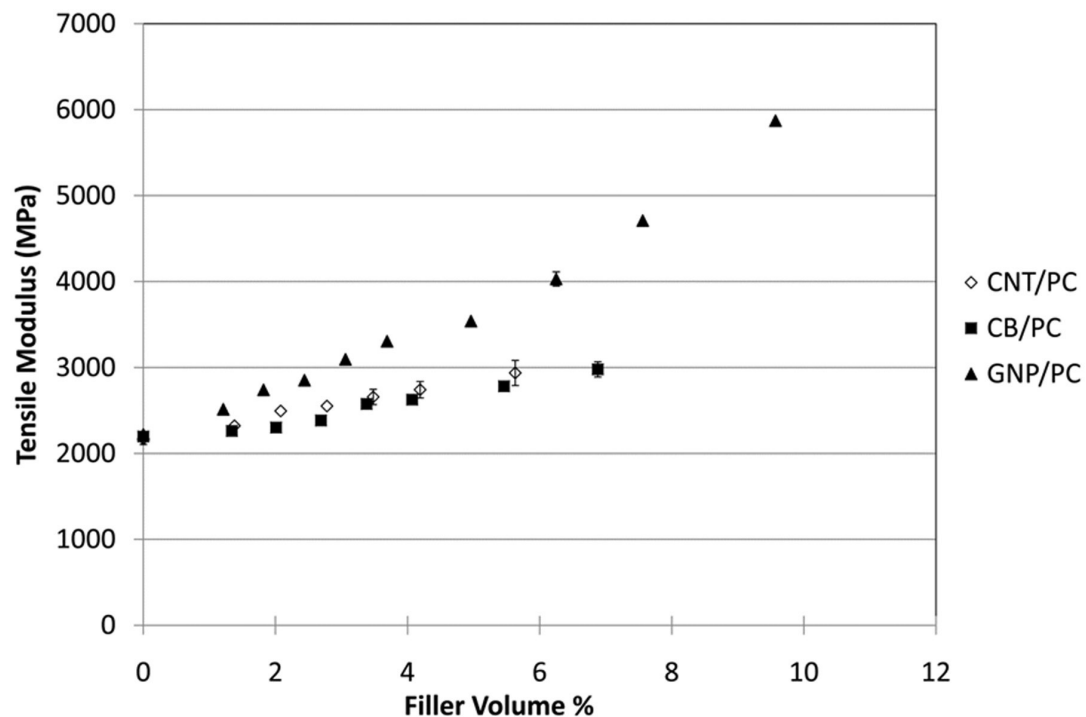


Figure 9.4: Tensile modulus of GNP/PC, CB/PC, and CNT/PC composites

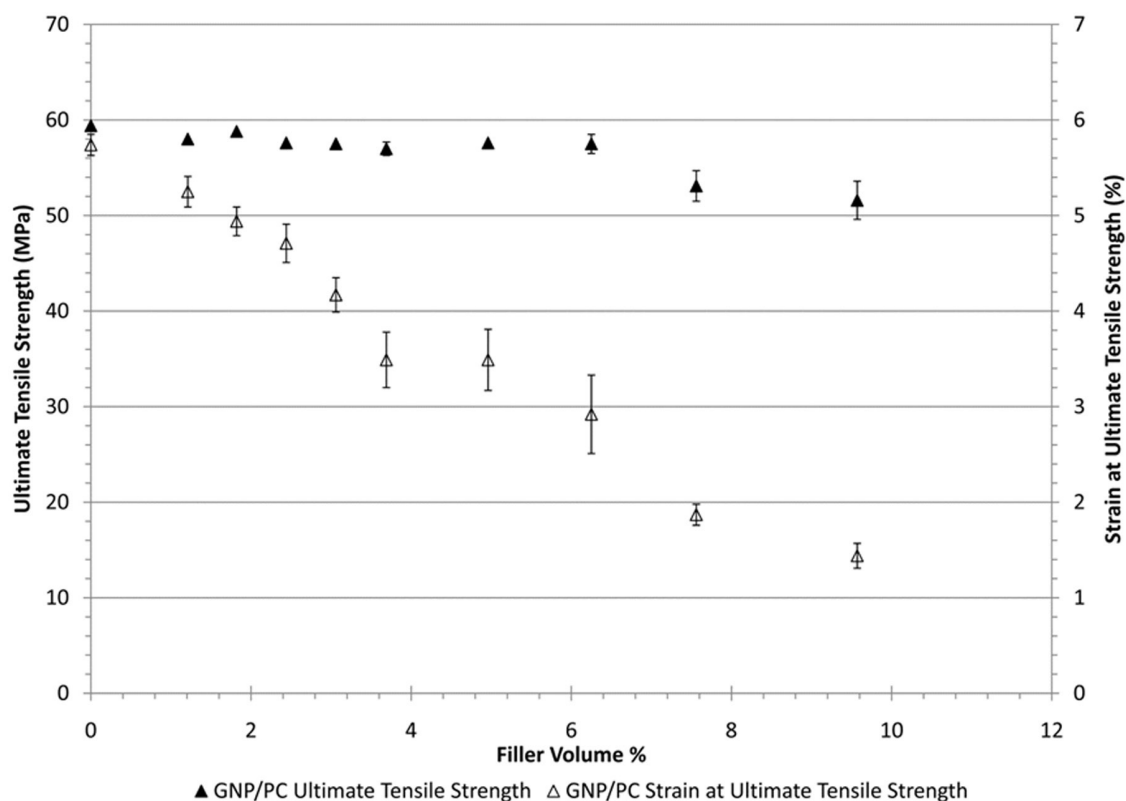


Figure 9.5: Ultimate tensile strength and strain at ultimate tensile strength for GNP/PC composites

The addition of GNP to PC increased the tensile modulus from 2.2 GPa for pure PC to 5.9 GPa for 15 wt% (9.6 vol%) GNP. When compared to CNT and CB, GNP has a larger effect on increasing the tensile modulus, at 5 vol% (8 wt%) GNP the composite has a tensile modulus of 3.5 GPa. At 5.6 vol% CNT (8 wt%) in PC, the tensile modulus is 2.9 GPa. At 5.5 vol% CB (8 wt%) in PC the tensile modulus is 2.8 GPa. A previous study of GNP in polypropylene by Kalaitzidou et al. found similar results as those seen in our GNP/PC composites (85).

As seen in Figure 9.5, the UTS of the GNP/PC composite stayed fairly constant at about 59 MPa for all formulations up to 10 wt% GNP. This compares similarly to the previous systems as seen in Figure 7.5. Above 10 wt% GNP, the composites became increasingly

brittle and the UTS and strain at UTS decreased. Figure 9.6 shows typical stress-strain curves for some of the GNP/PC composites. In this figure we can see that the ductile behavior of PC is maintained in GNP filled composites that contain less than 10 wt% GNP.

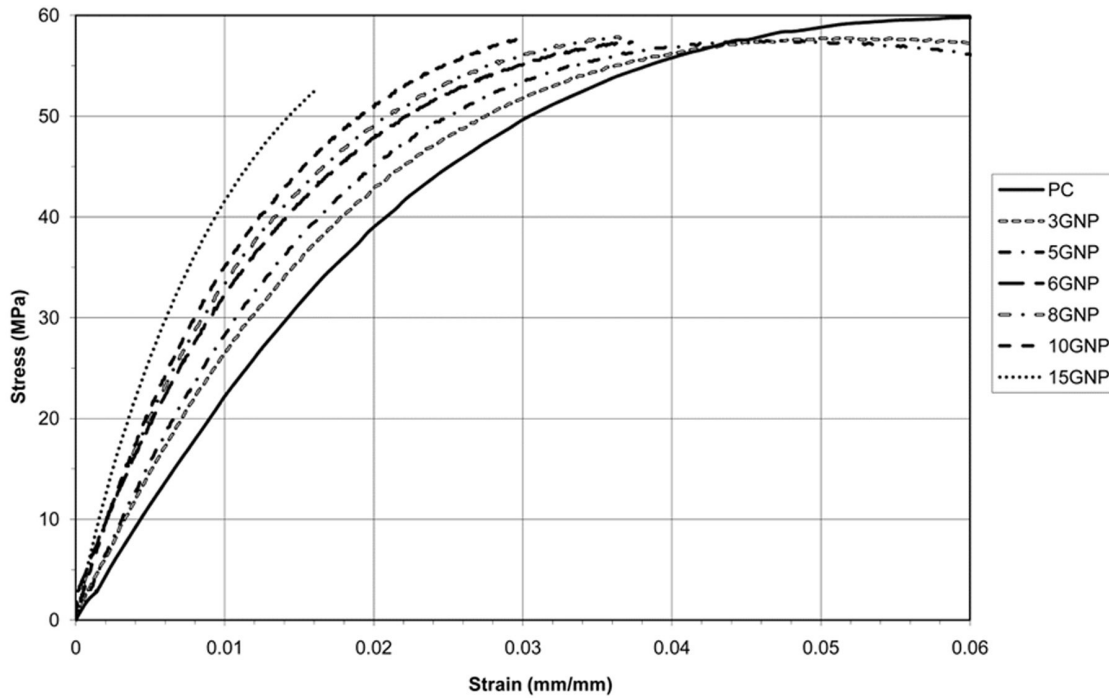


Figure 9.6: Tensile stress-strain curves for GNP/PC composites

9.5: Flexural Test Results

The flexural modulus of the GNP based composites is shown in Figure 9.7 along with the results for CNT and CB based composites for comparison. The ultimate flexural strengths (UFS) and the strains at the ultimate flexural strength for GNP/PC composites are shown in Figure 9.8. Both of these figures display the mean value along with error bars representing one standard deviation. In cases where the error bars are smaller than the marker size, they have been omitted. Detailed results for this data are given in Appendix K.

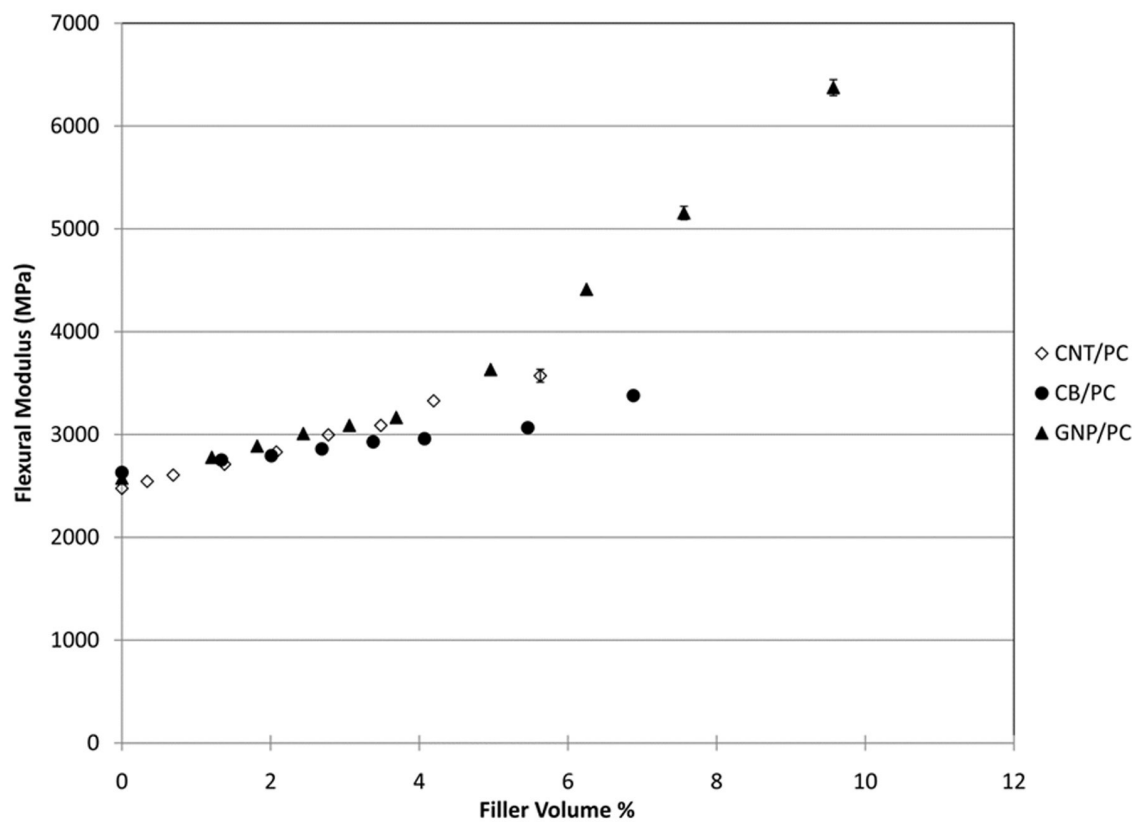


Figure 9.7: Flexural modulus for GNP/PC, CB/PC and CNT/PC composites

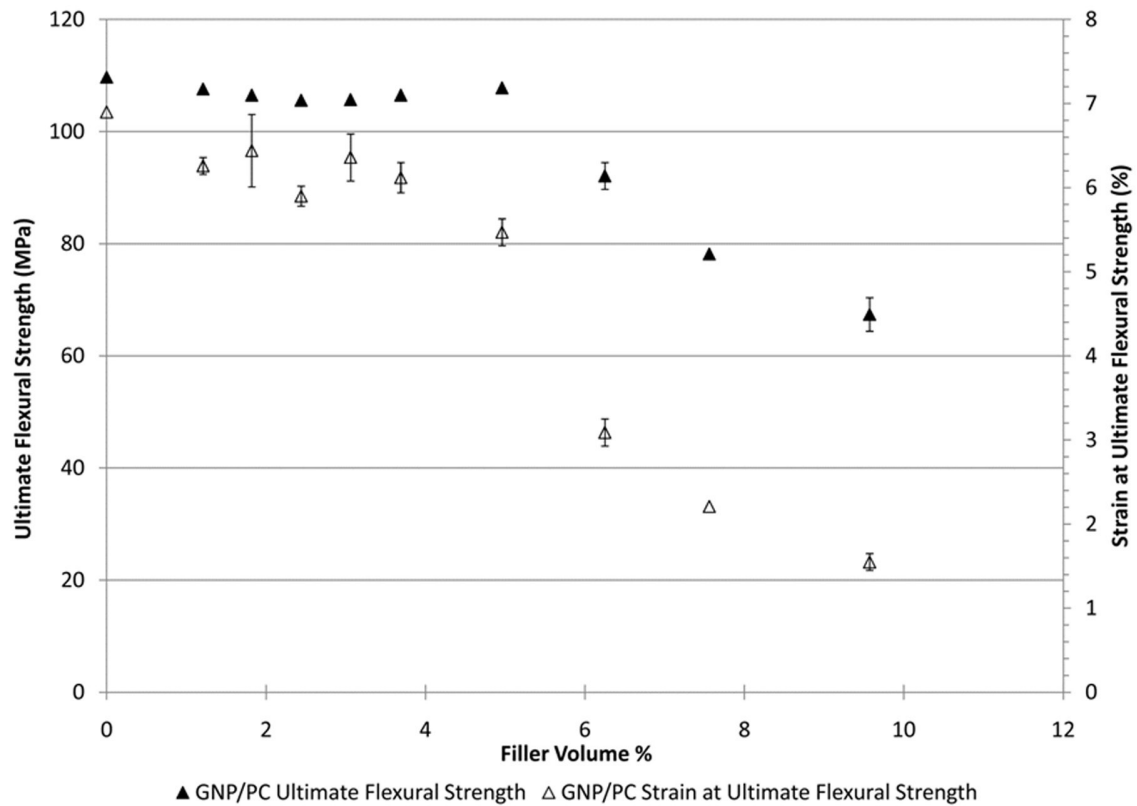


Figure 9.8: Ultimate flexural strength and strain at ultimate flexural strength for GNP/PC composites

In Figure 9.7 it is again seen that the trends in flexural modulus are similar to those in tensile modulus. The addition of GNP to PC increases the flexural modulus from 2.6 GPa for pure PC to 6.4 GPa for 15 wt% GNP (9.6 vol%). We see at high filler loadings that GNP has a larger effect on increasing the flexural modulus than either CNT or CB. At moderate filler loadings, it is similar to the other fillers. At 5 vol% GNP (8 wt%) in PC, the flexural modulus is 3.6 GPa. At 5.6 vol% CNT in PC the flexural modulus is also 3.6 GPa. CB is somewhat lower requiring 6.9 vol% to reach 3.4 GPa. Again the research of Kalitzidou et al. of GNP in polypropylene shows similar results as those seen here for GNP/PC (85).

As seen in Figure 9.8, the UFS for GNP/PC stayed fairly constant between 106 and 110 MPa for samples containing less than 10 wt% GNP. Samples with 10 wt% GNP or more again became increasingly brittle with decreasing UFS and strain at UFS. It is worth noting that the samples with 12 and 15 wt% GNP were quite viscous and difficult to injection mold.

9.6: Capillary Rheometer Results

Figure 9.9 shows the steady-shear viscosity master curve versus shear rate for GNP/PC composites. This figure shows all of the collected data points. This data is also listed in Appendix M. In the figure we see classical carbon filler in thermoplastic behavior where increased filler loading increases viscosity at all shear rates. We see common shear thinning behavior where the viscosity decreases at high shear rates. Also noticed is the common result in filled systems where the change in viscosity due to increased filler loading is more pronounced as shear rate decreases (note Figures 8.9 and 8.10 with CB in PC). The unusual viscosity reduction effects of CNT are not present in the GNP system.

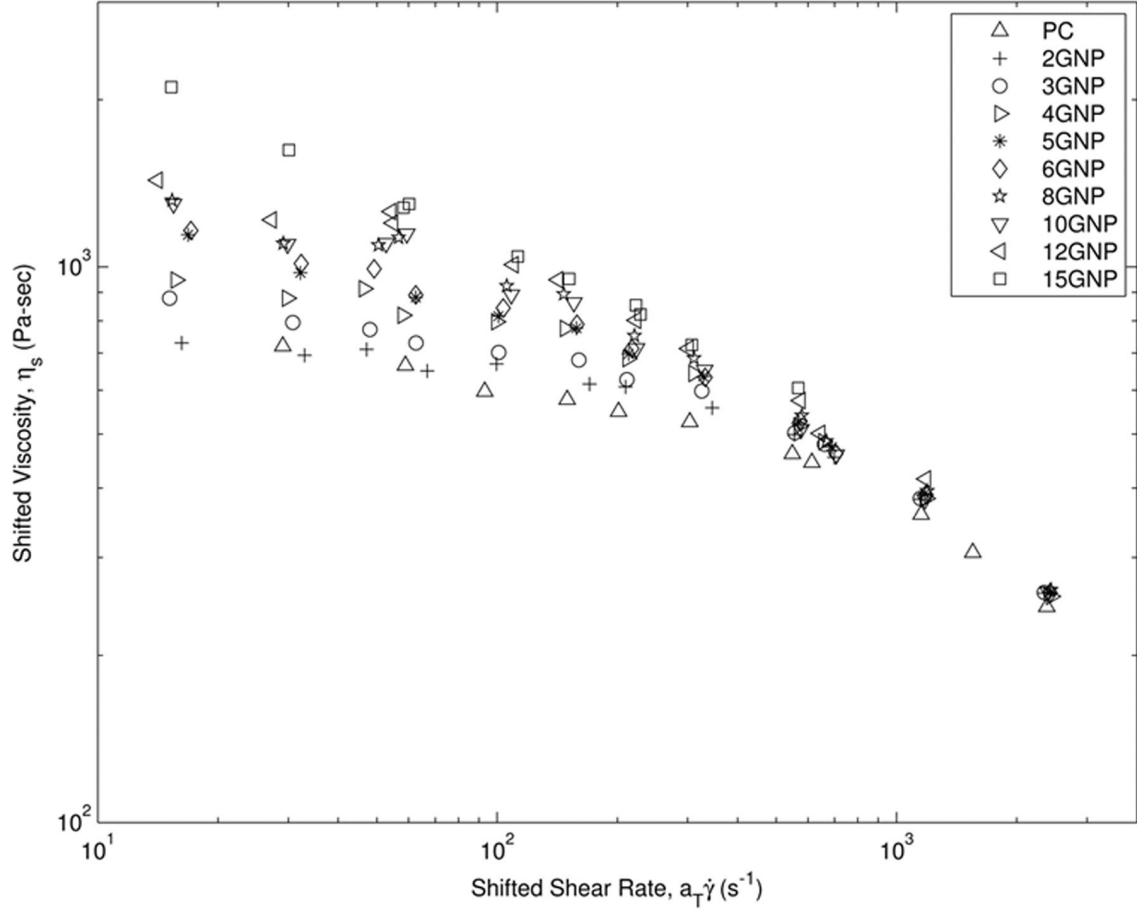


Figure 9.9: Time-temperature shifted steady-shear viscosity as a function of steady rate for GNP/PC composites studied at 270°C

To model the GNP/PC system, the Maron-Pierce model for relative viscosity versus filler fraction in a concentrated suspension is employed (86). This system is effective for shear-thinning systems as long as the comparison is done at a constant shear stress. The Maron-Pierce model is shown in Equation 9.1 below:

$$\eta_r = \frac{\eta(\phi)}{\eta(\phi = 0)} = \frac{1}{\left(1 - \frac{\phi}{\phi_m}\right)^2} \quad (9.1)$$

Where η_r is the reduced viscosity, $\eta(\phi)$ is the viscosity at filler volume, ϕ , and ϕ_m is the maximum packing fraction of the filler. This model was based off of Einstein's experiments with glass spheres in water flows thus it assumes volume filling effects as the sole cause for viscosity increase. A value of 0.637 for the maximum packing fraction corresponds to random close packing of spheres, a value of 0.44 corresponds to random packing of rough irregular particles. Flaky mica particles have been found to have a value of 0.047 for the maximum packing fraction (87). As GNP is a flake-like particle with a high aspect ratio, it is expected to exhibit behavior somewhere between mica and rough irregular particles. To study the behavior of GNP/PC we follow the work of Kitano et al. and employ a modification of the Maron-Pierce model where the maximum packing fraction, ϕ_m , is replaced with an adjustable parameter A as shown in Equation 9.2 (88).

$$\eta_r = \frac{\eta(\phi)}{\eta(\phi = 0)} = \frac{1}{\left(1 - \frac{\phi}{A}\right)^2} \quad (9.2)$$

This model was found to fit the GNP/PC data well with a value for A of 0.30. This model as well as the GNP/PC data is shown in Figure 9.10. The GNP/PC data shown in the figure corresponds to the viscosity of GNP/PC at a shear stress of 10^5 Pa. The value of 0.30 for GNP falls between the values for mica and rough irregular particles (0.047 and 0.44 respectively) as expected. The behavior of the GNP particles is more similar to that of rough irregular particles than flaky mica particles.

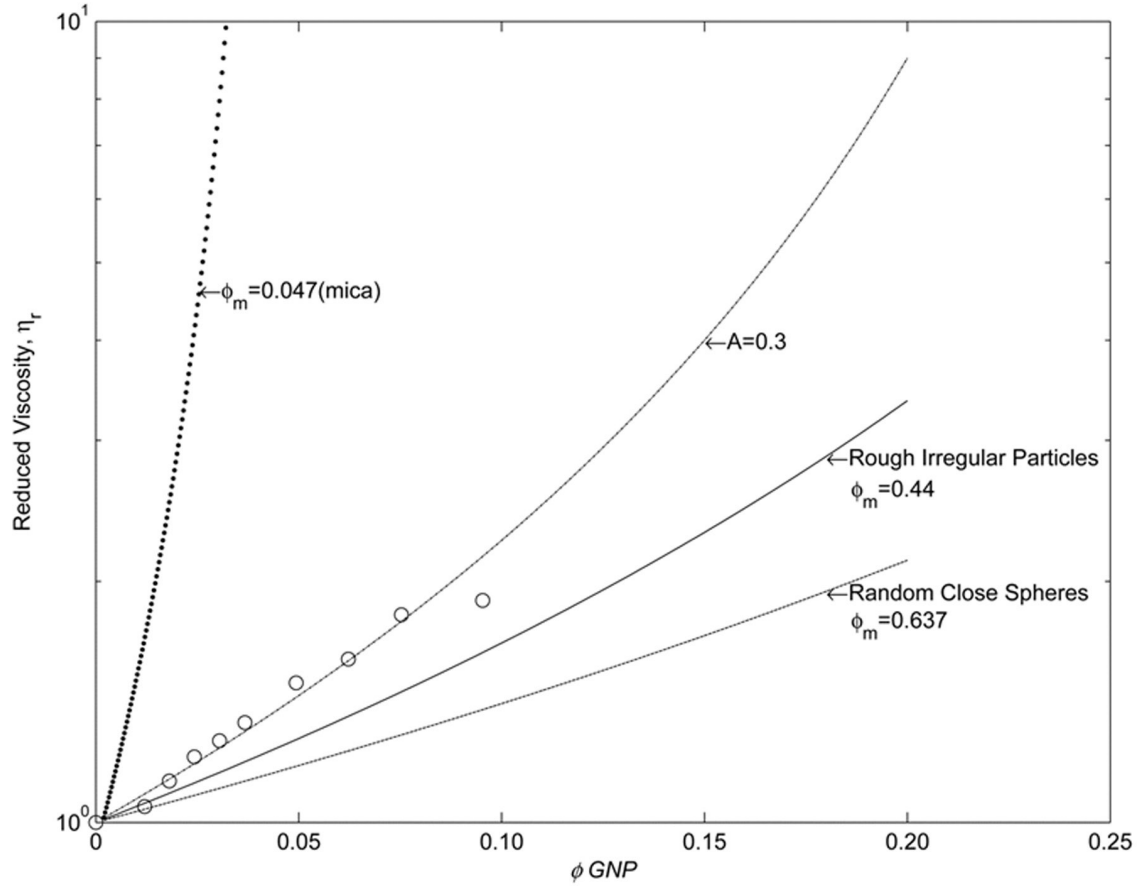


Figure 9.10: Reduced viscosity versus volume fraction, ϕ , GNP at a shear stress of 10^5 Pa for GNP/PC composites: experimental data along with Maron-Pierce models for various filler shapes and a Kitano-modified Maron-Pierce model ($A=0.3$)

9.7: Conclusions

The object of this portion of the project was to study the effects of GNP on PC and compare them to CNT and CB. Electrically, GNP has a substantially higher percolation threshold than either CNT or CB (4.0 vol% for GNP versus 1 vol% for CNT and 2.3 vol% for CB). GNP also had less of an effect on reducing the electrical resistivity of the composite only reducing the ER from $\sim 10^{17}$ ohm-cm for pure PC to 2.8×10^4 ohm-cm for 9.6 vol% GNP. GNP did have a relatively flat ER versus filler vol% curve and has high-end (8 to 15 wt% GNP) ER values that would place it in the electrostatic discharge range

(10^{10} to 10^3 ohm-cm). Adding GNP to PC also increased the thermal conductivity of the neat PC from 0.21 W/m·K to 0.49 W/m·K for 15 wt% GNP in PC.

Mechanically, GNP increased the tensile modulus of the resulting PC composite more than either CNT or CB reaching a value of 5.9 GPa for 15 wt% (9.6 vol%) GNP in PC up from 2.2 GPa for neat PC. The UTS for GNP remained constant at roughly 59 MPa for all GNP/PC composites with up to 10wt% GNP. Every composite containing less than 10 wt% GNP retained ductile behavior. The GNP also increased the flexural modulus of the resulting PC composite from 2.6 GPa for neat PC to 6.4 GPa for 15 wt% GNP in PC. The UFS stayed fairly constant at about 110 MPa for all composites containing up to 8 wt% GNP.

GNP/PC composites were found to exhibit classical shear-thinning carbon-filled thermoplastic behavior (similar to CB/PC). The increase in viscosity in GNP/PC composites is due to the volume filling effects of the GNP platelet morphology. The viscosity of GNP/PC composites was found to be well described by the Kitano-modified Maron-Pierce model with value of A of 0.3.

Chapter 10: Modeling the Electrical Conductivity of Carbon Black/Polycarbonate, Carbon Nanotube/Polycarbonate, and Exfoliated Graphite Nanoplatelet/Polycarbonate Composites

10.1: Electrical Conductivity (EC) Results

Table 10.1 shows the mean electrical conductivity, standard deviation of the electrical resistivity and number of samples that were tested for CB/PC, CNT/PC and GNP/PC. This data is plotted in Figures 10.1 through 10.3 respectively along with models that will be discussed later. The results for the individual samples are given in Appendices G and H. We see a typical electrical conductivity curves in these figures. At low conductive filler loadings, the electrical conductivity of the composite will be similar to that of the pure polymer. As the loading of the conductive filler increases, there is a point at which conductive networks begin to form and the conductivity increases dramatically over a very small range of filler loading. This point is known as the percolation threshold. After percolation occurs, the electrical conductivity of the composite levels out as additional conductive filler is added (7,60).

Table 10.1: CB/PC, CNT/PC and GNP/PC Electrical Resistivity Results

Formulation	Filler Wt %	Filler Vol %	Electrical Resistivity (ohm-cm)
PC	0	0.0	$9.37 \times 10^{16} \pm 2.00 \times 10^{16}$ n = 6
2CB	2	1.34	$4.05 \times 10^{16} \pm 2.66 \times 10^{16}$ n = 6
3CB	3	2.01	$2.85 \times 10^{15} \pm 4.58 \times 10^{14}$ n = 6
4CB	4	2.69	$1.17 \times 10^5 \pm 7.77 \times 10^4$ n = 8
5CB	5	3.38	2474 ± 646 n = 8
6CB	6	4.07	649 ± 18 n = 8
8CB	8	5.46	122 ± 4 n = 8
10CB	10	6.88	19.5 ± 0.5 n = 8
0.5CNT	0.5	0.34	$6.19 \times 10^{16} \pm 1.21 \times 10^{16}$ n = 6
1CNT	1	0.69	$2.02 \times 10^{16} \pm 6.62 \times 10^{15}$ n = 6
2CNT	2	1.38	4610 ± 1120 n = 6
3CNT	3	2.08	216 ± 44 n = 6
4CNT	4	2.78	73 ± 10 n = 6
5CNT	5	3.48	43 ± 7 n = 6
6CNT	6	4.19	18 ± 2 n = 6
8CNT	8	5.63	7.8 ± 0.4 n = 6
2GNP	2	1.21	$5.46 \times 10^{16} \pm 4.89 \times 10^{15}$ n = 6
3GNP	3	1.82	$3.23 \times 10^{16} \pm 7.22 \times 10^{15}$ n = 8
4GNP	4	2.44	$1.20 \times 10^{16} \pm 3.54 \times 10^{14}$ n = 6
5GNP	5	3.06	$3.76 \times 10^{15} \pm 2.83 \times 10^{14}$ n = 6
6GNP	6	3.69	$2.01 \times 10^{14} \pm 4.99 \times 10^{12}$ n = 6
8GNP	8	4.96	$3.95 \times 10^7 \pm 1.53 \times 10^7$ n = 8
10GNP	10	6.25	$1.74 \times 10^6 \pm 2.65 \times 10^5$ n = 8
12GNP	12	7.56	$3.07 \times 10^5 \pm 9.50 \times 10^3$ n = 5
15GNP	15	9.57	$2.79 \times 10^4 \pm 8.31 \times 10^3$ n = 8

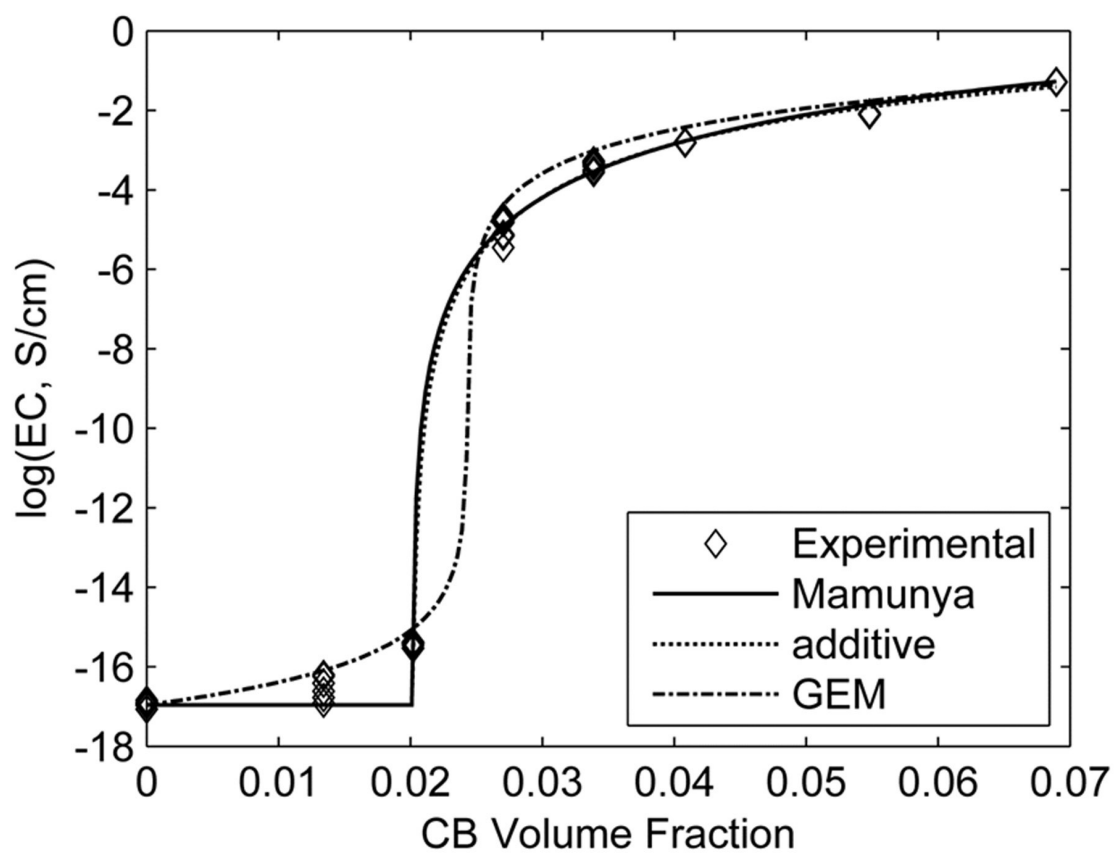


Figure 10.1: CB/PC electrical resistivity results along with Mamunya, additive and GEM models.

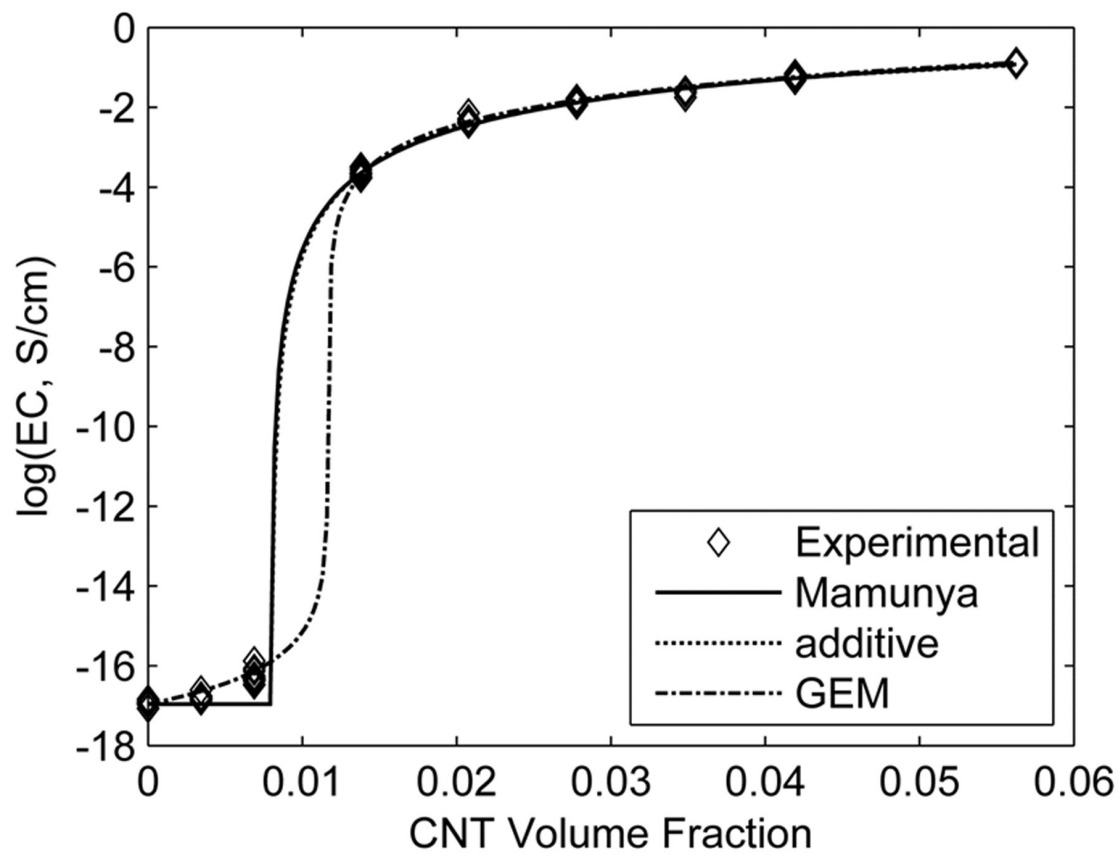


Figure 10.2: CNT/PC electrical resistivity results along with Mamunya, additive and GEM models.

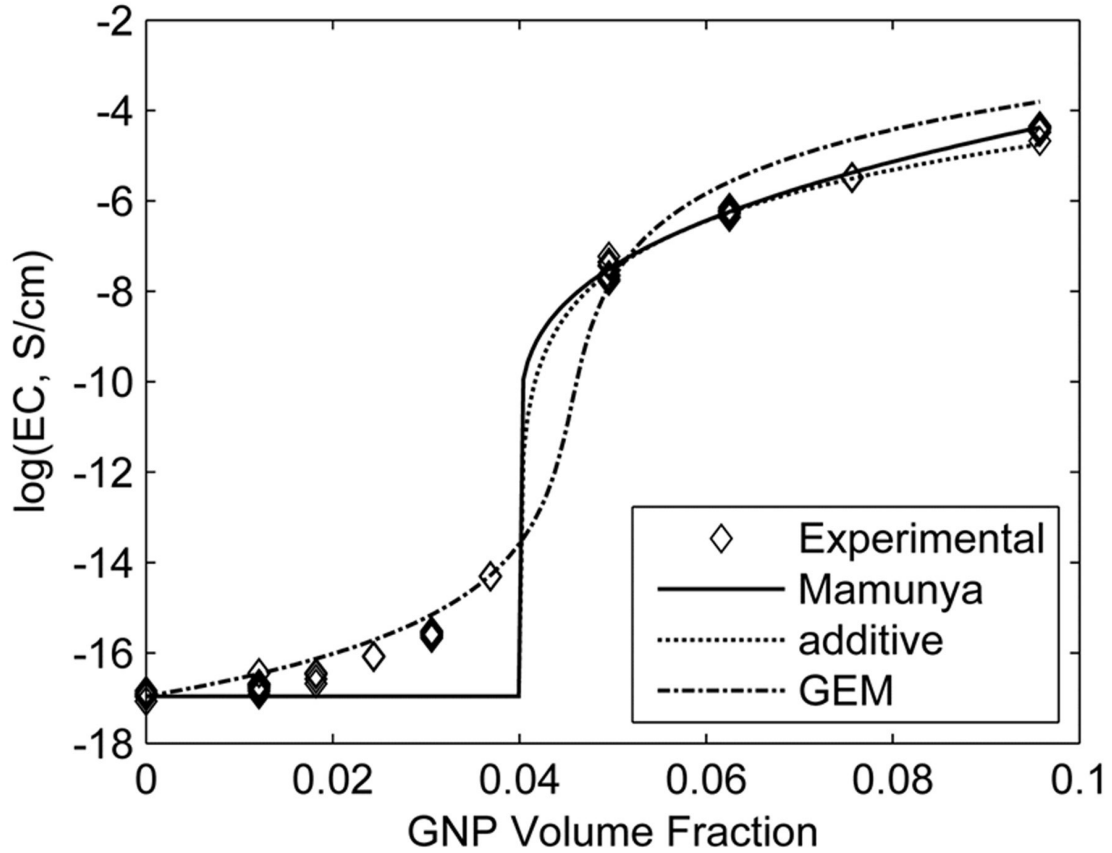


Figure 10.3: GNP/PC electrical resistivity results along with Mamunya, additive and GEM models.

In Figure 10.1 it is seen that CB decreases the ER of the composite at low loadings (percolation threshold 2.4 vol%) as discussed in Chapter 7. Figure 10.2 illustrates that CNT has a very low percolation threshold (1 vol%) and large effect on decreasing electrical conductivity (7.8 ohm-cm at 5.6 vol%) as discussed in Chapter 6. In Figure 10.3 we see that GNP has a higher percolation threshold than the other two fillers (4.6 vol%) as discussed in Chapter 9.

10.2: Electrical Conductivity Models

To model the electrical conductivity of these systems, we focused on a modified version of Mamunya et al.'s thermodynamic model (89,90), Clingerman et al.'s additive model (23,90) and McLachlan et al.'s General Effective Media (GEM) model (91-95). For all of these models, the adjustable parameters were chosen to minimize the total error as calculated by Equation 10.1 below:

$$\varepsilon = \sum_{i=1}^n (\log(\sigma_{calc}) - \log(\sigma_{measured}))^2 \quad (10.1)$$

where ε is the total error, σ_{calc} is the electrical conductivity for a formulation as predicted by the model and $\sigma_{measured}$ is the electrical conductivity of the same formulation as measured by experimentation. The total error as calculated by this method can also be used to compare the quality of fit of each model to each filler system. A lower total error would be indicative of a better quality of fit.

The modified Mamunya model is shown in Equation 10.2 below:

$$\begin{aligned} \log(\sigma) &= \log(\sigma_p) + [\log(\sigma_f) - \log(\sigma_p)] \left(\frac{\phi - \phi_c}{F - \phi_c} \right)^k & \text{if } \phi > \phi_c \\ \log(\sigma) &= \log(\sigma_p) & \text{if } \phi \leq \phi_c \end{aligned} \quad (10.2)$$

where σ is the composite electrical conductivity, σ_p is the electrical conductivity of the polymer, ϕ is the filler volume fraction, ϕ_c is the percolation threshold, F is the maximum filler volume fraction and σ_f is the electrical conductivity of the composite at F (89). For this model, k is given by Equation 10.3 below:

$$k = \frac{K\phi_c}{(\phi - \phi_c)^n} \quad (10.3)$$

where K and n are adjustable parameters (89). It is important to note that for this model, when the filler volume fraction is below the percolation threshold, the composite electrical conductivity is assumed to be equal to the polymer electrical conductivity. This indicates that the percolation threshold for this model is defined as the filler volume fraction at which the electrical conductivity of the composite begins to dramatically increase.

For all of the formulations, the electrical conductivity of the polymer was measured to be 1.07×10^{-17} S/cm. Figure 10.1 shows the fit of the Mamunya model to the CB/PC experimental data. For this fit, the percolation threshold, ϕ_c , is estimated to be 0.020, the maximum filler volume fraction, F , was 0.069, the electrical conductivity at F , σ_f , was 0.052 S/cm, K was set to 3.47 and n was set to 0.13. The Mamunya model resulted in a total error, ε , of $2.56 (\log \text{ S/cm})^2$ for the CB/PC system. Figure 10.2 shows the fit of the Mamunya model to the CNT/PC experimental data. For this fit, the percolation threshold, ϕ_c , is estimated to be 0.008, the maximum filler volume fraction, F , was 0.056, the electrical conductivity at F , σ_f , was 0.128 S/cm, K was set to 4.11 and n was set to 0.19. The Mamunya model resulted in a total error, ε , of $0.53 (\log \text{ S/cm})^2$ for the CNT/PC system. Figure 10.3 shows the fit of the Mamunya model to the GNP/PC experimental data. For this fit, the percolation threshold, ϕ_c , is estimated to be 0.040, the maximum filler volume fraction, F , was 0.096, the electrical conductivity at F , σ_f , was

3.59×10^{-5} S/cm, K was set to 6.42 and n was set to -0.099. The Mamunya model resulted in a total error, ε , of $10.1 (\log \text{ S/cm})^2$ for the GNP/PC system. This model shows good agreement with the bulk of data from all three systems. The majority of the error comes from the data where the filler volume fraction is less than the percolation threshold thus the electrical conductivity is assumed to be that of the pure polymer. This assumption has the largest effect on the GNP/PC system as the EC curve decreases more gradually than the other two systems.

Clingerman et al.'s additive model has been shown in Equation 10.4 below:

$$\begin{aligned} \log(\sigma) &= \log(\sigma_p) + H(\phi - \phi_c) \frac{G}{(\phi - \phi_c)^n} + E & \text{if } \phi \leq \phi_c \\ \log(\sigma) &= \log(\sigma_p) & \text{if } \phi \leq \phi_c \end{aligned} \quad (10.4)$$

where σ is the composite electrical conductivity, σ_p is the electrical conductivity of the polymer, ϕ is the filler volume fraction and ϕ_c is the percolation threshold (90). In this model, H , G , E and n are adjustable model parameters (90). Again it should be noted that, similarly to the Mamunya model, this model assumes that the electrical conductivity of any specimen with a filler volume fraction less than the percolation threshold is equal to the pure polymer electrical conductivity. This means again that the percolation threshold used in the model is defined as the filler volume fraction at which the electrical conductivity of the composite begins to dramatically increase.

For all of the formulations, the electrical conductivity of the polymer was measured to be 1.07×10^{-17} S/cm. Figure 10.1 shows the fit of the additive model to the CB/PC experimental data. For this fit, the percolation threshold, ϕ_c , is estimated to be 0.020, H

is 18.3, G is 2.72×10^{-2} , E is 0.0 and n is 0.23. The additive model resulted in a total error, ε , of $2.55 (\log \text{ S/cm})^2$ for the CB/PC system. Figure 10.2 shows the fit of the additive model to the CNT/PC experimental data. For this fit, the percolation threshold, ϕ_c , is estimated to be 0.008, H is 17.5, G is 1.28×10^{-2} , E is 0.0 and n is 0.28. The additive model resulted in a total error, ε , of $0.52 (\log \text{ S/cm})^2$ for the CNT/PC system. Figure 10.3 shows the fit of the additive model to the GNP/PC experimental data. For this fit, the percolation threshold, ϕ_c , is estimated to be 0.040, H is 17.5, G is 0.112, E is 0.0 and n is 0.040. The additive model resulted in a total error, ε , of $9.79 (\log \text{ S/cm})^2$ for the GNP/PC system. The additive model has a similar fit to the data as the Mamunya model did, fitting the bulk of the data for each system. Similarly to the Mamunya model, the majority of the total error comes from the assumption that the electrical conductivity of formulations with filler volume fractions less than the percolation threshold is equal to the electrical conductivity of the pure PC.

The GEM model is shown in Equation 10.5 below:

$$\frac{(1-\phi)(\sigma_p^{1/t} - \sigma_m^{1/t})}{\sigma_p^{1/t} - A\sigma_m^{1/t}} + \frac{\phi(\sigma_h^{1/t} - \sigma_m^{1/t})}{\sigma_h^{1/t} - A\sigma_m^{1/t}} = 0 \quad (10.5)$$

where σ_m is the electrical conductivity of the composite, σ_p is the electrical conductivity of the polymer, σ_h is the electrical conductivity of the filler and ϕ is the filler volume fraction (91-93). A is given by Equation 10.6 below:

$$A = \frac{1-\phi_c}{\phi_c} \quad (10.6)$$

where ϕ_c is the percolation threshold (91-93). t is a dimensionless critical component that can be used to determine the effects of the filler morphology and is given in Equation 10.7 below:

$$t = \frac{1 - \phi_c}{1 - L} \quad (10.7)$$

where L is the demagnification coefficient of the dispersion (91-93).

The GEM model requires the electrical conductivity of the polymer (1.07×10^{-17} S/cm) as well as the electrical conductivity of the conductive filler. CB has a conductivity of 100 S/cm as given in Table 3.3. CNTs have a wide range of reported values for EC. For this modeling, we used 100 S/cm as the EC (96-98). GNP has had measurements of the electrical conductivity range from 1 to 100 S/cm (99). For this project, we take the logarithmic average of these values, 10 S/cm for the EC of GNP.

It should be noted that due to the nature of the GEM model, the percolation threshold is assumed to be the inflection point of the large increase in electrical conductivity. This means that the values used for the percolation threshold for this model do not coincide with the values used for the Manmunya or additive models, but instead resembling the values we have been reporting as the percolation threshold in prior chapters. Figure 10.1 shows the fit of the GEM model to the CB/PC experimental data. For this fit, the percolation threshold, ϕ_c , is 0.024 and t is 2.5. The GEM model resulted in a total error, ε , of $0.55 (\log \text{ S/cm})^2$ for the CB/PC system. Figure 10.2 shows the fit of the GEM model to the CNT/PC experimental data. For this fit, the percolation threshold, ϕ_c , is

0.012 and t is 2.1. The GEM model resulted in a total error, ε , of $0.07 (\log S/\text{cm})^2$ for the CNT/PC system. Figure 10.3 shows the fit of the GEM model to the GNP/PC experimental data. For this fit, the percolation threshold, ϕ_c , is 0.046 and t is 3.8. The GEM model resulted in a total error, ε , of $1.04 (\log S/\text{cm})^2$ for the GNP/PC system. We can see from these parameters that t has a large influence on the slope of the EC curve near percolation with a larger value for t giving a more gradual slope. The GEM model showed the best quality of fit for all 3 systems as measured by the total errors. This was especially true for the GNP/PC system. These models have been studied before by this research group for other systems such as CB/polypropylene and CNT/polypropylene systems with similar results (100). These models were also used to study CB/liquid crystal polymer systems and again, the GEM model was found to fit the data well (94).

10.3: Conclusions

The purpose of this section of the project was to model the electrical conductivity of CB/PC, CNT/PC and GNP/PC systems with a modified Mamunya thermodynamic model, Clingerman et al.'s additive model, and the Generalized Effective Media (GEM) model. The Mamunya and additive models produced similar results and showed very good agreement with formulations that had filler volume fractions above the percolation threshold. The assumption present in each model that, with filler volume fractions below the percolation threshold, the electrical conductivity of the composite equals that of the pure polymer does not conform to experimental results. The GEM model does not include this assumption and thus models this area of the data quite well. While the GEM model does not model the region of the curves above the percolation threshold as well as

either the Mamunya or additive models, the ability to fit the data before the percolation threshold means it has a lower total error for all three filler systems. It is important to note that the percolation threshold for the GEM model coincides with the inflection point of the large increase of electrical conductivity versus filler volume fraction. This contrasts with the Mamunya and additive models which use the beginning of the large increase in electrical conductivity versus filler volume fraction as the percolation threshold. The GEM model has the benefit of not relying on the electrical conductivity of the highest filler loading composite in a system and is capable of being applied to multiple filler systems. The GEM model provides good estimations for CB/PC, CNT/PC and GNP/PC over a wide range of filler loadings (above and below the percolation threshold) and thus would be a good model for the formulation of materials for semiconductive and electrostatic discharge applications.

Chapter 11: Tensile Modulus Modeling of Carbon Black/Polycarbonate, Carbon Nanotube/Polycarbonate, and Exfoliated Graphite Nanoplatelet/Polycarbonate Composites

11.1: Electrical Conductivity and Percolation Models

Many of the most commonly used models to estimate the tensile modulus of filled composites require knowledge of the aspect ratio (typically length/diameter) of the filler. This is due to the filler aspect ratio having a significant effect on the tensile modulus of the composite. Typically, aspect ratios are known only for as-received materials. It is common knowledge that the high energy processing techniques used in composite manufacturing (i.e. extrusion, injection molding) causes some amount of filler degradation. It can be particularly difficult to determine the aspect ratio of nanomaterial fillers in polymer composites after processing. Nanomaterials are primarily too small to be optically imaged, and often have extreme geometries that are difficult to successfully measure using electron microscopy.

We hypothesize that the percolation threshold of the manufactured composite samples as calculated using electrical conductivity modeling can be used to calculate an effective aspect ratio for the fillers using modern percolation threshold modeling. For this calculation, we will assume that the degradation of the filler happens primarily in the extended dimensions of the filler. The extended dimensions of the fillers act as a long moment arm allowing for the moment felt by the particle during processing to be extremely high in these directions compared to the non-extended directions. Thus we

will use the GEM modeling from Chapter 10 to determine a percolation threshold for these systems that can then be used with percolation threshold modeling techniques.

Recently, CNT percolation thresholds have been modeled by incorporating a conductive interparticle distance (IPD) into an analytical method (101). This paper suggests that there is a particular distance that conductive particles can be separated from each other without a loss of electrical conductivity. This distance is related to the quantum mechanical electron tunneling distance through the non-conductive matrix. For this model, a simple cylindrical geometry was assumed for CNT. The model then creates cubic elements containing single CNTs and uses these elements to determine a percolation threshold. The resulting formula for the percolation threshold of CNT/PC composites is shown below in Equation 11.1 (101).

$$\phi_C = \frac{\pi d^2 L}{4 \left[\langle \cos^2 \theta \rangle \cdot (L + IPD) \right]^3} \quad (11.1)$$

For this project, the percolation threshold as calculated in the GEM model in Chapter 10 will be inserted into Equation 11.1 which will then be used to calculate an effective length and diameter (thus aspect ratio) for CNT in the CNT/PC system. Thus, ϕ_c is the percolation threshold as found in the GEM model (0.012), d is the diameter of the CNT (10 nm as given by the vendor), $\langle \cos^2 \theta \rangle$ is the average of the squared cosine of the orientation angle of the CNT (for a randomly distributed 3D system this is equal to 1/3), IPD is the electron tunneling distance (10 nm for many polymer systems) (101), and L is

the effective length of the CNT which is calculated to be 405 nm. The resulting aspect ratio that can be used in tensile modulus modeling of CNT/PC composites is thus 40.5.

GNP percolation threshold has also recently been modeled using a similar method involving the IPD in an analytical approach (102). Again it is suggested that the electron tunneling distance through the non-conductive polymer allows the conductive particles to be separated by a certain distance without losing conductivity. This model assumes a high aspect ratio disc-like geometry that is suitable for GNP. This geometry is then used to create cubic elements that contain a single GNP particle. These elements are then used to estimate the percolation threshold. The resulting formula for the percolation threshold of GNP/PC systems is shown in Equation 11.2 below.

$$\phi_c = \frac{27\pi d^2 t}{4(d + IPD)^3} \quad (11.2)$$

For this project, the percolation threshold as calculated in the GEM model in Chapter 10 will be inserted into Equation 11.2 which will then be used to calculate an effective thickness and diameter (thus aspect ratio) for GNP in the GNP/PC system. Thus, ϕ_c is the percolation threshold as found in the GEM model (0.046), t is the thickness of the GNP (7 nm), IPD is the electron tunneling distance (10 nm for many polymer systems) (102), and d is the effective diameter of the GNP which is calculated to be 3200 nm. The resulting aspect ratio that can be used in tensile modulus modeling of GNP/PC composites is thus 457.

11.2: Tensile Modulus Models

The Halpin-Tsai and Nielsen models will be investigated for this project. The Halpin-Tsai is a very common model used to estimate the tensile modulus of CNT based composites (103-105). It was originally developed as a modification of the Nielsen model as will be seen in the discussion.

As the Halpin-Tsai was based upon the Nielsen model, the Nielsen model will be discussed first. The Nielsen model requires the tensile modulus of the matrix, the tensile modulus of the filler, the volume fraction of the filler, the maximum volume fraction of the filler and the Einstein coefficient of the filler as inputs. The maximum packing fraction of CB and CNT have been determined in prior work to be 0.2 (37). The maximum packing fraction of GNP was determined using rheological analysis in prior work in Chapter 9 to be 0.3.

This Einstein coefficient, K_E , is related to the aspect ratio of the filler. For spherical particles such as CB, the Einstein coefficient is 2.5 (106). For rod-like fillers such as CNT, the Einstein coefficient is $2L/d$, where L/d is length/diameter (aspect ratio), or 81 for this system. For GNP the Einstein coefficient is calculated using Equation 11.3 (107) below.

$$K_E = 2.5 \left(\frac{d}{t} \right)^{0.645} \quad (11.3)$$

Where d is the diameter of the platelet (3200 nm from percolation threshold modeling), t is the thickness of the platelet (7 nm), and K_E is the Einstein coefficient which is found to be 130 for this system.

The Nielsen model uses these parameters to predict the tensile modulus of composites according to Equations 11.4 through 11.7 below.

$$\frac{E_C}{E_m} = \frac{1 + ABV_f}{1 - B\psi V_f} \quad (11.4)$$

$$A = K_E - 1 \quad (11.5)$$

$$B = \frac{(E_f/E_m) - 1}{(E_f/E_m) + A} \quad (11.6)$$

$$\psi = 1 + \frac{1 - \phi_m}{\phi_m^2} V_f \quad (11.7)$$

In these equations, E_C is the composite tensile modulus, E_m is the tensile modulus of the matrix, E_f is the tensile modulus of the filler, K_E is the Einstein coefficient of the filler, ϕ_m is the maximum packing fraction of the filler and V_f is the volume fraction of the filler (30,108-110).

For this project, E_m was the same value for all three systems, 2.20 GPa. Using experimental data from prior literature, CB composites used $E_f = 827$ GPa, $K_E = 2.5$, and $\phi_m = 0.2$ with the results of this modeling seen in Figure 11.1 (30,37,108). CNT composites used $E_f = 59.4$ GPa as determined from the Halpin-Tsai modeling discussed

later, $K_E = 81.0$, and $\phi_m = 0.2$ with the results being shown in Figure 11.2. For GNP composites the value for the tensile modulus of the filler, E_f , was set at the modulus of exfoliation of graphite, 36.5 GPa (38), K_E was set to 130, and ϕ_m was set to 0.3 with the results shown in Figure 11.3. Graphene sheets are often reported to have tensile moduli in the range of 1000 GPa in the plane of the graphene sheet (99). GNP is made of 10-15 graphene sheets stacked atop each other forming a graphite particle. When a tensile load is applied to the composite and the load is subsequently transferred to the GNP, it is likely that the weaker Van der Waals bonds between the graphene sheets will fail before the graphitic carbon-carbon bonds. This leads the effective modulus of the filler to be that of exfoliation of the plates, not the modulus of tearing of the individual plates. We see in Figures 11.1 through 11.3 that the Nielsen model shows good agreement for CB/PC and GNP/PC systems but consistently over-estimates the modulus for CNT/PC composites.

The Halpin-Tsai model takes the Nielsen model then assumes fiber geometry for all fillers and removes the volume filler parameter, Ψ , to create an equation describing the tensile modulus in the direction of fiber orientation and adds a second equation that determines the tensile modulus of the composite transverse to the fiber orientation. Scaling factors are then used to combine the two equations into a final composite modulus. This focus on fiber geometries makes the Halpin-Tsai model particularly effective at modeling CNT systems and has thus often been used for these systems (103-105). Equations 11.8 through 11.11 are used in the Halpin-Tsai model to determine the moduli of the composite in both the longitudinal and transverse directions of the fillers.

$$\frac{E_L}{E_M} = \frac{1 + 2(L/d)\eta_L V_f}{1 - \eta_L V_f} \quad (11.8)$$

$$\frac{E_T}{E_M} = \frac{1 + 2\eta_T V_f}{1 - \eta_T V_f} \quad (11.9)$$

$$\eta_L = \frac{(E_f/E_m) - 1}{(E_f/E_m) + 2(L/d)} \quad (11.10)$$

$$\eta_T = \frac{(E_f/E_m) - 1}{(E_f/E_m) + 2} \quad (11.11)$$

In the preceding equations, E_L is the longitudinal composite tensile modulus, E_T is the transverse composite tensile modulus, E_M is the tensile modulus of the matrix, E_f is the tensile modulus of the filler, L/d is the aspect ratio of the filler, and V_f is the volume fraction of the filler (111-114). It is apparent that Equation 11.8 when Equation 11.10 is incorporated is equivalent to Equation 11.4 after the incorporation of Equations 11.5 and 11.6 and the removal of Ψ when K_E is equal to $2(L/d)$. In order to better simulate the randomness of filler orientation within a composite system, the Halpin-Tsai model introduces two equations to determine the composite tensile modulus for primarily 2-dimensional systems (i.e. films) and for 3-dimensional systems (i.e. bulk materials and structures). These equations are shown as Equations 11.12 and 11.13 below with E_C being the composite tensile modulus.

$$E_C = \frac{3}{8}E_L + \frac{5}{8}E_T \quad \text{2D Randomly oriented fiber} \quad (11.12)$$

$$E_C = \frac{1}{5}E_L + \frac{4}{5}E_T \quad \text{3D Randomly oriented fiber} \quad (11.13)$$

For all the formulations in this project, E_m was set to be 2.20 GPa. For CB systems, $E_f = 827$ GPa and by following prior literature, $2(L/d)$ is replaced with the value 1.5 (30,37,108). The results for the CB system are shown in Figure 11.1 where we see a consistent underestimation of the tensile modulus.

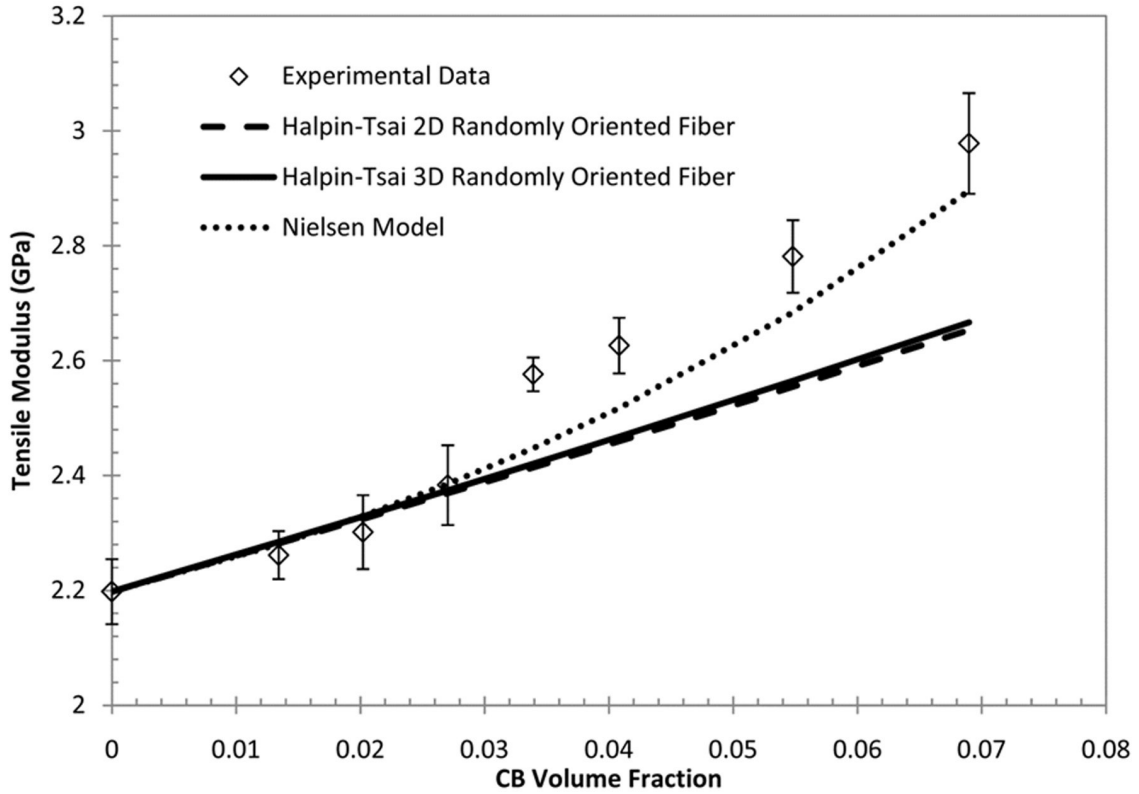


Figure 11.1: Tensile Modulus Results Along With Halpin-Tsai 2D and 3D Randomly Oriented Fiber and Nielsen Models for CB/PC Composites

For CNT systems, E_f has been reported to be anywhere from 12 GPa to 1000 GPa (115,116). For this reason, E_f was fit to minimize the error generated in the 3-dimensional Halpin-Tsai model. Error was defined as the sum of the absolute values of the differences between the experimental data and model values for each formulation. 3-dimensional random orientation was chosen for optimization due to the size difference between the filler and the tested sample. The smallest dimension of the sample, 3300 μm , is 330 times larger than the length of the as-received CNT (10 μm). Model fitting placed the value of E_f for the CNT system at 59.4 GPa, similar to the 12 to 50 GPa range given by Salvétat et al. (115). L/d was set to 40.5 as determined by the percolation threshold modeling shown earlier. The results for the CNT system are shown in Figure 11.2 where it can be seen that the 3-dimensional Halpin-Tsai model shows good agreement with the experimental data.

For GNP based systems, E_f is set to 36.5 GPa for the same reasons as it was in the Nielsen model. L/d was equated to d/t (diameter divided by thickness) and thus a value of 457 was used. The results for the GNP system are shown in Figure 11.3 where, similarly to CB systems, we see a consistent underestimation of the tensile modulus.

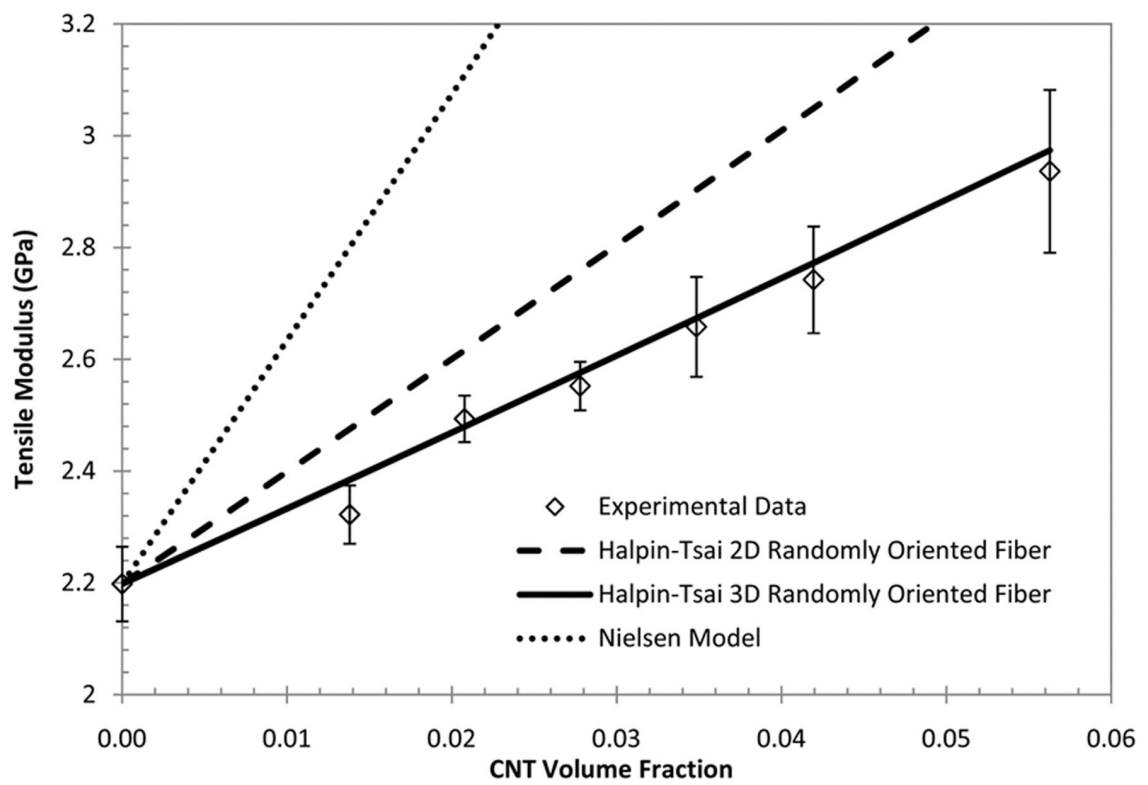


Figure 11.2: Tensile Modulus Results Along With Halpin-Tsai 2D and 3D Randomly Oriented Fiber and Nielsen Models for CNT/PC Composites

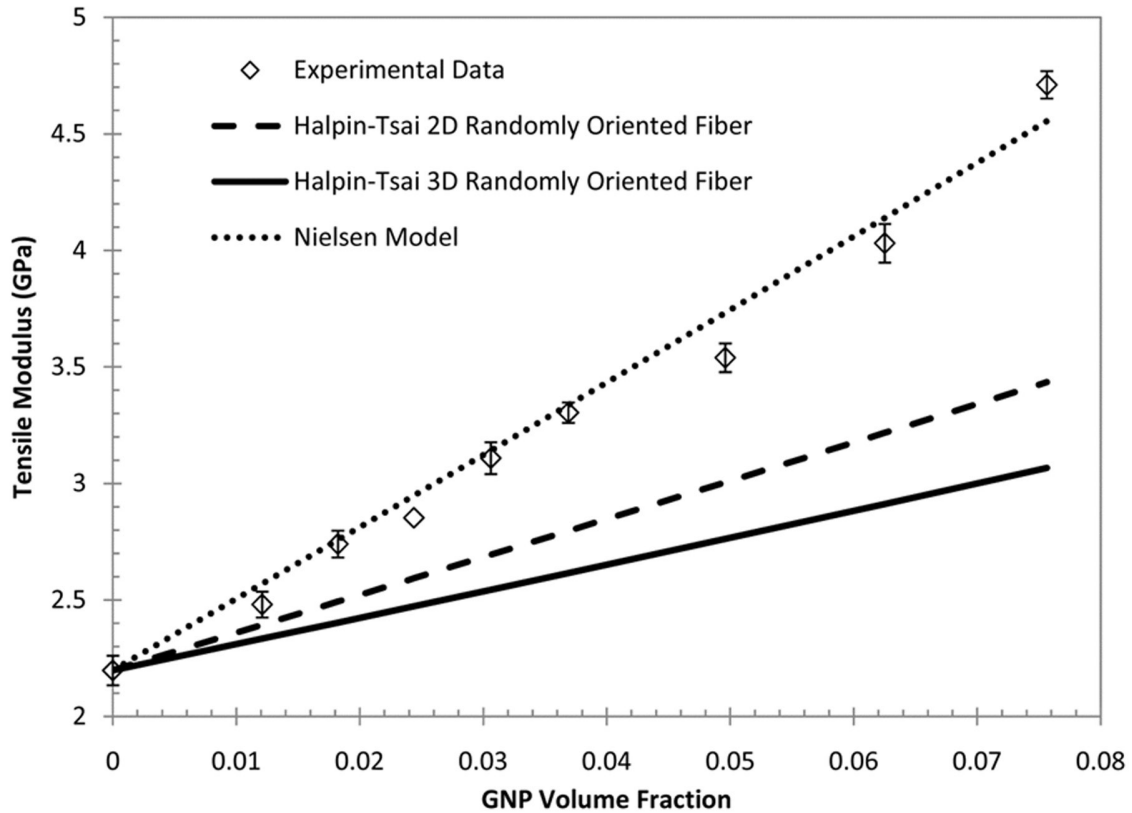


Figure 11.3: Tensile Modulus Results Along With Halpin-Tsai 2D and 3D Randomly Oriented Fiber and Nielsen Models for GNP/PC Composites

11.3: Conclusions

The purpose of this chapter is to measure the tensile moduli of single-filler PC composites (CB/PC, CNT/PC and GNP/PC) and apply the results to existing models (Nielsen and Halpin-Tsai) to determine which models are most applicable. Of these systems, GNP produced the largest increase in tensile modulus, followed by CNT, with CB having the least increase in tensile modulus.

The particular variation of the Halpin-Tsai model studied here assumes fiber-shaped filler geometry and is very commonly used to model the behavior of CNT in polymer systems. For the CNT/PC system studied here, the Halpin-Tsai model shows good agreement for all filler loadings. For the CB/PC (spherical filler) and GNP/PC (platelet filler) systems,

the Halpin-Tsai model was found to consistently underestimate the tensile modulus of the composites.

The Nielsen model is a precursor of the Halpin-Tsai model that does not assume the filler geometry. Instead of relying on assumptions for fiber geometry, the Nielsen model uses the Einstein coefficient of the filler and the maximum packing fraction to account for filler geometry and model the tensile modulus. Spherical particles like CB have a defined Einstein coefficient of 2.5. The Einstein coefficients of CNT and GNP are based upon the geometry of the filler particle, particularly the aspect ratio. The aspect ratio of the CNT and GNP in the PC was determined through modeling of the electrical percolation threshold as was determined previously using the GEM model as discussed in Chapter 10. Obtaining the model parameters using this method resulted in improved tensile models for the studied systems. The Einstein coefficient of the CNT in PC was calculated to be 81. GNP was calculated to have an Einstein coefficient of 130 in PC. The maximum packing fractions of the fillers were obtained in prior work. The Nielsen model was found to show good agreement with the CB/PC and GNP/PC composites, while consistently overestimating the tensile modulus of the CNT/PC composites.

Chapter 12: Effects of Multiple Fillers on the Electrical Resistivity, Thermal Conductivity and Tensile and Flexural Properties of Polycarbonate Based Composites

12.1: Transmission Electron Microscope (TEM) Results

Figure 12.1 shows a TEM bright field micrograph of a composite containing 5 wt% CB and 5 wt% CNT in PC. Figure 12.2 shows TEM bright field (a) and dark field (b) micrographs of a composite containing 5 wt% CB and 5 wt% GNP in PC. The dark field image is of the same region of the sample as the bright field. It was obtained by positioning the objective aperture off-center to isolate diffracted electrons from crystalline materials (GNP). This technique highlights only those crystalline particles that satisfy the Bragg condition, in this case, the GNP particle in the center of the image. Figure 12.3 similarly shows TEM bright field (a) and dark field (b) micrographs of a composite containing 5 wt% CNT and 5 wt% GNP in PC.

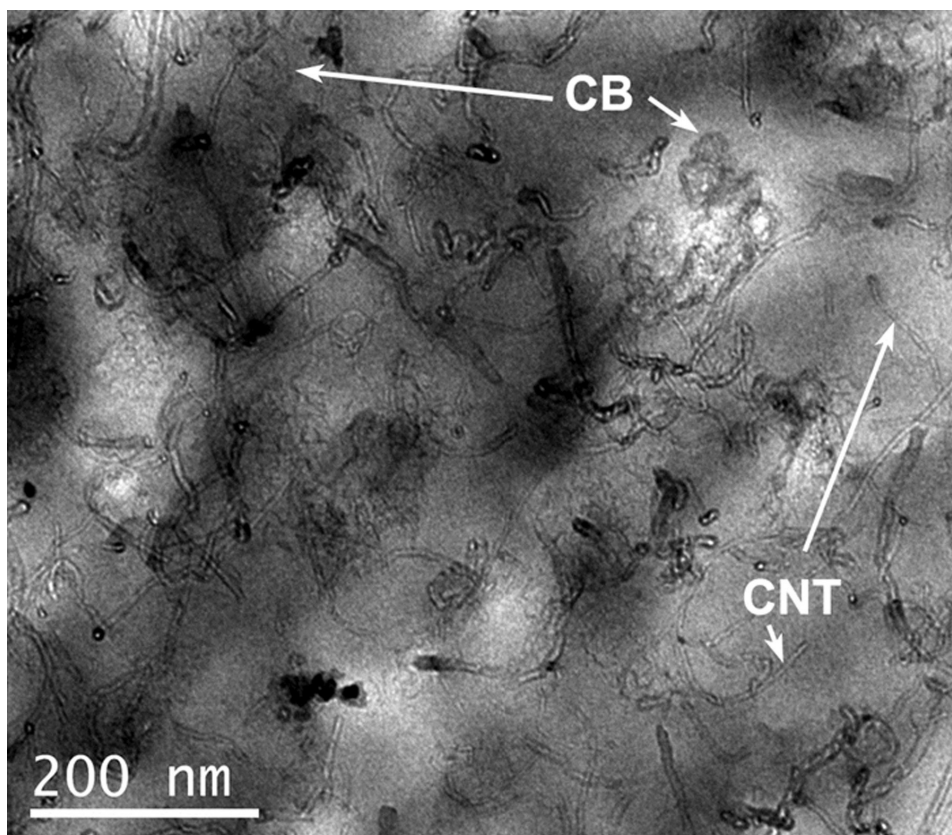


Figure 12.1: TEM Micrograph of Composite Containing 5 wt% CB and 5 wt% CNT in PC

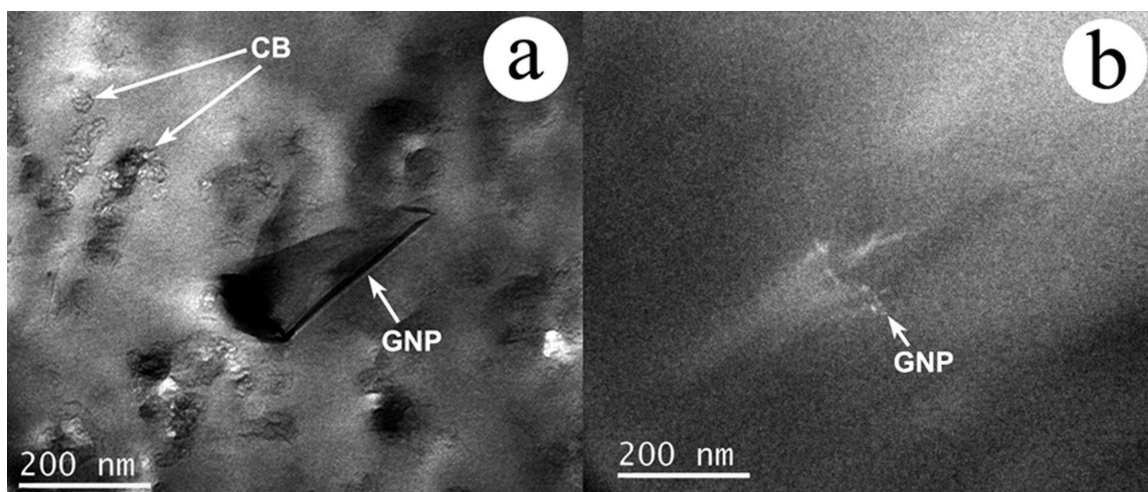


Figure 12.2: TEM Micrograph of Composite Containing 5 wt% CB and 5 wt% GNP in PC a) Bright Field Image b) Dark Field Image

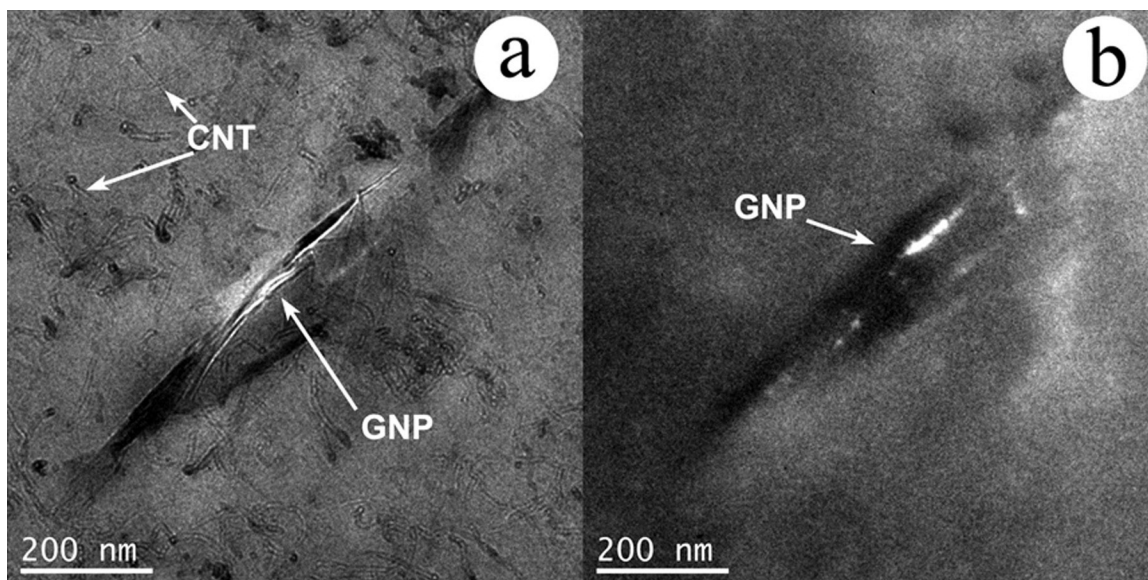


Figure 12.3: TEM Micrograph of Composite Containing 5 wt% CNT and 5 wt% GNP in PC a) Bright Field Image b) Dark Field Image

12.2: Electrical Resistivity (ER) Results

Table 12.1 shows the mean electrical resistivity, standard deviation of the electrical resistivity and number of samples that were tested for the 3^2 factorial design (2 filler, 3 level) composites containing both CB and CNT (CB/CNT). Table 12.2 shows these same data for factorial design composites containing both CB and GNP (CB/GNP). Table 12.3 shows the same data for the factorial design composites containing both CNT and GNP (CNT/GNP). Results for the individual samples are given in Appendices G and H. Comparing the data in these tables shows that a composite with 5 wt% CB and 5 wt% CNT has the lowest electrical resistivity with 15 ohm-cm. As a general rule, we note that composites containing GNP have a higher electrical resistivity than composites that contain CB and CNT.

Table 12.1: ER Results for Factorial Design Formulations Containing CB and CNT

Formulations	Constituents			Electrical Resistivity (ohm-cm)
No filler (PC)		Wt%	Vol%	
Original	PC	100	100	$1.26 \times 10^{17} \pm 3.35 \times 10^{16}$ n = 6
Replicate				$9.37 \times 10^{16} \pm 2.00 \times 10^{16}$ n = 6
2CB		Wt%	Vol%	
Original	CB	2	1.3	$4.05 \times 10^{16} \pm 2.66 \times 10^{16}$ n = 6
Replicate	PC	98	98.7	$2.36 \times 10^{16} \pm 1.25 \times 10^{16}$ n = 6
5CB		Wt%	Vol%	
Original	CB	5	3.4	3916 ± 233 n = 8
Replicate	PC	95	96.6	3972 ± 281 n = 8
1CNT		Wt%	Vol%	
Original	CNT	1	0.7	$2.04 \times 10^{16} \pm 7.48 \times 10^{15}$ n = 6
Replicate	PC	99	99.3	$2.02 \times 10^{16} \pm 6.62 \times 10^{15}$ n = 6
5CNT		Wt%	Vol%	
Original	CNT	5	3.1	163 ± 9 n = 6
Replicate	PC	95	96.9	177 ± 16 n = 6
2CB*1CNT		Wt%	Vol%	
Original	CB	2	1.3	$2.49 \times 10^5 \pm 5.28 \times 10^4$ n = 6
Replicate	CNT	1	0.7	$2.89 \times 10^5 \pm 7.28 \times 10^4$ n = 6
	PC	97	98.0	
2CB*5CNT		Wt%	Vol%	
Original	CB	2	1.4	74 ± 3 n = 6
Replicate	CNT	2	3.5	69 ± 2 n = 6
	PC	96	95.1	
5CB*1CNT		Wt%	Vol%	
Original	CB	5	3.4	433 ± 9 n = 4
Replicate	CNT	1	0.7	430 ± 7 n = 4
	PC	94	95.9	
5CB*5CNT		Wt%	Vol%	
Original	CB	5	3.5	15.9 ± 0.5 n = 6
Replicate	CNT	5	3.5	14.9 ± 0.5 n = 7
	PC	90	93.0	

Table 12.2: ER Results for Factorial Design Formulations Containing CB and GNP

Formulations	Constituents			Electrical Resistivity (ohm-cm)
No filler (PC)	Wt%	Vol%		
Original	PC	100	100	$1.26 \times 10^{17} \pm 3.35 \times 10^{16}$ n = 6
Replicate				$9.37 \times 10^{16} \pm 2.00 \times 10^{16}$ n = 6
2CB	Wt%	Vol%		
Original	CB	2	1.3	$4.05 \times 10^{16} \pm 2.66 \times 10^{16}$ n = 6
Replicate	PC	98	98.7	$2.36 \times 10^{16} \pm 1.25 \times 10^{16}$ n = 6
5CB	Wt%	Vol%		
Original	CB	5	3.4	3916 ± 233 n = 8
Replicate	PC	95	96.6	3972 ± 281 n = 8
2GNP	Wt%	Vol%		
Original	GNP	2	1.2	$5.46 \times 10^{16} \pm 4.89 \times 10^{15}$ n = 6
Replicate	PC	98	98.8	$5.20 \times 10^{16} \pm 2.25 \times 10^{16}$ n = 6
5GNP	Wt%	Vol%		
Original	GNP	5	3.1	$3.78 \times 10^{15} \pm 5.59 \times 10^{14}$ n = 6
Replicate	PC	95	96.9	$3.76 \times 10^{15} \pm 2.83 \times 10^{14}$ n = 6
2CB*2GNP	Wt%	Vol%		
Original	CB	2	1.4	$3.99 \times 10^{15} \pm 9.22 \times 10^{14}$ n = 6
Replicate	GNP	2	1.2	$3.77 \times 10^{15} \pm 1.31 \times 10^{15}$ n = 6
	PC	96	97.4	
2CB*5GNP	Wt%	Vol%		
Original	CB	2	1.4	$2.42 \times 10^7 \pm 3.14 \times 10^6$ n = 5
Replicate	GNP	5	3.1	$1.85 \times 10^7 \pm 4.31 \times 10^6$ n = 4
	PC	93	95.5	
5CB*2GNP	Wt%	Vol%		
Original	CB	5	3.4	1337 ± 16 n = 6
Replicate	GNP	2	1.2	1387 ± 32 n = 5
	PC	93	95.4	
5CB*5GNP	Wt%	Vol%		
Original	CB	5	3.5	729 ± 42 n = 5
Replicate	GNP	5	3.1	735 ± 40 n = 5
	PC	90	93.4	

Table 12.3: ER Results for Factorial Design Formulations Containing CNT and GNP

Formulations	Constituents		Electrical Resistivity (ohm-cm)
No filler (PC)	Wt%	Vol%	
Original	PC 100	100	$1.26 \times 10^{17} \pm 3.35 \times 10^{16}$ n=6
Replicate			$9.37 \times 10^{16} \pm 2.00 \times 10^{16}$ n = 6
1CNT	Wt%	Vol%	
Original	CNT 1	0.7	$2.04 \times 10^{16} \pm 7.48 \times 10^{15}$ n = 6
Replicate	PC 99	99.3	$2.02 \times 10^{16} \pm 6.62 \times 10^{15}$ n = 6
5CNT	Wt%	Vol%	
Original	CNT 5	3.1	163 ± 9 n = 6
Replicate	PC 95	96.9	177 ± 16 n = 6
2GNP	Wt%	Vol%	
Original	GNP 2	1.2	$5.46 \times 10^{16} \pm 4.89 \times 10^{15}$ n = 6
Replicate	PC 98	98.8	$5.20 \times 10^{16} \pm 2.25 \times 10^{16}$ n = 6
5GNP	Wt%	Vol%	
Original	GNP 5	3.1	$3.78 \times 10^{15} \pm 5.59 \times 10^{14}$ n = 6
Replicate	PC 95	96.9	$3.76 \times 10^{15} \pm 2.83 \times 10^{14}$ n = 6
1CNT*2GNP	Wt%	Vol%	
Original	CNT 1	0.7	$4.13 \times 10^{15} \pm 1.63 \times 10^{15}$ n = 7
Replicate	GNP 2	1.2	$5.03 \times 10^{15} \pm 1.82 \times 10^{15}$ n = 6
	PC 97	98.1	
1CNT*5GNP	Wt%	Vol%	
Original	CNT 1	0.7	$6.18 \times 10^6 \pm 1.34 \times 10^6$ n = 4
Replicate	GNP 5	3.1	$6.43 \times 10^6 \pm 9.02 \times 10^5$ n = 4
	PC 94	96.2	
5CNT*2GNP	Wt%	Vol%	
Original	CNT 5	3.5	210 ± 5 n = 7
Replicate	GNP 2	1.2	198 ± 6 n = 6
	PC 93	95.3	
5CNT*5GNP	Wt%	Vol%	
Original	CNT 5	3.6	126 ± 11 n = 6
Replicate	GNP 5	3.1	128 ± 9 n = 6
	PC 90	93.3	

Table 12.4 gives the results of regression analysis of Log(Log ER in ohm-cm) for the CB/CNT, CB/GNP and CNT/GNP systems. For this analysis the t-statistic and associated p-value for each case has been calculated and reported. The t-statistic is calculated by dividing the estimated value of a property (in this case ER) by the estimated standard error of the property. When the absolute value of the t-statistic is high, and the associated p-value is low, the conclusion is that the associated factor (a filler in this case) may have a significant effect on the property. Typically, a larger t-statistic value indicates greater significance of the factor. For this project, the significance level, α , is 0.05.

Table 12.4: 3² Regression Results for Log (Log Electrical Resistivity, ohm-cm)

Response	Correlation Term	Coefficient	t	p
Log (Log Electrical Resistivity, ohm-cm)	Correlation for CB/CNT Composites			
	Constant	1.34	26.9	0.000
	CB	-0.156	-9.7	0.000
	CNT	-0.195	-11.6	0.000
	CB*CNT	0.0194	3.6	0.003
	Correlation for CB/GNP Composites			
	Constant	1.27	47.3	0.000
	CB ²	-0.0284	-18.5	0.000
	GNP ²	-0.00646	-4.2	0.001
	Correlation for CNT/GNP Composites			
	Constant	1.29	39.8	0.000
	CNT	-0.177	-19.1	0.000
	GNP ²	-0.00624	-3.4	0.004

By studying the first part of Table 12.4 (ER of the CB/CNT system) more closely, we can see that both fillers individually (CB and CNT), as well as the interaction between the two fillers (CB*CNT), had a statistically significant interaction on the composite ER. As expected, the addition of either filler individually caused a statistically significant decrease (negative coefficient for both) in the composite ER. Of the two fillers, CNT caused a larger decrease in composite ER (as evidenced by the larger absolute coefficient). When CB and CNT are combined into a CB/CNT composite, the composite ER is higher (positive coefficient) than one would expect from the additive effect of each filler individually (117). The CB*CNT interaction is much smaller than the other two effects as seen by the lower absolute value of the coefficient. For the CB/CNT system, the Log(Log ER in ohm-cm) was found to vary with the filler percentage as shown in Equation 12.1 below:

$$\begin{aligned} \log(\log[ER, ohm - cm]) &= 1.34 - 0.156w_{CB} - 0.195w_{CNT} + 0.0194w_{CB}w_{CNT} \\ R^2 &= 0.954 \end{aligned} \quad (12.1)$$

where w_{CB} and w_{CNT} are the weight percentage of CB and CNT respectively. This correlation produced well behaved residuals and an R^2 value close to 1. Figure 12.4 shows a contour plot of Equation 12.1. It can be seen in the figure that CNT has a larger effect on decreasing the ER than CB. Additionally it is possible to see the small interaction effect of the fillers.

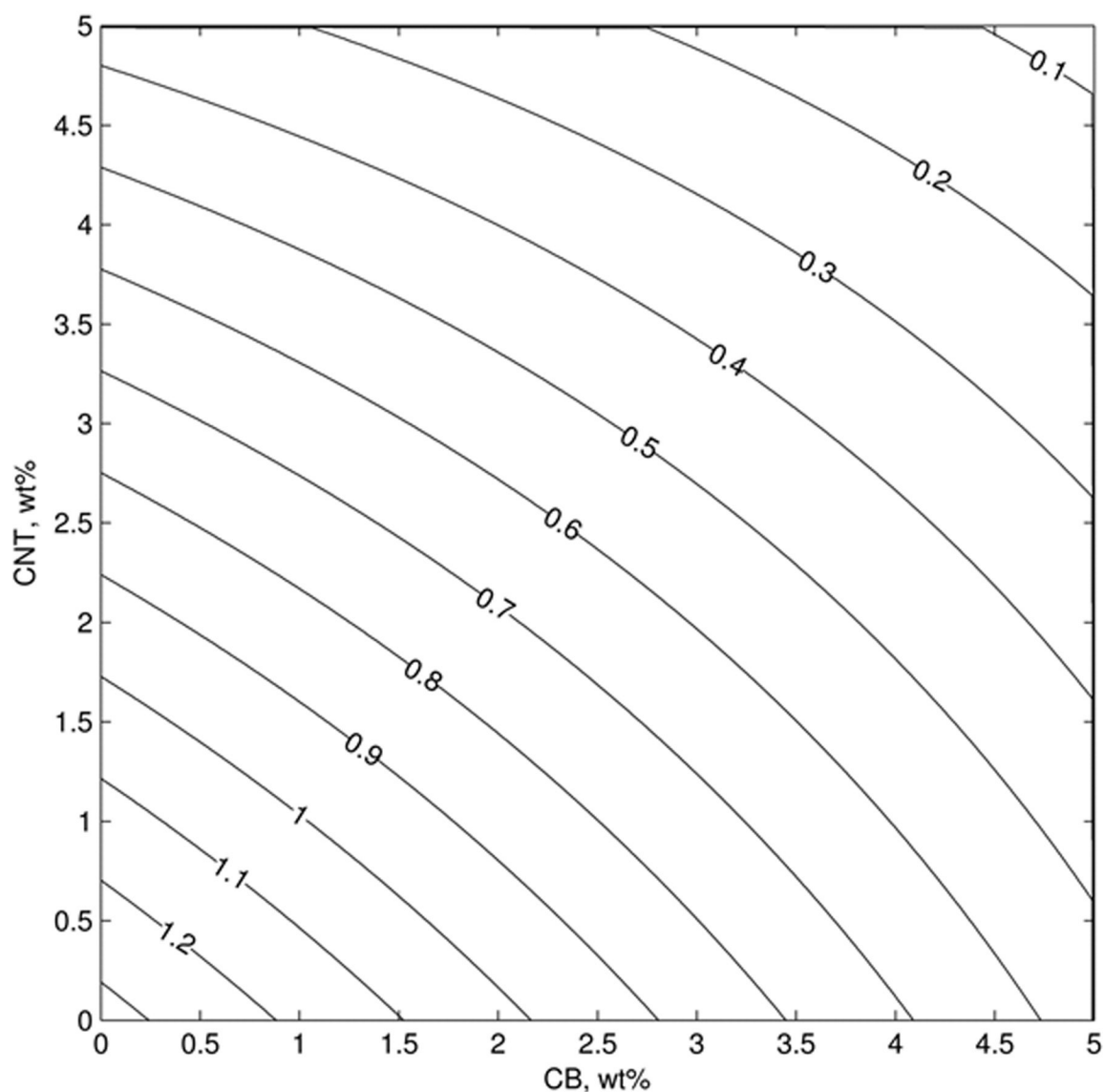


Figure 12.4. Contour Plot of Log (Log Electrical Resistivity, ohm-cm) for CB/CNT Composites

The second section of Table 12.4 (ER of the CB/GNP system) gives the results of regression analysis of Log(Log ER in ohm-cm) for the CB and GNP system. In this system, we see that both individual fillers, CB and GNP, had statistically significant effects on the ER of the composite as expected. The effect of each filler was best correlated using the square of the filler wt% versus the composite ER. CB had a larger effect on decreasing the composite ER than GNP as evidenced by the larger absolute

value of the coefficient. The CB/GNP system was found to be well correlated by the following Equation 12.2.

$$\begin{aligned} \text{Log}(\text{Log}[ER, ohm - cm]) &= 1.27 - 0.0284w_{CB}^2 - 0.00646w_{GNP}^2 \\ R^2 &= 0.960 \end{aligned} \quad (12.2)$$

In the previous equation, w_{CB} and w_{GNP} are the weight percentage of CB and GNP respectively.

The last section of Table 12.4 (ER of the CNT/GNP system) gives the results of regression analysis of Log(Log ER in ohm-cm) for the CNT and GNP system. Again both individual fillers had a statistically significant decrease on the composite ER. The CNT has a larger effect on decreasing the composite ER in a similar fashion as is discussed for the CNT/CB system. The CNT/GNP system was found to be correlated best by Equation 12.3 below:

$$\begin{aligned} \text{Log}(\text{Log}[ER, ohm - cm]) &= 1.29 - 0.177w_{CNT} - 0.00624w_{GNP}^2 \\ R^2 &= 0.962 \end{aligned} \quad (12.3)$$

where w_{CNT} and w_{GNP} are the weight percentage of CNT and GNP respectively. This equation is plotted in Figure 12.5. In this figure it can be seen again that CNT has a larger effect on decreasing the composite ER than the GNP. A related plot of Equation 12.2 has been omitted for brevity. When comparing Figures 12.4 and 12.5, we see that GNP has a smaller effect on reducing the composite ER than CNT or CB. Equations 12.1 through 12.3 could be used to estimate the ER of a theoretical formulation for material development purposes.

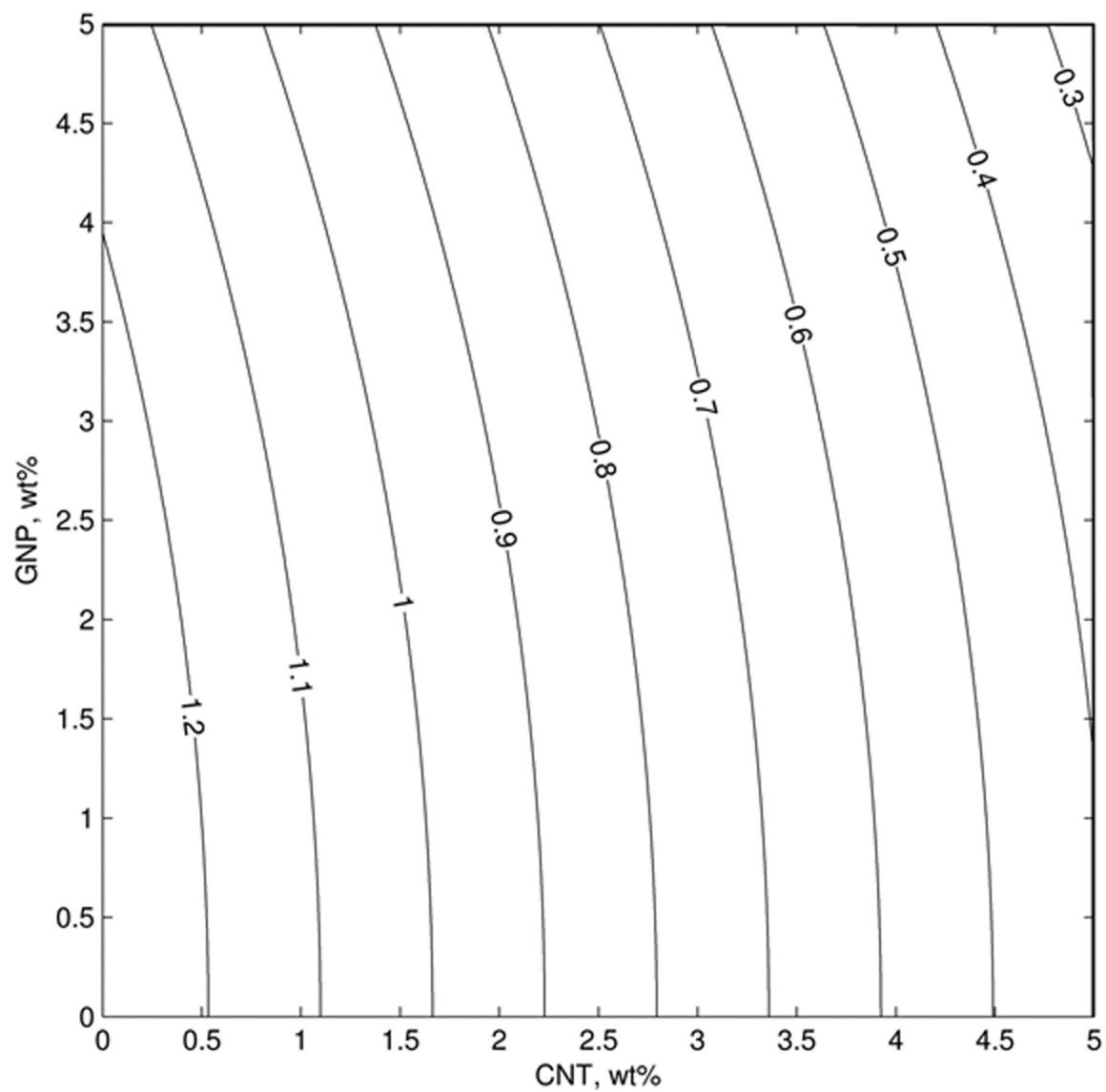


Figure 12.5. Contour Plot of Log (Log Electrical Resistivity, ohm-cm) for CNT/GNP Composites

12.3: Thermal Conductivity (TC) Results

Table 12.5 shows the mean thermal conductivity, standard deviation of the thermal conductivity and number of samples that were tested for the factorial design composites containing both CB and CNT (CB/CNT). Table 12.6 shows these same data for factorial design composites containing both CB and GNP (CB/GNP). Table 12.7 shows the same data for the factorial design composites containing both CNT and GNP (CNT/GNP). Results for the individual samples are given in Appendix I. We see from these tables that the best factorial design composite made roughly doubled the original PC thermal conductivity to 0.40 W/m·K from 0.21 W/m·K.

Table 12.8 gives the results of regression analysis of thermal conductivity for the CB/CNT, CB/GNP and CNT/GNP systems. Looking at the first third (CB/CNT system) we see that both fillers individually caused a statistically significant increase in composite TC. CNT caused a larger increase in TC as evidenced by the larger coefficient than CB, but it had a diminishing effect as additional CNT is added as evidenced by the negative coefficient for the CNT squared term. The TC of the CB/CNT system was found to be well correlated by Equation 12.4 below:

$$TC\left(\frac{W}{m \cdot K}\right) = 0.214 + 0.00822w_{CB} + 0.0136w_{CNT} - 0.000846w_{CNT}^2 \quad (12.4)$$
$$R^2 = 0.992$$

where w_{CB} and w_{CNT} are the weight percentage of CB and CNT respectively.

Table 12.5: TC Results for Factorial Design Formulations Containing CB and CNT

Formulations	Constituents			Thermal Conductivity (W/mK)
No filler (PC)		Wt%	Vol%	
Original	PC	100	100	0.214 ± 0.001 n = 5
Replicate				0.215 ± 0.002 n = 4
2CB		Wt%	Vol%	
Original	CB	2	1.3	0.228 ± 0.001 n = 5
Replicate	PC	98	98.7	0.232 ± 0.003 n = 4
5CB		Wt%	Vol%	
Original	CB	5	3.4	0.254 ± 0.001 n = 4
Replicate	PC	95	96.6	0.255 ± 0.004 n = 4
1CNT		Wt%	Vol%	
Original	CNT	1	0.7	0.224 ± 0.006 n = 4
Replicate	PC	99	99.3	0.226 ± 0.005 n = 4
5CNT		Wt%	Vol%	
Original	CNT	5	3.1	0.266 ± 0.003 n = 5
Replicate	PC	95	96.9	0.263 ± 0.003 n = 5
2CB*1CNT		Wt%	Vol%	
Original	CB	2	1.3	0.243 ± 0.002 n = 4
Replicate	CNT	1	0.7	0.243 ± 0.004 n = 4
	PC	97	98.0	
2CB*5CNT		Wt%	Vol%	
Original	CB	2	1.4	0.275 ± 0.005 n = 4
Replicate	CNT	2	3.5	0.271 ± 0.002 n = 4
	PC	96	95.1	
5CB*1CNT		Wt%	Vol%	
Original	CB	5	3.4	0.271 ± 0.003 n = 4
Replicate	CNT	1	0.7	0.268 ± 0.005 n = 4
	PC	94	95.9	
5CB*5CNT		Wt%	Vol%	
Original	CB	5	3.5	0.304 ± 0.002 n = 4
Replicate	CNT	5	3.5	0.300 ± 0.004 n = 4
	PC	90	93.0	

Table 12.6: TC Results for Factorial Design Formulations Containing CB and GNP

Formulations	Constituents			Thermal Conductivity (W/mK)
No filler (PC)		Wt%	Vol%	
Original	PC	100	100	0.214 ± 0.001 n = 5
Replicate				0.215 ± 0.002 n = 4
2CB		Wt%	Vol%	
Original	CB	2	1.3	0.228 ± 0.001 n = 5
Replicate	PC	98	98.7	0.232 ± 0.003 n = 4
5CB		Wt%	Vol%	
Original	CB	5	3.4	0.254 ± 0.001 n = 4
Replicate	PC	95	96.6	0.255 ± 0.004 n = 4
2GNP		Wt%	Vol%	
Original	GNP	2	1.2	0.251 ± 0.003 n = 5
Replicate	PC	98	98.8	0.252 ± 0.001 n = 4
5GNP		Wt%	Vol%	
Original	GNP	5	3.1	0.312 ± 0.004 n = 4
Replicate	PC	95	96.9	0.319 ± 0.001 n = 5
2CB*2GNP		Wt%	Vol%	
Original	CB	2	1.4	0.271 ± 0.009 n = 4
Replicate	GNP	2	1.2	0.269 ± 0.004 n = 4
	PC	96	97.4	
2CB*5GNP		Wt%	Vol%	
Original	CB	2	1.4	0.339 ± 0.006 n = 4
Replicate	GNP	5	3.1	0.337 ± 0.006 n = 4
	PC	93	95.5	
5CB*2GNP		Wt%	Vol%	
Original	CB	5	3.4	0.303 ± 0.003 n = 4
Replicate	GNP	2	1.2	0.301 ± 0.001 n = 4
	PC	93	95.4	
5CB*5GNP		Wt%	Vol%	
Original	CB	5	3.5	0.357 ± 0.001 n = 4
Replicate	GNP	5	3.1	0.366 ± 0.004 n = 4
	PC	90	93.4	

Table 12.7: TC Results for Factorial Design Formulations Containing CNT and GNP

Formulations	Constituents		Thermal Conductivity (W/mK)
No filler (PC)	Wt%	Vol%	
Original	PC 100	100	0.214 ± 0.001 n = 5
Replicate			0.215 ± 0.002 n = 4
1CNT	Wt%	Vol%	
Original	CNT 1	0.7	0.224 ± 0.006 n = 4
Replicate	PC 99	99.3	0.226 ± 0.005 n = 4
5CNT	Wt%	Vol%	
Original	CNT 5	3.1	0.266 ± 0.003 n = 5
Replicate	PC 95	96.9	0.263 ± 0.003 n = 5
2GNP	Wt%	Vol%	
Original	GNP 2	1.2	0.251 ± 0.003 n = 5
Replicate	PC 98	98.8	0.252 ± 0.001 n = 4
5GNP	Wt%	Vol%	
Original	GNP 5	3.1	0.312 ± 0.004 n = 4
Replicate	PC 95	96.9	0.319 ± 0.001 n = 5
1CNT*2GNP	Wt%	Vol%	
Original	CNT 1	0.7	0.268 ± 0.007 n = 4
Replicate	GNP 2	1.2	0.264 ± 0.006 n = 4
	PC 97	98.1	
1CNT*5GNP	Wt%	Vol%	
Original	CNT 1	0.7	0.328 ± 0.007 n = 4
Replicate	GNP 5	3.1	0.329 ± 0.002 n = 4
	PC 94	96.2	
5CNT*2GNP	Wt%	Vol%	
Original	CNT 5	3.5	0.318 ± 0.006 n = 4
Replicate	GNP 2	1.2	0.321 ± 0.005 n = 5
	PC 93	95.3	
5CNT*5GNP	Wt%	Vol%	
Original	CNT 5	3.6	0.396 ± 0.004 n = 4
Replicate	GNP 5	3.1	0.397 ± 0.007 n = 4
	PC 90	93.3	

Table 12.8: 3² Regression Results for Thermal Conductivity (W/m·K)

Response	Correlation Term	Coefficient	t	p
Thermal Conductivity, W/m·K	Correlation for CB/CNT Composites			
	Constant	0.214	161.9	0.000
	CB	0.00822	26.5	0.000
	CNT	0.0136	7.1	0.000
	CNT ²	-0.000846	-2.4	0.033
	Correlation for CB/GNP Composites			
	Constant	0.211	140.5	0.000
	CB	0.00913	23.6	0.000
	GNP	0.0211	54.4	0.000
	Correlation for CNT/GNP Composites			
	Constant	0.213	192.4	0.000
	CNT	0.0104	27.6	0.000
	GNP	0.0199	55.8	0.000
	CNT*GNP	0.00126	10.4	0.000

The second section of Table 12.8 (CB/GNP system) gives the results of regression analysis of TC for the CB and GNP system. Again each individual filler had a statistically significant increase in composite TC. For this system GNP caused a larger increase in composite TC than CB. The TC of the CB/GNP system was found to be correlated well by Equation 12.5 below:

$$TC\left(\frac{W}{m \cdot K}\right) = 0.211 + 0.00913w_{CB} + 0.0211w_{GNP} \quad (12.5)$$

$$R^2 = 0.996$$

where w_{CB} and w_{GNP} are the weight percentage of CB and GNP respectively.

The last section of Table 12.8 (CNT/GNP system) gives the results of regression analysis of TC for the CNT and GNP system. As expected we see that each individual filler

causes a statistically significant increase in composite TC. In this system GNP has a larger effect on increasing the composite TC than CNT. We also notice that there is a statistically significant interaction effect (CNT*GNP) that also increases the composite TC. This means that a composite with both CNT and GNP present would have a higher TC than would be expected solely from the additive effect of each individual filler (117). The TC of the CNT/GNP system was found to be correlated well by Equation 12.6 below:

$$TC\left(\frac{W}{m \cdot K}\right) = 0.213 + 0.0104w_{CNT} + 0.0199w_{GNP} + 0.00126w_{CNT}w_{GNP} \quad (12.6)$$

$$R^2 = 0.999$$

where w_{CNT} and w_{GNP} are the weight percentage of CNT and GNP respectively.

For all three systems the model R^2 values are very high (>0.99) indicating that the majority of the data variation is within expectation for the correlations. Equations 12.4 through 12.6 could be used to estimate the TC of a theoretical formulation for material development purposes.

12.4: Tensile Modulus Results

Table 12.9 shows the mean tensile modulus, standard deviation of the tensile modulus and number of samples that were tested for the factorial design composites containing both CB and CNT (CB/CNT). Table 12.10 shows these same data for factorial design composites containing both CB and GNP (CB/GNP). Table 12.11 shows the same data for the factorial design composites containing both CNT and GNP (CNT/GNP). Detailed results for this data are given in Appendix J.

Table 12.9: Tensile Modulus Results for Factorial Design Formulations Containing CB and CNT

Formulations	Constituents		Tensile Modulus (MPa)
No filler (PC)	Wt%	Vol%	
Original	PC 100	100	2198 ± 57 n = 6
Replicate			2222 ± 63 n = 4
2CB	Wt%	Vol%	
Original	CB 2	1.3	2365 ± 128 n = 6
Replicate	PC 98	98.7	2327 ± 52 n = 6
5CB	Wt%	Vol%	
Original	CB 5	3.4	2547 ± 35 n = 6
Replicate	PC 95	96.6	2575 ± 58 n = 6
1CNT	Wt%	Vol%	
Original	CNT 1	0.7	2484 ± 126 n = 6
Replicate	PC 99	99.3	2428 ± 25 n = 6
5CNT	Wt%	Vol%	
Original	CNT 5	3.1	2658 ± 89 n = 5
Replicate	PC 95	96.9	2746 ± 42 n = 4
2CB*1CNT	Wt%	Vol%	
Original	CB 2	1.3	2683 ± 103 n = 5
Replicate	CNT 1	0.7	2665 ± 119 n = 5
	PC 97	98.0	
2CB*5CNT	Wt%	Vol%	
Original	CB 2	1.4	2945 ± 49 n = 5
Replicate	CNT 5	3.5	2956 ± 75 n = 5
	PC 93	95.1	
5CB*1CNT	Wt%	Vol%	
Original	CB 5	3.4	2737 ± 11 n = 5
Replicate	CNT 1	0.7	2728 ± 46 n = 5
	PC 94	95.9	
5CB*5CNT	Wt%	Vol%	
Original	CB 5	3.5	3186 ± 73 n = 4
Replicate	CNT 5	3.5	3155 ± 49 n = 5
	PC 90	93.0	

Table 12.10: Tensile Modulus Results for Factorial Design Formulations Containing CB and GNP

Formulations	Constituents			Tensile Modulus (MPa)
No filler (PC)	Wt%	Vol%		
Original	PC	100	100	2198 ± 57 n = 6
Replicate				2222 ± 63 n = 4
2CB	Wt%	Vol%		
Original	CB	2	1.3	2365 ± 128 n = 6
Replicate	PC	98	98.7	2327 ± 52 n = 6
5CB	Wt%	Vol%		
Original	CB	5	3.4	2547 ± 35 n = 6
Replicate	PC	95	96.6	2575 ± 58 n = 6
2GNP	Wt%	Vol%		
Original	GNP	2	1.2	2514 ± 55 n = 5
Replicate	PC	98	98.8	2448 ± 45 n = 5
5GNP	Wt%	Vol%		
Original	GNP	5	3.1	3095 ± 64 n = 5
Replicate	PC	95	96.9	3123 ± 68 n = 7
2CB*2GNP	Wt%	Vol%		
Original	CB	2	1.4	2796 ± 98 n = 5
Replicate	GNP	2	1.2	2767 ± 73 n = 5
	PC	96	97.4	
2CB*5GNP	Wt%	Vol%		
Original	CB	2	1.4	3282 ± 55 n = 5
Replicate	GNP	5	3.1	3256 ± 36 n = 5
	PC	93	95.5	
5CB*2GNP	Wt%	Vol%		
Original	CB	5	3.4	3049 ± 59 n = 5
Replicate	GNP	2	1.2	3035 ± 76 n = 5
	PC	93	95.4	
5CB*5GNP	Wt%	Vol%		
Original	CB	5	3.5	3744 ± 77 n = 5
Replicate	GNP	5	3.1	3776 ± 137 n = 5
	PC	90	93.4	

Table 12.11: Tensile Modulus Results for Factorial Design Formulations Containing CNT and GNP

Formulations	Constituents			Tensile Modulus (MPa)
No filler (PC)	Wt%	Vol%		
Original	PC	100	100	2198 ± 57 n = 6
Replicate				2222 ± 63 n = 4
1CNT	Wt%	Vol%		
Original	CNT	1	0.7	2484 ± 126 n = 6
Replicate	PC	99	99.3	2428 ± 25 n = 6
5CNT	Wt%	Vol%		
Original	CNT	5	3.1	2658 ± 89 n = 5
Replicate	PC	95	96.9	2746 ± 42 n = 4
2GNP	Wt%	Vol%		
Original	GNP	2	1.2	2514 ± 55 n = 5
Replicate	PC	98	98.8	2448 ± 45 n = 5
5GNP	Wt%	Vol%		
Original	GNP	5	3.1	3095 ± 64 n = 5
Replicate	PC	95	96.9	3123 ± 68 n = 7
1CNT*2GNP	Wt%	Vol%		
Original	CNT	1	0.7	2769 ± 77 n = 5
Replicate	GNP	2	1.2	2783 ± 87 n = 5
	PC	97	98.1	
1CNT*5GNP	Wt%	Vol%		
Original	CNT	1	0.7	3447 ± 66 n = 5
Replicate	GNP	5	3.1 PC	3458 ± 94 n = 5
	94	96.2		
5CNT*2GNP	Wt%	Vol%		
Original	CNT	5	3.5	3069 ± 100 n = 5
Replicate	GNP	2	1.2	3018 ± 50 n = 5
	PC	93	95.3	
5CNT*5GNP	Wt%	Vol%		
Original	CNT	5	3.6	3490 ± 43 n = 5
Replicate	GNP	5	3.1	3482 ± 74 n = 5
	PC	90	93.3	

Table 12.12. 3² Regression Results for 3² Regression Results for Tensile Modulus (MPa)

Response	Correlation Term	Coefficient	t	p
Tensile Modulus, MPa	Correlation for CB/CNT Composites			
	Constant	2211	86.1	0.000
	CB	107	5.3	0.000
	CNT	268	8.5	0.000
	CB ²	-9.12	-2.5	0.030
	CNT ²	-33.7	-5.8	0.000
	CB*CNT	5.94	2.5	0.026
	Correlation for CB/GNP Composites			
	Constant	2192	87.6	0.000
	CB	76.2	9.5	0.000
	GNP	173	21.5	0.000
	CB*GNP	12.1	4.7	0.000
	Correlation for CNT/GNP Composites			
	Constant	2148	72.3	0.000
	CNT	361	9.3	0.000
	GNP	194	22.8	0.000
	CNT ²	-49.9	-6.9	0.000
	CNT*GNP	-6.96	-2.4	0.031

Table 12.12 gives the results of regression analysis of tensile modulus for the CB/CNT, CB/GNP and CNT/GNP systems. Looking at the first third (CB/CNT system) we see that both fillers individually caused a statistically significant increase in composite tensile modulus. CNT caused a larger increase in the composite tensile modulus than CB. The tensile modulus increasing effect of both fillers was found to diminish as more of the filler is added (as seen from the negative values for the coefficient of the squared term for each filler). We also found a statistically significant interaction between the two fillers that caused the composite tensile modulus to be higher than would be expected solely

from the additive effects of the individual fillers (117). The tensile modulus (E_t) of the CB/CNT system was found to be well correlated by Equation 12.7 below:

$$E_t (MPa) = 2211 + 107w_{CB} + 268w_{CNT} - 9.12w_{CB}^2 - 33.7w_{CNT}^2 + 5.94w_{CB}w_{CNT} \quad (12.7)$$

$$R^2 = 0.983$$

where w_{CB} and w_{CNT} are the weight percentage of CB and CNT respectively. Equation 12.7 is plotted in Figure 12.6. By studying this plot we see that CNT has a larger effect on increasing the tensile modulus than CB. At higher CNT loadings, we notice that above around 2.5 vol% CNT, additional CNT has a much smaller effect on the tensile modulus than it did at lower levels.

The second section of Table 12.12 (CB/GNP system) gives the results of regression analysis of tensile modulus for the CB and GNP system. Again each individual filler had a statistically significant increase in composite tensile modulus. For this system GNP caused a larger increase in composite tensile modulus than CB. There is also a statistically significant positive interaction effect between the two fillers. This positive interaction effect means that the tensile modulus of a composite containing both CB and GNP would have a tensile modulus higher than would be expected just from the additive effects of the two individual fillers (117). The tensile modulus (E_t) of the CB/GNP system was found to be correlated well by Equation 12.8 below:

$$E_t (MPa) = 2192 + 76.2w_{CB} + 173w_{GNP} + 12.1w_{CB}w_{GNP} \quad (12.4-2)$$

$$R^2 = 0.992$$

where w_{CB} and w_{GNP} are the weight percentage of CB and GNP respectively.

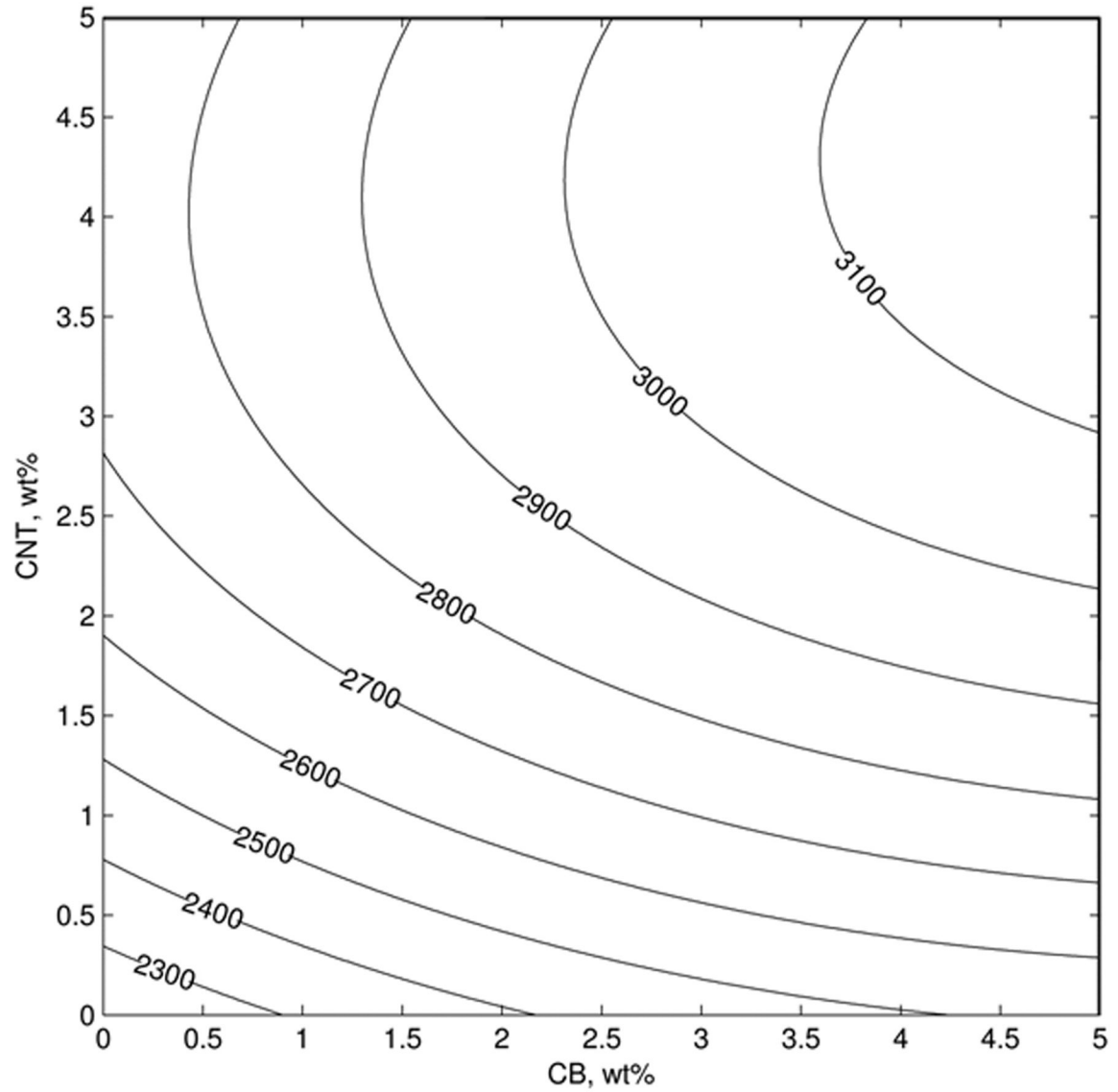


Figure 12.6: Contour Plot of Tensile Modulus (MPa) for CB/CNT Composites

Equation 12.8 is plotted in Figure 12.7. While studying this plot we can see that the GNP has a larger effect on increasing the composite tensile modulus than the CB does.

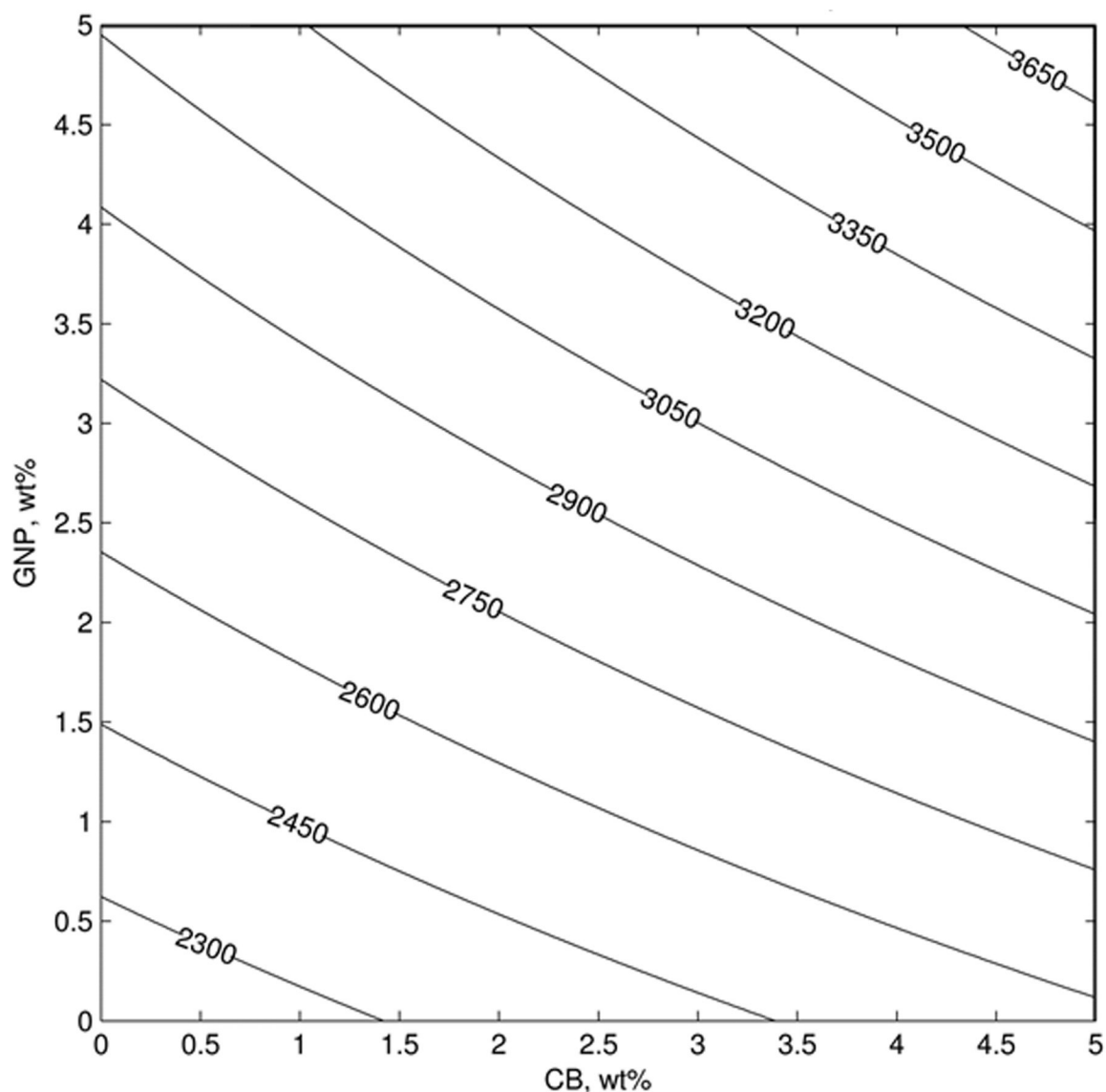


Figure 12.7: Contour Plot of Tensile Modulus (MPa) for CB/GNP Composites

The last section of Table 12.12 (CNT/GNP system) gives the results of regression analysis of tensile modulus for the CNT and GNP system. As expected we see that each individual filler causes a statistically significant increase in composite tensile modulus. In this system CNT has a larger effect on increasing the composite tensile modulus than GNP. We do notice that as the CNT loading is increased, the tensile modulus increasing effect diminishes (notice the negative coefficient on the CNT^2 term). We also notice that

there is a statistically significant negative interaction effect (CNT*GNP) that decreases the composite tensile modulus (note the negative coefficient for the CNT*GNP term). This means that a composite with both CNT and GNP present would have a lower tensile modulus than would be expected solely from the additive effect of each individual filler (117). The tensile modulus (E_t) of the CNT/GNP system was found to be correlated well by Equation 12.9 below:

$$E_t (MPa) = 2148 + 361w_{CNT} + 194w_{GNP} - 49.9w_{CNT}^2 - 6.96w_{CNT}w_{GNP}$$

$$R^2 = 0.988 \quad (12.9)$$

where w_{CNT} and w_{GNP} are the weight percentage of CNT and GNP respectively. For all 3 systems the R^2 values are greater than 0.98 indicating that the majority of the data variation is within expectation for the correlations. Equations 12.7 through 12.9 could be used to estimate the tensile modulus of a theoretical formulation for material development purposes.

12.5: Flexural Modulus Results

Table 12.13 shows the mean flexural modulus, standard deviation of the flexural modulus and number of samples that were tested for the factorial design composites containing both CB and CNT (CB/CNT). Table 12.14 shows these same data for factorial design composites containing both CB and GNP (CB/GNP). Table 12.15 shows the same data for the factorial design composites containing both CNT and GNP (CNT/GNP). Detailed results for this data are given in Appendix K.

Table 12.13: Flexural Modulus Results for Factorial Design Formulations Containing CB and CNT

Formulations	Constituents			Flexural Modulus (MPa)
No filler (PC)	Wt%	Vol%		
Original	PC	100	100	2479 ± 17 n = 5
Replicate				2474 ± 8 n = 5
2CB	Wt%	Vol%		
Original	CB	2	1.3	2599 ± 11 n = 10
Replicate	PC	98	98.7	2600 ± 14 n = 8
5CB	Wt%	Vol%		
Original	CB	5	3.4	2768 ± 13 n = 10
Replicate	PC	95	96.6	2772 ± 9 n = 8
1CNT	Wt%	Vol%		
Original	CNT	1	0.7	2606 ± 8 n = 10
Replicate	PC	99	99.3	2605 ± 14 n = 9
5CNT	Wt%	Vol%		
Original	CNT	5	3.1	3089 ± 24 n = 6
Replicate	PC	95	96.9	3067 ± 33 n = 5
2CB*1CNT	Wt%	Vol%		
Original	CB	2	1.3	2738 ± 37 n = 8
Replicate	CNT	1	0.7	2743 ± 16 n = 8
	PC	97	98.0	
2CB*5CNT	Wt%	Vol%		
Original	CB	2	1.4	3421 ± 106 n = 7
Replicate	CNT	5	3.5	3444 ± 64 n = 5
	PC	93	95.1	
5CB*1CNT	Wt%	Vol%		
Original	CB	5	3.4	2912 ± 12 n = 5
Replicate	CNT	1	0.7	2916 ± 29 n = 5
	PC	94	95.9	
5CB*5CNT	Wt%	Vol%		
Original	CB	5	3.5	3670 ± 63 n = 6
Replicate	CNT	5	3.5	3772 ± 71 n = 5
	PC	90	93.0	

Table 12.14: Flexural Modulus Results for Factorial Design Formulations Containing CB and GNP

Formulations	Constituents			Flexural Modulus (MPa)
No filler (PC)		Wt%	Vol%	
Original	PC	100	100	2479 ± 17 n = 5
Replicate				2474 ± 8 n = 5
2CB		Wt%	Vol%	
Original	CB	2	1.3	2599 ± 11 n = 10
Replicate	PC	98	98.7	2600 ± 14 n = 8
5CB		Wt%	Vol%	
Original	CB	5	3.4	2768 ± 13 n = 10
Replicate	PC	95	96.6	2772 ± 9 n = 8
2GNP		Wt%	Vol%	
Original	GNP	2	1.2	3005 ± 55 n = 4
Replicate	PC	98	98.8	2998 ± 31 n = 5
5GNP		Wt%	Vol%	
Original	GNP	5	3.1	3382 ± 17 n = 6
Replicate	PC	95	96.9	3401 ± 8 n = 5
2CB*2GNP		Wt%	Vol%	
Original	CB	2	1.4	3064 ± 12 n = 7
Replicate	GNP	2	1.2	3070 ± 15 n = 7
	PC	96	97.4	
2CB*5GNP		Wt%	Vol%	
Original	CB	2	1.4	3458 ± 22 n = 8
Replicate	GNP	5	3.1	3455 ± 20 n = 7
	PC	93	95.5	
5CB*2GNP		Wt%	Vol%	
Original	CB	5	3.4	3213 ± 23 n = 7
Replicate	GNP	2	1.2	3213 ± 30 n = 7
	PC	93	95.4	
5CB*5GNP		Wt%	Vol%	
Original	CB	5	3.5	3724 ± 42 n = 7
Replicate	GNP	5	3.1	3705 ± 24 n = 6
	PC	90	93.4	

Table 12.15: Flexural Modulus Results for Factorial Design Formulations Containing CNT and GNP

Formulations	Constituents		Flexural Modulus (MPa)
No filler (PC)	Wt%	Vol%	
Original	PC 100	100	2479 ± 17 n = 5
Replicate			2474 ± 8 n = 5
1CNT	Wt%	Vol%	
Original	CNT 1	0.7	2606 ± 8 n = 10
Replicate	PC 99	99.3	2605 ± 14 n = 9
5CNT	Wt%	Vol%	
Original	CNT 5	3.1	3089 ± 24 n = 6
Replicate	PC 95	96.9	3067 ± 33 n = 5
2GNP	Wt%	Vol%	
Original	GNP 2	1.2	3005 ± 55 n = 4
Replicate	PC 98	98.8	2998 ± 31 n = 5
5GNP	Wt%	Vol%	
Original	GNP 5	3.1	3382 ± 17 n = 6
Replicate	PC 95	96.9	3401 ± 8 n = 5
1CNT*2GNP	Wt%	Vol%	
Original	CNT 1	0.7	2938 ± 21 n = 5
Replicate	GNP 2	1.2	2925 ± 20 n = 5
	PC 97	98.1	
1CNT*5GNP	Wt%	Vol%	
Original	CNT 1	0.7	3398 ± 83 n = 5
Replicate	GNP 5	3.1	3406 ± 47 n = 5
	PC 94	96.2	
5CNT*2GNP	Wt%	Vol%	
Original	CNT 5	3.5	3592 ± 50 n = 7
Replicate	GNP 2	1.2	3632 ± 23 n = 6
	PC 93	95.3	
5CNT*5GNP	Wt%	Vol%	
Original	CNT 5	3.6	4312 ± 87 n = 6
Replicate	GNP 5	3.1	4364 ± 47 n = 5
	PC 90	93.3	

Table 12.16: 3² Regression Results for 3² Regression Results for Flexural Modulus (MPa)

Response	Correlation Term	Coefficient	t	p
Flexural Modulus, MPa	Correlation for CB/CNT Composites			
	Constant	2465	134	0.000
	CB	86.3	5.4	0.000
	CNT	127	22	0.000
	CB ²	-6.36	-2.2	0.049
	CB*CNT	14.3	7.7	0.000
	Correlation for CB/GNP Composites			
	Constant	2485	163	0.000
	CB	55.9	15.6	0.000
	GNP	278	19.9	0.000
	GNP ²	-19.4	-7.4	0.000
	Correlation for CNT/GNP Composites			
	Constant	2531	91.5	0.000
	GNP	220	8.4	0.000
	CNT ²	21.9	12.6	0.000
	GNP ²	-10.9	-2.3	0.040
	CNT*GNP	16.3	5.5	0.000

Table 12.16 gives the results of regression analysis of flexural modulus for the CB/CNT, CB/GNP and CNT/GNP systems. Looking at the first third (CB/CNT system) we see that both fillers individually caused a statistically significant increase in composite flexural modulus. CNT caused a larger increase in the composite flexural modulus than CB. The flexural modulus increasing effect of CB was found to diminish as more CB is added (as seen from the negative values for the coefficient of the squared term for CB). We also found a statistically significant positive interaction between the two fillers that caused the composite flexural modulus to be higher than would be expected solely from

the additive effects of the individual fillers (117). The flexural modulus (E_f) of the CB/CNT system was found to be well correlated by Equation 12.10 below:

$$E_f (MPa) = 2465 + 86.3w_{CB} + 127w_{CNT} - 6.36w_{CB}^2 + 14.3w_{CB}w_{CNT} \quad (12.10)$$

$$R^2 = 0.994$$

where w_{CB} and w_{CNT} are the weight percentage of CB and CNT respectively. Equation 12.10 is plotted in Figure 12.8. By studying this plot we see that CNT has a larger effect on increasing the flexural modulus than CB.

The second section of Table 12.16 (CB/GNP system) gives the results of regression analysis of flexural modulus for the CB and GNP system. Again each individual filler had a statistically significant increase in composite flexural modulus. For this system GNP caused a larger increase in composite flexural modulus than CB. We see a diminishing flexural modulus increasing effect as more GNP is added (as see from the negative coefficient of the GNP^2 term). The flexural modulus (E_f) of the CB/GNP system was found to be correlated well by Equation 12.11 below:

$$E_f (MPa) = 2485 + 55.9w_{CB} + 278w_{GNP} - 19.4w_{GNP}^2 \quad (12.11)$$

$$R^2 = 0.995$$

where w_{CB} and w_{GNP} are the weight percentage of CB and GNP respectively.

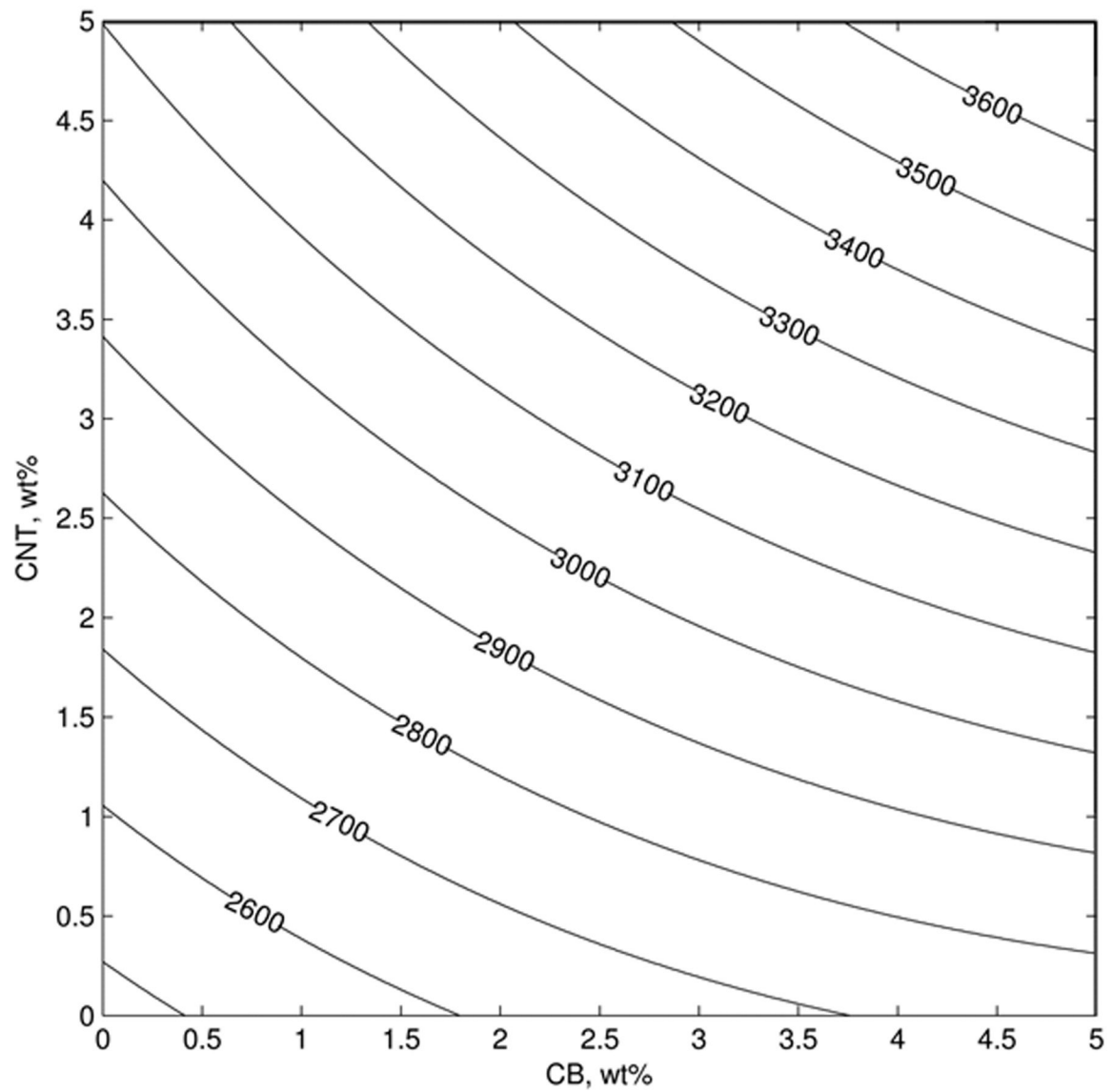


Figure 12.8: Contour Plot of Flexural Modulus (MPa) for CB/CNT Composites

Equation 12.11 is plotted in Figure 12.9. By studying this plot we see that GNP has a larger effect on increasing the flexural modulus than CB.

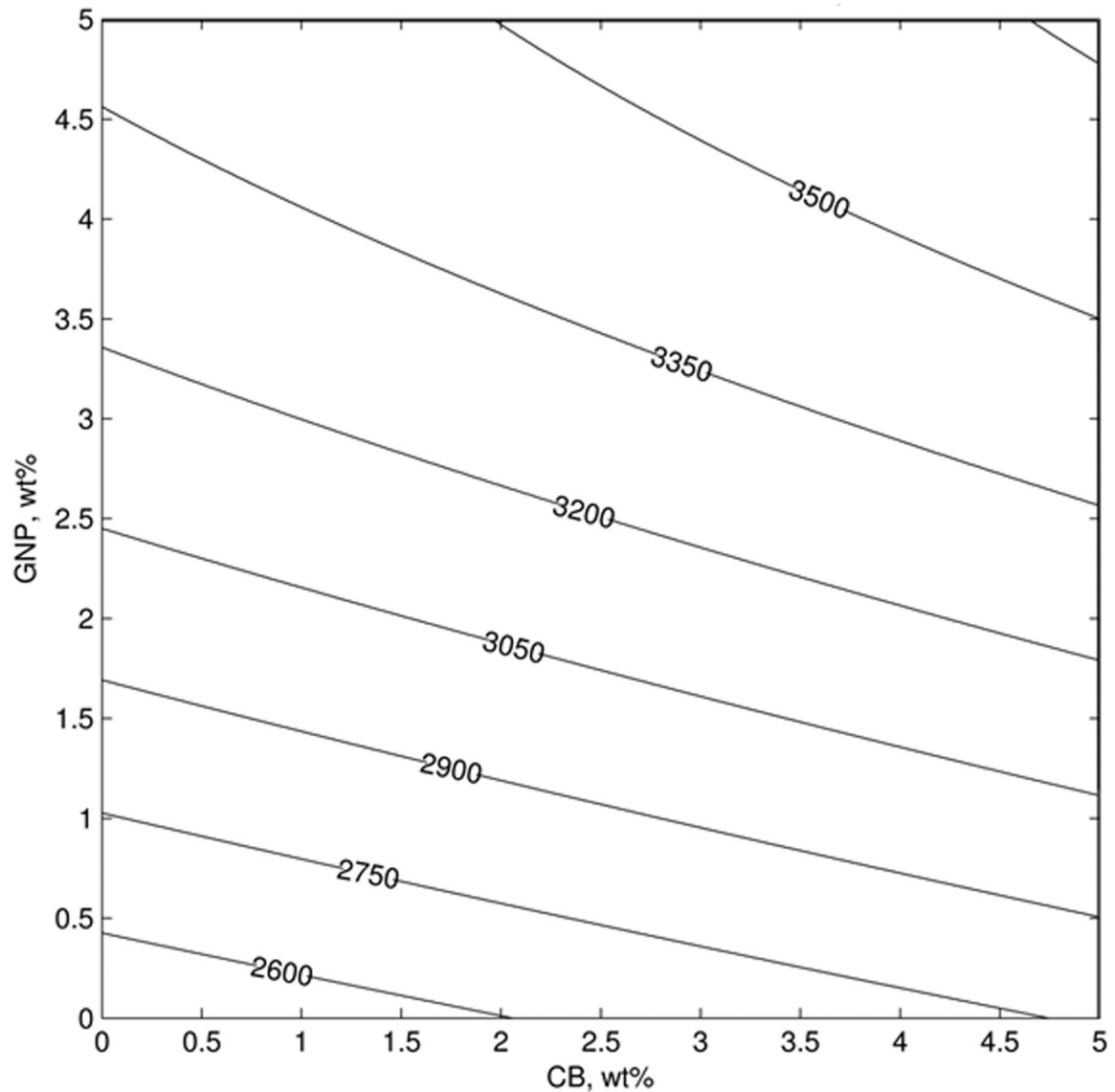


Figure 12.9: Contour Plot of Flexural Modulus (MPa) for CB/GNP Composites

The last section of Table 12.16 (CNT/GNP system) gives the results of regression analysis of flexural modulus for the CNT and GNP system. As expected we see that each individual filler causes a statistically significant increase in composite flexural modulus. In this system CNT has an increasing effect on increasing the flexural modulus as more CNT is added (as seen from the positive coefficient of the CNT^2 term). We do notice that as the GNP loading is increased, the flexural modulus increasing effect diminishes

(notice the negative coefficient on the GNP^2 term). We also notice that there is a statistically significant positive interaction effect (CNT*GNP) that decreases the composite flexural modulus (note the positive coefficient for the CNT*GNP term). This means that a composite with both CNT and GNP present would have a higher flexural modulus than would be expected solely from the additive effect of each individual filler (117). The flexural modulus (E_f) of the CNT/GNP system was found to be correlated well by Equation 12.12 below:

$$E_f (MPa) = 2531 + 220w_{GNP} + 21.9w_{CNT}^2 - 10.9w_{GNP}^2 + 16.3w_{CNT}w_{GNP} \quad (12.12)$$

$$R^2 = 0.992$$

where w_{CNT} and w_{GNP} are the weight percentage of CNT and GNP respectively. For all 3 systems the R^2 values are greater than 0.99 indicating that the majority of the data variation is within expectation for the correlations. Equations 12.10 through 12.12 could be used to estimate the flexural modulus of a theoretical formulation for material development purposes.

12.6: Conclusions

The purpose of this section of the project was to measure and model the effects of CB, CNT and GNP on PC using three 3^2 (2 factor, 3 level) factorial designs, one for each two-filler combination (CB/CNT, CB/GNP and CNT/GNP). In particular the effects on the electrical resistivity (ER), thermal conductivity (TC), tensile modulus and flexural modulus were measured and modeled. As seen in Tables 12.1 through 12.3 the filler loadings for the factorial design were 0, 2 and 5 wt% for CB, 0, 1 and 5 wt% for CNT and 0, 2 and 5 wt% for GNP. Electrically, all 3 fillers individually caused a statistically

significant decrease in the composite ER. Of the 3 fillers, CNT caused the largest decrease in composite ER. Thermally, all 3 individual fillers caused a statistically significant increase in TC. Of the fillers, GNP had the largest effect on increasing the TC. Additionally GNP and CNT together had a significant positive interaction effect that increased the TC of the 2-filler composite more than was expected due to the additive effects of GNP and CNT. Mechanically, all 3 fillers caused statistically significant increases in both tensile and flexural modulus. Among the fillers tested, GNP caused the greatest increase in both tensile and flexural modulus. The correlatoins that were created for each property and 2-filler system could be used to create conductive composites of PC with the desired electrical, thermal and mechanical properties.

Chapter 13: Effects of Multiple Fillers on the Rheology of Polycarbonate Based Resins

13.1: Capillary Rheometer Results

Figures 13.1 through 13.3 show the average values of the single filler steady-shear rheology data for the factorial design loadings. The standard deviations of these values are all less than 2% thus the error bars have been omitted for the sake of clarity. The composite with solely 5 wt% CB generated too high of a pressure at 2000 s^{-1} to be measured by the rheometer and thus this data point was omitted. Additionally the 5 wt% CNT formulation was unable to be measured at 50 s^{-1} shear rate due to flow instabilities at this shear rate and the data point was thus omitted. This data, along with the two-filler data is listed in Tables 13.1 through 13.3. More detailed results are listed in Appendix M.

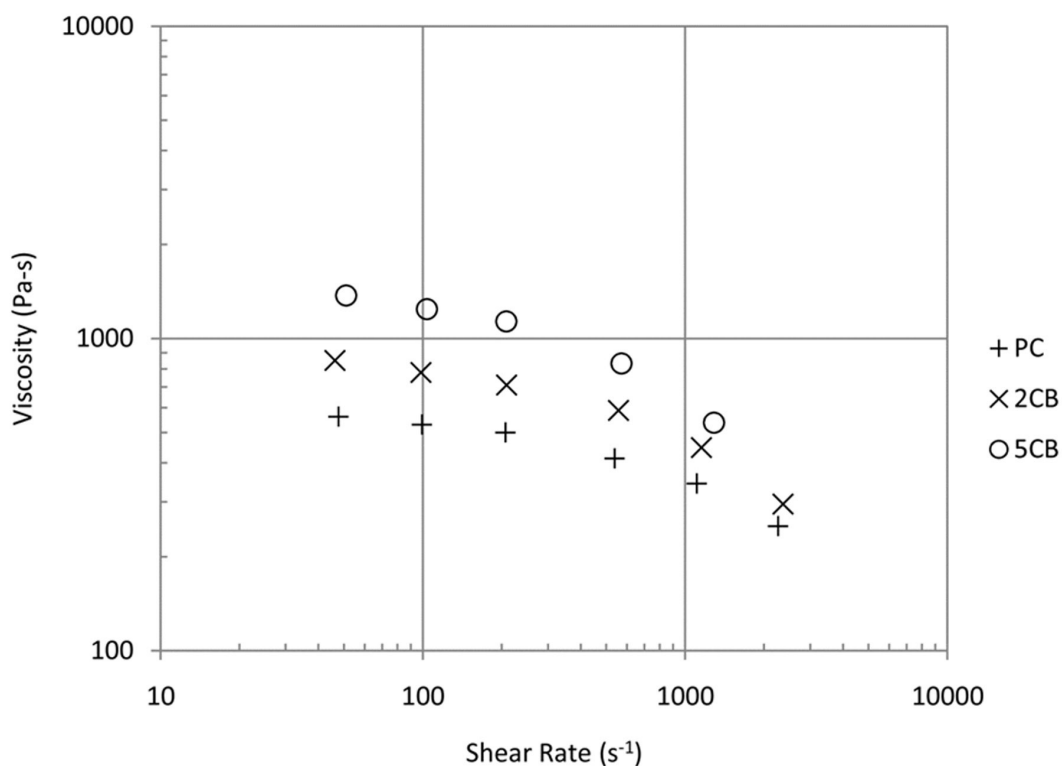


Figure 13.1: Viscosity versus Shear Rate for CB/PC Composites at 270°C

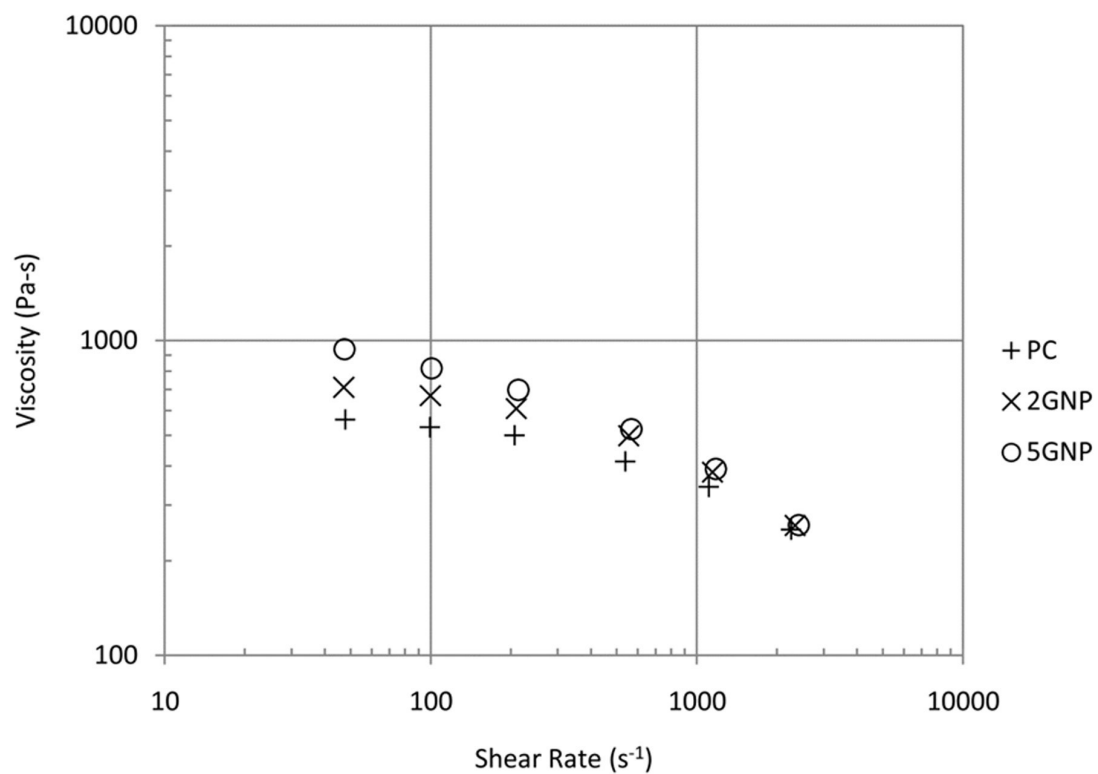


Figure 13.2: Viscosity versus Shear Rate for GNP/PC Composites at 270°C

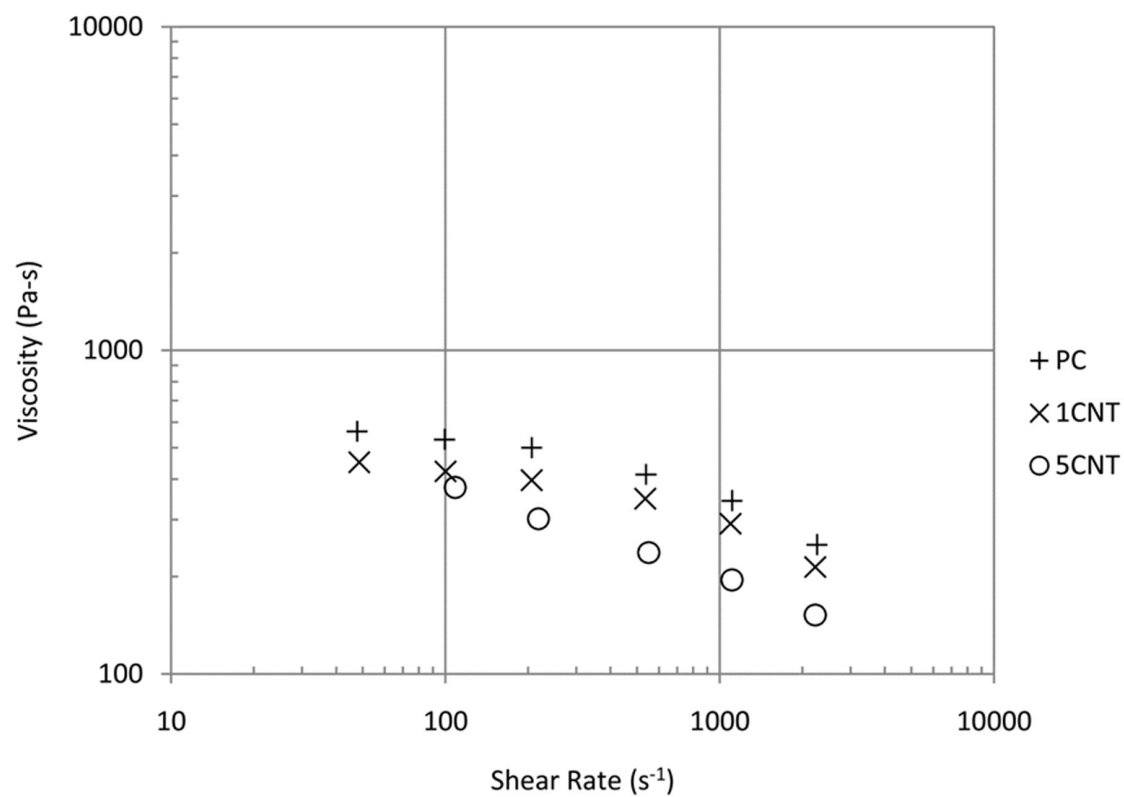


Figure 13.3: Viscosity versus Shear Rate for CNT/PC Composites at 270°C

Table 13.1: Newtonian Zero-Shear Plateau Results for Factorial Design Formulations Containing CB and GNP

Formulations	Constituents			Zero-Shear Plateau, η_0 (Pa-s)
No filler (PC)	Wt%	Vol%		
	PC	100	100	550
2CB	Wt%	Vol%		
	CB	2	1.3	850
	PC	98	98.7	
5CB	Wt%	Vol%		
	CB	5	3.4	≥ 1400
	PC	95	96.6	
2GNP	Wt%	Vol%		
	GNP	2	1.2	710
	PC	98	98.8	
5GNP	Wt%	Vol%		
	GNP	5	3.1	≥ 940
	PC	95	96.9	
2CB*2GNP	Wt%	Vol%		
	CB	2	1.4	≥ 970
	GNP	2	1.2	
	PC	96	97.4	
2CB*5GNP	Wt%	Vol%		
	CB	2	1.4	≥ 1200
	GNP	5	3.1	
	PC	93	95.5	
5CB*2GNP	Wt%	Vol%		
	CB	5	3.4	≥ 1500
	GNP	2	1.2	
	PC	97	95.4	
5CB*5GNP	Wt%	Vol%		
	CB	5	3.5	≥ 1900
	GNP	5	3.1	
	PC	90	93.4	

Table 13.2: Electrical Resistivity and Zero-Shear Viscosity Results for Factorial Design Formulations Containing CB and CNT

Formulations	Constituents			Zero-Shear Viscosity, η_0 (Pa-s)
No filler (PC)	PC	Wt% 100	Vol% 100	550
2CB	CB	Wt% 2	Vol% 1.3	850
	PC	98	98.7	
5CB	CB	Wt% 5	Vol% 3.4	≥ 1400
	PC	95	96.6	
1CNT	CNT	Wt% 1	Vol% 0.7	450
	PC	99	99.3	
5CNT	CNT	Wt% 5	Vol% 3.1	$\geq 380^\dagger$
	PC	95	96.9	
2CB*1CNT	CB	Wt% 2	Vol% 1.3	≥ 560
	CNT	1	0.7	
	PC	97	98.0	
2CB*5CNT	CB	Wt% 2	Vol% 1.4	$\geq 600^\dagger$
	CNT	2	3.5	
	PC	96	95.1	
5CB*1CNT	CB	Wt% 5	Vol% 3.4	≥ 880
	CNT	1	0.7	
	PC	94	95.9	
5CB*5CNT	CB	Wt% 5	Vol% 3.5	$\geq 1100^\dagger$
	CNT	5	3.5	
	PC	90	93.0	

[†] indicates formulations that have significant decreases in viscosity (relative to other formulations in table) at high shear rates.

Table 13.3: Electrical Resistivity and Zero-Shear Viscosity Results for Factorial Design Formulations Containing CNT and GNP

Formulations	Constituents		Zero-Shear Viscosity, η_0 (Pa-s)
No filler (PC)	Wt% PC 100	Vol% 100	550
1CNT	Wt% CNT 1 PC 99	Vol% 0.7 99.3	450
5CNT	Wt% CNT 5 PC 95	Vol% 3.1 96.9	$\geq 380^\dagger$
2GNP	Wt% GNP 2 PC 98	Vol% 1.2 98.8	710
5GNP	Wt% GNP 5 PC 95	Vol% 3.1 96.9	≥ 940
1CNT*2GNP	Wt% CNT 1 GNP 2 PC 97	Vol% 0.7 1.2 98.1	≥ 610
1CNT*5GNP	Wt% CNT 1 GNP 5 94	Vol% 0.7 3.1 96.2	≥ 820
5CNT*2GNP	Wt% CNT 5 GNP 2 PC 93	Vol% 3.5 1.2 95.3	$\geq 620^\dagger$
5CNT*5GNP	Wt% CNT 5 GNP 5 PC 90	Vol% 3.6 3.1 93.3	$\geq 690^\dagger$

† indicates formulations that have significant decreases in viscosity (relative to other formulations in table) at high shear rates.

Adding carbon fillers to thermoplastics typically increase the viscosity, especially at low shear rates (51). At higher shear rates as the polymer shear thins, the viscosity increase

due to the fillers is usually less pronounced. Figures 13.1 and 13.2 show CB and GNP respectively following this common behavior. The addition of 2 wt% CB increased the Newtonian zero-shear plateau to 850 Pa-s from the 550 Pa-s originally seen in the neat PC. When the CB loading is increased to 5 wt%, the Newtonian zero-shear plateau is increased to 1400 Pa-s. GNP shows a similar but lesser effect with 2 wt% GNP only increasing the Newtonian zero-shear plateau to 710 Pa-s and 5 wt% GNP increasing to 940 Pa-s. These values lead to the conclusion that CB increases the viscosity of the composite 100% more than the equivalent amount of GNP does. The viscosity increase due to either of these fillers diminish as the shear-rate increases. It is noteworthy that, for GNP, there is no apparent increase in viscosity at the highest shear rates measured.

As was discussed in Chapter 8 and seen again in Figure 13.3, CNT in PC does not follow the typical carbon filled thermoplastic behavior of increased viscosity with increased filler loading. Adding 1 wt% CNT to PC decreases the viscosity at all shear rates to below that of the neat PC while maintaining the shear-thinning behavior at high shear rates. Increasing the CNT loading to 5 wt% further reduces the viscosity of the composite for shear rates greater than 100 s^{-1} . The Newtonian zero-shear plateaus of the 1 wt% CNT and 5 wt% CNT composites are similar, but at the highest shear rate tested, the 1 wt% CNT has a viscosity of 210 Pa-s compared to then 150 Pa-s of 5 wt% CNT. As was discussed in Chapter 8, the reduction of viscosity due to the addition of CNT is thought to be laminarization of the flow due to CNT log-rolling and flow orientation.

Combination of the two classic fillers, CB and GNP, show additive behavior and increase the viscosity of the composite in all cases as shown in Figure 13.4. When the two

composites containing 7 wt% total carbon fillers are compared, we see that CB has a greater effect on increasing the viscosity of the composite as the 5 wt% CB, 2 wt% GNP (5CB*2GNP) composite has a higher viscosity than the 2 wt% CB, 5 wt% GNP (2CB*5GNP) composite for all shear rates. It is also interesting to note that at the highest shear-rates measured in Figure 13.4, GNP loading had no effect on the composite viscosity (i.e. 2CB*2GNP and 2CB*5GNP have roughly the same viscosity).

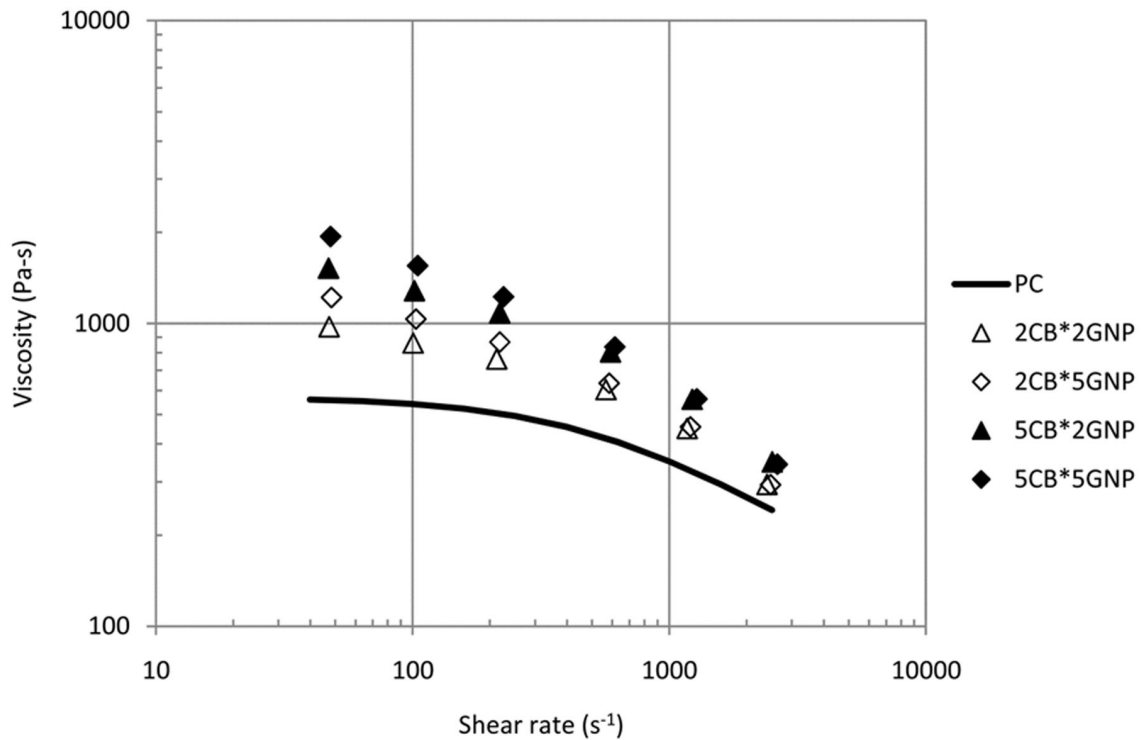


Figure 13.4: Viscosity versus Shear Rate for PC Composites with CB and GNP at 270°C

Figure 13.5 shows the results of the CB and CNT two-filler composites. We see that the unusual viscosity decreasing effect is present in all 4 filled systems. Studying Figure 13.5 we see that the addition of 1 wt% CNT to a composite with 2 wt% CB (As seen in Figure 13.1) completely negates all of the viscosity increasing effects of the CB and brings the composite viscosity back down to the level of the neat PC. When the CNT

loading is increased to 5 wt% CNT with 2 wt% CB, the viscosity of the composite is reduced to a level well below the neat PC viscosity at higher shear-rates. The addition of 1 wt% CNT to 5 wt% CB caused a significant decrease in viscosity bringing the Newtonian zero-shear plateau down from 1400 Pa-s for 5CB to 880 Pa-s for 5CB*1CNT. Again, the addition of further CNT to bring the CNT loading to 5 wt% CNT along with 5 wt% CB provides further viscosity reduction at higher shear rates (greater than 200 s^{-1}).

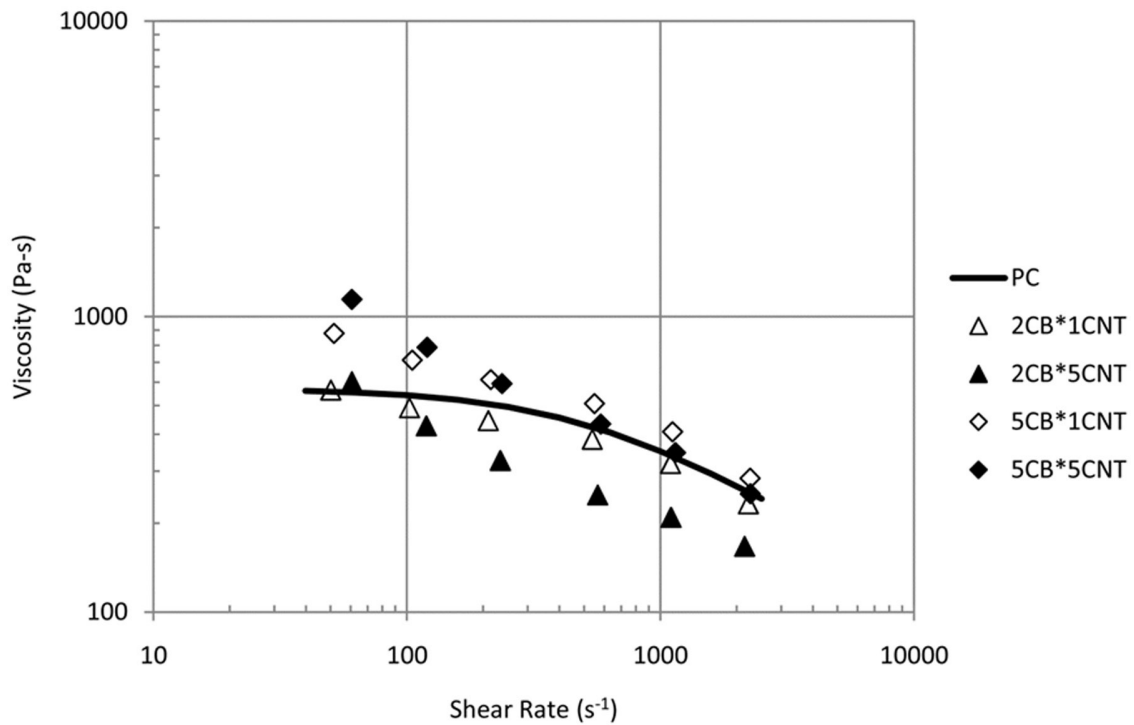


Figure 13.5: Viscosity versus Shear Rate PC Composites with CB and CNT at 270°C

The CNT and GNP two-filler system is summarized in Figure 13.6. Similarly to the CB/CNT system, we see that the addition of at least 1 wt% CNT to either 2 or 5 wt% GNP reduces the viscosity of the resulting composite versus the original GNP filled composite (as shown in Figure 13.2). Again, similarly to the CB/CNT system, the further addition of CNT to 5 wt% CNT with either loading of GNP increased the viscosity reduction at higher shear rates (greater than 100 s^{-1}). It is of note that both composites

with 5 wt% CNT (5CNT*2GNP and 5CNT*5GNP) have viscosities lower than that of neat PC at shear rates over 100 s^{-1} . The addition of CNT to the GNP systems has the added benefit of greatly reducing the electrical resistivity of the composites as shown in Table 12.3. For example, we see that adding just 1 wt% CNT to 5 wt% GNP can reduce the electrical resistivity from $4 \times 10^{15} \text{ ohm-cm}$ for 5GNP down to $6 \times 10^6 \text{ ohm-cm}$ for 1CNT*5GNP, which falls in the electrostatic dissipative range (10^{10} to 10^3 ohm-cm). The addition of 5 wt% CNT to 5 wt% GNP reduces the ER to 100 ohm-cm which places the 5CNT*5GNP composite in the semiconductive range (100 to 10 ohm-cm).

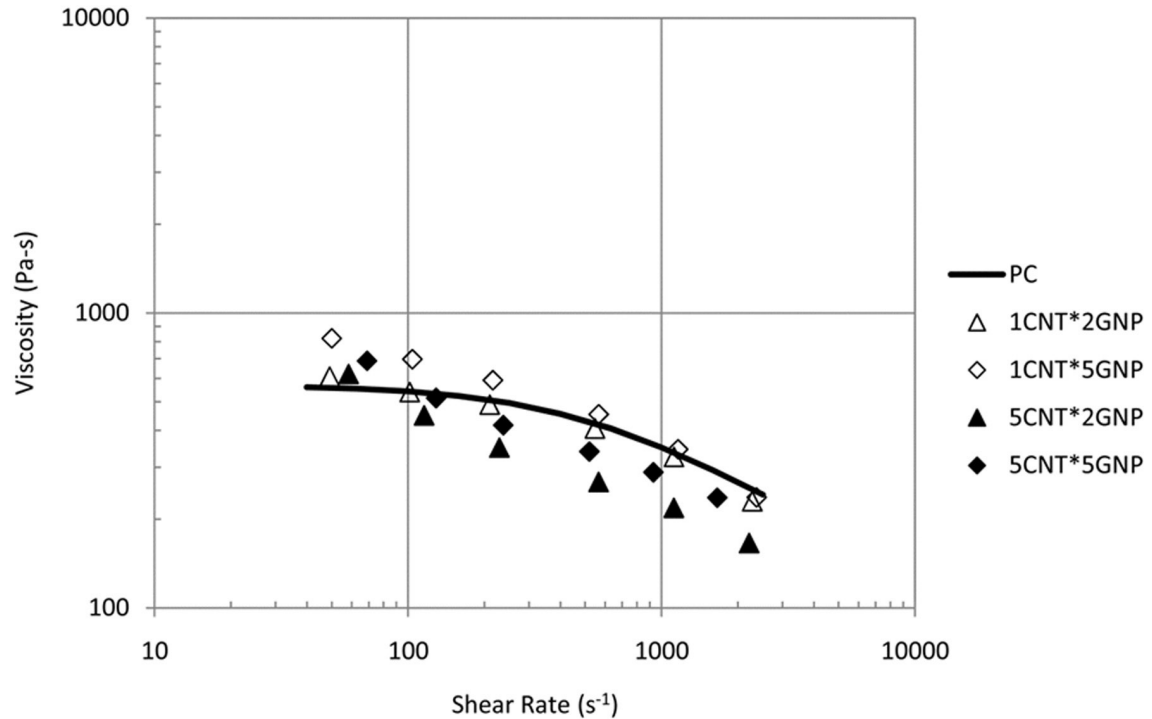


Figure 13.6: Viscosity versus Shear Rate for PC Composites with CNT and GNP at 270°C

Both the CB/CNT and CNT/GNP systems illustrate the viscosity reducing effect of CNT. Even at loadings as low as 1 wt%, CNTs can reduce the viscosity of filled or unfilled PC. Further addition of CNT up to 5 wt% to the systems can increase the

viscosity reduction effect, especially at higher shear rates. Viscosity is an indicator of processability for a composite. When the viscosity is lower, the composite is typically easier to process. The addition of 1 wt% CNT to neat PC, or PC with CB or GNP added can improve the processability of the material. It is also possible that the addition of 1 wt% CNT would allow for the processing of materials with loadings that are higher than are normally processable. An example of this possibility is seen in the CB/CNT system and illustrated in Figure 13.7. The addition of 1 wt% CNT to 2 wt% CB brings the viscosity down to the level of neat PC. The addition of 1 wt% CNT to 5 wt% CB brought the viscosity to roughly that of only 2 wt% CB in PC, the addition of 1 wt% CNT allowed for the addition of 3 wt% CB with a negligible change in viscosity. The addition of the CNT has the added benefit of decreasing the ER of the resultant compounds as seen in Tables 12.1 through 12.3. Looking back at the CB/CNT system, we see that when the addition of 1 wt% CNT to 2 wt% CB allowed us to increase the CB loading to 5 wt%, the ER decreased from 4×10^{16} ohm-cm for 2 wt% CB in PC to 400 ohm-cm for 1 wt% CNT and 5 wt% CB in PC. Of this 14 order of magnitude change, 13 orders of magnitude are due to the addition of the additional CB (ER of 2CB is 4×10^{16} ohm-cm, ER of 5CB is 4×10^3 ohm-cm).

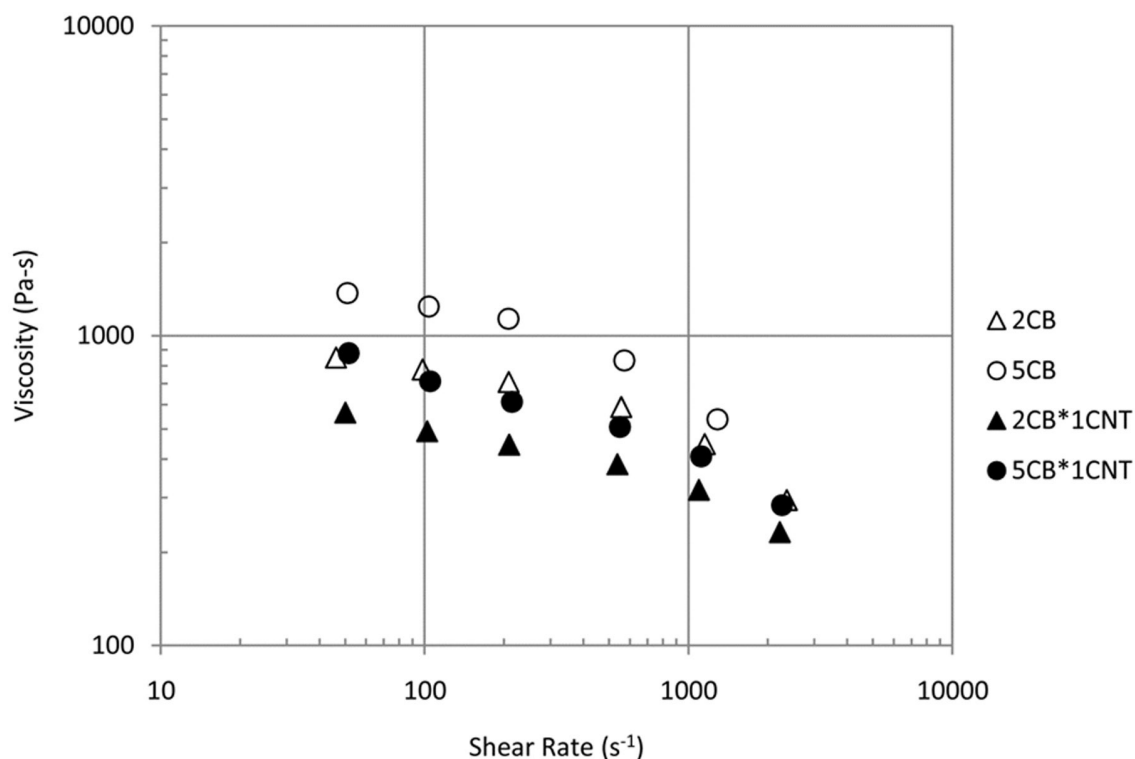


Figure 13.7: Viscosity versus Shear-Rate PC Composites with CB and CNT at 270°C: Illustrating the Effects of Adding 1 wt% CNT to CB/PC Composites

13.2: Conclusions

The purpose of this section of the project was to measure the effects of CB, CNT and GNP on the viscosity of PC using three 3^2 (2 factor, 3 level) factorial designs, one for each two-filler combination (CB/CNT, CB/GNP and CNT/GNP) while noting electrical resistivity changes. As seen in Tables 13.1-1 through 13.1-3 the filler loadings for the factorial design were 0, 2 and 5 wt% for CB, 0, 1 and 5 wt% for CNT and 0, 2 and 5 wt% for GNP. The addition of either CB or GNP to a system increased the viscosity of the resulting composite. Comparing CB and GNP, CB has a larger effect on increasing the viscosity of the composite than GNP. CNT exhibits unusual rheological behavior when added to PC. In filled or unfilled PC systems, the addition of as little as 1 wt% CNT reduces the viscosity of the resulting composite by up to 37%. The addition of further

CNT up to a total of 5 wt% CNT provides additional decreases in viscosity. This behavior is beneficial in that the addition of only 1 wt% CNT can allow for the further addition of a less expensive filler (such as CB or GNP) that follows classic behavior and increases the viscosity of the composite while maintaining high-shear processability (extrusion, injection molding, etc.). The properties of composites that are being enhanced by a filler such as CB or GNP could be enhanced by the addition of more of this filler as enabled by the addition of 1 wt% CNT.

Chapter 14: Conclusions and Future Work

14.1: Conclusions

14.1.1: Electrical Resistivity (ER)

When conductive carbon fillers are added to polymers, they decrease the electrical conductivity of the resulting composite. The resistivity of the composite begins near the neat polymer ER. The ER of the composite slowly decreases as filler is added until a point called the percolation threshold. At the percolation threshold the ER of the composite drops several orders of magnitude over a very narrow range of filler loadings. After this percolation threshold, the ER of the composite decreases at a much slower rate as it approaches the filler ER.

Carbon black (CB), carbon nanotubes (CNT) and graphene nanoplatelets (GNP) all exhibit percolation threshold behavior when added to polycarbonate (PC). Pure PC has an ER of about 10^{17} ohm-cm. CNT has the largest effect on reducing the ER of PC composites. The percolation threshold for CNT in PC is 1.0 vol%. The lowest ER measured for a CNT/PC formulation was 8 ohm-cm for 8 wt% (5.6 vol%) CNT in PC. CB had the next largest effect on decreasing ER. The percolation threshold for CB was about 2.4 vol%. The lowest ER measured for a CB/PC composite was 20 ohm-cm for 10 wt% (6.9 vol%) CB in PC. GNP had the least effect in decreasing the ER of PC composites. The GNP/PC system percolated at around 4.0 vol%, this is significantly higher than either CNT/PC or CB/PC. The lowest ER value measured for a GNP/PC composite was 2.8×10^4 ohm-cm for 15 wt% (9.6 vol%) GNP in PC.

When looking at two filler systems, the majority of the behavior of the systems is dominated by single filler effects. The CB/GNP and CNT/GNP formulations do not deviate from this behavior in any statistically significant way. The CB/CNT composite does exhibit an interaction effect between the two fillers. Specifically, the CB/CNT system shows a negative interaction in reducing the electrical resistivity of the resulting composite. This means that the ER of a composite containing both CB and CNT will have a higher ER than one would expect from just adding the ER effects of the individual fillers together.

14.1.2: Thermal Conductivity (TC)

Polymers are typically low thermal conductivity materials (compared to such materials as metals and carbons). Similarly to the electrical conductivity, the thermal conductivity of polymers can be increased by adding thermally conductive fillers to the polymer. Thermal conductivity deviates from electrical conductivity behavior by not being controlled by a percolation threshold and by the values for polymer and filler varying only a couple orders of magnitude, not 12 or more as electrical conductivity does.

CB, CNT and GNP all increase the thermal conductivity of polycarbonate. Polycarbonate itself has a TC of 0.20 W/m·K. GNP has the largest effect on increasing the thermal conductivity of polycarbonate composites. At 15 wt% (9.6 vol%) GNP in PC, the composite has a TC of 0.489 W/m·K. At 5.0 vol% (8 wt%) GNP increases the TC of the resulting PC composite to 0.374 W/m·K. CNT has the next largest effect on increasing the TC of PC composites. At the highest CNT loading, 5.6 vol% (8 wt%), CNT increases the TC of the resulting PC composite to 0.306 W/m·K, somewhat less

than the increase given by 5.0 vol% of GNP. CB has the smallest effect on increasing the TC of PC composites. 5.46 vol% (8 wt%) CB increases the TC of PC to 0.275 W/m·K. At the highest CB loading level, 10 wt% (6.9 vol%), CB increases the TC of PC to 0.291 W/m·K.

When looking at the two filler systems studied in this project, the thermal conductivity behavior of the composites is dominated by the single filler effects of the individual fillers. The CB/CNT and CB/GNP systems do not show any statistically significant interaction effects between the fillers. The CNT/GNP system does show a statistically significant positive interaction between the fillers. This means that when a composite contains both CNT and GNP, the TC of the composite is higher than would be expected from adding the individual effects of the single fillers together.

14.1.3: Tensile Properties

Adding fillers to polymers will often change the tensile properties of a material. The addition of strong and stiff fillers, such as carbons, will typically increase the tensile modulus and, to a lesser degree, tensile strength of the resulting composite.

CB, CNT and GNP all increase the tensile modulus of PC composites. All three fillers have little effect on the tensile strength of the composite. Neat PC has a tensile modulus of about 2.2 GPa. GNP has the largest effect on the tensile modulus of the composite, increasing the tensile modulus of the resulting composite to 5.9 GPa for the highest filled composite, 15 wt% (9.6 vol%) GNP in PC. When the GNP loading is 5.0 vol% (8 wt%) the tensile modulus is 3.5 GPa. CNT and CB have similar effects on increasing the tensile modulus of PC composites. At 5.6 vol % (8 wt%) CNT, the tensile modulus of

the PC composite is increased to 2.9 GPa. At 5.5 vol% (8 wt%) CB, the tensile modulus of the PC composite is increased to 2.8 GPa.

The two filler systems studied here all showed statistically significant interactions between the fillers in the composite. The CB/CNT system showed each filler increasing the tensile modulus of the system with diminishing effects as more of the individual filler was added. Additionally, there was a positive interaction effect between the CB and CNT. This means that a composite containing both CB and CNT would have a tensile modulus that would be higher than would be expected from adding the individual effects of the single fillers together. The CB/GNP system showed each filler increasing the tensile modulus of the filler as more of the filler was added. The CB/GNP system also showed a statistically significant positive interaction effect between the CB and GNP. This means that a composite containing both CB and GNP would have a tensile modulus that would be higher than would be expected from adding the individual effects of the single fillers together. The CNT/GNP system showed each filler increasing the tensile modulus of the composite with CNT exhibiting a diminishing effect as more CNT is added. The CNT/GNP system also displayed a statistically significant negative interaction between CNT and GNP. This means that a composite containing both CNT and GNP would have a tensile modulus that would be lower than would be expected from adding the individual effects of the single fillers together.

14.1.4: Flexural Properties

Adding fillers to polymers will often change the flexural properties of a material. The addition of strong and stiff fillers, such as carbons, will typically increase the flexural modulus and, to a lesser degree, flexural strength of the resulting composite.

CB, CNT and GNP all increase the flexural modulus of PC composites. All three fillers have little effect on the flexural strength of the composite. Neat PC has a flexural modulus of about 2.6 GPa. GNP has the largest effect on the flexural modulus of the composite at high loadings, increasing the flexural modulus of the resulting composite to 6.4 GPa for the highest filled composite, 15 wt% (9.6 vol%) GNP in PC. When the GNP loading is 5.0 vol% (8 wt%) the flexural modulus is similar to that of CNT with a value of 3.6 GPa. CNT has the second largest effect on increasing the tensile modulus of PC composites. At 5.6 vol % (8 wt%) CNT, the tensile modulus of the PC composite is increased to 3.6 GPa. CB has the least effect on increasing the flexural modulus of PC composites. At 5.5 vol% (8 wt%) CB, the tensile modulus of the PC composite is increased to 3.4 GPa, slightly less than the value for GNP or CNT.

The two filler composites all show the individual fillers increasing the flexural modulus of the resulting composites. The CB/CNT system shows CB having a diminishing effect as more CB is added. Additionally, the CB/CNT system exhibits a statistically significant positive interaction between CB and CNT. This means that a composite containing both CB and CNT would have a flexural modulus that would be higher than would be expected from adding the individual effects of the single fillers together. The CB/GNP system shows GNP having a diminishing effect on flexural modulus as

additional GNP is added to the composite. This system shows no statistically significant interaction effects. The CNT/GNP system shows GNP having a diminishing effect on flexural modulus as additional GNP is added. There is also a statistically significant positive interaction effect between the CNT and GNP. This means that a composite containing both CNT and GNP would have a flexural modulus that would be higher than would be expected from adding the individual effects of the single fillers together.

14.1.5: Rheological Properties

Pure polycarbonate shows very common shear-thinning polymeric behavior. As the shear rate applied to a polycarbonate sample increases, the viscosity of the sample decreases. As the shear rate decreases, the value of the viscosity levels out at a value known as the Newtonian zero-shear plateau. The addition of carbon fillers to a polymer typically increases the viscosity of the resulting composite. This increase in viscosity typically increases with increased filler loading. It is also common at low shear rates for carbon filled systems to exhibit a yield stress, seen on a log(stress) versus log(strain) curve as a straight line with a negative 1 slope.

CB and GNP show classic carbon filler behavior in PC. Both fillers increase the viscosity of the composite and exhibit yield stress behavior at low shear rates. CB has a larger effect on increasing the viscosity of the composite than GNP. CNT also shows a yield stress at low shear rates. At higher shear rates, CNT does not exhibit the expected carbon filler behavior. Instead, CNT reduces the viscosity of the resulting composite below the viscosity of the pure PC. This effect increases in strength with increased CNT

loading up to about 4 wt% CNT where the effect saturates and additional CNT does not change the high shear rate behavior of the material.

CB and GNP continue to act as expected in two filler systems, increasing the viscosity of the resulting composites, with larger increases for larger filler loadings. The CB/GNP system shows that both fillers act as expected for carbon fillers. The viscosity increasing effects are additive. When comparing the formulations within the CB/GNP system, it can be determined that CB has a larger effect on increasing the viscosity than GNP as described in Chapter 13. CNT in two filler systems acted similarly to its behavior as a single filler. In the GNP/PC system, we can see that as little as 1 wt% CNT can reduce the viscosity of a 2 wt% GNP in PC composite to below the level of the original pure PC. At high shear rates 1 wt% CNT can even negate the effect of up to 5 wt% GNP bringing the viscosity of a 1 wt% CNT, 5 wt% GNP in PC composite down to the level of pure PC. In this system 5 wt% CNT completely negates the effect of 5 wt% GNP bringing the viscosity of 5 wt% CNT and 5 wt% GNP in PC to below the of the original PC for all shear rates above 10 s^{-1} . In the CB/CNT system, we again see CNT acting to reduce the viscosity of the composite. 1 wt% CNT can bring the viscosity of a 2 wt% CB in PC composite down below the viscosity of pure PC. Of particular note for this system, when 1 wt% CNT is added to a 5 wt% CB in PC composite, the resulting viscosity for all shear rates is essentially the same as 2 wt% CB in PC. This means the addition of 1 wt% CNT to a 2 wt% CB in PC composite would allow for an additional 3 wt% CB to be added with no change to the viscosity.

14.1.6: Electrical Conductivity and Tensile Modulus Modeling

Electrical conductivity modeling for this project focused on applying the Mamunya model, additive model, and General Effective Media (GEM) model to the single filler systems. For all 3 systems the Mamunya model and additive model produced similar results. Both of these models generated significant amounts of error due to the assumption in both models that below the percolation threshold, the electrical conductivity of the composite is equal to that of the pure polymer. After the percolation threshold, both models have very good fits to the experimental data. The GEM model does not assume pure polymer electrical conductivity below the percolation threshold and was thus able to model this part of the data much better than the other two models. Above the percolation threshold the fit of the GEM model was inferior to the other two models. Overall the GEM model produced the best overall fit for all three filler systems.

Tensile modulus modeling for this project focused on applying the Halpin-Tsai models and Nielsen model to the single filler systems. Both of these models required information on the aspect ratio of the materials. In the Halpin-Tsai models, the aspect ratio is a direct input, for the Nielsen model, the aspect ratio is used to calculate the Einstein coefficient, a direct input to the model. Scanning and transmission electron microscopy of the materials showed that neither CNT nor GNP remain flat and straight in the composite. This led to ambiguity as to what the proper aspect ratio for these calculations would be. A solution was found using the previously mentioned electrical conductivity modeling. It is possible to estimate the percolation threshold of conductive fillers in a composite using an analytical model that models the fillers as simple cubic elements. Using the percolation threshold as determined from the GEM model for

electrical conductivity, the percolation threshold models could be reworked to solve for an effective filler aspect ratio. This method was tested on the GNP/PC system as there was accurate data for the maximum packing fraction (another direct input for the Nielsen model). This effective aspect ratio, combined with a literature value for the modulus of exfoliation of graphite (the hypothesized primary failure method) produced a model that had very good agreement with the experimental data. This method was also used for the CNT/PC system to allow the 3-dimensional randomly oriented Halpin-Tsai model to fit the experimental data very well. The CB/PC system did not require this modeling as the aspect ratio is assumed to be roughly 1 and the Einstein coefficient for spherical particles is assumed to be a constant. Overall, the percolation threshold modeling system allowed more accurate and meaningful tensile modulus modeling than has been previously seen in literature. The Halpin-Tsai model provided the best fit for CNT/PC while the Nielsen model provided the best fit for CB/PC and GNP/PC.

14.2: Recommendations for Future Work

The future of this research project should focus on extending the discoveries made therein to other systems. Primarily, the viscosity reducing effects of CNT in PC, and the electrical percolation threshold modeling approach to tensile modulus modeling, need to be extended to additional systems.

In this project we have shown that the addition of CNT can reduce the viscosity of PC, especially in the high shear rate domains that are consistent with extrusion and injection molding. We have also shown that CNT can be added to PC composites that already

have a different carbon filler to reduce the viscosity. This allows for additional amounts of the other carbon filler to be added to the composite without harming processability. Previous work with the same CNT in polypropylene (PP) did not exhibit this behavior. In CNT/PP systems, the CNT acted as a normal carbon filler to increase the viscosity of the composite. Experimentation needs to be done to determine what causes this different behavior. Looking at the structure of PC versus PP, PC contains benzene rings that are located in the backbone, as well as oxygen atoms both in the backbone, and carbonyl oxygen off the backbone while PP is fully aliphatic. This research should focus on materials that have one of these various differences to determine which of them cause the change.

Polyacrylonitrile is identical to PP except the methyl pendants are replaced with nitrile groups. If CNT reduced the viscosity of polyacrylonitrile systems, it would suggest the presence of hetero atoms in the structure cause the viscosity reduction effect.

Poly(p-xylene) contains benzene rings as a backbone element. If CNT reduced the viscosity of poly(p-xylene) systems, it would suggest the presence of benzene rings in the polymer backbone cause the viscosity reduction effect.

Polyformaldehyde contains oxygen as a backbone element. If CNT reduced the viscosity of polyformaldehyde systems, it would suggest the presence of oxygen in the polymer backbone cause the viscosity reduction effect.

Poly(phenylene oxide) has the combination of oxygen and benzene rings in the polymer backbone. If CNT reduced the viscosity of poly(phenylene oxide) systems, it would

suggest the presence of both oxygen and benzene rings in the polymer backbone cause the viscosity reduction effect.

There are dozens of combinations and countless types of polymers that could be tested for this behavior. These are just examples of materials that could be used as part of a Design of Experiments approach to test the various differences between PC and PP to determine how the CNT interacts with the polymer matrix to reduce the viscosity of the composite.

Additionally, it is important to test other fillers to determine their compatibility with the CNT viscosity reduction effect. In this project we have shown that the effect is compatible with nanoscale carbon fillers, particularly flake-like and spherical fillers. There are other geometries and materials that it is important to test.

Carbon nanofibers (CNF) are nanoscale rod-like fillers that would round out the knowledge of the geometries of carbon nanofillers as the CB is roughly zero dimensional, the GNP is roughly two dimensional and the carbon nanofibers are roughly one dimensional.

In addition to nanofillers, other carbon fillers should be tested. Carbon fiber is a very common reinforcement material for polymers. It is a rod-like filler like CNT or CNF, but it is on the micrometer scale. The size of the filler might change the viscosity reducing effects of CNT.

Synthetic graphite particles are rough irregular particles. They are roughly spherical, but may have aspect ratios up to 5. These particles are roughly 10 to 100 microns in size and again probe the interactions between CNT and larger particles.

It is possible that the CNT viscosity reduction effect could be compatible with other materials as well. Clay nanoplatelets represent a non-carbon version of the GNP studied in this project. Mica flakes represent a micrometer scale, non-carbon version of the GNP. Experimentation with both of these materials would help understand the compatibility of the CNT viscosity reduction effect.

There are other nanotubes that may exhibit this same viscosity reducing behavior. Boron nitride nanotubes in particular are quite similar to CNT in size and geometry. Experimentation with these nanotubes would help determine whether the effect is inherent to the CNT themselves, or their geometry and size.

The use of percolation threshold modeling to determine an effective aspect ratio for fillers within the composite was found to be very useful for this project. Testing the method on other systems would allow for the model to be used more universally. It would be most helpful to test the percolation threshold modeling method with other polymers and other fillers.

Similarly to the recommendations given for the CNT effect, this new tensile modeling tool should be applied to other polymer matrices. Specifically, it would be most beneficial to test it with polymer systems that are very dissimilar to polycarbonate. Polyethylene or polypropylene represent aliphatic polymers that may behave much differently than polycarbonate that contains benzene rings and oxygen atoms.

Polyimides/polyamides and polysulfones contain other kinds of hetero atoms (specifically nitrogen and sulfur respectively) and could behave differently than polycarbonate. Poly(p-xylene) has benzene rings but no atoms other than carbon and hydrogen and would help bridge the gap between the behavior of the aliphatic polymers and polycarbonate. Poly(p-xylene) would also help determine whether unsaturation or hetero atoms cause any behavior difference between the polymers.

It is also important to look at different fillers when applying this tensile modulus method. Particles that are larger sized, like synthetic graphite particles or carbon fiber, may behave differently than was seen in carbon nanoparticles in polycarbonate. Also, non-carbon materials that are both nanosized, such as clay nanoplatelets and boron-nitride nanotubes, and larger, such as calcium carbonate or fiberglass, may behave differently than carbon-based materials. It is also important to test this variety of different fillers in the different polymer systems.

As the percolation threshold modeling modification to tensile modulus modeling method is validated in other systems, it can become a useful tool for tensile modeling.

Chapter 15: References

- 1 Wright WM, Woodham GW. Conductive Polymers and Plastics. New York: Chapman and Hall; 1989.
- 2 Finan JM. Thermally conductive thermoplastic materials. In: Proceedings of the Society of Plastics Engineers Annual Technical Conference; 1999; New York. p. 1547-1550.
- 3 Taipalus T, Harmia M, Zhang Q, Friedrich K. The electrical conductivity of carbon-fibre-reinforced polypropylene/polyaniline complex-blends: experimental characterisation and modelling. *Composites Science and Technology*. 2001;61(6):801-814.
- 4 Agari Y, Uno T. Thermal-conductivity of polymer filled with carbon materials- effect of conductive particle chains on thermal-conductivity. *Journal of Applied Polymer Science*. 1985;30(5):2225-2236.
- 5 Bigg DM. Conductive polymeric compositions. *Polymer Engineering and Science*. 1977;30(12):842-847.
- 6 Bigg DM. The effect of compounding on the conductive properties of EMI shielding compounds. *Advanced Polymer Technology*. 1984;4(3-4):255-266.
- 7 Narkis M, Lodor G, Vaxman A, Zuri J. New injection moldable electrostatic dissipative (ESD) composites based on very low carbon black loadings. *Journal of Electrostatics*. 1999;47(4):201-214.
- 8 Nagata K, Iwabuchi H, Nigo H. Effect of particle size of graphites on electrical conductivity of graphite/polymer composite. *Composite Interfaces*. 1998;6(5):483-495.
- 9 Demain A. Thermal Conductivity of Polymer-Chopped Carbon Fibre Composites. Louvain-la-Neuve, Belgium: Universite Catholique de Louvain; 1994.
- 10 King JA, Tucker KW, Meyers JD, Weber EH, Clingerman ML, Ambrosius KR. Factorial design approach applied to electrically and thermally conductive nylon 6,6. *Polymer Composites*. 2001;22(1):142-154.

- 11 Murthy MV. Permanent EMI shielding of plastics using copper fibers. In: Proceedings of the Society of Plastics Engineers Annual Technical Conference; 1994; San Francisco. p. 1396-1401.
- 12 Simon RM. Thermally and electrically conductive flake filled plastics. *Polymer News*. 1985;11:102-108.
- 13 Mapleston P. Conductive composites get a growth boost from metallic fibers. *Modern Plastics*. 1992;69:80-83.
- 14 Donnet JB, Bansal RC, Wang MJ. *Carbon Black*. New York: Marcel Dekker; 1993.
- 15 Huang JC. Carbon black filled conducting polymers and polymer blends. *Advances in Polymer Technology*. 2002;21(4):299-313.
- 16 Bigg DM. The effect of chemical-exposure on the EMI shielding of conductive plastics. *Polymer Composites*. 1987;8(1):1-7.
- 17 King J, Johnson B, Via M, Ciarkowski C. Effects of carbon fillers in thermally conductive polypropylene based resins. *Polymer Composites*. 2010;31(3):497-506.
- 18 Chung DDL. *Composite Materials: Science and Applications (Engineering Materials and Processes)*. New York: Springer; 2010.
- 19 King JA, Via MD, Caspary JA, Jubinski MM, Miskioglu I, Mills OP, Bogucki GR. Electrical and thermal conductivity and tensile and flexural properties of carbon nanotube/polycarbonate resins. *Journal of Applied Polymer Science*. 2010;118(5):2512-2520.
- 20 Fried JR. *Polymer Science and Technology*. Upper Saddle River, New Jersey: Prentice Hall; 2003.
- 21 Boeing 787 Dreamliner Long-Range, Mid-Size Airliner, USA. [Internet]. [cited 2007 September 10]. Available from: <http://www.aerospace-technology.com/projects/dreamliner>.
- 22 Bigg DM. *Metal Filler Polymers: Properties and Applications*. New York: Marcel Dekker Inc.; 1986.

- 23 Clingerman ML, Weber EH, King JA, Schulz KH. Development of an additive equation for predicting the electrical conductivity of carbon-filled composites. *Journal of Applied Polymer Science*. 2003;88(9):2280-2299.
- 24 Broadbent SR, Hammersley JM. Percolation processes: I. Crystals and mazes. *Proceedings of the Cambridge Philosophical Society*. 1957;53:629-641.
- 25 Stauffer D. *Introduction of Percolation Theory*. London: Taylor and Francis; 1985.
- 26 Blunk RH, Lisi DJ, Yoo Y, Tucker III CL. Enhanced conductivity of fuel cell plates through controlled fiber orientation. *AIChE Journal*. 2003;49(1):18-29.
- 27 Ruschau GR, Newnham RE. Critical volume fractions in conductive composites. *Journal of Composite Materials*. 1992;26(18):2727-2735.
- 28 Bird RB, Stewart WE, Lightfoot EN. *Transport Phenomena*. 2nd ed. New York: Wiley; 2002.
- 29 Parrott JE, Stuckes AD. *Thermal Conductivity of Solids*. London: Pion Limited; 1975.
- 30 Bigg DM. Thermally conductive polymer compositions. *Polymer Composites*. 1986;7(3):125-140.
- 31 Hauser RA. *Synergistic Effects and Modeling of Thermally Conductive Resins for Fuel Cell Bipolar Plate Applications*. Houghton: Michigan Technological University; 2008.
- 32 Berman R. *Thermal Conduction in Solids*. Oxford: Clarendon Press; 1976.
- 33 Hone J, Llaguno MC, Nemes NM, Johnson AT, Fischer JE, Walters DA, Casavant MJ, Schmidt J, Smalley RE. Electrical and thermal transport properties of magnetically aligned single wall carbon nanotube films. *Applied Physics Letters*. 2000;77(5):666-668.
- 34 King JA, Johnson BA, Via MD, Ciarkowski CJ. Electrical conductivity of carbon-filled polypropylene-based resins. *Journal of Applied Polymer Science*. 2009;112(1):425-433.

- 35 King JA, Miller MG, Barton RL, Keith JM, Hauser RA, Peterson KR, Sutter LL. Thermal and electrical conductivity of carbon-filled liquid crystal polymer composites. *Journal of Applied Polymer Science*. 2006;99(4):1552-1558.
- 36 Agari Y, Ueda A, Nagai S. Thermal-conductivities of composites in several types of dispersion-systems. *Journal of Applied Polymer Science*. 1991;42(6):1665-1669.
- 37 Gaxiola DL, Jubinski MM, Keith JM, King JA, Miskioglu I. Effects of carbon fillers on tensile and flexural properties in polypropylene-based resins. *Journal of Applied Polymer Science*. 2010;118(3):1620-1633.
- 38 Marsh H, Rodriguez-Reinoso F. *Sciences of Carbon Materials*. San Vicente del Raspeig, Alicante, Spain: Universidad de Alicante; 2001.
- 39 Gupta M, Wang KK. Fiber orientation and mechanical-properties of short-fiber-reinforced injection-molded composites - Simulated and experimental results. *Polymer Composites*. 1993;14(5):367-382.
- 40 Ludwig HC, Fischer G, Becker H. A quantitative comparison of morphology and fibre orientation in push-pull processed and conventional injection-moulded parts. *Composites Science and Technology*. 1995;53(2):235-239.
- 41 Ryu SR, Lee DJ. Effects of fiber aspect ratio, fiber content, and bonding agent on tensile and tear properties of short-fiber reinforced rubber. *KSME International Journal*. 2001;15(1):35-43.
- 42 Sabic Innovative Plastics. PC Resin Product Brochure: Sabic-PLA-650. One Plastics Avenue, Pittsfield, MA, 01201 2008.
- 43 Hyperion Catalysis International. Fibrils Product Information. 38 Smith Place, Cambridge, MA 02138.
- 44 Spinelli F. *Plastics, Additives, and Modifiers Handbook*. New York: Chapman and Hall; 1996.
- 45 Burgess KA, Lyon F. *Encyclopedia of Polymer Science and Technology*. New York: John Wiley and Sons Inc.; 1985.
- 46 Akzo Nobel. Ketjenblack EC Product Brochure. Chicago, IL.
- 47 Kalaitzidou K, Fukushima H, Drzal LT. Mechanical properties and morphological

- characterization of exfoliated graphite-polypropylene nanocomposites. *Composites: Part A*. 2007;38(7):1675-1682.
- 48 Ovation Polymers, Inc. Extima GP MB PC 1530A Data Sheet. 1030 West Smith Rd, Medina, OH, 44256.
- 49 American Society for Testing and Materials. ASTM D792-98: Standard Test Methods for Density and Specific Gravity (Relative Density) of Plastics by Displacement. 1998.
- 50 American Society for Testing and Materials. ASTM D3835-96: Standard Test Method for Determination of Properties of Polymeric Materials by Means of a Capillary Rheometer. 1996.
- 51 Morrison FA. *Understanding Rheology*. New York: Oxford University Press; 2001.
- 52 International Organization for Standardization. ISO 6721-99: Plastics -- Determination of dynamic mechanical properties -- Part 10: Complex shear viscosity using a parallel-plate oscillatory rheometer. 1999.
- 53 Cox WP, Merz EH. Correlation of dynamic and steady flow viscosities. *Journal of Polymer Science*. 1958;28(118):619-622.
- 54 American Society for Testing and Materials. ASTM D257-99: Standard Test Methods for DC Resistance or Conductance of Insulating Materials. 1999.
- 55 American Society for Testing and Materials. ASTM D4496-04: Standard Test Method for D-C Resistance or Conductance of Moderately Conductive Materials. 2004.
- 56 American Society for Testing and Materials. ASTM F433-98: Standard Practice for Evaluating Thermal Conductivity of Gasket Materials. 1998.
- 57 Holometrix Inc. TCA 300 Operators Manual. Burlington, MA: Holometrix Inc.; 1994.
- 58 American Society for Testing and Materials. ASTM D638-03: Standard Test Method for Tensile Properties of Plastics. 2003.
- 59 American Society for Testing and Materials. ASTM D790-03: Standard Test Methods for Flexural Properties of Unreinforced and Reinforced Plastics and Electrical Insulating Materials. 2003.

- 60 Weber M, Kamal MR. Estimation of the volume resistivity of electrically conductive composites. *Polymer Composites*. 1997;18(6):711-725.
- 61 Hornbostel B, Potschke P, Koz J, Roth S. Single-walled carbon nanotubes/polycarbonate composites: basic electrical and mechanical properties. *Physica Status Solidi B-Basic Solid State Physics*. 2006;243(13):3445-3451.
- 62 Potschke P, Bhattacharyya A, Janke A. Melt mixing of polycarbonate with multiwalled carbon nanotubes: microscopic studies on the state of dispersion. *European Polymer Journal*. 2004;40(1):137-148.
- 63 Potshcke P, Bhattacharyya A, Janke A. Carbon nanotube-filled polycarbonate composites produced by melt mixing and their use in blends with polyethylene. *Carbon*. 2004;42(5-6):965-969.
- 64 Pegel S, Potshcke P, Petzold G, Alig I, Dudkin S, Lellinger D. Dispersion, agglomeration, and network formation of multiwalled carbon nanotubes in polycarbonate melts. *Polymer*. 2008;49(4):974-984.
- 65 Lee G, Lee J, Lee S, Park M, Kim J. Comparisons of thermal properties between inorganic filler and acid-treated multiwall nanotube/polymer composites. *Journal of Materials Science*. 2005;40(5):1259-1263.
- 66 Lopez Manchado M, Valentini L, Biagiotti J, Kenny J. Thermal and mechanical properties of single-walled carbon nanotubes–polypropylene composites prepared by melt processing. *Carbon*. 2005;43(7):1499-1505.
- 67 Fornes T, Baur J, Sabba Y, Thomas E. Morphology and properties of melt-spun polycarbonate fibers containing single- and multi-wall carbon nanotubes. *Polymer*. 2006;47(5):1704-1714.
- 68 Lee SH, Kim JH, Choi SH, Kim SY, Kim KW, Youn JR. Effects of filler geometry on internal structure and physical properties of polycarbonate composites prepared with various carbon fillers. *Polymer International*. 2009;58(4):354-361.

- 69 Potschke P, Abdel-Goad M, Pegel S, Jehnichen D, Mark JE, Zhou D, Heinrich G. Comparisons among electrical and rheological properties of melt-mixed composites containing various carbon nanostructures. *Journal of Macromolecular Science*. 2010;47(1):12-19.
- 70 Tchoudakov R, Breuer O, Narkis M. Conductive polymer blends with low carbon black loading: Polypropylene/polycarbonate. *Polymer Networks Blends*. 1996;6(1):1.
- 71 Ezquerro TA, Martinez-Salazar J, Balta Calleja FJ. Percolation-threshold of conductive polycarbonate carbon composites as revealed by electron microscopy. *Journal of Materials Science Letters*. 1986;5(10):1065-1066.
- 72 Balta Calleja FJ, Ezquerro TA, Rueda DR. Conductive polycarbonate-carbon composites. *Journal of Materials Science Letters*. 1984;3(2):165-168.
- 73 King JA, Johnson BA, Via MD, Ciarkowski CJ. Effects of carbon fillers in thermally conductive polypropylene based resins. *Polymer Composites*. 2010;31(3):497-506.
- 74 Keith JM, King JA, Lenhart KM, Zimny B. Thermal conductivity models for carbon/liquid crystal polymer composites. *Journal of Applied Polymer Science*. 2007;105(6):3309-3316.
- 75 Huang JC, Muangchareon P, Grossman SC. Effects of carbon black on mechanical properties of polycarbonate-polypropylene blends. *Journal of Polymer Engineering*. 2000;20(2):111.
- 76 Bird RB, Armstrong RC, Hassager O. *Dynamics of Polymeric Liquids*. New York: Wiley; 1987.
- 77 King JA, Via MD, Keith JM, Morrison FA. Effects of carbon fillers on rheology of polypropylene-based resins. *Journal of Composite Materials*. 2009;43(25):3073-3089.
- 78 King JA, Morrison FA, Keith JM, Miller MG, Smith RC, Cruz M, Neuhalfen AM, Barton RL. Electrical conductivity and rheology of carbon-filled liquid crystal polymer composites. *Journal of Applied Polymer Science*. 2006;101(4):2680-2688.

- 79 King JA, Tambling TM, Morrison FA, Keith JM, Cole AJ, Pagel RM. Effects of carbon fillers on the rheology of highly filled liquid-crystal polymer based resins. *Journal of Applied Polymer Science*. 2008;108(3):1646-1656.
- 80 Kunen E, Keith JM, Grant PW, King JA, Morrison FA. FEM calculations of capillary rheometer flow for carbon-filled liquid crystal polymer composites. *Journal of Applied Polymer Science*. 2007;106(1):433-438.
- 81 King JA, Tambling TM, Keith JM, Cole AJ, Morrison FA. Synergistic effects of multiple carbon fillers on the rheology of liquid crystal polymer based resins. *Polymer Composites*. 2009;30(1):111-119.
- 82 Shenvoy AV. *Rheology of Filled Polymer Systems*. Boston: Kluwer Academic Publishers; 1999.
- 83 Kalaitzidou K, Fukushima H, Drzal LT. A new compounding method for exfoliated graphite-polypropylene nanocomposites with enhanced flexural properties and lower percolation threshold. *Composites Science and Technology*. 2007;67(10):2045-2051.
- 84 Fukushima H, Drzal LT, Rook BP, Rich MJ. Thermal conductivity of exfoliated graphite nanocomposites. *Journal of Thermal Analysis and Calorimetry*. 2006;85(1):235-238.
- 85 Kalaitzidou K, Fukushima H, Miyagawa H, Drzal LT. Flexural and tensile moduli of polypropylene nanocomposites and comparison of experimental data to Halpin-Tsai and Tandon-Wang models. *Polymer Engineering and Science*. 2007;47(11):1796-1803.
- 86 Maron SH, Pierce PE. Application of ree-eyring generalized flow theory to suspensions of spherical particles. *Journal of Colloid Science*. 1956;11(1):80-95.
- 87 Fisa B, Vu-Khanh T, Remillard B. Extrusion of mica filled polypropylene. *Journal of Thermoplastic Composite Materials*. 1988;1(4):361-370.
- 88 Kitano T, Kataoka T, Shirota T. An empirical-equation of the relative viscosity of polymer melts filled with various inorganic fillers. *Rheologica Acta*. 1981;20(2):207-209.

- 89 Mamunya EP, Davidenko VV, Lebedev EV. Effect of polymer-filler interface interactions on percolation conductivity of thermoplastics filled with carbon black. *Composite Interfaces*. 1996;4(4):169-176.
- 90 Keith JM, King JA, Barton RL. Electrical conductivity modeling of carbon-filled liquid-crystalline polymer composites. *Journal of Applied Polymer Science*. 2006;102(4):3293-3300.
- 91 McLachlan DS, Newman RE. Electrical resistivity of composites. *Journal of the Americal Ceramic Society*. 1990;73(8):2187-2203.
- 92 McLachlan DS. Equation for the conductivity of metal-insulator mixtures. *Journal of Physics Part C: Solid State Physics*. 1985;18(9):1891-1898.
- 93 McLachlan DS. A new interpretation of percolation conductivity results with large critical regimes. *Solid State Communications*. 1986;60(10):821-825.
- 94 Barton RL, Keith JM, King JA. Development and modeling of electrically conductive carbon filled liquid crystal polymer composites for fuel cell bipolar plate applications. *Journal of New Materials for Electrochemical Systems*. 2007;10(4):225-229.
- 95 Barton RL, Keith JM, King JA. Electrical conductivity modeling of multiple carbon fillers in liquid crystal polymer composites for fuel cell bipolar plate applications. *Journal of New Materials for Electrochemical Systems*. 2008;11(3):181-186.
- 96 Dai H, Wong EW, Lieber CM. Probing electrical transport in nanomaterials: Conductivity of individual carbon nanotubes. *Science*. 1996;272(5261):523-526.
- 97 Thess A, Lee R, Nikolaev P, Dai H, Petit P, Robert J, Xu C, Lee YH, Kim SG, Rinzler AG, et al. Crystalline ropes of metallic carbon nanotubes. *Science*. 1996;273(5274):483-487.
- 98 Grunlan JC, Liu L, Kim YS. Tunable single-walled carbon nanotube microstructure in the liquid and solid states using poly(acrylic acid). *Nano Letters*. 2006;6(5):911-915.
- 99 XG Sciences Inc. xGnP Brand Graphene Nanoplatelets Product Information. East Lansing, Michigan: XG Sciences Inc.; 2010.
- 100 Keith JM, King JA, Johnson BA. Electrical conductivity modeling of carbon filled

- polypropylene based resins for fuel cell bipolar plate applications. *Journal of New Materials for Electrochemical Systems*. 2008;11(4):253-257.
- 101 Li J, Ma PC, Chow WS, To CK, Tang BZ, Kim JK. Correlations between percolation threshold, dispersion state, and aspect ratio of carbon nanotubes. *Advanced Functional Materials*. 2007;17(16):3207-3215.
 - 102 Li J, Kim JK. Percolation threshold of conducting polymer composites containing 3D randomly distributed graphite nanoplatelets. *Composites Science and Technology*. 2007;67(10):2114-2120.
 - 103 Thostenson ET, Chou TW. On the elastic properties of carbon nanotube-based composites: modelling and characterization. *Journal of Physics Part D: Applied Physics*. 2003;36(5):573-582.
 - 104 Gojny FH, Wichmann MHG, Kopke U, Fiedler B, Schulte K. Carbon nanotube-reinforced epoxy-compo sites: enhanced stiffness and fracture toughness at low nanotube content. *Composites Science and Technology*. 2004;64(15):2363-2371.
 - 105 Peeterbroeck S, Breugelmans L, Alandre M, Nagy JB, Viville P, Lazzaroni R, Dubois P. The influence of the matrix polarity on the morphology and properties of ethylene vinyl acetate copolymers-carbon nanotube nanocomposites. *Composites Science and Technology*. 2007;67(7-8):1659-1665.
 - 106 Nielsen LE. *Polymer Rheology*. New York: Marcel Dekker Inc.; 1977.
 - 107 Rao YQ, Pochan JM. Mechanics of polymer-clay nanocomposites. *Macromolecules*. 2007;40(2):290-296.
 - 108 Nielsen LE. The thermal and electrical conductivity of two-phase systems. *Industrial and Engineering Chemistry Fundamentals*. 1974;13(1):17-20.
 - 109 Nielsen LE, Landel RF. *Mechanical Properties of Polymers and Composites*. New York: Marcel Dekker Inc.; 1994.
 - 110 Nielsen LE. Generalized equation for the elastic moduli of composite materials. *Journal of Applied Physics*. 1970;41(11):4626-4627.

- 111 Halpin JC, Kardos JL. The Halpin-Tsai equations: A review. *Polymer Engineering and Science*. 1976;16(5):344-352.
- 112 Agarwal BD, Broutman LJ. *Analysis and Performance of Fiber Composites*. New York: Wiley; 1980.
- 113 Mallick PK. *Composites Engineering Handbook*. New York: Marcel Dekker Inc.; 1997.
- 114 Halpin JC. Stiffness and expansion estimates for oriented short fiber composites. *Journal of Composite Materials*. 1969;3(4):732-734.
- 115 Salvétat JP, Kulik AJ, Bonard JM, Briggs GAD, Stockli T, Metenier K, Bonnamy S, Beguin F, Bunham NA, Forro L. Elastic modulus of ordered and disordered multiwalled carbon nanotubes. *Advanced Materials*. 1999;11(2):161-165.
- 116 Lu JP. Elastic properties of carbon nanotubes and nanoropes. *Physical Review Letters*. 1997;79(7):1297-1300.
- 117 Montgomery DC. *Design and Analysis of Experiments*. New York: John Wiley and Sons Inc.; 2001.



Figure A.2: Extruder Screw Design 2-9-09 used on 5-6-09 and 5-7-09

Table A.1: Extrusion Conditions: Lexan HF1130-111 with Hyperion Fibrils MB6015-00

Material Number	BLE	BQ2L	BQ3L	BQ4L
Extrusion Date	5-6-09	5-6-09	5-6-09	5-6-09
Extruder RPM	250	250	250	250
Motor Amperage, %	55	54	54	54
Specific Energy, kW/(kg/h)	0.705	0.692	0.692	0.692
Melt Temperature, °C	305	304	302	302
Melt Pressure, psig	0	0	0	0
#3 Feeder Setting, lb/hr	10	10	10	10
Material in Feeder #3	Lexan HF1130-111	Lexan HF1130-111 & MB6015-00	Lexan HF1130-111 & MB6015-00	Lexan HF1130-111 & MB6015-00
Vacuum Port	1 atm	1 atm	1 atm	1 atm
Feed Section Temperature	H ₂ O Cooled	H ₂ O Cooled	H ₂ O Cooled	H ₂ O Cooled
Zone 1 Temperature, °C	200	200	200	200
Zone 2 Temperature, °C	270	270	270	270
Zone 3 Temperature, °C	270	270	270	270
Zone 4 Temperature, °C	240	240	240	240
Zone 5 Temperature, °C	240	240	240	240
Zone 6 Temperature, °C	240	240	240	240
Zone 7 Temperature, °C	240	240	240	240
Zone 8 Temperature, °C	240	240	240	240
Zone 9 Temperature, °C	270	270	270	270
Zone 10 Temperature, °C	270	270	270	270
Die Type and Gap	3x3 mm	3x3 mm	3x3 mm	3x3 mm
Pelletizer Setting	Warm H ₂ O bath	Warm H ₂ O bath	Warm H ₂ O bath	Warm H ₂ O bath
Output Rate, lbs/hr	10	10	10	10

Table A.1 : Extrusion Conditions: Lexan HF1130-111 with Hyperion Fibrils MB6015-00 continued

Material Number	BQ5L	BQ6L	BQ8L
Extrusion Date	5-7-09	5-7-09	5-7-09
Extruder RPM	250	250	250
Motor Amperage, %	53	54.5	56
Specific Energy, kW/(kg/h)	0.679	0.699	0.718
Melt Temperature, °C	303	300	300
Melt Pressure, psig	0	0	0
#3 Feeder Setting, lb/hr	10	10	10
Material in Feeder #3	Lexan HF1130-111 & MB6015-00	Lexan HF1130-111 & MB6015-00	Lexan HF1130-111 & MB6015-00
Vacuum Port	1 atm	1 atm	1 atm
Feed Section Temperature	H ₂ O Cooled	H ₂ O Cooled	H ₂ O Cooled
Zone 1 Temperature, °C	200	200	200
Zone 2 Temperature, °C	270	270	270
Zone 3 Temperature, °C	270	270	270
Zone 4 Temperature, °C	240	240	240
Zone 5 Temperature, °C	240	240	240
Zone 6 Temperature, °C	240	240	240
Zone 7 Temperature, °C	240	240	240
Zone 8 Temperature, °C	240	240	240
Zone 9 Temperature, °C	270	270	270
Zone 10 Temperature, °C	270	270	270
Die Type and Gap	3x3 mm	3x3 mm	3x3 mm
Pelletizer Setting	Warm H ₂ O bath	Warm H ₂ O bath	Warm H ₂ O bath
Output Rate, lbs/hr	10	10	10

Notes:

- 1) Hyperion MB6015-00 dried 6 at 250F=121C Bry Air Dryer, stored in moisture barrier bags.
- 2) Lexan HF11301111 dried 12 hrs at 250F=121C Bry Air Dryer, stored in moisture barrier bags.
- 3) Extruded materials dried 12 hrs at 250F=121C Bry Air Dryer, stored in moisture barrier bags. 4) Lexan HF1130-111 and MB6015-00 mixed in V cone blender for 4 min at 24 rpm in 3.0 lb batches and then placed in Feeder 3.
- 5) Approximately 15 lbs of each extruded material was produced, except only 10 lbs of BLE (extruded Lexan HF1130-111) was made. Pelletizer ran well.
- 6) Feeder 3 helix: 0.5" open helix with end stub and 0.75" nozzle side discharge.
- 7) Extruder screw 2-9-09 design used.
- 8) Dyna- Purge E used at end of extrusion runs to clean out extruder on 5-6-09 and 5-7-09.
- 9) Specific energy is calculated using the equation shown below.

Leistriz
Micro 27mm / GL 40:1 L/D
Michigan Technological University 10/30/09





Figure A.4: Twin Screw Extruder Screw named 10-30-09

Table A.2: Extrusion Conditions: Lexan HF1130-111 with Ketjenblack EC-600 JD

Material Number	BLE2	BA2L	BA3L	BA4L
Extrusion Date	11-5-09	11-5-09	11-5-09	11-5-09
Extruder RPM	250	250	250	250
Motor Amperage, %	58	58	61	63
Specific Energy, kW/(kg/h)	0.743	0.743	0.781	0.807
Melt Temperature, °C	298	298	298	299
Melt Pressure, psig	0	0	30	60
#3 Feeder Setting, lb/hr	10	9.8	9.7	9.6
Material in Feeder #3	Lexan HF1130-111	Lexan HF1130-111	Lexan HF1130-111	Lexan HF1130-111
#4 Feeder Setting, lb/hr	0	0.2	0.3	0.4
Material in Feeder #4	Empty	Ketjenblack EC-600 JD	Ketjenblack EC-600 JD	Ketjenblack EC-600 JD
Zone 5 Side Stuffer, rpm	300	300	300	300
Feeder at Zone 5	Feeder 4	Feeder 4	Feeder 4	Feeder 4
Feed Section Temperature	H ₂ O Cooled	H ₂ O Cooled	H ₂ O Cooled	H ₂ O Cooled
Zone 1 Temperature, °C	200	200	200	200
Zone 2 Temperature, °C	270	270	270	270
Zone 3 Temperature, °C	270	270	270	270
Zone 4 Temperature, °C	240	240	240	240
Zone 5 Temperature, °C	240	240	240	240
Zone 6 Temperature, °C	240	240	240	240
Zone 7 Temperature, °C	240	240	240	240
Zone 8 Temperature, °C	240	240	240	240
Zone 9 Temperature, °C	270	270	270	270
Zone 10 Temperature, °C	270	270	270	270
Die Type and Gap	2 x 3 mm dia	2 x 3 mm dia	2 x 3 mm dia	2 x 3 mm dia
Pelletizer Setting	Warm H ₂ O bath	Warm H ₂ O bath	Warm H ₂ O bath	Warm H ₂ O bath
Output Rate, lbs/hr	10	10	10	10

Table A.2: Extrusion Conditions: Lexan HF1130-111 with Ketjenblack EC-600 JD continued

Material Number	BA5L	BA6L	BA8L	BA10L
Extrusion Date	11-11-09	11-11-09	11-11-09	11-11-09
Extruder RPM	250	250	250	250
Motor Amperage, %	65	68	74	82
Specific Energy, kW/(kg/h)	0.832	0.871	0.948	1.050
Melt Temperature, °C	299	297	296	294
Melt Pressure, psig	90	130	250	430
#3 Feeder Setting, lb/hr	9.5	9.4	9.2	9
Material in Feeder #3	Lexan HF1130-111	Lexan HF1130-111	Lexan HF1130-111	Lexan HF1130-111
#4 Feeder Setting, lb/hr	0.5	0.6	0.8	1.0
Material in Feeder #4	Ketjenblack EC-600 JD	Ketjenblack EC-600 JD	Ketjenblack EC-600 JD	Ketjenblack EC-600 JD
Zone 5 Side Stuffer, rpm	300	300	300	300
Feeder at Zone 5	Feeder 4	Feeder 4	Feeder 4	Feeder 4
Vacuum Port	1 atm	1 atm	1 atm	1 atm
Feed Section Temperature	H ₂ O Cooled	H ₂ O Cooled	H ₂ O Cooled	H ₂ O Cooled
Zone 1 Temperature, °C	200	200	200	200
Zone 2 Temperature, °C	270	270	270	270
Zone 3 Temperature, °C	270	270	270	270
Zone 4 Temperature, °C	240	240	240	240
Zone 5 Temperature, °C	240	240	240	240
Zone 6 Temperature, °C	240	240	240	240
Zone 7 Temperature, °C	240	240	240	240
Zone 8 Temperature, °C	240	240	240	240
Zone 9 Temperature, °C	270	270	270	270
Zone 10 Temperature, °C	270	270	270	270
Die Type and Gap	2 x 3 mm dia	2 x 3 mm dia	2 x 3 mm dia	2 x 3 mm dia
Pelletizer Setting	Warm H ₂ O bath	Warm H ₂ O bath	Warm H ₂ O bath	Warm H ₂ O bath
Output Rate, lbs/hr	10	10	10	10

Notes:

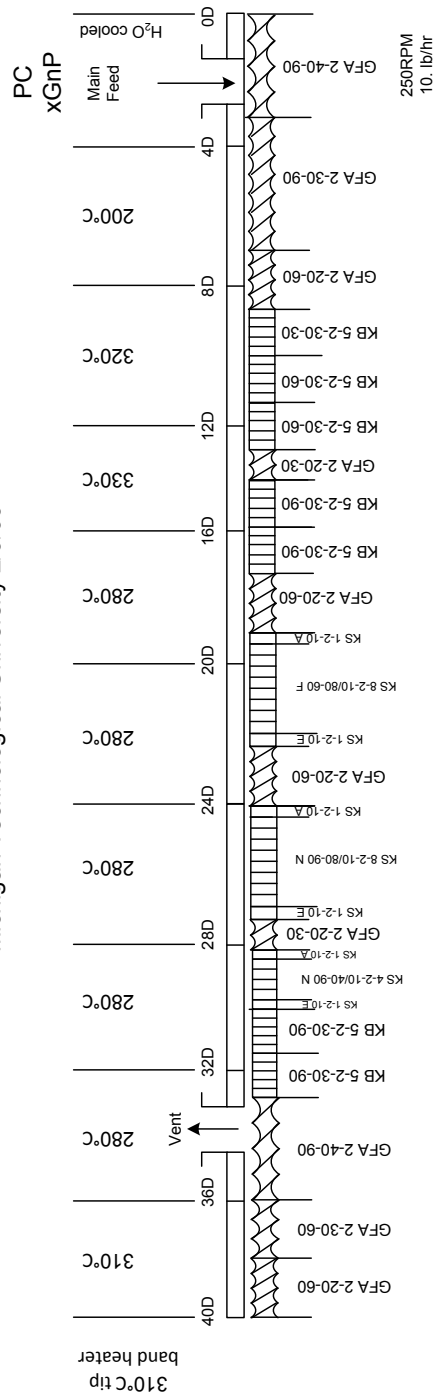
- 1) Ketjenblack EC-600 JD carbon black used as received.
- 2) Lexan HF1130-111 dried 12 hrs at 250°F=121°C Bry Air Dryer, stored in moisture barrier bags.
- 3) Extruded materials dried 12 hrs at 250°F=121°C Bry Air Dryer, stored in moisture barrier bags.
- 4) Approximately 13 lbs of each extruded material was produced, except only 10 lbs of BLE2 (extruded Lexan HF1130-111) was made. Pelletizer ran well.
- 5) Feeder 4 helix: 0.5" open helix with 0.75" vinyl nozzle and support and 40:1 gear ratio: for Ketjenblack EC-600 JD- ran on manual. Feeder 4 ran well. We got what we wanted as confirmed by pail and scale method and with AccuRate Scale reading vs. time on control panel.
- 6) Feeder 3 helix: 0.5" open helix with end stub and 0.75" nozzle side discharge: for Lexan – ran on automatic on loss in weight
- 7) Extruder screw 10-30-09 design used.
- 8) Dyna- Purge E used at end of extrusion runs to clean out extruder on 11-5-09 and 11-11-09.
- 9) Specific energy is calculated using the equation shown below.

Appendix A.3: Polycarbonate with Graphite Nanoplatelets

Leistritz

Micro 27mm / GL 40:1 L/D

Michigan Technological University 2/9/09



For Screw Type Elements

GFA-d-ee-ff

G = co-rotating

G = co-rotating
F = conveying

F = conveying

A = Free-Meshing

d = number of threads

ee = pitch (length in mill

ff = length of screw elements in millimeters

 l = length of screw elements in millimeters

Kneading Blocks

KBj-d-kk-II

KBj-U-KK-II
KB = kneading block

KB = kneading block
i = number of kneading segments

j = number of kneading
d = number of threads

d = number of threads
k = length of kneading block

k = length of kneading blocks in millimeters
 l = twisting angle ($^{\circ}$) of the individual kneading segments

 θ = twisting angle (°) of the individual kneading segments

Kneading Disks

KS1-d-hh-i

KS1-U-III-F
KS1 = Kneading disk

$KS1$ = Kheading disk
d = number of threads

d = number of threads

h = length of kneading disk in millimeter

Zones

0D to 4D is Zone 1

4D to 8D is Zone 2 and Heating Zone 1

4D to 8D is Zone 2 and Heating Zone 2
8D to 12D is Zone 3 and Heating Zone 2

8D to 12D is Zone 3 and Heating Zone 2
12D to 16D is Zone 4 and Heating Zone 3

12D to 16D is Zone 4 and Heating Zone 3

16D to 20D is Zone 5 and Heating Zone 4

20D to 24D is Zone 6 and Heating Zone 5

24D to 28D is Zone 7 and Heating Zone 6

28D to 32 D is Zone 8 and Heating Zone 7

32D to 36D is Zone 9 and Heating Zone 8

36D to 40D is Zone 10 and Heating Zone 9

Nozzle is Heating Zone

Figure A.5: Extruder Screw Design 2-9-09 used on 5-26-10 and 5-27-10

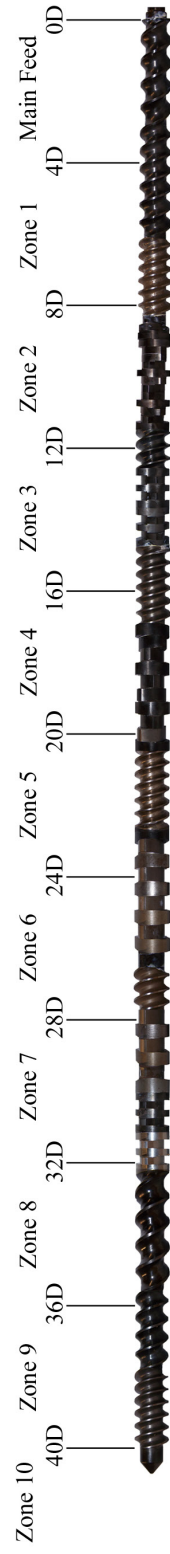


Figure A.6: Twin Screw Extruder Screw named 2-9-09

Table A.3: Extrusion Conditions: Lexan HF1130-111 with GNP

Material Number	BLE3	BG2L	BG3L	BG4L
Extrusion Date	5-26-10	5-26-10	5-26-10	5-26-10
Extruder RPM	250	250	250	250
Motor Amperage, %	64	63	63	63
Specific Energy, kW/(kg/h)	0.821	0.808	0.808	0.808
Melt Temperature, °C	300	299	298	294
Melt Pressure, psig	0	0	0	10
#3 Feeder Setting, lb/hr	10	10	10	10
Material in Feeder #3	Lexan HF1130-111	Lexan HF1130-111+ GP MB PC 1515A	Lexan HF1130-111+ GP MB PC 1515A	Lexan HF1130-111+ GP MB PC 1515A
Vacuum Port	1 atm	1 atm	1 atm	1 atm
Feed Section Temperature	H ₂ O Cooled	H ₂ O Cooled	H ₂ O Cooled	H ₂ O Cooled
Zone 1 Temperature, °C	200	200	200	200
Zone 2 Temperature, °C	270	270	270	270
Zone 3 Temperature, °C	270	270	270	270
Zone 4 Temperature, °C	240	240	240	240
Zone 5 Temperature, °C	240	240	240	240
Zone 6 Temperature, °C	240	240	240	240
Zone 7 Temperature, °C	240	240	240	240
Zone 8 Temperature, °C	240	240	240	240
Zone 9 Temperature, °C	270	270	270	270
Zone 10 Temperature, °C	265	265	265	265
Die Type and Gap	2 x 3 mm dia	2 x 3 mm dia	2 x 3 mm dia	2 x 3 mm dia
Pelletizer Setting	Warm H ₂ O bath @105F	Warm H ₂ O bath @105F	Warm H ₂ O bath @105F	Warm H ₂ O bath @105F
Output Rate, lbs/hr	10	10	10	10

Table A.3: Extrusion Conditions: Lexan HF1130-111 with GNP continued

Material Number	BG5L	BG6L	BG8L	BG10L
Extrusion Date	5-26-10	5-27-10	5-27-10	5-27-10
Extruder RPM	250	250	250	250
Motor Amperage, %	64	65	67	69
Specific Energy, kW/(kg/h)	0.821	0.834	0.860	0.885
Melt Temperature, °C	295	293	292	293
Melt Pressure, psig	30	50	70	90
#3 Feeder Setting, lb/hr	10	10	10	10
Material in Feeder #3	Lexan HF1130-111+ GP MB PC 1515A	Lexan HF1130-111+ GP MB PC 1515A	Lexan HF1130-111+ GP MB PC 1515A	Lexan HF1130-111+ GP MB PC 1515A
Vacuum Port	1 atm	1 atm	1 atm	1 atm
Feed Section Temperature	H ₂ O Cooled	H ₂ O Cooled	H ₂ O Cooled	H ₂ O Cooled
Zone 1 Temperature, °C	200	200	200	200
Zone 2 Temperature, °C	270	270	270	270
Zone 3 Temperature, °C	270	270	270	270
Zone 4 Temperature, °C	240	240	240	240
Zone 5 Temperature, °C	240	240	240	240
Zone 6 Temperature, °C	240	240	240	240
Zone 7 Temperature, °C	240	240	240	240
Zone 8 Temperature, °C	240	240	240	240
Zone 9 Temperature, °C	270	270	270	270
Zone 10 Temperature, °C	265	265	265	265
Die Type and Gap	2 x 3 mm dia	2 x 3 mm dia	2 x 3 mm dia	2 x 3 mm dia
Pelletizer Setting	Warm H ₂ O bath@105F	Warm H ₂ O bath @105F	Warm H ₂ O bath @105F	Warm H ₂ O bath @105F
Output Rate, lbs/hr	10	10	10	10

Notes:

- 1) The Ovation Extima™ GP MB PC 1515B (15wt% exfoliated graphene nanoplatelets from XG Sciences in polycarbonate) was dried in the Bry Air System indirect heated dehumidifying drying oven at 121°C (250°F) for 6 hours.
- 2) Lexan HF1130-111 dried 12 hrs at 250°F=121°C Bry Air Dryer, stored in moisture barrier bags.
- 3) Extruded materials dried 12 hrs at 250°F=121°C Bry Air Dryer, stored in moisture barrier bags.
- 4) Approximately 12 lbs of each extruded material was produced, except only 10 lbs of BLE3 (extruded Lexan HF1130-111) was made. Pelletizer ran well.
- 5) Feeder 3 helix: 0.5" open helix with end stub and 0.75" nozzle side discharge: ran on automatic on loss in weight on laptop.
- 6) Extruder screw 2-9-09 design used.
- 7) Dyna- Purge E used at end of extrusion runs to clean out extruder on 5-27-10.
- 8) Extruder was cleaned in sand bath before May 26, 2010 so started out with a totally clean extruder screw.
- 9) Per Sabic, keep T melt < 305C.
- 10) Specific energy is calculated using the equation shown below.

Appendix A.4: Polycarbonate with Multiple Fillers

Leistritz

Micro 27mm / GL 40:1 L/D

Michigan Technological University 2/9/09

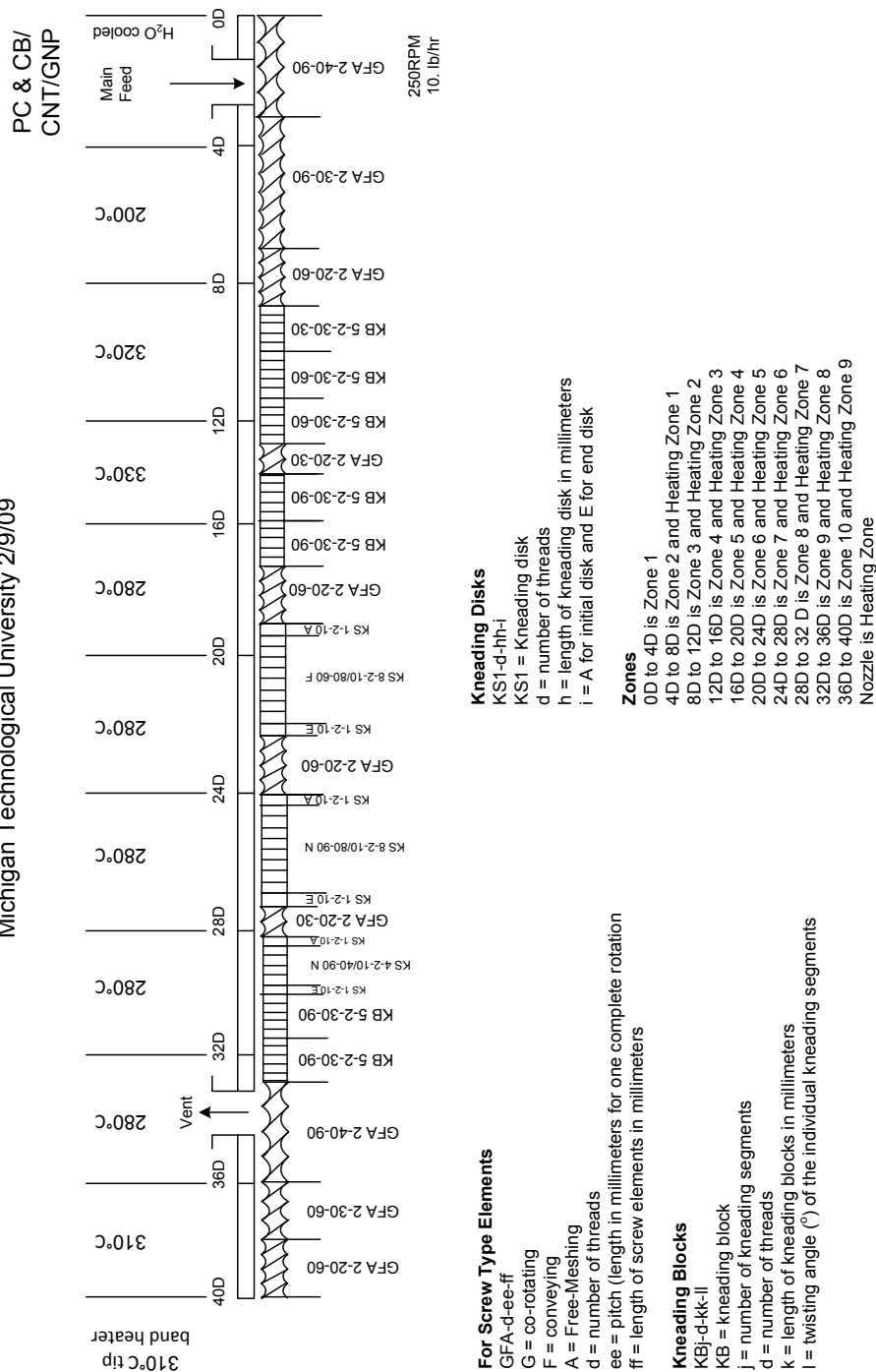


Figure A.7: Extruder Screw Design 2-9-09

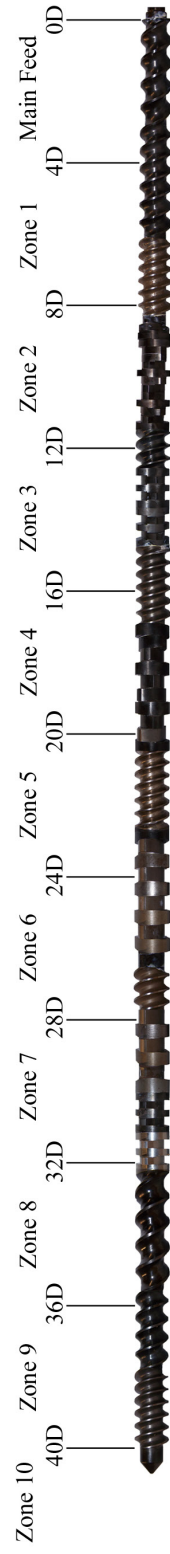


Figure A.8: Twin Screw Extruder Screw named 2-9-09

Table A.4: Extrusion Conditions: Lexan HF1130-111 with 8 wt% Ketjenblack EC-600 JD in Lexan HF1130-111 Masterbatch (extruder screw used = 10-30-09)

Material Number	BA8LR
Extrusion Date	4-14-10
Extruder RPM	250
Motor Amperage, %	71
Specific Energy, kW/(kg/h)	0.91
Melt Temperature, °C	296
Melt Pressure, psig	250
#3 Feeder Setting, lb/hr	9.2
Material in Feeder #3	Lexan HF1130-111
#4 Feeder Setting, lb/hr	0.8
Material in Feeder #4	Ketjenblack EC-600 JD
Vacuum Port	1 atm
Feed Section Temperature	H ₂ O Cooled
Zone 1 Temperature, °C	200
Zone 2 Temperature, °C	270
Zone 3 Temperature, °C	270
Zone 4 Temperature, °C	240
Zone 5 Temperature, °C	240
Zone 6 Temperature, °C	240
Zone 7 Temperature, °C	240
Zone 8 Temperature, °C	240
Zone 9 Temperature, °C	270
Zone 10 Temperature, °C	269
Die Type and Gap	2 x 3 mm dia
Pelletizer Setting	Warm H ₂ O bath @105F
Output Rate, lbs/hr	10

Notes:

- 1) The Ketjenblack EC-600 JD was used as received. The Ketjenblack EC-600 JD was used in Feeder 4 running on manual at 49%. New carbon black was placed in Feeder 4 on April 14, 2010 (nothing was left in the feeder 4 hopper before or after the extrusion run).
- 2) Feeder 4 used the 0.5" open helix with 0.75" vinyl nozzle and support (40:1 gear ratio).
- 3) Lexan HF1130-111 dried 12 hrs at 250°F=121°C Bry Air Dryer, stored in moisture barrier bags.
- 4) Extruded materials dried 12 hrs at 250°F=121°C Bry Air Dryer, stored in moisture barrier bags.
- 5) Approximately 60 lbs of BA8LR was produced. Pelletizer ran well.
- 6) Feeder 3 helix: 0.5" open helix with end stub and 0.75" nozzle side discharge: ran on automatic on loss in weight on laptop.
- 7) Extruder screw 10-30-09 design used.
- 8) Dyna- Purge E used at end of the extrusion run on April 14, 2010 to clean out extruder.
- 9) Extruder was cleaned in sand bath before April 14, 2010 so we started out with a totally clean extruder screw.
- 10) Per Sabic, keep T melt < 305C.
- 11) Specific energy is calculated using the equation shown below.

—

Table A.5: Extrusion Conditions: Lexan HF1130-111 Carbon Fillers for Factorial Design (extruder screw used = 2-9-09)

Material Number	BQ0.5L	BQ1L	BQ1G2L	BQ1G5L
Extrusion Date	6-30-10	6-30-10	7-1-10	7-1-10
Extruder RPM	250	250	250	250
Motor Amperage, %	60	60	60	64
Specific Energy, kW/(kg/h)	0.77	0.77	0.77	0.82
Melt Temperature, °C	301	301	302	301
Melt Pressure, psig	0	0	0	10
#3 Feeder Setting, lb/hr	10	10	10	10
Material in Feeder #3	Lexan HF1130-111+ MB 6015-00	Lexan HF1130-111+ MB 6015-00	Lexan HF1130-111+ GP MB PC 1515A + MB6015-00	Lexan HF1130-111+ GP MB PC 1515A + MB6015-00
Vacuum Port	1 atm	1 atm	1 atm	1 atm
Feed Section Temperature	H ₂ O Cooled	H ₂ O Cooled	H ₂ O Cooled	H ₂ O Cooled
Zone 1 Temperature, °C	200	200	200	200
Zone 2 Temperature, °C	270	270	270	270
Zone 3 Temperature, °C	270	270	270	270
Zone 4 Temperature, °C	240	240	240	240
Zone 5 Temperature, °C	240	240	240	240
Zone 6 Temperature, °C	240	240	240	240
Zone 7 Temperature, °C	240	240	240	240
Zone 8 Temperature, °C	240	240	240	240
Zone 9 Temperature, °C	270	270	270	270
Zone 10 Temperature, °C	268	268	265	265
Die Type and Gap	2 x 3 mm dia	2 x 3 mm dia	2 x 3 mm dia	2 x 3 mm dia
Pelletizer Setting	Warm H ₂ O bath @105F	Warm H ₂ O bath @105F	Warm H ₂ O bath @105F	Warm H ₂ O bath @105F
Output Rate, lbs/hr	10	10	10	10

Table A.5: Extrusion Conditions: Lexan HF1130-111 Carbon Fillers for Factorial Design (extruder screw used = 2-9-09)
continued

Material Number	BQ5G2L	BQ5G5L	BA2G2L	BA2G5L
Extrusion Date	7-1-10	7-1-10	7-6-10	7-6-10
Extruder RPM	250	250	250	250
Motor Amperage, %	58	61	67	71
Specific Energy, kW/(kg/h)	0.74	0.78	0.860	0.91
Melt Temperature, °C	301	299	299	299
Melt Pressure, psig	10	50	20	60
#3 Feeder Setting, lb/hr	10	10	10	10
Material in Feeder #3	Lexan HF1130-111+ GP MB PC 1515A+ MB6015-00	Lexan HF1130-111+ GP MB PC 1515A + MB6015-00	Lexan HF1130-111+ GP MB PC 1515A + BA8LR	Lexan HF1130-111+ GP MB PC 1515A + BA8LR
Vacuum Port	1 atm	1 atm	1 atm	1 atm
Feed Section Temperature	H ₂ O Cooled	H ₂ O Cooled	H ₂ O Cooled	H ₂ O Cooled
Zone 1 Temperature, °C	200	200	200	200
Zone 2 Temperature, °C	270	270	270	270
Zone 3 Temperature, °C	270	270	270	270
Zone 4 Temperature, °C	240	240	240	240
Zone 5 Temperature, °C	240	240	240	240
Zone 6 Temperature, °C	240	240	240	240
Zone 7 Temperature, °C	240	240	240	240
Zone 8 Temperature, °C	240	240	240	240
Zone 9 Temperature, °C	270	270	270	270
Zone 10 Temperature, °C	265	265	265	265
Die Type and Gap	2 x 3 mm dia	2 x 3 mm dia	2 x 3 mm dia	2 x 3 mm dia
Pelletizer Setting	Warm H ₂ O bath @105F	Warm H ₂ O bath @105F	Warm H ₂ O bath @105F	Warm H ₂ O bath @105F
Output Rate, lbs/hr	10	10	10	10

Table A.5: Extrusion Conditions: Lexan HF1130-111 Carbon Fillers for Factorial Design (extruder screw used = 2-9-09)
continued

Material Number	BA5G2L	BA5G5L	BA2Q1L	BA2Q5L
Extrusion Date	7-6-10	7-6-10	7-6-10	7-7-10
Extruder RPM	250	250	250	250
Motor Amperage, %	80	83	60	61
Specific Energy, kW/(kg/h)	1.03	1.06	0.77	0.78
Melt Temperature, °C	299	297	300	302
Melt Pressure, psig	110	170	0	10
#3 Feeder Setting, lb/hr	10	10	10	10
Material in Feeder #3	Lexan HF1130-111+ GP MB PC 1515A+ BA8LR	Lexan HF1130-111+ GP MB PC 1515A+ BA8LR	Lexan HF1130-111 + BA8LR + MB6015-00	Lexan HF1130-111+ BA8LR+MB6015-00
Vacuum Port	1 atm	1 atm	1 atm	1 atm
Feed Section Temperature	H2O Cooled	H2O Cooled	H2O Cooled	H2O Cooled
Zone 1 Temperature, °C	200	200	200	200
Zone 2 Temperature, °C	270	270	270	270
Zone 3 Temperature, °C	270	270	270	270
Zone 4 Temperature, °C	240	240	240	240
Zone 5 Temperature, °C	240	240	240	240
Zone 6 Temperature, °C	240	240	240	240
Zone 7 Temperature, °C	240	240	240	240
Zone 8 Temperature, °C	240	240	240	240
Zone 9 Temperature, °C	270	270	270	270
Zone 10 Temperature, °C	265	265	265	265
Die Type and Gap	2 x 3 mm dia Warm H2O bath @105F	2 x 3 mm dia Warm H2O bath @105F	2 x 3 mm dia Warm H2O bath @105F	2 x 3 mm dia Warm H2O bath @105F
Pelletizer Setting				
Output Rate, lbs/hr	10	10	10	10

Table A.5: Extrusion Conditions: Lexan HF1130-111 Carbon Fillers for Factorial Design (extruder screw used = 2-9-09)
continued

Material Number	BA5Q1L	BA5Q5L	BA2LR	BA5LR
Extrusion Date	7-7-10	7-7-10	7-7-10	7-8-10
Extruder RPM	250	250	250	250
Motor Amperage, %	72	75	63	78
Specific Energy, kW/(kg/h)	0.92	0.96	0.81	1.00
Melt Temperature, °C	305	302	306	305
Melt Pressure, psig	20	130	0	80
#3 Feeder Setting, lb/hr	10	10	10	10
Material in Feeder #3	Lexan HF1130-111+ BA8LR + MB6015-00	Lexan HF1130-111+ BA8LR + MB6015-00	Lexan HF1130-111+ BA8LR	Lexan HF1130-111+ BA8LR
Vacuum Port	1 atm	1 atm	1 atm	1 atm
Feed Section Temperature	H2O Cooled	H2O Cooled	H2O Cooled	H2O Cooled
Zone 1 Temperature, °C	200	200	200	200
Zone 2 Temperature, °C	270	270	270	270
Zone 3 Temperature, °C	270	270	270	270
Zone 4 Temperature, °C	240	240	240	240
Zone 5 Temperature, °C	240	240	240	240
Zone 6 Temperature, °C	240	240	240	240
Zone 7 Temperature, °C	240	240	240	240
Zone 8 Temperature, °C	240	240	240	240
Zone 9 Temperature, °C	270	270	270	270
Zone 10 Temperature, °C	265	265	257	257
Die Type and Gap	2 x 3 mm dia	2 x 3 mm dia	2 x 3 mm dia	2 x 3 mm dia
Pelletizer Setting	Warm H2O bath@105F	Warm H2O bath @105F	Warm H2O bath @105F	Warm H2O bath @105F
Output Rate, lbs/hr	10	10	10	10

Table A.5: Extrusion Conditions: Lexan HF1130-111 Carbon Fillers for Factorial Design (extruder screw used = 2-9-09)
continued

Material Number	BQ5LR	BG12L	BG15L
Extrusion Date	6-30-10	7-8-10	7-8-10
Extruder RPM	250	250	250
Motor Amperage, %	56	71	75
Specific Energy, kW/(kg/h)	0.72	0.91	0.96
Melt Temperature, °C	300	305	305
Melt Pressure, psig	0	70	90
#3 Feeder Setting, lb/hr	10	10	10
Material in Feeder #3	Lexan HF1130-111+ MB 6015-00	Lexan HF1130-111+ GP MB PC 1515A	Lexan HF1130-111+ GP MB PC 1515A
Vacuum Port	1 atm	1 atm	1 atm
Feed Section Temperature	H2O Cooled	H2O Cooled	H2O Cooled
Zone 1 Temperature, °C	200	200	200
Zone 2 Temperature, °C	270	270	270
Zone 3 Temperature, °C	270	270	270
Zone 4 Temperature, °C	240	240	240
Zone 5 Temperature, °C	240	240	240
Zone 6 Temperature, °C	240	240	240
Zone 7 Temperature, °C	240	240	240
Zone 8 Temperature, °C	240	240	240
Zone 9 Temperature, °C	270	270	270
Zone 10 Temperature, °C	268	257	256
Die Type and Gap	2 x 3 mm dia	2 x 3 mm dia	2 x 3 mm dia
Pelletizer Setting	Warm H2O bath @105F	Warm H2O bath @105F	Warm H2O bath @105F
Output Rate, lbs/hr	10	10	10

Notes:

- 1) The Ovation Extima™ GP MB PC 1515B (15wt% exfoliated graphene nanoplatelets from XG Sciences in polycarbonate, 5 micron diameter) was dried in the Bry Air System indirect heated dehumidifying drying oven at 121°C (250°F) for 6 hours. The Hyperion Fibrils MB6015-00 was the Bry Air System indirect heated dehumidifying drying oven at 121°C (250°F) for 6 hours. The BA8LR masterbatch made on 4-14-10 at MTU was dried in the Bry Air System indirect heated dehumidifying drying oven at 121°C (250°F) for 12 hours. The materials were premixed in a V cone mixer at 24 rpm for 4 min in 3 lb batches prior to adding to Zone 1.
- 2) Lexan HF1130-111 dried 12 hrs at 250°F=121°C Bry Air Dryer, stored in moisture barrier bags.
- 3) Extruded materials dried 12 hrs at 250°F=121°C Bry Air Dryer, stored in moisture barrier bags.
- 4) Approximately 12 lbs of each extruded material was produced. Pelletizer ran well.
- 5) Feeder 3 helix: 0.5" open helix with end stub and 0.75" nozzle side discharge: ran on automatic on loss in weight on laptop.
- 6) Extruder screw 2-9-09 design used.
- 7) Dyna- Purge E used at end of extrusion runs to clean out extruder on 5-27-10.
- 8) Extruder was cleaned in sand bath before 6-30-2009 so started out with a totally clean extruder screw.
- 9) Per Sabic, keep T melt < 305C.
- 10) Between each 'family' of materials, the extruder screw was purged with DynaPurge E, and then pulled out and cleaned with a wire brush.
- 11) Specific energy is calculated using the equation shown below.

Appendix B: Injection Molding Run Conditions

Appendix B.1: Polycarbonate with Carbon Nanotubes

Table B.1: Injection Molding Conditions for CNT/PC Composites

Notation	Injection Molding Conditions	BL	BLE	BQ2L	BQ3L
T _{mold}	Mold Temperature (F)	190	190	190	190
E1	Zone 1 Temperature (F) (nozzle)	580	580	580	580
E2	Zone 2 Temperature (F)	570	570	570	570
E3	Zone 3 Temperature (F)	554	554	554	554
E4	Zone 4 Temperature (F) (feed zone)	536	536	536	536
P1	Injection pressure (psi)	15,827	15,827	15,827	15,827
P2	Hold Pressure (psi)	15,827	15,827	15,827	15,827
P7	Back Pressure (psi)	45.22	45.22	45.22	45.22
S1	Shot size (mm)	40	40	40	40
S2	Pullback before (mm)	2.5	2.5	2.5	2.5
S3	Pullback after (mm)	5	5	5	5
S6	Width of mold (mm)	196	196	196	196
S8	Screw Position to Switch from P1 to P2 (mm)	15	15	15	15
T1	Injection Time (s)	15	15	15	15
T2	Cool Time (s)	25	25	25	25
T3	Interval Time (s)	2	2	2	2
T6	Retraction Time (s)	0	0	0	0
T7	Nozzle Retraction Delay Time (s)	0	0	0	0
T8	Injection Delay Time (s)	0	0	0	0
T9	Charge Delay Time (s)	0	0	0	0
V1	Injection Velocity (in ³ /s)	3.732	3.732	3.732	3.732
V6	Screw Rotation (rpm)	60	60	60	60
V9	Retraction Velocity (%)	25	25	25	25
V10	Advance Velocity (%)	90	90	90	90
V11	Retraction Velocity (%)	90	90	90	90
CF	Clamp Force (US tons)	80	80	80	80

Table B.1: Injection Molding Conditions for CNT/PC Composites continued

Notation	Injection Molding Conditions	BQ4L	BQ5L	BQ6L	BQ8L
T _{mold}	Mold Temperature (F)	190	190	190	190
E1	Zone 1 Temperature (F) (nozzle)	580	580	580	600
E2	Zone 2 Temperature (F)	570	570	570	600
E3	Zone 3 Temperature (F)	554	554	554	570
E4	Zone 4 Temperature (F) (feed zone)	536	536	536	550
P1	Injection pressure (psi)	15,827	18,088	20,349	22,383
P2	Hold Pressure (psi)	15,827	15,827	15,827	15,827
P7	Back Pressure (psi)	45.22	45.22	45.22	45.22
S1	Shot size (mm)	40	40	45	47
S2	Pullback before (mm)	2.5	2.5	0	0
S3	Pullback after (mm)	5	5	0	0
S6	Width of mold (mm)	196	196	196	196
S8	Screw Position to Switch from P1 to P2 (mm)	15	15	15	15
T1	Injection Time (s)	15	15	15	15
T2	Cool Time (s)	25	25	25	25
T3	Interval Time (s)	2	2	2	2
T6	Retraction Time (s)	0	0	0	0
T7	Nozzle Retraction Delay Time (s)	0	0	0	0
T8	Injection Delay Time (s)	0	0	0	0
T9	Charge Delay Time (s)	0	0	0	0
V1	Injection Velocity (in ³ /s)	3.732	3.732	3.732	3.732
V6	Screw Rotation (rpm)	60	60	60	60
V9	Retraction Velocity (%)	25	25	25	25
V10	Advance Velocity (%)	90	90	90	90
V11	Retraction Velocity (%)	90	90	90	90
CF	Clamp Force (US tons)	80	80	80	80

Notes:

For all formulations, about 30 2.5” diameter disks, 30 tensile bars, and 30 flexural bars molded.

After each formulation, the feed hopper was run until it was empty and no material was in screw. Then we discarded 5 transition shots, and then started collecting the next formulation.

Appendix B.2: Polycarbonate with Carbon Black

Table B.2: Injection Molding Conditions for CB/PC Composites

Notation	Injection Molding Conditions	BL2 12-4-09†	BLE2 12-4-09†	BA2L 12-4-09†	BA3L 12-4-09†
T _{mold}	Mold Temperature (F)	160	160	160	160
E1	Zone 1 Temperature (F) (nozzle)	610	610	610	610
E2	Zone 2 Temperature (F)	570	570	570	570
E3	Zone 3 Temperature (F)	554	554	554	554
E4	Zone 4 Temperature (F) (feed zone)	536	536	536	536
P1	Injection pressure (psi)	70% = 15,827	70% = 15,827	70% = 15,827	70% = 15,827
P2	Hold Pressure (psi)	55% = 12,436	55% = 12,436	55% = 12,436	55% = 12,436
P7	Back Pressure (psi)	0.2% = 45.2	0.2% = 45.2	0.2% = 45.2	0.2% = 45.2
S1	Shot size (mm)	20	20	20	20
S2	Pullback before (mm)	0	0	0	0
S3	Pullback after (mm)	0.1	0.1	0.1	0.1
S6	Width of mold (mm)	202	202	202	202
S8	Screw Position to Switch from P1 to P2 (mm)	8 for tensile, 10 for flex, 12 for disk	8 for tensile, 10 for flex, 12 for disk	8 for tensile, 10 for flex, 12 for disk	8 for tensile, 10 for flex, 12 for disk
T1	Injection Time (s)	9	9	9	9
T2	Cool Time (s)	20	20	20	20
T3	Interval Time (s)	0.5	0.5	0.5	0.5
T6	Retraction Time (s)	0	0	0	0
T7	Nozzle Retraction Delay Time (s)	0	0	0	0
T8	Injection Delay Time (s)	0	0	0	0
T9	Charge Delay Time (s)	0	0	0	0
V1	Injection Velocity (in ³ /s)	30% = 1.866	30% = 1.866	30% = 1.866	30% = 1.866
V6	Screw Rotation (rpm)	19% = 60	19% = 60	19% = 60	19% = 60
V9	Retraction Velocity (%)	20	20	20	20
V10	Advance Velocity (%)	90	90	90	90
V11	Retraction Velocity (%)	90	90	90	90
CF	Clamp Force (US tons)	80	80	80	80

Table B.2: Injection Molding Conditions for CB/PC Composites continued

Notation	Injection Molding Conditions	BL2 12-4-09+	BLE2 12-4-09+	BA2L 12-4-09+	BA3L 12-4-09+
P-5-1	Inj Start, mm	--	--	--	--
P-5-1	Cushion, mm	--	--	--	--
P-5-1	P1 → P2 Fill time, sec	--	--	--	--
P-5-1	P1 Actual Pressure, %	--	--	--	--
P-5-1	Charge time, sec	--	--	--	--

Table B.2: Injection Molding Conditions for CB/PC Composites continued

Notation	Injection Molding Conditions	BA4L 12-4-09†	BA5L 12-4-09†	BA6L 12-4-09†	BA8L 12-4-09†	BA10L 12-4-09†
T _{mold}	Mold Temperature (F)	160	160	160	180	200
E1	Zone 1 Temperature (F) (nozzle)	610	610	610	610	630
E2	Zone 2 Temperature (F)	570	570	570	580	630
E3	Zone 3 Temperature (F)	554	554	554	570	610
E4	Zone 4 Temperature (F) (feed zone)	536	536	536	560	610
P1	Injection pressure (psi)	75% = 16,958	75% = 16,958	80% = 18,088	90% = 20,349	99% = 22,384
P2	Hold Pressure (psi)	55% = 12,436	55% = 12,436	55% = 12,436	55% = 12,436	55% = 12,436
P7	Back Pressure (psi)	0.2% = 45.2	0.2% = 45.2	0.2% = 45.2	0.5% = 113	0.5% = 113
S1	Shot size (mm)	20	20	20	20 flex and disk, 22 tensile	22 flex and tensile, 20 disk
S2	Pullback before (mm)	0	0	0	0	0
S3	Pullback after (mm)	0.1	0.1	0.1	0.1	0.1
S6	Width of mold (mm)	202	202	202	202	202
S8	Screw Position to Switch from P1 to P2 (mm)	8 for tensile, 10 for flex, 12 for disk	8 for tensile, 10 for flex, 12 for disk	8 for tensile, 10 for flex, 12 for disk	7 for tensile, 10 for flex, 12 for disk	12 for tensile, 14 for flex, 18 for disk
T1	Injection Time (s)	8*	8*	8*	8*	8*
T2	Cool Time (s)	16*	16*	16*	16*	16*
T3	Interval Time (s)	0.1*	0.1*	0.1*	0.1*	0.1*
T6	Retraction Time (s)	0	0	0	0	0
T7	Nozzle Retraction Delay Time (s)	0	0	0	0	0
T8	Injection Delay Time (s)	0	0	0	0	0
T9	Charge Delay Time (s)	0	0	0	0	0
V1	Injection Velocity (in ³ /s)	30% = 1.866	30% = 1.866	10% = 0.622	10% = 0.622	10% = 0.622
V6	Screw Rotation (rpm)	19% = 60	19% = 60	19% = 60	19% = 60	19% = 60
V9	Retraction Velocity (%)	20	20	20	20	20
V10	Advance Velocity (%)	90	90	50	50	50
V11	Retraction Velocity (%)	90	90	90	90	90

Table B.2: Injection Molding Conditions for CB/PC Composites continued

Notation	Injection Molding Conditions	BA4L 12-4-09†	BA5L 12-4-09†	BA6L 12-4-09†	BA8L 12-4-09†	BA10L 12-4-09†
CF	Clamp Force (US tons)	80	80	80	80	80
P-5-1	Inj Start, mm	21	20.8 tensile 20.8 flex 20.9 disk	21 tensile 21 flex 20.9 disk	22.5 tensile 20.1 flex 20.3 disk	22.1 tensile 22.1 flex 20.1 disk
P-5-1	Cushion, mm	2.5	2.1 tensile 3.9 flex 3.1 disk	2.3 tensile 4 flex 3.2 disk	3.9 tensile 3.0 flex 2.8 disk	2.0 tensile 2.0 flex 2.0 disk
P-5-1	P1 → P2 Fill time, sec	0.75	1.0 tensile 0.65 flex 0.56 disk	2.4 tensile 2.1 flex 1.7 disk	2.81 tensile 1.94 flex 1.6 disk	1.81 tensile 1.53 flex 0.56 disk
P-5-1	P1 Actual Pressure, %	68	60 tensile 60 flex 48 disk	57 tensile 47 flex 36 disk	86 tensile 51 flex 38 disk	48 tensile 39 flex 17 disk
P-5-1	Charge time, sec	3.3	3.3 tensile 2.9 flex 3.0 disk	3.4 tensile 3.4 flex 3.3 disk	3.7 tensile 3.5 flex 3.4 disk	3.6 tensile 3.2 flex 3.4 disk

Notes:

- 1) For all formulations, about 30 2.5" diameter disks, 30 tensile bars, and 30 flexural bars molded. Each sample was individually molded. The injection molding machine ran on the fully automatic mode all day on Dec 4, 2009.
- 2) After each formulation, the feed hopper was run until it was empty and no material was in screw. Then we discarded 5 transition shots, and then started collecting the next formulation.
- 3) *Can use for T1= injection time= 8 seconds, T2= Cool time= 16 seconds, and T3= time between shots=0.1 seconds for all inj molding done on Dec 4, 2009. This reduces cycle time.
- 4) Did not record P-5-1 values until started BA4L formulation.
- 5) Formulation BA10L did not mold 'pretty samples' but it was the best we could do. Formulation is too viscous.
- 6) Formulation BA8L was starting to get much more viscous too. We had to make several temperature changes, etc.
- 7) † is injection molding date

Appendix B.3: Polycarbonate with Graphite Nanoplatelets

Table B.3: Injection Molding conditions for GNP/PC composites

Notation	Injection Molding Conditions	BL3	BLE3	BG2L	BG3L	BG4L
T _{mold}	Mold Temperature (F)	160	160	160	160	160
E1	Zone 1 Temperature (F) (nozzle)	610	610	610	610	610
E2	Zone 2 Temperature (F)	570	570	570	570	570
E3	Zone 3 Temperature (F)	554	554	554	554	554
E4	Zone 4 Temperature (F) (feed zone)	536	536	536	536	536
P1	Injection pressure (psi)	70% = 15,827	70% = 15,827	70% = 15,827	70% = 15,827	70% = 15,827
P2	Hold Pressure (psi)	55% = 12,436	55% = 12,436	55% = 12,436	55% = 12,436	55% = 12,436
P7	Back Pressure (psi)	0.2% = 45.2	0.2% = 45.2	0.2% = 45.2	0.2% = 45.2	0.2% = 45.2
S1	Shot size (mm)	20	20	20	20	20
S2	Pullback before (mm)	0	0	0	0	0
S3	Pullback after (mm)	0.1	0.1	0.1	0.1	0.1
S6	Width of mold (mm)	202	202	202	202	202
S8	Screw Position to Switch from P1 to P2 (mm)	8 for tensile, 10 for flex, 12 for disk	8 for tensile, 10 for flex, 12 for disk	8 for tensile, 10 for flex, 12 for disk	8 for tensile, 10 for flex, 12 for disk	8 for tensile, 10 for flex, 12 for disk
T1	Injection Time (s)	8	8	8	8	8
T2	Cool Time (s)	16	16	16	16	16
T3	Interval Time (s)	0.1	0.1	0.1	0.1	0.1
T6	Retraction Time (s)	0	0	0	0	0
T7	Nozzle Retraction Delay Time (s)	0	0	0	0	0
T8	Injection Delay Time (s)	0	0	0	0	0
T9	Charge Delay Time (s)	0	0	0	0	0
V1	Injection Velocity (in ³ /s)	30% = 1.866	30% = 1.866	30% = 1.866	30% = 1.866	30% = 1.866
V6	Screw Rotation (rpm)	19% = 60	19% = 60	19% = 60	19% = 60	19% = 60
V9	Retraction Velocity (%)	20	20	20	20	20
V10	Advance Velocity (%)	50	50	50	50	50
V11	Retraction Velocity (%)	90	90	90	90	90

Table B.3: Injection Molding conditions for GNP/PC composites continued

Notation	Injection Molding Conditions	BL3	BLE3	BG2L	BG3L	BG4L
CF	Clamp Force (US tons)	80	80	80	80	80
P-5-1	Actual Cycle Time, sec	30.6 tensile 30.6 flex 30.8 disk	30.9 tensile 30.9 flex 31.0 disk	31.1 tensile 31.1 flex 31.1 disk	31.3 tensile 31.1 flex 31.1 disk	31.5 tensile 31.5 flex 31.5 disk
P-5-1	Inj Start, mm	20.1 tensile 20.1 flex 20.2 disk	20.3 tensile 20.7 flex 20.7 disk	20.3 tensile 20.8 flex 20.9 disk	20.8 tensile 20.8 flex 20.9 disk	20.8 tensile 20.8 flex 20.9 disk
P-5-1	Cushion, mm	1.2 tensile 3.0 flex 2.0 disk	1.9 tensile 3.6 flex 2.2 disk	1.5 tensile 3.8 flex 2.9 disk	2.2 tensile 3.9 flex 3.3 disk	2.1 tensile 3.9 flex 3.1 disk
P-5-1	P1 → P2 Fill time, sec	0.68 tensile 0.58 flex 0.48 disk	0.70 tensile 0.60 flex 0.48 disk	0.68 tensile 0.61 flex 0.53 disk	0.70 tensile 0.63 flex 0.55 disk	0.70 tensile 0.66 flex 0.51 disk
P-5-1	P1 Actual Pressure P1 → P2, kg/cm ²	52 tensile 46 flex 36 disk	55 tensile 49 flex 40 disk	57 tensile 51 flex 40 disk	61 tensile 60 flex 58 disk	63 tensile 61 flex 50 disk
P-5-1	Charge time, sec	4.1 tensile 3.3 flex 3.5 disk	3.4 tensile 3.1 flex 3.5 disk	3.6 tensile 3.2 flex 3.3 disk	4.0 tensile 3.6 flex 3.5 disk	4.0 tensile 4.0 flex 4.0 disk
P-5-1	Injection Peak Pressure P1, kg/cm ²	--	--	--	83 tensile	99 tensile 96 flex 50 disk

Table B.3: Injection Molding conditions for GNP/PC composites continued

Notation	Injection Molding Conditions	BG5L	BG6L	BG8L	BG10L
T _{mold}	Mold Temperature (F)	160	160	180	200
E1	Zone 1 Temperature (F) (nozzle)	610	620	Tensile 630 Flex, disk 620	630
E2	Zone 2 Temperature (F)	Tensile 580 Flex, disk 570	590	Tensile 630 Flex, disk 590	630
E3	Zone 3 Temperature (F)	554	570	Tensile 600 Flex, disk 570	610
E4	Zone 4 Temperature (F) (feed zone)	536	536	Tensile 550 Flex, disk 536	550
P1	Injection pressure (psi)	70% =15,827	75% =16,958	Tensile 90% =20,349 Flex, disks 75%=16,958	99% =22,384
P2	Hold Pressure (psi)	55% = 12,436	55% = 12,436	55% = 12,436	55% = 12,436
P7	Back Pressure (psi)	0.2% = 45.2	0.5% = 113	0.5% = 113	0.5% = 113
S1	Shot size (mm)	20	20	20	20
S2	Pullback before (mm)	0	0	0	0
S3	Pullback after (mm)	0.1	0.1	0.1	0.1
S6	Width of mold (mm)	202	202	202	202
S8	Screw Position to Switch from P1 to P2 (mm)	8 for tensile, 10 for flex, 12 for disk	8 for tensile, 10 for flex, 12 for disk	8 for tensile, 10 for flex, 12 for disk	8 for tensile, 10 for flex, 12 for disk
T1	Injection Time (s)	8	8	8	8
T2	Cool Time (s)	16	16	16	16
T3	Interval Time (s)	0.1	0.1	0.1	0.1
T6	Retraction Time (s)	0	0	0	0
T7	Nozzle Retraction Delay Time (s)	0	0	0	0
T8	Injection Delay Time (s)	0	0	0	0
T9	Charge Delay Time (s)	0	0	0	0
V1	Injection Velocity (in ³ /s)	30% = 1.866	30% = 1.866	Tensile 10% = 0.622 Flex, disk 30% =1.866	10% = 0.622
V6	Screw Rotation (rpm)	19% = 60	19% = 60	19% = 60	19% = 60
V9	Retraction Velocity (%)	20	20	20	20

Table B.3: Injection Molding conditions for GNP/PC composites continued

Notation	Injection Molding Conditions	BG5L	BG6L	BG8L	BG10L
V10	Advance Velocity (%)	50	50	50	50
V11	Retraction Velocity (%)	90	90	90	90
CF	Clamp Force (US tons)	80	80	80	80
P-5-1	Actual Cycle Time, sec	30.4 tensile 31.8 flex 31.6 disk	30.7 tensile 30.6 flex 30.6 disk	30.5 tensile 30.7 flex 30.6 disk	30.7 tensile 30.4 flex 30.4 disk
P-5-1	Inj Start, mm	20.8 tensile 20.8 flex 20.9 disk	20.5 tensile 20.7 flex 20.6 disk	20.9 tensile 20.9 flex 20.9 disk	20.7 tensile 20.7 flex 20.7 disk
P-5-1	Cushion, mm	2.1 tensile 3.9 flex 3.1 disk	2.1 tensile 3.5 flex 2.9 disk	1.6 tensile 3.8 flex 2.8 disk	1.6 tensile 3.3 flex 2.5 disk
P-5-1	P1 → P2 Fill time, sec	1.0 tensile 0.65 flex 0.56 disk	0.70 tensile 0.61 flex 0.51 disk	2.0 tensile 0.6 flex 0.51 disk	1.99 tensile 1.70 flex 1.41 disk
P-5-1	P1 Actual Pressure P1 → P2, kg/cm ²	60 tensile 60 flex 48 disk	57 tensile 46 flex 39 disk	34 tensile 50 flex 42 disk	35 tensile 29 flex 22 disk
P-5-1	Charge time, sec	3.3 tensile 2.9 flex 3.0 disk	3.8 tensile 3.2 flex 3.4 disk	3.2 tensile 3.2 flex 3.2 disk	3.1 tensile 2.8 flex 2.9 disk
P-5-1	Injection Peak Pressure P1, kg/cm ²	98 tensile 56 flex 46 disk	57 tensile 46 flex 39 disk	34 tensile 50 flex 42 disk	35 tensile 29 flex 22 disk

Notes:

- 1) For all formulations, about 30 2.5" diameter disks, 30 tensile bars, and 20 flexural bars molded. Each sample was individually molded. The injection molding machine ran on the fully automatic mode.
- 2) After each formulation, the feed hopper was run until it was empty and no material was in screw. Then we discarded 5 transition shots, and then started collecting the next formulation.
- 3) If injection mold again, try different conditions for BG5L and BG6L. Maybe increase P1 to 90%, etc.

Appendix B.4: Polycarbonate with Multiple Fillers

Table B.4: Injection Molding Conditions for Combinations in PC

Notation	Injection Molding Conditions	BL4	BQ0.5L	BQ1L
T _{mold}	Mold Temperature (F)	160	160	160
E1	Zone 1 Temperature (F) (nozzle)	610	610	610
E2	Zone 2 Temperature (F)	570	570	570
E3	Zone 3 Temperature (F)	554	554	554
E4	Zone 4 Temperature (F) (feed zone)	536	536	536
P1	Injection pressure (psi)	70% = 15,827	70% = 15,827	70% = 15,827
P2	Hold Pressure (psi)	55% = 12,436	55% = 12,436	55% = 12,436
P7	Back Pressure (psi)	0.2% = 45.2	0.2% = 45.2	0.2% = 45.2
S1	Shot size (mm)	20	20	20
S2	Pullback before (mm)	0	0	0
S3	Pullback after (mm)	0.1	0.1	0.1
S6	Width of mold (mm)	202	202	202
S8	Screw Position to Switch from P1 to P2 (mm)	8 for tensile, 10 for flex, 12 for disk	8 for tensile, 10 for flex, 12 for disk	8 for tensile, 10 for flex, 12 for disk
T1	Injection Time (s)	8	8	8
T2	Cool Time (s)	16	16	16
T3	Interval Time (s)	0.1	0.1	0.1
T6	Retraction Time (s)	0	0	0
T7	Nozzle Retraction Delay Time (s)	0	0	0
T8	Injection Delay Time (s)	0	0	0
T9	Charge Delay Time (s)	0	0	0
V1	Injection Velocity (in ³ /s)	30% = 1.866	20% for disk, 30% for rest	20% for disk, 30% = 1.866 for tensile, flex
V6	Screw Rotation (rpm)	19% = 60	19% = 60	19% = 60
V9	Retraction Velocity (%)	20	20	20
V10	Advance Velocity (%)	50	50	50
V11	Retraction Velocity (%)	90	90	90
CF	Clamp Force (US tons)	80	80	80

Table B.4: Injection Molding Conditions for Combinations in PC continued

Notation	Injection Molding Conditions	BL4	BQ0.5L	BQ1L
P-5-1	Actual Cycle Time, sec	30.8 tensile 30.8 flex 30.1 disk	30.9 tensile 30.9 flex 31.0 disk	31.1 tensile 31.1 flex 31.1 disk
P-5-1	Inj Start, mm	20.1 tensile 20.1 flex 20.1 disk	20.7 tensile 20.5 flex 20.4 disk	20.8 tensile 20.8 flex 20.9 disk
P-5-1	Cushion, mm	1.3 tensile 3.0 flex 2.0 disk	1.6 tensile 3.3 flex 2.9 disk	1.9 tensile 3.8 flex 2.9 disk
P-5-1	P1 → P2 Fill time, sec	0.68 tensile 0.58 flex 0.50 disk	0.70 tensile 0.60 flex 0.73 disk	0.68 tensile 0.61 flex 0.73 disk
P-5-1	P1 Actual Pressure P1 → P2, kg/cm ²	73 tensile 64 flex 63 disk	67 tensile 63 flex 49 disk	64 tensile 59 flex 47 disk
P-5-1	Charge time, sec	3.9 tensile 3.9 flex 5.1 disk	3.6 tensile 3.1 flex 3.1 disk	3.6 tensile 3.2 flex 3.3 disk
P-5-1	Injection Peak Pressure P1, kg/cm ²	73 tensile 64 flex 63 disk	67 tensile 63 flex 49 disk	64 tensile 59 flex 47 disk

Table B.4: Injection Molding Conditions for Combinations in PC continued

Notation	Injection Molding Conditions	BA2LR 7-26-10*	BA5LR 7-26-10*	BA2Q1L 7-26-10*
T _{mold}	Mold Temperature (F)	160	160	160
E1	Zone 1 Temperature (F) (nozzle)	610	610	610
E2	Zone 2 Temperature (F)	570	570	570
E3	Zone 3 Temperature (F)	554	554	554
E4	Zone 4 Temperature (F) (feed zone)	536	536	536
P1	Injection pressure (psi)	70% = 15,827	75% = 16,958	75% = 16,958
P2	Hold Pressure (psi)	55% = 12,436	55% = 12,436	55% = 12,436
P7	Back Pressure (psi)	0.2% = 45.2	0.2% = 45.2	0.2% = 45.2
S1	Shot size (mm)	20	20	20
S2	Pullback before (mm)	0	0	0
S3	Pullback after (mm)	0.1	0.1	0.1
S6	Width of mold (mm)	202	202	202
S8	Screw Position to Switch from P1 to P2 (mm)	8 for tensile, 10 for flex, 12 for disk	8 for tensile, 10 for flex, 12 for disk	8 for tensile, 10 for flex, 12 for disk
T1	Injection Time (s)	8	8	8
T2	Cool Time (s)	16	16	16
T3	Interval Time (s)	0.1	0.1	0.1
T6	Retraction Time (s)	0	0	0
T7	Nozzle Retraction Delay Time (s)	0	0	0
T8	Injection Delay Time (s)	0	0	0
T9	Charge Delay Time (s)	0	0	0
V1	Injection Velocity (in ³ /s)	30% = 1.866	30% = 1.866	30% = 1.866
V6	Screw Rotation (rpm)	19% = 60	19% = 60	19% = 60
V9	Retraction Velocity (%)	20	20	20
V10	Advance Velocity (%)	50	50	50
V11	Retraction Velocity (%)	90	90	90
CF	Clamp Force (US tons)	80	80	80

Table B.4: Injection Molding Conditions for Combinations in PC continued

Notation	Injection Molding Conditions	BA2LR 7-26-10*	BA5LR 7-26-10*	BA2Q1L 7-26-10*
P-5-1	Actual Cycle Time, sec	30.9 tensile 30.7 flex 30.6 disk	30.7 tensile 30.8 flex 30.6 disk	30.9 tensile 30.7 flex 30.6 disk
P-5-1	Inj Start, mm	30.9 tensile 30.7 flex 30.6 disk	30.7 tensile 30.8 flex 30.6 disk	30.9 tensile 30.7 flex 30.6 disk
P-5-1	Cushion, mm	20.8 tensile 20.8 flex 20.9 disk	20.0 tensile 20.0 flex 20.0 disk	20.8 tensile 20.8 flex 20.9 disk
P-5-1	P1 → P2 Fill time, sec	2.0 tensile 3.9 flex 3.3 disk	1.7 tensile 3.1 flex 2.7 disk	1.6 tensile 3.3.3 flex 2.5 disk
P-5-1	P1 Actual Pressure P1 → P2, kg/cm ²	0.70 tensile 0.60 flex 0.51 disk	0.70 tensile 0.61 flex 0.51 disk	0.70 tensile 0.60 flex 0.51 disk
P-5-1	Charge time, sec	70 tensile 65 flex 58 disk	81 tensile 71 flex 63 disk	52 tensile 44 flex 38 disk
P-5-1	Injection Peak Pressure P1, kg/cm ²	4.0 tensile 3.6 flex 3.5 disk	5.5 tensile 5.3 flex 4.1 disk	3.4 tensile 2.9 flex 3.2 disk
P-5-1	Inj Start, mm	70 tensile 65 flex 58 disk	81 tensile 71 flex 63 disk	52 tensile 44 flex 38 disk

Table B.4: Injection Molding Conditions for Combinations in PC continued

Notation	Injection Molding Conditions	BA5Q1L 7-26-10 for disk and flex*	BA5Q1L 8-25-10 and 8-6-10 tensile only*	BA2Q5L 8-6-10 and 8-25-10*
T _{mold}	Mold Temperature (F)	160	160	160
E1	Zone 1 Temperature (F) (nozzle)	610	590	590
E2	Zone 2 Temperature (F)	570	570	570
E3	Zone 3 Temperature (F)	554	554	554
E4	Zone 4 Temperature (F) (feed zone)	536	536	536
P1	Injection pressure (psi)	75% = 16,958	75% = 16,958, 80% = 18,088 worked too	Tensile, flex 75% = 16,958 disks 50% = 11,305
P2	Hold Pressure (psi)	55% = 12,436	55% = 12,436	55% = 12,436 flex, tensile 45% = 10,175 disks
P7	Back Pressure (psi)	0.2% = 45.2	0.2% or 5%	Set point 5.0% = 1100 but actual was 1 kgf/cm ²
S1	Shot size (mm)	20	22	22
S2	Pullback before (mm)	0	0	0
S3	Pullback after (mm)	0.1	0.4	0.4
S6	Width of mold (mm)	202	202	202
S8	Screw Position to Switch from P1 to P2 (mm)	10 for flex, 12 for disk	7 for tensile	7 for tensile, 10 for flex, 12 for disk
T1	Injection Time (s)	8	8	8
T2	Cool Time (s)	16	16 or 20	16 or 20
T3	Interval Time (s)	0.1	0.1	0.1
T6	Retraction Time (s)	0	0	0
T7	Nozzle Retraction Delay Time (s)	0	0	0
T8	Injection Delay Time (s)	0	0	0
T9	Charge Delay Time (s)	0	0	0
V1	Injection Velocity (in ³ /s)	30% = 1.866	30% = 1.866	30% = 1.866
V6	Screw Rotation (rpm)	19% = 60	19% = 60	19% = 60
V9	Retraction Velocity (%)	20	20	20
V10	Advance Velocity (%)	50	50	50
V11	Retraction Velocity (%)	90	90	90
CF	Clamp Force (US tons)	80	80	80

Table B.4: Injection Molding Conditions for Combinations in PC continued

Notation	Injection Molding Conditions	BA5Q1L 7-26-10 for disk and flex*	BA5Q1L 8-25-10 and 8-6-10 tensile only*	BA2Q5L 8-6-10 and 8-25-10*
P-5-1	Actual Cycle Time, sec	31.8 flex 31.6 disk	35.1 or 31.3 tensile	35.1 or 31.3 tensile 35.1 flex 35.1 disk
P-5-1	Inj Start, mm	20.8 flex 20.9 disk	22.4 tensile	22.5 tensile 22.5 flex 22.5 disk
P-5-1	Cushion, mm	3.5 flex 2.7 disk	3.5 tensile	3.3 tensile 5.0 flex 4.0 disk
P-5-1	P1 → P2 Fill time, sec	0.6 flex 0.5 disk	0.80 tensile	0.78 tensile 0.65 flex 0.56 disk
P-5-1	P1 Actual Pressure P1 → P2, kgf/cm ²	56 flex 48 disk	65 tensile	42 tensile 33 flex 26 disk
P-5-1	Charge time, sec	3.3 flex 3.5 disk	3.8 tensile	3.2 tensile 3.2 flex 3.2 disk
P-5-1	Injection Peak Pressure P1, kg/cm ²	56 flex 48 disk	65 tensile	42 tensile 33 flex 26 disk

Table B.4: Injection Molding Conditions for Combinations in PC continued

Notation	Injection Molding Conditions	BA5Q5L 8-6-10 and 8-25-10*	BG2L 9-9-10Tensile and flex only*	BG5L 9-9-10 tensile and flex*
T _{mold}	Mold Temperature (F)	160	160	160
E1	Zone 1 Temperature (F) (nozzle)	620	610	620
E2	Zone 2 Temperature (F)	590	570	590
E3	Zone 3 Temperature (F)	560	554	560
E4	Zone 4 Temperature (F) (feed zone)	550	536	550
P1	Injection pressure (psi)	Tensile, flex 75% =16,958 disks 50%=11,305	70%=15,827	75% =16,958
P2	Hold Pressure (psi)	55% = 12,436 flex, tensile 45% =10,175 disks	55%=12,436	55% = 12,436
P7	Back Pressure (psi)	Set point 5.0% =1100 but actual was 1 kgf/cm ²	Set point 5.0% =1100 but actual was 1 kgf/cm ²	Set point 5.0% =1100 but actual was 1 kgf/cm ²
S1	Shot size (mm)	22	22	22
S2	Pullback before (mm)	0	0	0
S3	Pullback after (mm)	0.4	0.4	0.4
S6	Width of mold (mm)	202	202	202
S8	Screw Position to Switch from P1 to P2 (mm)	7 for tensile, 10 for flex, 12 for disk	7 for tensile, 10 for flex	7 for tensile, 10 for flex
T1	Injection Time (s)	8	8	8
T2	Cool Time (s)	24	16	20
T3	Interval Time (s)	0.1	0.1	0.1
T6	Retraction Time (s)	0	0	0
T7	Nozzle Retraction Delay Time (s)	0	0	0
T8	Injection Delay Time (s)	0	0	0
T9	Charge Delay Time (s)	0	0	0
V1	Injection Velocity (in ³ /s)	55% =3.69 tensile 30% =1.866 disk, flex	30% = 1.866	8%=0.54
V6	Screw Rotation (rpm)	19% = 60	19% = 60	19% = 60

Table B.4: Injection Molding Conditions for Combinations in PC continued

Notation	Injection Molding Conditions	BA5Q5L 8-6-10 and 8-25-10*	BG2L 9-9-10 Tensile and flex only*	BG5L 9-9-10 tensile and flex*
V9	Retraction Velocity (%)	20	20	20
V10	Advance Velocity (%)	50	50	50
V11	Retraction Velocity (%)	90	90	90
CF	Clamp Force (US tons)	80	80	80
P-5-1	Actual Cycle Time, sec	38.7 tensile 38.7 flex 38.7 disk	30.9 tensile 30.6 flex	34.8
P-5-1	Inj Start, mm	22.5 tensile 22.5 flex 22.5 disk	22.4	22.5
P-5-1	Cushion, mm	3.3 tensile 5.0 flex 4.0 disk	3.5 tensile 5.3 flex	3.5 tensile 5.3 flex
P-5-1	P1 → P2 Fill time, sec	0.50 tensile 0.65 flex 0.56 disk	0.8 tensile 0.68 flex	3.6 tensile 2.8 flex
P-5-1	P1 Actual Pressure P1 → P2, kg/cm ²	64 tensile 46 flex 34 disk	67 tensile 54 flex	47 tensile 35 flex
P-5-1	Charge time, sec	3.9 tensile 3.5 flex 3.5 disk	3.5 tensile 3.3 flex	3.3 tensile 2.9 flex
P-5-1	Injection Peak Pressure P1, kg/cm ²	64 tensile 46 flex 34 disk	67 tensile 54 flex	47 tensile 35 flex

Table B.4: Injection Molding Conditions for Combinations in PC continued

Notation	Injection Molding Conditions	BG12L 8-18-10*	BG15L 8-18-10*	BQ5LR 8-25-10*
T _{mold}	Mold Temperature (F)	200	200	160
E1	Zone 1 Temperature (F) (nozzle)	630	640	590
E2	Zone 2 Temperature (F)	640	650	570
E3	Zone 3 Temperature (F)	610	610	554
E4	Zone 4 Temperature (F) (feed zone)	550	550	536
P1	Injection pressure (psi)	99%=22,384	99%=22,384	Tensile, flex 70%=15,827 disks 50%=11,305
P2	Hold Pressure (psi)	55% = 12,436	55% = 12,436 flex, tensile 45% disks	55% = 12,436 flex, tensile 45% disks
P7	Back Pressure (psi)	Set point 5.0% =1100 but actual was 1 kgf/cm ²	Set point 5.0% =1100 but actual was 1 kgf/cm ²	Set point 5.0% =1100 but actual was 1 kgf/cm ²
S1	Shot size (mm)	22	22	22
S2	Pullback before (mm)	0	0	0
S3	Pullback after (mm)	0.4	0.4	0.4
S6	Width of mold (mm)	202	202	202
S8	Screw Position to Switch from P1 to P2 (mm)	7 for tensile 10 for flex 12 for disk	7 for tensile, 10 for flex, 12 for disk	7 for tensile, 10 for flex, 12 for disk
T1	Injection Time (s)	8	8	8
T2	Cool Time (s)	16	16	16
T3	Interval Time (s)	0.1	0.1	0.1
T6	Retraction Time (s)	0	0	0
T7	Nozzle Retraction Delay Time (s)	0	0	0
T8	Injection Delay Time (s)	0	0	0
T9	Charge Delay Time (s)	0	0	0
V1	Injection Velocity (in ³ /s)	8%=0.54	8%=0.54	30%=1.866
V6	Screw Rotation (rpm)	19% = 60	19% = 60	19% = 60
V9	Retraction Velocity (%)	20	20	20
V10	Advance Velocity (%)	50	50	50
V11	Retraction Velocity (%)	90	90	90

CF	Clamp Force (US tons)	80	80	80
----	-----------------------	----	----	----

Table B.4: Injection Molding Conditions for Combinations in PC continued

Notation	Injection Molding Conditions	BG12L 8-18-10*	BG15L 8-18-10*	BQ5LR 8-25-10 *
P-5-1	Actual Cycle Time, sec	31	31	31
P-5-1	Inj Start, mm	22.4	22.4	22.5
P-5-1	Cushion, mm	3.0 tensile 4.9 flex 4.1 disk	3.3 tensile 5.0 flex 4.0 disk	3.4 tensile 5.0 flex 4.0 disk
P-5-1	P1 → P2 Fill time, sec	3.5 tensile 2.9 flex 2.4 disk	3.5 tensile 2.9 flex 2.4 disk	0.78 tensile 0.65 flex 0.56 disk
P-5-1	P1 Actual Pressure P1 → P2, kg/cm ²	42 tensile 30 flex 19 disk	40 tensile 28 flex 17 disk	42 tensile 37 flex 22 disk
P-5-1	Charge time, sec	3.0	3.2 tensile 3.2 flex 3.2 disk	3.5
P-5-1	Injection Peak Pressure P1, kg/cm ²	42 tensile 30 flex 19 disk	40 tensile 28 flex 17 disk	42 tensile 37 flex 22 disk

Table B.4: Injection Molding Conditions for Combinations in PC continued

Notation	Injection Molding Conditions	BA2G2L 8-18-10 and 8-6-10*	BA2G5L 8-18-10 and 8-6-10*	BA5G2L 8-18-10 and 8-6-10*
T _{mold}	Mold Temperature (F)	160	160	160
E1	Zone 1 Temperature (F) (nozzle)	620	620	620
E2	Zone 2 Temperature (F)	590	590	590
E3	Zone 3 Temperature (F)	560	560	560
E4	Zone 4 Temperature (F) (feed zone)	550	550	550
P1	Injection pressure (psi)	75%=16,958	75%=16,958 flex, tensile 50%=11,305 disk	75%=16,958 flex, tensile 50%=11,305 disk
P2	Hold Pressure (psi)	55% = 12,436	55% = 12,436 tensile, flex 45% disk	55% = 12,436 tensile, flex 45% disk
P7	Back Pressure (psi)	Set point 5.0% =1100 but actual was 1 kgf/cm ²	Set point 5.0% =1100 but actual was 1 kgf/cm ²	Set point 5.0% =1100 but actual was 1 kgf/cm ²
S1	Shot size (mm)	22	22	22
S2	Pullback before (mm)	0	0	0
S3	Pullback after (mm)	0.4	0.4	0.4
S6	Width of mold (mm)	202	202	202
S8	Screw Position to Switch from P1 to P2 (mm)	7 for tensile 10 for flex 12 for disk	7 for tensile 10 for flex 12 for disk	7 for tensile, 10 for flex, 12 for disk
T1	Injection Time (s)	8	8	8
T2	Cool Time (s)	16	16	16
T3	Interval Time (s)	0.1	0.1	0.1
T6	Retraction Time (s)	0	0	0
T7	Nozzle Retraction Delay Time (s)	0	0	0
T8	Injection Delay Time (s)	0	0	0
T9	Charge Delay Time (s)	0	0	0
V1	Injection Velocity (in ³ /s)	30%=1.866 disk 55%=3.69 flex and tensile	30% disk=1.866 55%=3.69 flex and tensile	8%=0.54 tensile, flex 30%=1.866 disk
V6	Screw Rotation (rpm)	19% = 60	19% = 60	19% = 60
V9	Retraction Velocity (%)	20	20	20
V10	Advance Velocity (%)	50	50	50

Table B.4: Injection Molding Conditions for Combinations in PC continued

Notation	Injection Molding Conditions	BA2G2L 8-18-10 and 8-6-10*	BA2G5L 8-18-10 and 8-6-10*	BA5G2L 8-18-10 and 8-6-10*
V11	Retraction Velocity (%)	90	90	90
CF	Clamp Force (US tons)	80	80	80
P-5-1	Actual Cycle Time, sec	31	31	31
P-5-1	Inj Start, mm	22.4	22.4	22.4
P-5-1	Cushion, mm	3.0 tensile 4.9 flex 4.1 disk	4.1 tensile 4.9 flex 4.1 disk	4.0 tensile 5.7 flex 5.8 disk
P-5-1	P1 → P2 Fill time, sec	0.5 tensile 0.4 flex 0.36 disk	0.56 tensile 0.43 flex 0.51 disk	3.5 tensile 2.9 flex 0.6 disk
P-5-1	P1 Actual Pressure P1 → P2, kg/cm ²	83 tensile 70 flex 53 disk	85 tensile 72 flex 40 disk	63 tensile 48 flex 46 disk
P-5-1	Charge time, sec	3.0	3.0	3.2 tensile 3.2 flex 3.2 disk
P-5-1	Injection Peak Pressure P1, kg/cm ²	83 tensile 70 flex 53 disk	85 tensile 72 flex 40 disk	63 tensile 48 flex 46 disk

Table B.4: Injection Molding Conditions for Combinations in PC continued

Notation	Injection Molding Conditions	BA5G5L 8-18-10 and 8-6-10*	BQ1G2L 8-18-10 and 8-6-10*	BQ1G5L 8-18-10 and 8-6- 10*
T _{mold}	Mold Temperature (F)	160	160	160
E1	Zone 1 Temperature (F) (nozzle)	620	620	620
E2	Zone 2 Temperature (F)	590	590	590
E3	Zone 3 Temperature (F)	560	560	560
E4	Zone 4 Temperature (F) (feed zone)	550	550	550
P1	Injection pressure (psi)	Tensile, flex 70%=15,827 disks 50%=11,305	75%=16,958	75%=16,958
P2	Hold Pressure (psi)	55% = 12,436 flex, tensile 45% disks	55% = 12,436	55% = 12,436
P7	Back Pressure (psi)	Set point 5.0% =1100 but actual was 1 kgf/cm ²	Set point 5.0% =1100 but actual was 1 kgf/cm ²	Set point 5.0% =1100 but actual was 1 kgf/cm ²
S1	Shot size (mm)	22	22	22
S2	Pullback before (mm)	0	0	0
S3	Pullback after (mm)	0.4	0.4	0.4
S6	Width of mold (mm)	202	202	202
S8	Screw Position to Switch from P1 to P2 (mm)	7 for tensile, 10 for flex, 12 for disk	7 for tensile 10 for flex 12 for disk	7 for tensile 10 for flex 12 for disk
T1	Injection Time (s)	8	8	8
T2	Cool Time (s)	16	16	16
T3	Interval Time (s)	0.1	0.1	0.1
T6	Retraction Time (s)	0	0	0
T7	Nozzle Retraction Delay Time (s)	0	0	0
T8	Injection Delay Time (s)	0	0	0
T9	Charge Delay Time (s)	0	0	0
V1	Injection Velocity (in ³ /s)	8%=0.54	8%=0.54	8%=0.54
V6	Screw Rotation (rpm)	19% = 60	19% = 60	19% = 60
V9	Retraction Velocity (%)	20	20	20
V10	Advance Velocity (%)	50	50	50
V11	Retraction Velocity (%)	90	90	90
CF	Clamp Force (US tons)	80	80	80

Table B.4: Injection Molding Conditions for Combinations in PC continued

Notation	Injection Molding Conditions	BA5G5L 8-18-10 and 8-6-10*	BQ1G2L 8-18-10 and 8-6-10*	BQ1G5L 8-18-10 and 8-6- 10*
P-5-1	Actual Cycle Time, sec	31	31	31
P-5-1	Inj Start, mm	22.5	22.4	22.8
P-5-1	Cushion, mm	3.0 tensile 5.0 flex 4.0 disk	3.0 tensile 4.9 flex 4.1 disk	3.6 tensile 5.3 flex 4.5 disk
P-5-1	P1 → P2 Fill time, sec	3.5 tensile 2.9 flex 2.4 disk	3.5 tensile 2.8 flex 2.4 disk	3.5 tensile 2.8 flex 2.4 disk
P-5-1	P1 Actual Pressure P1 → P2, kg/cm ²	65 tensile 48 flex 31 disk	34 tensile 26 flex 17 disk	41 tensile 30 flex 18 disk
P-5-1	Charge time, sec	3.5	3.0	3.0
P-5-1	Injection Peak Pressure P1, kg/cm ²	65 tensile 48 flex 31 disk	34 tensile 26 flex 17 disk	41 tensile 30 flex 18 disk

Table B.4: Injection Molding Conditions for Combinations in PC continued

Notation	Injection Molding Conditions	BQ2LR 7-26-10 flex only*	BQ3LR 7-26-10 flex only*	BQ5G2L 9-9-10 and 8-6- 10*
T _{mold}	Mold Temperature (F)	160	160	160
E1	Zone 1 Temperature (F) (nozzle)	610	610	620
E2	Zone 2 Temperature (F)	570	570	590
E3	Zone 3 Temperature (F)	554	554	560
E4	Zone 4 Temperature (F) (feed zone)	536	536	550
P1	Injection pressure (psi)	70%=15,827	70%=15,827	75%=16,958
P2	Hold Pressure (psi)	55% = 12,436	55% = 12,436	55% = 12,436
P7	Back Pressure (psi)	0.2% = 45.2	0.2% = 45.2	Set point 5.0% =1100 but actual was 1 kgf/cm ²
S1	Shot size (mm)	20	20	22
S2	Pullback before (mm)	0	0	0
S3	Pullback after (mm)	0.1	0.1	0.4
S6	Width of mold (mm)	202	202	202
S8	Screw Position to Switch from P1 to P2 (mm)	10 flex	10 flex	7 for tensile 10 for flex, 12 disk
T1	Injection Time (s)	8	8	8
T2	Cool Time (s)	16	16	20
T3	Interval Time (s)	0.1	0.1	0.1
T6	Retraction Time (s)	0	0	0
T7	Nozzle Retraction Delay Time (s)	0	0	0
T8	Injection Delay Time (s)	0	0	0
T9	Charge Delay Time (s)	0	0	0
V1	Injection Velocity (in ³ /s)	30%= 1.866	30%= 1.866	8%=0.54
V6	Screw Rotation (rpm)	19% = 60	19% = 60	19% = 60
V9	Retraction Velocity (%)	20	20	20
V10	Advance Velocity (%)	50	50	50
V11	Retraction Velocity (%)	90	90	90
CF	Clamp Force (US tons)	80	80	80

Table B.4: Injection Molding Conditions for Combinations in PC continued

Notation	Injection Molding Conditions	BQ2LR 7-26-10 flex only*	BQ3LR 7-26-10 flex only*	BQ5G2L 9-9-10 and 8-6- 10*
P-5-1	Actual Cycle Time, sec	31 flex	31 flex	35
P-5-1	Inj Start, mm	20.6	20.6	22.4
P-5-1	Cushion, mm	3.4	3.4	3.2 tensile 4.8 flex
P-5-1	P1 → P2 Fill time, sec	0.61	0.61	3.6 tensile 2.9 flex
P-5-1	P1 Actual Pressure P1 → P2, kg/cm ²	57	57	27 tensile 21 flex
P-5-1	Charge time, sec	2.9	2.9	3.9
P-5-1	Injection Peak Pressure P1, kg/cm ²	57	57	27 tensile 21 flex

Table B.4: Injection Molding Conditions for Combinations in PC continued

Notation	Injection Molding Conditions	BQ5G5L 9-9-10 and 8- 6-10*	BQ4LR 8-25-10 flex only*	BQ6LR 8-25-10 flex only*
T _{mold}	Mold Temperature (F)	160	160	160
E1	Zone 1 Temperature (F) (nozzle)	620	610	610
E2	Zone 2 Temperature (F)	590	570	570
E3	Zone 3 Temperature (F)	560	554	554
E4	Zone 4 Temperature (F) (feed zone)	550	536	536
P1	Injection pressure (psi)	75%= 16,958	70%=15,827	70%=15,827
P2	Hold Pressure (psi)	55%= 12,436	55% = 12,436	55% = 12,436
P7	Back Pressure (psi)	Set point 5.0% =1100 but actual was 1 kgf/cm ²	Set point 5.0% =1100 but actual was 1 kgf/cm ²	Set point 5.0% =1100 but actual was 1 kgf/cm ²
S1	Shot size (mm)	22	22	22
S2	Pullback before (mm)	0	0	0
S3	Pullback after (mm)	0.4	0.4	0.4
S6	Width of mold (mm)	202	202	202
S8	Screw Position to Switch from P1 to P2 (mm)	7 for tensile 10 for flex, 12 disk	10 flex	10 flex
T1	Injection Time (s)	8	8	8
T2	Cool Time (s)	20	16	20
T3	Interval Time (s)	0.1	0.1	0.1
T6	Retraction Time (s)	0	0	0
T7	Nozzle Retraction Delay Time (s)	0	0	0
T8	Injection Delay Time (s)	0	0	0
T9	Charge Delay Time (s)	0	0	0
V1	Injection Velocity (in ³ /s)	8%=0.54	30%=1.866	30%=1.866
V6	Screw Rotation (rpm)	19% = 60	19% = 60	19% = 60
V9	Retraction Velocity (%)	20	20	20
V10	Advance Velocity (%)	50	50	50
V11	Retraction Velocity (%)	90	90	90
CF	Clamp Force (US tons)	80	80	80

Table B.4: Injection Molding Conditions for Combinations in PC continued

Notation	Injection Molding Conditions	BQ5G5L 9-9-10 and 8-6-10*	BQ4LR 8-25-10 flex only*	BQ6LR 8-25-10 flex only*
P-5-1	Actual Cycle Time, sec	35	31 flex only	31 flex only
P-5-1	Inj Start, mm	22.4	22.4	22.4
P-5-1	Cushion, mm	3.0 tensile 4.9 flex	5.1	5.1
P-5-1	P1 → P2 Fill time, sec	3.7 tensile 3.0 flex	0.66 flex	0.66 flex
P-5-1	P1 Actual Pressure P1 → P2, kg/cm ²	32 tensile 26 flex	40 flex	40 flex
P-5-1	Charge time, sec	3.7	3.2	3.2
P-5-1	Injection Peak Pressure P1, kg/cm ²	32 tensile 26 flex	40 flex	40 flex

Table B.4: Injection Molding Conditions for Combinations in PC continued

Notation	Injection Molding Conditions	BQ8LR 8-25-10 flex only*
T _{mold}	Mold Temperature (F)	180
E1	Zone 1 Temperature (F) (nozzle)	610
E2	Zone 2 Temperature (F)	570
E3	Zone 3 Temperature (F)	554
E4	Zone 4 Temperature (F) (feed zone)	536
P1	Injection pressure (psi)	80%= 18,088
P2	Hold Pressure (psi)	55% = 12,436
P7	Back Pressure (psi)	Set point 5.0% =1100 but actual was 1 kgf/cm ²
S1	Shot size (mm)	22
S2	Pullback before (mm)	0
S3	Pullback after (mm)	0.4
S6	Width of mold (mm)	202
S8	Screw Position to Switch from P1 to P2 (mm)	10 flex
T1	Injection Time (s)	8
T2	Cool Time (s)	20
T3	Interval Time (s)	0.1
T6	Retraction Time (s)	0
T7	Nozzle Retraction Delay Time (s)	0
T8	Injection Delay Time (s)	0
T9	Charge Delay Time (s)	0
V1	Injection Velocity (in ³ /s)	30%=1.866
V6	Screw Rotation (rpm)	19% = 60
V9	Retraction Velocity (%)	20
V10	Advance Velocity (%)	50
V11	Retraction Velocity (%)	90
CF	Clamp Force (US tons)	80
P-5-1	Actual Cycle Time, sec	35 flex only
P-5-1	Inj Start, mm	22.4
P-5-1	Cushion, mm	5.1
P-5-1	P1 → P2 Fill time, sec	0.66 flex
P-5-1	P1 Actual Pressure P1 → P2, kg/cm ²	35 flex
P-5-1	Charge time, sec	3.2
P-5-1	Injection Peak Pressure P1, kg/cm ²	35 flex

Notes:

- 1) For each formulation, typically about 30 2.5” diameter disks, 30 tensile bars, and 20 flexural bars molded. Each sample was individually molded. The injection molding machine ran on the fully automatic mode.
- 2) After each formulation, the feed hopper was run until it was empty and no material was in screw. Then we discarded 5 transition shots, and then started collecting the next formulation.
- 3) Between each ‘family’, we cleaned with DynaPurge E, and then Lexan HF1130-111.
- 4) * is injection molding date

Appendix C: Density Data

Appendix C.1: Polycarbonate with Carbon Nanotubes

Table C.1: Density Results for Lexan HF1130-111:BL: Injection Molded May 26, 2009

Test Date	Sample Number	Theoretical Density (g/ml)	Actual Density (g/ml)
6/26/2009	BL-TC-15	1.200	1.195
6/26/2009	BL-TC-18	1.200	1.192
6/26/2009	BL-TC-21	1.200	1.191
6/26/2009	BL-TC-26	1.200	1.192
6/26/2009	BL-TC-31	1.200	1.191
		Average	1.1923
		Standard Deviation	0.0016
		Number of Samples	5

Table C.2: Density Results for Extruded Lexan HF1130-111:BLE: Injection Molded May 26, 2009

Test Date	Sample Number	Theoretical Density (g/ml)	Actual Density (g/ml)
6/26/2009	BLE-TC-12	1.200	1.193
6/26/2009	BLE-TC-14	1.200	1.194
6/26/2009	BLE-TC-19	1.200	1.193
6/26/2009	BLE-TC-22	1.200	1.195
6/26/2009	BLE-TC-24	1.200	1.194
		Average	1.1938
		Standard Deviation	0.0008
		Number of Samples	5

Table C.3: Density Results for 2 wt% fibrils in Lexan HF1130-111: BQ2L: Injection Molded May 26, 2009

Test Date	Sample Number	Theoretical Density (g/ml)	Actual Density (g/ml)
5/26/2009	BQ2L-TC-19	1.210	1.202
5/26/2009	BQ2L-TC-14	1.210	1.201
5/26/2009	BQ2L-TC-16	1.210	1.201
5/26/2009	BQ2L-TC-13	1.210	1.202
5/26/2009	BQ2L-TC-29	1.210	1.201
5/26/2009	BQ2L-TC-31	1.210	1.202
5/26/2009	BQ2L-TC-17	1.210	1.201
5/26/2009	BQ2L-TC-27	1.210	1.202
		Average	1.2015
		Standard Deviation	0.0005
		Number of Samples	8

Table C.4: Density Results for 3 wt% fibrils in Lexan HF1130-111: BQ3L: Injection Molded May 26, 2009

Test Date	Sample Number	Theoretical Density (g/ml)	Actual Density (g/ml)
5/26/2009	BQ3L-TC-21	1.215	1.206
5/26/2009	BQ3L-TC-26	1.215	1.204
5/26/2009	BQ3L-TC-11	1.215	1.204
5/26/2009	BQ3L-TC-22	1.215	1.205
5/26/2009	BQ3L-TC-12	1.215	1.206
5/26/2009	BQ3L-TC-17	1.215	1.206
		Average	1.2052
		Standard Deviation	0.0010
		Number of Samples	6

Table C.5: Density Results for 4 wt% fibrils in Lexan HF1130-111: BQ4L: Injection Molded May 26, 2009

Test Date	Sample Number	Theoretical Density (g/ml)	Actual Density (g/ml)
6/26/2009	BQ4L-TC-13	1.220	1.213
6/26/2009	BQ4L-TC-18	1.220	1.210
6/26/2009	BQ4L-TC-24	1.220	1.213
6/26/2009	BQ4L-TC-28	1.220	1.213
6/26/2009	BQ4L-TC-32	1.220	1.213
		Average	1.2123
		Standard Deviation	0.0013
		Number of Samples	5

Table C.6: Density Results for 5 wt% fibrils in Lexan HF1130-111: BQ5L: Injection Molded May 26, 2009

Test Date	Sample Number	Theoretical Density (g/ml)	Actual Density (g/ml)
6/26/2009	BQ5L-TC-12	1.225	1.217
6/26/2009	BQ5L-TC-18	1.225	1.217
6/26/2009	BQ5L-TC-20	1.225	1.216
6/26/2009	BQ5L-TC-28	1.225	1.217
6/26/2009	BQ5L-TC-32	1.225	1.217
		Average	1.2168
		Standard Deviation	0.0004
		Number of Samples	5

Table C.7: Density Results for 6 wt% fibrils in Lexan HF1130-111: BQ6L: Injection Molded May 26, 2009

Test Date	Sample Number	Theoretical Density (g/ml)	Actual Density (g/ml)
6/26/2009	BQ6L-TC-12	1.224	1.221
6/26/2009	BQ6L-TC-20	1.224	1.222
6/26/2009	BQ6L-TC-26	1.224	1.222
6/26/2009	BQ6L-TC-29	1.224	1.221
6/26/2009	BQ6L-TC-33	1.224	1.221
		Average	1.2214
		Standard Deviation	0.0004
		Number of Samples	5

Table C.8: Density Results for 8 wt% fibrils in Lexan HF1130-111: BQ8L: Injection Molded May 26, 2009

Test Date	Sample Number	Theoretical Density (g/ml)	Actual Density (g/ml)
6/26/2009	BQ8L-TC-11	1.225	1.231
6/26/2009	BQ8L-TC-19	1.225	1.232
6/26/2009	BQ8L-TC-24	1.225	1.231
6/26/2009	BQ8L-TC-29	1.225	1.231
6/26/2009	BQ8L-TC-33	1.225	1.232
		Average	1.2313
		Standard Deviation	0.0005
		Number of Samples	5

Appendix C.2: Polycarbonate with Carbon Black

Table C.9: Density Results for Lexan HF1130-111:BL2: Injection Molded December 4, 2009

Test Date	Sample	Actual Density (g/cc)	Theoretical Density (g/cc)
12/16/2009	BL2-TC-7	1.1963	1.20
12/16/2009	BL2-TC-20	1.1958	1.20
12/16/2009	BL2-TC-21	1.1953	1.20
12/16/2009	BL2-TC-26	1.1955	1.20
12/16/2009	BL2-TC-32	1.1955	1.20
12/16/2009	BL2-TC-36	1.1959	1.20
	Average	1.1957	
	Std Dev	0.0004	
	Number	6	

Table C.10: Density Results for Extruded Lexan HF1130-111:BLE2: Extruded Nov 5, 2009; Injection Molded December 4, 2009

Test Date	Sample	Actual Density (g/cc)	Theoretical Density (g/cc)
12/16/2009	BLE2-TC-9	1.1957	1.20
12/16/2009	BLE2-TC-11	1.1957	1.20
12/16/2009	BLE2-TC-13	1.1957	1.20
12/16/2009	BLE2-TC-14	1.1960	1.20
12/16/2009	BLE2-TC-19	1.1962	1.20
12/16/2009	BLE2-TC-20	1.1958	1.20
12/16/2009	BLE2-TC-25	1.1957	1.20
	Average	1.1958	
	Std Dev	0.0002	
	Number	7	

Table C.11: Density Results for 2 wt% Ketjenblack EC-600 JD in Lexan HF1130-111:
BA2L: Extruded November 5, 2009; Injection Molded December 4, 2009

Test Date	Sample	Actual Density (g/cc)	Theoretical Density (g/cc) *	Theoretical Density (g/cc)**
12/16/2009	BA2L-TC-11	1.2037	1.208	1.204
12/16/2009	BA2L-TC-19	1.2030	1.208	1.204
12/16/2009	BA2L-TC-22	1.2036	1.208	1.204
12/16/2009	BA2L-TC-25	1.2026	1.208	1.204
12/16/2009	BA2L-TC-27	1.2032	1.208	1.204
12/16/2009	BA2L-TC-28	1.2033	1.208	1.204
12/16/2009	BA2L-TC-30	1.2034	1.208	1.204
	Average	1.2032		
	Std Dev	0.0004		
	Number	7		

* using 1.20 g/cc for Lexan

** using 1.196 g/cc for
Lexan

Table C.12: Density Results for 3 wt% Ketjenblack EC-600 JD in Lexan HF1130-111:
BA3L: Extruded November 5, 2009; Injection Molded December 4, 2009

Test Date	Sample	Actual Density (g/cc)	Theoretical Density (g/cc) *	Theoretical Density (g/cc)**
12/16/2009	BA3L-TC-14	1.2081	1.212	1.208
12/16/2009	BA3L-TC-16	1.2079	1.212	1.208
12/16/2009	BA3L-TC-18	1.2077	1.212	1.208
12/16/2009	BA3L-TC-21	1.2082	1.212	1.208
12/16/2009	BA3L-TC-24	1.2080	1.212	1.208
12/16/2009	BA3L-TC-29	1.2080	1.212	1.208
	Average	1.2080		
	Std Dev	0.0001		
	Number	6		

* using 1.20 g/cc for Lexan

** using 1.196 g/cc for Lexan

Table C.13: Density Results for 4 wt% Ketjenblack EC-600 JD in Lexan HF1130-111:
BA4L: Extruded November 5, 2009; Injection Molded December 4, 2009

Test Date	Sample	Actual Density (g/cc)	Theoretical Density (g/cc) *	Theoretical Density (g/cc)**
12/16/2009	BA4L-TC-10	1.2113	1.216	1.212
12/16/2009	BA4L-TC-16	1.2123	1.216	1.212
12/16/2009	BA4L-TC-18	1.2113	1.216	1.212
12/16/2009	BA4L-TC-24	1.2126	1.216	1.212
12/16/2009	BA4L-TC-27	1.2115	1.216	1.212
12/16/2009	BA4L-TC-30	1.2126	1.216	1.212
	Average	1.2119		
	Std Dev	0.0007		
	Number	6		

* using 1.20 g/cc for Lexan

** using 1.196 g/cc for
Lexan

Table C.15: Density Results for 5 wt% Ketjenblack EC-600 JD in Lexan HF1130-111:
BA5L: Extruded November 11, 2009; Injection Molded December 4, 2009

Test Date	Sample	Actual Density (g/cc)	Theoretical Density (g/cc) *	Theoretical Density (g/cc)**
12/16/2009	BA5L-TC-15	1.2155	1.220	1.216
12/16/2009	BA5L-TC-16	1.2153	1.220	1.216
12/16/2009	BA5L-TC-22	1.2151	1.220	1.216
12/16/2009	BA5L-TC-25	1.2153	1.220	1.216
12/16/2009	BA5L-TC-26	1.2153	1.220	1.216
12/16/2009	BA5L-TC-30	1.2155	1.220	1.216
	Average	1.2153		
	Std Dev	0.0001		
	Number	6		

* using 1.20 g/cc for Lexan

** using 1.196 g/cc for
Lexan

Table C.14: Density Results for 6 wt% Ketjenblack EC-600 JD in Lexan HF1130-111:
BA6L: Extruded November 11, 2009; Injection Molded December 4, 2009

Test Date	Sample	Actual Density (g/cc)	Theoretical Density (g/cc) *	Theoretical Density (g/cc)**
12/16/2009	BA6L-TC-12	1.2184	1.224	1.221
12/16/2009	BA6L-TC-16	1.2188	1.224	1.221
12/16/2009	BA6L-TC-18	1.2190	1.224	1.221
12/16/2009	BA6L-TC-23	1.2189	1.224	1.221
12/16/2009	BA6L-TC-24	1.2193	1.224	1.221
	Average	1.2189		
	Std Dev	0.0004		
	Number	5		

* using 1.20 g/cc for Lexan

** using 1.196 g/cc for

Lexan

Table C.16: Density Results for 8 wt% Ketjenblack EC-600 JD in Lexan HF1130-111:
BA8L: Extruded November 11, 2009; Injection Molded December 4, 2009

Test Date	Sample	Actual Density (g/cc)	Theoretical Density (g/cc) *	Theoretical Density (g/cc)**
12/16/2009	BA8L-TC-20	1.2265	1.233	1.229
12/16/2009	BA8L-TC-24	1.2268	1.233	1.229
12/16/2009	BA8L-TC-26	1.2272	1.233	1.229
12/16/2009	BA8L-TC-28	1.2268	1.233	1.229
12/16/2009	BA8L-TC-30	1.2266	1.233	1.229
	Average	1.2268		
	Std Dev	0.0002		
	Number	5		

* using 1.20 g/cc for Lexan

** using 1.196 g/cc for

Lexan

Table C.17: Density Results for 10 wt% Ketjenblack EC-600 JD in Lexan HF1130-111:
BA10L: Extruded November 11, 2009; Injection Molded December 4, 2009

Test Date	Sample	Actual Density (g/cc)	Theoretical Density (g/cc) *	Theoretical Density (g/cc)**
12/16/2009	BA10L-TC-12	1.2372	1.241	1.238
12/16/2009	BA10L-TC-16	1.2372	1.241	1.238
12/16/2009	BA10L-TC-24	1.2374	1.241	1.238
12/16/2009	BA10L-TC-27	1.2378	1.241	1.238
12/16/2009	BA10L-TC-29	1.2372	1.241	1.238
	Average	1.2373		
	Std Dev	0.0003		
	Number	5		

* using 1.20 g/cc for Lexan

** using 1.196 g/cc for Lexan

Appendix C.3: Polycarbonate with Graphene Nanoplatelets

Table C.18: Density Results for Lexan HF1130-111:BL3: Injection Molded June 3, 2010

Test Date	Sample Number	Theoretical Density (g/ml)	Actual Density (g/ml)
6/4/2010	BL3-TC-20	1.200	1.1957
6/4/2010	BL3-TC-15	1.200	1.1938
6/4/2010	BL3-TC-18	1.200	1.1956
6/4/2010	BL3-TC-7	1.200	1.1941
6/4/2010	BL3-TC-25	1.200	1.1941
		Average	1.1947
		Standard Deviation	0.0009
		Number of Samples	5

Table C.19: Density Results for Extruded Lexan HF1130-111:BLE3: Extruded May 26, 2010; Injection Molded June 3, 2010

Test Date	Sample Number	Theoretical Density (g/ml)	Actual Density (g/ml)
6/4/2010	BLE3-TC-17	1.200	1.1940
6/4/2010	BLE3-TC-16	1.200	1.1946
6/4/2010	BLE3-TC-12	1.200	1.1938
6/4/2010	BLE3-TC-20	1.200	1.1938
6/4/2010	BLE3-TC-18	1.200	1.1946
		Average	1.1942
		Standard Deviation	0.0004
		Number of Samples	5

Table C.20: Density Results for 2 wt% xGnP in Lexan HF1130-111: BG2L: Extruded May 26, 2010; Injection Molded June 3, 2010

Test Date	Sample Number	Theoretical Density (g/ml)*	Theoretical Density (g/ml)**	Actual Density (g/ml)
6/4/2010	BG2L-TC-8	1.2097	1.2044	1.2041
6/4/2010	BG2L-TC-13	1.2097	1.2044	1.2029
6/4/2010	BG2L-TC-29	1.2097	1.2044	1.2029
6/4/2010	BG2L-TC-19	1.2097	1.2044	1.2018
6/4/2010	BG2L-TC-11	1.2097	1.2044	1.2021
		Average		1.2027
		Standard Deviation		0.0009
		Number of Samples		5

* using 1.20 g/cc for Lexan

** using 1.1947 g/cc for Lexan

Table C.21: Density Results for 3 wt% xGnP in Lexan HF1130-111: BG3L: Extruded May 26, 2010; Injection Molded June 3, 2010

Test Date	Sample Number	Theoretical Density (g/ml)*	Theoretical Density (g/ml)**	Actual Density (g/ml)
6/4/2010	BG3L-TC-8	1.2146	1.2093	1.2059
6/4/2010	BG3L-TC-10	1.2146	1.2093	1.2060
6/4/2010	BG3L-TC-28	1.2146	1.2093	1.2063
6/4/2010	BG3L-TC-20	1.2146	1.2093	1.2061
6/4/2010	BG3L-TC-16	1.2146	1.2093	1.2075
6/4/2010	BG3L-TC-23	1.2146	1.2093	1.2056
		Average		1.2062
		Standard Deviation		0.0007
		Number of Samples		6

* using 1.20 g/cc for Lexan

** using 1.1947 g/cc for Lexan

Table C.22: Density Results for 4 wt% xGnP in Lexan HF1130-111: BG4L: Extruded May 26, 2010; Injection Molded June 3, 2010

Test Date	Sample Number	Theoretical Density (g/ml)*	Theoretical Density (g/ml)**	Actual Density (g/ml)
6/4/2010	BG4L-TC-11	1.2195	1.2143	1.2104
6/4/2010	BG4L-TC-24	1.2195	1.2143	1.2110
6/4/2010	BG4L-TC-14	1.2195	1.2143	1.2107
6/4/2010	BG4L-TC-18	1.2195	1.2143	1.2108
6/4/2010	BG4L-TC-21	1.2195	1.2143	1.2125
6/4/2010	BG4L-TC-15	1.2195	1.2143	1.2069
		Average		1.2104
		Standard Deviation		0.0019
		Number of Samples		6

* using 1.20 g/cc for Lexan

** using 1.1947 g/cc for Lexan

Table C.23: Density Results for 5 wt% xGnP in Lexan HF1130-111: BG5L: Extruded May 26, 2010; Injection Molded June 3, 2010

Test Date	Sample Number	Theoretical Density (g/ml)*	Theoretical Density (g/ml)**	Actual Density (g/ml)
6/4/2010	BG5L-TC-30	1.2245	1.2192	1.2156
6/4/2010	BG5L-TC-20	1.2245	1.2192	1.2152
6/4/2010	BG5L-TC-15	1.2245	1.2192	1.2156
6/4/2010	BG5L-TC-26	1.2245	1.2192	1.2159
6/4/2010	BG5L-TC-10	1.2245	1.2192	1.2146
		Average		1.2154
		Standard Deviation		0.0005
		Number of Samples		5

* using 1.20 g/cc for Lexan

** using 1.1947 g/cc for Lexan

Table C.24: Density Results for 6 wt% xGnP in Lexan HF1130-111: BG5L: Extruded May 27, 2010; Injection Molded June 8, 2010

Test Date	Sample Number	Theoretical Density (g/ml)*	Theoretical Density (g/ml)**	Actual Density (g/ml)
6/8/2009	BG6L-TC-11	1.2295	1.2243	1.2224
6/8/2009	BG6L-TC-16	1.2295	1.2243	1.2232
6/8/2009	BG6L-TC-19	1.2295	1.2243	1.2226
6/8/2009	BG6L-TC-29	1.2295	1.2243	1.2224
6/8/2009	BG6L-TC-23	1.2295	1.2243	1.2237
		Average		1.2229
		Standard Deviation		0.0006
		Number of Samples		5

* using 1.20 g/cc for Lexan

** using 1.1947 g/cc for Lexan

Table C.25: Density Results for 8 wt% xGnP in Lexan HF1130-111: BG5L: Extruded May 27, 2010; Injection Molded June 8, 2010

Test Date	Sample Number	Theoretical Density (g/ml)*	Theoretical Density (g/ml)**	Actual Density (g/ml)
6/8/2009	BG8L-TC-15	1.2397	1.2345	1.2308
6/8/2009	BG8L-TC-28	1.2397	1.2345	1.2307
6/8/2009	BG8L-TC-20	1.2397	1.2345	1.2311
6/8/2009	BG8L-TC-9	1.2397	1.2345	1.2298
6/8/2009	BG8L-TC-25	1.2397	1.2345	1.2306
		Average		1.2306
		Standard Deviation		0.0005
		Number of Samples		5

* using 1.20 g/cc for Lexan

** using 1.1947 g/cc for Lexan

Table C.26: Density Results for 10 wt% xGnP in Lexan HF1130-111: BG5L: Extruded May 27, 2010; Injection Molded June 8, 2010

Test Date	Sample Number	Theoretical Density (g/ml)*	Theoretical Density (g/ml)**	Actual Density (g/ml)
6/8/2009	BG10L-TC-33	1.2500	1.2448	1.2411
6/8/2009	BG10L-TC-41	1.2500	1.2448	1.2411
6/8/2009	BG10L-TC-19	1.2500	1.2448	1.2395
6/8/2009	BG10L-TC-32	1.2500	1.2448	1.2396
6/8/2009	BG10L-TC-11	1.2500	1.2448	1.2399
		Average		1.2402
		Standard Deviation		0.0008
		Number of Samples		5

* using 1.20 g/cc for Lexan

** using 1.1947 g/cc for Lexan

Appendix C.4: Polycarbonate with Multiple Fillers

Table C.27: Density Results for Lexan HF1130-111:BL4: Injection Molded July 26, 2010

Test Date	Sample Number	Theoretical Density (g/ml)	Actual Density (g/ml)
7/30/2010	BL4-TC-3	1.200	1.1935
7/30/2010	BL4-TC-9	1.200	1.1924
7/30/2010	BL4-TC-4	1.200	1.1927
7/30/2010	BL4-TC-6	1.200	1.1930
7/30/2010	BL4-TC-1	1.200	1.1942
7/30/2010	BL4-TC-5	1.200	1.1929
7/30/2010	BL4-TC-2	1.200	1.1922
		Average	1.1930
		Standard Deviation	0.0007
		Number of Samples	7

Table C.28: Density Results for BA2LR: Extruded 7-8-10; Injection Molded 7-26-10

Test Date	Sample Number	Theoretical Density (g/ml)	Actual Density (g/ml)
7/30/2010	BA2LR-TC-9	1.2011	1.2022
7/30/2010	BA2LR-TC-5	1.2011	1.2019
7/30/2010	BA2LR-TC-15	1.2011	1.2017
7/30/2010	BA2LR-TC-23	1.2011	1.2016
7/30/2010	BA2LR-TC-28	1.2011	1.2017
7/30/2010	BA2LR-TC-32	1.2011	1.2019
7/30/2010	BA2LR-TC-13	1.2011	1.2017
		Average	1.2018
		Standard Deviation	0.0002
		Number of Samples	7

Table C29: Density Results for BA5LR: Extruded 7-8-10; Injection Molded 7-26-10

Test Date	Sample Number	Theoretical Density (g/ml)	Actual Density (g/ml)
7/30/2010	BA5LR-TC-21	1.2135	1.2142
7/30/2010	BA5LR-TC-27	1.2135	1.2144
7/30/2010	BA5LR-TC-13	1.2135	1.2138
7/30/2010	BA5LR-TC-30	1.2135	1.2148
7/30/2010	BA5LR-TC-14	1.2135	1.2132
7/30/2010	BA5LR-TC-10	1.2135	1.2129
7/30/2010	BA5LR-TC-25	1.2135	1.2141
		Average	1.2139
		Standard Deviation	0.0006
		Number of Samples	7

Table C.30: Density Results for BG12L: Extruded 7-8-10; Injection Molded 8-18-10

Test Date	Sample Number	Theoretical Density (g/ml)	Actual Density (g/ml)
8/31/2010	BG12L-TC-22	1.2537	1.2519
8/31/2010	BG12L-TC-28	1.2537	1.2520
8/31/2010	BG12L-TC-30	1.2537	1.2523
8/31/2010	BG12L-TC-11	1.2537	1.2521
8/31/2010	BG12L-TC-12	1.2537	1.2523
		Average	1.2521
		Standard Deviation	0.0002
		Number of Samples	5

Table C.31: Density Results for BG15L: Extruded 7-8-10; Injection Molded 8-18-10

Test Date	Sample Number	Theoretical Density (g/ml)	Actual Density (g/ml)
8/31/2010	BG15L-TC-5	1.2699	1.2685
8/31/2010	BG15L-TC-24	1.2699	1.2680
8/31/2010	BG15L-TC-19	1.2699	1.2686
8/31/2010	BG15L-TC-12	1.2699	1.2687
8/31/2010	BG15L-TC-1	1.2699	1.2682
8/31/2010	BG15L-TC-14	1.2699	1.2681
		Average	1.2683
		Standard Deviation	0.0003
		Number of Samples	6

Table C.32: Density Results for BA2Q1L: Extruded 7-7-10; Injection Molded June 26, 2010

Test Date	Sample Number	Theoretical Density (g/ml)	Actual Density (g/ml)
7/30/2010	BA2Q1L-TC-34	1.2050	1.2067
7/30/2010	BA2Q1L-TC-17	1.2050	1.2071
7/30/2010	BA2Q1L-TC-27	1.2050	1.2074
7/30/2010	BA2Q1L-TC-31	1.2050	1.2072
7/30/2010	BA2Q1L-TC-2	1.2050	1.2074
7/30/2010	BA2Q1L-TC-40	1.2050	1.2080
7/30/2010	BA2Q1L-TC-9	1.2050	1.2079
		Average	1.2074
		Standard Deviation	0.0004
		Number of Samples	7

Table C.33: Density Results for BA2Q5L: Extruded 7-7-10; Injection Molded 8-25-10

Test Date	Sample Number	Theoretical Density (g/ml)	Actual Density (g/ml)
8/26/2010	BA2Q5L-TC-24	1.2207	1.2250
8/26/2010	BA2Q5L-TC-21	1.2207	1.2282
8/26/2010	BA2Q5L-TC-7	1.2207	1.2221
8/26/2010	BA2Q5L-TC-18	1.2207	1.2259
8/26/2010	BA2Q5L-TC-15	1.2207	1.2253
8/26/2010	BA2Q5L-TC-10	1.2207	1.2247
		Average	1.2252
		Standard Deviation	0.0020
		Number of Samples	6

Table C.34: Density Results for BA5Q1L: Extruded 7-7-10; Injection Molded 7-26-10

Test Date	Sample Number	Theoretical Density (g/ml)	Actual Density (g/ml)
7/30/2010	BA5Q1L-TC-17	1.2174	1.2188
7/30/2010	BA5Q1L-TC-21	1.2174	1.2194
7/30/2010	BA5Q1L-TC-16	1.2174	1.2191
7/30/2010	BA5Q1L-TC-10	1.2174	1.2191
7/30/2010	BA5Q1L-TC-26	1.2174	1.2192
7/30/2010	BA5Q1L-TC-28	1.2174	1.2195
		Average	1.2192
		Standard Deviation	0.0002
		Number of Samples	6

Table C.35: Density Results for BA5Q5L: Extruded 7-7-10; Injection Molded 8-25-10

Test Date	Sample Number	Theoretical Density (g/ml)	Actual Density (g/ml)
8/26/2010	BA5Q5L-TC-9	1.2334	1.2353
8/26/2010	BA5Q5L-TC-17	1.2334	1.2384
8/26/2010	BA5Q5L-TC-23	1.2334	1.2388
8/26/2010	BA5Q5L-TC-25	1.2334	1.2384
8/26/2010	BA5Q5L-TC-15	1.2334	1.2385
		Average	1.2379
		Standard Deviation	0.0015
		Number of Samples	5

Table C.36: Density Results for BA2G2L: Extruded 7-6-10; Injection Molded 8-18-10

Test Date	Sample Number	Theoretical Density (g/ml)	Actual Density (g/ml)
8/18/2010	BA2G2L-TC-12	1.2109	1.2095
8/18/2010	BA2G2L-TC-6	1.2109	1.2098
8/18/2010	BA2G2L-TC-1	1.2109	1.2091
8/18/2010	BA2G2L-TC-20	1.2109	1.2090
8/18/2010	BA2G2L-TC-13	1.2109	1.2090
8/18/2010	BA2G2L-TC-4	1.2109	1.2096
		Average	1.2093
		Standard Deviation	0.0004
		Number of Samples	6

Table C.37: Density Results for BA2G5L: Extruded 7-6-10; Injection Molded 8-18-10

Test Date	Sample Number	Theoretical Density (g/ml)	Actual Density (g/ml)
8/18/2010	BA2G5L-TC-7	1.2260	1.2240
8/18/2010	BA2G5L-TC-30	1.2260	1.2259
8/18/2010	BA2G5L-TC-20	1.2260	1.2256
8/18/2010	BA2G5L-TC-17	1.2260	1.2249
8/18/2010	BA2G5L-TC-6	1.2260	1.2254
		Average	1.2252
		Standard Deviation	0.0008
		Number of Samples	5

Table C.38: Density Results for BA5G2L: Extruded 7-6-10; Injection Molded 8-18-10

Test Date	Sample Number	Theoretical Density (g/ml)	Actual Density (g/ml)
8/18/2010	BA5G2L-TC-24	1.2235	1.2238
8/18/2010	BA5G2L-TC-17	1.2235	1.2234
8/18/2010	BA5G2L-TC-3	1.2235	1.2258
8/18/2010	BA5G2L-TC-10	1.2235	1.2242
8/18/2010	BA5G2L-TC-25	1.2235	1.2235
8/18/2010	BA5G2L-TC-14	1.2235	1.2245
		Average	1.2241
		Standard Deviation	0.0010
		Number of Samples	6

Table C.39: Density Results for BA5G5L: Extruded 7-6-10; Injection Molded 8-18-10

Test Date	Sample Number	Theoretical Density (g/ml)	Actual Density (g/ml)
8/18/2010	BA5G5L-TC-19	1.2389	1.2387
8/18/2010	BA5G5L-TC-7	1.2389	1.2381
8/18/2010	BA5G5L-TC-16	1.2389	1.2377
8/18/2010	BA5G5L-TC-28	1.2389	1.2388
		Average	1.2382
		Standard Deviation	0.0005
		Number of Samples	4

Table C.40: Density Results for BQ1G2L: Extruded 7-1-10; Injection Molded 8-18-10

Test Date	Sample Number	Theoretical Density (g/ml)	Actual Density (g/ml)
8/18/2010	BQ1G2L-TC-8	1.2066	1.2050
8/18/2010	BQ1G2L-TC-4	1.2066	1.2053
8/18/2010	BQ1G2L-TC-11	1.2066	1.2057
8/18/2010	BQ1G2L-TC-23	1.2066	1.2047
		Average	1.2053
		Standard Deviation	0.0004
		Number of Samples	4

Table C.41: Density Results for BQ1G5L: Extruded 7-1-10; Injection Molded 8-18-10

Test Date	Sample Number	Theoretical Density (g/ml)	Actual Density (g/ml)
8/18/2010	BQ1G5L-TC-19	1.2215	1.2192
8/18/2010	BQ1G5L-TC-4	1.2215	1.2195
8/18/2010	BQ1G5L-TC-10	1.2215	1.2197
8/18/2010	BQ1G5L-TC-27	1.2215	1.2193
		Average	1.2194
		Standard Deviation	0.0002
		Number of Samples	4

Table C.42: Density Results for BQ5G2L: Extruded 7-1-10; Injection Molded 8-18-10

Test Date	Sample Number	Theoretical Density (g/ml)	Actual Density (g/ml)
8/19/2010	BQ5G2L-TC-22	1.2223	1.2231
8/19/2010	BQ5G2L-TC-14	1.2223	1.2222
8/19/2010	BQ5G2L-TC-9	1.2223	1.2233
8/19/2010	BQ5G2L-TC-3	1.2223	1.2224
8/19/2010	BQ5G2L-TC-17	1.2223	1.2236
8/19/2010	BQ5G2L-TC-25	1.2223	1.2228
		Average	1.2229
		Standard Deviation	0.0006
		Number of Samples	6

Table C.43: Density Results for BQ5G5L: Extruded 7-1-10; Injection Molded 8-18-10

Test Date	Sample Number	Theoretical Density (g/ml)	Actual Density (g/ml)
8/19/2010	BQ5G5L-TC-12	1.2377	1.2370
8/19/2010	BQ5G5L-TC-23	1.2377	1.2378
8/19/2010	BQ5G5L-TC-30	1.2377	1.2379
8/19/2010	BQ5G5L-TC-16	1.2377	1.2380
		Average	1.2376
		Standard Deviation	0.0005
		Number of Samples	4

Appendix D: Melt Flow Indexing Results

Appendix D.1: Polycarbonate with Carbon Nanotubes

Table D.1: MFI Results for BL at 300°C

BL	weight (g)	MFI (g/10min)
1	0.7886	31.544
2	0.8187	32.748
3	0.8087	32.348
4	0.8021	32.084
5	0.8392	33.568
6	0.7541	30.164
7	0.8046	32.184
Average	0.80	32.09
Stdev	0.03	1.06
Count	7	7

Conditions

Dwell

time 360 s

Collect

Time 15 s

Temp 300 °C

Mass 1.25 kg

Table D.2: MFI Results for BLE at 300°C

BLE	weight (g)	MFI (g/10min)
1	0.8777	35.108
2	0.8479	33.916
3	0.8965	35.86
4	0.876	35.04
5	0.8273	33.092
6	0.852	34.08
7	0.8868	35.472
Average	0.87	34.65
Stdev	0.02	0.98
Count	7	7

Conditions

Dwell

time 360 s

Collect

Time 15 s

Temp 300 °C

Mass 1.25 kg

Table D.3: MFI Results for BQ2L at 320°C

BQ2L	weight (g)	collection time (s)	MFI (g/10min)
1	7.0399	16.10	262.36
2	7.5509	16.36	276.93
3	6.8234	12.77	320.60
4	6.4848	11.80	329.74
5	7.377	16.41	269.73
Average	7.0552	14.69	291.87
Stdev	0.4267889	2.22	31.00
Count	5	5	5

Conditions

Dwell time 360 s
Temp 320 °C
Mass 5 kg

Table D.4: MFI Results for BQ3L at 320°C

BQ3L	weight (g)	collection time (s)	MFI (g/10min)
1	7.5219	19.21	234.94
2	7.1056	16.29	261.72
3	7.7166	18.21	254.25
4	7.0722	16.89	251.23
5	7.2726	17.98	242.69
6	7.2386	19.58	221.82
7	7.1151	16.80	254.11
Average	7.2918	17.85	245.82
Stdev	0.2417704	1.25	13.70
Count	7	7	7

Conditions

Dwell time 360 s
Temp 320 °C
Mass 5 kg

Table D.5: MFI Results for BQ4L at 320°C

BQ4L	weight (g)	collection time (s)	MFI (g/10min)
1	7.8128	31.32	149.67
2	7.6709	25.35	181.56
3	7.8292	25.12	187.00
4	7.9561	26.52	180.00
5	7.5923	25.76	176.84
6	7.7082	27.97	165.35
7	7.786	27.80	168.04
Average	7.7650714	27.12	172.64
Stdev	0.1192148	2.17	12.65
Count	7	7	7

Conditions

Dwell time 360 s

Temp 320 °C

Mass 5 kg

Table D.6: MFI Results for BQ5L at 320°C

BQ5L	weight	collection time (s)	MFI (g/10min)
1	8.7469	50.05	104.86
2	8.5612	42.52	120.81
3	8.5034	42.63	119.68
4	8.4834	45.44	112.02
5	8.5521	42.87	119.69
6	8.551	40.96	125.26
7	6.8488	35.87	114.56
8	8.5386	46.39	110.44
9	8.7448	50.91	103.06
Average	8.3922444	44.18	114.49
Stdev	0.5866946	4.64	7.55
Count	9	9	9

Conditions

Dwell time 360 s

Temp 320 °C

Mass 5 kg

Table D.7: MFI Results for BQ6L at 320°C

BQ6L	weight	collection time (s)	MFI (g/10min)
1	9.0341	94.12	57.59
2	8.8972	84.47	63.20
3	8.938	93.64	57.27
4	9.2136	115.01	48.07
5	8.9946	93.58	57.67
6	9.0947	126.63	43.09
7	8.8359	92.00	57.63
Average	9.0011571	99.92	54.93
Stdev	0.1272244	15.03	6.87
Count	7	7	7

Conditions

Dwell time 360 s

Temp 320 °C

Mass 5 kg

Appendix D.2: Polycarbonate with Carbon Black

Table D.8: MFI Results for BA2L at 320°C

BA2L	Weight (g)	Collection time (s)	MFI (g/10min)
1	7.424	30.43	146.38
2	7.5022	31.75	141.77
3	5.3803	20.97	153.94
4	7.4205	30.17	147.57
5	4.1336	16.45	150.77
Average			148.09
Stdev			4.60
Count			5

Conditions

Dwell time 360 s

Temp 320 °C

Wt 5 kg

Table D.9: MFI Results for BA3L at 320°C

BA3L	Weight (g)	Collection time (s)	MFI (g/10min)
1	6.1856	34.64	107.14
2	6.4552	34.73	111.52
3	4.468	22.33	120.05
4	6.824	35.28	116.05
5	6.0563	32.1	113.20
6	6.1082	35.36	103.65
Average			111.94
Stdev			5.94
Count			6

Conditions

Dwell time 360 s

Temp 320 °C

Weight 5 kg

Table D.10: MFI Results for BA4L at 320°C

BA4L	Weight (g)	Collection time (s)	MFI (g/10min)
1	7.7919	54.44	85.88
2	6.3183	42.21	89.81
3	7.0031	47.26	88.91
4	6.4195	45.20	85.21
5	7.2145	50.7	85.38
6	7.5645	50.37	90.11
Average			87.55
Stdev			2.30
Count			6

Conditions

Dwell time 360 s

Temp 320 °C

Weight 5 kg

Table D.11: MFI Results for BA5L at 320°C

BA5L	Weight (g)	Collection time (s)	MFI (g/10min)
1	1.6637	15.0	66.55
2	6.2791	61.63	61.13
3	2.0807	20.0	62.42
4	1.6109	15.0	64.44
5	2.1543	20.0	64.63
6	2.1407	20.32	62.15
Average			63.55
Stdev			2.00
Count			6

Conditions

Dwell time 360 s

Temp 320 °C

Weight 5 kg

Table D.12: MFI Results for BA6L at 320°C

BA6L	Weight (g)	Collection time (s)	MFI (g/10min)
1	7.7246	131.3	35.30
2	6.5882	102.6	38.53
3	5.5827	98.7	33.94
4	6.3849	98.2	39.01
5	6.2436	99.38	37.69
6	7.6590	120.0	38.30
Average			37.13
Stdev			2.03
Count			6

Conditions

Dwell time 360 s

Temp 320 °C

Weight 5 kg

Appendix D.3: Polycarbonate with Graphene Nanoplatelets

Table D.13: MFI Results for BLE3 at 300°C

BLE3	Weight (g)	MFI (g/10min)	Conditions	
1	0.8653	34.612	Dwell time	360 s
2	0.8647	34.588	Collect	
3	0.823	32.92	Time	15 s
4	0.8309	33.236	Temp	300 °C
5	0.8847	35.388	Weight	1.25 kg
6	0.8153	32.612		
7	0.864	34.56		
Average	0.85	33.99		
Stdev	0.03	1.05		
Count	7	7		

Table D.14: MFI Results for BG2L at 320°C

BG2L	Weight (g)	Collection Time (s)	MFI (g/10min)	Conditions	
1	6.5055	24.45	159.64	Dwell time	360 s
2	6.4991	27.02	144.32	Temp	320 °C
3	5.8066	22.00	158.36	Weight	5 kg
4	6.65	24.39	163.59		
5	5.8219	23.33	149.73		
Average	6.25662	24.24	155.13		
Stdev	0.4083458	1.85	7.88		
Count	5	5	5		

Table D.15: MFI Results for BG3L at 320°C

BG3L	Weight (g)	Collection Time (s)	MFI (g/10min)
1	6.7809	27.86	146.04
2	6.3482	27.15	140.29
3	6.4	27.32	140.56
4	6.564	27.20	144.79
Average	6.523275	27.38	142.92
Stdev	0.1948308	0.33	2.93
Count	4	4	4

Conditions

Dwell time 360 s
Temp 320 °C
Weight 5 kg

Table D.16: MFI Results for BG4L at 320°C

BG4L	Weight (g)	Collection Time (s)	MFI (g/10min)
1	6.5626	30.49	129.14
2	6.249	30.48	123.01
3	6.268	29.19	128.84
4	6.2607	28.72	130.79
5	6.2837	29.75	126.73
Average	6.3248	29.73	127.70
Stdev	0.1335278	0.78	2.99
Count	5	5	5

Conditions

Dwell time 360 s
Temp 320 °C
Weight 5 kg

Table D.17: MFI Results for BG5L at 320°C

BG5L	Weight (g)	Collection Time (s)	MFI (g/10min)
1	6.7978	35.31	115.51
2	6.3043	31.22	121.16
3	6.2818	32.87	114.67
4	6.2872	31.97	118.00
5	6.0184	31.81	113.52
Average	6.3379	32.64	116.57
Stdev	0.2830349	1.61	3.05
Count	5	5	5

Conditions

Dwell time 360 s
Temp 320 °C
Weight 5 kg

Table D.18: MFI Results for BG6L at 320°C

BG6L	Weight (g)	Collection Time (s)	MFI (g/10min)
1	6.5994	38.82	102.00
2	6.5142	36.64	106.67
3	6.6678	36.62	109.25
4	6.3793	35.26	108.55
5	6.7822	37.86	107.48
Average	6.58858	37.04	106.79
Stdev	0.1526533	1.36	2.85
Count	5	5	5

Conditions

Dwell time 360 s
Temp 320 °C
Weight 5 kg

Table D.19: MFI Results for BG8L at 320°C

BG8L	Weight (g)	Collection Time (s)	MFI (g/10min)
1	7.2204	55.29	78.35
2	6.8595	47.21	87.18
3	6.8792	50.51	81.72
4	7.0451	48.53	87.10
5	6.8555	48.87	84.17
Average	6.97194	50.08	83.70
Stdev	0.1595983	3.14	3.75
Count	5	5	5

Conditions

Dwell time 360 s
Temp 320 °C
Weight 5 kg

Table D.20: MFI Results for BG10L at 320°C

BG10L	Weight (g)	Collection Time (s)	MFI (g/10min)
1	6.9704	61.05	68.51
2	6.7229	57.80	69.79
3	7.2966	61.44	71.26
4	6.6696	55.99	71.47
5	6.7842	56.92	71.51
Average	6.88874	58.64	70.51
Stdev	0.254692	2.47	1.33
Count	5	5	5

Conditions

Dwell time 360 s
Temp 320 °C
Weight 5 kg

Appendix D.4: Polycarbonate with Multiple Fillers

Table D.21: MFI Results for BA2LR

BA2LR	Mass (g)	Collection Time (s)	MFI (g/10min)
1	5.6484	22.48	150.758
2	5.7247	23.49	146.225
3	6.5661	27.01	145.859
4	7.3149	31.02	141.487
5	5.9090	25.14	141.026
Average	6.2326	16.14	145.071
STDEV	0.7047	3.37	3.984
Count	5	5	5

Conditions:

Dwell

Time: 360 s

Melt Temp: 320 °C

Mass: 5 kg

Table D.22: MFI Results for BA5LR

BA5LR	Mass (g)	Collection Time (s)	MFI (g/10min)
1	6.7137	58.25	69.154
2	7.5117	68.78	65.528
3	7.0857	61.70	68.905
4	7.3767	61.49	71.980
Average	7.1720	16.14	68.892
STDEV	0.3535	4.44	2.641
Count	4	4	4

Conditions:

Dwell

Time: 360 s

Melt Temp: 320 °C

Mass: 5 kg

Table D.23: MFI Results for BQ0.5L

BQ0.5L	weight (g)	collection time (s)	MFI (g/10min)
1	5.6229	10.35	325.97
2	5.0695	10.27	296.17
3	4.8193	9.10	317.76
4	4.1398	7.51	330.74
5	5.7201	9.57	358.63
Average	5.07432	9.36	325.85
Stdev	0.6434978	1.16	22.61
Count	5	5	5

Conditions

Dwell time 360 s

Temp 320 °C

Mass 5 kg

extruded 6-30-10

2-9-09

screw

Table D.24: MFI Results for BQ1L

BQ1L	weight (g)	collection time (s)	MFI (g/10min)
1	5.4763	11.86	277.05
2	5.3404	10.10	317.25
3	6.1525	10.31	358.05
4	4.9803	9.25	323.05
5	5.1941	9.54	326.67
Average	5.42872	10.21	320.41
Stdev	0.4444234	1.01	28.95
Count	5	5	5

Conditions

Dwell time 360 s
Temp 320 °C
Mass 5 kg

extruded 6-30-10
2-9-09
screw

Table D.25: MFI Results for BG12L

BG12L	Mass (g)	Collection Time (s)	MFI (g/10min)
1	6.7200	73.43	54.909
2	7.0295	75.12	56.146
3	7.0785	75.42	56.313
4	6.8060	74.12	55.094
5	6.6946	70.58	56.911
Average	6.8657	73.73	55.875
STDEV	0.1776	1.93	0.848
Count	5	5	5

Conditions:

Dwell
Time: 360 s
Melt Temp: 320 °C
Mass: 5 kg

Table D.26: MFI Results for BG15L

BG15L	Mass (g)	Collection Time (s)	MFI (g/10min)
1	7.9222	149.03	31.895
2	8.4803	152.44	33.378
3	8.2269	165.56	29.815
4	8.0704	162.99	29.709
5	7.1327	126.01	33.963
Average	7.9665	151.21	31.752
STDEV	0.5098	15.70	1.967
Count	5	5	5

Conditions:

Dwell
Time: 360 s
Melt Temp: 320 °C
Mass: 5 kg

Table D.27: MFI Results for BA2Q1L

BA2Q1L	Mass (g)	Collection Time (s)	MFI (g/10min)
1	4.0725	8.43	289.858
2	6.2589	12.80	293.386
3	6.4543	13.50	286.858
4	6.1503	12.67	291.253
5	6.3000	12.48	302.885
Average	5.8472	11.98	292.848
STDEV	0.9981	2.02	6.091
Count	5	5	5

Conditions:

Dwell

Time: 360 s

Melt Temp: 320 °C

Mass: 5 kg

Table D.28: MFI Results for BA2Q5L

BA2Q5L	Mass (g)	Collection Time (s)	MFI (g/10min)
1	7.2307	67.97	63.828
2	6.3634	52.12	73.255
3	6.5801	53.02	74.464
4	6.7000	64.42	62.403
5	6.1862	50.02	74.205
Average	6.6121	57.51	69.631
STDEV	0.3983	8.10	5.986
Count	5	5	5

Conditions:

Dwell

Time: 360 s

Melt Temp: 320 °C

Mass: 5 kg

Table D.29: MFI Results for BA5Q1L

BA5Q1L	Mass (g)	Collection Time (s)	MFI (g/10min)
1	6.4642	30.47	127.290
2	6.9321	35.70	116.506
3	6.5939	34.18	115.750
4	6.1080	31.90	114.884
5	7.1207	35.45	120.520
Average	6.6438	33.54	118.990
STDEV	0.3976	2.28	5.117
Count	5	5	5

Conditions:

Dwell

Time: 360 s

Melt Temp: 320 °C

Mass: 5 kg

Table D.30: MFI Results for BA2G2L

BA2G2L	Mass (g)	Collection Time (s)	MFI (g/10min)
1	5.5844	31.42	106.640
2	4.7933	24.67	116.578
3	5.4900	30.17	109.181
4	5.9189	31.92	111.258
5	5.4177	31.00	104.859
Average	5.4409	29.84	109.703
STDEV	0.4097	2.96	4.550
Count	5	5	5

Conditions:

Dwell

Time: 360 s

Melt Temp: 320 °C

Mass: 5 kg

Table D.31: MFI Results for BA2G5L

BA2G5L	Mass (g)	Collection Time (s)	MFI (g/10min)
1	6.1636	45.47	81.332
2	6.3866	46.83	81.827
3	5.4733	41.41	79.304
4	6.1589	44.56	82.930
5	5.3509	41.10	78.115
Average	5.9067	43.87	80.702
STDEV	0.4628	2.53	1.954
Count	5	5	5

Conditions:

Dwell

Time: 360 s

Melt Temp: 320 °C

Mass: 5 kg

Table D.32: MFI Results for BA5G2L

BA5G2L	Mass (g)	Collection Time (s)	MFI (g/10min)
1	7.8549	99.25	47.486
2	8.0947	102.83	47.232
3	8.1574	95.66	51.165
4	7.9282	95.30	49.915
5	7.1263	81.76	52.297
Average	7.8323	94.96	49.619
STDEV	0.4131	7.99	2.230
Count	5	5	5

Conditions:

Dwell

Time: 360 s

Melt Temp: 320 °C

Mass: 5 kg

Table D.33: MFI Results for BA5G5L

BA5G5L	Mass (g)	Collection Time (s)	MFI (g/10min)
1	6.5516	197.51	19.903
2	7.4600	172.18	25.996
3	8.1355	214.36	22.772
4	8.6637	248.38	20.928
5	7.1263	208.62	20.496
Average	7.5874	208.21	22.019
STDEV	0.8307	27.68	2.468
Count	5	5	5

Conditions:

Dwell

Time: 360 s

Melt Temp: 320 °C

Mass: 5 kg

Table D.34: MFI Results for BQ1G2L

BQ1G2L	Mass (g)	Collection Time (s)	MFI (g/10min)
1	4.9825	14.82	201.721
2	4.5854	12.10	227.375
3	4.9918	12.98	230.746
4	4.8379	12.63	229.829
5	5.1504	15.09	204.787
Average	4.9096	16.14	218.892
STDEV	0.2123	1.35	14.369
Count	5	5	5

Conditions:

Dwell

Time: 360 s

Melt Temp: 320 °C

Mass: 5 kg

Table D.35: MFI Results for BQ1G5L

BQ1G5L	Mass (g)	Collection Time (s)	MFI (g/10min)
1	5.5200	20.55	161.168
2	5.3902	20.27	159.552
3	5.7949	21.77	159.712
4	5.8422	21.23	165.112
5	4.9440	18.93	156.704
Average	5.4983	16.14	160.450
STDEV	0.3625	1.08	3.067
Count	5	5	5

Conditions:

Dwell

Time: 360 s

Melt Temp: 320 °C

Mass: 5 kg

Table D.36: MFI Results for BQ5G2L

BQ5G2L	Mass (g)	Collection Time (s)	MFI (g/10min)
1	7.0572	32.06	132.075
2	6.7910	27.72	146.991
3	7.0427	27.84	151.782
4	6.4428	27.54	140.366
5	7.1681	28.98	148.408
Average	6.9004	16.14	143.924
STDEV	0.2906	1.89	7.816
Count	5	5	5

Conditions:

Dwell

Time: 360 s

Melt Temp: 320 °C

Mass: 5 kg

Table D.37: MFI Results for BQ5G5L

BQ5G5L	Mass (g)	Collection Time (s)	MFI (g/10min)
1	7.0087	72.03	58.382
2	7.3604	70.47	62.668
3	7.4759	74.70	60.047
4	7.2946	80.42	54.424
5	6.7267	65.68	61.450
Average	7.1733	16.14	59.394
STDEV	0.3032	5.44	3.206
Count	5	5	5

Conditions:

Dwell

Time: 360 s

Melt Temp: 320 °C

Mass: 5 kg

Appendix E: Sample Differential Scanning Calorimetry (DSC) Results

Appendix E.1: Polycarbonate with Carbon Nanotubes

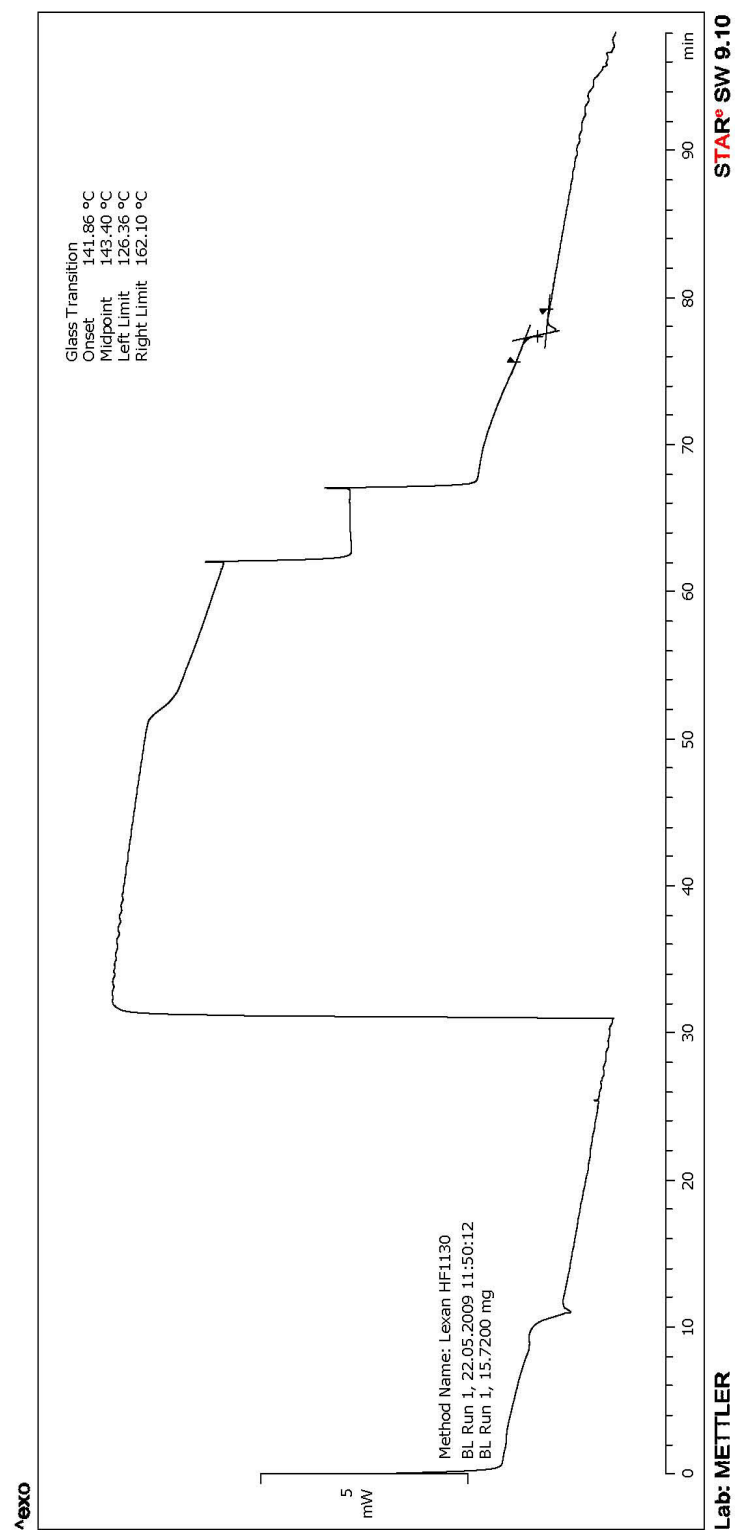


Figure E.1: DSC for Lexan HF1130-111 (BL) Run 1 vs. Time

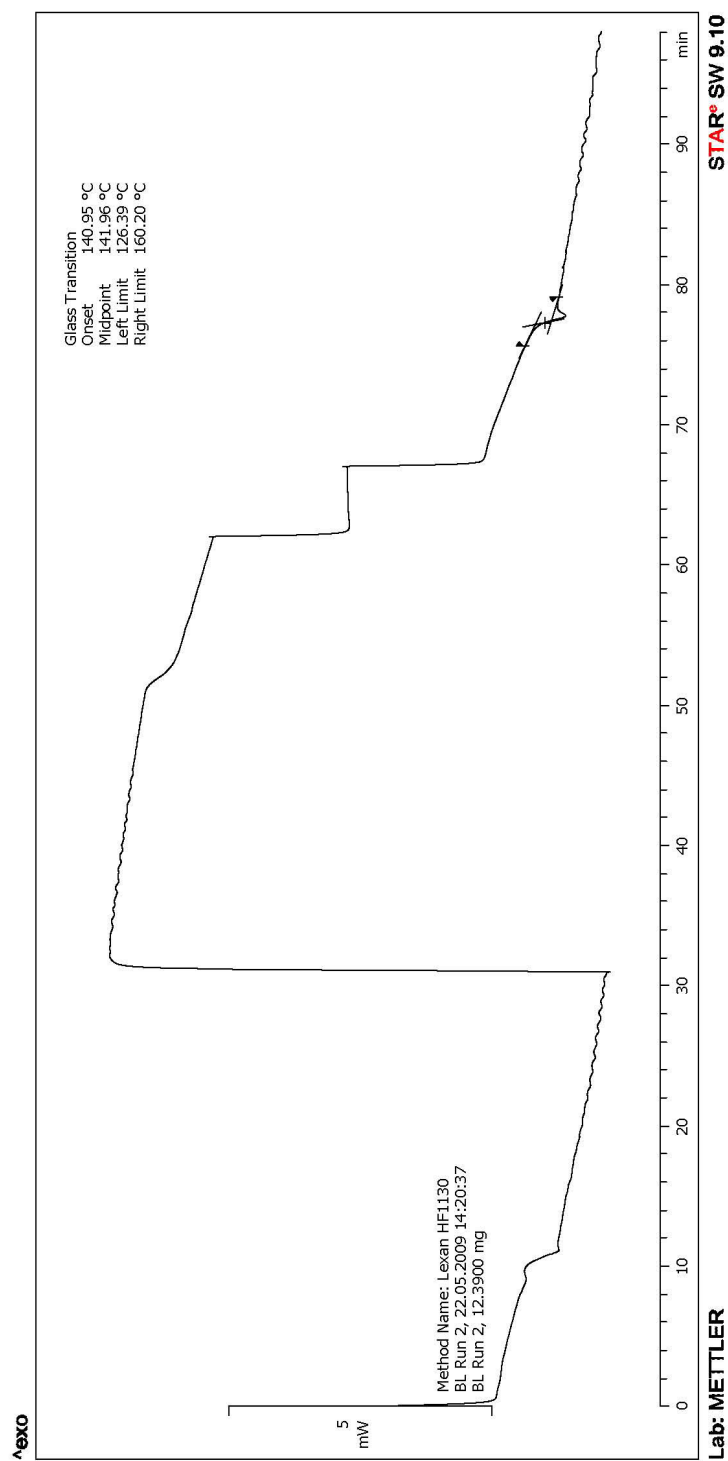


Figure E.2: DSC for Lexan HF1130-111 (BL) Run 2 vs. Time

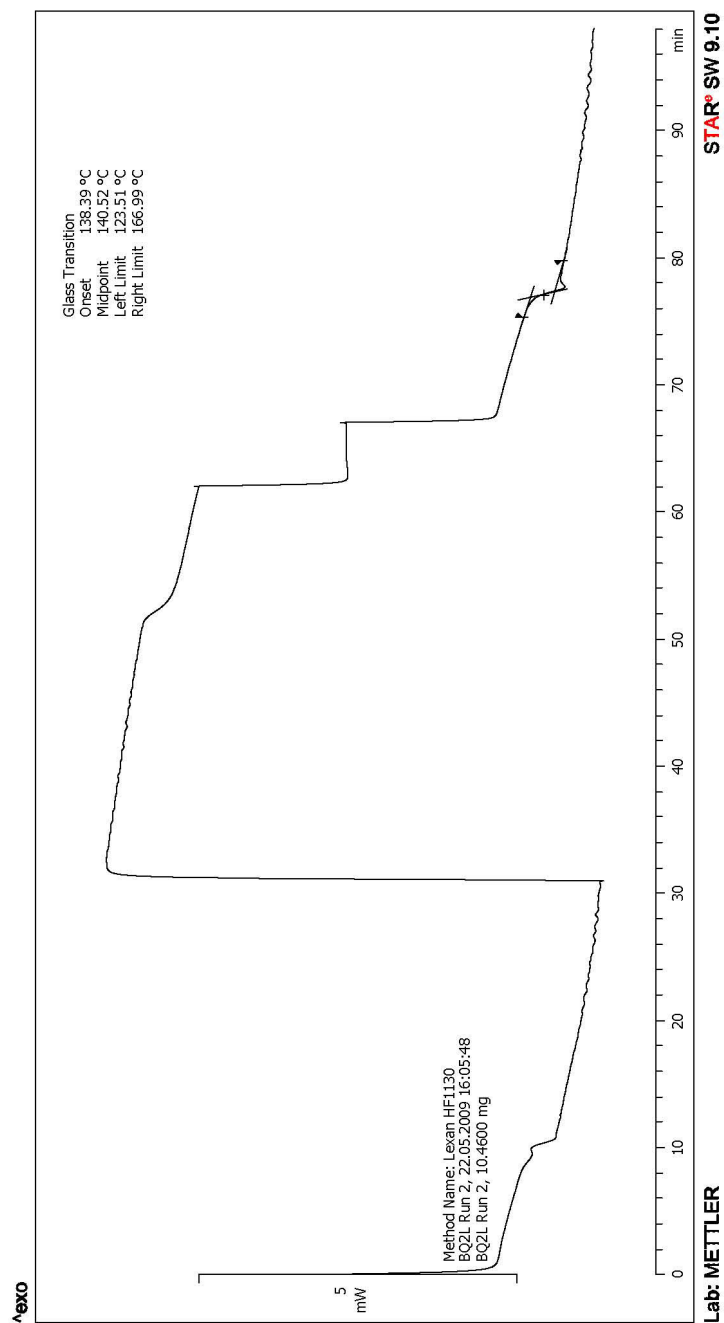


Figure E.3: DSC for BQ2L Run 1 vs. Time

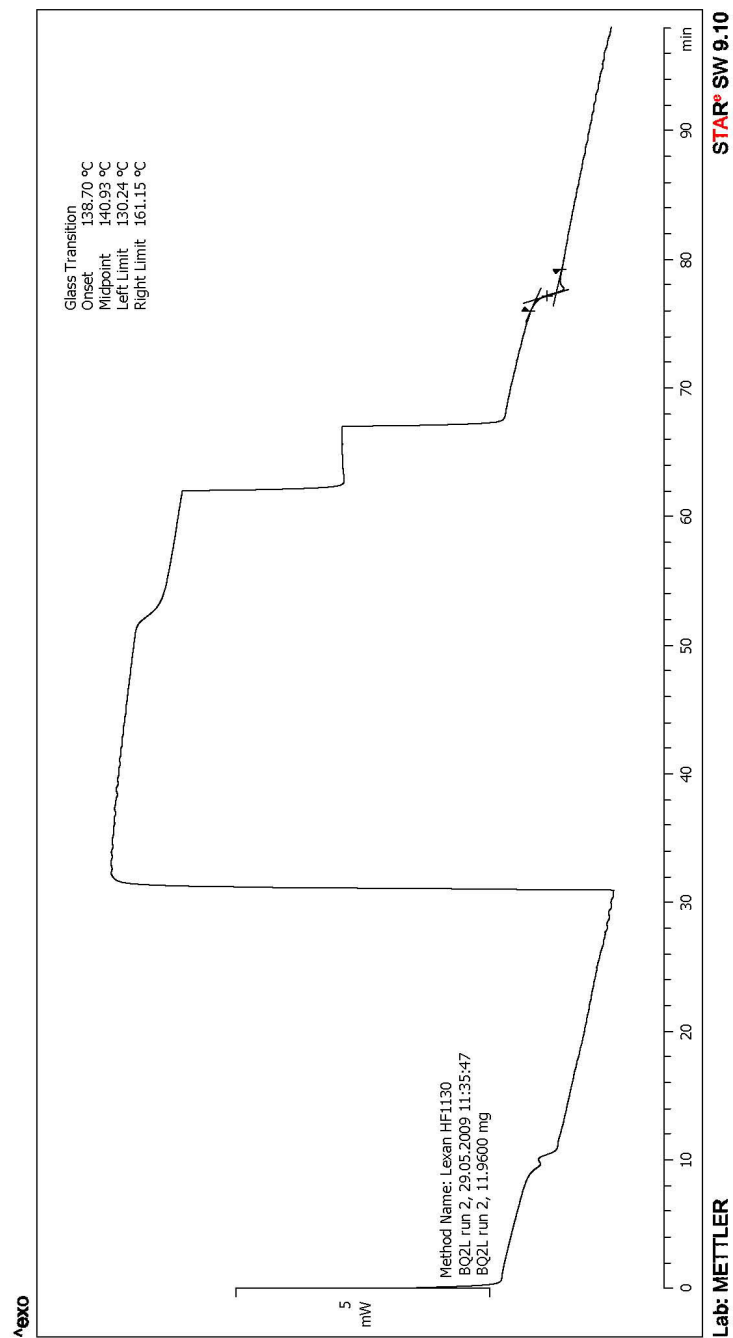


Figure E.4: DSC for BQ2L Run 2 vs. Time

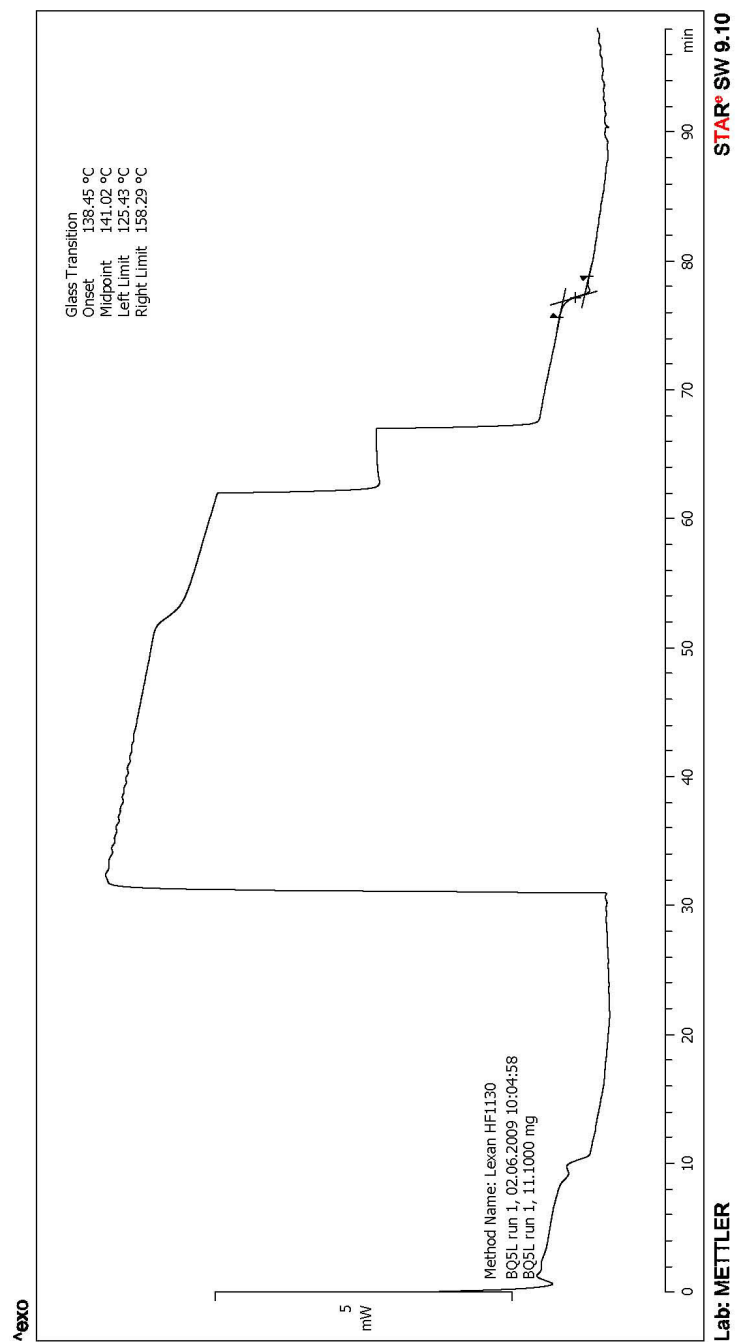


Figure E.5: DSC for BQ5L Run 1 vs. Time

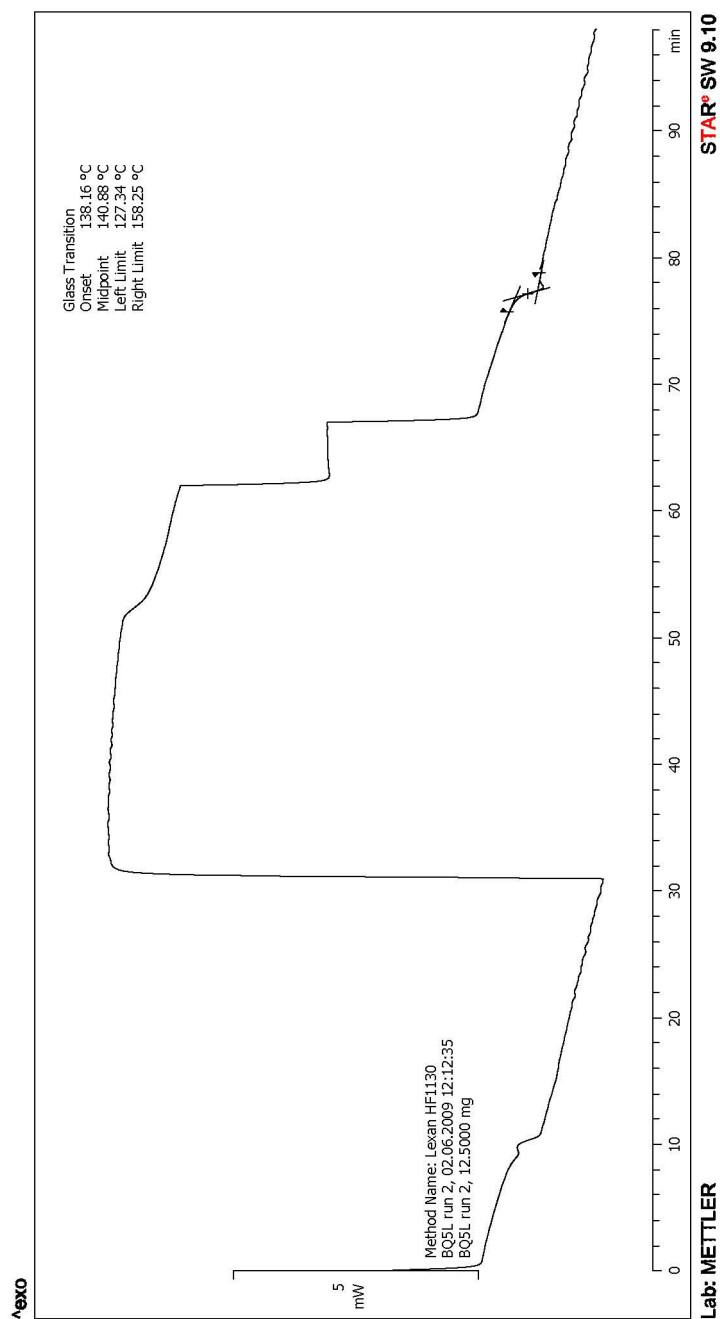


Figure E.6: DSC for BQ5L Run 2 vs. Time

Appendix E.2: Polycarbonate with Carbon Black

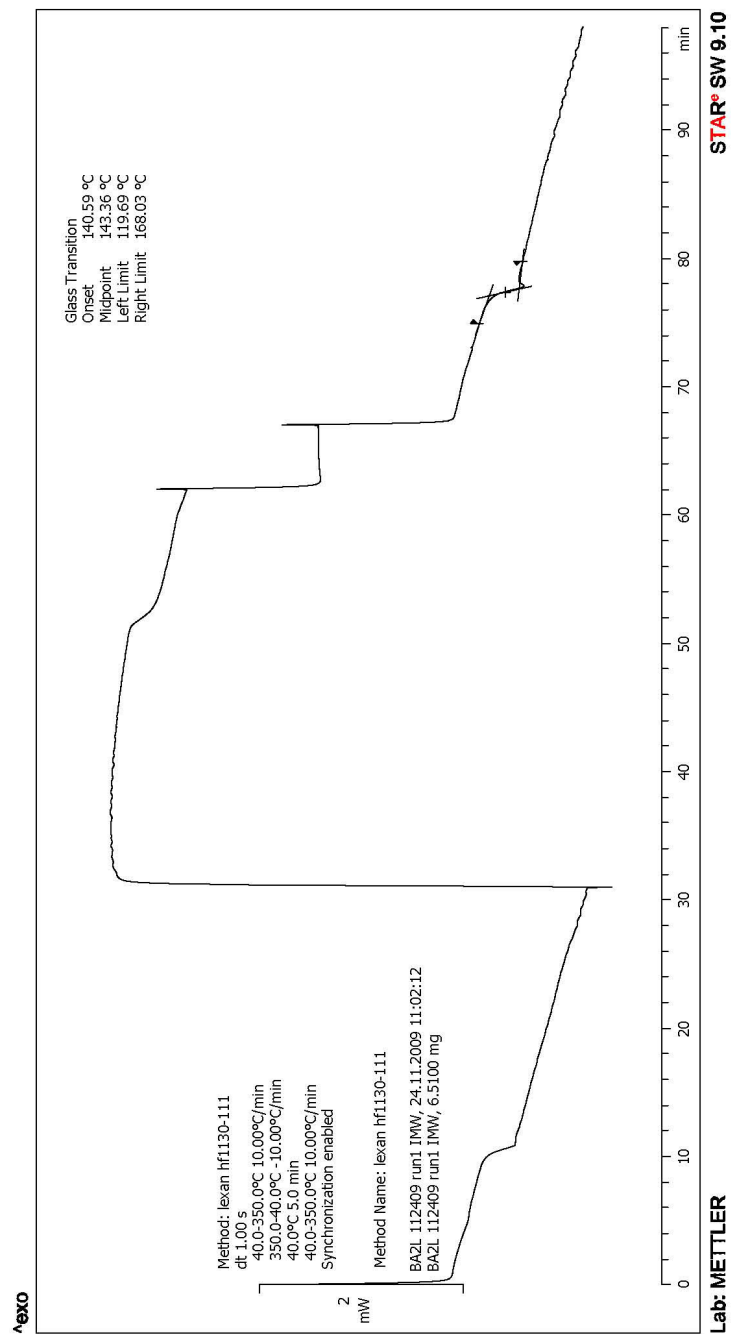


Figure E.7: DSC for BA2L Run 1 vs. Time

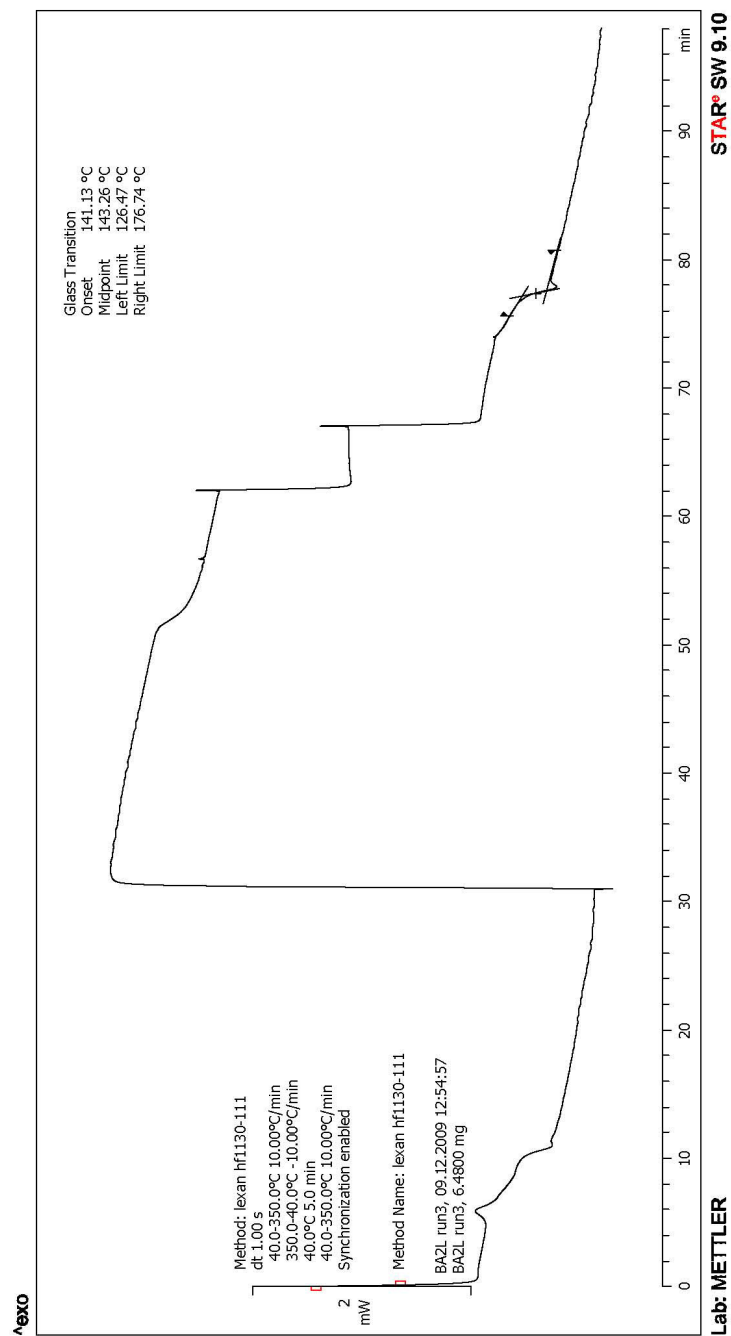


Figure E.8: DSC for BA2L Run 2 vs. Time

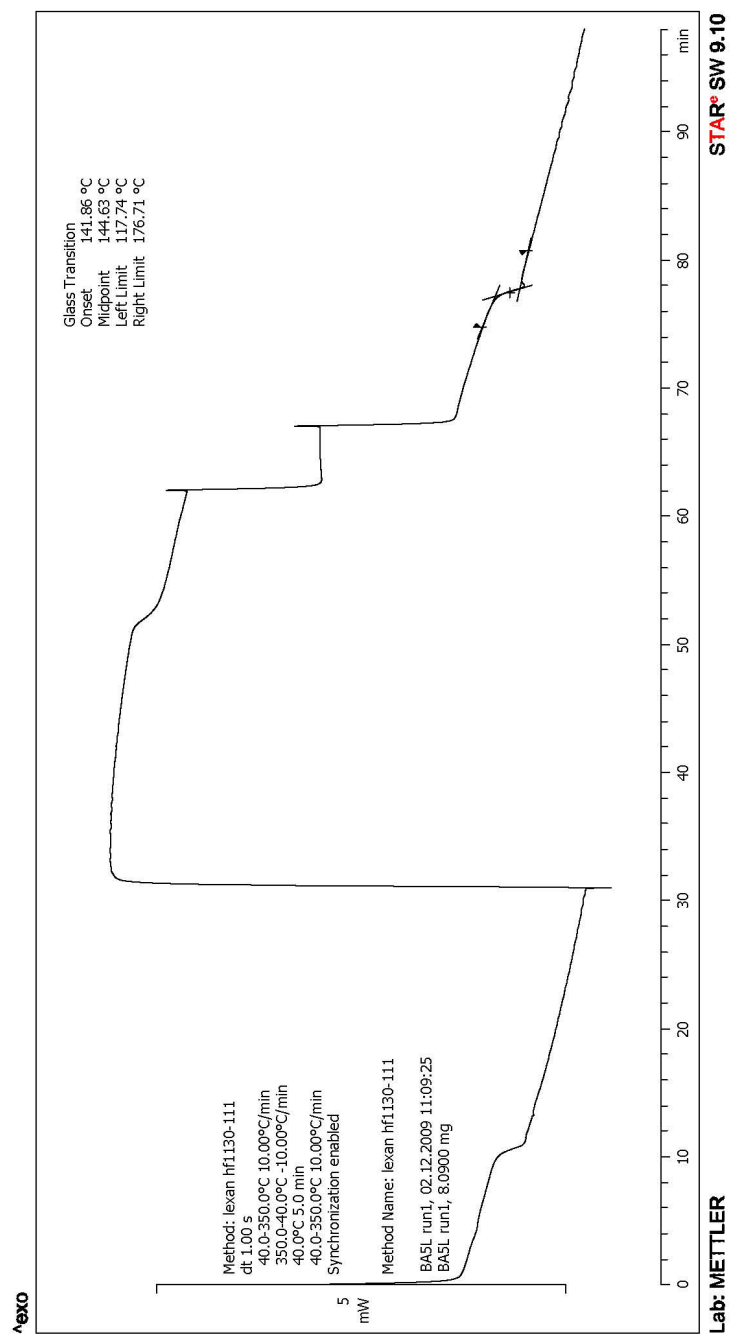


Figure E.9: DSC for BA5L Run 1 vs. Time

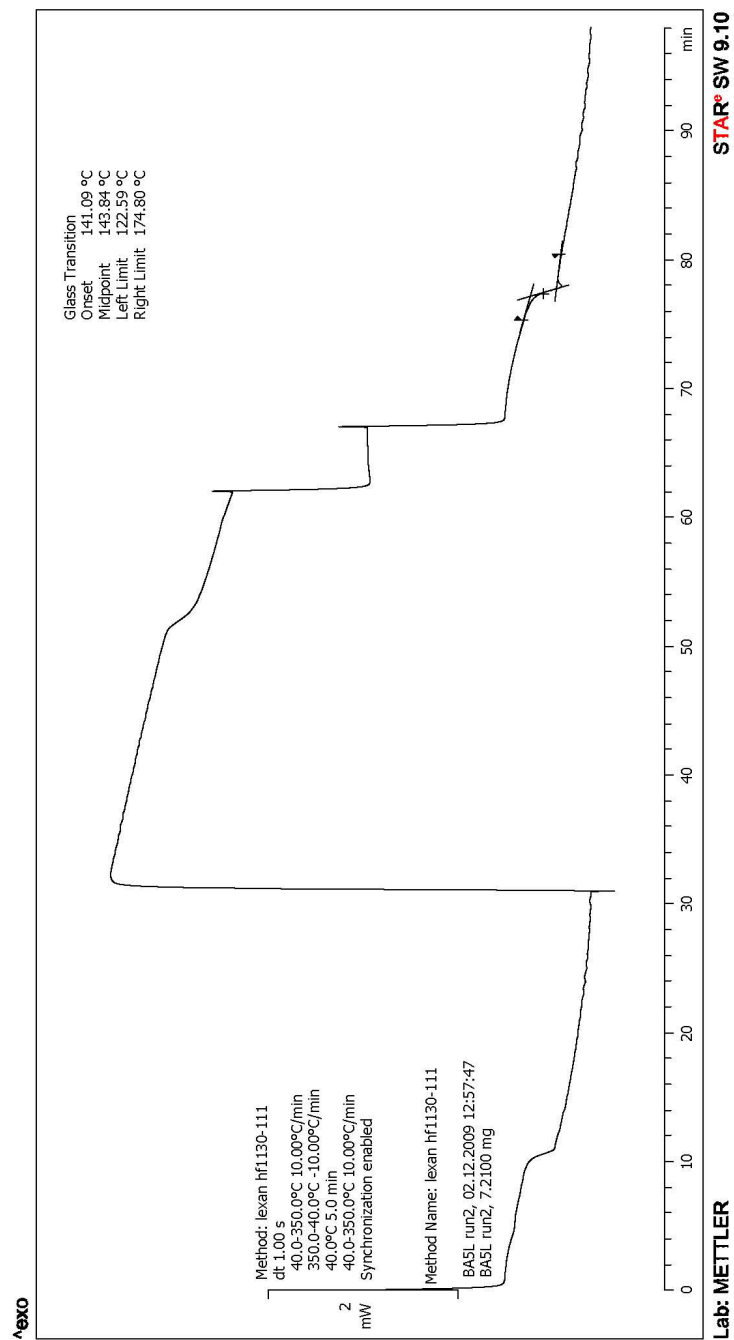


Figure E.10: DSC for BA5L Run 2 vs. Time

Appendix E.3: Polycarbonate with Graphene Nanoplatelets

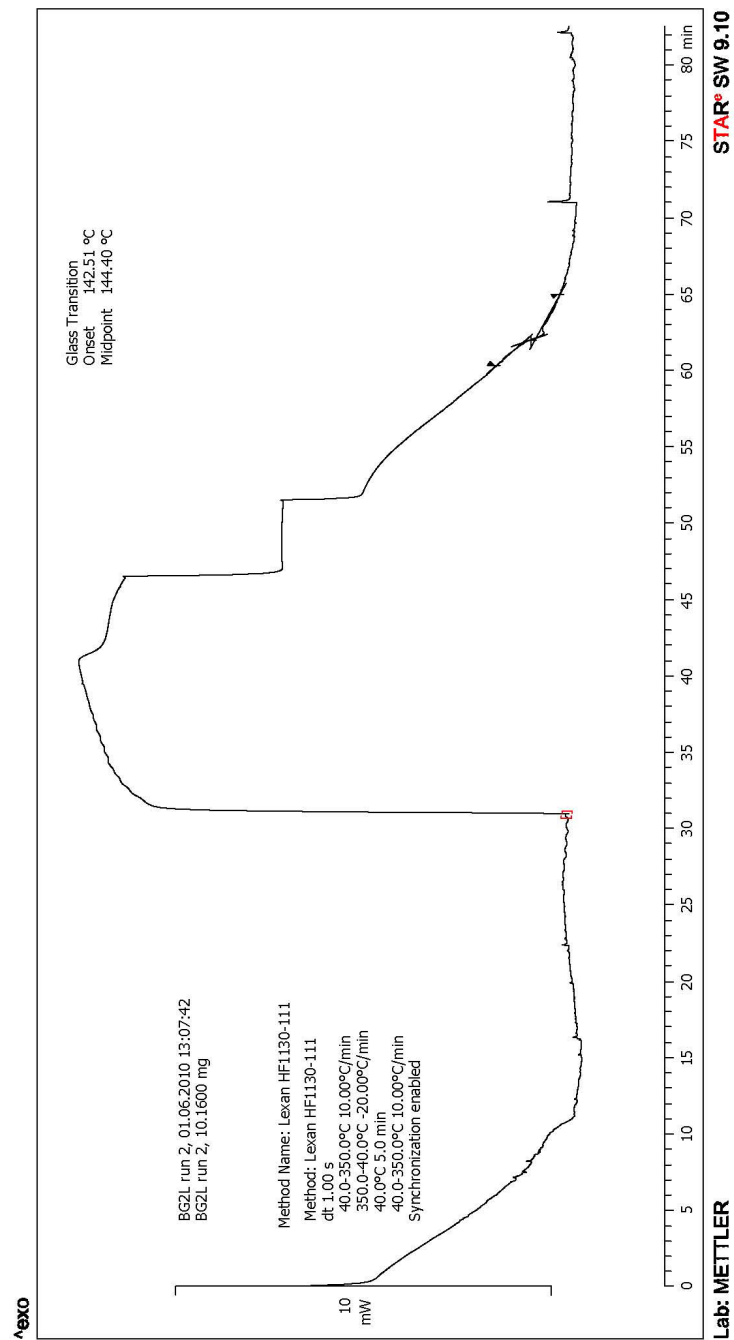


Figure E.11: DSC for BG2L Run 1 vs. Time

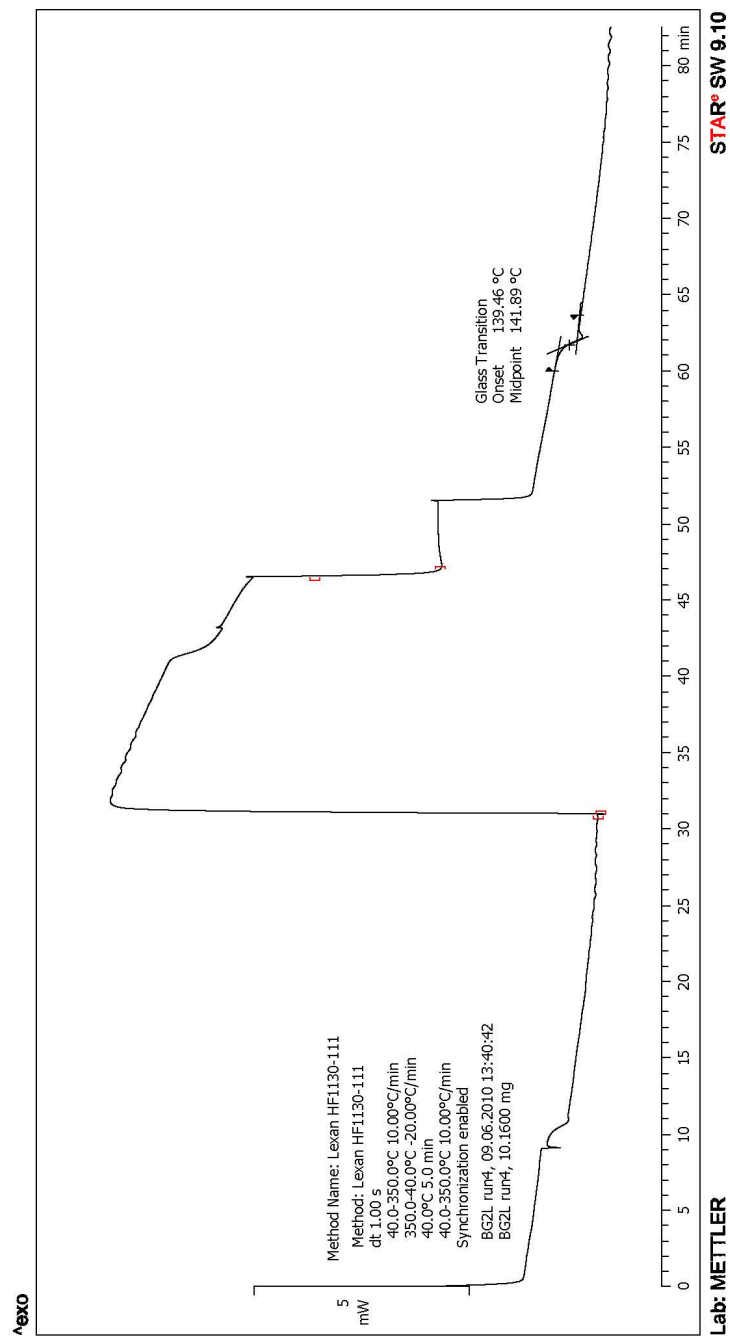


Figure E.12: DSC for BG2L Run 2 vs. Time

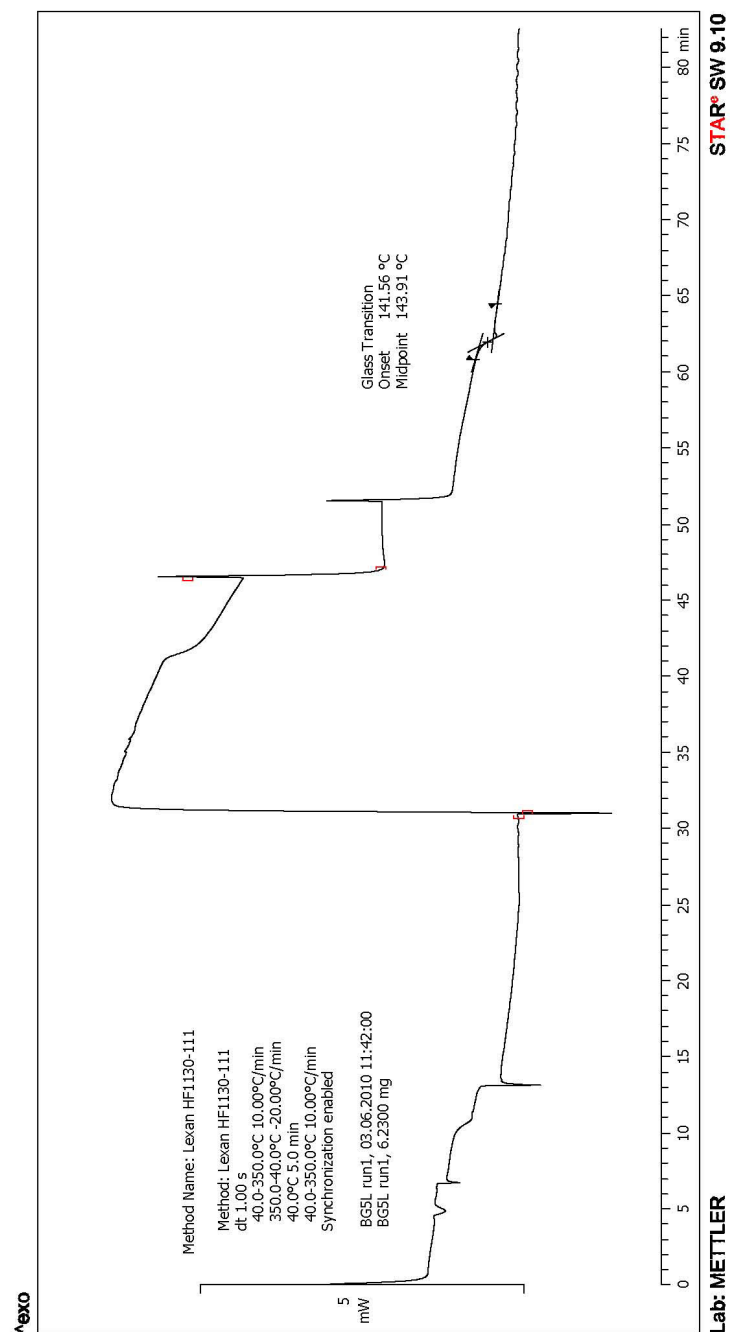


Figure E.13: DSC for BG5L Run 1 vs. Time

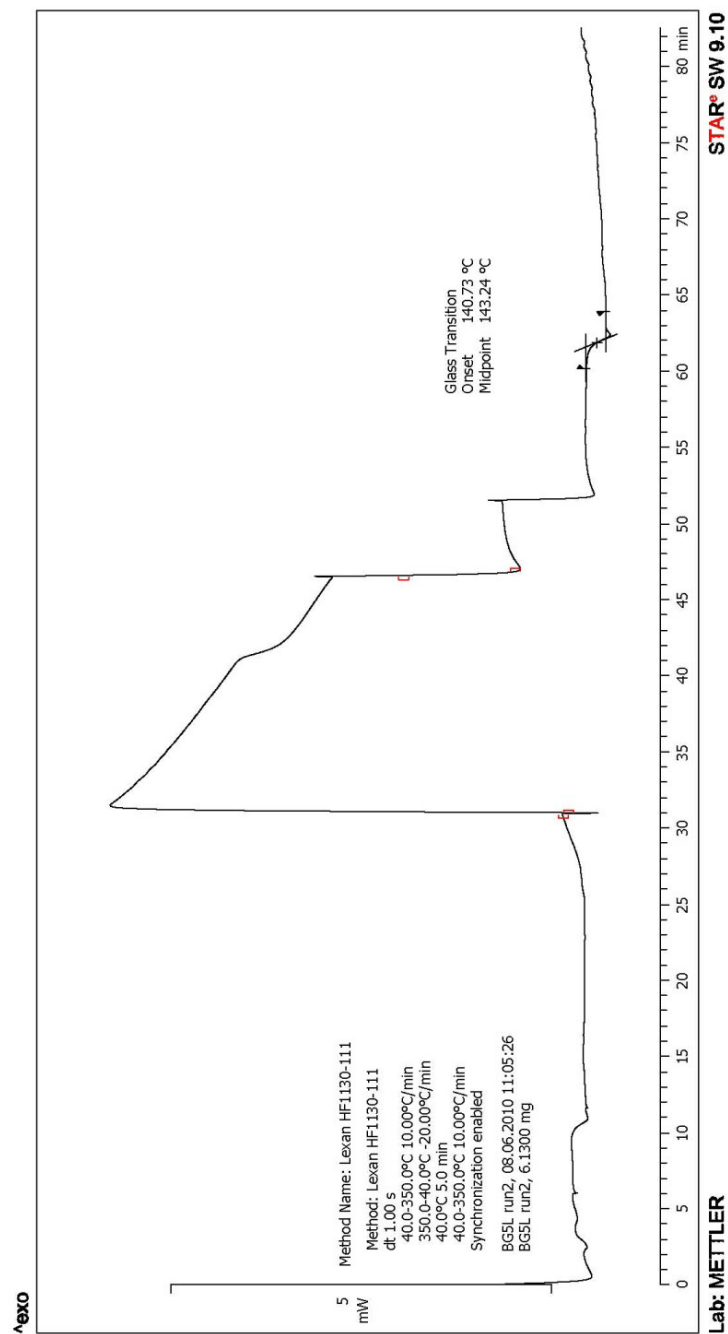


Figure E.14: DSC for BG5L Run 2 vs. Time

Appendix E.4: Polycarbonate with Multiple Fillers

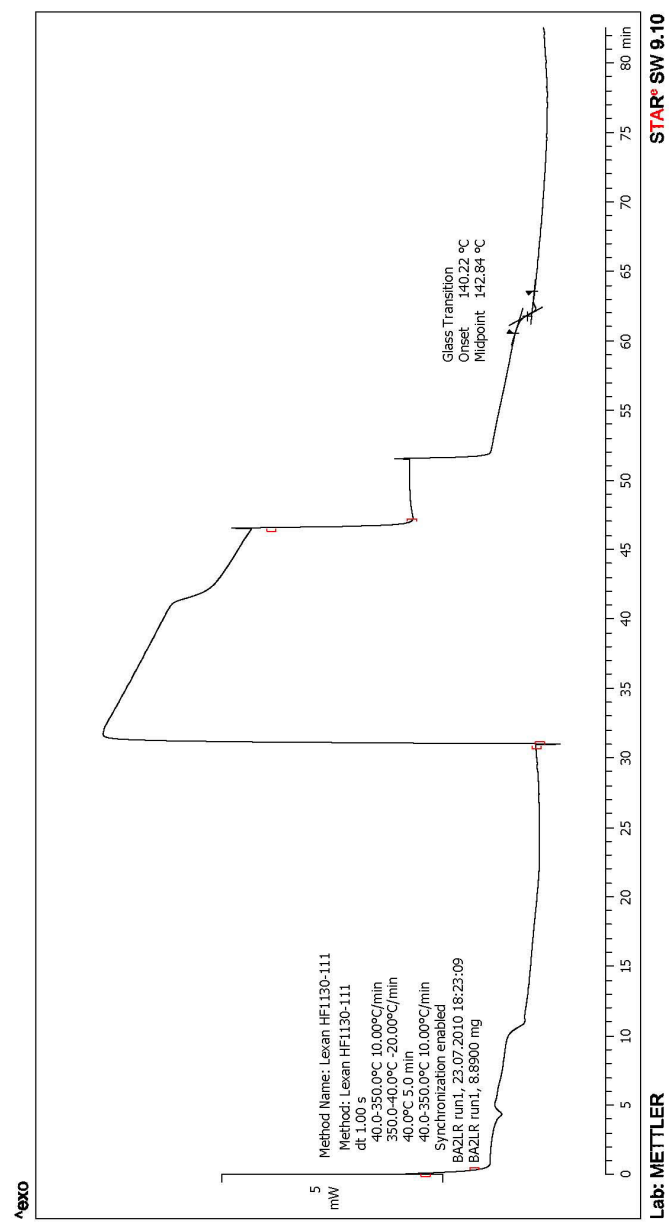


Figure E.15: DSC for BA2LR Run 1 vs. Time

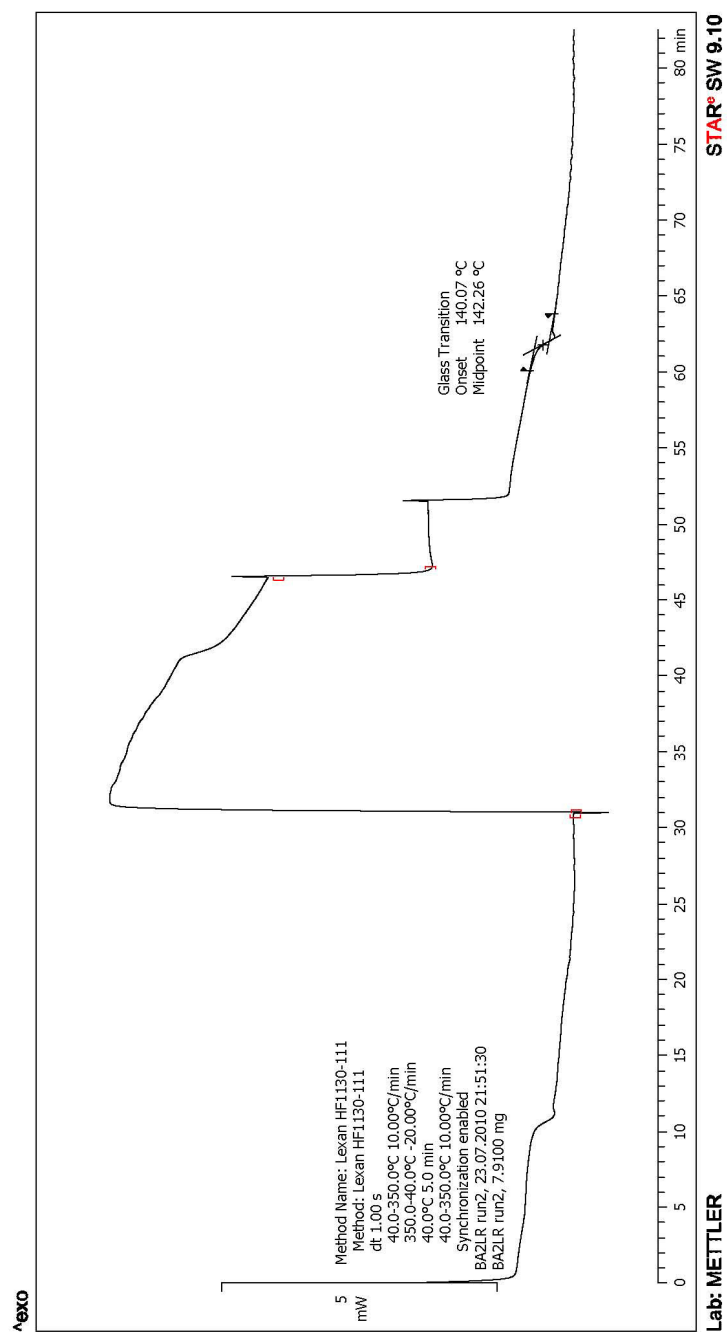


Figure E.16: DSC for BA2LR Run 2 vs. Time

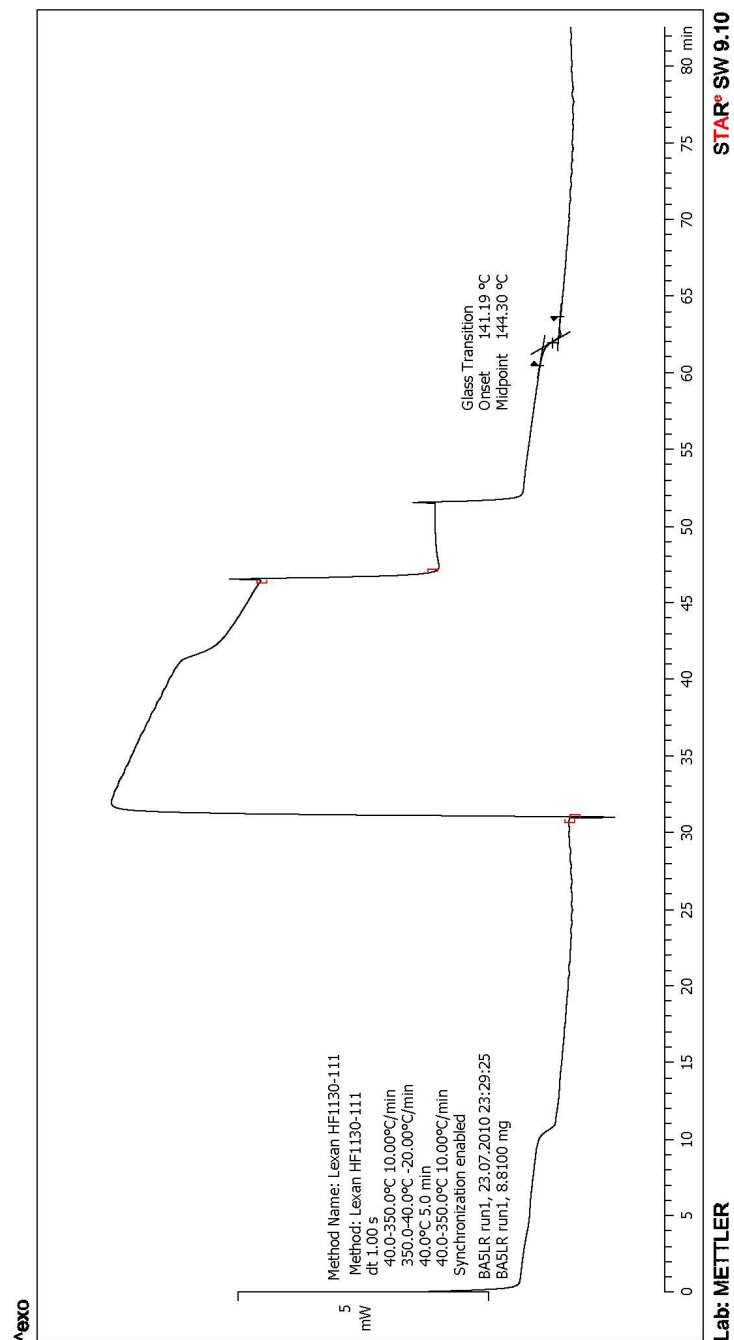


Figure E.17: DSC for BA5LR Run 1 vs. Time

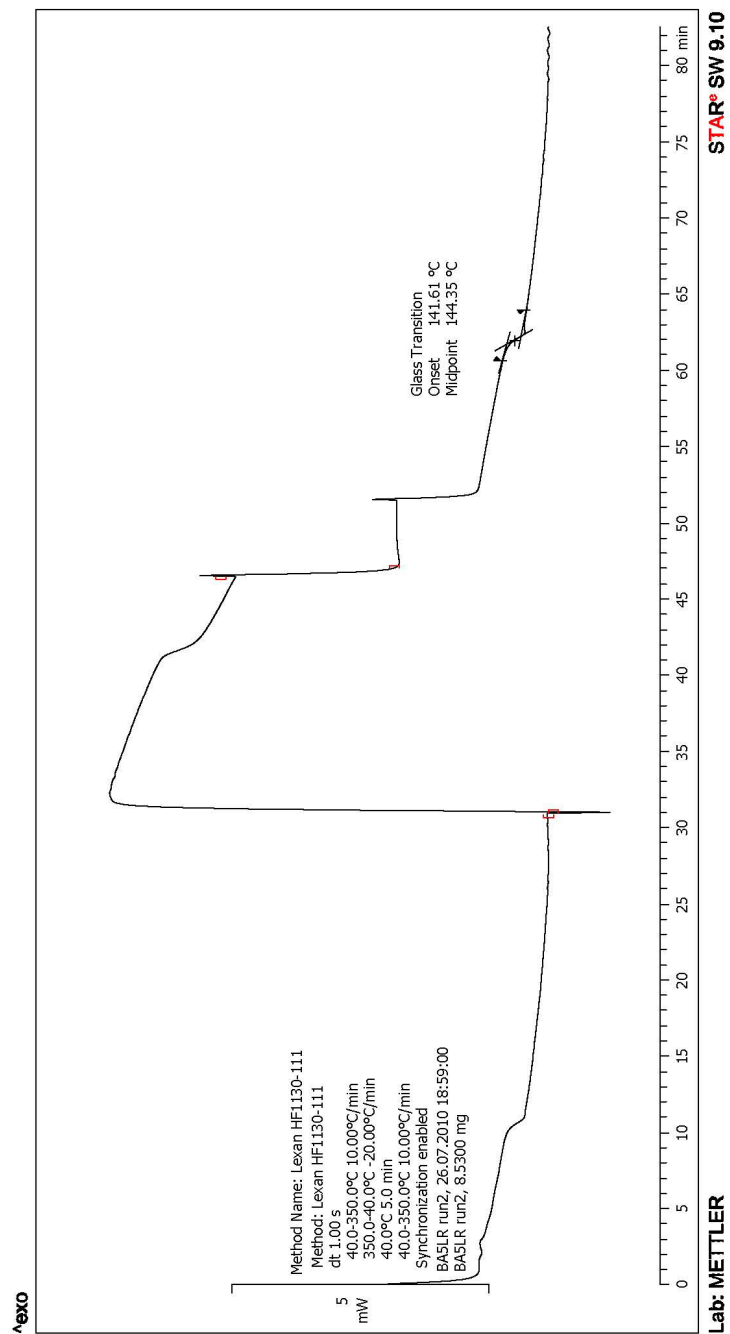


Figure E.18: DSC for BA5LR Run 2 vs. Time

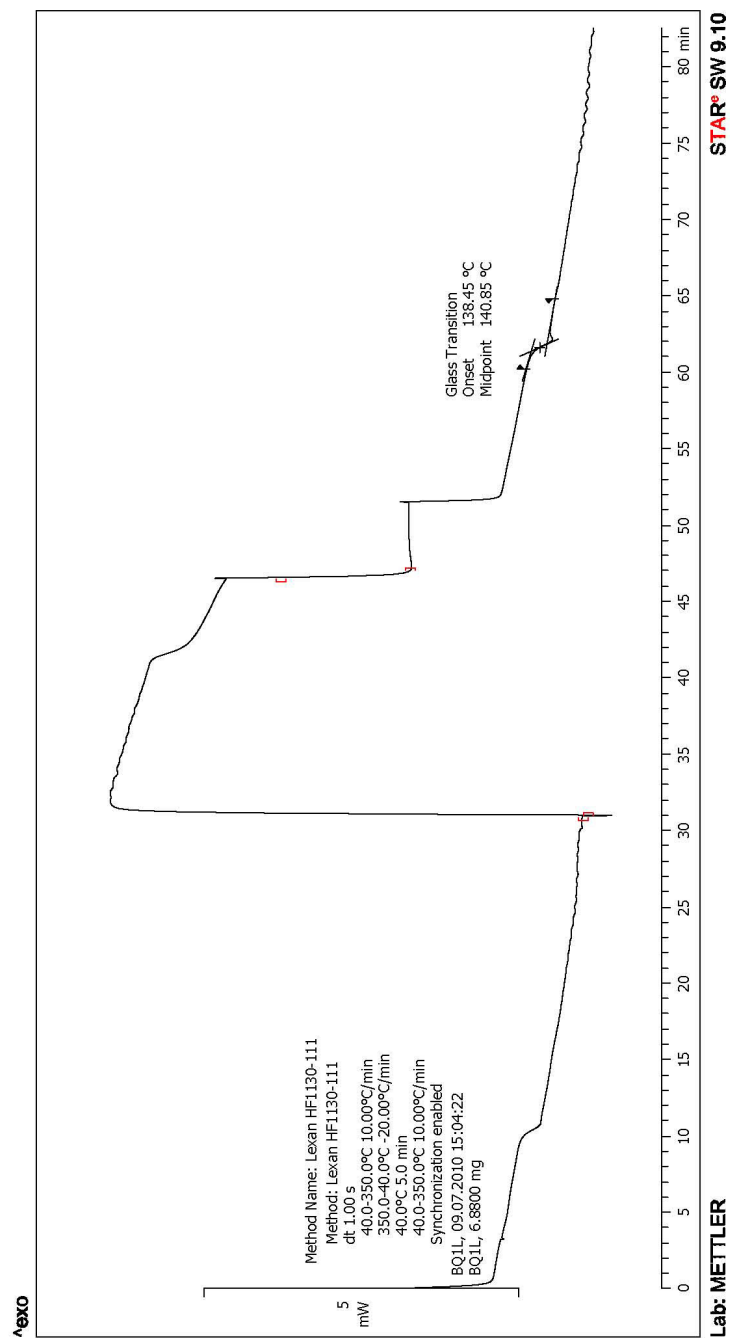


Figure E.19: DSC for BQ1L Run 1 vs. Time

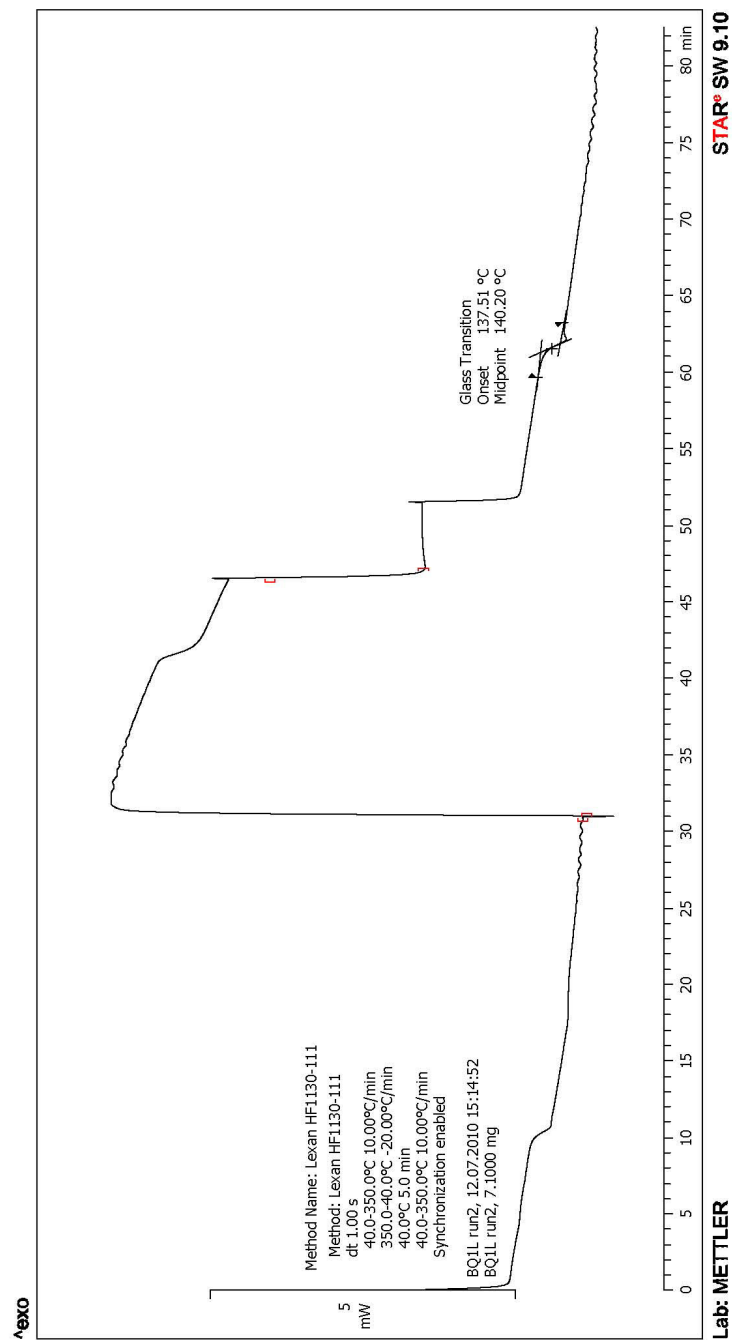


Figure E.20: DSC for BQ1L Run 2 vs. Time

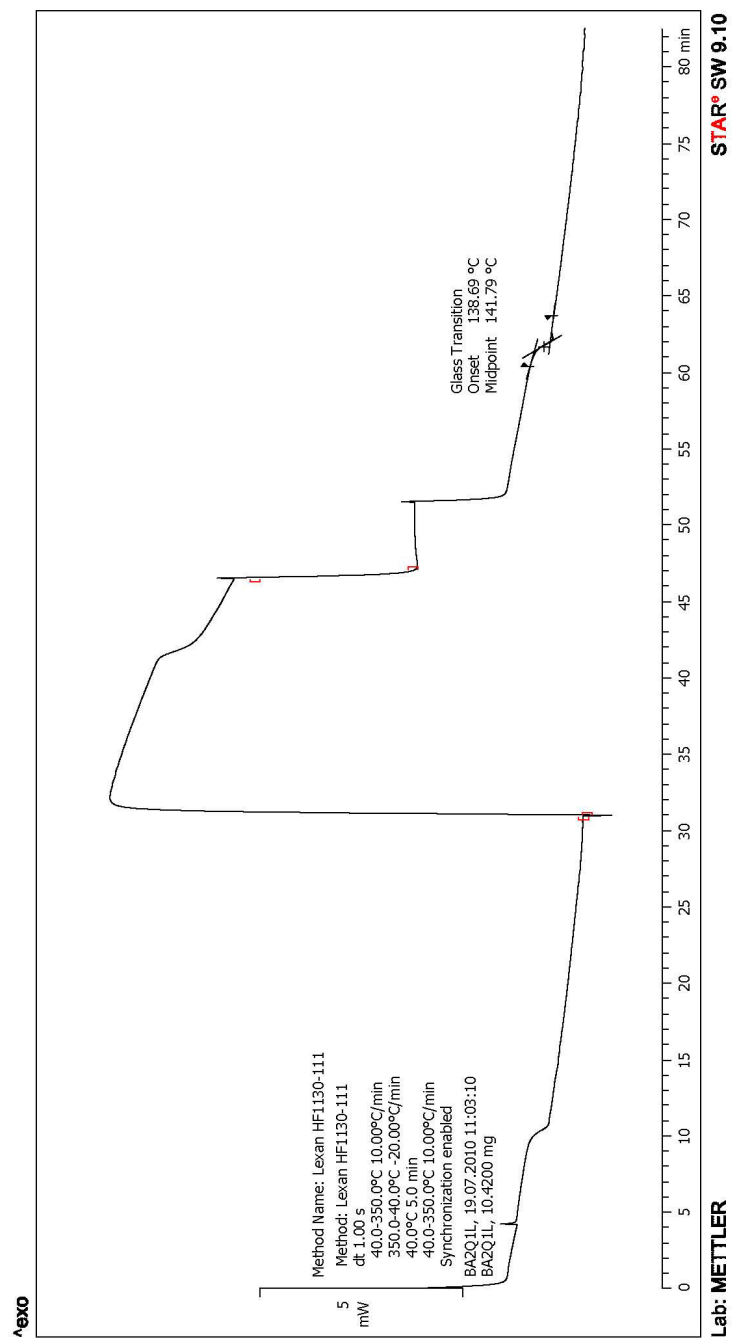


Figure E.21: DSC for BA2Q1L Run 1 vs. Time

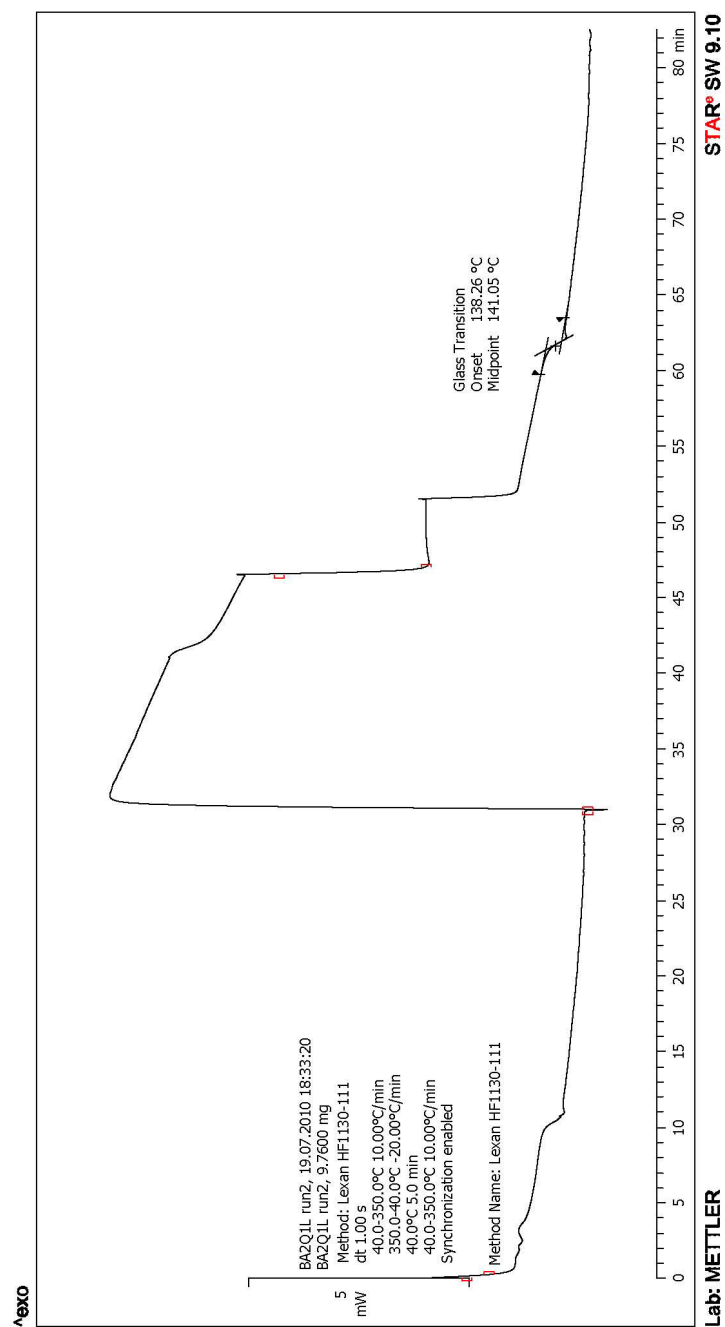


Figure E.22: DSC for BA2Q1L Run 2 vs. Time

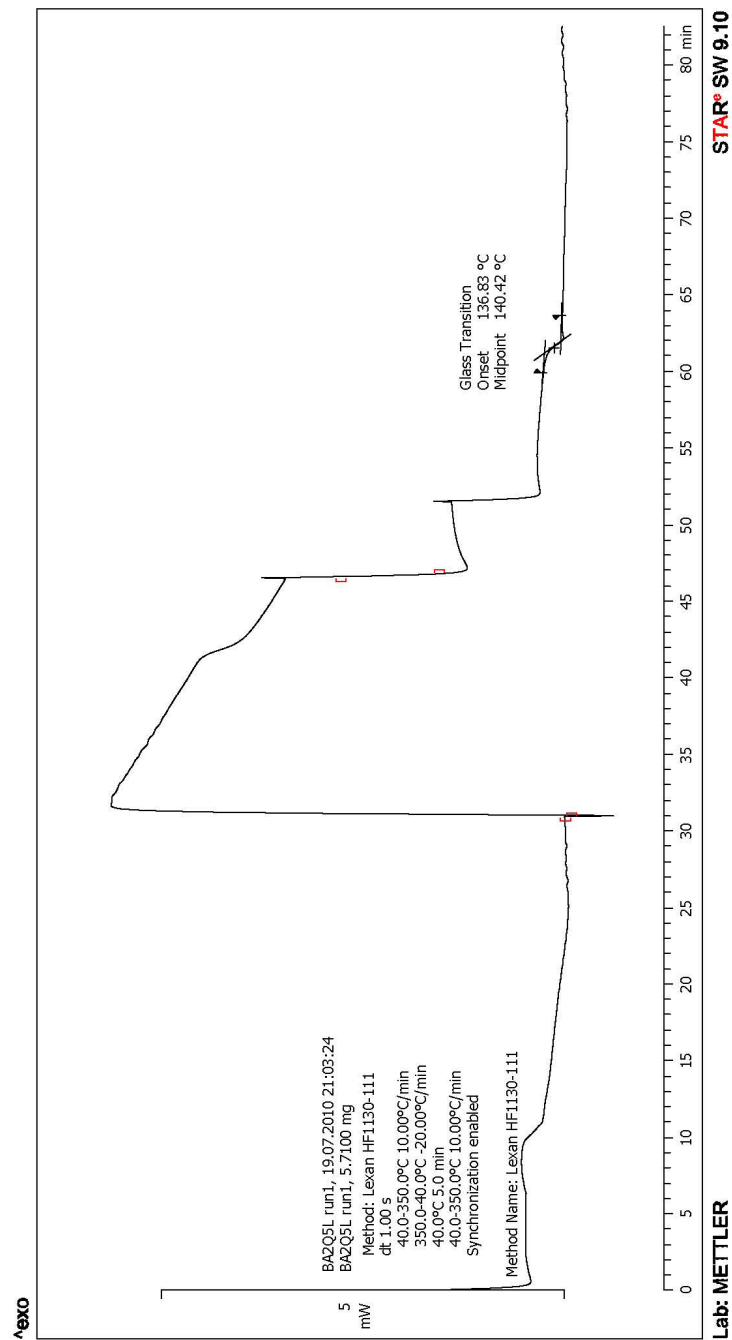


Figure E.23: DSC for BA2Q5L Run 1 vs. Time

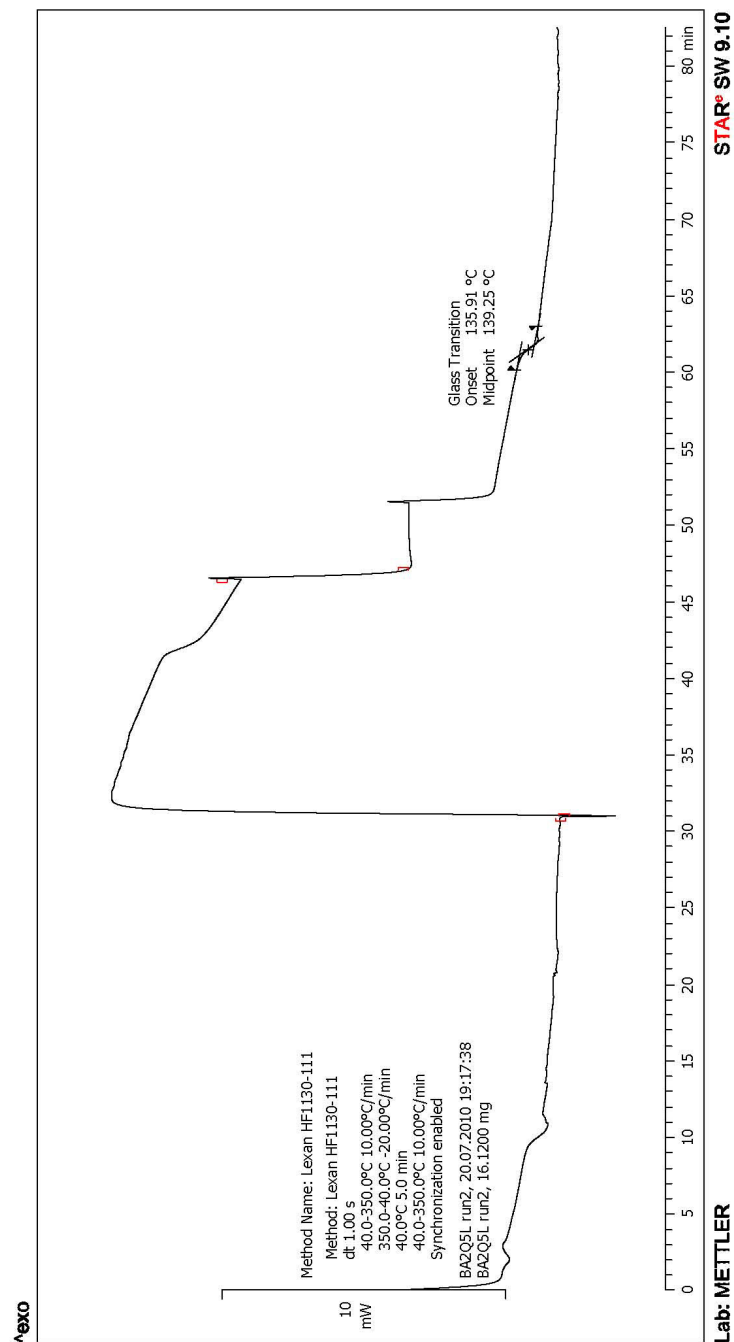


Figure E.24: DSC for BA2Q5L Run 2 vs. Time

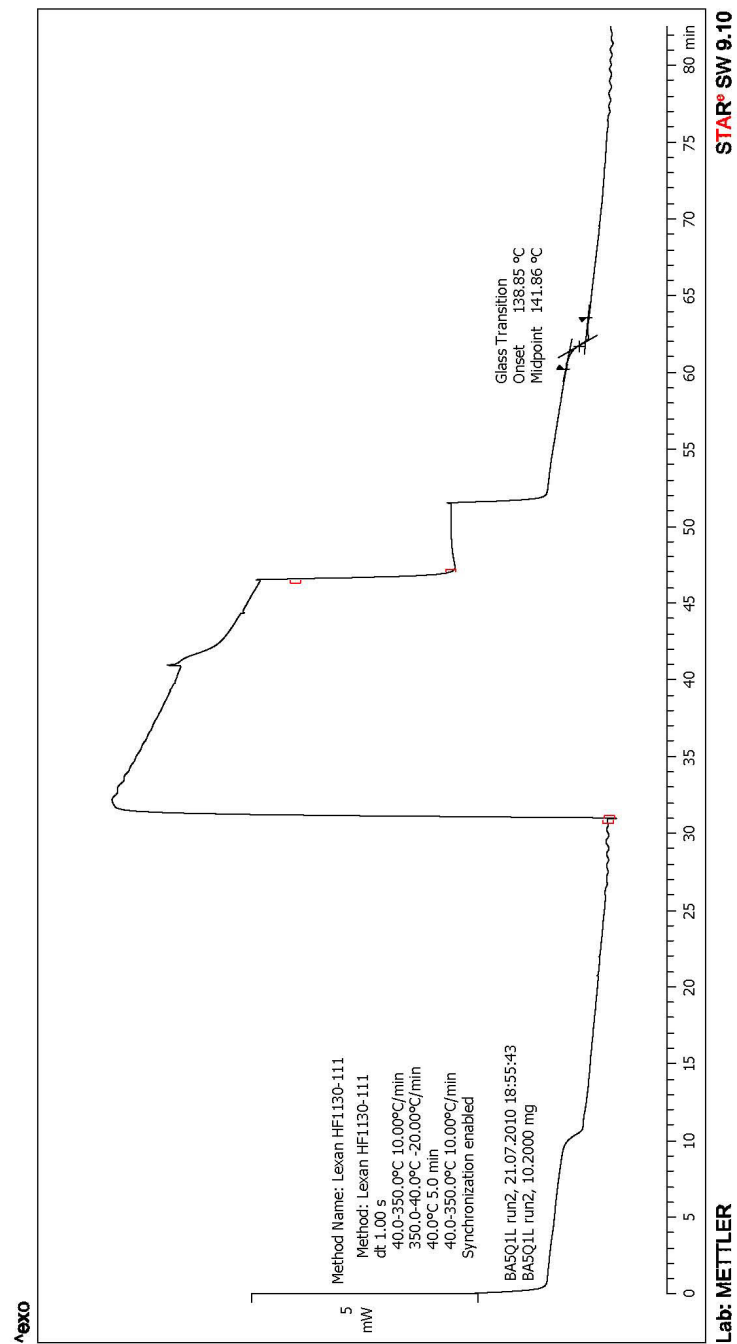


Figure E.25: DSC for BA5Q1L Run 1 vs. Time

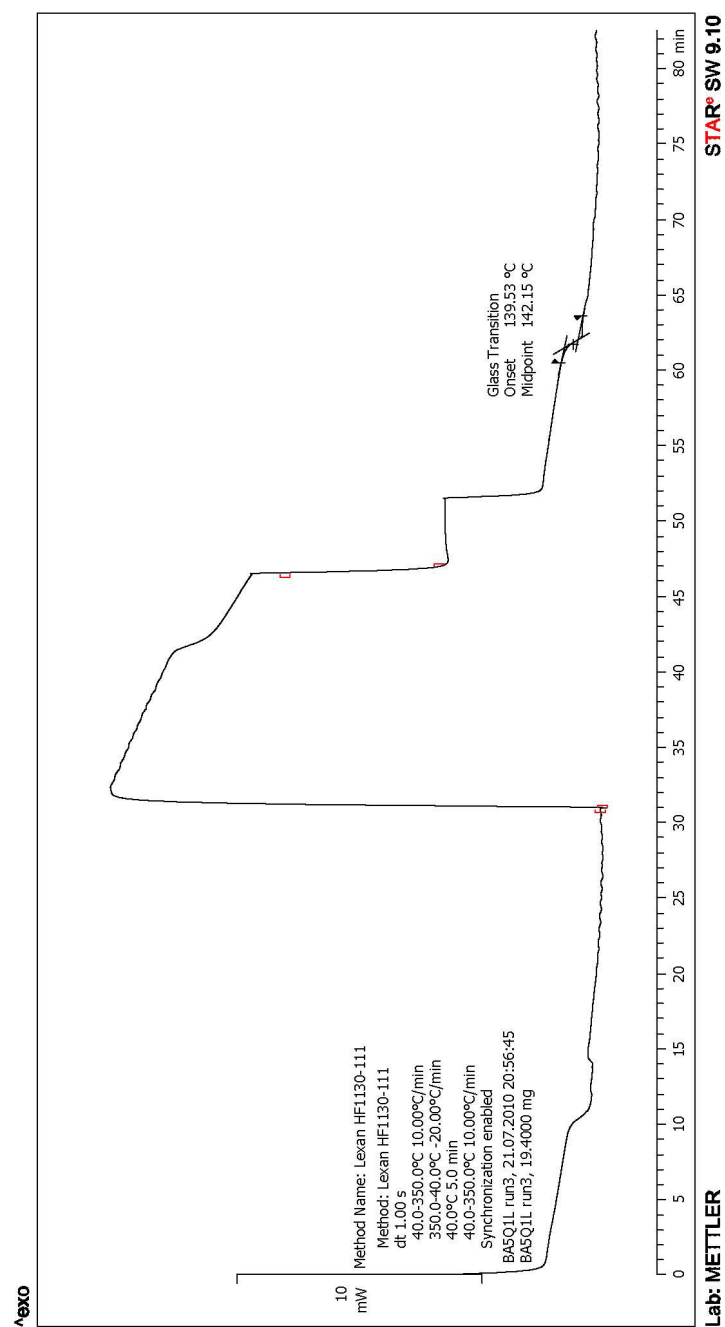


Figure E.26: DSC for BA5QIL Run 2 vs. Time

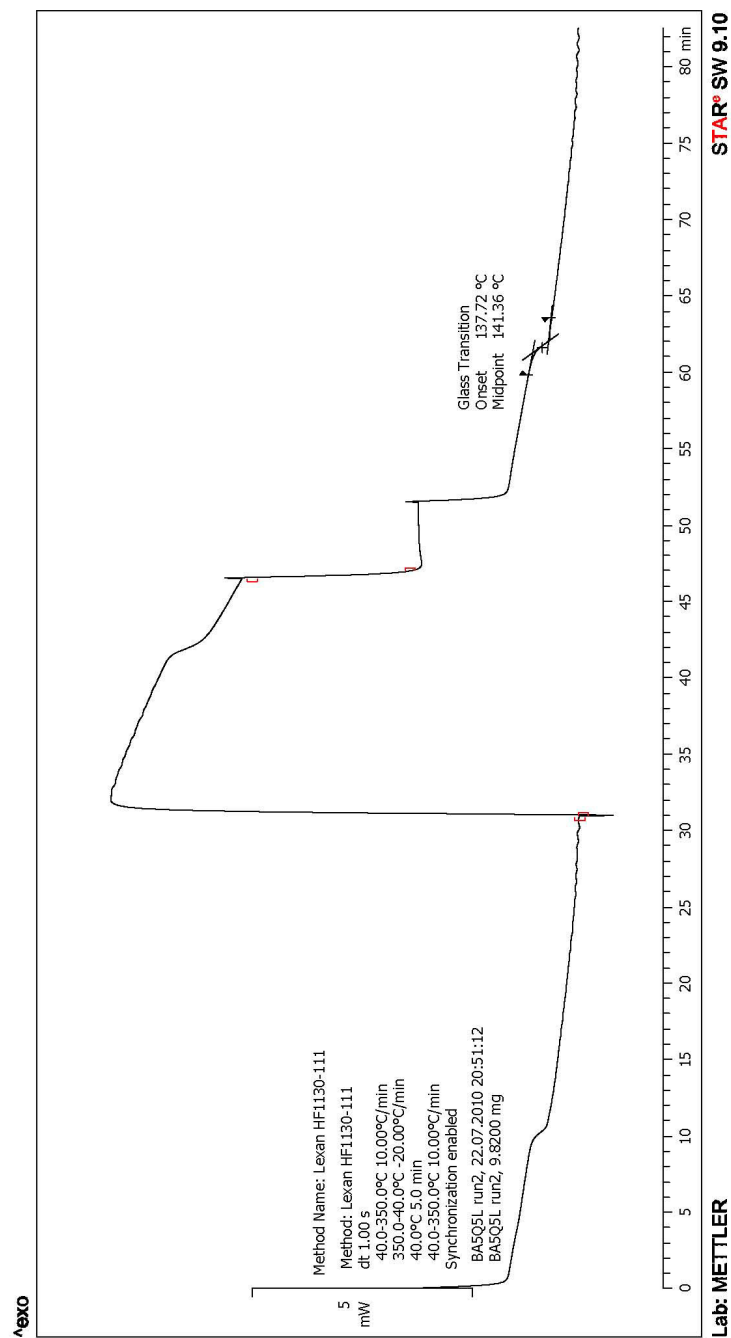


Figure E.27: DSC for BA5Q5L Run 1 vs. Time

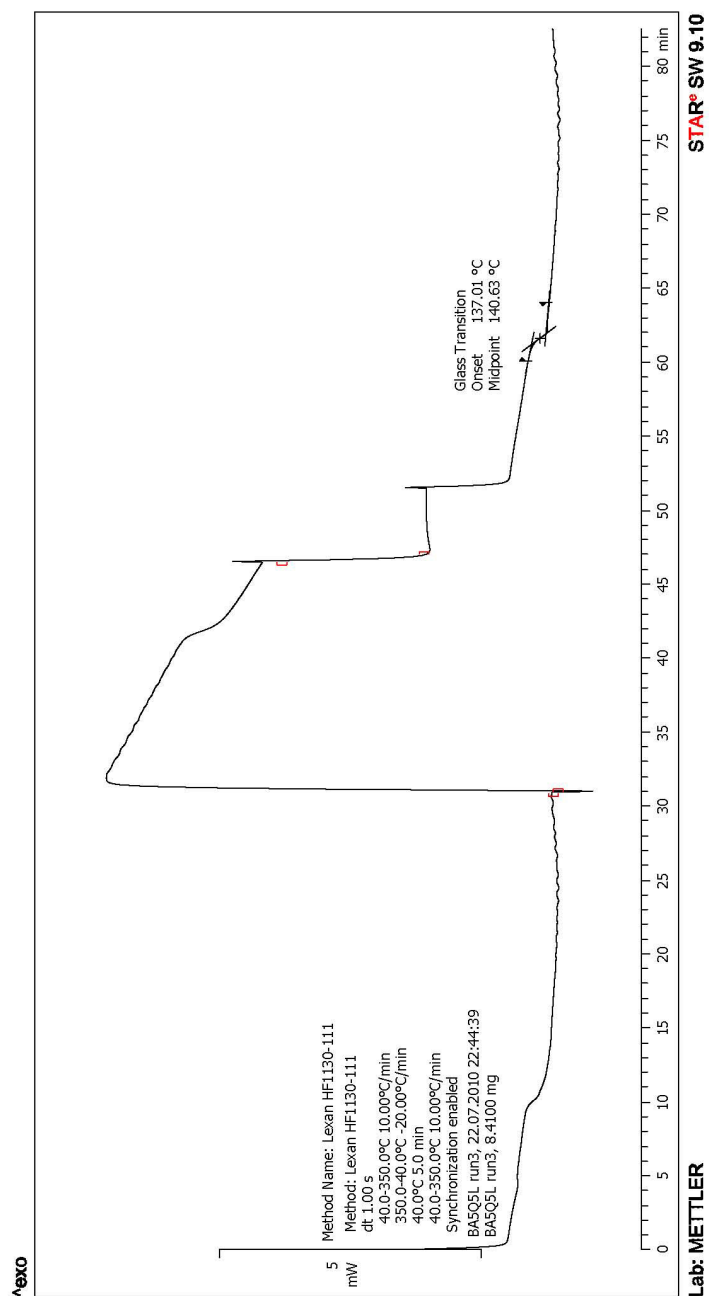


Figure E.28: DSC for BA5Q5L Run 2 vs. Time

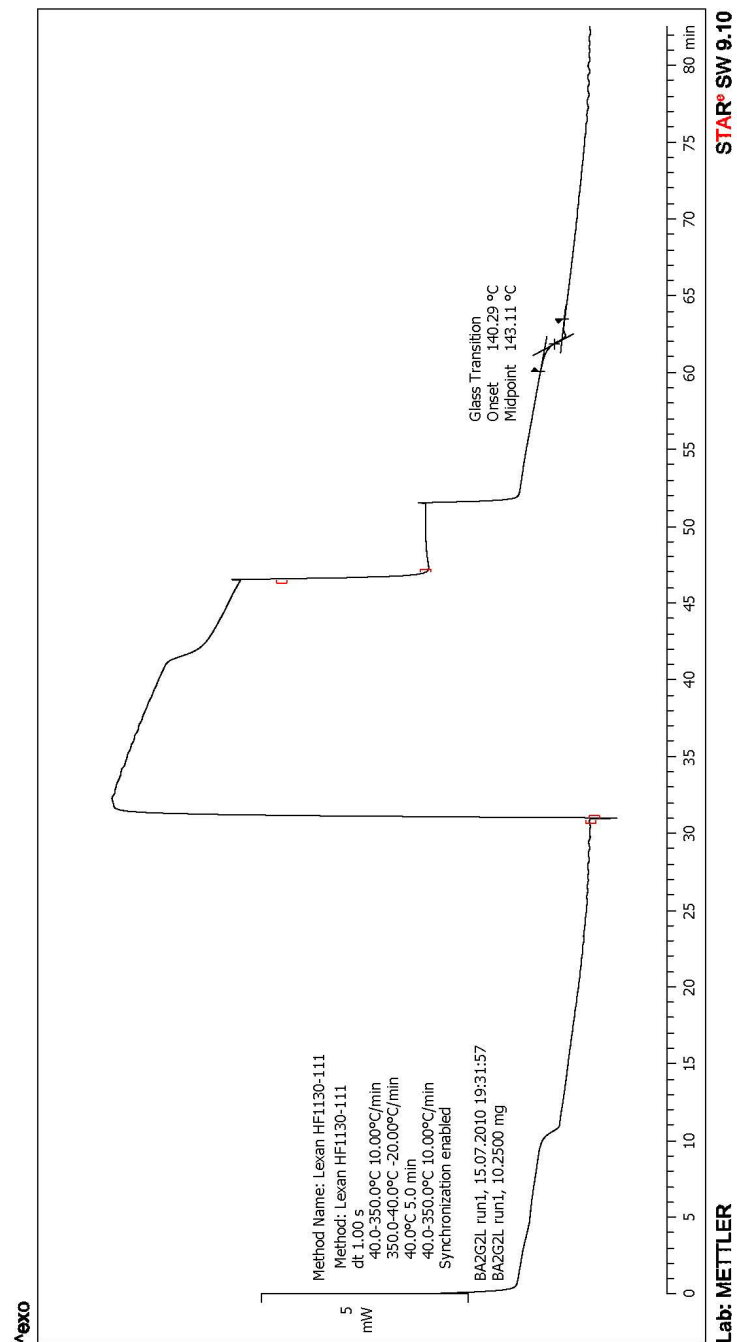


Figure E.29: DSC for BA2G2L Run 1 vs. Time

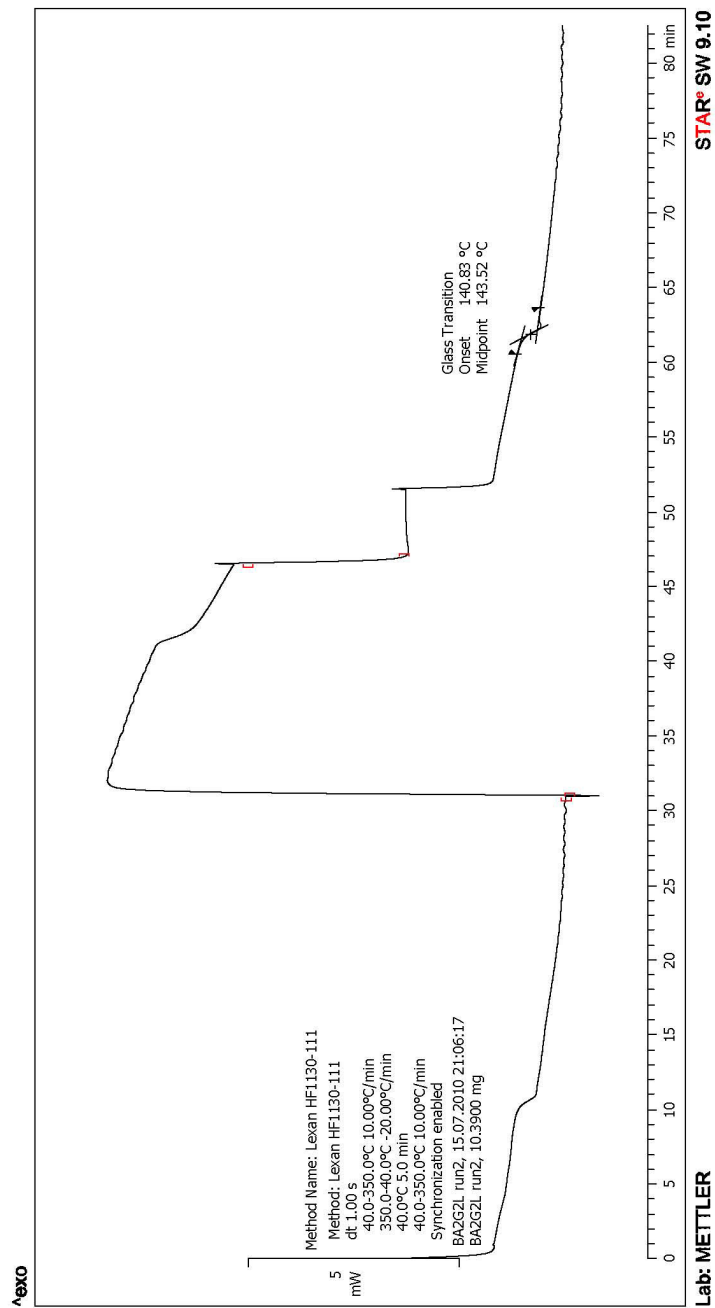


Figure E.30: DSC for BA2G2L Run 2 vs. Time

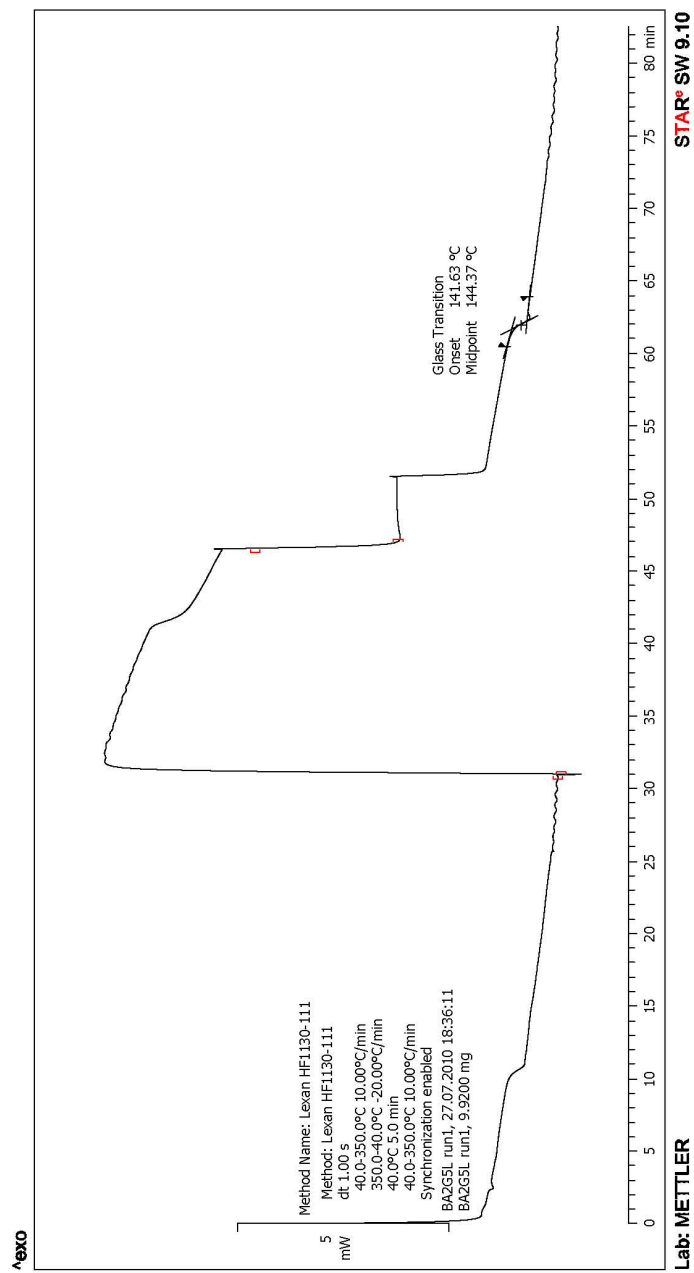


Figure E.31: DSC for BA2G5L Run 1 vs. Time

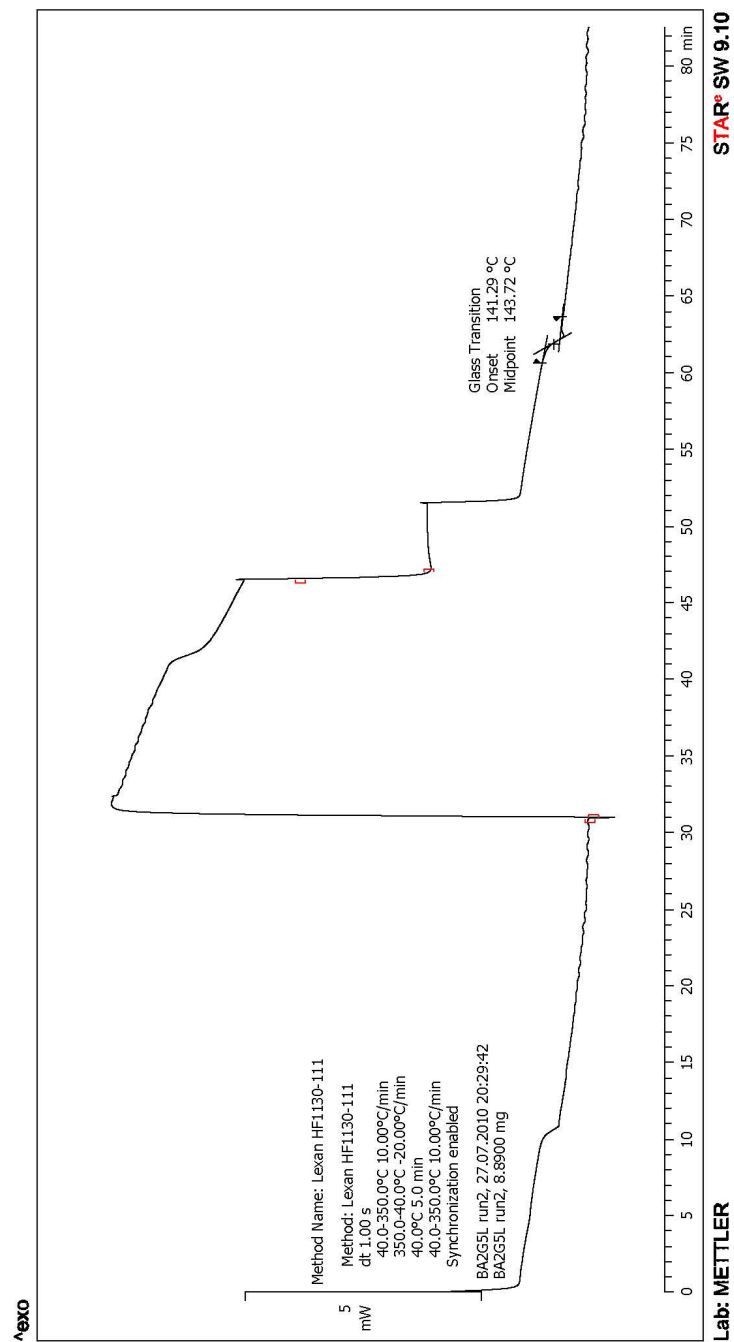


Figure E.32: DSC for BA2G5L Run 2 vs. Time

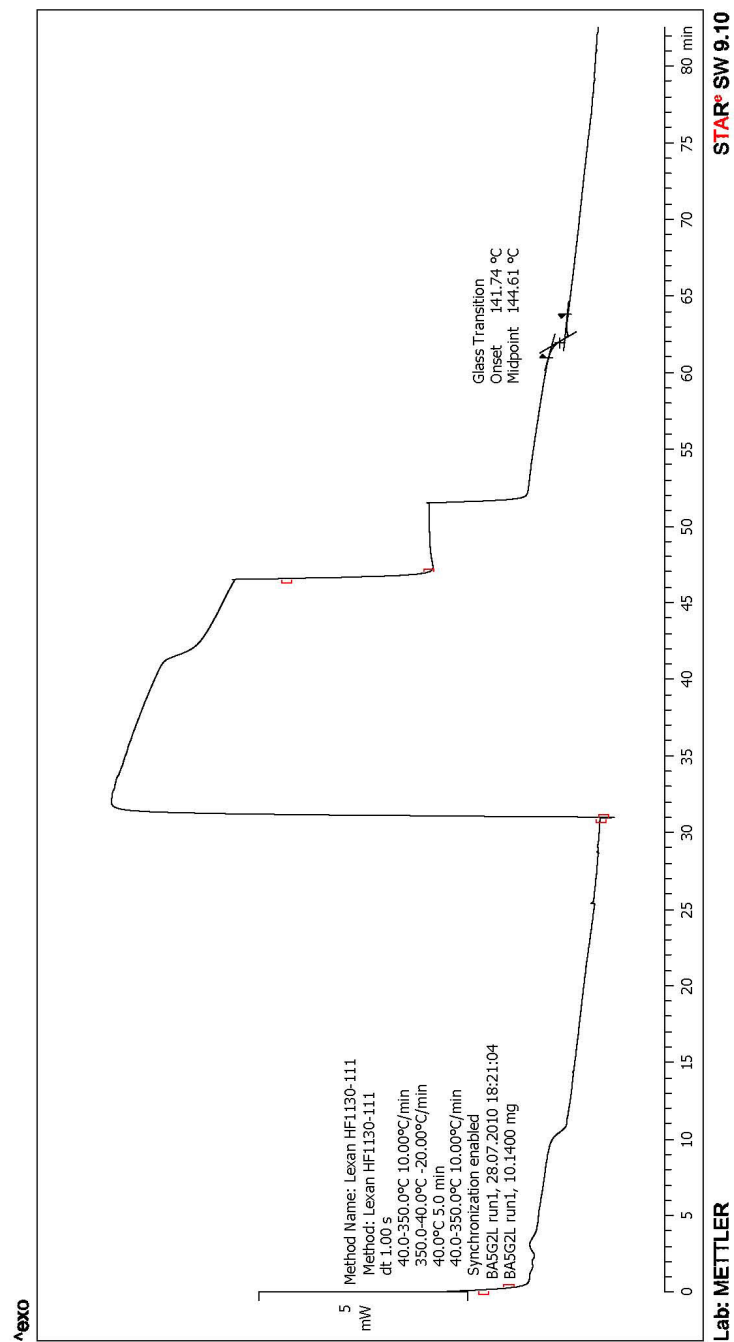


Figure E.33: DSC for BA5G2L Run 1 vs. Time

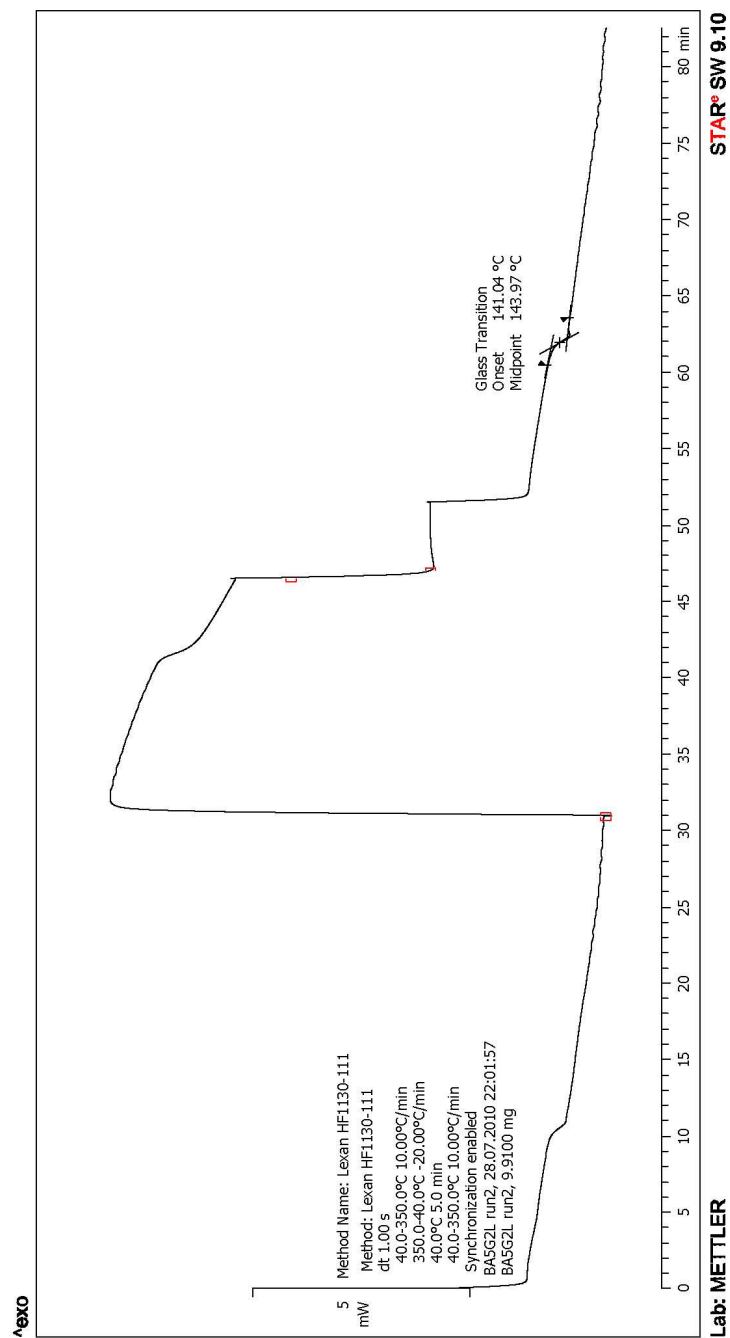


Figure E.34: DSC for BA5G2L Run 2 vs. Time

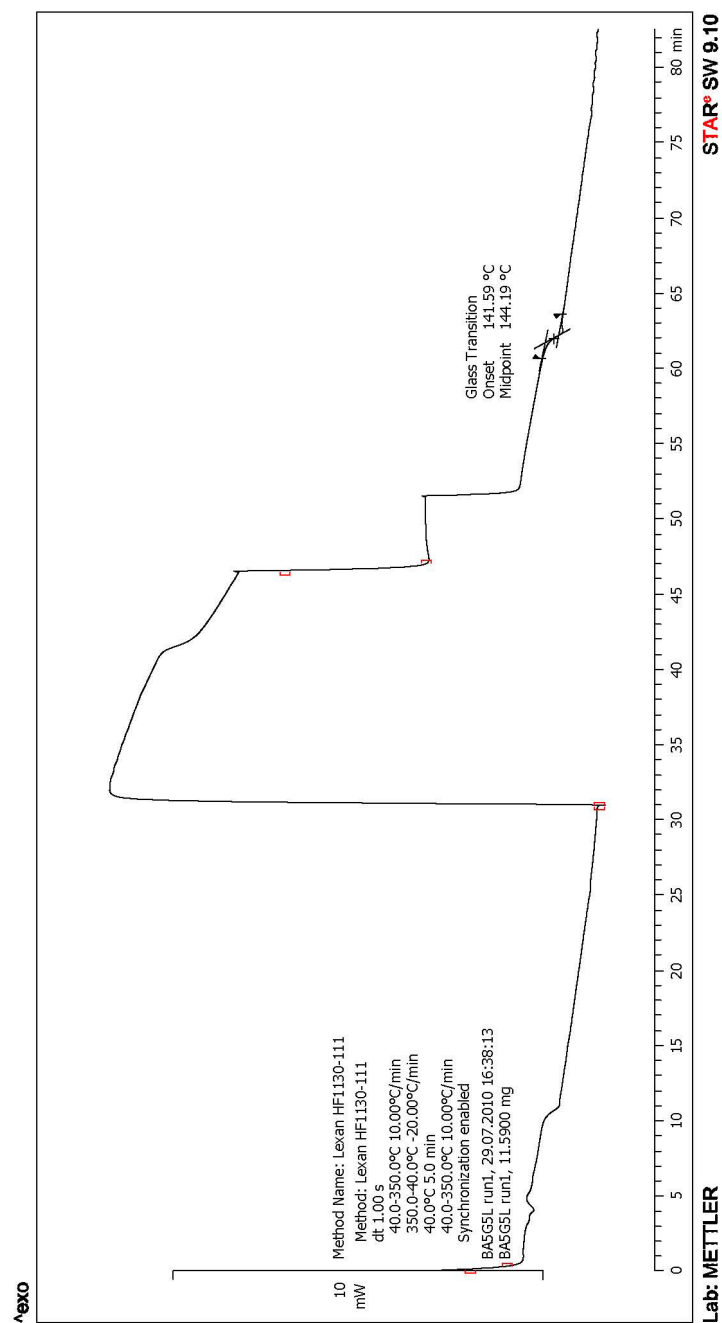


Figure E.35: DSC for BA5G5L Run 1 vs. Time

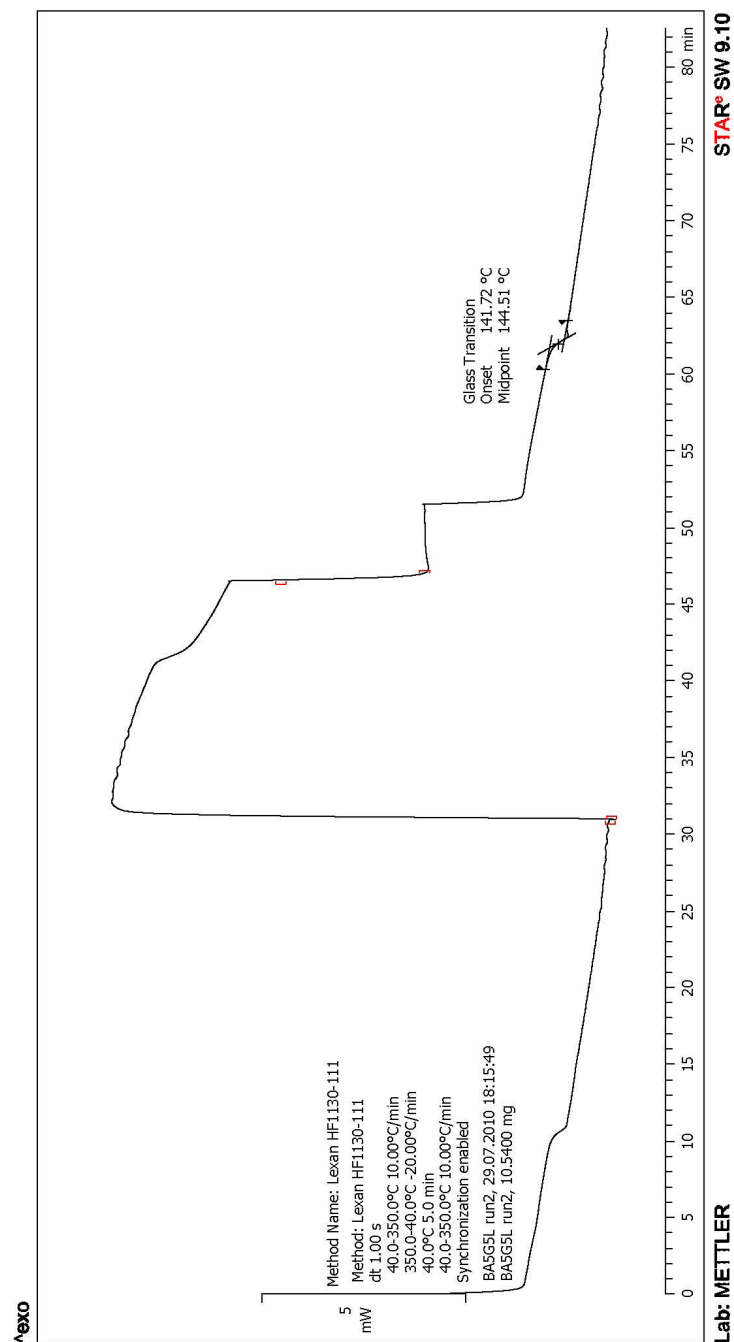


Figure E.36: DSC for BA5G5L Run 2 vs. Time

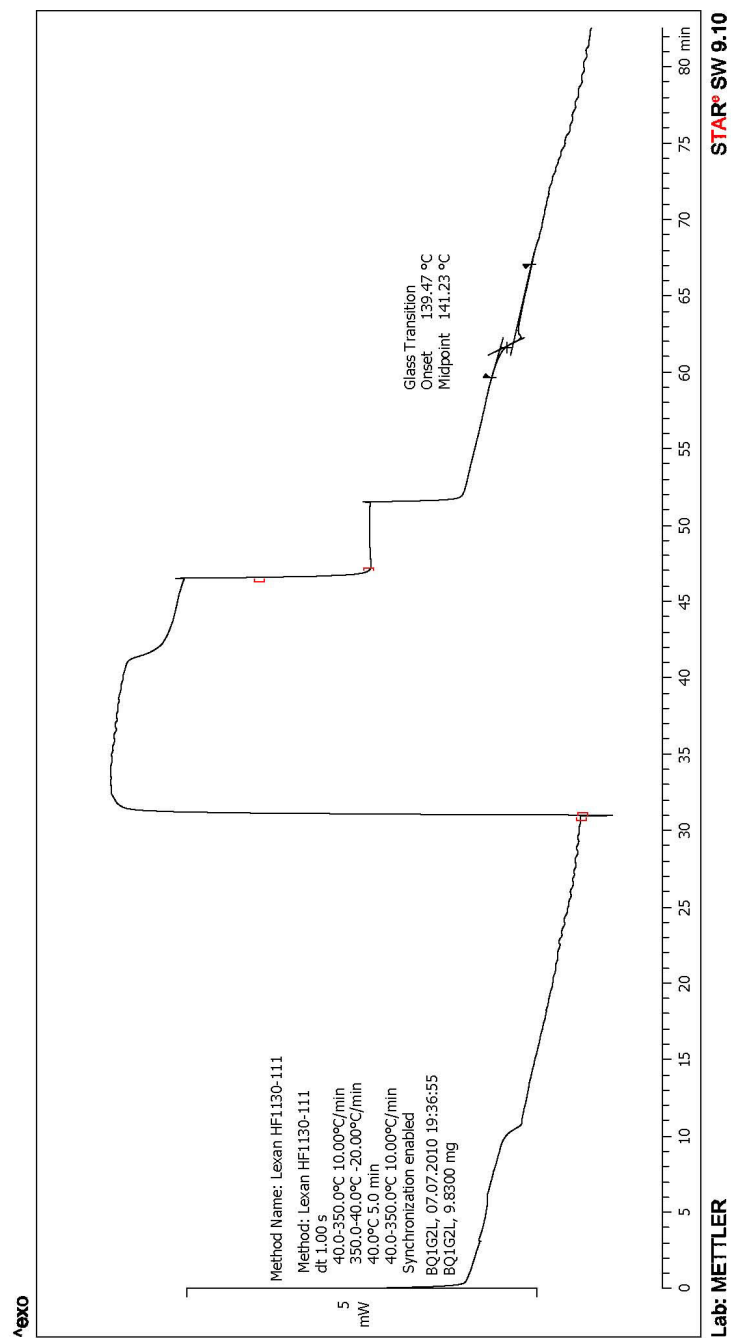


Figure E.37: DSC for BQ1G2L Run 1 vs. Time

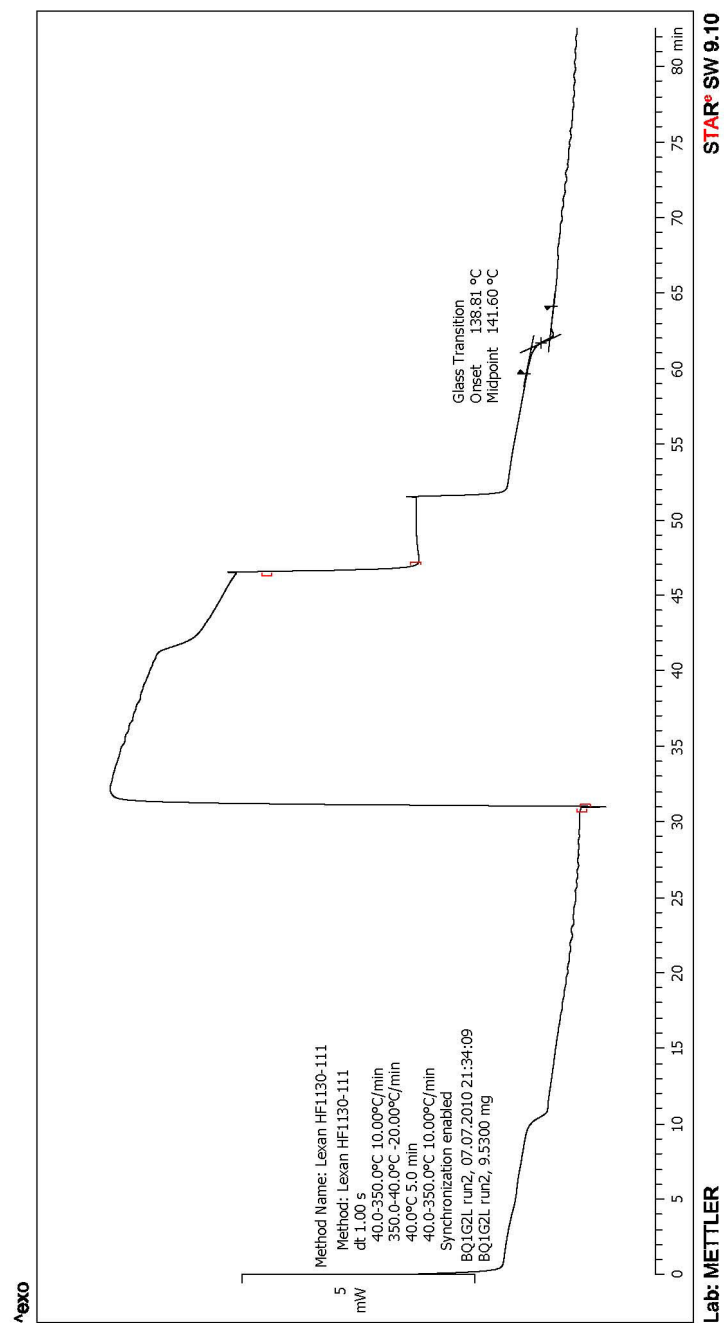


Figure E.38: DSC for BQ1G2L Run 2 vs. Time

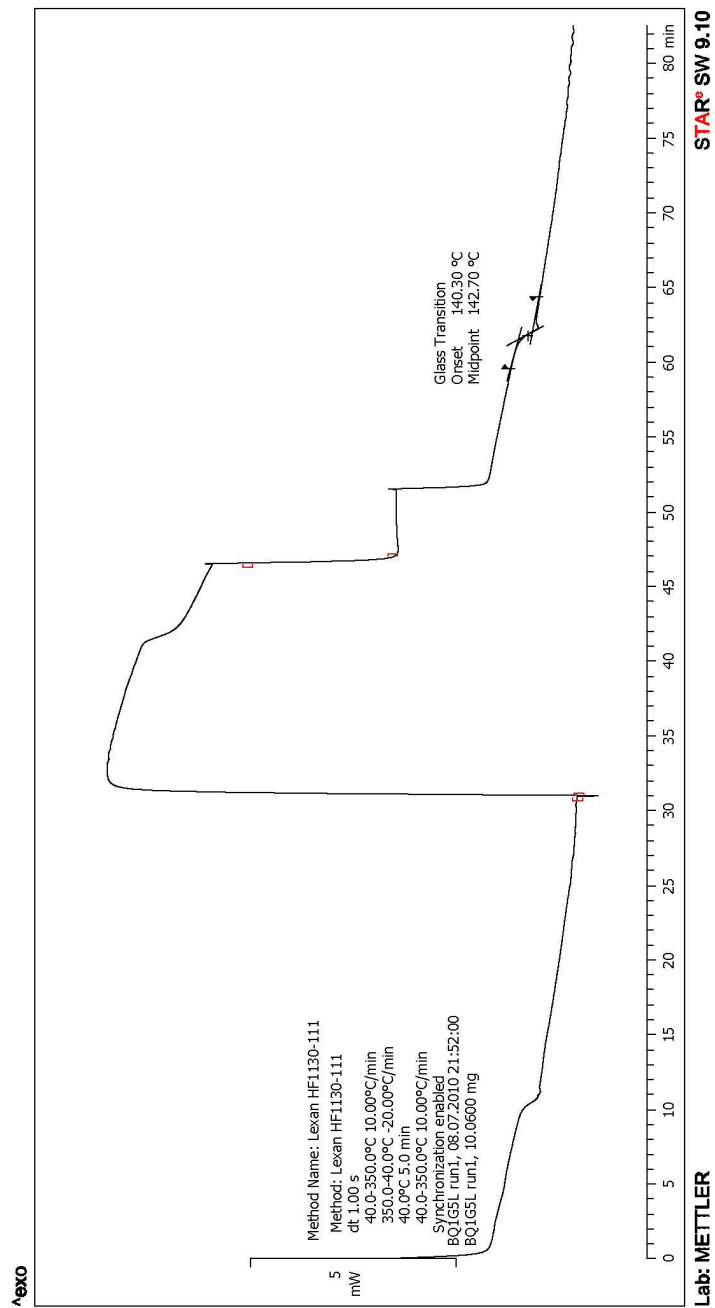


Figure E.39: DSC for BQ1G5L Run 1 vs. Time

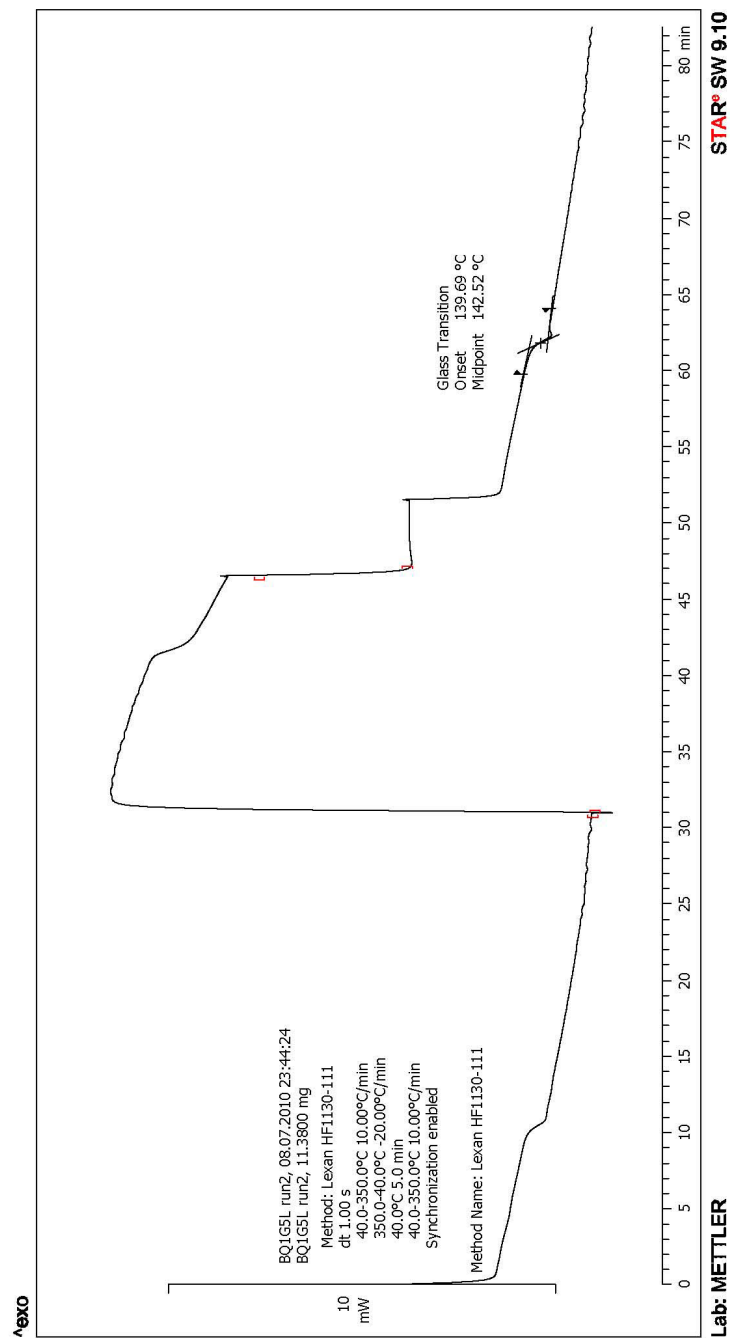


Figure E.40: DSC for BQ1G5L Run 2 vs. Time

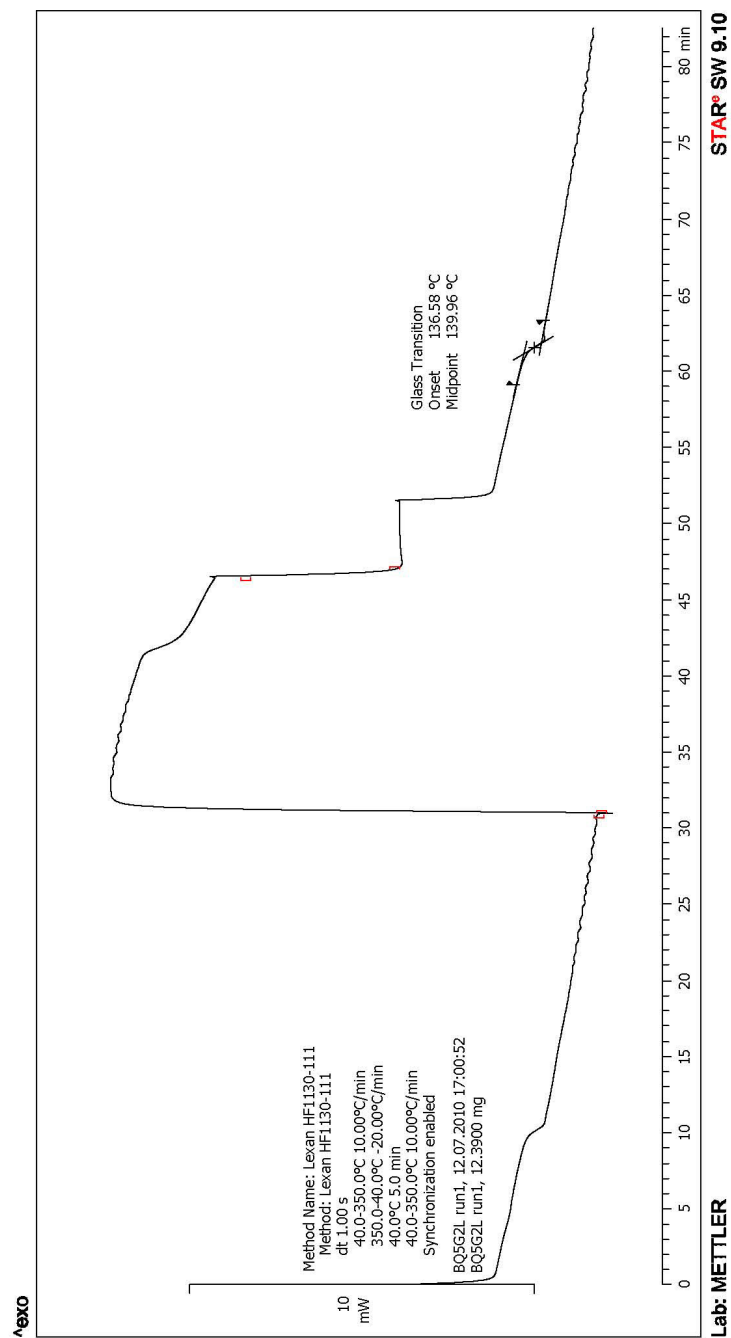


Figure E.41: DSC for BQ5G2L Run 1 vs. Time

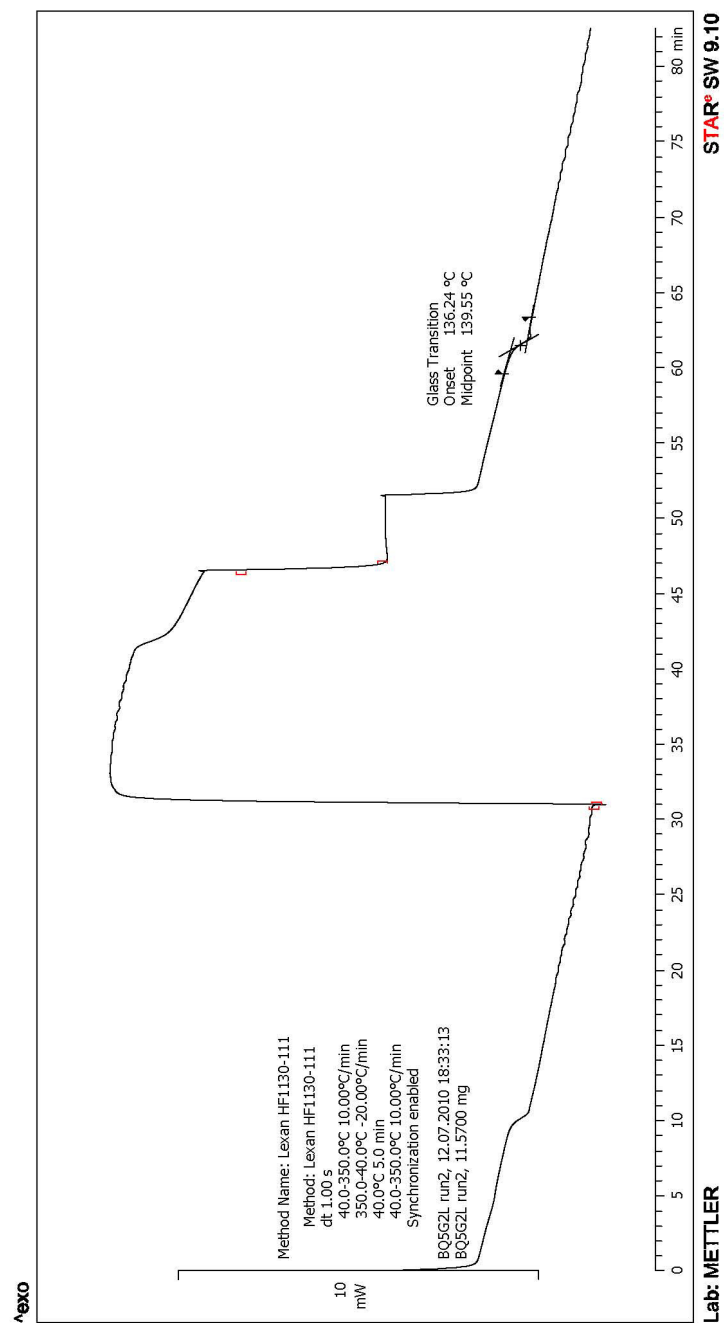


Figure E.42: DSC for BQ5G2L Run 2 vs. Time

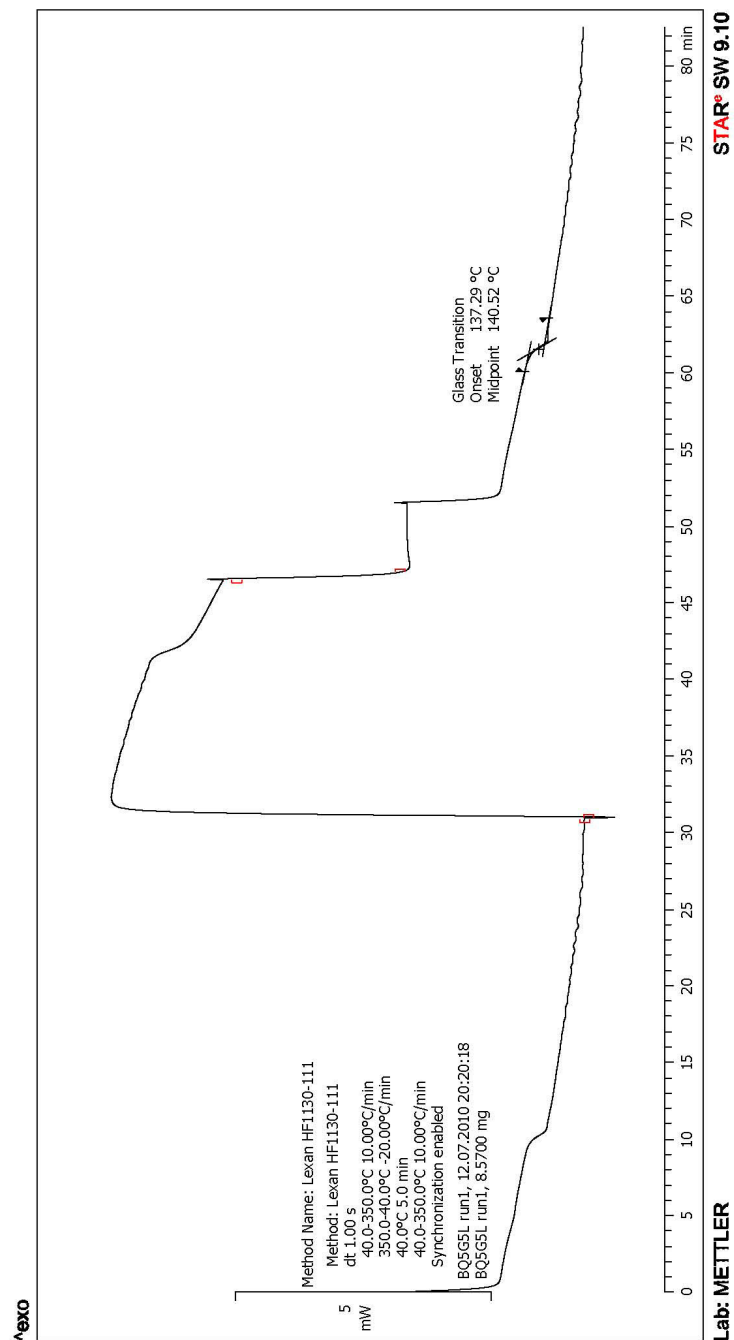


Figure E.43: DSC for BQ5G5L Run 1 vs. Time

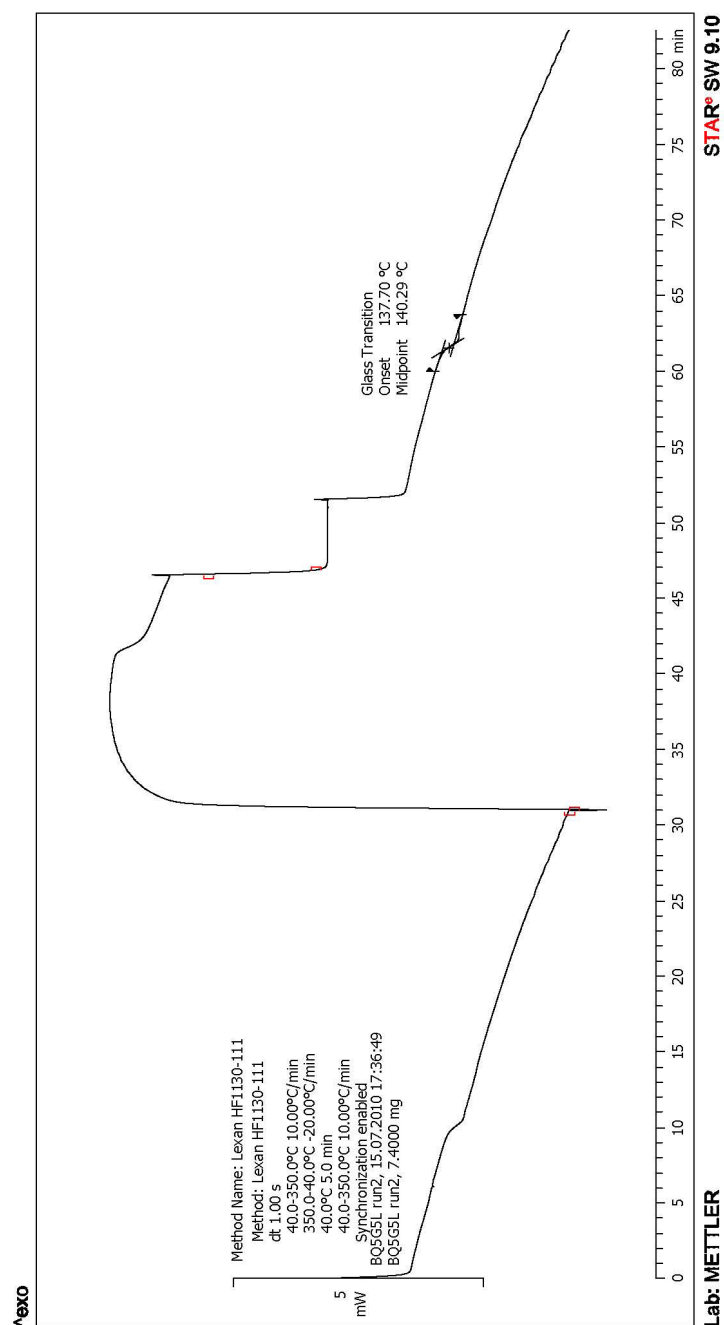


Figure E.44: DSC for BQ5G5L Run 2 vs. Time

Appendix F: In-Plane Electrical Resistivity (Two-Probe) Results on Extruded Rods

Appendix F.1: Polycarbonate with Carbon Black

Table F.1: Two Point Two Probe In-Plane Electrical Resistivity Results for BA2L: 2 wt% Ketjenblack EC-600 JD in Lexan HF1130-111: Extruded Rods: Extruded Nov 5, 2009

Test Date	Sample Number	Length (cm)	Diameter (cm)	Gross Sectional Area (cm ²)	Amps (A)	Volts (V)	Volume ER (ohm-cm)
11/18/2009	BA2L-1	6.02	0.15	0.01767	<1.00E-09	20	5.871E+07
	BA2L-2	6.1	0.13	0.01327	<1.00E-09	20	4.352E+07
	BA2L-3	6.1	0.14	0.01539	<1.00E-09	20	5.047E+07
	BA2L-4	6.1	0.14	0.01539	<1.00E-09	20	5.047E+07
	BA2L-5	6	0.13	0.01327	<1.00E-09	20	4.424E+07
	BA2L-6	6	0.13	0.01327	<1.00E-09	20	4.424E+07
Average							4.861E+07
Std Dev							5.882E+06
Number							6

Table F.2: Two Point Two Probe In-Plane Electrical Resistivity Results for BA3L: 3 wt% Ketjenblack EC-600 JD in Lexan HF1130-111: Extruded Rods: Extruded Nov 5, 2009

Test Date	Sample Number	Length (cm)	Diameter (cm)	Cross Sectional Area (cm ²)	Amps (A)	Volts (V)	Volume ER (ohm-cm)
11/18/2009	BA3L-1	6.04	0.17	0.02270	3.79E-05	3	297.46
	BA3L-3	6.08	0.14	0.01539	2.12E-05	3	358.28
	BA3L-4	5.95	0.14	0.01539	9.30E-06	3	834.58
	BA3L-6	6.02	0.14	0.01539	1.31E-05	3	585.60
	BA3L-8	6.04	0.15	0.01767	9.10E-06	3	964.53
Average							608.09
Std Dev							290.58
Number							5

Table F.3: Two Point Two Probe In-Plane Electrical Resistivity Results for BA4L: 4 wt% Ketjenblack EC-600 JD in Lexan HF1130-111: Extruded Rods: Extruded Nov 5, 2009

Test Date	Sample Number	Length (cm)	Diameter (cm)	Cross Sectional Area (cm ²)	Amps (A)	Volts (V)	Volume ER (ohm-cm)
12/22/2009	BA4L-1	6.08	0.14	0.01539	2.47E-05	1	102.51
	BA4L-2	6.18	0.15	0.01767	2.70E-05	1	105.91
	BA4L-3	6	0.14	0.01539	3.84E-05	1	66.81
	BA4L-4	6.2	0.14	0.01539	2.76E-05	1	89.96
	BA4L-5	6.07	0.15	0.01767	2.66E-05	1	109.45
	BA4L-6	5.95	0.13	0.01327	1.85E-05	1	120.58
	BA4L-7	6.13	0.15	0.01767	3.57E-05	1	80.75
	BA4L-8	6.15	0.14	0.01539	2.12E-05	1	118.07
Average							99.25
Std Dev							18.70
Number							8

Table F.4: Two Point Two Probe In-Plane Electrical Resistivity Results for BA5L: 5 wt% Ketjenblack EC-600 JD in Lexan HF1130-111: Extruded Rods: Extruded Nov 11, 2009

Test Date	Sample Number	Length (cm)	Diameter (cm)	Cross Sectional Area (cm ²)	Amps (A)	Volts (V)	Volume ER (ohm-cm)
12/22/2009	BA5L-1	6.3	0.15	0.01767	3.47E-05	0.3	24.25
	BA5L-2	5.7	0.18	0.02544	3.99E-05	0.3	33.57
	BA5L-3	6.14	0.17	0.02270	4.22E-05	0.3	26.28
	BA5L-4	5.93	0.16	0.02011	4.03E-05	0.3	25.24
	BA5L-5	5.9	0.16	0.02011	3.79E-05	0.3	26.97
	BA5L-6	6.16	0.15	0.01767	3.64E-05	0.3	23.64
	BA5L-7	6.26	0.16	0.02011	3.47E-05	0.3	27.77
Average							26.82
Std Dev							3.31
Number							7

Table F.5: Two Point Two Probe In-Plane Electrical Resistivity Results for BA6L: 6 wt% Ketjenblack EC-600 JD in Lexan HF1130-111: Extruded Rods: Extruded Nov 11, 2009

Test Date	Sample Number	Length (cm)	Diameter (cm)	Cross Sectional Area (cm ²)	Amps (A)	Volts (V)	Volume ER (ohm-cm)
12/22/2009	BA6L-1	5.91	0.18	0.02545	3.38E-05	0.1	12.74
	BA6L-2	6.04	0.17	0.02270	2.99E-05	0.1	12.57
	BA6L-3	6.1	0.18	0.02544	2.76E-05	0.1	15.11
	BA6L-4	6.25	0.18	0.02544	3.36E-05	0.1	12.12
	BA6L-5	6.1	0.17	0.02270	2.34E-05	0.1	15.90
	BA6L-6	6	0.17	0.02270	2.28E-05	0.1	16.59
	BA6L-7	6	0.17	0.02270	2.68E-05	0.1	14.12
	BA6L-8	6.02	0.18	0.02544	3.16E-05	0.1	13.38
Average							14.07
Std Dev							1.65
Number							8

Table F.6: Two Point Two Probe In-Plane Electrical Resistivity Results for BA8L: 8 wt% Ketjenblack EC-600 JD in Lexan HF1130-111: Extruded Rods: Extruded Nov 11, 2009

Test Date	Sample Number	Length (cm)	Diameter (cm)	Cross Sectional Area (cm ²)	Amps (A)	Volts (V)	Volume ER (ohm-cm)
12/22/2009	BA8L-1	6.02	0.25	0.04909	3.85E-05	0.03	6.35
	BA8L-2	5.96	0.25	0.04909	4.06E-05	0.03	6.09
	BA8L-3	6.62	0.25	0.04900	3.75E-05	0.03	5.93
	BA8L-4	6.04	0.24	0.04524	3.66E-05	0.03	6.14
	BA8L-5	6	0.245	0.04714	4.07E-05	0.03	5.79
	BA8L-6	5.98	0.245	0.04714	4.11E-05	0.03	5.75
	BA8L-7	6.04	0.245	0.04714	3.91E-05	0.03	5.99
Average							6.01
Std Dev							0.21
Number							7

Table F.7: Two Point Two Probe In-Plane Electrical Resistivity Results for BA10L: 10 wt% Ketjenblack EC-600 JD in Lexan HF1130-111: Extruded Rods: Extruded Nov 11, 2009

Test Date	Sample Number	Length (cm)	Diameter (cm)	Cross Sectional Area (cm ²)	Amps (A)	Volts (V)	Volume ER (ohm-cm)
12/22/2009	BA10L-1	6.08	0.295	0.06835	3.28E-05	0.01	3.43
	BA10L-2	6	0.29	0.06605	3.36E-05	0.01	3.28
	BA10L-3	5.96	0.27	0.05726	2.89E-05	0.01	3.32
	BA10L-4	6.23	0.288	0.06514	3.27E-05	0.01	3.20
	BA10L-5	6.06	0.285	0.06379	3.27E-05	0.01	3.22
	BA10L-6	6	0.265	0.05515	2.94E-05	0.01	3.13
Average							3.26
Std Dev							0.11
Number							6

Appendix F.2: Polycarbonate with Graphene Nanoplatelets

Table F.8: Two Point Two Probe In-Plane Electrical Resistivity Results for Ovation Polymers Extima GP MB PC 1515B As-Received Pellets: 15 wt% xGnP in Lexan HF1130-111

Test Date	Sample Number	Length (cm)	Diameter (cm)	Cross Sectional Area (cm ²)	Amps (A)	Volts (V)	Volume ER (ohm-cm)
5/21/2010	1	0.293	0.285	0.06379	3.88E-05	0.03	1.683E+02
	2	0.421	0.243	0.04638	2.45E-05	0.03	1.349E+02
	3	0.363	0.241	0.04562	2.85E-05	0.03	1.323E+02
	4	0.330	0.250	0.04909	4.85E-05	0.03	9.201E+01
	5	0.360	0.250	0.04909	1.86E-05	0.03	2.199E+02
Average							1.495E+02
Std Dev							4.778E+01
Number							5

Table F.9: Two Point Two Probe In-Plane Electrical Resistivity Results for BG8L: 8 wt% xGnP in Lexan HF1130-111: Extruded Rods: Extruded May 27, 2010

Test Date	Sample Number	Length (cm)	Diameter (cm)	Cross Sectional Area (cm ²)	Amps (A)	Volts (V)	Volume ER (ohm-cm)
6/3/2010	BG8L-1	5.922	0.180	0.02545	1.68E-06	20	5.125E+04
	BG8L-2	5.985	0.182	0.02602	1.75E-06	20	4.971E+04
	BG8L-3	5.923	0.173	0.02351	1.35E-06	20	5.901E+04
	BG8L-4	6.025	0.176	0.02433	1.54E-06	20	5.258E+04
	BG8L-5	5.855	0.175	0.02405	1.15E-06	20	7.169E+04
	BG8L-6	5.965	0.175	0.02405	1.52E-06	20	5.295E+04
	BG8L-7	5.944	0.179	0.02516	1.52E-06	20	5.585E+04
	BG8L-8	6.014	0.173	0.02351	1.35E-06	20	5.803E+04
	BG8L-9	5.992	0.166	0.02164	1.18E-06	20	6.122E+04
	BG8L-10	5.966	0.176	0.02433	1.32E-06	20	6.202E+04
Average							5.743E+04
Std Dev							6.547E+03
Number							10

Table F.10: Two Point Two Probe In-Plane Electrical Resistivity Results for BG10L: 10 wt% xGnP in Lexan HF1130-111:
Extruded Rods: Extruded May 27, 2010

Test Date	Sample Number	Length (cm)	Diameter (cm)	Cross Sectional Area (cm ²)	Amps (A)	Volts (V)	Volume ER (ohm-cm)
6/3/2010	BG10L-1	5.952	0.168	0.02217	2.29E-05	20	3.260E+03
	BG10L-2	6.006	0.165	0.02138	2.07E-05	20	3.443E+03
	BG10L-3	5.999	0.175	0.02405	2.47E-05	20	3.248E+03
	BG10L-4	5.929	0.168	0.02217	2.48E-05	20	3.015E+03
	BG10L-5	5.851	0.172	0.02324	2.56E-05	20	3.105E+03
	BG10L-6	6.003	0.172	0.02324	2.72E-05	20	2.849E+03
	BG10L-7	6.014	0.175	0.02405	2.51E-05	20	3.186E+03
	BG10L-8	5.925	0.173	0.02351	2.45E-05	20	3.244E+03
	BG10L-9	6.069	0.173	0.02351	2.63E-05	20	2.943E+03
	BG10L-10	5.932	0.173	0.02351	2.92E-05	20	2.716E+03
Average							3.101E+03
Std Dev							2.199E+02
Number							10

Appendix F.3: Polycarbonate with Multiple Fillers

Table F.11: Two Point Two Probe In-Plane Electrical Resistivity Results for BA5LR Extruded Rods: Extruded on 7-8-10

Test Date	Sample Number	Length (cm)	Diameter (cm)	Gross Sectional Area (cm ²)	Amps (A)	Volts (V)	Volume ER (ohm-cm)
7/15/2010	BA5LR-1	5.887	0.175	0.024052819	1.87E-05	0.3	6.565E+01
	BA5LR-2	6.044	0.17	0.022698007	1.98E-05	0.3	5.684E+01
	BA5LR-5	5.924	0.175	0.024052819	2.35E-05	0.3	5.188E+01
	BA5LR-6	6.017	0.18	0.0254469	1.88E-05	0.3	6.734E+01
	BA5LR-8	6.034	0.17	0.022698007	1.87E-05	0.3	6.032E+01
	BA5LR-9	5.971	0.185	0.026880252	1.86E-05	0.3	7.261E+01
	BA5LR-10	6.069	0.185	0.026880252	1.99E-05	0.3	6.674E+01
Average							6.305E+01
Std Dev							7.083E+00
Number							7

Table F.12: Two Point Two Probe In-Plane Electrical Resistivity Results for BA8LR Extruded Rods: Extruded on 4-14-10 Masterbatch

Test Date	Sample Number	Length (cm)	Diameter (cm)	Cross Sectional Area (cm ²)	Amps (A)	Volts (V)	Volume ER (ohm-cm)
4/20/2010	BA8LR-1	6.03	0.25	0.049087385	4.16E-05	0.03	5.87
	BA8LR-2	6.14	0.26	0.053092916	4.23E-05	0.03	6.13
	BA8LR-3	6.02	0.26	0.053092916	4.12E-05	0.03	6.43
	BA8LR-4	6.05	0.26	0.053092916	4.32E-05	0.03	6.09
	BA8LR-5	5.99	0.25	0.049087385	4.00E-05	0.03	6.14
	BA8LR-6	6.02	0.25	0.049087385	4.02E-05	0.03	6.09
	BA8LR-7	6.01	0.25	0.049087385	4.19E-05	0.03	5.85
	BA8LR-8	6.08	0.27	0.057255526	4.39E-05	0.03	6.44
	BA8LR-9	5.99	0.25	0.049087385	4.10E-05	0.03	6.00
	BA8LR-10	5.99	0.26	0.053092916	4.17E-05	0.03	6.38
	BA8LR-11	6.13	0.25	0.049087385	4.12E-05	0.03	5.83
	BA8LR-12	5.99	0.25	0.049087385	4.19E-05	0.03	5.87
	BA8LR-13	6.03	0.25	0.049087385	4.03E-05	0.03	6.06
	BA8LR-14	6	0.26	0.053092916	4.19E-05	0.03	6.34
	BA8LR-15	6.08	0.26	0.053092916	4.20E-05	0.03	6.24
	BA8LR-16	6.02	0.25	0.049087385	4.19E-05	0.03	5.84
Average							6.10
Std Dev							0.22
Number							16

Table F.13: Two Point Two Probe In-Plane Electrical Resistivity Results for BG12L Extruded Rods: Extruded on 7-8-10

Test Date	Sample Number	Length (cm)	Diameter (cm)	Cross Sectional Area (cm ²)	Amps (A)	Volts (V)	Volume ER (ohm-cm)
7/15/2010	BG12L-1	5.999	0.180	0.02545	7.04E-05	10	6.023E+02
	BG12L-2	6.206	0.185	0.02688	6.97E-05	10	6.212E+02
	BG12L-3	6.007	0.180	0.02545	7.79E-05	10	5.442E+02
	BG12L-4	5.959	0.175	0.02405	6.91E-05	10	5.845E+02
	BG12L-5	5.892	0.180	0.02545	6.31E-05	10	6.848E+02
	BG12L-6	5.947	0.180	0.02545	7.12E-05	10	6.006E+02
	BG12L-7	6.043	0.180	0.02545	8.05E-05	10	5.229E+02
	BG12L-8	6.032	0.180	0.02545	6.08E-05	10	6.943E+02
	BG12L-9	6.002	0.180	0.02545	6.40E-05	10	6.630E+02
	BG12L-10	5.996	0.180	0.02545	7.29E-05	10	5.819E+02
Average							6.100E+02
Std Dev							5.690E+01
Number							10

Table F.14: Two Point Two Probe In-Plane Electrical Resistivity Results for BG15L Extruded Rods: Extruded on 7-8-10

Test Date	Sample Number	Length (cm)	Diameter (cm)	Cross Sectional Area (cm ²)	Amps (A)	Volts (V)	Volume ER (ohm-cm)
7/15/2010	BG15L-1	5.997	0.180	0.02545	4.30E-05	2	1.976E+02
	BG15L-2	6.008	0.190	0.02835	5.38E-05	2	1.756E+02
	BG15L-3	6.011	0.185	0.02688	4.17E-05	2	2.143E+02
	BG15L-4	6.015	0.180	0.02545	4.27E-05	2	1.981E+02
	BG15L-5	6.018	0.190	0.02835	4.96E-05	2	1.899E+02
	BG15L-6	5.955	0.190	0.02835	4.96E-05	2	1.921E+02
	BG15L-7	6.016	0.175	0.02405	4.81E-05	2	1.664E+02
	BG15L-8	6.078	0.185	0.02688	4.33E-05	2	2.043E+02
	BG15L-9	6.037	0.185	0.02688	4.15E-05	2	2.146E+02
	BG15L-10	5.977	0.185	0.02688	4.69E-05	2	1.919E+02
Average							1.945E+02
Std Dev							1.527E+01
Number							10

Table F.15: Two Point Two Probe In-Plane Electrical Resistivity Results for Ovation Polymers Extima GP MB PC 1515B As-Received Pellets: 15 wt% xGnP in Lexan HF1130-111

Test Date	Sample Number	Length (cm)	Diameter (cm)	Cross Sectional Area (cm ²)	Amps (A)	Volts (V)	Volume ER (ohm-cm)
5/21/2010	PC1515B-1	0.293	0.285	0.06379	3.88E-05	0.03	1.683E+02
	PC1515B-2	0.421	0.243	0.04638	2.45E-05	0.03	1.349E+02
	PC1515B-3	0.363	0.241	0.04562	2.85E-05	0.03	1.323E+02
	PC1515B-4	0.330	0.250	0.04909	4.85E-05	0.03	9.201E+01
	PC1515B-5	0.360	0.250	0.04909	1.86E-05	0.03	2.199E+02
					Average		1.495E+02
					Std Dev		4.778E+01
					Number		5

Table F.16: Two Point Two Probe In-Plane Electrical Resistivity Results for BA2Q1L: Extruded Rods: Extruded 7-7-10

Test Date	Sample Number	Length (cm)	Diameter (cm)	Cross Sectional Area (cm ²)	Amps (A)	Volts (V)	Volume ER (ohm-cm)
7/16/2010	BA2Q1L-1	6.061	0.195	0.029864765	3.83E-05	2	2.576E+02
	BA2Q1L-2	6.035	0.195	0.029864765	2.63E-05	2	3.759E+02
	BA2Q1L-3	5.971	0.19	0.028352874	2.67E-05	2	3.556E+02
	BA2Q1L-5	6.147	0.19	0.028352874	3.72E-05	2	2.480E+02
	BA2Q1L-8	6.005	0.18	0.0254469	3.20E-05	2	2.649E+02
					Average		3.004E+02
					Std Dev		6.039E+01
					Number		5

Table F.17: Two Point Two Probe In-Plane Electrical Resistivity Results for BA2Q5L: Extruded Rods: Extruded 7-7-10

Test Date	Sample Number	Length (cm)	Diameter (cm)	Cross Sectional Area (cm ²)	Amps (A)	Volts (V)	Volume ER (ohm-cm)
7/16/2010	BA2Q5L-1	6.034	0.265	0.055154586	1.92E-05	0.01	4.773E+00
	BA2Q5L-2	6.012	0.27	0.057255526	2.02E-05	0.01	4.710E+00
	BA2Q5L-3	6.113	0.27	0.057255526	1.92E-05	0.01	4.886E+00
	BA2Q5L-4	6.042	0.265	0.055154586	1.93E-05	0.01	4.725E+00
	BA2Q5L-5	6.015	0.275	0.059395736	2.05E-05	0.01	4.829E+00
	BA2Q5L-6	6.003	0.275	0.059395736	1.95E-05	0.01	5.084E+00
	BA2Q5L-7	6.005	0.27	0.057255526	1.97E-05	0.01	4.847E+00
	BA2Q5L-8	5.96	0.27	0.057255526	2.06E-05	0.01	4.657E+00
	BA2Q5L-9	5.977	0.27	0.057255526	2.03E-05	0.01	4.724E+00
	BA2Q5L-10	6.044	0.26	0.053092916	1.88E-05	0.01	4.680E+00
Average							4.791E+00
Std Dev							1.273E-01
Number							10

Table F.18: Two Point Two Probe In-Plane Electrical Resistivity Results for BA5Q1L: Extruded Rods: Extruded 7-7-10

Test Date	Sample Number	Length (cm)	Diameter (cm)	Cross Sectional Area (cm ²)	Amps (A)	Volts (V)	Volume ER (ohm-cm)
7/16/2010	BA5Q1L-1	5.985	0.275	0.059395736	2.61E-05	0.05	1.899E+01
	BA5Q1L-2	6.015	0.27	0.057255526	2.81E-05	0.05	1.696E+01
	BA5Q1L-3	6.122	0.275	0.059395736	2.75E-05	0.05	1.762E+01
	BA5Q1L-4	6.003	0.275	0.059395736	2.70E-05	0.05	1.833E+01
	BA5Q1L-5	6.046	0.27	0.057255526	2.40E-05	0.05	1.972E+01
	BA5Q1L-6	6.046	0.265	0.055154586	2.67E-05	0.05	1.707E+01
	BA5Q1L-7	5.9	0.27	0.057255526	2.68E-05	0.05	1.812E+01
	BA5Q1L-8	6.074	0.275	0.059395736	2.61E-05	0.05	1.872E+01
	BA5Q1L-9	6.059	0.275	0.059395736	2.79E-05	0.05	1.754E+01
	BA5Q1L-10	6.012	0.275	0.059395736	2.58E-05	0.05	1.918E+01
Average							1.823E+01
Std Dev							9.290E-01
Number							10

Table F.19: Two Point Two Probe In-Plane Electrical Resistivity Results for BA5Q5L: Extruded Rods: Extruded 7-7-10

Test Date	Sample Number	Length (cm)	Diameter (cm)	Cross Sectional Area (cm ²)	Amps (A)	Volts (V)	Volume ER (ohm-cm)
7/16/2010	BA5Q5L-1	5.953	0.285	0.063793966	3.40E-05	0.01	3.153E+00
	BA5Q5L-2	5.985	0.28	0.061575216	3.46E-05	0.01	2.977E+00
	BA5Q5L-3	6.084	0.28	0.061575216	3.60E-05	0.01	2.810E+00
	BA5Q5L-4	5.998	0.28	0.061575216	3.66E-05	0.01	2.804E+00
	BA5Q5L-5	6.008	0.285	0.063793966	3.61E-05	0.01	2.943E+00
	BA5Q5L-6	6.145	0.28	0.061575216	3.47E-05	0.01	2.887E+00
	BA5Q5L-7	5.941	0.28	0.061575216	3.55E-05	0.01	2.923E+00
	BA5Q5L-8	6.287	0.275	0.059395736	3.39E-05	0.01	2.789E+00
	BA5Q5L-9	6.072	0.28	0.061575216	3.50E-05	0.01	2.901E+00
	BA5Q5L-10	6.093	0.28	0.061575216	3.43E-05	0.01	2.948E+00
Average							2.913E+00
Std Dev							1.067E-01
Number							10

Table F.20: Two Point Two Probe In-Plane Electrical Resistivity Results for BA2G5L: Extruded Rods: Extruded 7-6-10

Test Date	Sample Number	Length (cm)	Diameter (cm)	Cross Sectional Area (cm ²)	Amps (A)	Volts (V)	Volume ER (ohm-cm)
7/15/2010	BA2G5L-2	5.908	0.185	0.026880252	2.56E-05	5	8.897E+02
	BA2G5L-3	5.98	0.195	0.029864765	3.88E-05	5	6.437E+02
	BA2G5L-4	5.952	0.185	0.026880252	3.57E-05	5	6.329E+02
	BA2G5L-5	6.011	0.19	0.028352874	3.23E-05	5	7.295E+02
	BA2G5L-6	5.983	0.18	0.0254469	3.83E-05	5	5.552E+02
	BA2G5L-8	5.963	0.175	0.024052819	3.52E-05	5	5.733E+02
	BA2G5L-9	6.057	0.185	0.026880252	2.79E-05	5	7.956E+02
	BA2G5L-10	6.02	0.18	0.0254469	2.96E-05	5	7.148E+02
Average							6.918E+02
Std Dev							1.136E+02
Number							8

Table F.21: Two Point Two Probe In-Plane Electrical Resistivity Results for BA5G2L: Extruded Rods: Extruded 7-6-10

Test Date	Sample Number	Length (cm)	Diameter (cm)	Cross Sectional Area (cm ²)	Amps (A)	Volts (V)	Volume ER (ohm-cm)
7/15/2010	BA5G2L-1	6.019	0.19	0.028352874	3.87E-05	0.2	2.432E+01
	BA5G2L-2	5.964	0.19	0.028352874	4.36E-05	0.2	2.182E+01
	BA5G2L-3	6.033	0.19	0.028352874	3.71E-05	0.2	2.531E+01
	BA5G2L-5	6.028	0.19	0.028352874	4.40E-05	0.2	2.138E+01
	BA5G2L-6	6.056	0.19	0.028352874	4.36E-05	0.2	2.149E+01
	BA5G2L-7	5.996	0.185	0.026880252	3.96E-05	0.2	2.263E+01
	BA5G2L-9	5.999	0.19	0.028352874	4.68E-05	0.2	2.021E+01
	BA5G2L-10	6.021	0.19	0.028352874	4.90E-05	0.2	1.922E+01
Average							2.205E+01
Std Dev							2.011E+00
Number							8

Table F.22: Two Point Two Probe In-Plane Electrical Resistivity Results for BA5G5L: Extruded Rods: Extruded 7-6-10

Test Date	Sample Number	Length (cm)	Diameter (cm)	Cross Sectional Area (cm ²)	Amps (A)	Volts (V)	Volume ER (ohm-cm)
7/16/2010	BA5G5L-1	6.013	0.2	0.031415927	4.59E-05	0.1	1.139E+01
	BA5G5L-2	6.038	0.2	0.031415927	4.56E-05	0.1	1.142E+01
	BA5G5L-3	5.966	0.195	0.029864765	4.32E-05	0.1	1.160E+01
	BA5G5L-4	5.977	0.2	0.031415927	4.61E-05	0.1	1.140E+01
	BA5G5L-5	6.016	0.2	0.031415927	4.81E-05	0.1	1.087E+01
	BA5G5L-6	6.002	0.2	0.031415927	4.73E-05	0.1	1.108E+01
	BA5G5L-7	6.027	0.195	0.029864765	4.82E-05	0.1	1.029E+01
	BA5G5L-8	6.02	0.2	0.031415927	4.65E-05	0.1	1.122E+01
	BA5G5L-9	6.011	0.195	0.029864765	4.57E-05	0.1	1.087E+01
	BA5G5L-10	5.954	0.2	0.031415927	4.62E-05	0.1	1.143E+01
Average							1.116E+01
Std Dev							3.909E-01
Number							10

Table F.23: Two Point Two Probe In-Plane Electrical Resistivity Results for BQ1G5L: Extruded Rods: Extruded 7-1-10

Test Date	Sample Number	Length (cm)	Diameter (cm)	Cross Sectional Area (cm ²)	Amps (A)	Volts (V)	Volume ER (ohm-cm)
7/16/2010	BQ1G5L-4	5.892	0.195	0.029864765	3.72E-05	10	1.362E+03
	BQ1G5L-6	5.95	0.19	0.028352874	4.89E-05	10	9.739E+02
	BQ1G5L-7	6.185	0.19	0.028352874	3.86E-05	10	1.189E+03
	BQ1G5L-8	5.952	0.19	0.028352874	6.17E-05	10	7.726E+02
	BQ1G5L-9	5.972	0.19	0.028352874	6.27E-05	10	7.578E+02
	BQ1G5L-10	6.06	0.19	0.028352874	4.69E-05	10	9.970E+02
Average							1.009E+03
Std Dev							2.356E+02
Number							6

Table F.24: Two Point Two Probe In-Plane Electrical Resistivity Results for BQ5G2L: Extruded Rods: Extruded 7-1-10

Test Date	Sample Number	Length (cm)	Diameter (cm)	Cross Sectional Area (cm ²)	Amps (A)	Volts (V)	Volume ER (ohm-cm)
7/16/2010	BQ5G2L-1	6.006	0.2	0.031415927	2.18E-05	0.02	4.810E+00
	BQ5G2L-2	6.027	0.215	0.03630503	2.41E-05	0.02	5.007E+00
	BQ5G2L-3	5.993	0.215	0.03630503	2.51E-05	0.02	4.833E+00
	BQ5G2L-4	6.023	0.215	0.03630503	2.42E-05	0.02	4.980E+00
	BQ5G2L-5	6.092	0.215	0.03630503	2.40E-05	0.02	4.962E+00
	BQ5G2L-6	5.967	0.205	0.033006358	2.10E-05	0.02	5.273E+00
	BQ5G2L-7	5.979	0.21	0.034636059	2.37E-05	0.02	4.897E+00
	BQ5G2L-8	6.062	0.21	0.034636059	2.35E-05	0.02	4.856E+00
	BQ5G2L-9	6.048	0.2	0.031415927	2.28E-05	0.02	4.567E+00
	BQ5G2L-10	6.03	0.21	0.034636059	2.33E-05	0.02	4.935E+00
Average							4.912E+00
Std Dev							1.784E-01
Number							10

Table F.25: Two Point Two Probe In-Plane Electrical Resistivity Results for BQ5G5L: Extruded Rods: Extruded 7-1-10

Test Date	Sample Number	Length (cm)	Diameter (cm)	Cross Sectional Area (cm ²)	Amps (A)	Volts (V)	Volume ER (ohm-cm)
7/16/2010	BQ5G5L-1	6.08	0.225	0.039760782	2.26E-05	0.01	2.899E+00
	BQ5G5L-2	6.02	0.23	0.041547563	2.53E-05	0.01	2.724E+00
	BQ5G5L-3	6.023	0.23	0.041547563	2.51E-04	0.01	2.746E-01
	BQ5G5L-4	6.007	0.225	0.039760782	2.35E-05	0.01	2.821E+00
	BQ5G5L-5	6.096	0.23	0.041547563	2.37E-05	0.01	2.879E+00
	BQ5G5L-6	6.023	0.23	0.041547563	2.45E-05	0.01	2.821E+00
	BQ5G5L-7	6.028	0.23	0.041547563	2.38E-05	0.01	2.902E+00
	BQ5G5L-8	6.196	0.23	0.041547563	2.32E-05	0.01	2.894E+00
	BQ5G5L-9	6.079	0.225	0.039760782	2.26E-05	0.01	2.899E+00
Average							2.568E+00
Std Dev							8.621E-01
Number							9

Appendix G: Through Plane Electrical Resistivity (ASTM D257) Results

Appendix G.1: Polycarbonate with Carbon Nanotubes

Table G.1: ASTM D257 Through Plane Electrical Resistivity Results for BL: Lexan HF1130-111: Injection Molded May 26, 2009

Test Date	Sample Number	Applied Voltage (V)	Through-Plane Surface Electrical Resistivity (Ω/square)	Through-Plane Volume Electrical Resistivity ($\Omega\text{-cm}$)
6/10/2009	BL-TC-12	100	1.33E+16	1.50E+16
6/10/2009	BL-TC-15	100	2.44E+16	3.00E+16
6/10/2009	BL-TC-17	100	1.53E+17	1.79E+17
6/10/2009	BL-TC-21	100	4.26E+16	5.38E+16
6/19/2009	BL-TC-13	100	1.59E+17	1.74E+17
6/19/2009	BL-TC-30	100	6.44E+16	7.96E+16
6/10/2009	BL-TC-31	100	1.67E+17	2.09E+17
Average			8.918E+16	1.057E+17
Standard Deviation			6.806E+16	7.963E+16
Number of Samples			7	7

Table G.2: ASTM D257 Through Plane Electrical Resistivity Results for BLE: Extruded Lexan HF1130-111: Injection Molded May 26, 2009

Test Date	Sample Number	Applied Voltage (V)	Through-Plane Surface Electrical Resistivity (Ω /square)	Through-Plane Volume Electrical Resistivity (Ω -cm)
6/10/2009	BLE-TC-13	100	1.94E+16	2.39E+16
6/11/2009	BLE-TC-16	100	6.78E+16	8.48E+16
6/11/2009	BLE-TC-17	100	4.88E+16	5.92E+16
6/11/2009	BLE-TC-20	100	1.18E+17	1.50E+17
6/11/2009	BLE-TC-22	100	2.67E+16	3.19E+16
6/11/2009	BLE-TC-24	100	6.12E+16	7.48E+16
		Average	5.703E+16	7.068E+16
		Standard Deviation	3.546E+16	4.530E+16
		Number of Samples	6	6

Appendix G.2: Polycarbonate with Carbon Black

Table G.3: ASTM D257 Through Plane Electrical Resistivity Results for BL2: Lexan HF1130-111: Injection Molded December 4, 2009

Test Date	Sample Number	Applied Voltage (V)	Through-Plane Surface Electrical Resistivity (Ω/square)	Through-Plane Volume Electrical Resistivity ($\Omega\text{-cm}$)
12/7/2009	BL2-TC-40	100	8.8010E+16	9.6089E+16
12/7/2009	BL2-TC-22	100	5.5567E+16	1.4034E+17
12/7/2009	BL2-TC-9	100	1.7208E+17	8.6133E+16
12/7/2009	BL2-TC-25	100	1.0728E+17	1.3089E+17
12/7/2009	BL2-TC-29	100	1.0565E+17	1.2183E+17
12/7/2009	BL2-TC-27	100	1.3064E+17	1.7982E+17
Average			1.0987E+17	1.2585E+17
Standard Deviation			3.9377E+16	3.3548E+16
Number of Samples			6	6

Table G.4: ASTM D257 Through Plane Electrical Resistivity Results for BLE2: Extruded Lexan HF1130-111: Extruded Nov 5, 2009; Injection Molded December 4, 2009

Test Date	Sample Number	Applied Voltage (V)	Through-Plane Surface Electrical Resistivity (Ω /square)	Through-Plane Volume Electrical Resistivity (Ω -cm)
12/17/2009	BLE2-TC-14	100	2.3979E+16	4.0569E+17
12/17/2009	BLE2-TC-11	100	3.4927E+16	1.2131E+17
12/17/2009	BLE2-TC-7	100	2.5512E+16	2.6558E+17
12/17/2009	BLE2-TC-17	100	2.0976E+16	4.4475E+17
12/17/2009	BLE2-TC-9	100	3.0226E+16	1.3335E+17
12/17/2009	BLE2-TC-21	100	9.5520E+15	1.8589E+17
		Average	2.4195E+16	2.5943E+17
		Standard Deviation	8.6961E+15	1.3868E+17
		Number of Samples	6	6

Table G.5: ASTM D257 Through Plane Electrical Resistivity Results for BA2L: 2 wt% Ketjenblack EC-600 JD in Lexan HF1130-111: Injection Molded December 4, 2009

Test Date	Sample Number	Applied Voltage (V)	Through-Plane Surface Electrical Resistivity (Ω /square)	Through-Plane Volume Electrical Resistivity (Ω -cm)
12/18/2009	BA2L-TC-24	100	2.4674E+17	2.5957E+16
12/18/2009	BA2L-TC-27	100	3.1627E+16	1.7383E+16
12/18/2009	BA2L-TC-5	100	1.1845E+16	5.9889E+16
12/18/2009	BA2L-TC-9	100	2.4993E+16	1.5829E+16
12/18/2009	BA2L-TC-30	100	1.1959E+16	8.2963E+16
12/18/2009	BA2L-TC-19	100	1.1826E+16	4.1130E+16
		Average	5.6498E+16	4.0525E+16
		Standard Deviation	9.3570E+16	2.6586E+16
		Number of Samples	6	6

Table G.6: ASTM D257 Through Plane Electrical Resistivity Results for BA3L: 3 wt% Ketjenblack EC-600 JD in Lexan HF1130-111: Injection Molded December 4, 2009

Test Date	Sample Number	Applied Voltage (V)	Through-Plane Surface Electrical Resistivity (Ω /square)	Through-Plane Volume Electrical Resistivity (Ω -cm)
12/18/2009	BA3L-TC-28	100	6.2420E+15	2.3907E+15
12/18/2009	BA3L-TC-24	100	3.6602E+15	2.5925E+15
12/18/2009	BA3L-TC-20	100	2.6216E+15	2.8664E+15
12/18/2009	BA3L-TC-7	100	3.9430E+15	2.4510E+15
12/18/2009	BA3L-TC-11	100	2.3223E+15	3.3838E+15
12/18/2009	BA3L-TC-4	100	2.6606E+15	3.4235E+15
		Average	3.5750E+15	2.8513E+15
		Standard Deviation	1.4540E+15	4.5838E+14
		Number of Samples	6	6

Appendix G.3: Polycarbonate with Graphite Nanoparticles

Table G.7: ASTM D257 Through Plane Electrical Resistivity Results for BL3: Lexan HF1130-111: Injection Molded 6-3-10

Test Date	Sample Number	Applied Voltage (V)	Through-Plane Surface Electrical Resistivity (Ω/square)	Through-Plane Volume Electrical Resistivity ($\Omega\text{-cm}$)
6/4/2010	BL3-TC-12	100	8.9746E+16	1.1695E+17
6/4/2010	BL3-TC-23	100	8.9015E+14	9.4655E+16
6/8/2010	BL3-TC-18	100	3.0826E+16	1.1713E+17
6/8/2010	BL3-TC-27	100	2.6199E+17	6.9047E+16
6/8/2010	BL3-TC-28	100	3.6130E+17	8.5692E+16
6/8/2010	BL3-TC-29	100	5.5683E+17	7.8509E+16
		Average	2.1693E+17	9.3664E+16
		Standard Deviation	2.1720E+17	1.9965E+16
		Number of Samples	6	6

Table G.8: ASTM D257 Through Plane Electrical Resistivity Results for BLE3: Extruded Lexan HF1130-111: Extruded 5-26-10; Injection Molded 6-3-10

Test Date	Sample Number	Applied Voltage (V)	Through-Plane Surface Electrical Resistivity (Ω /square)	Through-Plane Volume Electrical Resistivity (Ω -cm)
6/8/2010	BLE3-TC-5	100	6.3781E+15	6.3695E+16
6/8/2010	BLE3-TC-6	100	2.0715E+17	9.9061E+16
6/8/2010	BLE3-TC-7	100	1.2488E+17	9.7042E+16
6/8/2010	BLE3-TC-8	100	2.4365E+17	9.2231E+16
6/8/2010	BLE3-TC-9	100	5.6273E+16	1.0422E+17
6/8/2010	BLE3-TC-4	100	5.0379E+16	2.0189E+17
6/8/2010	BLE3-TC-3	100	2.1701E+17	9.8937E+16
6/8/2010	BLE3-TC-11	100	1.2729E+16	7.7092E+16
		Average	1.1481E+17	1.0427E+17
		Standard Deviation	9.6680E+16	4.1692E+16
		Number of Samples	8	8

Table G.9: ASTM D257 Through Plane Electrical Resistivity Results for BG2L: 2 wt% xGnP in Lexan HF1130-111: Injection Molded 6-3-10

Test Date	Sample Number	Applied Voltage (V)	Through-Plane Surface Electrical Resistivity (Ω /square)	Through-Plane Volume Electrical Resistivity (Ω -cm)
6/8/2010	BG2L-TC-15	100	9.6444E+14	5.0799E+16
6/8/2010	BG2L-TC-13	100	4.3584E+16	5.4010E+16
6/8/2010	BG2L-TC-24	100	9.8499E+16	5.3507E+16
6/8/2010	BG2L-TC-23	100	5.6887E+16	6.2724E+16
6/8/2010	BG2L-TC-22	100	1.6322E+17	4.9213E+16
6/8/2010	BG2L-TC-21	100	3.1959E+16	5.7554E+16
		Average	6.5852E+16	5.4635E+16
		Standard Deviation	5.7414E+16	4.8934E+15
		Number of Samples	6	6

Table G.10: ASTM D257 Through Plane Electrical Resistivity Results for BG3L: 3 wt% xGnP in Lexan HF1130-111: Injection Molded 6-3-10

Test Date	Sample Number	Applied Voltage (V)	Through-Plane Surface Electrical Resistivity (Ω/square)	Through-Plane Volume Electrical Resistivity ($\Omega\text{-cm}$)
6/9/2010	BG3L-TC-12	100	7.0386E+16	2.7572E+16
6/9/2010	BG3L-TC-27	100	8.9686E+16	2.8229E+16
6/9/2010	BG3L-TC-19	100	5.3263E+16	2.9993E+16
6/9/2010	BG3L-TC-30	100	2.7196E+16	3.7716E+16
6/9/2010	BG3L-TC-15	100	2.0123E+16	4.8140E+16
6/9/2010	BG3L-TC-25	100	1.0754E+17	2.8534E+16
6/9/2010	BG3L-TC-20	100	4.3133E+16	3.0276E+16
6/9/2010	BG3L-TC-18	100	2.2539E+17	2.7590E+16
		Average	7.9590E+16	3.2256E+16
		Standard Deviation	6.6040E+16	7.2204E+15
		Number of Samples	8	8

Table G.11: ASTM D257 Through Plane Electrical Resistivity Results for BG4L: 4 wt% xGnP in Lexan HF1130-111: Injection Molded 6-3-10

Test Date	Sample Number	Applied Voltage (V)	Through-Plane Surface Electrical Resistivity (Ω/square)	Through-Plane Volume Electrical Resistivity ($\Omega\text{-cm}$)
6/9/2010	BG4L-TC-21	100	9.4799E+16	1.1575E+16
6/9/2010	BG4L-TC-20	100	7.5057E+16	1.1796E+16
6/9/2010	BG4L-TC-19	100	9.0056E+16	1.2164E+16
6/9/2010	BG4L-TC-18	100	9.2462E+16	1.2126E+16
6/9/2010	BG4L-TC-16	100	5.5037E+16	1.2539E+16
6/9/2010	BG4L-TC-13	100	9.1579E+16	1.1732E+16
		Average	8.3165E+16	1.1989E+16
		Standard Deviation	1.5472E+16	3.5400E+14
		Number of Samples	6	6

Table G.12: ASTM D257 Through Plane Electrical Resistivity Results for BG5L: 5 wt% xGnP in Lexan HF1130-111: Injection Molded 6-3-10

Test Date	Sample Number	Applied Voltage (V)	Through-Plane Surface Electrical Resistivity (Ω /square)	Through-Plane Volume Electrical Resistivity (Ω -cm)
6/10/2010	BG5L-TC-8	100	2.4495E+16	4.7090E+15
6/10/2010	BG5L-TC-11	100	2.4791E+16	4.0782E+15
6/10/2010	BG5L-TC-19	100	2.2501E+16	3.9044E+15
6/10/2010	BG5L-TC-18	100	2.0221E+16	3.4275E+15
6/10/2010	BG5L-TC-14	100	1.8767E+16	3.2874E+15
6/10/2010	BG5L-TC-12	100	1.9863E+16	3.3011E+15
		Average	2.1773E+16	3.7846E+15
		Standard Deviation	2.5354E+15	5.5921E+14
		Number of Samples	6	6

Table G.13: ASTM D257 Through Plane Electrical Resistivity Results for BG6L: 6 wt% xGnP in Lexan HF1130-111: Injection Molded 6-8-10

Test Date	Sample Number	Applied Voltage (V)	Through-Plane Surface Electrical Resistivity (Ω /square)	Through-Plane Volume Electrical Resistivity (Ω -cm)
6/10/2010	BG6L-TC-22	100	1.7140E+15	2.0798E+14
6/10/2010	BG6L-TC-26	100	3.4737E+15	1.9682E+14
6/10/2010	BG6L-TC-19	100	3.2758E+15	1.9705E+14
6/10/2010	BG6L-TC-16	100	3.3674E+15	2.0585E+14
6/10/2010	BG6L-TC-23	100	3.6406E+15	1.9690E+14
6/10/2010	BG6L-TC-11	100	3.0990E+15	1.9927E+14
		Average	3.0951E+15	2.0065E+14
		Standard Deviation	7.0074E+14	4.9873E+12
		Number of Samples	6	6

Appendix G.4: Polycarbonate with Multiple Fillers

Table G.14: ASTM D257 Through Plane Electrical Resistivity Results for BA2LR:
Extruded 7-8-10, Injection Molded 7-26-10

Test Date	Sample Number	Applied Voltage (V)	Through-Plane Surface Electrical Resistivity (Ω /square)	Through-Plane Volume Electrical Resistivity (Ω -cm)
8/2/2010	BA2LR-TC-11	100	1.3994E+16	1.0845E+16
8/2/2010	BA2LR-TC-9	100	2.8471E+16	1.5032E+16
8/2/2010	BA2LR-TC-20	100	2.8633E+16	1.3669E+16
8/2/2010	BA2LR-TC-8	100	1.3855E+16	3.9620E+16
8/2/2010	BA2LR-TC-19	100	1.1641E+16	2.5462E+16
8/2/2010	BA2LR-TC-27	100	3.6494E+16	3.7168E+16
		Average	2.2181E+16	2.3633E+16
		Standard Deviation	1.0330E+16	1.2481E+16
		Number of Samples	6	6

Table G.15: ASTM D257 Through Plane Electrical Resistivity Results for BQ0.5L:
Extruded 6-30-10, Injection Molded 7-26-10

Test Date	Sample Number	Applied Voltage (V)	Through-Plane Surface Electrical Resistivity (Ω /square)	Through-Plane Volume Electrical Resistivity (Ω -cm)
7/30/2010	BQ0.5L-TC-26	100	7.637E+16	4.097E+16
7/30/2010	BQ0.5L-TC-15	100	3.670E+16	6.188E+16
7/30/2010	BQ0.5L-TC-18	100	4.716E+16	5.720E+16
7/30/2010	BQ0.5L-TC-31	100	6.643E+16	7.594E+16
7/30/2010	BQ0.5L-TC-11	100	2.304E+17	6.609E+16
7/30/2010	BQ0.5L-TC-9	100	2.114E+17	6.921E+16
		Average	1.114E+17	6.188E+16
		Standard Deviation	8.616E+16	1.207E+16
		Number of Samples	6	6

Table G.16: ASTM D257 Through Plane Electrical Resistivity Results for BQ1L Set 1:
Extruded 6-30-10, Injection Molded 7-26-10

Test Date	Sample Number	Applied Voltage (V)	Through-Plane Surface Electrical Resistivity (Ω /square)	Through-Plane Volume Electrical Resistivity (Ω -cm)
7/30/2010	BQ1L-TC-24	100	1.146E+16	1.802E+16
7/30/2010	BQ1L-TC-29	100	1.719E+16	2.028E+16
7/30/2010	BQ1L-TC-4	100	2.461E+16	2.410E+16
7/30/2010	BQ1L-TC-22	100	1.440E+16	2.999E+16
7/30/2010	BQ1L-TC-27	100	1.273E+16	2.218E+16
7/30/2010	BQ1L-TC-15	100	4.375E+15	7.540E+15
		Average	1.413E+16	2.035E+16
		Standard Deviation	6.686E+15	7.482E+15
		Number of Samples	6	6

Table G.17: ASTM D257 Through Plane Electrical Resistivity Results for BQ1L Set 2:
Extruded 6-30-10, Injection Molded 7-26-10

Test Date	Sample Number	Applied Voltage (V)	Through-Plane Surface Electrical Resistivity (Ω /square)	Through-Plane Volume Electrical Resistivity (Ω -cm)
8/16/2010	BQ1L-TC-19	100	2.187E+15	1.180E+16
8/16/2010	BQ1L-TC-1	100	3.631E+15	1.364E+16
8/16/2010	BQ1L-TC-5	100	1.987E+16	2.968E+16
8/16/2010	BQ1L-TC-8	100	4.156E+15	2.217E+16
8/16/2010	BQ1L-TC-12	100	2.853E+15	2.359E+16
8/16/2010	BQ1L-TC-20	100	1.994E+15	2.054E+16
		Average	5.782E+15	2.024E+16
		Standard Deviation	6.950E+15	6.618E+15
		Number of Samples	6	6

Table G.18: ASTM D257 Through Plane Electrical Resistivity Results for BG2L Set 2:
Extruded 5-26-10, Injection Molded 6-3-10

Test Date	Sample Number	Applied Voltage (V)	Through-Plane Surface Electrical Resistivity (Ω /square)	Through-Plane Volume Electrical Resistivity (Ω -cm)
8/17/2010	BG2L-TC-17	100	6.5513E+16	4.8041E+16
8/17/2010	BG2L-TC-28	100	3.1168E+16	8.3672E+16
8/17/2010	BG2L-TC-27	100	7.8210E+16	5.2731E+16
8/17/2010	BG2L-TC-10	100	4.0170E+15	2.8324E+16
8/17/2010	BG2L-TC-16	100	3.4634E+16	7.1192E+16
8/17/2010	BG2L-TC-12	100	3.4313E+15	2.7823E+16
		Average	3.6162E+16	5.1964E+16
		Standard Deviation	3.0859E+16	2.2507E+16
		Number of Samples	6	6

Table G.19: ASTM D257 Through Plane Electrical Resistivity Results for BG5L Set 2:
Extruded 5-26-10, Injection Molded 6-3-10

Test Date	Sample Number	Applied Voltage (V)	Through-Plane Surface Electrical Resistivity (Ω /square)	Through-Plane Volume Electrical Resistivity (Ω -cm)
8/17/2010	BG5L-TC-13	100	1.1369E+16	3.6390E+15
8/17/2010	BG5L-TC-15	100	1.7158E+16	3.6826E+15
8/17/2010	BG5L-TC-17	100	7.6844E+15	4.3248E+15
8/17/2010	BG5L-TC-21	100	1.9709E+16	3.6472E+15
8/17/2010	BG5L-TC-24	100	1.6271E+16	3.5443E+15
8/17/2010	BG5L-TC-27	100	1.6329E+16	3.7105E+15
		Average	1.4753E+16	3.7581E+15
		Standard Deviation	4.3943E+15	2.8331E+14
		Number of Samples	6	6

Table G.20: ASTM D257 Through Plane Electrical Resistivity Results for BA2G2L set 1: Extruded 7-6-10, Injection Molded 8-18-10

Test Date	Sample Number	Applied Voltage (V)	Through-Plane Surface Electrical Resistivity (Ω /square)	Through-Plane Volume Electrical Resistivity (Ω -cm)
8/20/2010	BA2G2L-TC-6	100	9.4365E+15	3.7396E+15
8/20/2010	BA2G2L-TC-14	100	8.0971E+14	2.3171E+15
8/20/2010	BA2G2L-TC-11	100	1.2262E+16	4.4191E+15
8/20/2010	BA2G2L-TC-1	100	4.5653E+15	3.9580E+15
8/20/2010	BA2G2L-TC-13	100	4.7833E+15	4.8149E+15
8/20/2010	BA2G2L-TC-3	100	6.5848E+15	4.7114E+15
		Average	6.4069E+15	3.9934E+15
		Standard Deviation	4.0212E+15	9.2166E+14
		Number of Samples	6	6

Table G.21: ASTM D257 Through Plane Electrical Resistivity Results for BA2G2L set 2: Extruded 7-6-10, Injection Molded 8-18-10

Test Date	Sample Number	Applied Voltage (V)	Through-Plane Surface Electrical Resistivity (Ω /square)	Through-Plane Volume Electrical Resistivity (Ω -cm)
8/20/2010	BA2G2L-TC-2	100	7.4870E+14	2.0260E+15
8/20/2010	BA2G2L-TC-16	100	6.6779E+15	5.5933E+15
8/20/2010	BA2G2L-TC-15	100	5.5963E+15	3.5137E+15
8/20/2010	BA2G2L-TC-5	100	2.1389E+16	3.7288E+15
8/20/2010	BA2G2L-TC-7	100	3.6256E+15	4.9054E+15
8/20/2010	BA2G2L-TC-4	100	7.7504E+14	2.8706E+15
		Average	6.4688E+15	3.7730E+15
		Standard Deviation	7.7025E+15	1.3062E+15
		Number of Samples	6	6

Table G.22: ASTM D257 Through Plane Electrical Resistivity Results for BQ1G2L set 1: Extruded 7-1-10, Injection Molded 8-18-10

Test Date	Sample Number	Applied Voltage (V)	Through-Plane Surface Electrical Resistivity (Ω /square)	Through-Plane Volume Electrical Resistivity (Ω -cm)
8/20/2010	BQ1G2L-TC-17	100	1.9206E+15	1.7656E+15
8/20/2010	BQ1G2L-TC-18	100	2.9728E+15	5.6134E+15
8/20/2010	BQ1G2L-TC-19	100	2.9754E+15	3.2043E+15
8/20/2010	BQ1G2L-TC-24	100	1.4475E+15	6.4033E+15
8/20/2010	BQ1G2L-TC-23	100	5.4451E+14	2.9981E+15
8/20/2010	BQ1G2L-TC-25	100	5.3023E+14	3.8702E+15
8/20/2010	BQ1G2L-TC-9	100	3.8504E+15	5.0674E+15
		Average	2.0345E+15	4.1318E+15
		Standard Deviation	1.2848E+15	1.6352E+15
		Number of Samples	7	7

Table G.23: ASTM D257 Through Plane Electrical Resistivity Results for BQ1G2L set 2: Extruded 7-1-10, Injection Molded 8-18-10

Test Date	Sample Number	Applied Voltage (V)	Through-Plane Surface Electrical Resistivity (Ω /square)	Through-Plane Volume Electrical Resistivity (Ω -cm)
8/20/2010	BQ1G2L-TC-12	100	2.6538E+15	4.0712E+15
8/20/2010	BQ1G2L-TC-11	100	1.2402E+15	7.3240E+15
8/20/2010	BQ1G2L-TC-13	100	4.9092E+15	3.5794E+15
8/20/2010	BQ1G2L-TC-16	100	1.8394E+15	7.4054E+15
8/20/2010	BQ1G2L-TC-14	100	4.3601E+15	4.1251E+15
8/20/2010	BQ1G2L-TC-21	100	1.9085E+15	3.6652E+15
		Average	2.8185E+15	5.0284E+15
		Standard Deviation	1.4868E+15	1.8226E+15
		Number of Samples	6	6

Appendix H: In-Plane Electrical Resistivity (Two-Probe) Results

Appendix H.1: Polycarbonate with Carbon Nanotubes

Table H.1: Two Point Two Probe In-Plane Electrical Resistivity Results for BQ2L: 2 wt% fibrils in Lexan HF1130-111: Injection Molded May 26, 2009

Test Date	Sample Number	Length (cm)	Thickness (cm)	Width (cm)	Amps (A)	Volts (V)	Volume ER (ohm-cm)
6/11/2009	BQ2L-T-15	6.04	0.336	1.26	1.25E-05	1	5607.42
6/11/2009	BQ2L-T-18	6.06	0.336	1.26	1.16E-05	1	6022.53
6/11/2009	BQ2L-T-23	6.08	0.336	1.26	2.23E-05	1	3122.49
6/11/2009	BQ2L-T-24	6.04	0.336	1.26	1.60E-05	1	4380.79
6/11/2009	BQ2L-T-25	6.06	0.336	1.26	1.91E-05	1	3657.66
6/11/2009	BQ2L-T-26	6.12	0.336	1.26	1.43E-05	1	4837.52
Average							4604.74
Std Dev							1114.80
Number							6

Table H.2: Two Point Two Probe In-Plane Electrical Resistivity Results for BQ3L: 3 wt% fibrils in Lexan HF1130-111: Injection Molded May 26, 2009

Test Date	Sample Number	Length (cm)	Thickness (cm)	Width (cm)	Amps (A)	Volts (V)	Volume ER (ohm-cm)
6/11/2009	BQ3L-T-15	6.12	0.334	1.26	3.09E-05	0.1000	222.54
6/11/2009	BQ3L-T-19	6.06	0.334	1.26	3.57E-05	0.1000	194.53
6/11/2009	BQ3L-T-26	6.04	0.334	1.26	2.91E-05	0.1000	239.43
6/11/2009	BQ3L-T-27	6.03	0.334	1.26	5.00E-05	0.1000	139.58
6/11/2009	BQ3L-T-29	6.08	0.334	1.26	2.64E-05	0.1000	262.19
6/11/2009	BQ3L-T-20	6.06	0.334	1.26	2.93E-05	0.1000	237.26
Average							215.92
Std Dev							43.54
Number							6

Table H.3: Two Point Two Probe In-Plane Electrical Resistivity Results for BQ4L: 4 wt% fibrils in Lexan HF1130-111: Injection Molded May 26, 2009

Test Date	Sample Number	Length (cm)	Thickness (cm)	Width (cm)	Amps (A)	Volts (V)	Volume ER (ohm-cm)
6/11/2009	BQ4L-T-11	6.06	0.335	1.26	4.57E-05	0.05	76.21
6/11/2009	BQ4L-T-13	6.06	0.335	1.26	3.98E-05	0.05	87.50
6/11/2009	BQ4L-T-17	6.09	0.335	1.26	4.63E-05	0.05	74.85
6/11/2009	BQ4L-T-24	6.07	0.335	1.26	4.46E-05	0.05	77.96
6/11/2009	BQ4L-T-26	6.03	0.335	1.26	5.74E-05	0.05	60.98
6/11/2009	BQ4L-T-30	6.07	0.335	1.26	5.74E-05	0.05	60.57
Average							73.01
Std Dev							10.47
Number							6

Table H.4: Two Point Two Probe In-Plane Electrical Resistivity Results for BQ5L: 5 wt% fibrils in Lexan HF1130-111: Injection Molded May 26, 2009

Test Date	Sample Number	Length (cm)	Thickness (cm)	Width (cm)	Amps (A)	Volts (V)	Volume ER (ohm-cm)
6/11/2009	BQ5L-T-11	6.10	0.335	1.26	8.65E-05	0.0500	40.00
6/11/2009	BQ5L-T-14	5.98	0.335	1.26	6.27E-05	0.0500	56.29
6/11/2009	BQ5L-T-18	6.02	0.335	1.26	7.90E-05	0.0500	44.38
6/11/2009	BQ5L-T-21	6.06	0.335	1.26	8.92E-05	0.0500	39.04
6/11/2009	BQ5L-T-22	6.11	0.335	1.26	8.70E-05	0.0500	39.70
6/11/2009	BQ5L-T-25	6.08	0.335	1.26	9.29E-05	0.0500	37.37
Average							42.80
Std Dev							7.01
Number							6.00

Table H.5: Two Point Two Probe In-Plane Electrical Resistivity Results for BQ6L: 6 wt% fibrils in Lexan HF1130-111: Injection Molded May 26, 2009

Test Date	Sample Number	Length (cm)	Thickness (cm)	Width (cm)	Amps (A)	Volts (V)	Volume ER (ohm-cm)
6/11/2009	BQ6L-T-12	6.02	0.336	1.26	8.45E-05	0.02	16.65
6/11/2009	BQ6L-T-15	6.05	0.336	1.26	7.31E-05	0.02	19.15
6/11/2009	BQ6L-T-23	6.06	0.336	1.26	6.62E-05	0.02	21.11
6/11/2009	BQ6L-T-29	6.04	0.336	1.26	7.15E-05	0.02	19.61
6/11/2009	BQ6L-T-30	6.07	0.336	1.26	9.58E-05	0.02	14.56
6/11/2009	BQ6L-T-33	6.05	0.336	1.26	8.09E-05	0.02	17.30
Average							18.06
Std Dev							2.35
Number							6

Table H.6: Two Point Two Probe In-Plane Electrical Resistivity Results for BQ8L: 8 wt% fibrils in Lexan HF1130-111: Injection Molded May 26, 2009

Test Date	Sample Number	Length (cm)	Thickness (cm)	Width (cm)	Amps (A)	Volts (V)	Volume ER(ohm-cm)
6/11/2009	BQ8L-T-16	6.12	0.334	1.26	3.35E-05	0.004	8.211
6/11/2009	BQ8L-T-21	6.19	0.334	1.26	3.57E-05	0.004	7.618
6/11/2009	BQ8L-T-27	5.95	0.334	1.26	3.57E-05	0.004	7.925
6/11/2009	BQ8L-T-23	6.14	0.334	1.26	3.56E-05	0.004	7.701
6/11/2009	BQ8L-T-30	6.27	0.334	1.26	3.74E-05	0.004	7.179
6/11/2009	BQ8L-T-33	6.22	0.334	1.26	3.23E-05	0.004	8.379
Average							7.835
Std Dev							0.434
Number							6

Appendix H.2: Polycarbonate with Carbon Black

Table H.7: Two Point Two Probe In-Plane Electrical Resistivity (ER) Results for BA2L: 2 wt% Ketjenblack EC-600 JD in Lexan HF1130-111: Tensile Bars: Injection Molded Dec 4, 2009

Test Date	Sample Number	Length (cm)	Thickness (cm)	Width (cm)	Amps (A)	Volts (V)	Volume ER (ohm-cm)
12/10/2009	BA2L-T-7	6.09	0.335	1.26	<1.00E-09	20	>1.386E+09
12/10/2009	BA2L-T-9	6.19	0.335	1.26	<1.00E-09	20	>1.364E+09
12/10/2009	BA2L-T-10	6.17	0.335	1.26	<1.00E-09	20	>1.368E+09
12/10/2009	BA2L-T-15	6.24	0.335	1.26	<1.00E-09	20	>1.353E+09
12/10/2009	BA2L-T-20	6.18	0.335	1.26	<1.00E-09	20	>1.366E+09
12/10/2009	BA2L-T-25	6.22	0.335	1.26	<1.00E-09	20	>1.357E+09
12/10/2009	BA2L-T-27	6.16	0.335	1.26	<1.00E-09	20	>1.370E+09
12/10/2009	BA2L-T-30	6.13	0.335	1.26	<1.00E-09	20	>1.377E+09
Average							>1.368E+09
Std Dev							1.060E+07
Number							8

Table H.8: Two Point Two Probe In-Plane Electrical Resistivity Results for BA3L: 3 wt% Ketjenblack EC-600 JD in Lexan HF1130-111: Tensile Bars: Injection Molded Dec 4, 2009

Test Date	Sample Number	Length (cm)	Thickness (cm)	Width (cm)	Amps (A)	Volts (V)	Volume ER (ohm-cm)
12/10/2009	BA3L-T-5	6.23	0.335	1.26	<1.00E-09	20	>1.355E+09
12/10/2009	BA3L-T-9	6.18	0.335	1.26	<1.00E-09	20	>1.366E+09
12/10/2009	BA3L-T-16	6.20	0.335	1.26	<1.00E-09	20	>1.362E+09
12/10/2009	BA3L-T-20	6.22	0.335	1.26	<1.00E-09	20	>1.357E+09
12/10/2009	BA3L-T-23	6.20	0.335	1.26	<1.00E-09	20	>1.362E+09
12/10/2009	BA3L-T-29	6.24	0.335	1.26	<1.00E-09	20	>1.353E+09
12/10/2009	BA3L-T-18	6.19	0.335	1.26	8.70E-08	20	1.568E+07
12/10/2009	BA3L-T-21	6.20	0.335	1.26	5.90E-08	20	2.308E+07
Average							1.024E+09
Std Dev							6.202E+08
Number							8

Table H.9: Two Point Two Probe In-Plane Electrical Resistivity Results for BA4L: 4 wt% Ketjenblack EC-600 JD in Lexan HF1130-111: Tensile Bars: Injection Molded Dec 4, 2009

Test Date	Sample Number	Length (cm)	Thickness (cm)	Width (cm)	Amps (A)	Volts (V)	Volume ER (ohm-cm)
12/22/2009	BA4L-T-6	6.23	0.335	1.26	5.150E-06	10	1.316E+05
12/22/2009	BA4L-T-7	6.18	0.335	1.26	1.010E-05	10	6.762E+04
12/22/2009	BA4L-T-11	6.25	0.335	1.26	2.400E-06	10	2.814E+05
12/22/2009	BA4L-T-13	6.19	0.335	1.26	4.860E-06	10	1.403E+05
12/22/2009	BA4L-T-15	6.16	0.335	1.26	1.080E-05	10	6.345E+04
12/22/2009	BA4L-T-17	6.24	0.335	1.26	4.640E-06	10	1.458E+05
12/22/2009	BA4L-T-20	6.24	0.335	1.26	1.430E-05	10	4.730E+04
12/22/2009	BA4L-T-24	6.15	0.335	1.26	1.186E-05	10	5.787E+04
Average							1.169E+05
Std Dev							7.771E+04
Number							8

Table H.10: Two Point Two Probe In-Plane Electrical Resistivity Results for BA5L: 5 wt% Ketjenblack EC-600 JD in Lexan HF1130-111: Tensile Bars: Injection Molded Dec 4, 2009

Test Date	Sample Number	Length (cm)	Thickness (cm)	Width (cm)	Amps (A)	Volts (V)	Volume ER (ohm-cm)
12/22/2009	BA5L-T-5	6.24	0.335	1.26	1.842E-05	1	3.672E+03
12/22/2009	BA5L-T-10	6.23	0.335	1.26	3.332E-05	1	2.033E+03
12/22/2009	BA5L-T-11	6.19	0.335	1.26	3.110E-05	1	2.193E+03
12/22/2009	BA5L-T-17	6.20	0.335	1.26	2.109E-05	1	3.228E+03
12/22/2009	BA5L-T-18	6.22	0.335	1.26	3.380E-05	1	2.008E+03
12/22/2009	BA5L-T-22	6.18	0.335	1.26	2.670E-05	1	2.558E+03
12/22/2009	BA5L-T-26	6.18	0.335	1.26	3.080E-05	1	2.218E+03
12/22/2009	BA5L-T-31	6.14	0.335	1.26	3.660E-05	1	1.878E+03
Average							2.474E+03
Std Dev							6.462E+02
Number							8

Table H.11: Two Point Two Probe In-Plane Electrical Resistivity Results for BA6L: 6 wt% Ketjenblack EC-600 JD in Lexan HF1130-111: Tensile Bars: Injection Molded Dec 4, 2009

Test Date	Sample Number	Length (cm)	Thickness (cm)	Width (cm)	Amps (A)	Volts (V)	Volume ER (ohm-cm)
12/22/2009	BA6L-T-6	6.20	0.335	1.26	5.225E-05	0.5	6.515E+02
12/22/2009	BA6L-T-14	6.20	0.335	1.26	5.292E-05	0.5	6.432E+02
12/22/2009	BA6L-T-17	6.13	0.335	1.26	5.196E-05	0.5	6.626E+02
12/22/2009	BA6L-T-20	6.16	0.335	1.26	5.094E-05	0.5	6.726E+02
12/22/2009	BA6L-T-21	6.20	0.335	1.26	5.102E-05	0.5	6.672E+02
12/22/2009	BA6L-T-22	6.20	0.335	1.26	5.472E-05	0.5	6.221E+02
12/22/2009	BA6L-T-29	6.16	0.335	1.26	5.336E-05	0.5	6.421E+02
12/22/2009	BA6L-T-30	6.23	0.335	1.26	5.360E-05	0.5	6.320E+02
Average							6.492E+02
Std Dev							1.762E+01
Number							8

Table H.12: Two Point Two Probe In-Plane Electrical Resistivity Results for BA8L: 8 wt% Ketjenblack EC-600 JD in Lexan HF1130-111: Tensile Bars: Injection Molded Dec 4, 2009

Test Date	Sample Number	Length (cm)	Thickness (cm)	Width (cm)	Amps (A)	Volts (V)	Volume ER (ohm-cm)
12/22/2009	BA8L-T-8	6.16	0.335	1.26	2.640E-05	0.05	1.298E+02
12/22/2009	BA8L-T-10	6.20	0.335	1.26	2.700E-05	0.05	1.261E+02
12/22/2009	BA8L-T-17	6.20	0.335	1.26	2.827E-05	0.05	1.204E+02
12/22/2009	BA8L-T-24	6.35	0.335	1.26	2.700E-05	0.05	1.231E+02
12/22/2009	BA8L-T-26	6.22	0.335	1.26	2.850E-05	0.05	1.191E+02
12/22/2009	BA8L-T-27	6.07	0.335	1.26	2.870E-05	0.05	1.211E+02
12/22/2009	BA8L-T-30	6.17	0.335	1.26	2.910E-05	0.05	1.175E+02
12/22/2009	BA8L-T-31	6.19	0.335	1.26	2.834E-05	0.05	1.203E+02
Average							1.222E+02
Std Dev							4.012E+00
Number							8

Table H.13: Two Point Two Probe In-Plane Electrical Resistivity Results for BA10L: 10 wt% Ketjenblack EC-600 JD in Lexan HF1130-111: Tensile Bars: Injection Molded Dec 4, 2009

Test Date	Sample Number	Length (cm)	Thickness (cm)	Width (cm)	Amps (A)	Volts (V)	Volume ER (ohm-cm)
12/22/2009	BA10L-T-8	6.12	0.34	1.26	3.518E-05	0.01	1.990E+01
12/22/2009	BA10L-T-16	5.84	0.34	1.26	3.650E-05	0.01	2.010E+01
12/22/2009	BA10L-T-12	6.04	0.34	1.26	3.720E-05	0.01	2.010E+01
12/22/2009	BA10L-T-19	6.15	0.34	1.26	3.580E-05	0.01	1.946E+01
12/22/2009	BA10L-T-20	6.08	0.34	1.26	3.550E-05	0.01	1.985E+01
12/22/2009	BA10L-T-25	6.15	0.34	1.26	3.650E-05	0.01	1.908E+01
12/22/2009	BA10L-T-30	5.93	0.34	1.26	3.800E-05	0.01	1.901E+01
12/22/2009	BA10L-T-32	5.98	0.34	1.26	3.800E-05	0.01	1.885E+01
Average							1.954E+01
Std Dev							5.087E-01
Number							8

Appendix H.3: Polycarbonate with Graphite Nanoparticles

Table H.14: Two Point Two Probe In-Plane Electrical Resistivity (ER) Results for BG8L: 8 wt% xGnP in Lexan HF1130-111: Tensile Bars: Injection Molded June 8, 2010

Test Date	Sample Number	Length (cm)	Thickness (cm)	Width (cm)	Amps (A)	Volts (V)	Volume ER (ohm-cm)
6/15/2010	BG8L-T-23	6.10	0.335	1.26	5.100E-08	20	2.714E+07
6/15/2010	BG8L-T-34	6.10	0.335	1.26	6.130E-08	20	2.258E+07
6/15/2010	BG8L-T-38	6.18	0.335	1.26	8.000E-08	20	1.708E+07
6/15/2010	BG8L-T-43	6.10	0.335	1.26	2.550E-08	20	5.427E+07
6/15/2010	BG8L-T-47	5.96	0.335	1.26	2.400E-08	20	5.902E+07
6/15/2010	BG8L-T-53	6.04	0.335	1.26	3.020E-08	20	4.628E+07
6/15/2010	BG8L-T-56	6.12	0.335	1.26	3.000E-08	20	4.598E+07
6/15/2010	BG8L-T-57	6.05	0.335	1.26	3.200E-08	20	4.361E+07
Average							3.949E+07
Std Dev							1.534E+07
Number							8

Table H.15: Two Point Two Probe In-Plane Electrical Resistivity (ER) Results for BG10L: 10 wt% xGnP in Lexan HF1130-111:
Tensile Bars: Injection Molded June 8, 2010

Test Date	Sample Number	Length (cm)	Thickness (cm)	Width (cm)	Amps (A)	Volts (V)	Volume ER (ohm-cm)
6/15/2010	BG10L-T-10	6.10	0.335	1.26	6.048E-07	20	2.288E+06
6/15/2010	BG10L-T-12	6.13	0.335	1.26	7.150E-07	20	1.926E+06
6/15/2010	BG10L-T-13	6.10	0.335	1.26	8.080E-07	20	1.713E+06
6/15/2010	BG10L-T-16	6.09	0.335	1.26	8.340E-07	20	1.662E+06
6/15/2010	BG10L-T-18	6.08	0.335	1.26	7.900E-07	20	1.758E+06
6/15/2010	BG10L-T-26	6.06	0.335	1.26	8.790E-07	20	1.585E+06
6/15/2010	BG10L-T-29	6.11	0.335	1.26	9.770E-07	20	1.414E+06
6/15/2010	BG10L-T-30	6.04	0.335	1.26	8.710E-07	20	1.605E+06
Average							1.744E+06
Std Dev							2.648E+05
Number							8

Appendix H.4: Polycarbonate with Multiple Fillers

Table H.16: Two Point Two Probe In-Plane Electrical Resistivity (ER) Results for BA5LR set 1: 5 wt% Ketjenblack EC-600 JD in Lexan HF1130-111: Tensile Bars: Injection Molded July 26, 2010; Extruded 7-8-10; 2-9-09 extruder screw

Test Date	Sample Number	Length (cm)	Thickness (cm)	Width (cm)	Amps (A)	Volts (V)	Volume ER (ohm-cm)
8/26/2010	BA5LR-T-24	6.057	0.335	1.26	1.864E-05	1	3.739E+03
8/26/2010	BA5LR-T-27	6.152	0.335	1.26	1.794E-05	1	3.825E+03
8/26/2010	BA5LR-T-30	6.101	0.335	1.26	1.816E-05	1	3.825E+03
8/26/2010	BA5LR-T-33	6.156	0.335	1.26	1.863E-05	1	3.680E+03
8/26/2010	BA5LR-T-52	6.130	0.335	1.26	1.783E-05	1	3.862E+03
8/26/2010	BA5LR-T-53	6.170	0.335	1.26	1.682E-05	1	4.067E+03
8/4/2010	BA5LR-T-23	6.035	0.335	1.26	3.570E-05	2	3.918E+03
8/4/2010	BA5LR-T-3	6.069	0.335	1.26	4.726E-05	3	4.415E+03
Average							3916.326
Std Dev							232.514
Number							8

Table H.17: Two Point Two Probe In-Plane Electrical Resistivity (ER) Results for BA5LR set 2: 5 wt% Ketjenblack EC-600 JD in Lexan HF1130-111: Tensile Bars: Injection Molded July 26, 2010; Extruded 7-8-10; 2-9-09 extruder screw

Test Date	Sample Number	Length (cm)	Thickness (cm)	Width (cm)	Amps (A)	Volts (V)	Volume ER (ohm-cm)
9/1/2010	BA5LR-T-7	6.199	0.335	1.26	1.622E-05	1	4198.004
9/1/2010	BA5LR-T-15	6.199	0.335	1.26	1.779E-05	1	3827.523
9/1/2010	BA5LR-T-16	6.113	0.335	1.26	1.270E-05	1	3827.523
9/1/2010	BA5LR-T-28	6.304	0.335	1.26	1.744E-05	1	3839.305
9/1/2010	BA5LR-T-30	6.152	0.335	1.26	1.690E-05	1	4059.872
9/1/2010	BA5LR-T-34	6.226	0.335	1.26	1.878E-05	1	3610.029
9/1/2010	BA5LR-T-43	6.225	0.335	1.26	1.742E-05	1	3892.493
9/1/2010	BA5LR-T-55	6.346	0.335	1.26	1.472E-05	1	4518.637
Average							3971.673
Std Dev							281.402
Number							8

Table H.18: Two Point Two Probe In-Plane Electrical Resistivity (ER) Results for BQ5LR set 1: Tensile Bars: Injection Molded 8-25-10; Extruded 7-8-10; 2-9-09 extruder screw

Test Date	Sample Number	Length (cm)	Thickness (cm)	Width (cm)	Amps (A)	Volts (V)	Volume ER (ohm-cm)
9/1/2010	BQ5LR-T-6	5.818	0.335	1.26	2.19E-05	0.05	165.72
9/1/2010	BQ5LR-T-8	6.012	0.335	1.26	2.05E-05	0.05	170.91
9/1/2010	BQ5LR-T-16	6.108	0.335	1.26	2.35E-05	0.05	147.35
9/1/2010	BQ5LR-T-20	6.022	0.335	1.26	2.15E-05	0.05	163.01
9/1/2010	BQ5LR-T-21	6.141	0.335	1.26	2.01E-05	0.05	170.90
9/1/2010	BQ5LR-T-24	6.000	0.335	1.26	2.19E-05	0.05	160.40
Average							163.05
Std Dev							8.76
Number							6.00

Table H.19: Two Point Two Probe In-Plane Electrical Resistivity (ER) Results for BQ5LR set 2: Tensile Bars: Injection Molded 8-25-10; Extruded 7-8-10; 2-9-09 extruder screw

Test Date	Sample Number	Length (cm)	Thickness (cm)	Width (cm)	Amps (A)	Volts (V)	Volume ER (ohm-cm)
9/7/2010	BQ5LR-T-27	6.108	0.335	1.26	1.85E-05	0.05	187.08
9/7/2010	BQ5LR-T-13	5.850	0.335	1.26	2.44E-05	0.05	147.86
9/7/2010	BQ5LR-T-14	6.230	0.335	1.26	1.99E-05	0.05	170.40
9/7/2010	BQ5LR-T-17	6.160	0.335	1.26	1.80E-05	0.05	190.34
9/7/2010	BQ5LR-T-26	6.230	0.335	1.26	1.87E-05	0.05	181.16
9/7/2010	BQ5LR-T-30	6.250	0.335	1.26	1.80E-05	0.05	187.60
Average							177.41
Std Dev							16.13
Number							6.00

Table H.20: Two Point Two Probe In-Plane Electrical Resistivity (ER) Results for BG12L: 12 wt% xGnP in Lexan HF1130-111:
Tensile Bars: Injection Molded 8-18-10; Extruded 7-8-10; 2-9-09 extruder screw

Test Date	Sample Number	Length (cm)	Thickness (cm)	Width (cm)	Amps (A)	Volts (V)	Volume ER (ohm-cm)
9/1/2010	BG12L-T-5	6.187	0.335	1.26	4.300E-06	20	3.173E+05
9/1/2010	BG12L-T-12	6.091	0.335	1.26	4.740E-06	20	2.924E+05
9/1/2010	BG12L-T-14	6.155	0.335	1.26	4.500E-06	20	3.048E+05
9/1/2010	BG12L-T-15	6.164	0.335	1.26	4.430E-06	20	3.092E+05
9/1/2010	BG12L-T-16	6.164	0.335	1.26	4.380E-06	20	3.127E+05
Average							3.073E+05
Std Dev							9.502E+03
Number							5

Table H.21: Two Point Two Probe In-Plane Electrical Resistivity (ER) Results for BG15L: 15 wt% xGnP in Lexan HF1130-111:
Tensile Bars: Injection Molded 8-18-10; Extruded 7-8-10; 2-9-09 extruder screw

Test Date	Sample Number	Length (cm)	Thickness (cm)	Width (cm)	Amps (A)	Volts (V)	Volume ER (ohm-cm)
9/1/2010	BG15L-T-5	5.998	0.335	1.26	1.483E-05	10	4.745E+04
9/1/2010	BG15L-T-6	6.009	0.335	1.26	2.326E-05	10	3.020E+04
9/1/2010	BG15L-T-7	5.950	0.335	1.26	2.712E-05	10	2.616E+04
9/1/2010	BG15L-T-8	5.965	0.335	1.26	2.726E-05	10	2.596E+04
9/1/2010	BG15L-T-11	6.027	0.335	1.26	2.877E-05	10	2.434E+04
9/1/2010	BG15L-T-14	6.062	0.335	1.26	3.052E-05	10	2.281E+04
9/1/2010	BG15L-T-15	5.964	0.335	1.26	3.201E-05	10	2.211E+04
9/1/2010	BG15L-T-21	6.026	0.335	1.26	2.947E-05	10	2.377E+04
Average							2.785E+04
Std Dev							8.311E+03
Number							8

Table H.22: Two Point Two Probe In-Plane Electrical Resistivity (ER) Results for BA2Q1L Set 1: Tensile Bars: Injection Molded 7-26-10

Test Date	Sample Number	Length (cm)	Thickness (cm)	Width (cm)	Amps (A)	Volts (V)	Volume ER (ohm-cm)
8/4/2010	BA2Q1L-T-20	6.124	0.335	1.26	4.35E-06	20	3.169E+05
8/4/2010	BA2Q1L-T-23	6.086	0.335	1.26	5.02E-06	20	2.763E+05
8/4/2010	BA2Q1L-T-32	6.143	0.335	1.26	5.10E-06	20	2.695E+05
8/4/2010	BA2Q1L-T-38	6.042	0.335	1.26	5.46E-06	20	2.559E+05
8/4/2010	BA2Q1L-T-46	6.120	0.335	1.26	6.95E-06	20	1.985E+05
8/4/2010	BA2Q1L-T-51	6.136	0.335	1.26	7.88E-06	20	1.746E+05
Average							2.486E+05
Std Dev							5.275E+04
Number							6

Table H.23: Two Point Two Probe In-Plane Electrical Resistivity (ER) Results for BA2Q1L Set 2: Tensile Bars: Injection Molded 7-26-10

Test Date	Sample Number	Length (cm)	Thickness (cm)	Width (cm)	Amps (A)	Volts (V)	Volume ER (ohm-cm)
8/18/2010	BA2Q1L-T-19	5.99	0.335	1.26	4.98E-06	20	2.830E+05
8/18/2010	BA2Q1L-T-21	6.02	0.335	1.26	4.39E-06	20	3.194E+05
8/18/2010	BA2Q1L-T-24	5.78	0.335	1.26	4.17E-06	20	3.503E+05
8/18/2010	BA2Q1L-T-31	5.93	0.335	1.26	3.81E-06	20	3.737E+05
8/18/2010	BA2Q1L-T-40	5.86	0.335	1.26	6.80E-06	20	2.119E+05
8/18/2010	BA2Q1L-T-44	6.01	0.335	1.26	7.17E-06	20	1.959E+05
8/18/2010	BA2Q1L-T-49	5.89	0.335	1.26	8.37E-06	20	1.712E+05
Average							2.890E+05
Std Dev							7.280E+04
Number							6

Table H.24: Two Point Two Probe In-Plane Electrical Resistivity (ER) Results for BA2Q5L Set 1: Tensile Bars: Injection Molded 8-6-10

Test Date	Sample Number	Length (cm)	Thickness (cm)	Width (cm)	Amps (A)	Volts (V)	Volume ER (ohm-cm)
8/13/2010	BA2Q5L-T-6	6.00	0.335	1.26	1.90E-05	0.02	74.053
8/13/2010	BA2Q5L-T-9	5.99	0.335	1.26	1.91E-05	0.02	73.788
8/13/2010	BA2Q5L-T-12	5.99	0.335	1.26	2.00E-05	0.02	70.467
8/13/2010	BA2Q5L-T-15	6.05	0.335	1.26	1.98E-05	0.02	70.473
8/13/2010	BA2Q5L-T-16	6.01	0.335	1.26	1.83E-05	0.02	76.757
8/13/2010	BA2Q5L-T-17	6.00	0.335	1.26	1.83E-05	0.02	76.885
Average							73.737
Std Dev							2.845
Number							6

Table H.25: Two Point Two Probe In-Plane Electrical Resistivity (ER) Results for BA2Q5L Set 2: Tensile Bars: Injection Molded 8-6-10

Test Date	Sample Number	Length (cm)	Thickness (cm)	Width (cm)	Amps (A)	Volts (V)	Volume ER (ohm-cm)
8/18/2010	BA2Q5L-T-1	6.05	0.335	1.26	2.91E-05	0.03	71.926
8/18/2010	BA2Q5L-T-2	5.97	0.335	1.26	3.15E-05	0.03	67.337
8/18/2010	BA2Q5L-T-4	6.05	0.335	1.26	3.06E-05	0.03	68.401
8/18/2010	BA2Q5L-T-5	5.74	0.335	1.26	3.29E-05	0.03	67.055
8/18/2010	BA2Q5L-T-11	5.88	0.335	1.26	3.15E-05	0.03	68.367
8/18/2010	BA2Q5L-T-18	6.08	0.335	1.26	2.98E-05	0.03	69.890
Average							68.829
Std Dev							1.816
Number							6

Table H.26: Two Point Two Probe In-Plane Electrical Resistivity (ER) Results for BA5Q1L Set 1: Tensile Bars: Injection Molded 8-25-10

Test Date	Sample Number	Length (cm)	Thickness (cm)	Width (cm)	Amps (A)	Volts (V)	Volume ER (ohm-cm)
9/1/2010	BA5Q1L-T-20	6.244	0.335	1.26	1.54E-05	0.1	437.830
9/1/2010	BA5Q1L-T-22	6.112	0.335	1.26	1.57E-05	0.1	439.039
9/1/2010	BA5Q1L-T-25	6.139	0.335	1.26	1.58E-05	0.1	436.000
9/1/2010	BA5Q1L-T-35	6.209	0.335	1.26	1.62E-05	0.1	419.901
						Average	433.192
						Std Dev	8.949
						Number	4

Table H.27: Two Point Two Probe In-Plane Electrical Resistivity (ER) Results for BA5Q1L Set 2: Tensile Bars: Injection Molded 8-25-10

Test Date	Sample Number	Length (cm)	Thickness (cm)	Width (cm)	Amps (A)	Volts (V)	Volume ER (ohm-cm)
9/1/2010	BA5Q1L-T-36	6.278	0.335	1.26	1.60E-05	0.1	420.480
9/1/2010	BA5Q1L-T-40	6.160	0.335	1.26	1.60E-05	0.1	427.199
9/1/2010	BA5Q1L-T-42	6.164	0.335	1.26	1.58E-05	0.1	433.407
9/1/2010	BA5Q1L-T-44	6.194	0.335	1.26	1.56E-05	0.1	436.837
						Average	429.481
						Std Dev	7.205
						Number	4

Table H.28: Two Point Two Probe In-Plane Electrical Resistivity (ER) Results for BA5Q5L Set 1: Tensile Bars: Injection Molded 8-6-10

Test Date	Sample Number	Length (cm)	Thickness (cm)	Width (cm)	Amps (A)	Volts (V)	Volume ER (ohm-cm)
8/13/2010	BA5Q5L-T-6	6.116	0.335	1.26	2.10E-05	0.005	16.432
8/13/2010	BA5Q5L-T-8	6.092	0.335	1.26	2.15E-05	0.005	16.113
8/13/2010	BA5Q5L-T-11	6.269	0.335	1.26	2.18E-05	0.005	15.443
8/13/2010	BA5Q5L-T-13	5.991	0.335	1.26	2.28E-05	0.005	15.451
8/13/2010	BA5Q5L-T-16	6.083	0.335	1.26	2.13E-05	0.005	16.289
8/13/2010	BA5Q5L-T-18	5.947	0.335	1.26	2.29E-05	0.005	15.497
Average							15.871
Std Dev							0.458
Number							7

Table H.29: Two Point Two Probe In-Plane Electrical Resistivity (ER) Results for BA5Q5L Set 2: Tensile Bars: Injection Molded 8-26-10

Test Date	Sample Number	Length (cm)	Thickness (cm)	Width (cm)	Amps (A)	Volts (V)	Volume ER (ohm-cm)
9/1/2010	BA5Q5L-T-11	6.240	0.335	1.26	2.15E-05	0.005	15.731
9/1/2010	BA5Q5L-T-15	6.063	0.335	1.26	2.32E-05	0.005	15.004
9/1/2010	BA5Q5L-T-16	6.210	0.335	1.26	2.31E-05	0.005	14.712
9/1/2010	BA5Q5L-T-18	6.143	0.335	1.26	2.33E-05	0.005	14.745
9/1/2010	BA5Q5L-T-19	6.127	0.335	1.26	2.29E-05	0.005	15.042
9/1/2010	BA5Q5L-T-21	6.043	0.335	1.26	2.32E-05	0.005	15.054
9/1/2010	BA5Q5L-T-22	6.156	0.335	1.26	2.42E-05	0.005	14.167
Average							14.922
Std Dev							0.472
Number							7

Table H.30 Two Point Two Probe In-Plane Electrical Resistivity (ER) Results for BA2G5L Set 1: Tensile Bars: Injection Molded 8-18-10

Test Date	Sample Number	Length (cm)	Thickness (cm)	Width (cm)	Amps (A)	Volts (V)	Volume ER (ohm-cm)
9/1/2010	BA2G5L-T-6	5.979	0.335	1.26	4.90E-08	20	2.882E+07
9/1/2010	BA2G5L-T-7	6.068	0.335	1.26	5.70E-08	20	2.441E+07
9/1/2010	BA2G5L-T-21	6.032	0.335	1.26	7.00E-08	20	1.999E+07
9/1/2010	BA2G5L-T-10	5.891	0.335	1.26	6.00E-08	20	2.388E+07
9/1/2010	BA2G5L-T-12	5.954	0.335	1.26	6.00E-08	20	2.363E+07
Average							2.415E+07
Std Dev							3.140E+06
Number							5

Table H.31: Two Point Two Probe In-Plane Electrical Resistivity (ER) Results for BA2G5L Set 2: Tensile Bars: Injection Molded 8-18-10

Test Date	Sample Number	Length (cm)	Thickness (cm)	Width (cm)	Amps (A)	Volts (V)	Volume ER (ohm-cm)
9/1/2010	BA2G5L-T-8	5.975	0.335	1.26	5.90E-08	20	2.395E+07
9/1/2010	BA2G5L-T-13	6.068	0.335	1.26	7.00E-08	20	1.987E+07
9/1/2010	BA2G5L-T-28	5.983	0.335	1.26	9.00E-08	20	1.568E+07
9/1/2010	BA2G5L-T-29	5.831	0.335	1.26	1.00E-07	20	1.448E+07
Average							1.849E+07
Std Dev							4.309E+06
Number							4

Table H.32: Two Point Two Probe In-Plane Electrical Resistivity (ER) Results for BA5G2L Set 1: Tensile Bars: Injection Molded 8-18-10

Test Date	Sample Number	Length (cm)	Thickness (cm)	Width (cm)	Amps (A)	Volts (V)	Volume ER (ohm-cm)
9/1/2010	BA5G2L-T-5	6.085	0.335	1.26	2.58E-05	0.5	1344.327
9/1/2010	BA5G2L-T-6	6.237	0.335	1.26	2.57E-05	0.5	1316.669
9/1/2010	BA5G2L-T-7	6.110	0.335	1.26	2.58E-05	0.5	1338.827
9/1/2010	BA5G2L-T-8	6.022	0.335	1.26	2.62E-05	0.5	1337.653
9/1/2010	BA5G2L-T-9	6.128	0.335	1.26	2.60E-05	0.5	1324.626
9/1/2010	BA5G2L-T-10	6.076	0.335	1.26	2.55E-05	0.5	1362.158
Average							1337.377
Std Dev							15.849
Number							6

Table H.33: Two Point Two Probe In-Plane Electrical Resistivity (ER) Results for BA5G2L Set 2: Tensile Bars: Injection Molded 8-18-10

Test Date	Sample Number	Length (cm)	Thickness (cm)	Width (cm)	Amps (A)	Volts (V)	Volume ER (ohm-cm)
9/1/2010	BA5G2L-T-11	6.130	0.335	1.26	2.58E-05	0.5	1334.459
9/1/2010	BA5G2L-T-13	6.025	0.335	1.26	2.53E-05	0.5	1384.547
9/1/2010	BA5G2L-T-14	6.156	0.335	1.26	2.47E-05	0.5	1388.001
9/1/2010	BA5G2L-T-17	6.131	0.335	1.26	2.45E-05	0.5	1405.038
9/1/2010	BA5G2L-T-22	6.016	0.335	1.26	2.47E-05	0.5	1420.302
						Average	1386.469
						Std Dev	32.406
						Number	5

Table H.34: Two Point Two Probe In-Plane Electrical Resistivity (ER) Results for BA5G5L Set 1: Tensile Bars: Injection Molded 8-18-10

Test Date	Sample Number	Length (cm)	Thickness (cm)	Width (cm)	Amps (A)	Volts (V)	Volume ER (ohm-cm)
9/1/2010	BA5G5L-T-4	6.147	0.335	1.26	1.74E-05	0.2	790.646
9/1/2010	BA5G5L-T-17	6.155	0.335	1.26	1.98E-05	0.2	692.711
9/1/2010	BA5G5L-T-19	6.081	0.335	1.26	2.02E-05	0.2	686.917
9/1/2010	BA5G5L-T-7	6.184	0.335	1.26	1.84E-05	0.2	741.116
9/1/2010	BA5G5L-T-8	6.192	0.335	1.26	1.86E-05	0.2	733.390
						Average	728.956
						Std Dev	41.995
						Number	5

Table H.35: Two Point Two Probe In-Plane Electrical Resistivity (ER) Results for BA5G5L Set 2: Tensile Bars: Injection Molded 8-18-10

Test Date	Sample Number	Length (cm)	Thickness (cm)	Width (cm)	Amps (A)	Volts (V)	Volume ER (ohm-cm)
9/1/2010	BA5G5L-T-10	5.973	0.335	1.26	1.94E-05	0.2	730.419
9/1/2010	BA5G5L-T-12	6.164	0.335	1.26	1.92E-05	0.2	713.315
9/1/2010	BA5G5L-T-16	6.221	0.335	1.26	1.99E-05	0.2	682.947
9/1/2010	BA5G5L-T-5	6.091	0.335	1.26	1.79E-05	0.2	774.723
9/1/2010	BA5G5L-T-6	6.065	0.335	1.26	1.80E-05	0.2	773.719
					Average		735.025
					Std Dev		39.616
					Number		5

Table H.36: Two Point Two Probe In-Plane Electrical Resistivity (ER) Results for BQ1G5L Set 1: Tensile Bars: Injection Molded 8-18-10

Test Date	Sample Number	Length (cm)	Thickness (cm)	Width (cm)	Amps (A)	Volts (V)	Volume ER (ohm-cm)
9/1/2010	BQ1G5L-T-31	6.006	0.335	1.265	3.30E-07	20	4.276E+06
9/1/2010	BQ1G5L-T-19	6.102	0.335	1.265	2.24E-07	20	6.201E+06
9/1/2010	BQ1G5L-T-17	6.072	0.335	1.265	1.94E-07	20	7.195E+06
9/1/2010	BQ1G5L-T-15	6.092	0.335	1.265	1.98E-07	20	7.027E+06
					Average		6.175E+06
					Std Dev		1.338E+06
					Number		4

Table H.37: Two Point Two Probe In-Plane Electrical Resistivity (ER) Results for BQ1G5L Set 2: Tensile Bars: Injection Molded 8-18-10

Test Date	Sample Number	Length (cm)	Thickness (cm)	Width (cm)	Amps (A)	Volts (V)	Volume ER (ohm-cm)
9/7/2010	BQ1G5L-T-21	6.140	0.335	1.265	2.16E-07	20	6.391E+06
9/7/2010	BQ1G5L-T-23	6.120	0.335	1.265	2.17E-07	20	6.382E+06
9/7/2010	BQ1G5L-T-25	6.200	0.335	1.265	2.54E-07	20	5.382E+06
9/7/2010	BQ1G5L-T-13	6.072	0.335	1.265	1.84E-07	20	7.586E+06
					Average		6.435E+06
					Std Dev		9.016E+05
					Number		4

Table H.38: Two Point Two Probe In-Plane Electrical Resistivity (ER) Results for BQ5G2L Set 1: Tensile Bars: Injection Molded 8-18-10

Test Date	Sample Number	Length (cm)	Thickness (cm)	Width (cm)	Amps (A)	Volts (V)	Volume ER (ohm-cm)
9/1/2010	BQ5G2L-T-4	6.091	0.335	1.265	1.64E-05	0.05	212.116
9/1/2010	BQ5G2L-T-5	6.156	0.335	1.265	1.66E-05	0.05	207.347
9/1/2010	BQ5G2L-T-7	6.088	0.335	1.265	1.58E-05	0.05	220.558
9/1/2010	BQ5G2L-T-11	6.081	0.335	1.265	1.65E-05	0.05	210.666
9/1/2010	BQ5G2L-T-13	5.981	0.335	1.265	1.73E-05	0.05	204.661
9/1/2010	BQ5G2L-T-14	6.100	0.335	1.265	1.67E-05	0.05	207.501
9/1/2010	BQ5G2L-T-15	6.031	0.335	1.265	1.69E-05	0.05	207.642
					Average		210.070
					Std Dev		5.224
					Number		7

Table H.39: Two Point Two Probe In-Plane Electrical Resistivity (ER) Results for BQ5G2L Set 2: Tensile Bars: Injection Molded 8-18-10

Test Date	Sample Number	Length (cm)	Thickness (cm)	Width (cm)	Amps (A)	Volts (V)	Volume ER (ohm-cm)
9/1/2010	BQ5G2L-T-16	6.043	0.335	1.265	1.73E-05	0.05	202.795
9/1/2010	BQ5G2L-T-19	6.097	0.335	1.265	1.69E-05	0.05	205.759
9/1/2010	BQ5G2L-T-28	5.997	0.335	1.265	1.81E-05	0.05	195.422
9/1/2010	BQ5G2L-T-32	6.059	0.335	1.265	1.75E-05	0.05	199.947
9/1/2010	BQ5G2L-T-35	6.075	0.335	1.265	1.80E-05	0.05	193.448
9/1/2010	BQ5G2L-T-36	5.985	0.335	1.265	1.87E-05	0.05	189.524
Average							197.816
Std Dev							6.099
Number							6

Table H.40: Two Point Two Probe In-Plane Electrical Resistivity (ER) Results for BQ5G5L Set 1: Tensile Bars: Injection Molded 9-9-10

Test Date	Sample Number	Length (cm)	Thickness (cm)	Width (cm)	Amps (A)	Volts (V)	Volume ER (ohm-cm)
9/14/2010	BQ5G5L-T-32	6.206	0.335	1.265	1.40E-05	0.025	121.850
9/14/2010	BQ5G5L-T-15	6.203	0.335	1.265	1.54E-05	0.025	111.050
9/14/2010	BQ5G5L-T-16	6.150	0.335	1.265	1.30E-05	0.025	132.309
9/14/2010	BQ5G5L-T-17	6.244	0.335	1.265	1.45E-05	0.025	117.097
9/14/2010	BQ5G5L-T-21	6.232	0.335	1.265	1.32E-05	0.025	128.788
9/14/2010	BQ5G5L-T-30	6.182	0.335	1.265	1.21E-05	0.025	141.632
Average							125.454
Std Dev							11.047
Number							6

Table H.41: Two Point Two Probe In-Plane Electrical Resistivity (ER) Results for BQ5G5L Set 2: Tensile Bars: Injection Molded 9-9-10

Test Date	Sample Number	Length (cm)	Thickness (cm)	Width (cm)	Amps (A)	Volts (V)	Volume ER (ohm-cm)
9/14/2010	BQ5G5L-T-14	6.260	0.335	1.265	1.52E-05	0.025	111.488
9/14/2010	BQ5G5L-T-33	6.316	0.335	1.265	1.30E-05	0.025	129.030
9/14/2010	BQ5G5L-T-35	6.205	0.335	1.265	1.39E-05	0.025	123.277
9/14/2010	BQ5G5L-T-45	6.189	0.335	1.265	1.24E-05	0.025	138.049
9/14/2010	BQ5G5L-T-47	6.134	0.335	1.265	1.31E-05	0.025	131.844
9/14/2010	BQ5G5L-T-50	6.213	0.335	1.265	1.29E-05	0.025	132.597
Average							127.714
Std Dev							9.299
Number							6

Appendix I: Through-Plane Thermal Conductivity (ASTM F433) Test Results

Appendix I.1: Polycarbonate with Carbon Nanotubes

Table I.1: Through-Plane Thermal Conductivity at 55°C using Holometrix TCA-300 Guarded Heat Flow Meter Method for Lexan HF1130-111 (BL): Injection Molded May 26, 2009

Test Date	Sample Number	Through Plane Thermal Conductivity (W/m•K)
7/2/2009	BL-TC-10	0.2181
7/2/2009	BL-TC-16	0.2167
7/2/2009	BL-TC-22	0.2174
7/2/2009	BL-TC-34	0.2181
7/2/2009	BL-TC-37	0.2206
	Average	0.2182
	Standard Deviation	0.0015
	Number of Samples	5

Table I.2: Through-Plane Thermal Conductivity at 55°C using Holometrix TCA-300 Guarded Heat Flow Meter Method for Extruded Lexan HF1130-111 (BLE): Injection Molded May 26, 2009

Test Date	Sample Number	Through Plane Thermal Conductivity (W/m•K)
7/2/2009	BLE-TC-13	0.2161
7/2/2009	BLE-TC-21	0.2161
7/6/2009	BLE-TC-22	0.2180
7/2/2009	BLE-TC-24	0.2170
7/2/2009	BLE-TC-26	0.2178
	Average	0.2170
	Standard Deviation	0.0009
	Number of Samples	5

Table I.3: Through-Plane Thermal Conductivity at 55°C using Holometrix TCA-300 Guarded Heat Flow Meter Method for 2 wt% Hyperion Fibrils in Lexan HF1130-111 (BQ2L): Injection Molded May 26, 2009

Test Date	Sample Number	Through Plane Thermal Conductivity (W/m•K)
7/1/2009	BQ2L-TC-16	0.2293
7/1/2009	BQ2L-TC-19	0.2334
7/6/2009	BQ2L-TC-21	0.2307
7/6/2009	BQ2L-TC-29	0.2333
7/2/2009	BQ2L-TC-30	0.2329
	Average	0.2319
	Standard Deviation	0.0018
	Number of Samples	5

Table I.4: Through-Plane Thermal Conductivity at 55°C using Holometrix TCA-300 Guarded Heat Flow Meter Method for 3 wt% Hyperion Fibrils in Lexan HF1130-111 (BQ3L): Injection Molded May 26, 2009

Test Date	Sample Number	Through Plane Thermal Conductivity (W/m•K)
7/1/2009	BQ3L-TC-13	0.2372
7/1/2009	BQ3L-TC-16	0.2373
7/1/2009	BQ3L-TC-19	0.2411
7/1/2009	BQ3L-TC-20	0.2431
7/1/2009	BQ3L-TC-32	0.2445
	Average	0.2406
	Standard Deviation	0.0033
	Number of Samples	5

Table I.5: Through-Plane Thermal Conductivity at 55°C using Holometrix TCA-300 Guarded Heat Flow Meter Method for 4 wt% Hyperion Fibrils in Lexan HF1130-111 (BQ4L): Injection Molded May 26, 2009

Test Date	Sample Number	Through Plane Thermal Conductivity (W/m•K)
7/1/2009	BQ4L-TC-13	0.2533
7/6/2009	BQ4L-TC-19	0.2540
7/1/2009	BQ4L-TC-24	0.2560
7/1/2009	BQ4L-TC-29	0.2542
7/1/2009	BQ4L-TC-32	0.2565
	Average	0.2548
	Standard Deviation	0.0014
	Number of Samples	5

Table I.6: Through-Plane Thermal Conductivity at 55°C using Holometrix TCA-300 Guarded Heat Flow Meter Method for 5 wt% Hyperion Fibrils in Lexan HF1130-111 (BQ5L): Injection Molded May 26, 2009

Test Date	Sample Number	Through Plane Thermal Conductivity (W/m•K)
6/30/2009	BQ5L-TC-15	0.2684
7/6/2009	BQ5L-TC-19	0.2612
6/30/2009	BQ5L-TC-21	0.2700
6/30/2009	BQ5L-TC-27	0.2646
6/30/2009	BQ5L-TC-30	0.2660
	Average	0.2660
	Standard Deviation	0.0034
	Number of Samples	5

Table I.7: Through-Plane Thermal Conductivity at 55°C using Holometrix TCA-300 Guarded Heat Flow Meter Method for 6 wt% Hyperion Fibrils in Lexan HF1130-111 (BQ6L): Injection Molded May 26, 2009

Test Date	Sample Number	Through Plane Thermal Conductivity (W/m•K)
6/30/2009	BQ6L-TC-12	0.2717
6/30/2009	BQ6L-TC-15	0.2721
6/30/2009	BQ6L-TC-20	0.2772
6/30/2009	BQ6L-TC-29	0.2766
6/30/2009	BQ6L-TC-33	0.2761
	Average	0.2747
	Standard Deviation	0.0026
	Number of Samples	5

Table I.8: Through-Plane Thermal Conductivity at 55°C using Holometrix TCA-300 Guarded Heat Flow Meter Method for 8 wt% Hyperion Fibrils in Lexan HF1130-111 (BQ8L): Injection Molded May 26, 2009

Test Date	Sample Number	Through Plane Thermal Conductivity (W/m•K)
7/6/2009	BQ8L-TC-18	0.3085
6/30/2009	BQ8L-TC-21	0.3079
6/30/2009	BQ8L-TC-22	0.3040
6/30/2009	BQ8L-TC-26	0.3008
6/30/2009	BQ8L-TC-35	0.3078
	Average	0.3058
	Standard Deviation	0.0033
	Number of Samples	5

Appendix I.2: Polycarbonate with Carbon Black

Table I.9: Through-Plane Thermal Conductivity at 55°C using Holometrix TCA-300 Guarded Heat Flow Meter Method for Lexan HF1130-111 (BL2): Injection Molded December 4, 2009

Test Date	Sample Number	Through Plane Thermal Conductivity (W/m•K)
12/21/2009	BL2-TC-19	0.2149
12/21/2009	BL2-TC-37	0.2126
12/21/2009	BL2-TC-10	0.2126
12/21/2009	BL2-TC-24	0.2141
12/21/2009	BL2-TC-30	0.2136
	Average	0.2136
	Standard Deviation	0.0010
	Number of Samples	5

Table I.10: Through-Plane Thermal Conductivity at 55°C using Holometrix TCA-300 Guarded Heat Flow Meter Method for Extruded Lexan HF1130-111 (BLE2): Injection Molded Dec 4, 2009

Test Date	Sample Number	Through Plane Thermal Conductivity (W/m•K)
12/21/2009	BLE2-TC-12	0.2140
12/21/2009	BLE2-TC-16	0.2150
12/21/2009	BLE2-TC-23	0.2151
12/21/2009	BLE2-TC-22	0.2157
12/21/2009	BLE2-TC-13	0.2124
	Average	0.2144
	Standard Deviation	0.0013
	Number of Samples	5

Table I.11: Through-Plane Thermal Conductivity at 55°C using Holometrix TCA-300 Guarded Heat Flow Meter Method for 2 wt% Ketjenblack EC-600 JD in Lexan HF1130-111 (BA2L): Injection Molded Dec 4, 2009

Test Date	Sample Number	Through Plane Thermal Conductivity (W/m•K)
12/22/2009	BA2L-TC-26	0.2268
12/22/2009	BA2L-TC-16	0.2276
12/22/2009	BA2L-TC-15	0.2291
12/22/2009	BA2L-TC-29	0.2282
12/22/2009	BA2L-TC-12	0.2284
	Average	0.2280
	Standard Deviation	0.0009
	Number of Samples	5

Table I.12: Through-Plane Thermal Conductivity at 55°C using Holometrix TCA-300 Guarded Heat Flow Meter Method for 3 wt% Ketjenblack EC-600 JD in Lexan HF1130-111 (BA3L): Injection Molded Dec 4, 2009

Test Date	Sample Number	Through Plane Thermal Conductivity (W/m•K)
12/22/2009	BA3L-TC-10	0.2363
12/22/2009	BA3L-TC-19	0.2319
12/22/2009	BA3L-TC-12	0.2331
12/22/2009	BA3L-TC-27	0.2355
	Average	0.2342
	Standard Deviation	0.0020
	Number of Samples	4

Table I.13: Through-Plane Thermal Conductivity at 55°C using Holometrix TCA-300 Guarded Heat Flow Meter Method for 4 wt% Ketjenblack EC-600 JD in Lexan HF1130-111 (BA4L): Injection Molded Dec 4, 2009

Test Date	Sample Number	Through Plane Thermal Conductivity (W/m•K)
12/23/2009	BA4L-TC-11	0.2453
12/23/2009	BA4L-TC-15	0.2451
12/23/2009	BA4L-TC-17	0.2444
12/23/2009	BA4L-TC-22	0.2448
	Average	0.2449
	Standard Deviation	0.0004
	Number of Samples	4

Table I.14: Through-Plane Thermal Conductivity at 55°C using Holometrix TCA-300 Guarded Heat Flow Meter Method for 5 wt% Ketjenblack EC-600 JD in Lexan HF1130-111 (BA5L): Injection Molded Dec 4, 2009

Test Date	Sample Number	Through Plane Thermal Conductivity (W/m•K)
12/23/2009	BA5L-TC-13	0.2541
12/23/2009	BA5L-TC-20	0.2551
12/23/2009	BA5L-TC-23	0.2525
12/23/2009	BA5L-TC-26	0.2533
	Average	0.2538
	Standard Deviation	0.0011
	Number of Samples	4

Table I.15: Through-Plane Thermal Conductivity at 55°C using Holometrix TCA-300 Guarded Heat Flow Meter Method for 6 wt% Ketjenblack EC-600 JD in Lexan HF1130-111 (BA6L): Injection Molded Dec 4, 2009

Test Date	Sample Number	Through Plane Thermal Conductivity (W/m•K)
1/4/2010	BA6L-TC-18	0.2599
1/4/2010	BA6L-TC-23	0.2595
1/4/2010	BA6L-TC-28	0.2601
1/4/2010	BA6L-TC-31	0.2614
	Average	0.2602
	Standard Deviation	0.0008
	Number of Samples	4

Table I.16: Through-Plane Thermal Conductivity at 55°C using Holometrix TCA-300 Guarded Heat Flow Meter Method for 8 wt% Ketjenblack EC-600 JD in Lexan HF1130-111 (BA8L): Injection Molded Dec 4, 2009

Test Date	Sample Number	Through Plane Thermal Conductivity (W/m•K)
1/4/2010	BA8L-TC-13	0.2765
1/4/2010	BA8L-TC-18	0.2767
1/4/2010	BA8L-TC-20	0.2709
1/4/2010	BA8L-TC-25	0.2774
	Average	0.2754
	Standard Deviation	0.0030
	Number of Samples	4

Table I.17: Through-Plane Thermal Conductivity at 55°C using Holometrix TCA-300 Guarded Heat Flow Meter Method for 10 wt% Ketjenblack EC-600 JD in Lexan HF1130-111 (BA10L): Injection Molded Dec 4, 2009

Test Date	Sample Number	Through Plane Thermal Conductivity (W/m•K)
1/5/2010	BA10L-TC-19	0.2888
1/5/2010	BA10L-TC-21	0.2944
1/5/2010	BA10L-TC-24	0.2892
1/5/2010	BA10L-TC-27	0.2908
	Average	0.2908
	Standard Deviation	0.0026
	Number of Samples	4

Appendix I.3: Polycarbonate with Graphite Nanoparticles

Table I.18: Through-Plane Thermal Conductivity at 55°C using Holometrix TCA-300 Guarded Heat Flow Meter Method for Lexan HF1130-111 (BL3): Injection Molded June 3, 2010

Test Date	Sample Number	Through Plane Thermal Conductivity (W/m•K)
6/15/2010	BL3-TC-10	0.2126
6/15/2010	BL3-TC-16	0.2181
6/15/2010	BL3-TC-19	0.2158
6/15/2010	BL3-TC-8	0.2136
	Average	0.2150
	Standard Deviation	0.0024
	Number of Samples	4

Table I.19: Through-Plane Thermal Conductivity at 55°C using Holometrix TCA-300 Guarded Heat Flow Meter Method for Extruded Lexan HF1130-111 (BLE3): Injection Molded June 3, 2010

Test Date	Sample Number	Through Plane Thermal Conductivity (W/m•K)
6/15/2010	BLE3-TC-5	0.2141
6/15/2010	BLE3-TC-6	0.2176
6/15/2010	BLE3-TC-18	0.2167
6/15/2010	BLE3-TC-2	0.2182
6/15/2010	BLE3-TC-3	0.2187
	Average	0.2171
	Standard Deviation	0.0018
	Number of Samples	5

Table I.20: Through-Plane Thermal Conductivity at 55°C using Holometrix TCA-300 Guarded Heat Flow Meter Method for 2 wt% xGnP in Lexan HF1130-111 (BG2L): Injection Molded June 3, 2010

Test Date	Sample Number	Through Plane Thermal Conductivity (W/m•K)
6/16/2010	BG2L-TC-23	0.2527
6/16/2010	BG2L-TC-13	0.2498
6/16/2010	BG2L-TC-21	0.2479
6/16/2010	BG2L-TC-22	0.2479
6/16/2010	BG2L-TC-24	0.254
	Average	0.2505
	Standard Deviation	0.0028
	Number of Samples	5

Table I.21: Through-Plane Thermal Conductivity at 55°C using Holometrix TCA-300 Guarded Heat Flow Meter Method for 3 wt% xGnP in Lexan HF1130-111 (BG3L): Injection Molded June 3, 2010

Test Date	Sample Number	Through Plane Thermal Conductivity (W/m•K)
6/16/2010	BG3L-TC-18	0.278
6/16/2010	BG3L-TC-20	0.2781
6/16/2010	BG3L-TC-25	0.2695
6/16/2010	BG3L-TC-29	0.2676
6/16/2010	BG3L-TC-30	0.2695
	Average	0.2725
	Standard Deviation	0.0051
	Number of Samples	5

Table I.22: Through-Plane Thermal Conductivity at 55°C using Holometrix TCA-300 Guarded Heat Flow Meter Method for 4 wt% xGnP in Lexan HF1130-111 (BG4L): Injection Molded June 3, 2010

Test Date	Sample Number	Through Plane Thermal Conductivity (W/m•K)
6/16/2010	BG4L-TC-16	0.301
6/16/2010	BG4L-TC-19	0.2931
6/16/2010	BG4L-TC-18	0.2971
6/16/2010	BG4L-TC-20	0.2985
6/16/2010	BG4L-TC-21	0.3008
	Average	0.2981
	Standard Deviation	0.0032
	Number of Samples	5

Table I.23: Through-Plane Thermal Conductivity at 55°C using Holometrix TCA-300 Guarded Heat Flow Meter Method 5 wt% xGnP in Lexan HF1130-111 (BG5L): Injection Molded June 3, 2010

Test Date	Sample Number	Through Plane Thermal Conductivity (W/m•K)
6/17/2010	BG5L-TC-8	0.3148
6/17/2010	BG5L-TC-14	0.3172
6/17/2010	BG5L-TC-18	0.3067
6/17/2010	BG5L-TC-12	0.3083
6/17/2010	BG5L-TC-11	0.3123
	Average	0.3119
	Standard Deviation	0.0044
	Number of Samples	5

Table I.24: Through-Plane Thermal Conductivity at 55°C using Holometrix TCA-300 Guarded Heat Flow Meter Method for 6 wt% xGnP in Lexan HF1130-111 (BG6L): Injection Molded June 8, 2010

Test Date	Sample Number	Through Plane Thermal Conductivity (W/m•K)
6/17/2010	BG6L-TC-23	0.3438
6/17/2010	BG6L-TC-22	0.3459
6/17/2010	BG6L-TC-26	0.3427
6/18/2010	BG6L-TC-16	0.3405
6/18/2010	BG6L-TC-19	0.3449
	Average	0.3436
	Standard Deviation	0.0021
	Number of Samples	5

Table I.25: Through-Plane Thermal Conductivity at 55°C using Holometrix TCA-300 Guarded Heat Flow Meter Method for 8 wt% xGnP in Lexan HF1130-111 (BG8L): Injection Molded June 8, 2010

Test Date	Sample Number	Through Plane Thermal Conductivity (W/m•K)
6/18/2010	BG8L-TC-23	0.371
6/18/2010	BG8L-TC-26	0.3817
6/18/2010	BG8L-TC-24	0.3694
6/18/2010	BG8L-TC-14	0.3822
6/18/2010	BG8L-TC-12	0.3679
	Average	0.3744
	Standard Deviation	0.0069
	Number of Samples	5

Table I.26: Through-Plane Thermal Conductivity at 55°C using Holometrix TCA-300 Guarded Heat Flow Meter Method for 10 wt% xGnP in Lexan HF1130-111 (BG10L): Injection Molded June 8, 2010

Test Date	Sample Number	Through Plane Thermal Conductivity (W/m•K)
6/18/2010	BG10L-TC-39	0.4229
6/18/2010	BG10L-TC-26	0.4171
6/18/2010	BG10L-TC-20	0.4176
6/18/2010	BG10L-TC-15	0.419
6/18/2010	BG10L-TC-14	0.4209
	Average	0.4195
	Standard Deviation	0.0024
	Number of Samples	5

Appendix I.4: Polycarbonate with Multiple Fillers

Table I.27: Through-Plane Thermal Conductivity at 55°C using Holometrix TCA-300 Guarded Heat Flow Meter Method for BQ0.5L: Injection Molded 7-26-10

Test Date	Sample Number	Through Plane Thermal Conductivity (W/m•K)
8/13/2010	BQ0.5L-TC-25	0.2176
8/13/2010	BQ0.5L-TC-26	0.2213
8/13/2010	BQ0.5L-TC-29	0.2172
8/13/2010	BQ0.5L-TC-15	0.2173
	Average	0.2184
	Standard Deviation	0.0020
	Number of Samples	4

Table I.28: Through-Plane Thermal Conductivity at 55°C using Holometrix TCA-300 Guarded Heat Flow Meter Method for BQ1L Set 1: Injection Molded 7-26-10

Test Date	Sample Number	Through Plane Thermal Conductivity (W/m•K)
8/13/2010	BQ1L-TC-21	0.2167
8/13/2010	BQ1L-TC-9	0.2206
8/13/2010	BQ1L-TC-29	0.2296
8/13/2010	BQ1L-TC-7	0.2281
	Average	0.2238
	Standard Deviation	0.0061
	Number of Samples	4

Table I.29: Through-Plane Thermal Conductivity at 55°C using Holometrix TCA-300 Guarded Heat Flow Meter Method for BQ1L Set 2: Injection Molded 7-26-10

Test Date	Sample Number	Through Plane Thermal Conductivity (W/m•K)
8/13/2010	BQ1L-TC-30	0.2304
8/13/2010	BQ1L-TC-3	0.2202
8/13/2010	BQ1L-TC-23	0.2232
8/13/2010	BQ1L-TC-24	0.2282
	Average	0.2255
	Standard Deviation	0.0046
	Number of Samples	4

Table I.30: Through-Plane Thermal Conductivity at 55°C using Holometrix TCA-300 Guarded Heat Flow Meter Method for BQ5L Set 2

Test Date	Sample Number	Through Plane Thermal Conductivity (W/m•K)
8/17/2010	BQ5L-TC-10	0.2608
8/17/2010	BQ5L-TC-11	0.265
8/17/2010	BQ5L-TC-19	0.2639
8/17/2010	BQ5L-TC-20	0.2656
8/18/2010	BQ5L-TC-44	0.2595
	Average	0.2630
	Standard Deviation	0.0027
	Number of Samples	5

Table I.31: Through-Plane Thermal Conductivity at 55°C using Holometrix TCA-300 Guarded Heat Flow Meter Method for BG2L Set 2: Injection Molded 6-3-10

Test Date	Sample Number	Through Plane Thermal Conductivity (W/m•K)
8/17/2010	BG2L-TC-9	0.259
8/17/2010	BG2L-TC-14	0.258
8/17/2010	BG2L-TC-18	0.2498
8/17/2010	BG2L-TC-20	0.2416
	Average	0.2521
	Standard Deviation	0.0081
	Number of Samples	4

Table I.32: Through-Plane Thermal Conductivity at 55°C using Holometrix TCA-300 Guarded Heat Flow Meter Method for BG5L Set 2: Injection Molded 6-3-10

Test Date	Sample Number	Through Plane Thermal Conductivity (W/m•K)
8/17/2010	BG5L-TC-22	0.3184
8/17/2010	BG5L-TC-23	0.3166
8/17/2010	BG5L-TC-9	0.3184
8/17/2010	BG5L-TC-29	0.3197
8/17/2010	BG5L-TC-20	0.3198
	Average	0.3186
	Standard Deviation	0.0013
	Number of Samples	5

Table I.33: Through-Plane Thermal Conductivity at 55°C using Holometrix TCA-300 Guarded Heat Flow Meter Method for BG12L: Injection Molded 8-18-10

Test Date	Sample Number	Through Plane Thermal Conductivity (W/m•K)
8/20/2010	BG12L-TC-1	0.4729
8/20/2010	BG12L-TC-4	0.4527
8/20/2010	BG12L-TC-5	0.4667
8/20/2010	BG12L-TC-6	0.4379
	Average	0.4576
	Standard Deviation	0.0156
	Number of Samples	4

Table I.34: Through-Plane Thermal Conductivity at 55°C using Holometrix TCA-300 Guarded Heat Flow Meter Method for BG15L: Injection Molded 8-18-10

Test Date	Sample Number	Through Plane Thermal Conductivity (W/m•K)
8/20/2010	BG15L-TC-23	0.4895
8/20/2010	BG15L-TC-6	0.4727
8/20/2010	BG15L-TC-15	0.5098
8/20/2010	BG15L-TC-18	0.4832
	Average	0.4888
	Standard Deviation	0.0156
	Number of Samples	4

Table I.35: Through-Plane Thermal Conductivity at 55°C using Holometrix TCA-300 Guarded Heat Flow Meter Method for BA2Q1L set 1: Injection Molded 7-26-10

Test Date	Sample Number	Through Plane Thermal Conductivity (W/m•K)
8/13/2010	BA2Q1L-TC-17	0.2401
8/13/2010	BA2Q1L-TC-31	0.2436
8/13/2010	BA2Q1L-TC-2	0.2442
8/13/2010	BA2Q1L-TC-12	0.2444
	Average	0.2431
	Standard Deviation	0.0020
	Number of Samples	4

Table I.36: Through-Plane Thermal Conductivity at 55°C using Holometrix TCA-300 Guarded Heat Flow Meter Method for BA2Q1L set 2: Injection Molded 7-26-10

Test Date	Sample Number	Through Plane Thermal Conductivity (W/m•K)
8/13/2010	BA2Q1L-TC-35	0.2432
8/13/2010	BA2Q1L-TC-25	0.2429
8/13/2010	BA2Q1L-TC-10	0.2437
8/13/2010	BA2Q1L-TC-33	0.2428
	Average	0.2432
	Standard Deviation	0.0004
	Number of Samples	4

Table I.37: Through-Plane Thermal Conductivity at 55°C using Holometrix TCA-300 Guarded Heat Flow Meter Method for BA2Q5L set 1: Injection Molded 8-25-10

Test Date	Sample Number	Through Plane Thermal Conductivity (W/m•K)
9/2/2010	BA2Q5L-TC-7	0.2718
	BA2Q5L-TC-13	0.2718
	BA2Q5L-TC-11	0.2833
	BA2Q5L-TC-15	0.2746
	Average	0.2754
	Standard Deviation	0.0054
	Number of Samples	4

Table I.38: Through-Plane Thermal Conductivity at 55°C using Holometrix TCA-300 Guarded Heat Flow Meter Method for BA2Q5L set 2: Injection Molded 8-25-10

Test Date	Sample Number	Through Plane Thermal Conductivity (W/m•K)
9/2/2010	BA2Q5L-TC-22	0.2707
	BA2Q5L-TC-8	0.2688
	BA2Q5L-TC-23	0.274
	BA2Q5L-TC-18	0.2719
	Average	0.2714
	Standard Deviation	0.0022
	Number of Samples	4

Table I.4-39: Through-Plane Thermal Conductivity at 55°C using Holometrix TCA-300 Guarded Heat Flow Meter Method for BA5Q1L set 1: Injection Molded 7-26-10

Test Date	Sample Number	Through Plane Thermal Conductivity (W/m•K)
8/13/2010	BA5Q1L-TC-24	0.2666
8/13/2010	BA5Q1L-TC-30	0.2722
8/13/2010	BA5Q1L-TC-19	0.2715
8/13/2010	BA5Q1L-TC-16	0.2718
	Average	0.2705
	Standard Deviation	0.0026
	Number of Samples	4

Table I.4-40: Through-Plane Thermal Conductivity at 55°C using Holometrix TCA-300 Guarded Heat Flow Meter Method for BA5Q1L set 2: Injection Molded 7-26-10

Test Date	Sample Number	Through Plane Thermal Conductivity (W/m•K)
8/13/2010	BA5Q1L-TC-23	0.2708
8/13/2010	BA5Q1L-TC-28	0.2701
8/13/2010	BA5Q1L-TC-13	0.2709
8/13/2010	BA5Q1L-TC-9	0.2605
	Average	0.2681
	Standard Deviation	0.0051
	Number of Samples	4

Table I.41: Through-Plane Thermal Conductivity at 55°C using Holometrix TCA-300 Guarded Heat Flow Meter Method for BA5Q5L set 1: Injection Molded 8-25-10

Test Date	Sample Number	Through Plane Thermal Conductivity (W/m•K)
9/3/2010	BA5Q5L-TC-15	0.3041
	BA5Q5L-TC-27	0.3034
	BA5Q5L-TC-16	0.3015
	BA5Q5L-TC-24	0.306
	Average	0.3038
	Standard Deviation	0.0019
	Number of Samples	4

Table I.42: Through-Plane Thermal Conductivity at 55°C using Holometrix TCA-300 Guarded Heat Flow Meter Method for BA5Q5L set 2: Injection Molded 8-25-10

Test Date	Sample Number	Through Plane Thermal Conductivity (W/m•K)
9/3/2010	BA5Q5L-TC-9	0.2959
	BA5Q5L-TC-20	0.3064
	BA5Q5L-TC-11	0.299
	BA5Q5L-TC-21	0.2997
	Average	0.3003
	Standard Deviation	0.0044
	Number of Samples	4

Table I.43: Through-Plane Thermal Conductivity at 55°C using Holometrix TCA-300 Guarded Heat Flow Meter Method for BA2G2L set 1: Injection Molded 8-18-10

Test Date	Sample Number	Through Plane Thermal Conductivity (W/m•K)
8/23/2010	BA2G2L-TC-6	0.2799
8/23/2010	BA2G2L-TC-9	0.2766
8/23/2010	BA2G2L-TC-19	0.2616
8/23/2010	BA2G2L-TC-15	0.2667
	Average	0.2712
	Standard Deviation	0.0085
	Number of Samples	4

Table I.44: Through-Plane Thermal Conductivity at 55°C using Holometrix TCA-300 Guarded Heat Flow Meter Method for BA2G2L set 2: Injection Molded 8-18-10

Test Date	Sample Number	Through Plane Thermal Conductivity (W/m•K)
8/23/2010	BA2G2L-TC-10	0.2732
8/23/2010	BA2G2L-TC-7	0.2704
8/23/2010	BA2G2L-TC-16	0.2641
8/23/2010	BA2G2L-TC-8	0.2684
	Average	0.2690
	Standard Deviation	0.0038
	Number of Samples	4

Table I.45: Through-Plane Thermal Conductivity at 55°C using Holometrix TCA-300 Guarded Heat Flow Meter Method for BA2G5L set 1: Injection Molded 8-18-10

Test Date	Sample Number	Through Plane Thermal Conductivity (W/m•K)
8/20/2010	BA2G5L-TC-4	0.3346
8/20/2010	BA2G5L-TC-7	0.3312
8/20/2010	BA2G5L-TC-9	0.3443
8/20/2010	BA2G5L-TC-10	0.3426
8/20/2010	BA2G5L-TC-17	0.3429
	Average	0.3391
	Standard Deviation	0.0058
	Number of Samples	5

Table I.46: Through-Plane Thermal Conductivity at 55°C using Holometrix TCA-300 Guarded Heat Flow Meter Method for BA2G5L set 2: Injection Molded 8-18-10

Test Date	Sample Number	Through Plane Thermal Conductivity (W/m•K)
8/20/2010	BA2G5L-TC-21	0.3339
8/20/2010	BA2G5L-TC-28	0.3417
8/20/2010	BA2G5L-TC-29	0.3419
8/20/2010	BA2G5L-TC-30	0.3291
	Average	0.3367
	Standard Deviation	0.0063
	Number of Samples	4

Table I.47: Through-Plane Thermal Conductivity at 55°C using Holometrix TCA-300 Guarded Heat Flow Meter Method for BA5G2L set 1: Injection Molded 8-18-10

Test Date	Sample Number	Through Plane Thermal Conductivity (W/m•K)
8/24/2010	BA5G2L-TC-8	0.3076
8/24/2010	BA5G2L-TC-18	0.3015
8/24/2010	BA5G2L-TC-12	0.3015
8/24/2010	BA5G2L-TC-15	0.3028
	Average	0.3034
	Standard Deviation	0.0029
	Number of Samples	4

Table I.48: Through-Plane Thermal Conductivity at 55°C using Holometrix TCA-300 Guarded Heat Flow Meter Method for BA5G2L set 2: Injection Molded 8-18-10

Test Date	Sample Number	Through Plane Thermal Conductivity (W/m•K)
8/24/2010	BA5G2L-TC-25	0.3008
8/24/2010	BA5G2L-TC-14	0.3016
8/24/2010	BA5G2L-TC-24	0.2996
8/24/2010	BA5G2L-TC-21	0.3025
	Average	0.3011
	Standard Deviation	0.0012
	Number of Samples	4

Table I.49: Through-Plane Thermal Conductivity at 55°C using Holometrix TCA-300 Guarded Heat Flow Meter Method for BA5G5L set 1: Injection Molded 8-18-10

Test Date	Sample Number	Through Plane Thermal Conductivity (W/m•K)
8/26/2010	BA5G5L-TC-10	0.3708
8/26/2010	BA5G5L-TC-22	0.3518
8/26/2010	BA5G5L-TC-23	0.3526
8/26/2010	BA5G5L-TC-9	0.3511
	Average	0.3566
	Standard Deviation	0.0095
	Number of Samples	4

Table I.50: Through-Plane Thermal Conductivity at 55°C using Holometrix TCA-300 Guarded Heat Flow Meter Method for BA5G5L set 2: Injection Molded 8-18-10

Test Date	Sample Number	Through Plane Thermal Conductivity (W/m•K)
8/26/2010	BA5G5L-TC-25	0.3687
8/26/2010	BA5G5L-TC-15	0.3683
8/26/2010	BA5G5L-TC-6	0.3599
8/26/2010	BA5G5L-TC-14	0.3667
	Average	0.3659
	Standard Deviation	0.0041
	Number of Samples	4

Table I.51: Through-Plane Thermal Conductivity at 55°C using Holometrix TCA-300 Guarded Heat Flow Meter Method for BQ1G2L set 1: Injection Molded 8-18-10

Test Date	Sample Number	Through Plane Thermal Conductivity (W/m•K)
8/27/2010	BQ1G2L-TC-16	0.258
8/27/2010	BQ1G2L-TC-18	0.2704
8/27/2010	BQ1G2L-TC-19	0.2732
8/27/2010	BQ1G2L-TC-10	0.2682
	Average	0.2675
	Standard Deviation	0.0066
	Number of Samples	4

Table I.52: Through-Plane Thermal Conductivity at 55°C using Holometrix TCA-300 Guarded Heat Flow Meter Method for BQ1G2L set 2: Injection Molded 8-18-10

Test Date	Sample Number	Through Plane Thermal Conductivity (W/m•K)
8/27/2010	BQ1G2L-TC-23	0.2726
8/27/2010	BQ1G2L-TC-11	0.261
8/27/2010	BQ1G2L-TC-25	0.2607
8/27/2010	BQ1G2L-TC-22	0.263
	Average	0.2643
	Standard Deviation	0.0056
	Number of Samples	4

Table I-53: Through-Plane Thermal Conductivity at 55°C using Holometrix TCA-300 Guarded Heat Flow Meter Method for BQ1G5L set 1: Injection Molded 8-18-10

Test Date	Sample Number	Through Plane Thermal Conductivity (W/m•K)
8/30/2010	BQ1G5L-TC-6	0.329
	BQ1G5L-TC-19	0.3254
	BQ1G5L-TC-14	0.3357
	BQ1G5L-TC-13	0.3201
	Average	0.3276
	Standard Deviation	0.0065
	Number of Samples	4

Table I.54: Through-Plane Thermal Conductivity at 55°C using Holometrix TCA-300 Guarded Heat Flow Meter Method for BQ1G5L set 2: Injection Molded 8-18-10

Test Date	Sample Number	Through Plane Thermal Conductivity (W/m•K)
8/30/2010	BQ1G5L-TC-29	0.3278
	BQ1G5L-TC-15	0.3261
	BQ1G5L-TC-17	0.3304
	BQ1G5L-TC-25	0.3311
	Average	0.3289
	Standard Deviation	0.0023
	Number of Samples	4

Table I.55: Through-Plane Thermal Conductivity at 55°C using Holometrix TCA-300 Guarded Heat Flow Meter Method for BQ5G2L set 1: Injection Molded 8-18-10

Test Date	Sample Number	Through Plane Thermal Conductivity (W/m•K)
8/31/2010	BQ5G2L-TC-25	0.3194
	BQ5G2L-TC-21	0.3165
	BQ5G2L-TC-14	0.3116
	BQ5G2L-TC-24	0.3254
	Average	0.3182
	Standard Deviation	0.0058
	Number of Samples	4

Table I.56: Through-Plane Thermal Conductivity at 55°C using Holometrix TCA-300 Guarded Heat Flow Meter Method for BQ5G2L set 2: Injection Molded 8-18-10

Test Date	Sample Number	Through Plane Thermal Conductivity (W/m•K)
8/31/2010	BQ5G2L-TC-15	0.319
	BQ5G2L-TC-13	0.3147
	BQ5G2L-TC-19	0.3279
	BQ5G2L-TC-20	0.3231
	BQ5G2L-TC-11	0.3196
	Average	0.3209
	Standard Deviation	0.0049
	Number of Samples	5

Table I.57: Through-Plane Thermal Conductivity at 55°C using Holometrix TCA-300 Guarded Heat Flow Meter Method for BQ5G5L set 1: Injection Molded 8-18-10

Test Date	Sample Number	Through Plane Thermal Conductivity (W/m•K)
9/1/2010	BQ5G5L-TC-17	0.3908
	BQ5G5L-TC-21	0.3986
	BQ5G5L-TC-24	0.3965
	BQ5G5L-TC-5	0.3977
	Average	0.3959
	Standard Deviation	0.0035
	Number of Samples	4

Table I.58: Through-Plane Thermal Conductivity at 55°C using Holometrix TCA-300 Guarded Heat Flow Meter Method for BQ5G5L set 2: Injection Molded 8-18-10

Test Date	Sample Number	Through Plane Thermal Conductivity (W/m•K)
9/1/2010	BQ5G5L-TC-27	0.4017
	BQ5G5L-TC-19	0.3899
	BQ5G5L-TC-10	0.4042
	BQ5G5L-TC-15	0.3905
	Average	0.3966
	Standard Deviation	0.0074
	Number of Samples	4

Appendix J: Mechanical Tensile Property Results

Appendix J.1: Polycarbonate with Carbon Nanotubes

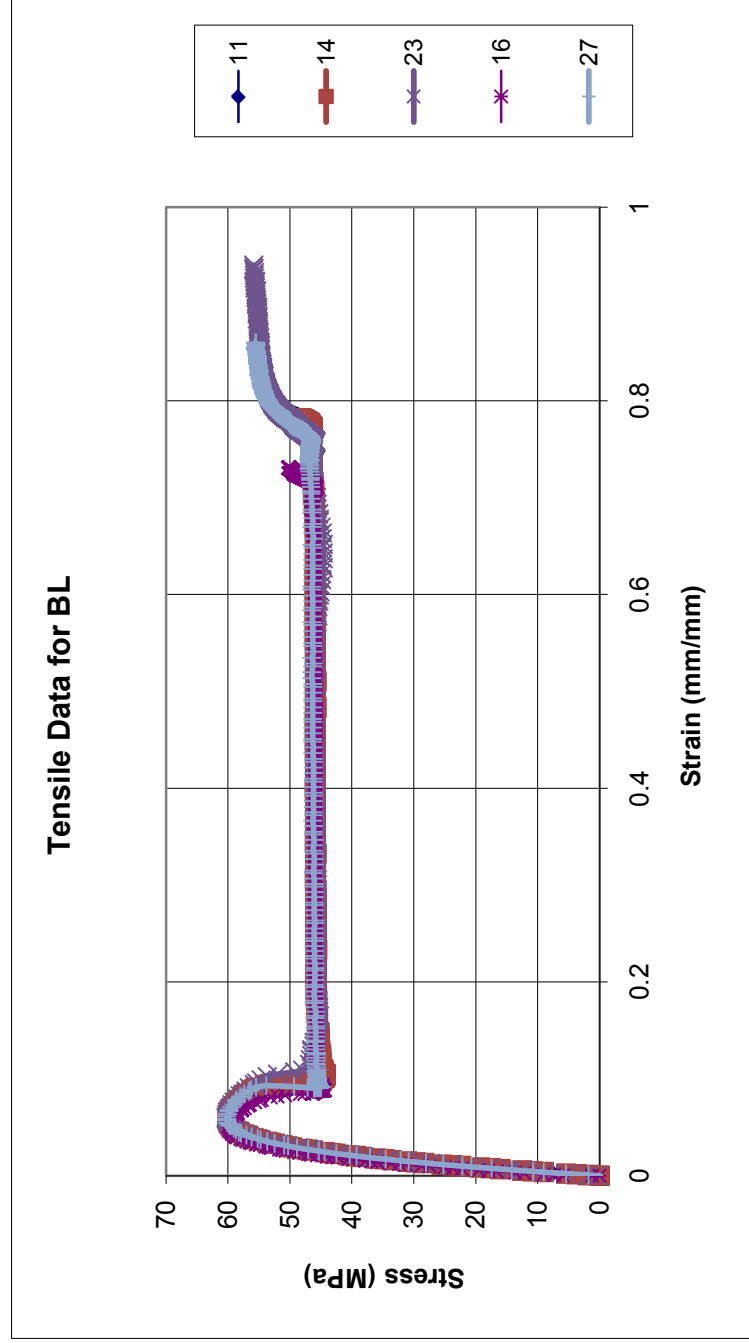


Figure J.1: Tensile Results for BL: Lexan HF1130-111: Injection Molded 5-26-09

Table J.1: Tensile Results for BL: Lexan HF1130-111: Injection Molded 5-26-09

Sample	Specimen	Tensile Ultimate Stress (MPa)	Tensile Strain at Ultimate Stress (%)	Tensile Fracture Stress (MPa)	Tensile Strain at Fracture Stress (%)	Tensile Modulus (MPa)
BL	11	60.173	5.80	52.788	80.28	2177.2
	14	60.053	5.80	49.703	79.01	2152.5
	23	60.294	5.92	55.841	93.55	2138.7
	16	59.933	5.00	50.185	73.08	2282.3
	27	60.174	5.74	55.600	85.33	2107.2
Average		60.13	5.65	52.82	82.25	2171.58
Standard Deviation		0.14	0.37	2.89	7.67	66.86
Number		5	5	5	5	5

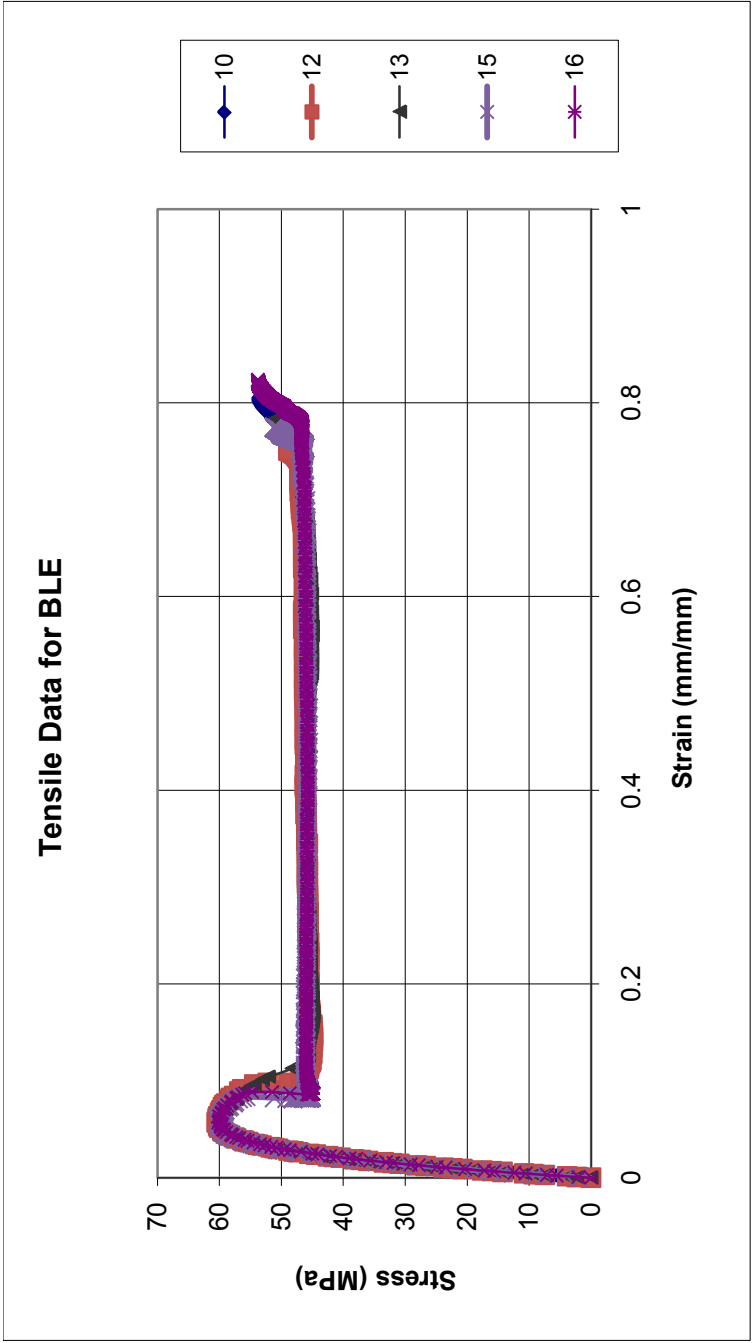


Figure J.2: Tensile Results for BLE: Extruded Lexan HF1130-111: Injection Molded 5-26-09

Table J.2: Tensile Results for BLE: Extruded Lexan HF1130-111 : Injection Molded 5-26-09

Sample	Specimen	Tensile Ultimate Stress (MPa)	Tensile Strain at Ultimate Stress (%)	Tensile Fracture Stress (MPa)	Tensile Strain at Fracture Stress (%)	Tensile Modulus (MPa)
BLE	10	60.414	5.55	53.675	80.33	2090.1
	12	60.414	5.68	50.787	76.03	2113.6
	13	60.294	5.64	51.388	78.22	2182.1
	15	60.053	5.44	51.148	77.44	2158.8
	16	60.174	5.70	53.795	82.19	2093.8
Average		60.27	5.60	52.16	78.84	2127.68
Standard Deviation		0.16	0.11	1.46	2.43	40.89
Number		5	5	5	5	5

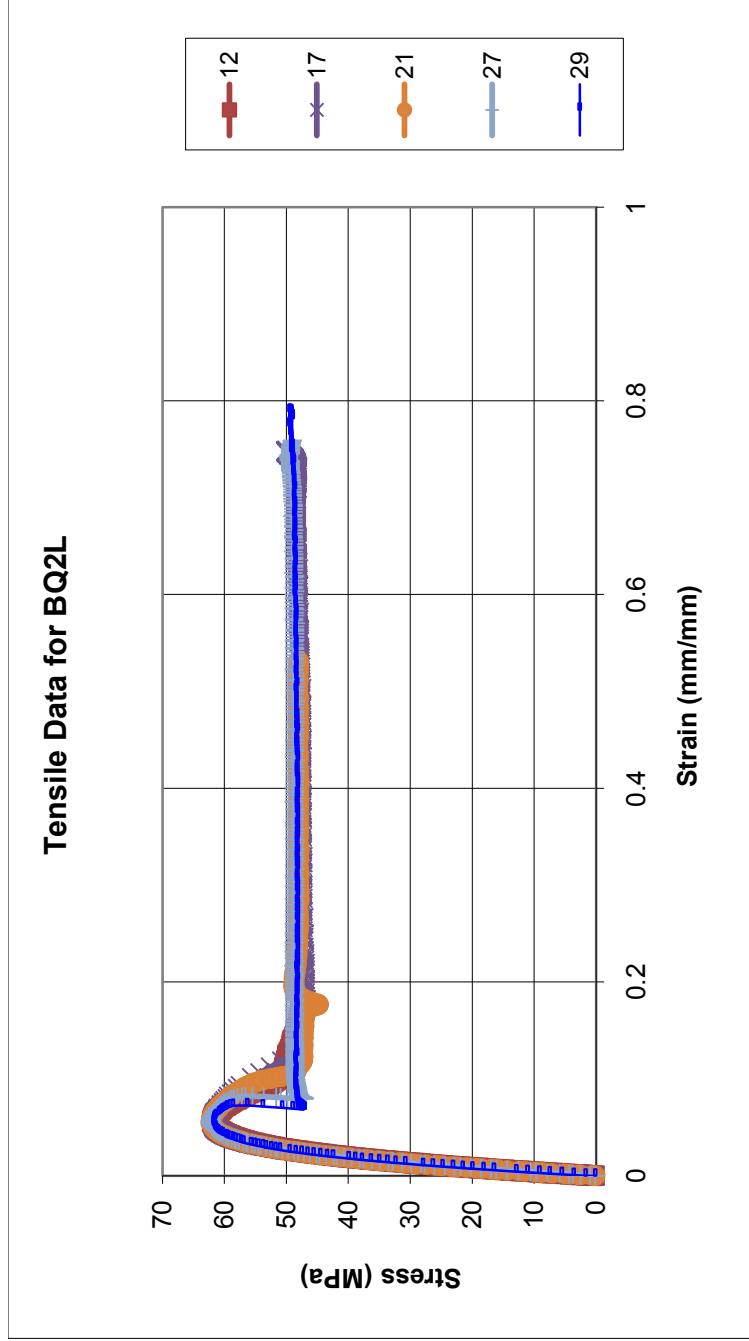


Figure J.3: Tensile Results for BQ2L: 2 wt% fibrils (carbon nanotubes) in Lexan HF1130-111: Injection Molded 5-26-09

Table J.3: Tensile Results for BQ2L: 2 wt% fibrils (carbon nanotubes) in Lexan HF1130-111: Injection Molded 5-26-09

Sample	Specimen	Tensile Ultimate Stress (MPa)	Tensile Strain at Ultimate Stress (%)	Tensile Fracture Stress (MPa)	Tensile Strain at Fracture Stress (%)	Tensile Modulus (MPa)
BQ2L	12	61.979	5.61	46.093	22.69	2389.3
	17	61.979	5.48	49.944	74.85	2272.8
	21	62.220	5.51	48.019	51.93	2346.8
	27	62.220	5.40	49.102	75.63	2266
	29	61.738	5.25	49.342	78.97	2336.3
Average		62.03	5.45	48.50	60.81	2322.24
Standard Deviation		0.20	0.13	1.52	23.87	52.21
Number		5	5	5	5	5

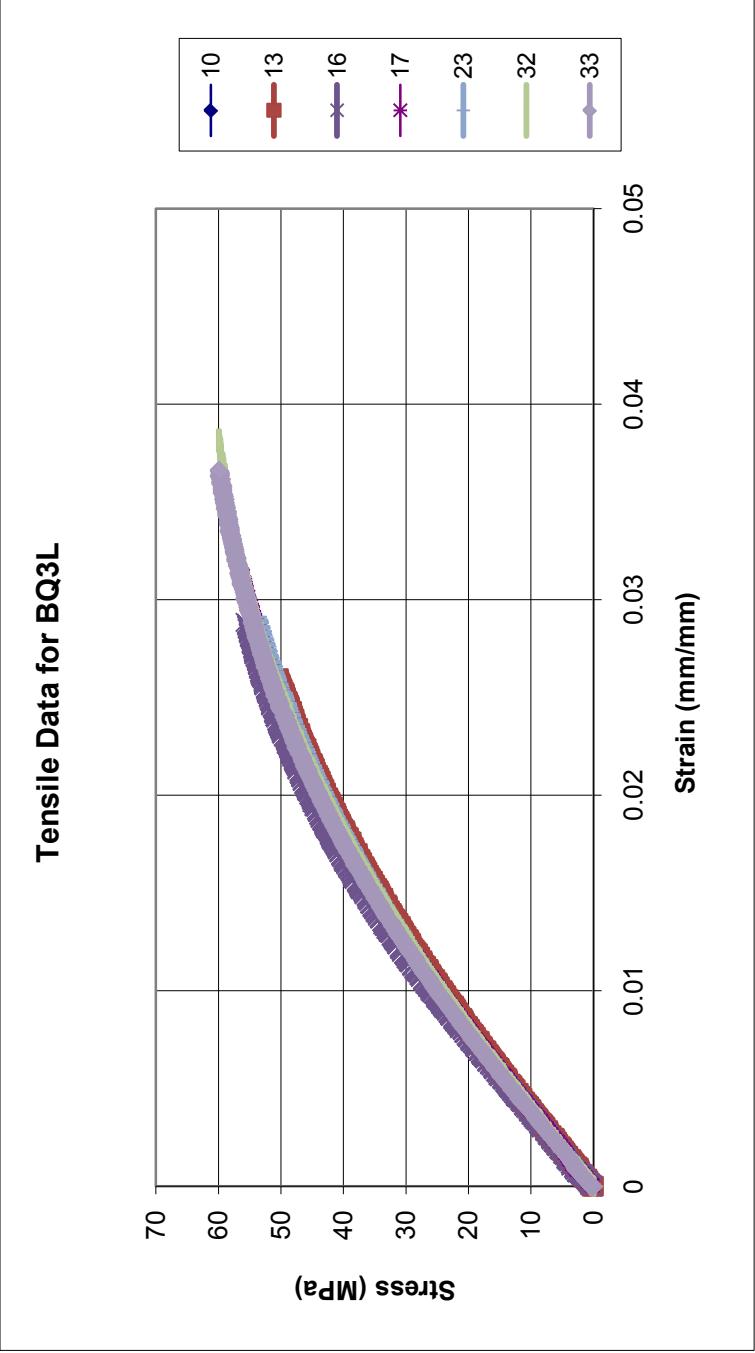


Figure J.4: Tensile Results for BQ3L: 3 wt% fibrils (carbon nanotubes) in Lexan HF1130-111: Injection Molded 5-26-09

Table J.4: Tensile Results for BQ3L: 3 wt% fibrils (carbon nanotubes) in Lexan HF1130-111: Injection Molded 5-26-09

Sample	Specimen	Tensile Ultimate Stress (MPa)	Tensile Strain at Ultimate Stress (%)	Tensile Fracture Stress (MPa)	Tensile Strain at Fracture Stress (%)	Tensile Modulus (MPa)
BQ3L	10	53.795	2.91	53.795	2.91	2494.8
	13	54.277	2.99	54.277	2.99	2452.3
	16	55.721	2.88	55.721	2.88	2578.2
	17	56.202	3.12	56.202	3.12	2475.3
	23	53.795	2.91	53.795	2.91	2509.8
	32	60.053	3.83	60.053	3.83	2473.2
	33	59.813	3.63	59.813	3.66	2471.9
Average		56.24	3.18	56.24	3.19	2493.64
Standard Deviation		2.69	0.39	2.69	0.39	41.53
Number		7	7	7	7	7

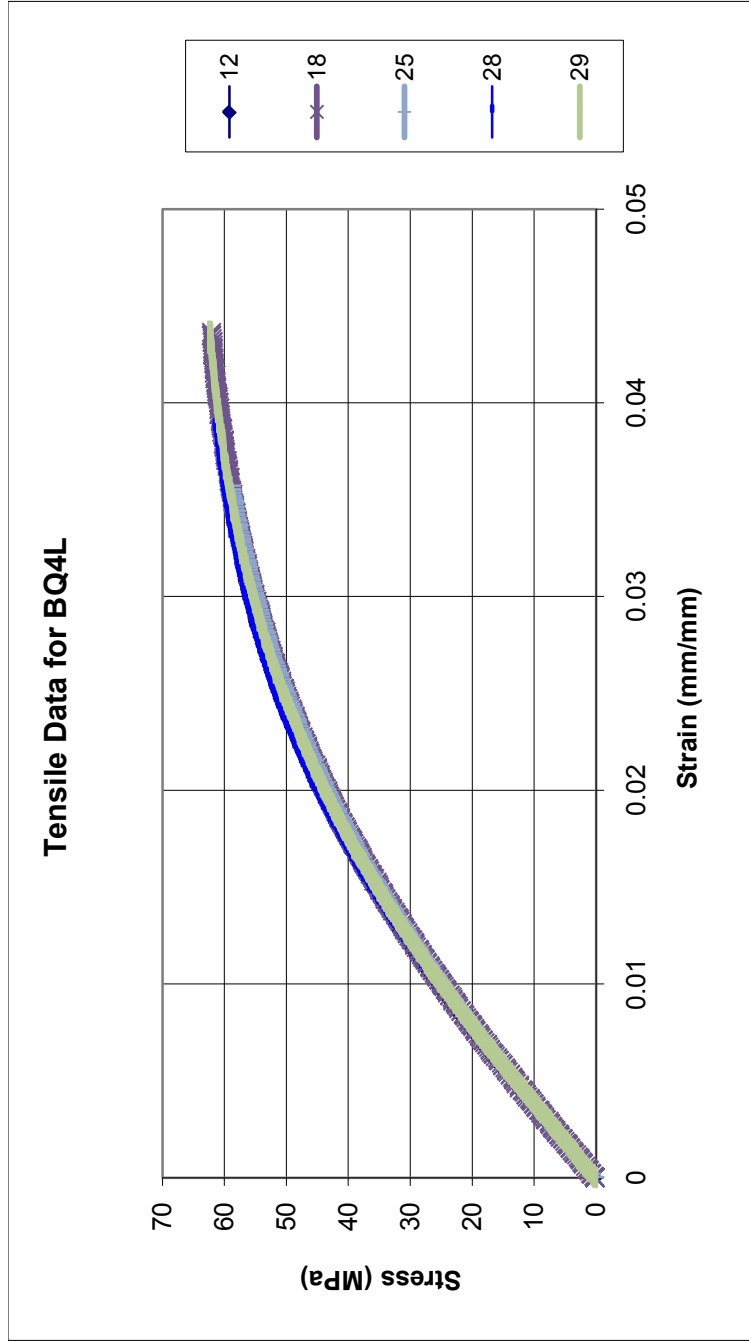


Figure J.5: Tensile Results for BQ4L: 4 wt% fibrils (carbon nanotubes) in Lexan HF1130-111: Injection Molded 5-26-09

Table J.5: Tensile Results for BQ4L: 4 wt% fibrils (carbon nanotubes) in Lexan HF1130-111: Injection Molded 5-26-09

Sample	Specimen	Tensile Ultimate Stress (MPa)	Tensile Strain at Ultimate Stress (%)	Tensile Fracture Stress (MPa)	Tensile Strain at Fracture Stress (%)	Tensile Modulus (MPa)
BQ4L	12	57.285	3.17	57.285	3.17	2602.2
	18	62.099	4.35	62.099	4.35	2535.5
	25	58.850	3.53	58.850	3.53	2503.4
	28	61.738	3.95	61.738	3.95	2593.2
	29	62.460	4.39	62.460	4.39	2526.7
Average		60.49	3.88	60.49	3.88	2552.20
Standard Deviation		2.29	0.52	2.29	0.52	43.28
Number		5	5	5	5	5

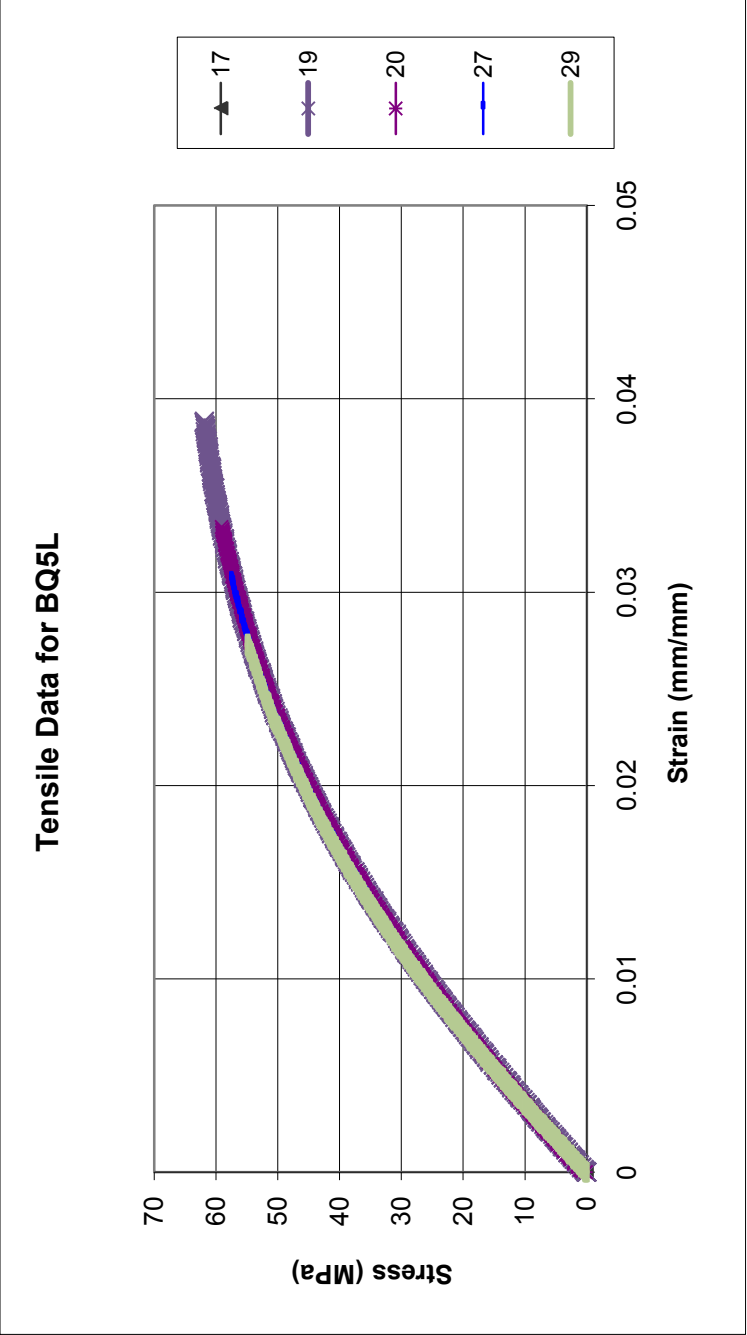


Figure J.6: Tensile Results for BQ5L: 5 wt% fibrils (carbon nanotubes) in Lexan HF1130-111: Injection Molded 5-26-09

Table J.6: Tensile Results for BQ5L: 5 wt% fibrils (carbon nanotubes) in Lexan HF1130-111: Injection Molded 5-26-09

Sample	Specimen	Tensile Ultimate Stress (MPa)	Tensile Strain at Ultimate Stress (%)	Tensile Fracture Stress (MPa)	Tensile Strain at Fracture Stress (%)	Tensile Modulus (MPa)
BQ5L	17	51.629	2.42	51.629	2.42	2714.9
	19	61.979	3.88	61.979	3.88	2630.4
	20	59.091	3.34	59.091	3.34	2527.5
	27	58.007	3.13	58.007	3.13	2655.7
	29	54.878	2.72	54.878	2.73	2762.5
Average		57.12	3.10	57.12	3.10	2658.20
Standard Deviation		3.98	0.56	3.98	0.56	89.38
Number		5	5	5	5	5

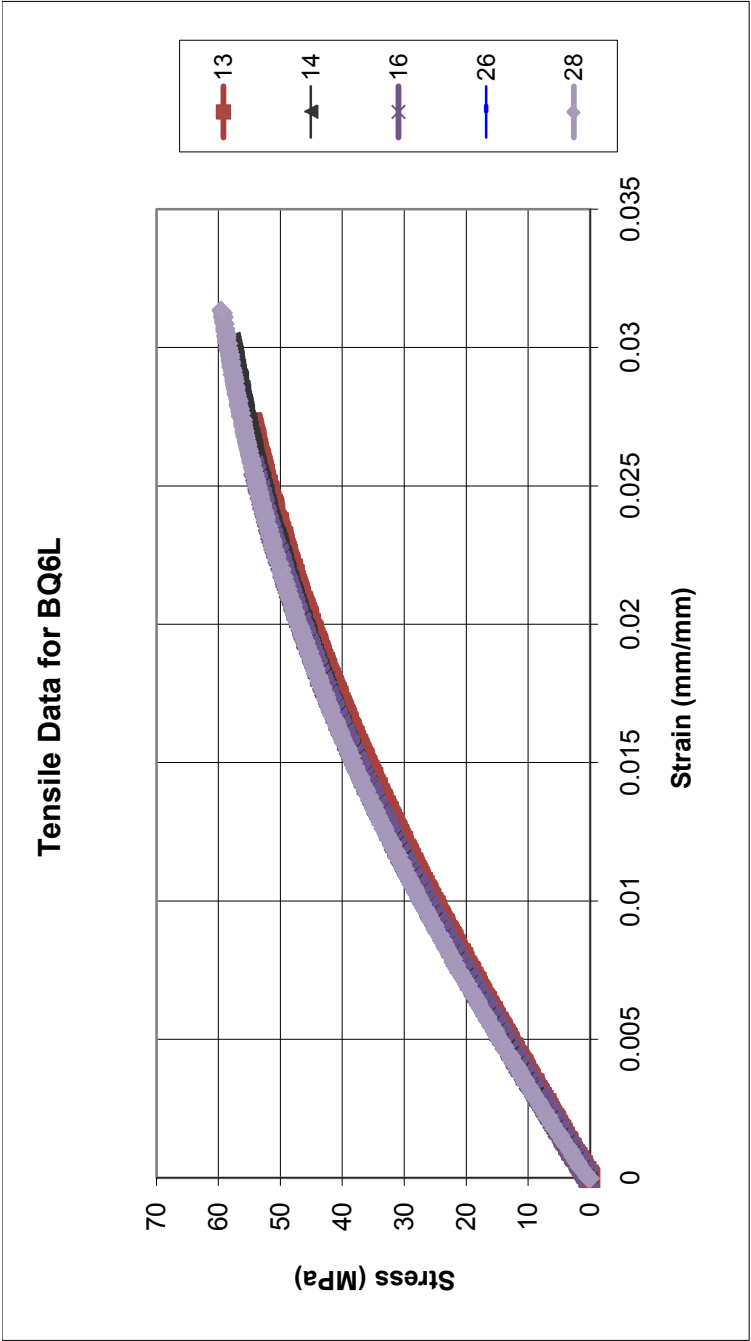


Figure J.7: Tensile Results for BQ6L: 6 wt% fibrils (carbon nanotubes) in Lexan HF1130-111: Injection Molded 5-26-09

Table J.7: Tensile Results for BQ6L: 6 wt% fibrils (carbon nanotubes) in Lexan HF1130-111: Injection Molded 5-26-09

Sample	Specimen	Tensile Ultimate Stress (MPa)	Tensile Strain at Ultimate Stress (%)	Tensile Fracture Stress (MPa)	Tensile Strain at Fracture Stress (%)	Tensile Modulus (MPa)
BQ6L	13	54.595	2.73	54.595	2.73	2648.2
	14	57.594	3.01	57.594	3.01	2698.3
	16	54.355	2.57	54.355	2.57	2707.7
	26	51.835	2.37	51.835	2.37	2759.6
	28	59.514	3.13	59.514	3.13	2897.9
Average		55.58	2.76	55.58	2.76	2742.34
Standard Deviation		3.00	0.31	3.00	0.31	95.52
Number		5	5	5	5	5

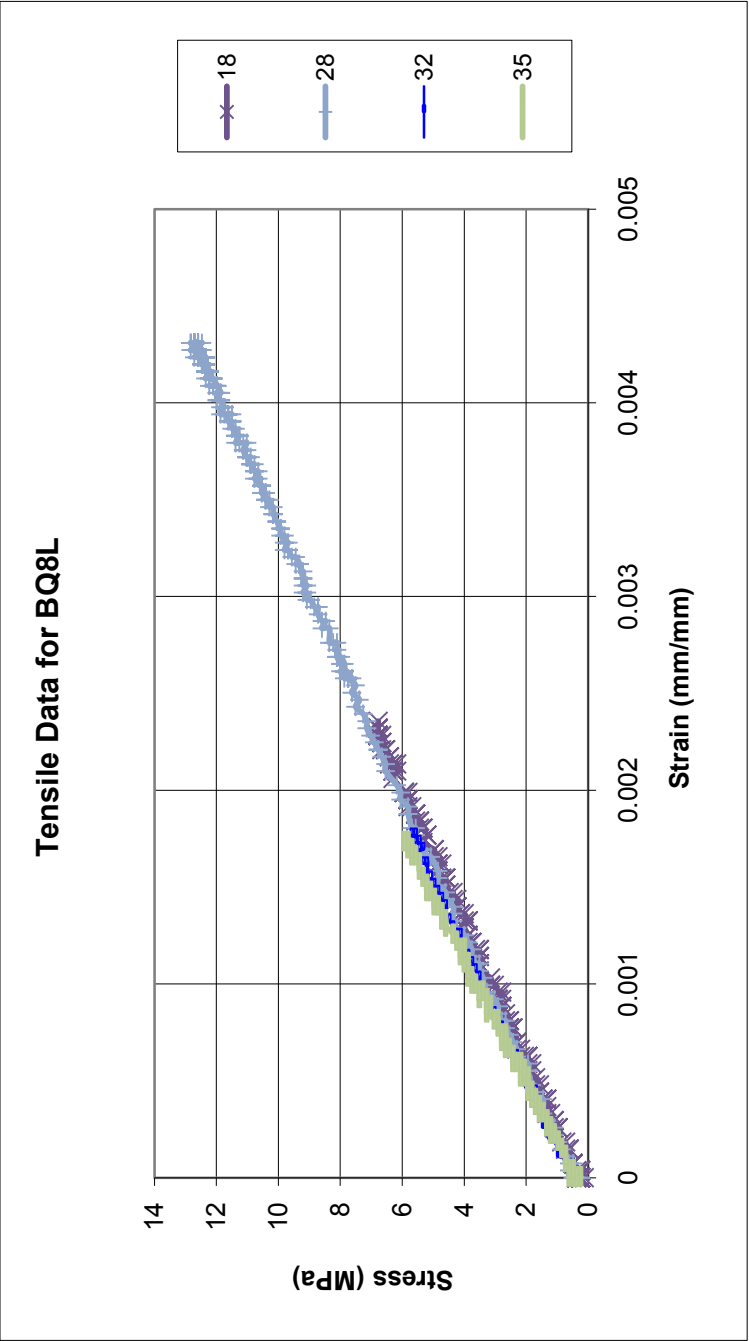


Figure J.8: Tensile Results for BQ8L: 8 wt% fibrils (carbon nanotubes) in Lexan HF1130-111: Injection Molded 5-26-09

Table J.8: Tensile Results for BQ8L: 8 wt% fibrils (carbon nanotubes) in Lexan HF1130-111: Injection Molded 5-26-09 (all these samples broke in the grips)

Sample	Specimen	Tensile Ultimate Stress (MPa)	Tensile Strain at Ultimate Stress (%)	Tensile Fracture Stress (MPa)	Tensile Strain at Fracture Stress (%)	Tensile Modulus (MPa)
BQ8L	18	7.628	0.26	5.327	0.13	2842.2
	28	12.834	0.43	11.139	0.36	2842.6
	32	6.296	0.20	5.327	0.12	2911.9
	35	6.175	0.18	2.906	0.01	3149.3
Average		8.23	0.27	6.17	0.15	2936.50
Standard Deviation		3.14	0.11	3.50	0.15	145.60
Number		4	4	4	4	4

Appendix J.2: Polycarbonate with Carbon Black

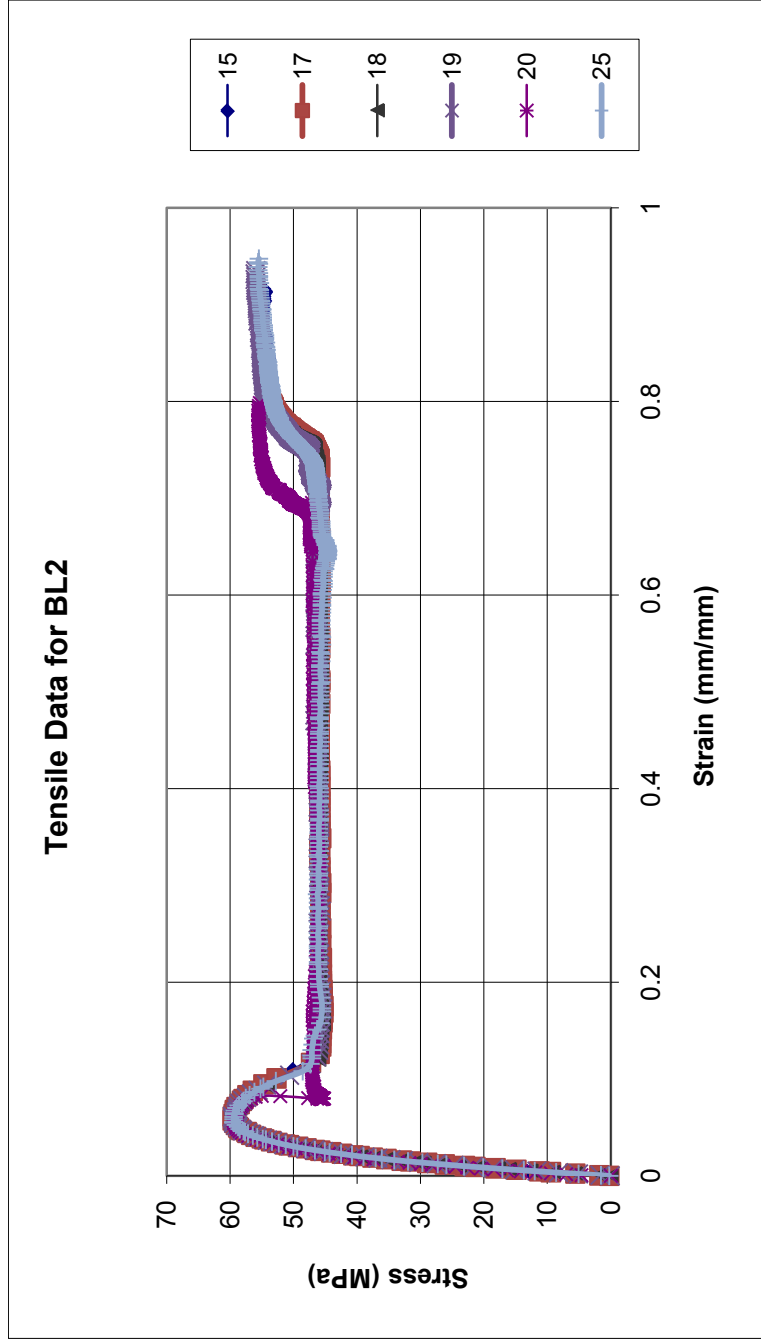


Figure J.9: Tensile Results for BL2: Lexan HF1130-111: Injection Molded 12-4-09

Table J.9: Tensile Results for BL2: Lexan HF1130-111: Injection Molded 12-4-09

Sample	Specimen	Tensile Ultimate Stress (MPa)	Tensile Strain at Ultimate Stress (%)	Tensile Fracture Stress (MPa)	Tensile Strain at Fracture Stress (%)	Tensile Modulus (MPa)
BL2	15	59.701	5.62	55.220	92.33	2301
	17	59.580	5.73	54.978	88.66	2162.6
	18	59.338	5.51	55.584	90.19	2190
	19	59.580	5.88	56.068	92.58	2221.5
	20	59.459	5.75	55.462	78.79	2166
	25	59.459	5.48	55.584	93.55	2147.6
Average		59.52	5.66	55.48	89.35	2198.12
Standard Deviation		0.13	0.16	0.37	5.47	56.64
Number		6	6	6	6	6

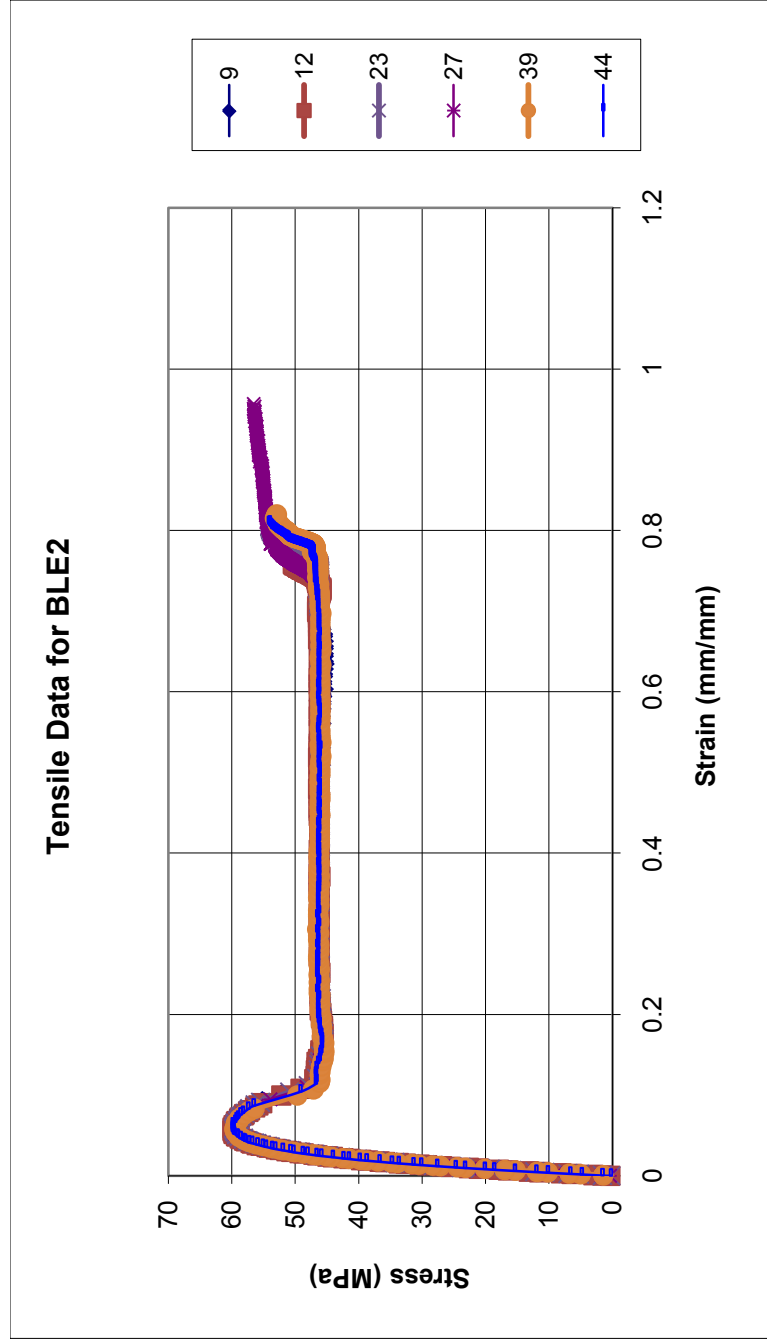


Figure J.10: Tensile Results for BLE2: Extruded Lexan HF1130-111: Extruded 11-5-09, Injection Molded 12-4-09

Table J.10: Tensile Results for BLE2: Extruded Lexan HF1130-111: Extruded 11-5-09, Injection Molded 12-4-09

Sample	Specimen	Tensile Ultimate Stress (MPa)	Tensile Strain at Ultimate Stress (%)	Tensile Fracture Stress (MPa)	Tensile Strain at Fracture Stress (%)	Tensile Modulus (MPa)
BLE2	9	59.822	5.55	54.130	81.09	2248.9
	12	59.822	5.52	53.404	77.82	2212.1
	23	59.701	5.78	54.009	80.62	2149.3
	27	59.822	5.62	56.552	95.07	2173.9
	39	59.580	5.78	53.041	81.65	2224.8
	44	59.822	5.55	54.252	81.17	2294.5
Average		59.76	5.63	54.23	82.90	2217.25
Standard Deviation		0.10	0.12	1.23	6.12	52.06
Number		6	6	6	6	6

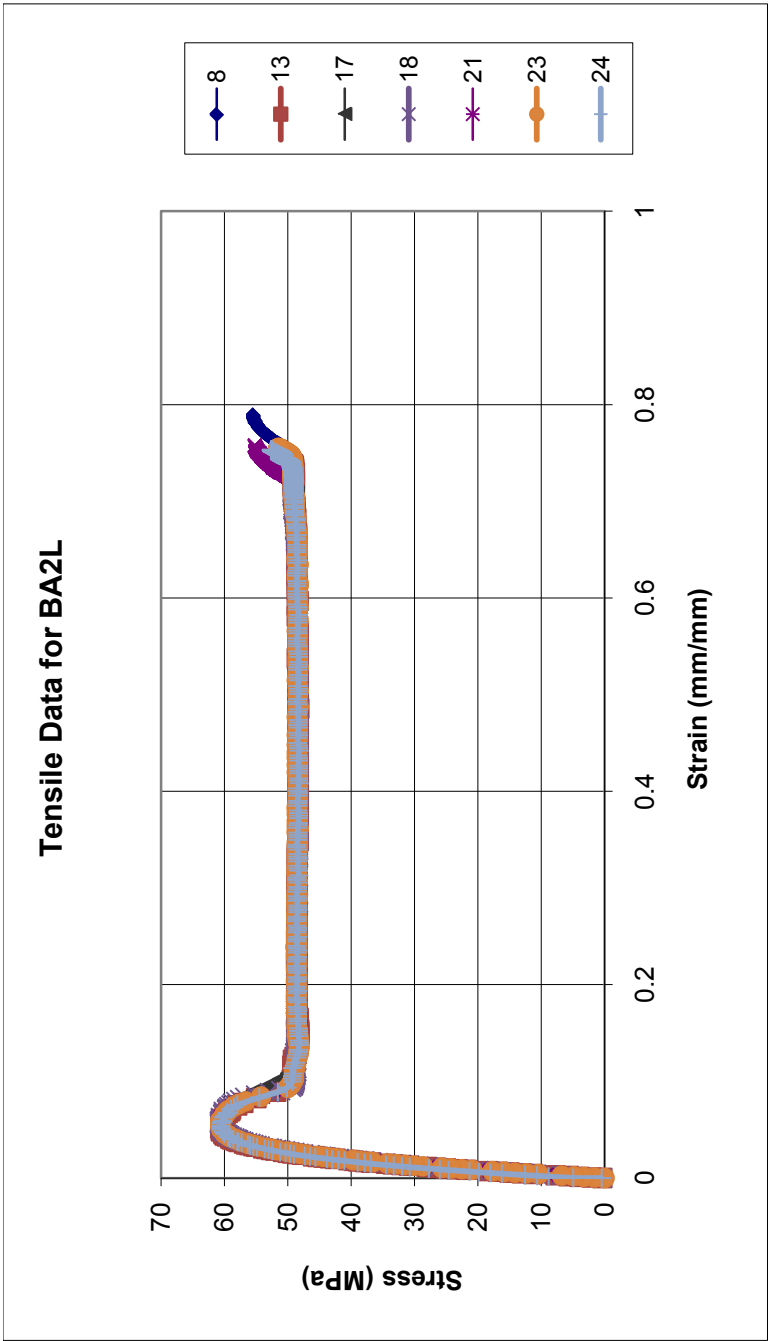


Figure J.11: Tensile Results for BA2L: 2 wt% Ketjenblack EC-600 JD (carbon black) in Lexan HF1130-111: Injection Molded 12-4-09

Table J.11: Tensile Results for BA2L: 2 wt% Ketjenblack EC-600 JD (carbon black) in Lexan HF1130-111: Injection Molded 12-4-09

Sample	Specimen	Tensile Ultimate Stress (MPa)	Tensile Strain at Ultimate Stress (%)	Tensile Fracture Stress (MPa)	Tensile Strain at Fracture Stress (%)	Tensile Modulus (MPa)
BA2L	8	60.791	5.34	55.462	78.72	2222.5
	13	60.670	5.17	51.466	74.72	2332.7
	17	60.912	5.58	50.740	74.10	2282.8
	18	60.791	5.60	49.650	73.83	2217.2
	21	60.912	5.28	55.220	75.67	2229
	23	60.670	5.41	51.466	75.49	2281.8
	24	60.549	5.15	52.556	75.26	2266.1
Average		60.76	5.36	52.37	75.40	2261.73
Standard Deviation		0.13	0.18	2.21	1.62	41.82
Number		7	7	7	7	7

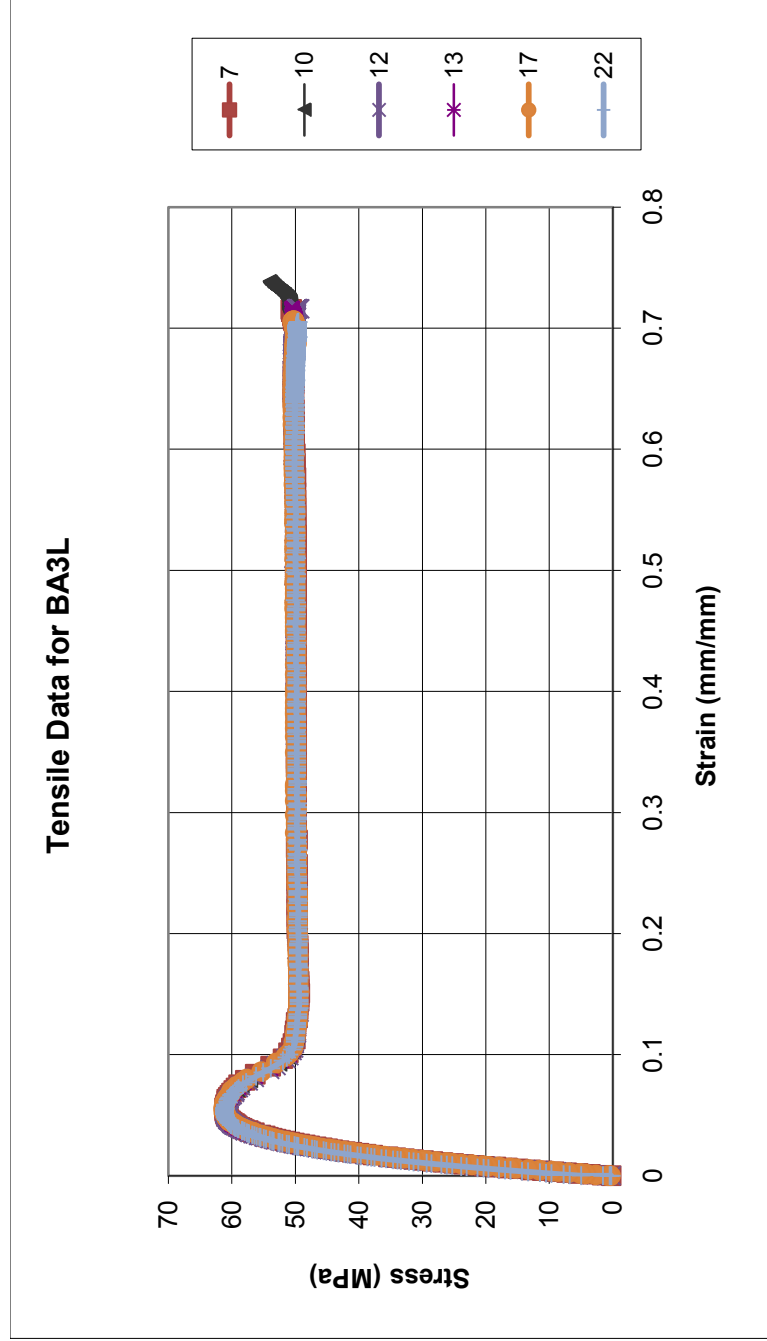


Figure J.12: Tensile Results for BA3L: 3 wt% Ketjenblack EC-600 JD (carbon black) in Lexan HF1130-111: Injection Molded 12-4-09

Table J.12: Tensile Results for BA3L: 3 wt% Ketjenblack EC-600 JD (carbon black) in Lexan HF1130-111: Injection Molded 12-4-09

Sample	Specimen	Tensile Ultimate Stress (MPa)	Tensile Strain at Ultimate Stress (%)	Tensile Fracture Stress (MPa)	Tensile Strain at Fracture Stress (%)	Tensile Modulus (MPa)
BA3L	7	61.154	5.35	51.103	72.11	2257.3
	10	60.912	5.09	54.009	73.77	2307.5
	12	61.154	5.17	49.529	71.61	2341.5
	13	61.154	5.02	50.498	71.67	2408
	17	61.275	5.22	50.255	70.62	2248.1
	22	61.154	5.07	49.650	70.27	2247.9
Average		61.13	5.15	50.84	71.67	2301.72
Standard Deviation		0.12	0.12	1.66	1.24	64.27
Number		6	6	6	6	6

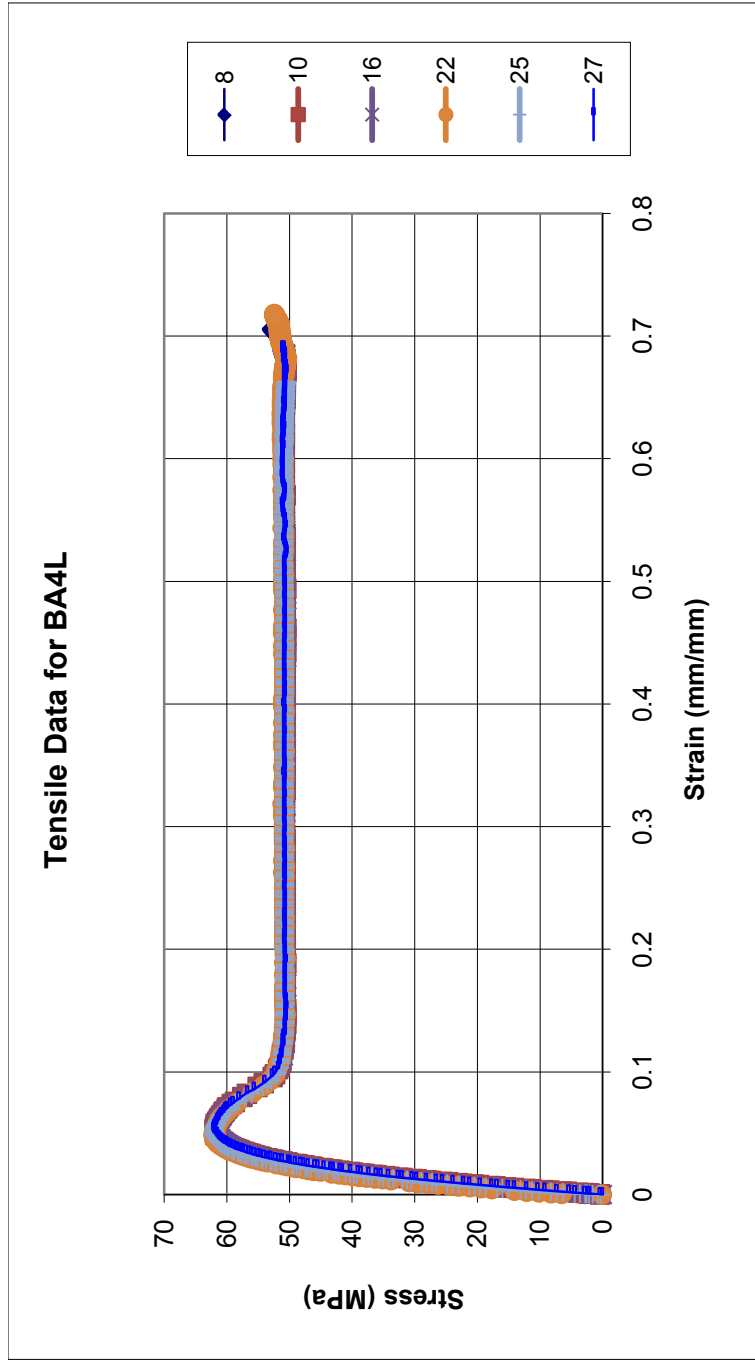


Figure J.13: Tensile Results for BA4L: 4 wt% Ketjenblack EC-600 JD (carbon black) in Lexan HF1130-111: Injection Molded
12-4-09

Table J.13: Tensile Results for BA4L: 4 wt% Ketjenblack EC-600 JD (carbon black) in Lexan HF1130-111: Injection Molded 12-4-09

Sample	Specimen	Tensile Ultimate Stress (MPa)	Tensile Strain at Ultimate Stress (%)	Tensile Fracture Stress (MPa)	Tensile Strain at Fracture Stress (%)	Tensile Modulus (MPa)
BA4L	8	61.760	4.90	53.283	70.57	2389.5
	10	62.002	5.32	50.376	68.93	2350.9
	16	61.881	5.20	50.740	68.50	2327.4
	22	62.123	4.89	52.435	71.71	2450.1
	25	62.123	5.06	50.498	66.03	2479.1
	27	62.123	5.25	50.982	69.12	2304.4
Average		62.00	5.10	51.39	69.14	2383.57
Standard Deviation		0.15	0.18	1.19	1.94	69.39
Number		6	6	6	6	6

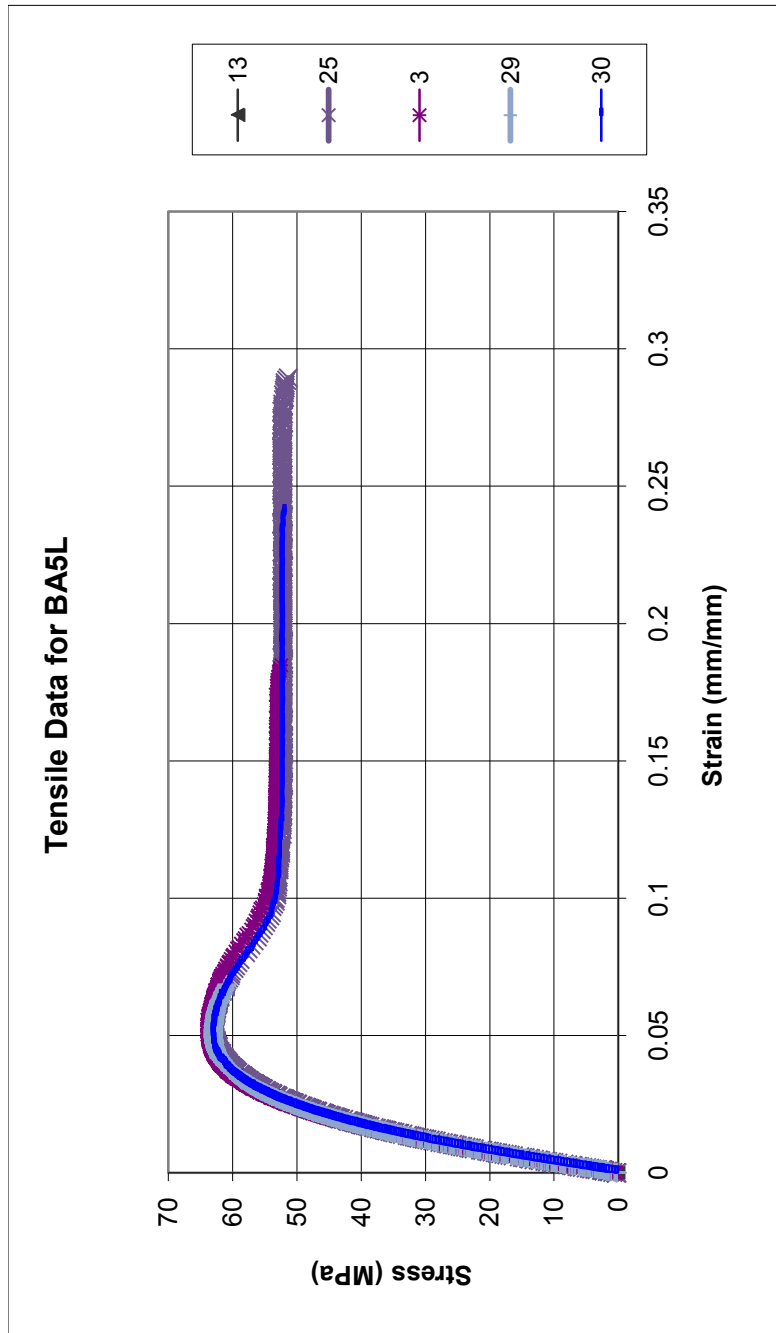


Figure J.14: Tensile Results for BA5L: 5 wt% Ketjenblack EC-600 JD (carbon black) in Lexan HF1130-111: Injection Molded 12-4-09

Table J.14: Tensile Results for BA5L: 5 wt% Ketjenblack EC-600 JD (carbon black) in Lexan HF1130-111: Injection Molded 12-4-09

Sample	Specimen	Tensile Ultimate Stress (MPa)	Tensile Strain at Ultimate Stress (%)	Tensile Fracture Stress (MPa)	Tensile Strain at Fracture Stress (%)	Tensile Modulus (MPa)
BA5L	13	63.092	4.79	63.092	4.79	2570.1
	25	62.971	5.01	51.587	28.85	2546.7
	3	63.917	5.03	52.659	18.30	2551.3
	29	63.092	4.92	60.912	6.83	2604.8
	30	63.092	5.00	51.224	24.81	2609.3
Average		63.23	4.95	55.89	16.72	2576.44
Standard Deviation		0.39	0.10	5.65	10.67	29.33
Number		5	5	5	5	5

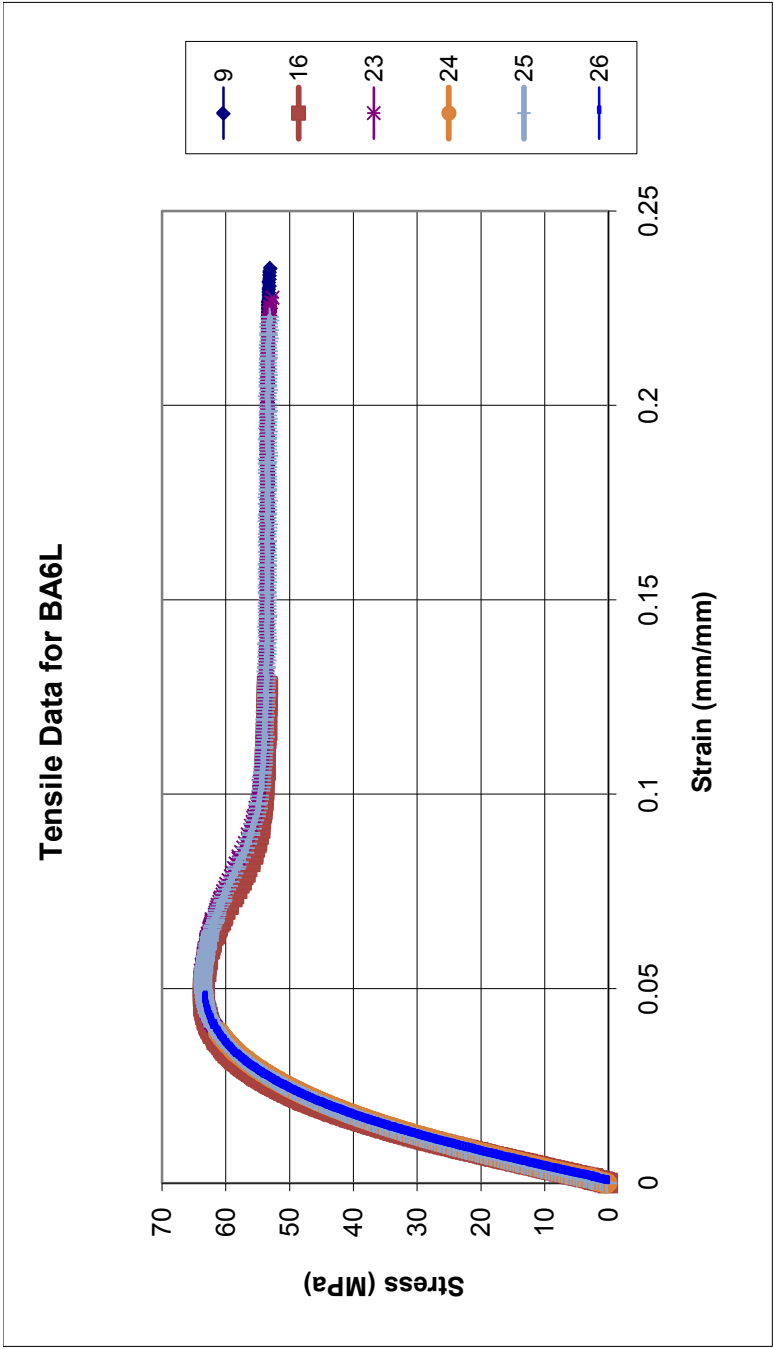


Figure J.15: Tensile Results for BA6L: 6 wt% Ketjenblack EC-600 JD (carbon black) in Lexan HF1130-111: Injection Molded 12-4-09

Table J.15: Tensile Results for BA6L: 6 wt% Ketjenblack EC-600 JD (carbon black) in Lexan HF1130-111: Injection Molded 12-4-09

Sample	Specimen	Tensile Ultimate Stress (MPa)	Tensile Strain at Ultimate Stress (%)	Tensile Fracture Stress (MPa)	Tensile Strain at Fracture Stress (%)	Tensile Modulus (MPa)
BA6L	9	63.818	5.19	53.162	23.08	2598.8
	16	63.576	4.78	53.041	16.78	2662.9
	23	63.939	5.29	52.919	22.65	2550.3
	24	61.154	3.87	61.154	3.87	2609.4
	25	63.576	5.01	53.162	21.93	2670.3
	26	63.455	4.80	63.455	4.80	2667.2
Average		63.25	4.82	56.15	15.52	2626.48
Standard Deviation		1.04	0.51	4.82	8.96	48.51
Number		6	6	6	6	6

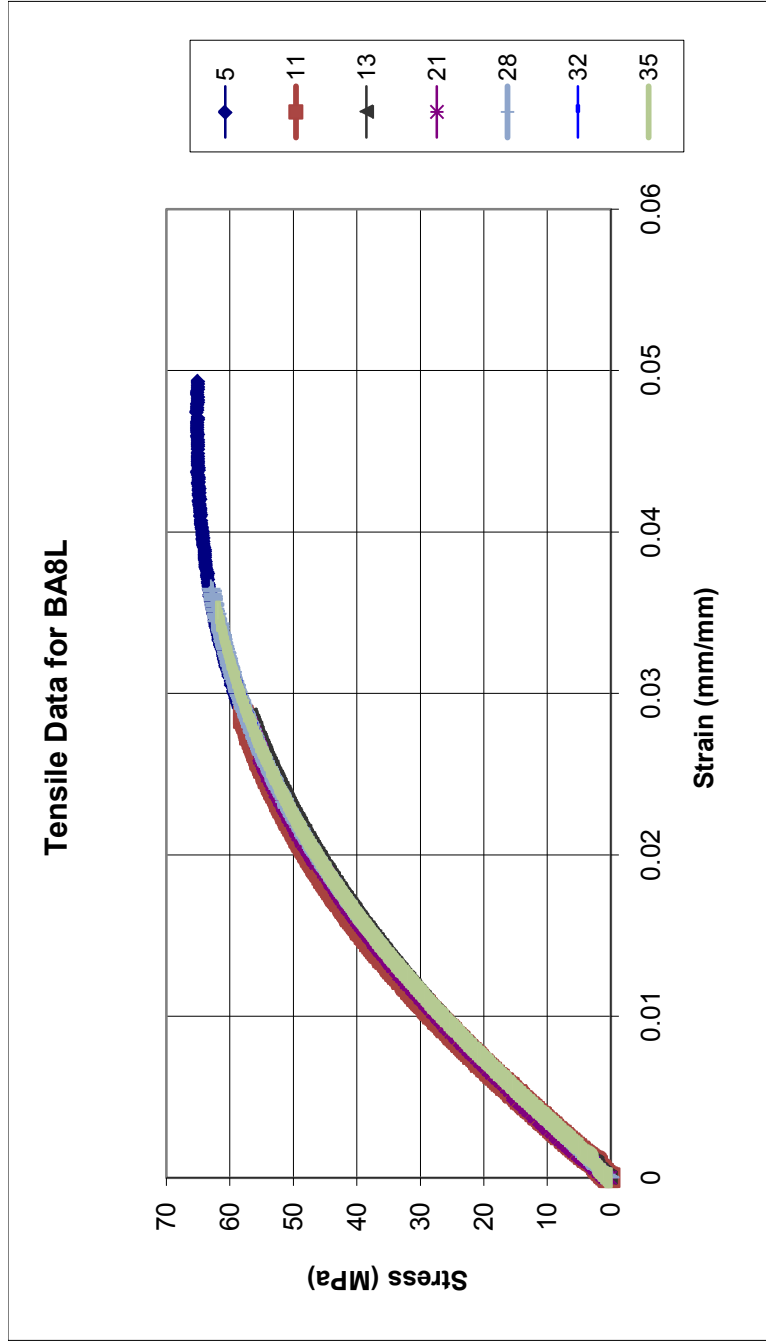


Figure J.16: Tensile Results for BA8L: 8 wt% Ketjenblack EC-600 JD (carbon black) in Lexan HF1130-111: Injection Molded 12-4-09

Table J.16: Tensile Results for BA8L: 8 wt% Ketjenblack EC-600 JD (carbon black) in Lexan HF1130-111: Injection Molded 12-4-09

Sample	Specimen	Tensile Ultimate Stress (MPa)	Tensile Strain at Ultimate Stress (%)	Tensile Fracture Stress (MPa)	Tensile Strain at Fracture Stress (%)	Tensile Modulus (MPa)
BA8L	5	65.271	4.74	65.029	4.89	2823.7
	11	61.760	3.39	61.760	3.39	2864.9
	13	56.795	2.86	56.795	2.86	2784.8
	21	57.037	2.83	57.037	2.83	2748.1
	28	62.971	3.65	62.971	3.65	2693.3
	32	59.095	3.11	59.095	3.11	2834.6
Average	35	61.517	3.44	61.881	3.49	2722.2
		60.64	3.43	60.65	3.46	2781.66
		3.14	0.65	3.10	0.70	63.22
Standard Deviation						
Number		7	7	7	7	7

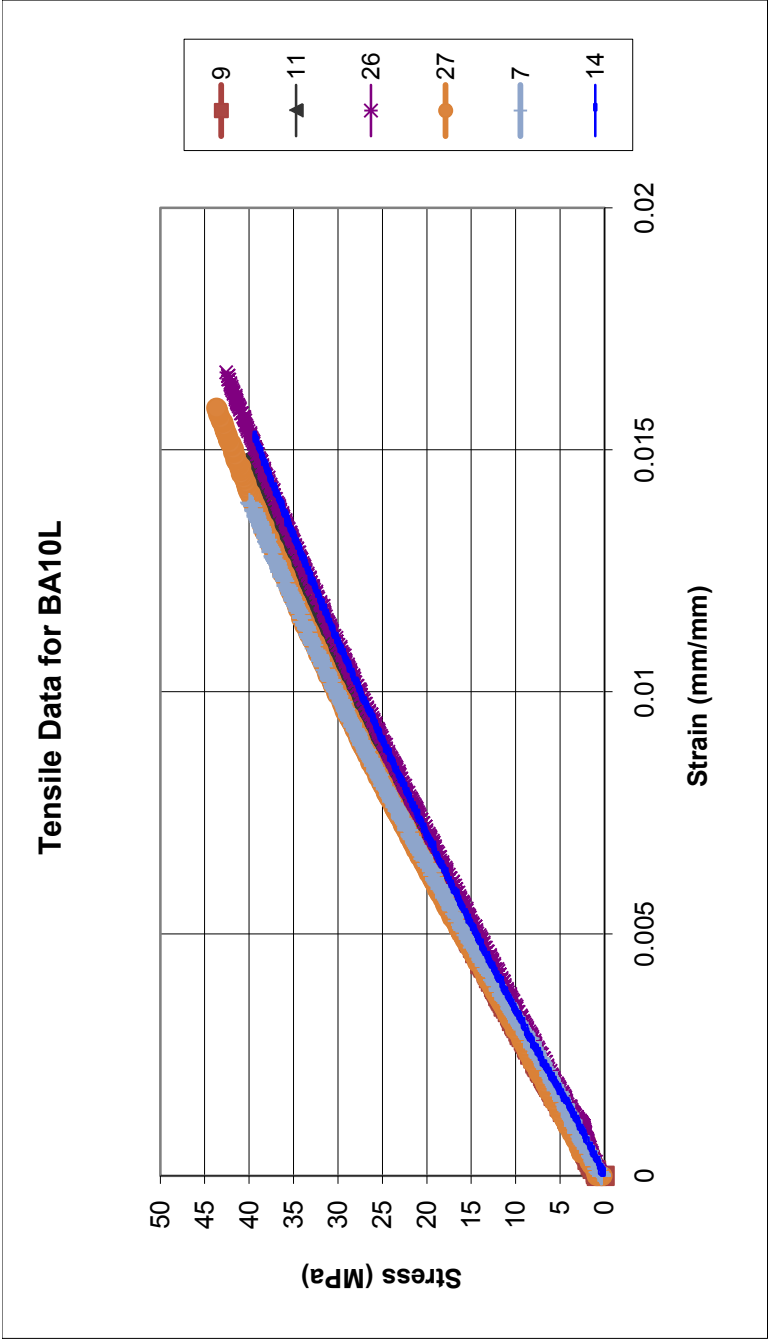


Figure J.17: Tensile Results for BA10L: 10 wt% Ketjenblack EC-600 JD (carbon black) in Lexan HF1130-111: Injection Molded 12-4-09

Table J.17: Tensile Results for BA10L: 10 wt% Ketjenblack EC-600 JD (carbon black) in Lexan HF1130-111: Injection Molded 12-4-09

Sample	Specimen	Tensile Ultimate Stress (MPa)	Tensile Strain at Ultimate Stress (%)	Tensile Fracture Stress (MPa)	Tensile Strain at Fracture Stress (%)	Tensile Modulus (MPa)
BA10L	9	44.022	1.67	44.022	1.67	3081.6
	11	40.443	1.48	40.443	1.48	3057.3
	26	42.710	1.66	42.710	1.66	2878.4
	27	43.664	1.59	43.664	1.59	2978.5
	7	39.962	1.39	39.962	1.39	2873.7
	14	39.966	1.55	39.966	1.55	3001.6
Average		41.79	1.56	41.79	1.56	2978.52
Standard Deviation		1.89	0.11	1.89	0.11	87.61
Number		6	6	6	6	6

Appendix J.3: Polycarbonate with Graphite Nanoparticles

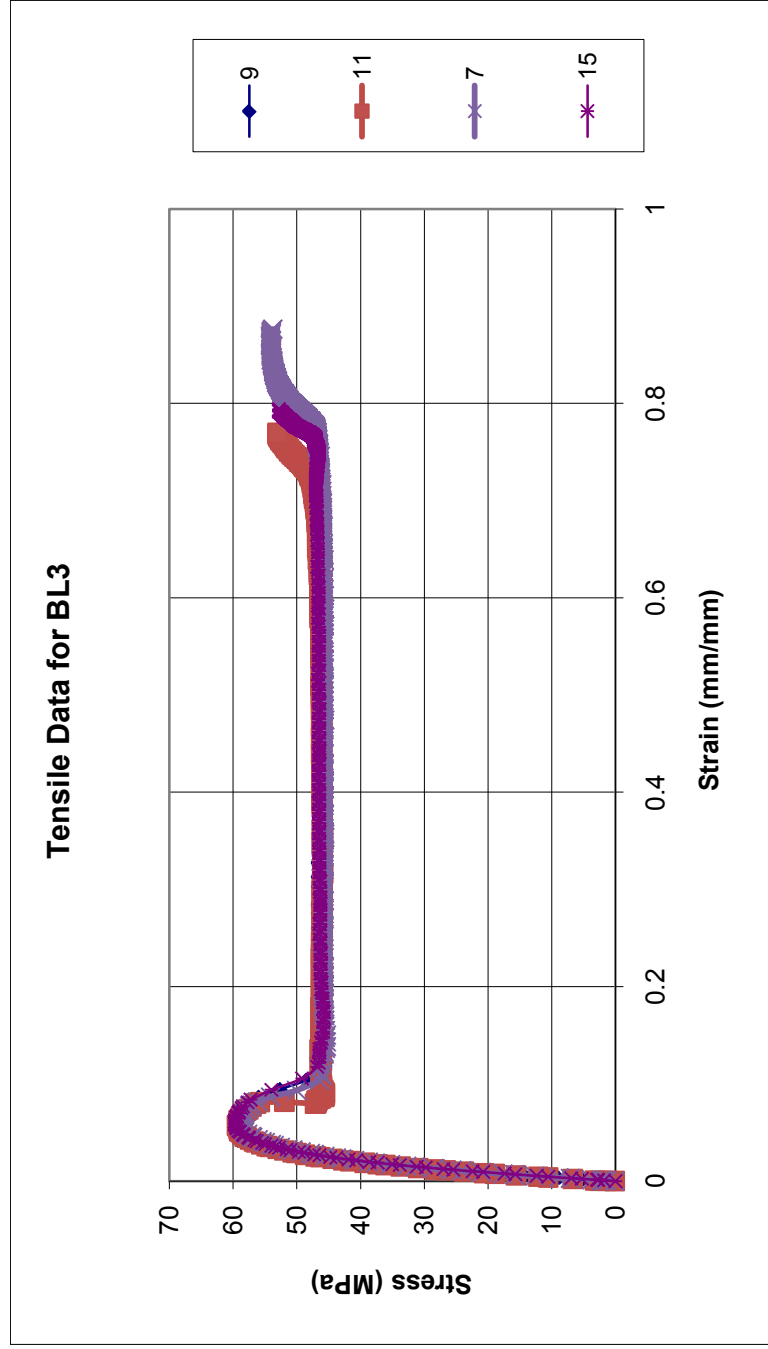


Figure J.18: Tensile Results for BL3: Lexan HF1130-111: Injection Molded 6-3-10

Table J.18: Tensile Results for BL3: Lexan HF1130-111: Injection Molded 6-3-10

Sample	Specimen	Tensile Ultimate Stress (MPa)	Tensile Strain at Ultimate Stress (%)	Tensile Fracture Stress (MPa)	Tensile Strain at Fracture Stress (%)	Tensile Modulus (MPa)
BL3	9	59.755	5.72	49.796	78.52	2217.50
	11	59.395	5.73	54.476	84.47	2309.40
	7	58.805	5.62	53.884	87.53	2200.00
	15	59.755	5.89	52.796	79.20	2159.50
Average		59.43	5.74	52.74	82.43	2221.60
Standard Deviation		0.45	0.11	2.08	4.31	63.37
Number		4	4	4	4	4

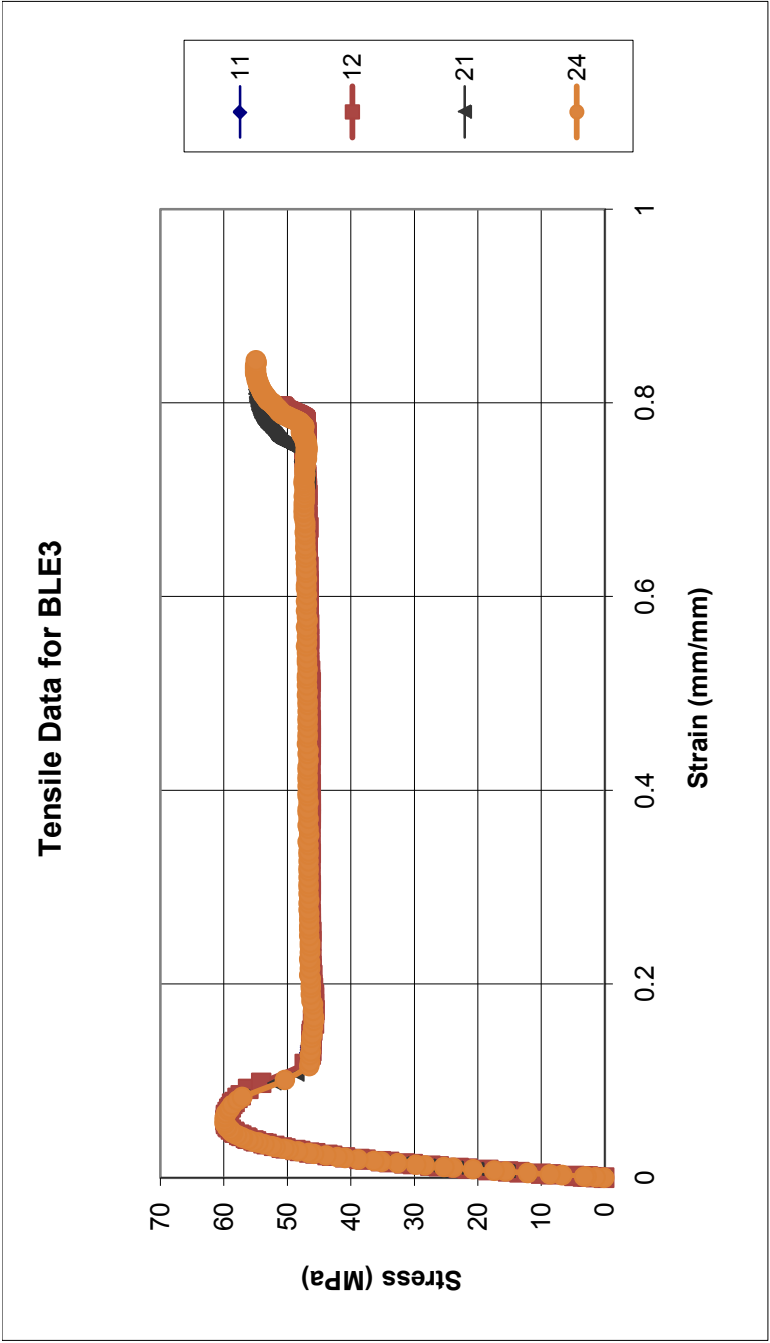


Figure J.19: Tensile Results for BLE3: Extruded Lexan HF1130-111: Extruded 5-26-10, Injection Molded 6-3-10

Table J.19: Tensile Results for BLE3: Extruded Lexan HF1130-111: Extruded 5-26-10, Injection Molded 6-3-10

Sample	Specimen	Tensile Ultimate Stress (MPa)	Tensile Strain at Ultimate Stress (%)	Tensile Fracture Stress (MPa)	Tensile Strain at Fracture Stress (%)	Tensile Modulus (MPa)
BLE3	11	60.235	5.86	48.356	78.82	2307.6
	12	59.755	5.94	53.876	81.31	2216.5
	21	60.115	5.73	54.956	80.96	2297.6
	24	59.875	5.56	54.956	83.95	2233.3
Average		60.00	5.77	53.04	81.26	2263.75
Standard Deviation		0.22	0.16	3.16	2.10	45.56
Number		4	4	4	4	4

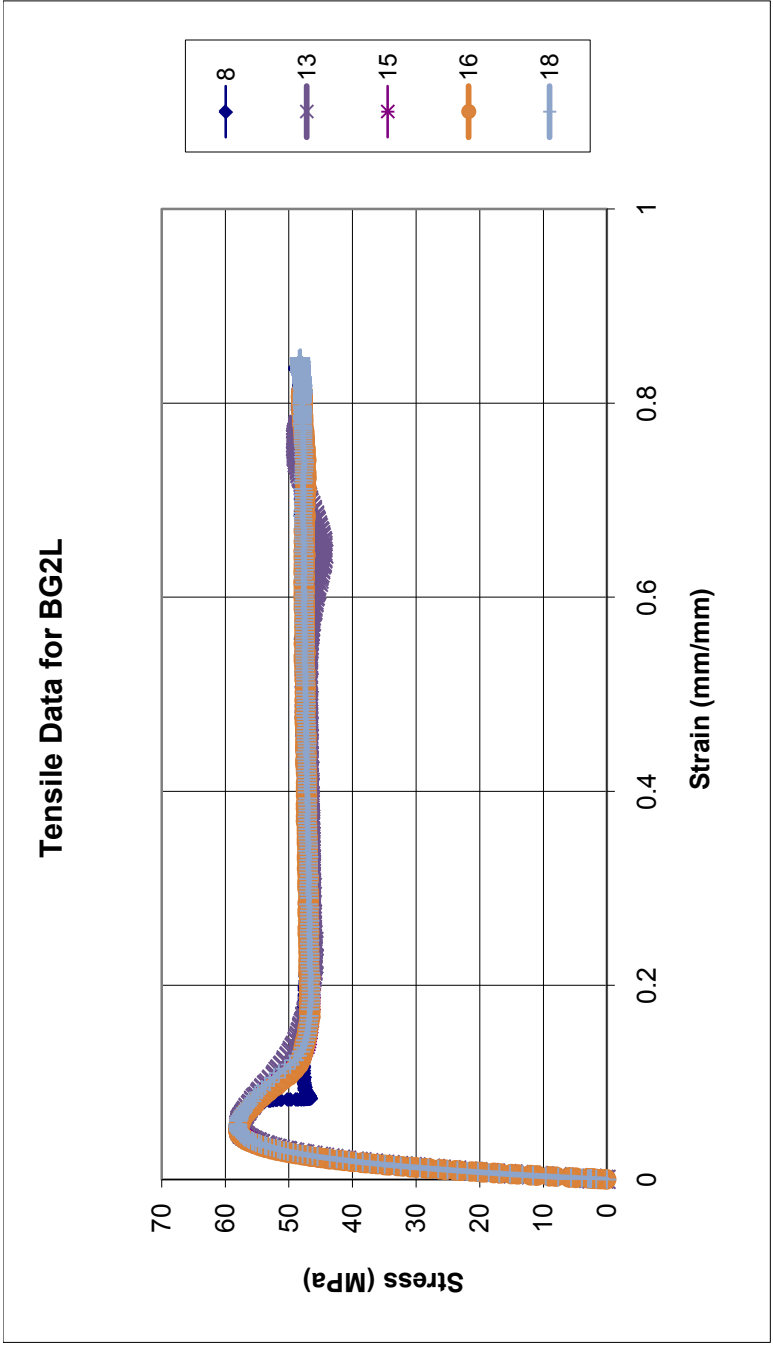


Figure J.20: Tensile Results for BG2L: 2 wt% xGnP in Lexan HF1130-111: Injection Molded 6-3-10, Extruded 5-26-10

Table J.20: Tensile Results for BG2L: 2 wt% xGnP in Lexan HF1130-111: Injection Molded 6-3-10, Extruded 5-26-10

Sample	Specimen	Tensile Ultimate Stress (MPa)	Tensile Strain at Ultimate Stress (%)	Tensile Fracture Stress (MPa)	Tensile Strain at Fracture Stress (%)	Tensile Modulus (MPa)
BG2L	8	58.436	5.27	48.956	83.53	2483.4
	13	57.836	5.19	48.476	77.55	2461
	15	57.836	5.38	47.996	81.37	2487.7
	16	57.956	5.01	47.996	81.11	2599.6
	18	58.076	5.42	48.236	84.60	2536.3
Average		58.03	5.25	48.33	81.63	2513.60
Standard Deviation		0.25	0.16	0.40	2.71	55.36
Number		5	5	5	5	5

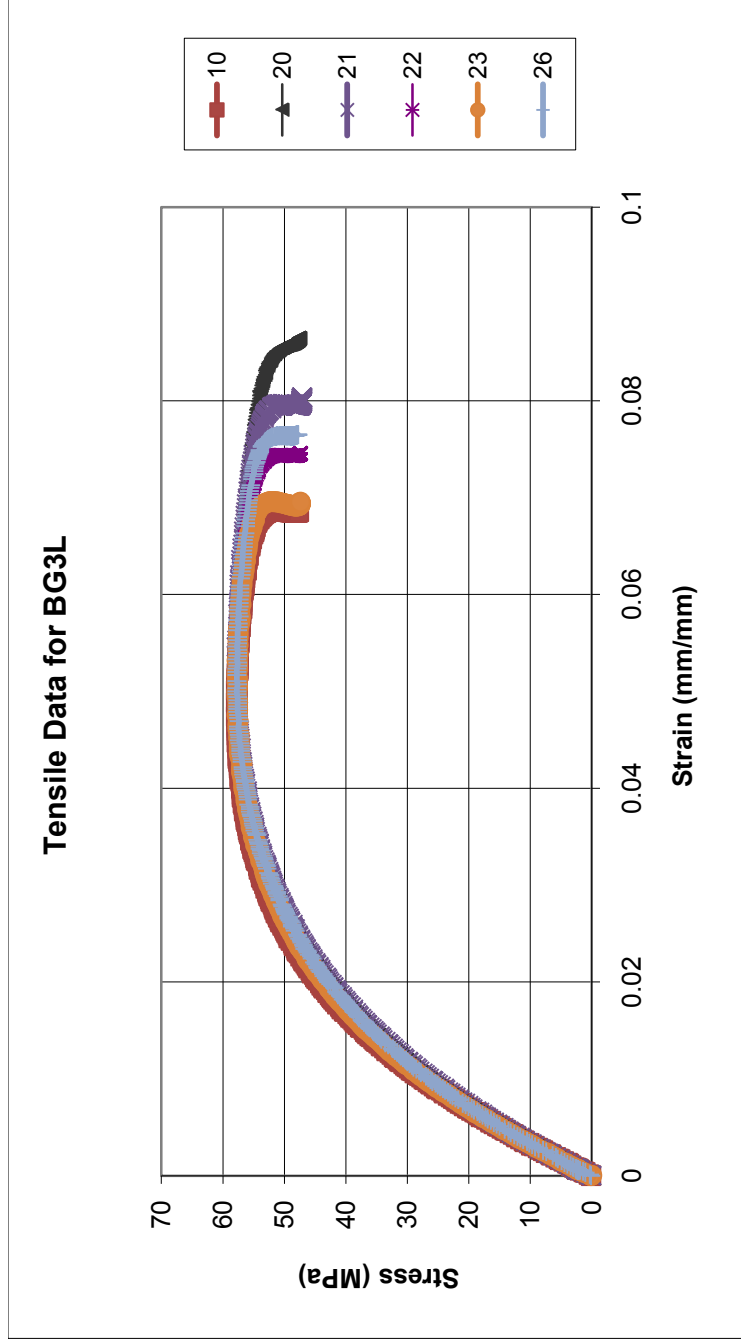


Figure J.21: Tensile Results for BG3L: 3 wt% xGnP in Lexan HF1130-111: Injection Molded 6-3-10, Extruded 5-26-10

Table J.21: Tensile Results for BG3L: 3 wt% xGnP in Lexan HF1130-111: Injection Molded 6-3-10, Extruded 5-26-10

Sample	Specimen	Tensile Ultimate Stress (MPa)	Tensile Strain at Ultimate Stress (%)	Tensile Fracture Stress (MPa)	Tensile Strain at Fracture Stress (%)	Tensile Modulus (MPa)
BG3L	10	57.836	4.74	46.676	6.88	2816.7
	20	57.836	5.05	46.196	8.69	2709.5
	21	57.836	5.11	46.916	8.07	2664.1
	22	57.716	5.01	46.316	7.45	2770.6
	23	57.716	4.76	47.276	7.05	2779.5
	26	57.716	4.97	47.156	7.87	2701.8
Average		57.78	4.94	46.76	7.67	2740.37
Standard Deviation		0.07	0.15	0.44	0.68	57.50
Number		6	6	6	6	6

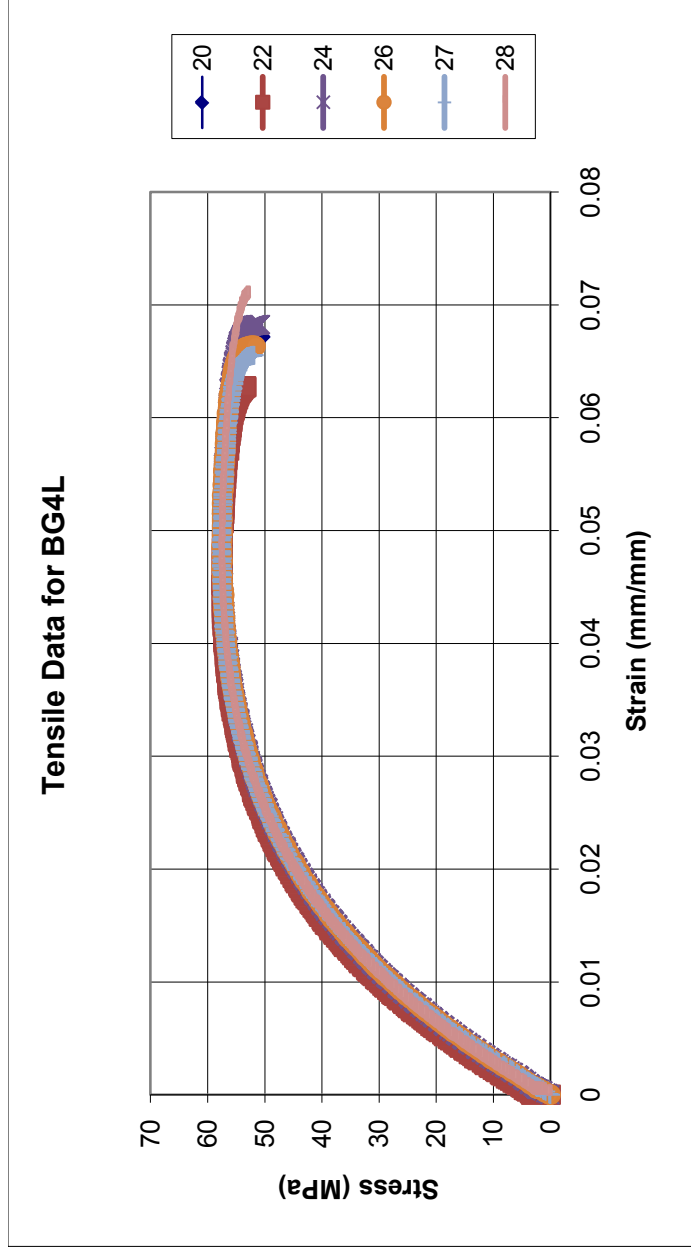


Figure J.22: Tensile Results for BG4L: 4 wt% xGnP in Lexan HF1130-111: Injection Molded 6-3-10, Extruded 5-26-10

Table J.22: Tensile Results for BG4L: 4 wt% xGnP in Lexan HF1130-111: Injection Molded 6-3-10, Extruded 5-26-10

Sample	Specimen	Tensile Ultimate Stress (MPa)	Tensile Strain at Ultimate Stress (%)	Tensile Fracture Stress (MPa)	Tensile Strain at Fracture Stress (%)	Tensile Modulus (MPa)
BG4L	20	57.596	4.75	48.236	6.68	2834.5
	22	57.596	4.52	48.356	6.26	2832.4
	24	57.596	5.07	49.076	6.80	2858.2
	26	57.596	4.67	49.556	6.61	2877
	27	57.596	4.56	49.076	6.53	2883.9
	28	57.596	4.70	48.356	7.04	2827.7
Average		57.60	4.71	48.78	6.65	2852.28
Standard Deviation		0.00	0.20	0.54	0.26	24.34
Number		6	6	6	6	6

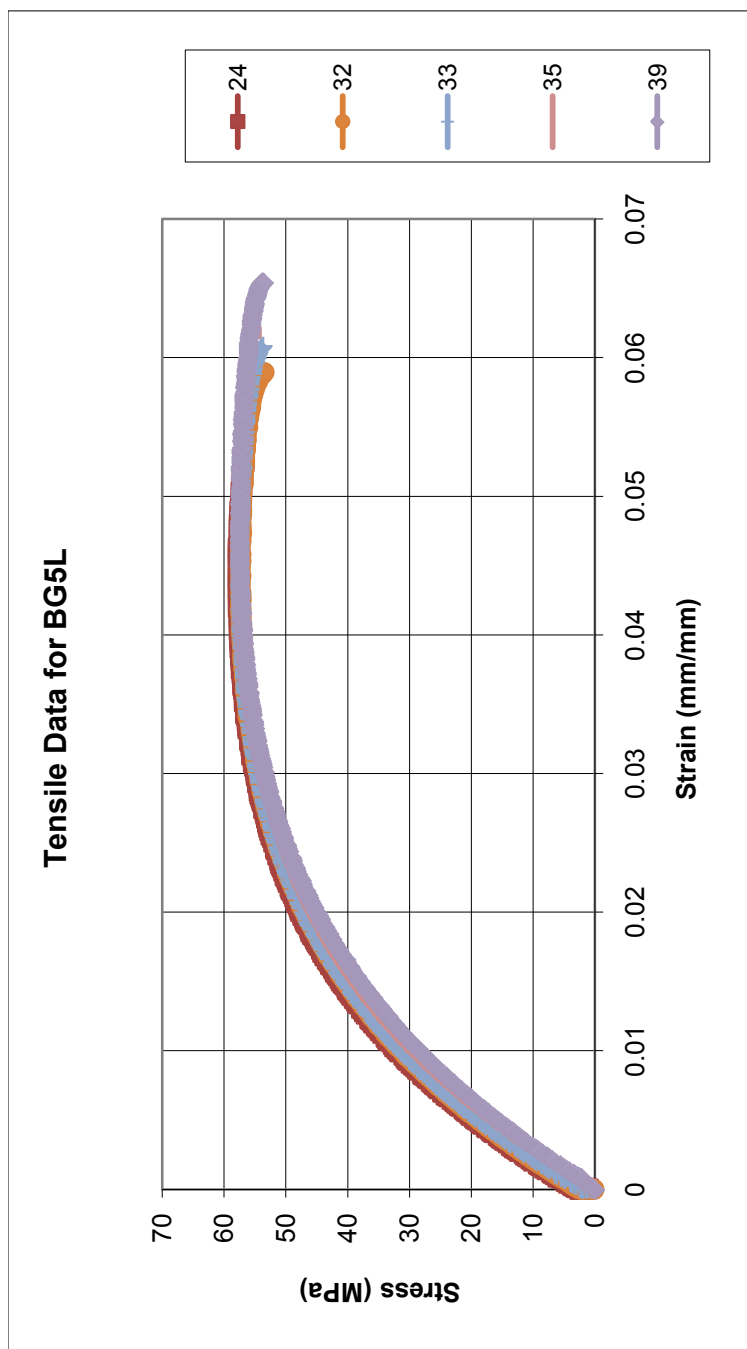


Figure J.23: Tensile Results for BG5L: 5 wt% xGnP in Lexan HF1130-111: Injection Molded 6-3-10, Extruded 5-26-10

Table J.23: Tensile Results for BG5L: 5 wt% xGnP in Lexan HF1130-111: Injection Molded 6-3-10, Extruded 5-26-10

Sample	Specimen	Tensile Ultimate Stress (MPa)	Tensile Strain at Ultimate Stress (%)	Tensile Fracture Stress (MPa)	Tensile Strain at Fracture Stress (%)	Tensile Modulus (MPa)
BG5L	24	57.716	4.20	53.036	5.82	3108.8
	32	57.356	4.16	52.076	5.91	3055.1
	33	57.476	4.18	52.676	6.10	3149.3
	35	57.596	4.41	54.836	6.16	3155.4
	39	57.476	3.90	53.756	6.54	3004.3
Average		57.52	4.17	53.28	6.10	3094.58
Standard Deviation		0.14	0.18	1.06	0.28	64.43
Number		5	5	5	5	5

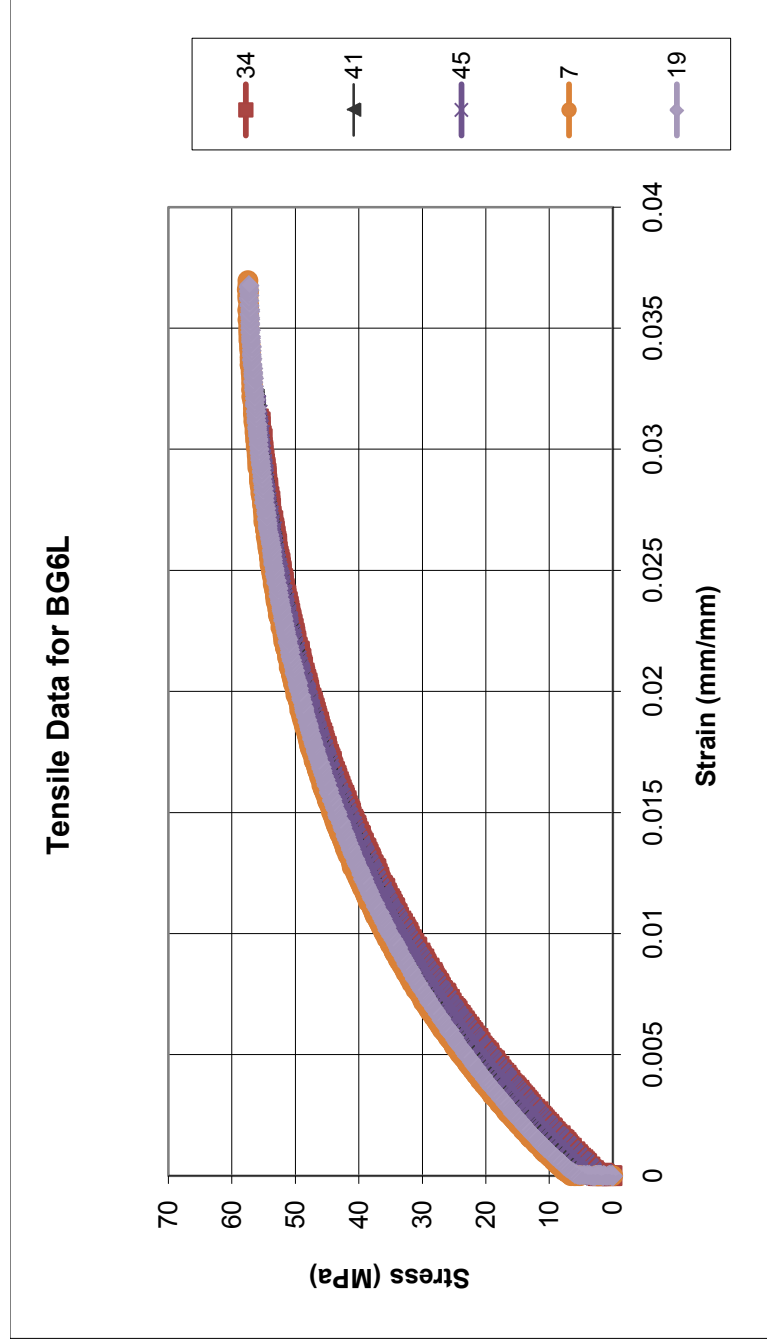


Figure J.24: Tensile Results for BG6L: 6 wt% xGnP in Lexan HF1130-111: Injection Molded 6-8-10, Extruded 5-27-10

Table J.24: Tensile Results for BG6L: 6 wt% xGnP in Lexan HF1130-111: Injection Molded 6-8-10, Extruded 5-27-10

Sample	Specimen	Tensile Ultimate Stress (MPa)	Tensile Strain at Ultimate Stress (%)	Tensile Fracture Stress (MPa)	Tensile Strain at Fracture Stress (%)	Tensile Modulus (MPa)
BG6L	34	57.476	3.74	57.476	3.74	3263.9
	41	56.156	3.21	56.156	3.21	3274.4
	45	56.156	3.14	56.156	3.16	3294.2
	7	57.596	3.66	57.476	3.63	3374.2
	19	57.356	3.69	57.356	3.62	3315.8
Average		56.95	3.49	56.92	3.47	3304.50
Standard Deviation		0.73	0.29	0.70	0.27	43.72
Number		5	5	5	5	5

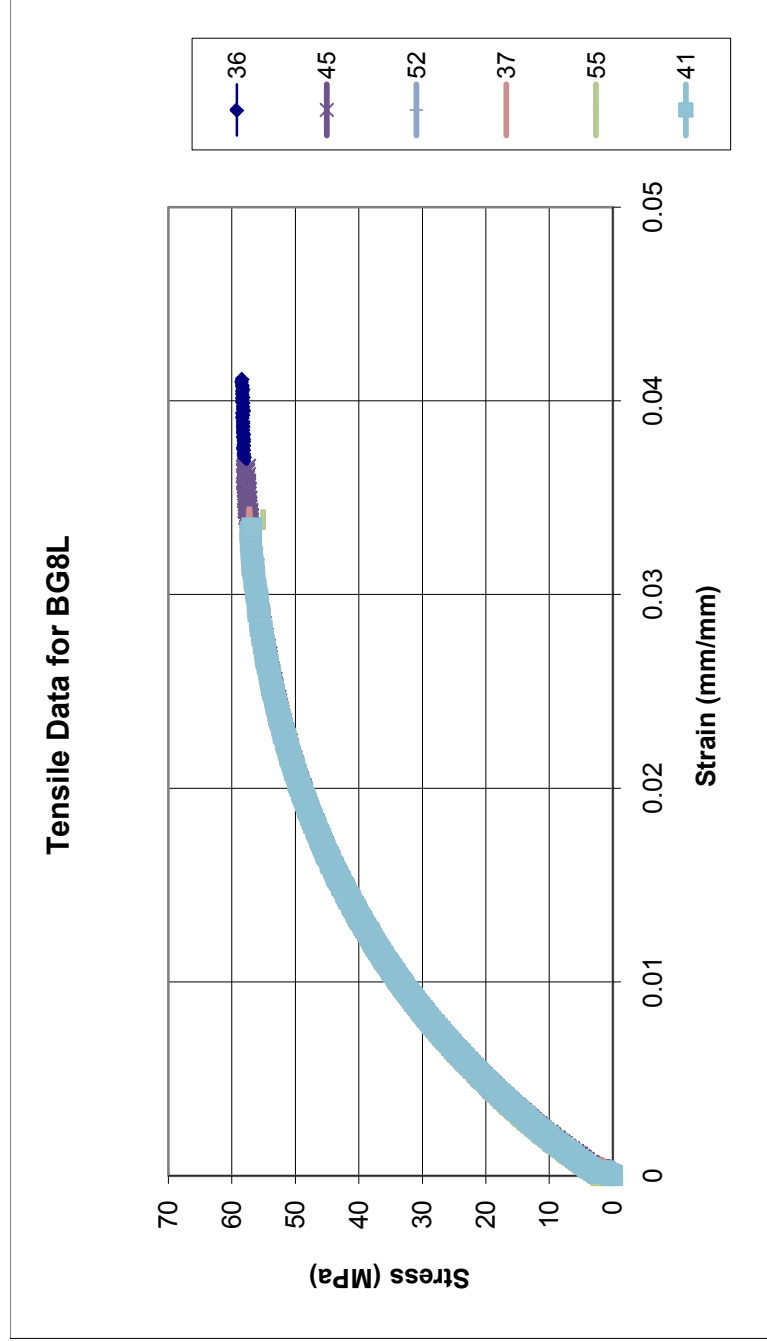


Figure J.25: Tensile Results for BG8L: 8 wt% xGnP in Lexan HF1130-111: Injection Molded 6-8-10, Extruded 5-27-10

Table J.25: Tensile Results for BG8L: 8 wt% xGnP in Lexan HF1130-111: Injection Molded 6-8-10, Extruded 5-27-10

Sample	Specimen	Tensile Ultimate Stress (MPa)	Tensile Strain at Ultimate Stress (%)	Tensile Fracture Stress (MPa)	Tensile Strain at Fracture Stress (%)	Tensile Modulus (MPa)
BG8L	36	58.445	4.10	58.445	4.10	3582
	45	57.836	3.59	57.836	3.60	3542.4
	52	56.996	3.29	56.996	3.29	3494.3
	37	57.365	3.37	57.245	3.35	3635.1
	55	57.596	3.31	57.596	3.31	3520.4
	41	57.116	3.27	57.116	3.31	3464.3
Average		57.56	3.49	57.54	3.49	3539.75
Standard Deviation		0.53	0.32	0.54	0.32	61.67
Number		6	6	6	6	6

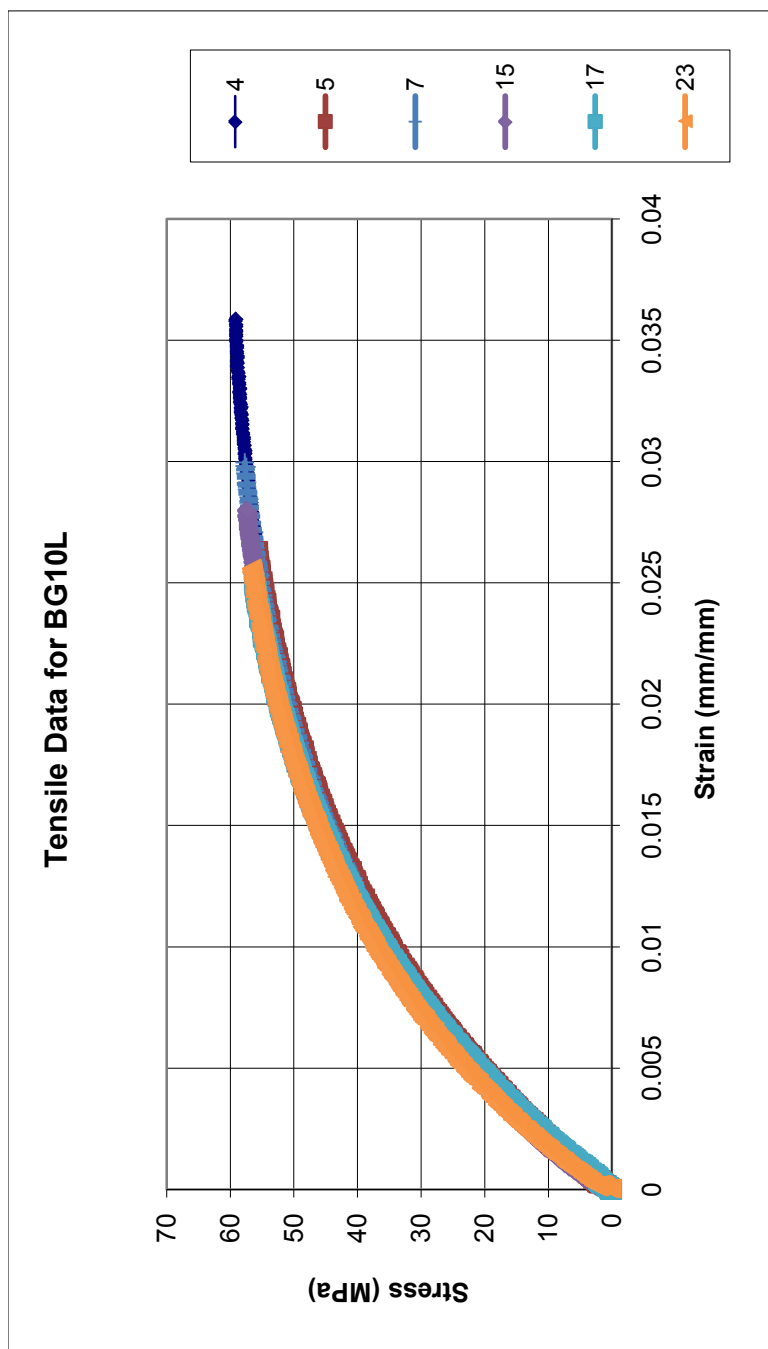


Figure J.26: Tensile Results for BG10L: 10 wt% xGnP in Lexan HF1130-111: Injection Molded 6-8-10, Extruded 5-27-10

Table J.26: Tensile Results for BG10L: 10 wt% xGnP in Lexan HF1130-111: Injection Molded 6-8-10, Extruded 5-27-10

Sample	Specimen	Tensile Ultimate Stress (MPa)	Tensile Strain at Ultimate Stress (%)	Tensile Fracture Stress (MPa)	Tensile Strain at Fracture Stress (%)	Tensile Modulus (MPa)
BG10L	4	59.165	3.58	59.165	3.58	3940.6
	5	58.085	3.15	58.085	3.15	3944.9
	7	57.725	2.98	57.725	2.98	4055.3
	15	57.356	2.77	57.356	2.77	4017
	17	56.276	2.51	56.276	2.51	4068.2
	23	56.636	2.54	56.636	2.54	4160
Average		57.54	2.92	57.54	2.92	4031.00
Standard Deviation		1.04	0.41	1.04	0.41	82.94
Number		6	6	6	6	6

Appendix J.4: Polycarbonate with Multiple Fillers

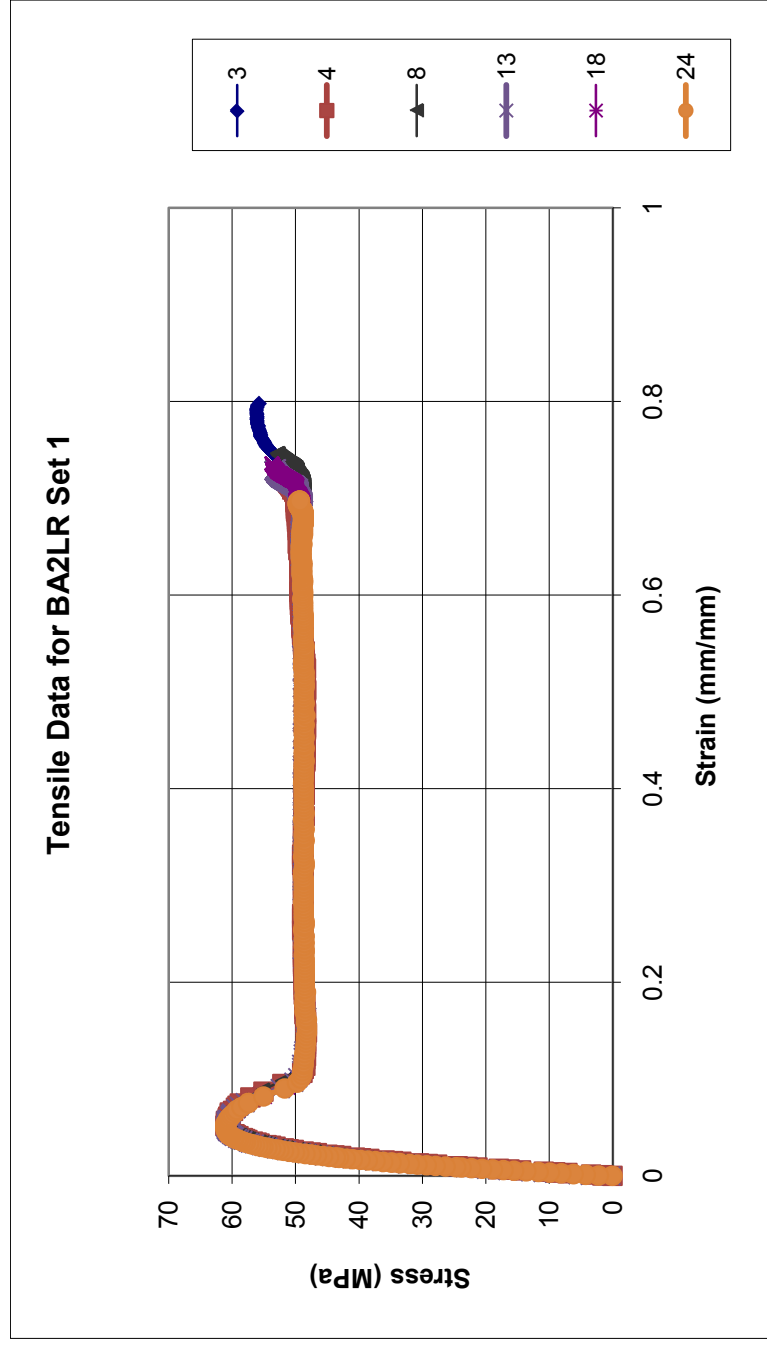


Figure J.27: Tensile Results for BA2LR Set 1: Extruded 7-8-10, Injection Molded 7-26-10

Table J.27: Tensile Results for BA2LR Set 1 : Extruded 7-8-10, Injection Molded 7-26-10

Sample	Specimen	Tensile Ultimate Stress (MPa)	Tensile Strain at Ultimate Stress (%)	Tensile Fracture Stress (MPa)	Tensile Strain at Fracture Stress (%)	Tensile Modulus (MPa)
BA2LR Set 1	3	61.059	5.28	56.017	79.42	2259.8
	4	61.059	5.17	53.376	74.09	2311.9
	8	60.939	5.70	52.896	74.56	2202.3
	13	61.059	5.04	53.136	72.99	2415.2
	18	60.819	4.74	53.736	73.54	2526.1
	24	61.059	4.85	49.294	69.72	2476.8
Average		61.00	5.13	53.08	74.05	2365.35
Standard Deviation		0.10	0.34	2.17	3.14	127.54
Number		6	6	6	6	6

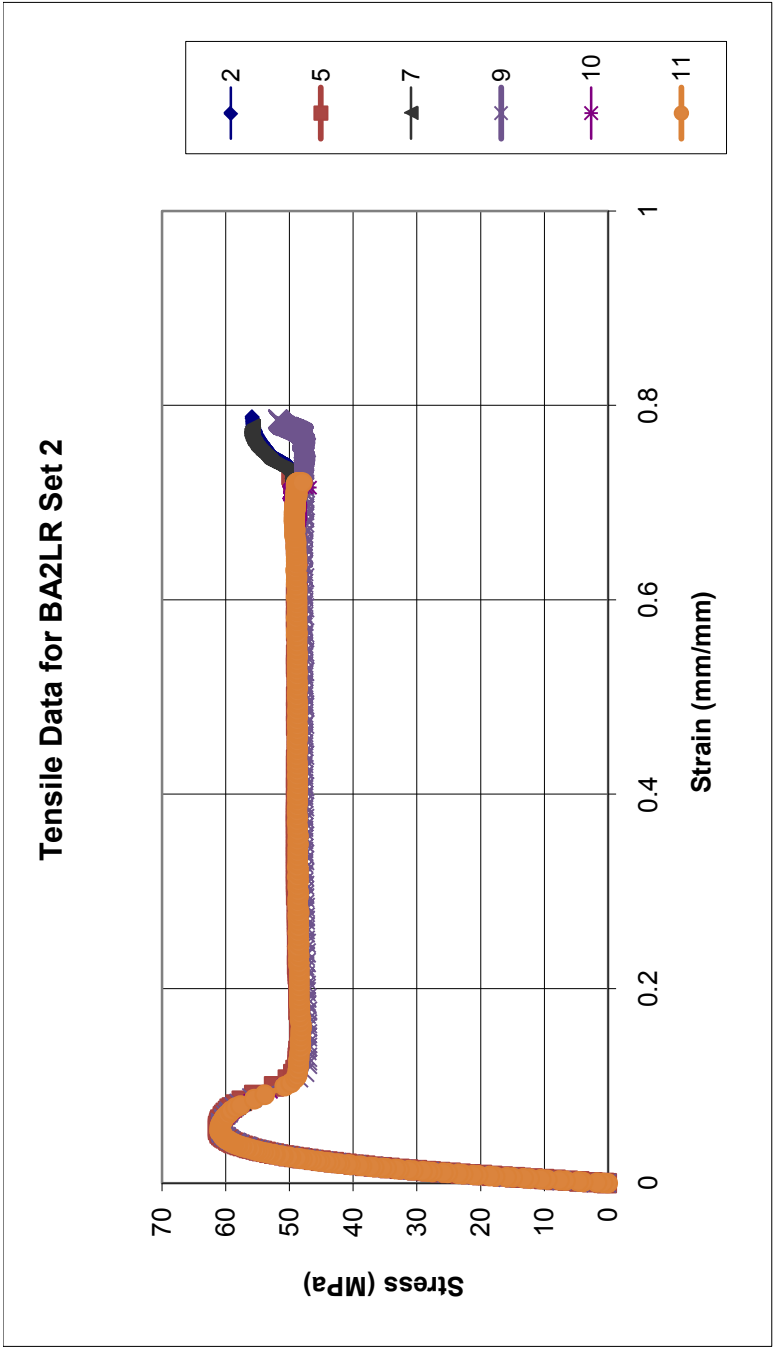


Figure J.28: Tensile Results for BA2LR Set 2: Extruded 7-8-10, Injection Molded 7-26-10

Table J.28: Tensile Results for BA2LR Set 2: Extruded 7-8-10, Injection Molded 7-26-10

Sample	Specimen	Tensile Ultimate Stress (MPa)	Tensile Strain at Ultimate Stress (%)	Tensile Fracture Stress (MPa)	Tensile Strain at Fracture Stress (%)	Tensile Modulus (MPa)
BA2LR Set 2	2	61.059	5.31	55.897	78.75	2386
	5	61.179	5.46	49.174	73.28	2275.5
	7	61.059	5.14	55.897	77.45	2369.5
	9	60.819	5.35	51.815	78.54	2278.5
	10	60.939	5.17	47.373	71.58	2286.7
	11	60.939	5.30	48.214	72.07	2367.4
Average		61.00	5.29	51.39	75.28	2327.27
Standard Deviation		0.13	0.12	3.79	3.33	52.05
Number		6	6	6	6	6

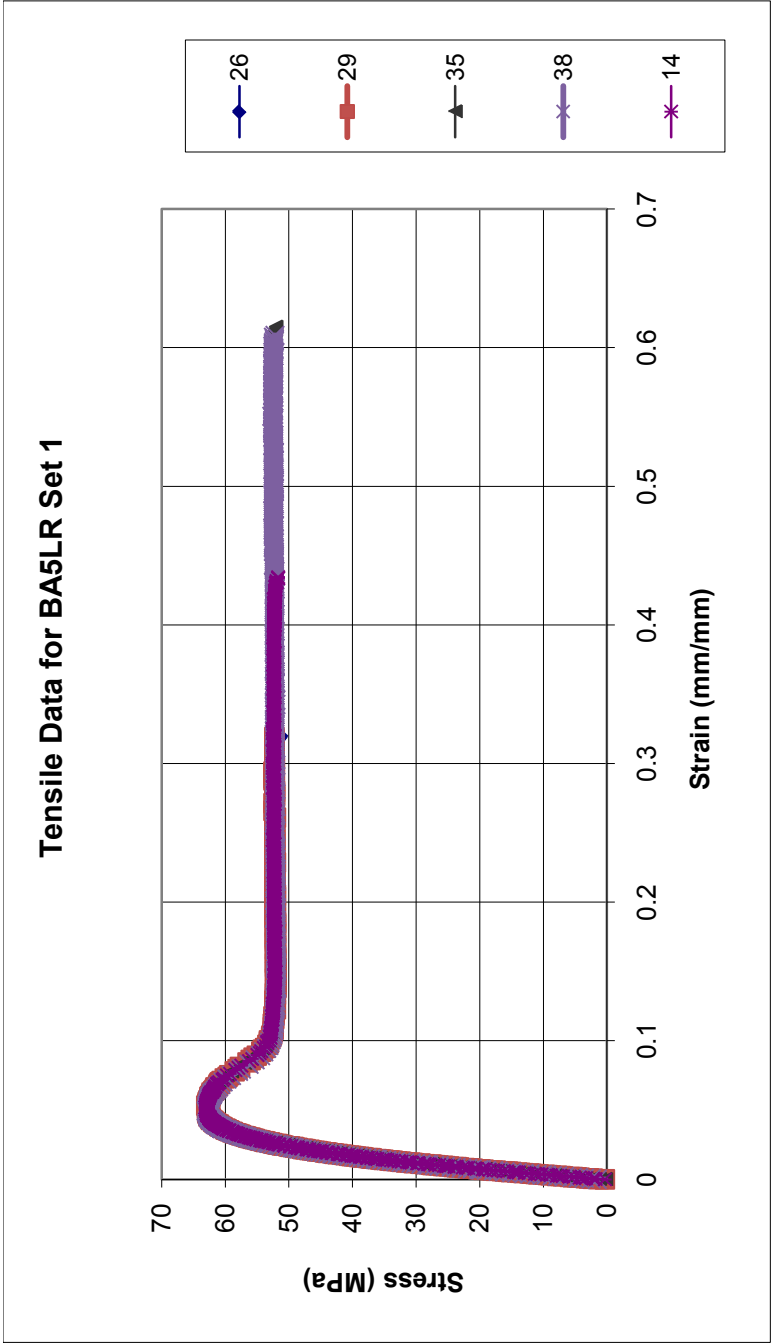


Figure J.29: Tensile Results for BA5LR Set 1: Extruded 7-8-10, Injection Molded 7-26-10

Table J.29: Tensile Results for BA5LR Set 1 : Extruded 7-8-10, Injection Molded 7-26-10

Sample	Specimen	Tensile Ultimate Stress (MPa)	Tensile Strain at Ultimate Stress (%)	Tensile Fracture Stress (MPa)	Tensile Strain at Fracture Stress (%)	Tensile Modulus (MPa)
BA5LR Set 1	26	63.100	4.89	51.335	31.90	2584.4
	29	62.980	5.33	51.815	38.21	2509.6
	35	62.980	5.08	52.175	61.20	2561.1
	38	62.980	4.94	52.415	60.23	2510.6
	14	63.100	5.04	51.695	43.34	2571.5
Average		63.03	5.06	51.89	46.98	2547.44
Standard Deviation		0.07	0.17	0.42	13.18	35.07
Number		5	5	5	5	5

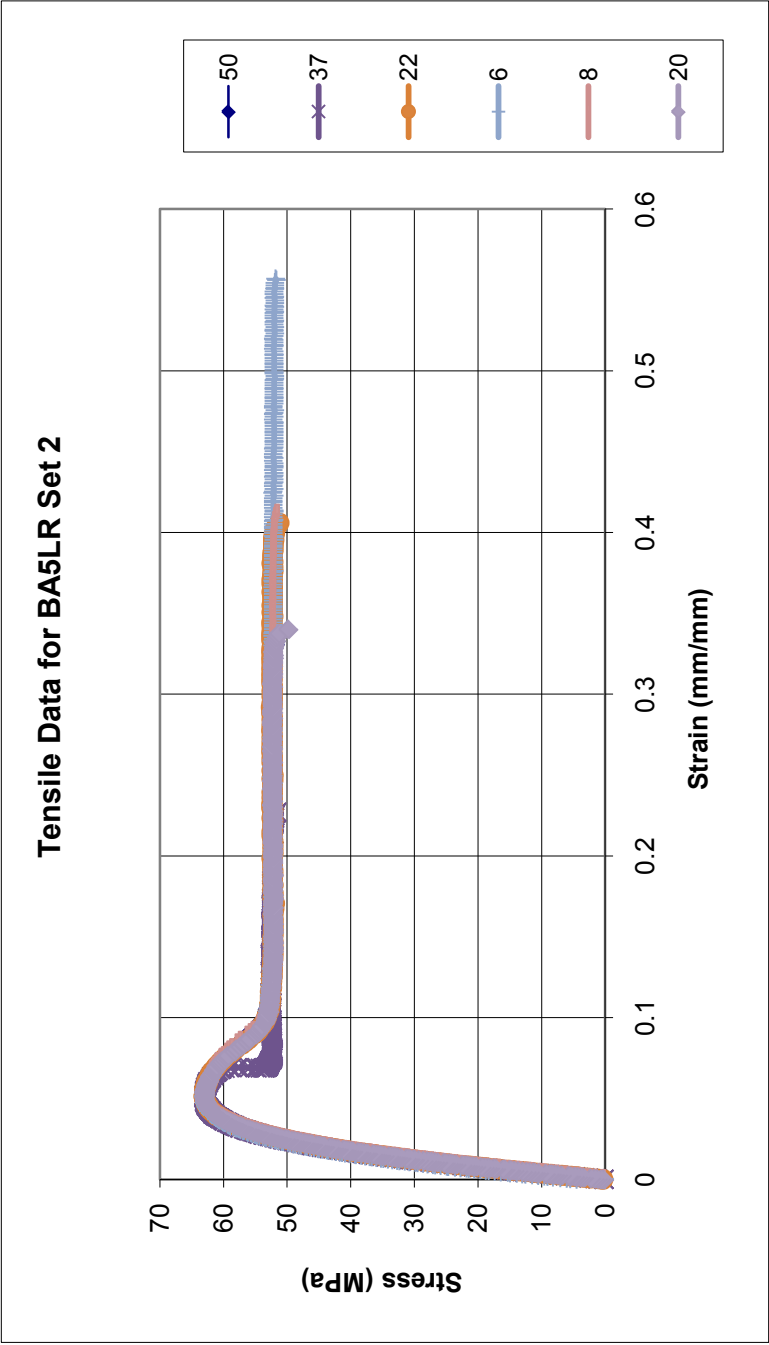


Figure J.30: Tensile Results for BA5LR Set 2: Extruded 7-8-10, Injection Molded 7-26-10

Table J.30: Tensile Results for BA5LR Set 2: Extruded 7-8-10, Injection Molded 7-26-10

Sample	Specimen	Tensile Ultimate Stress (MPa)	Tensile Strain at Ultimate Stress (%)	Tensile Fracture Stress (MPa)	Tensile Strain at Fracture Stress (%)	Tensile Modulus (MPa)
BA5LR Set 2	50	63.340	5.00	51.695	32.88	2656
	37	63.100	5.03	51.695	22.65	2623
	22	63.100	5.12	51.695	40.36	2564.9
	6	63.100	5.08	51.815	55.69	2584.4
	8	63.100	5.19	51.575	41.05	2509.6
	20	63.100	5.03	51.455	33.62	2514.8
Average		63.14	5.08	51.66	37.71	2575.45
Standard Deviation		0.10	0.07	0.12	11.03	58.23
Number		6	6	6	6	6

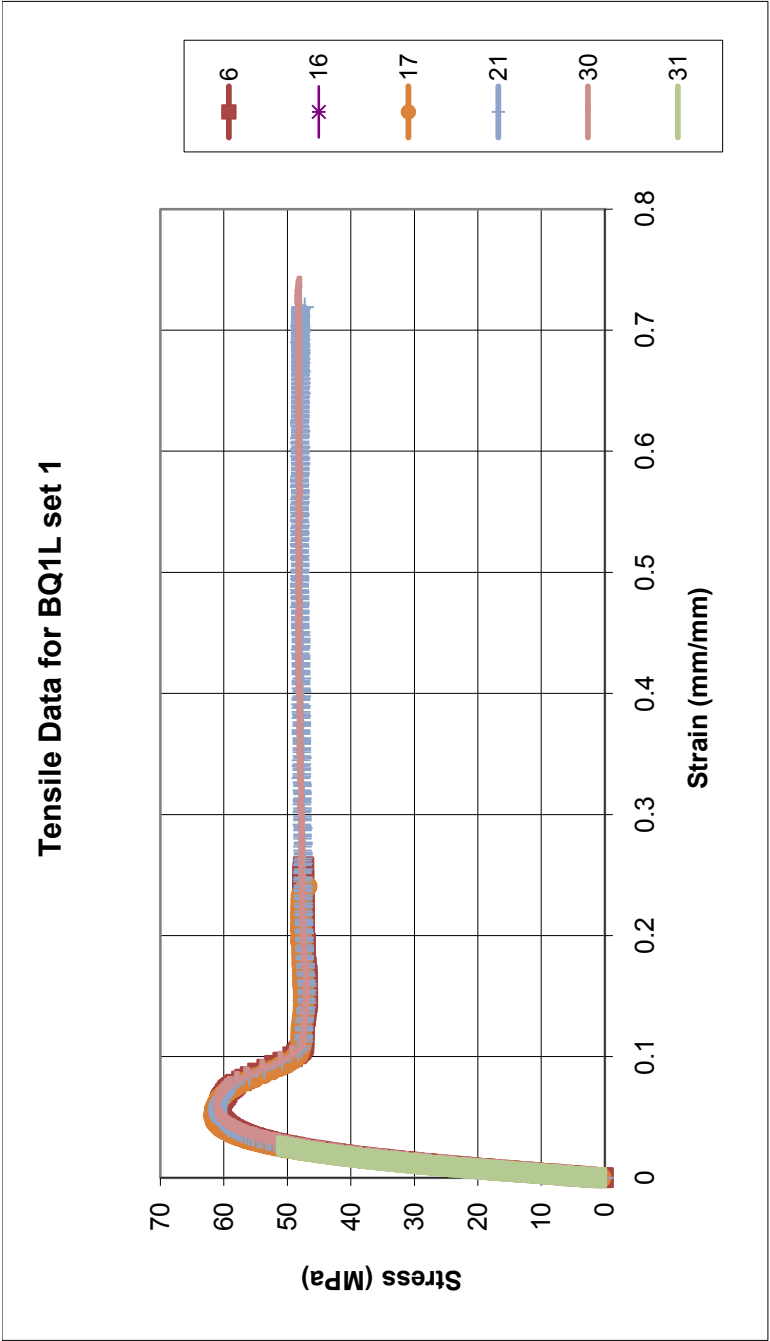


Figure J.31: Tensile Results for BQ1L Set 1: Extruded 6-30-10, Injection Molded 7-26-10

Table J.31: Tensile Results for BQ1L Set 1: Extruded 6-30-10, Injection Molded 7-26-10

Sample	Specimen	Tensile Ultimate Stress (MPa)	Tensile Strain at Ultimate Stress (%)	Tensile Fracture Stress (MPa)	Tensile Strain at Fracture Stress (%)	Tensile Modulus (MPa)
BQ1L Set 1	6	60.939	5.38	45.812	31.87	2349.9
	10	61.419	4.59	47.733	68.57	2628.4
	11	58.658	3.38	58.658	3.38	2633.4
	16	52.415	2.82	52.415	2.82	2404
	17	61.660	5.15	47.133	23.90	2510
	21	61.059	5.63	47.853	71.74	2377.2
Average		59.36	4.49	49.93	33.71	2483.82
Standard Deviation		3.57	1.15	4.82	30.45	126.20
Number		6	6	6	6	6

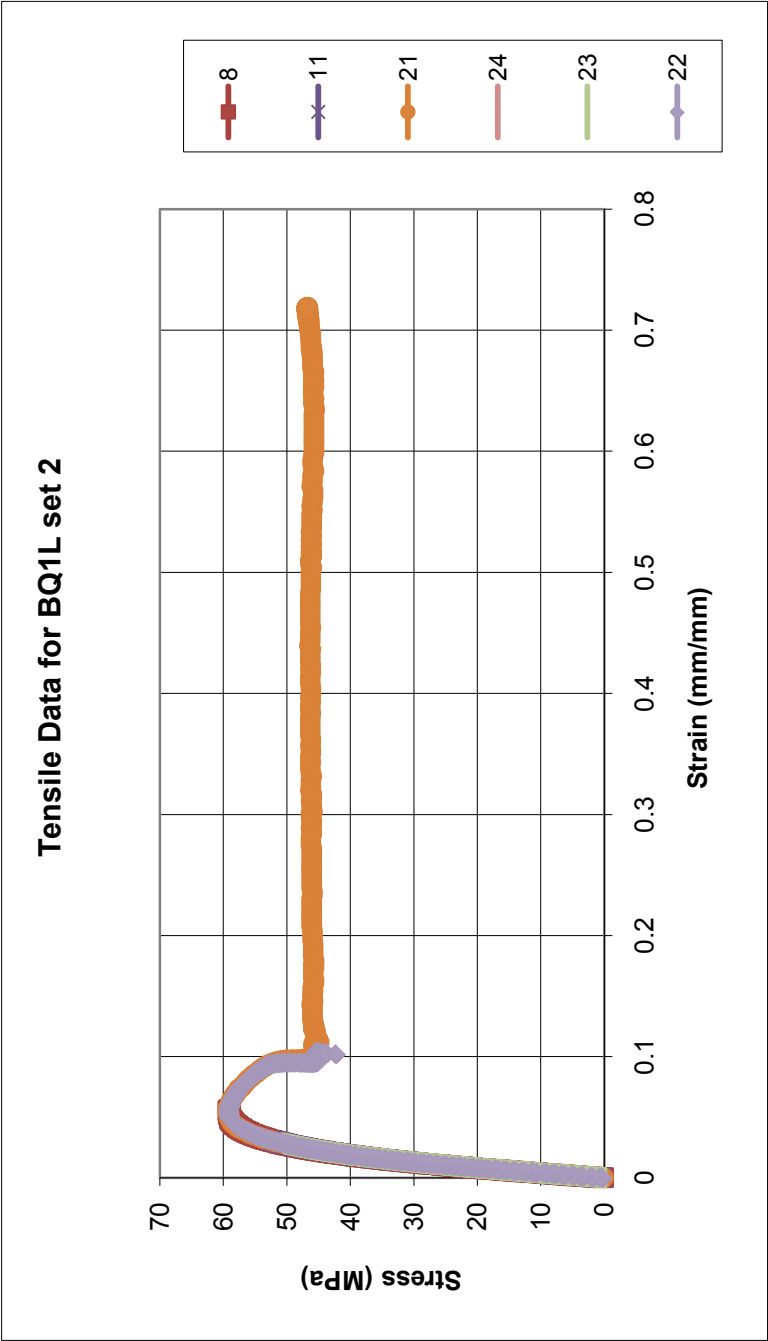


Figure J.32: Tensile Results for BQ1L Set 2: Extruded 6-30-10, Injection Molded 7-26-10

Table J.32: Tensile Results for BQ1L Set 2: Extruded 6-30-10, Injection Molded 7-26-10

Sample	Specimen	Tensile Ultimate Stress (MPa)	Tensile Strain at Ultimate Stress (%)	Tensile Fracture Stress (MPa)	Tensile Strain at Fracture Stress (%)	Tensile Modulus (MPa)
BQ1L Set 2	8	59.285	5.52	57.845	6.79	2457.8
	11	52.564	3.13	52.564	3.13	2383.7
	21	59.285	5.34	46.804	71.85	2444.5
	24	50.644	2.88	50.644	2.88	2418.8
	23	50.284	2.82	50.284	2.82	2433.1
	22	59.165	5.22	43.924	10.29	2427.5
Average		55.20	4.15	50.34	16.29	2427.57
Standard Deviation		4.49	1.33	4.80	27.38	25.43
Number		6	6	6	6	6

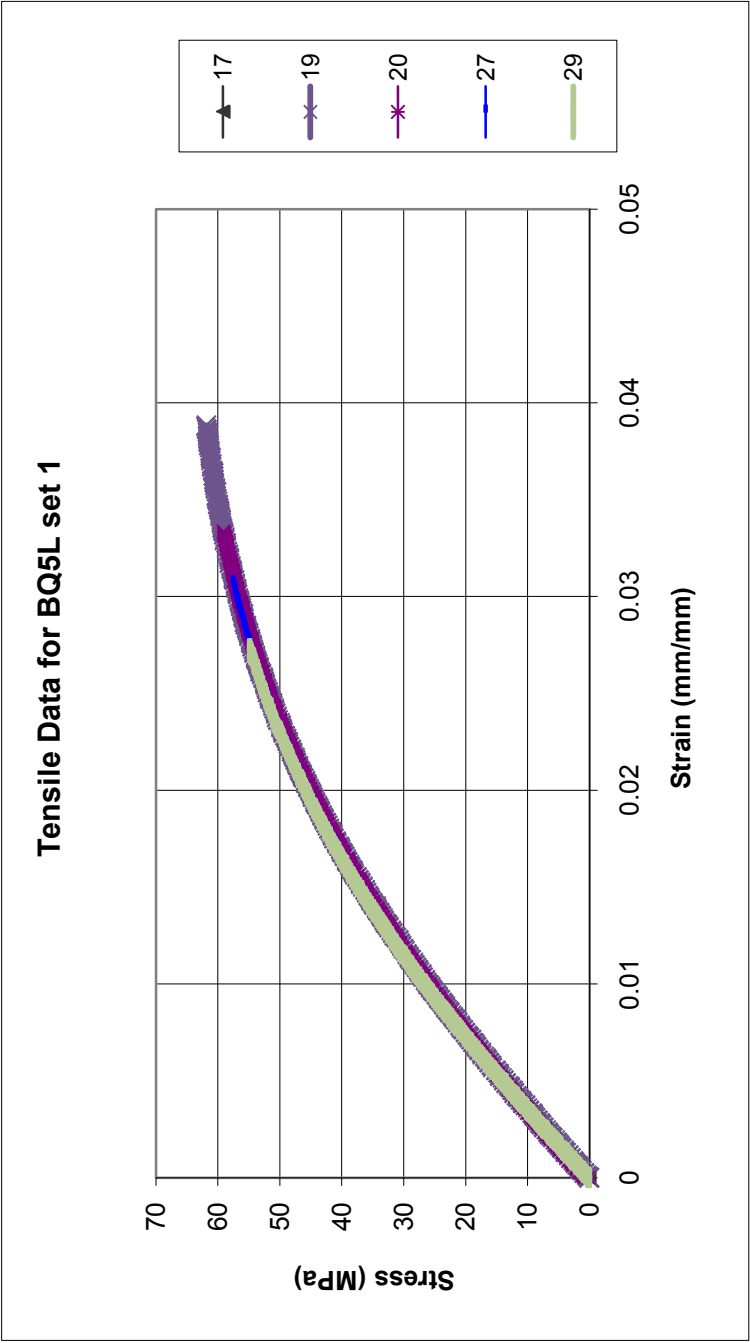


Figure J.33: Tensile Results for BQ5L Set 1: Extruded May 2009, Injection Molded 5-26-09

Table J.33: Tensile Results for BQ5L Set 1: Extruded May 2009, Injection Molded 5-26-09

Sample	Specimen	Tensile Ultimate Stress (MPa)	Tensile Strain at Ultimate Stress (%)	Tensile Fracture Stress (MPa)	Tensile Strain at Fracture Stress (%)	Tensile Modulus (MPa)
BQ5L Set 1	17	51.629	2.42	51.629	2.42	2714.9
	19	61.979	3.88	61.979	3.88	2630.4
	20	59.091	3.34	59.091	3.34	2527.5
	27	58.007	3.13	58.007	3.13	2655.7
	29	54.878	2.72	54.878	2.73	2762.5
Average		57.12	3.10	57.12	3.10	2658.20
Standard Deviation		3.98	0.56	3.98	0.56	89.38
Number		5	5	5	5	5

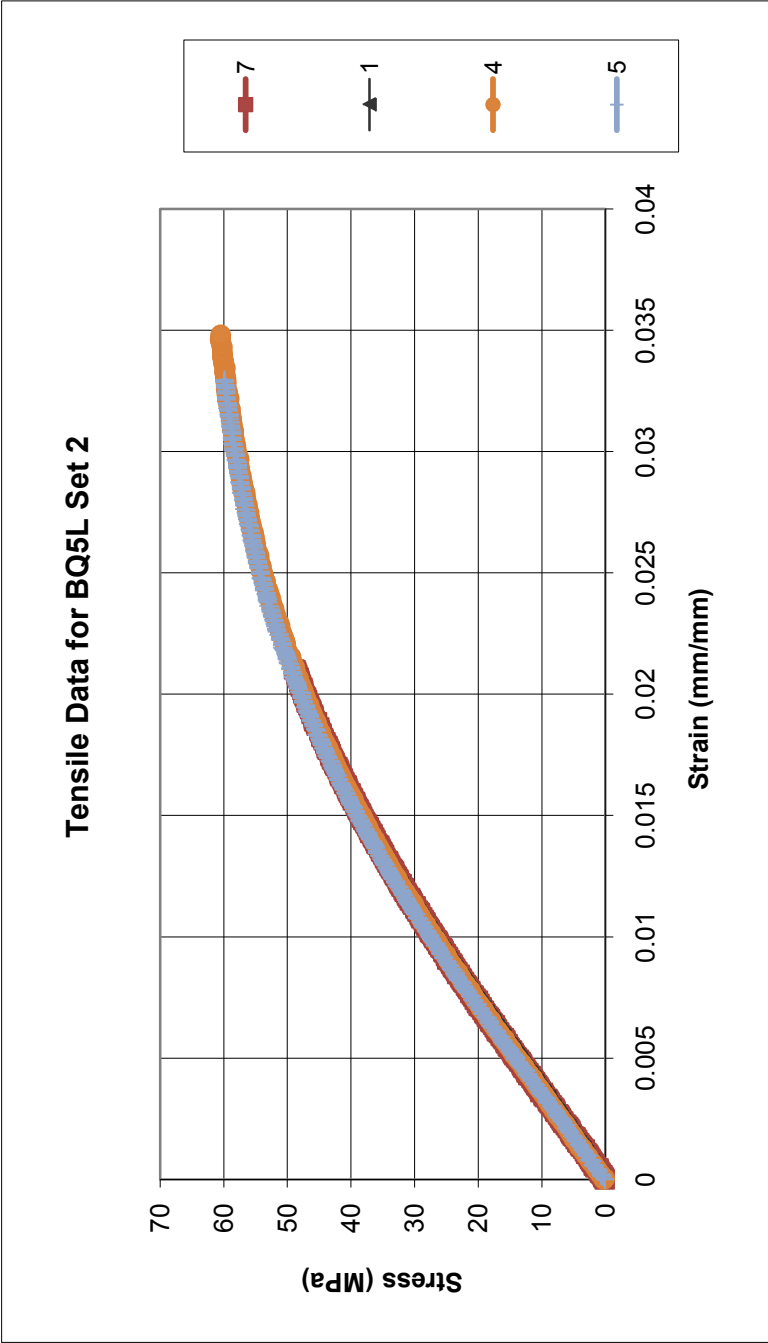


Figure J.34: Tensile Results for BQ5L Set 2: Extruded May 2009, Injection Molded 5-26-09

Table J.34: Tensile Results for BQ5L Set 2: Extruded May 2009, Injection Molded 5-26-09

Sample	Specimen	Tensile Ultimate Stress (MPa)	Tensile Strain at Ultimate Stress (%)	Tensile Fracture Stress (MPa)	Tensile Strain at Fracture Stress (%)	Tensile Modulus (MPa)
BQ5L Set 2	7	53.280	2.43	53.280	2.43	2758.8
	1	59.280	3.15	59.280	3.15	2698.9
	4	60.720	3.50	60.720	3.50	2728.2
	5	59.880	3.28	59.880	3.28	2797.1
Average		58.29	3.09	58.29	3.09	2745.75
Standard Deviation		3.39	0.46	3.39	0.46	42.07
Number		4	4	4	4	4

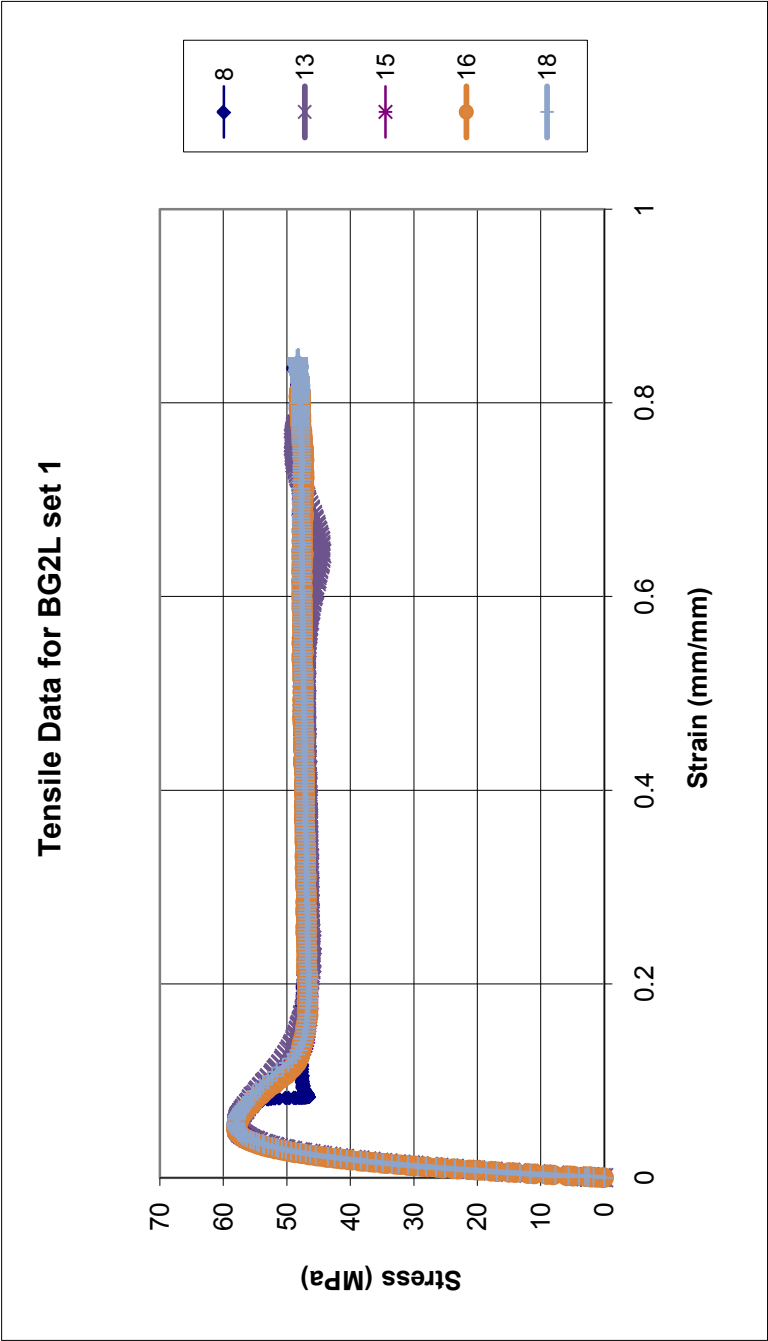


Figure J.35: Tensile Results for BG2L set 1: 2 wt% xGnP in Lexan HF1130-111: Injection Molded 6-3-10, Extruded 5-26-10

Table J.35: Tensile Results for BG2L set 1: 2 wt% xGnP in Lexan HF1130-111: Injection Molded 6-3-10, Extruded 5-26-10

Sample	Specimen	Tensile Ultimate Stress (MPa)	Tensile Strain at Ultimate Stress (%)	Tensile Fracture Stress (MPa)	Tensile Strain at Fracture Stress (%)	Tensile Modulus (MPa)
BG2L Set 1	8	58.436	5.27	48.956	83.53	2483.4
	13	57.836	5.19	48.476	77.55	2461
	15	57.836	5.38	47.996	81.37	2487.7
	16	57.956	5.01	47.996	81.11	2599.6
	18	58.076	5.42	48.236	84.60	2536.3
Average		58.03	5.25	48.33	81.63	2513.60
Standard Deviation		0.25	0.16	0.40	2.71	55.36
Number		5	5	5	5	5

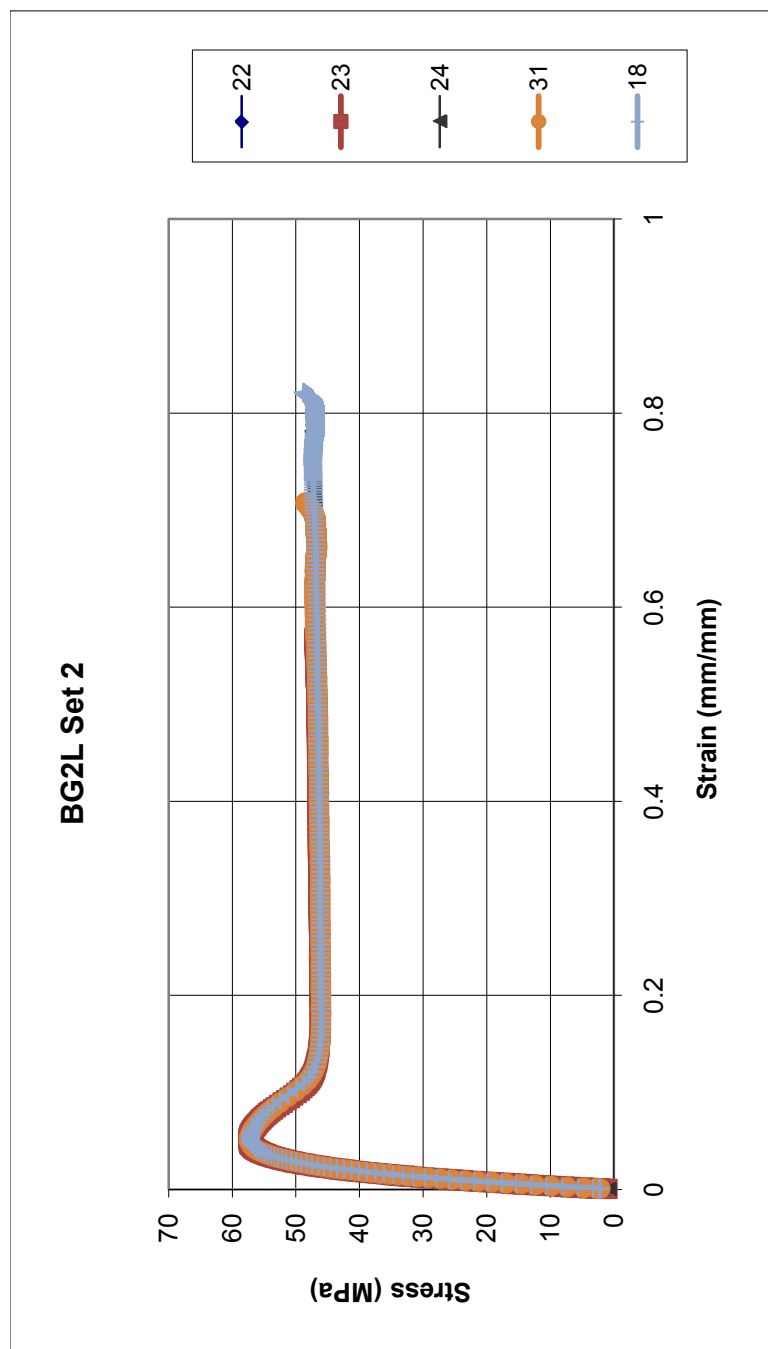


Figure J.36: Tensile Results for BG2L set 2: 2 wt% xGnP in Lexan HF1130-111: Injection Molded 9-9-10, Extruded 5-26-10

Table J.36: Tensile Results for BG2L set 2: 2 wt% xGnP in Lexan HF1130-111: Injection Molded 9-9-10, Extruded 5-26-10

Sample	Specimen	Tensile Ultimate Stress (MPa)	Tensile Strain at Ultimate Stress (%)	Tensile Fracture Stress (MPa)	Tensile Strain at Fracture Stress (%)	Tensile Modulus (MPa)
BG2L Set 2	22	57.610	5.08	50.046	75.34	2393.3
	23	57.403	5.05	47.156	61.91	2478.6
	24	57.172	5.38	47.532	78.16	2500.5
	31	57.337	5.14	48.493	70.77	2454.2
	18	57.148	5.07	48.849	82.14	2412.6
Average		57.33	5.15	48.42	73.66	2447.84
Standard Deviation		0.19	0.13	1.14	7.77	44.65
Number		5	5	5	5	5

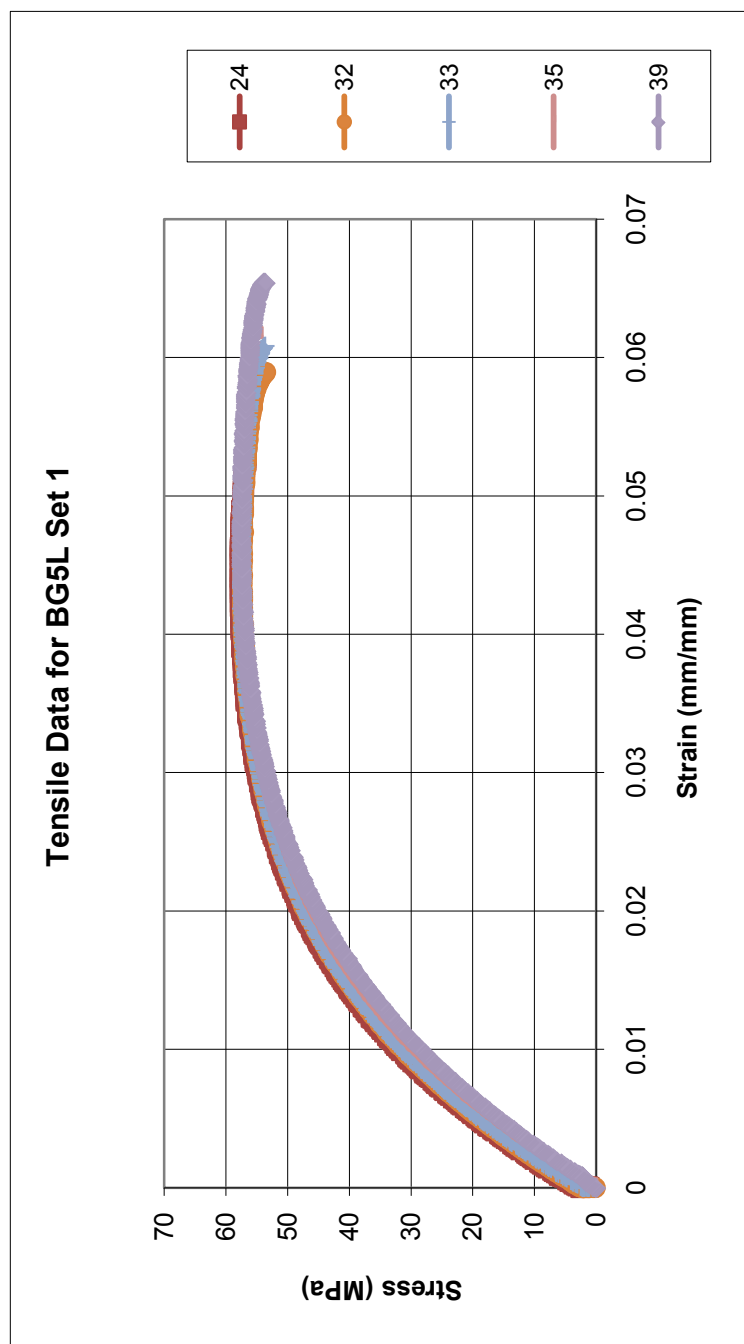


Figure J.37: Tensile Results for BG5L Set 1: 5 wt% xGnP in Lexan HF1130-111: Injection Molded 6-3-10, Extruded 5-26-10

Table J.37: Tensile Results for BG5L set 1: 5 wt% xGnP in Lexan HF1130-111: Injection Molded 6-3-10, Extruded 5-26-10

Sample	Specimen	Tensile Ultimate Stress (MPa)	Tensile Strain at Ultimate Stress (%)	Tensile Fracture Stress (MPa)	Tensile Strain at Fracture Stress (%)	Tensile Modulus (MPa)
BG5L Set 1	24	57.716	4.20	53.036	5.82	3108.8
	32	57.356	4.16	52.076	5.91	3055.1
	33	57.476	4.18	52.676	6.10	3149.3
	35	57.596	4.41	54.836	6.16	3155.4
	39	57.476	3.90	53.756	6.54	3004.3
Average		57.52	4.17	53.28	6.10	3094.58
Standard Deviation		0.14	0.18	1.06	0.28	64.43
Number		5	5	5	5	5

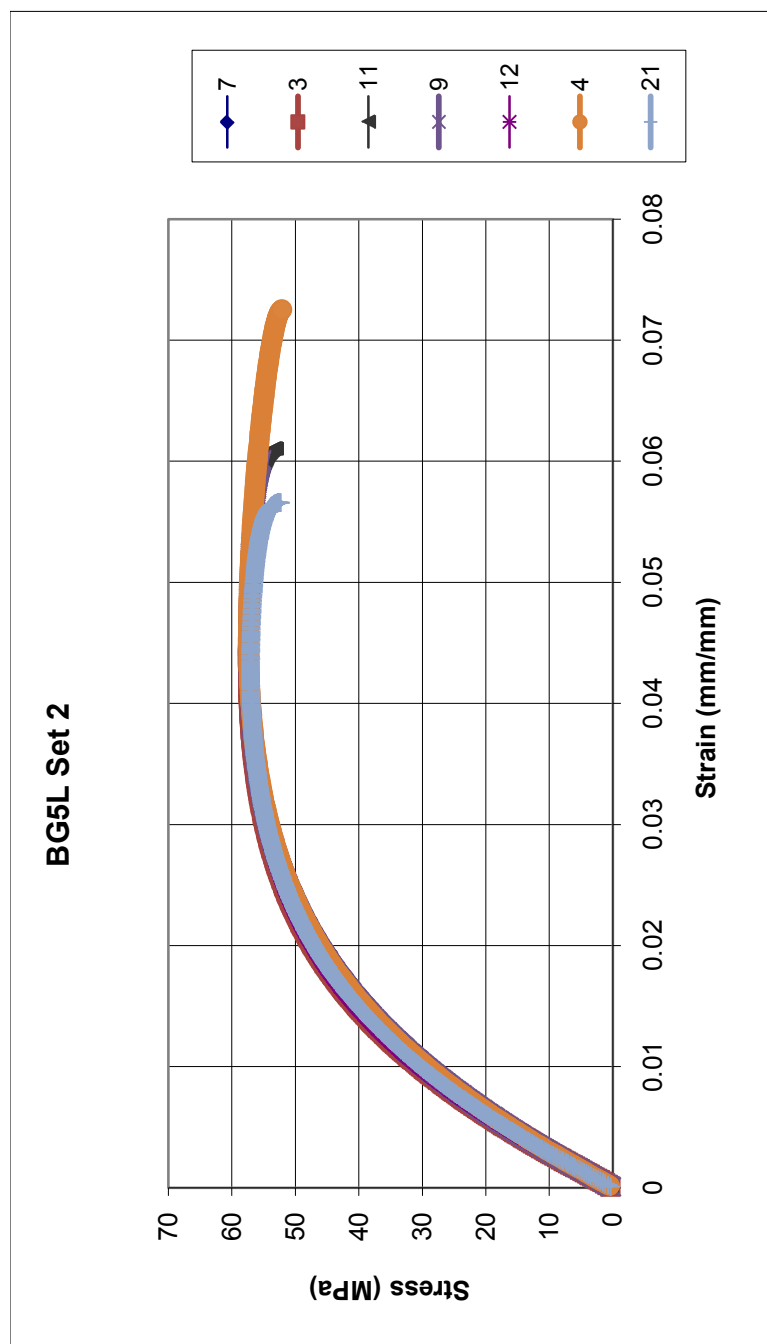


Figure J.38: Tensile Results for BG5L set 2: 2 wt% xGnP in Lexan HF1130-111: Extruded 5-26-10

Table J.38: Tensile Results for BG5L set 2: 2 wt% xGnP in Lexan HF1130-111: Extruded 5-26-10

Sample	Specimen	Tensile Ultimate Stress (MPa)	Tensile Strain at Ultimate Stress (%)	Tensile Fracture Stress (MPa)	Tensile Strain at Fracture Stress (%)	Tensile Modulus (MPa)
BG5L Set 2	7	57.351	4.49	53.930	5.96	3143.6
	3	57.427	4.47	53.638	6.54	3165.6
	11	57.332	4.42	53.125	6.10	3014.9
	9	57.453	4.60	55.357	6.00	3086.5
	12	57.176	4.43	56.261	5.17	3190.2
	4	57.395	4.59	52.255	7.25	3065.3
	21	57.067	4.29	52.464	5.66	3193.3
Average		57.31	4.47	53.86	6.10	3122.77
Standard Deviation		0.14	0.11	1.48	0.66	68.37
Number		7	7	7	7	7

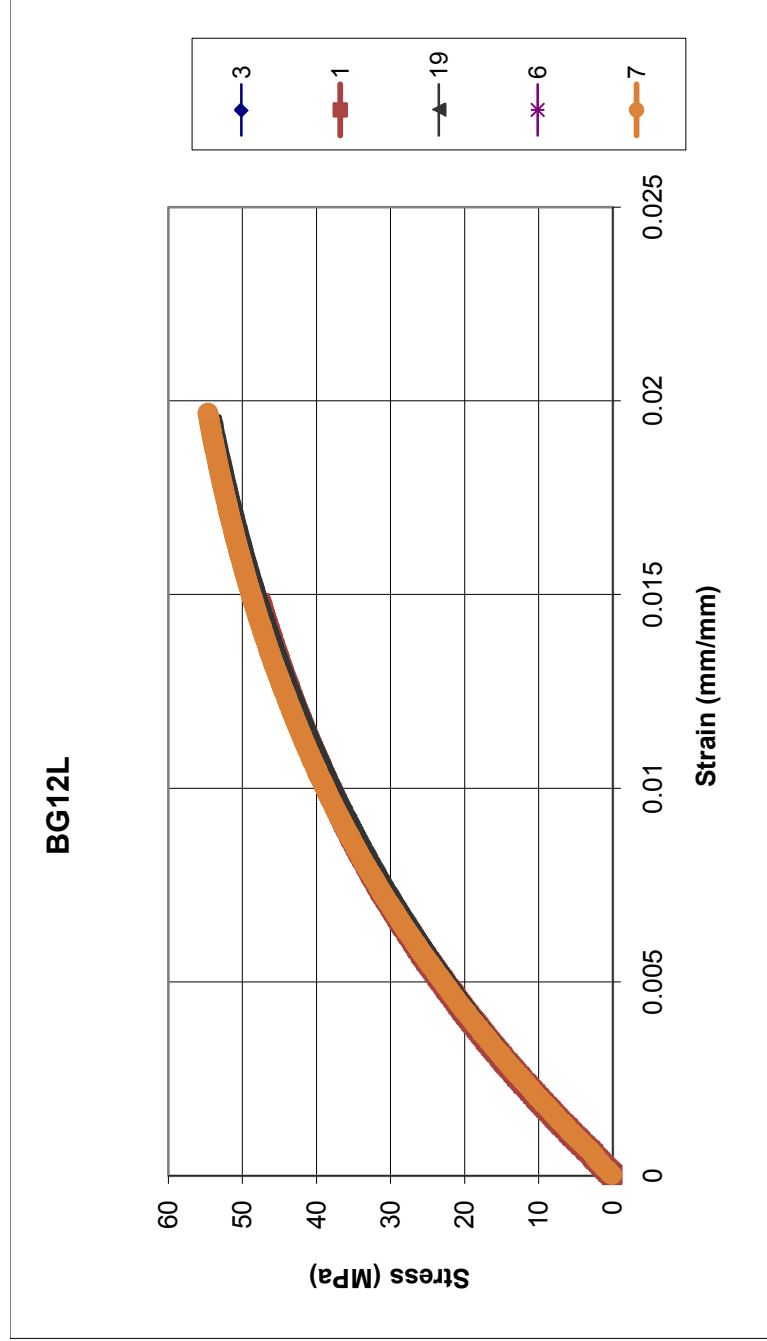


Figure J.39: Tensile Results for BG12L: 12 wt% xGnP in Lexan HF1130-111: Injection Molded 8-18-10, Extruded 7-8-10

Table J.39: Tensile Results for BG12L: 12 wt% xGnP in Lexan HF1130-111: Injection Molded 8-18-10, Extruded 7-8-10

Sample	Specimen	Tensile Ultimate Stress (MPa)	Tensile Strain at Ultimate Stress (%)	Tensile Fracture Stress (MPa)	Tensile Strain at Fracture Stress (%)	Tensile Modulus (MPa)
BG12L	3	52.249	1.83	52.249	1.83	4662.9
	1	50.762	1.70	50.762	1.70	4755.9
	19	53.900	1.95	53.900	1.95	4634.4
	6	53.895	1.90	53.895	1.90	4768.1
	7	54.737	1.98	54.737	1.98	4730.4
Average		53.11	1.87	53.11	1.87	4710.34
Standard Deviation		1.59	0.11	1.59	0.11	58.80
Number		5	5	5	5	5

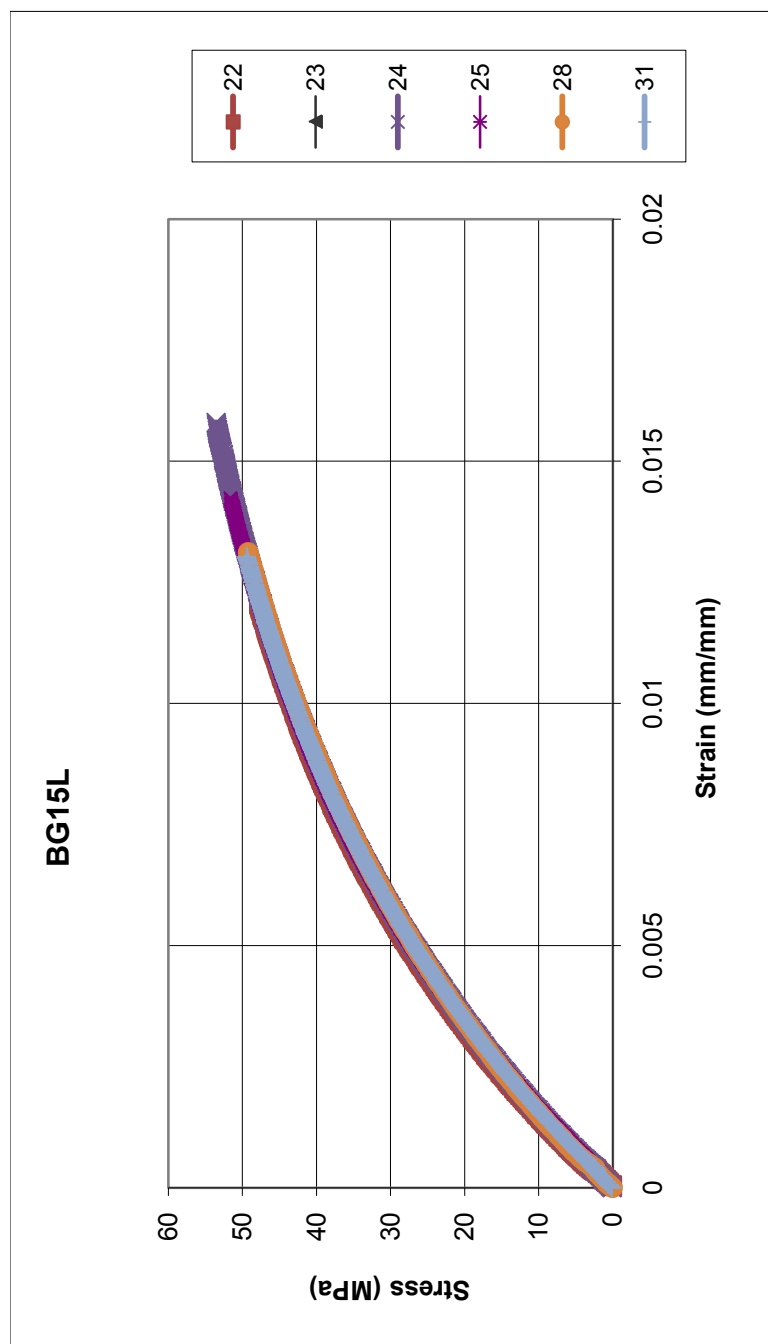


Figure J.40: Tensile Results for BG15L: 15 wt% xGnP in Lexan HF1130-111: Injection Molded 8-18-10, Extruded 7-8-10

Table J.40: Tensile Results for BG15L: 15 wt% xGnP in Lexan HF1130-111: Injection Molded 8-18-10, Extruded 7-8-10

Sample	Specimen	Tensile Ultimate Stress (MPa)	Tensile Strain at Ultimate Stress (%)	Tensile Fracture Stress (MPa)	Tensile Strain at Fracture Stress (%)	Tensile Modulus (MPa)
BG15L	22	50.908	1.39	50.908	1.39	5832.1
	23	52.619	1.48	52.619	1.48	5928.3
	24	53.677	1.59	53.677	1.59	5869.1
	25	53.576	1.58	53.576	1.58	5894.6
	28	49.318	1.31	49.318	1.31	5854.5
	31	49.500	1.30	49.500	1.30	5855.1
Average		51.60	1.44	51.60	1.44	5872.28
Standard Deviation		1.97	0.13	1.97	0.13	34.27
Number		6	6	6	6	6

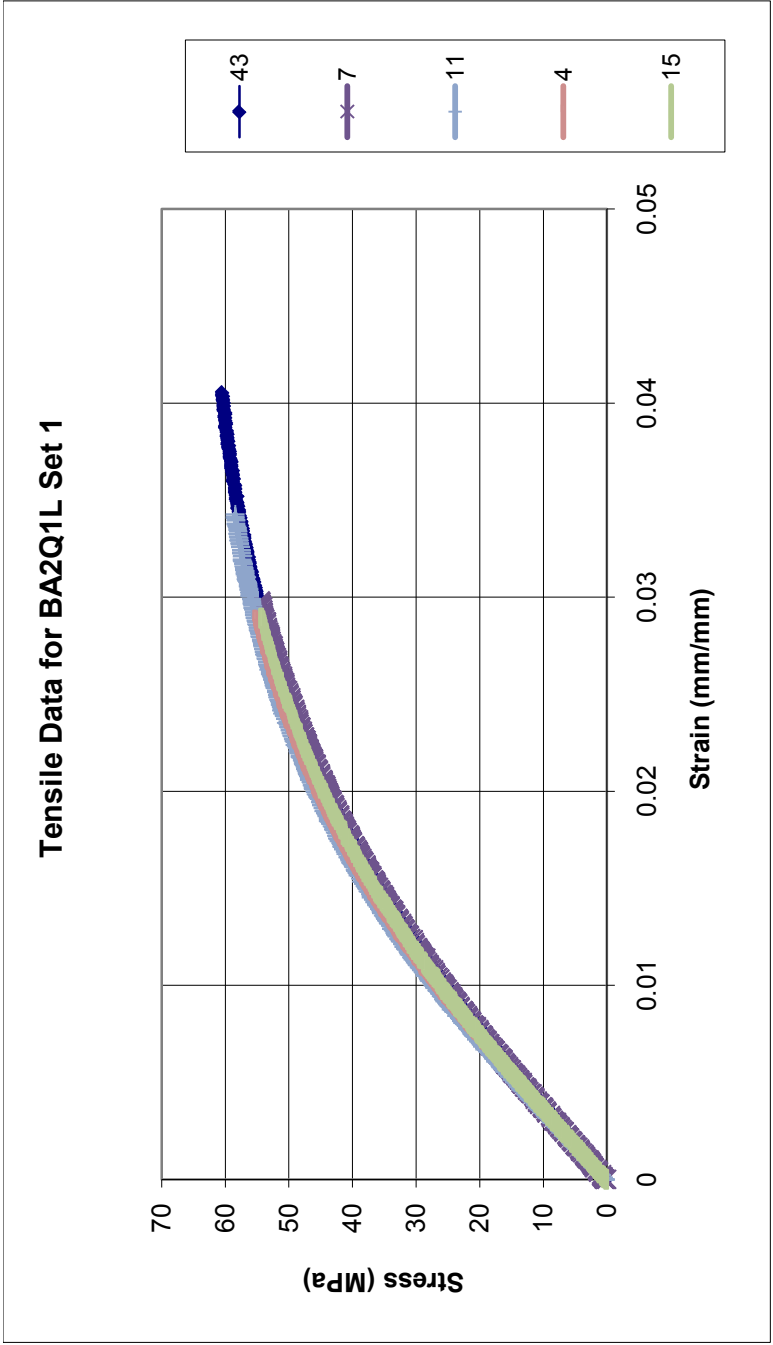


Figure J.41: Tensile Results for BA2Q1L set 1: Injection Molded 7-26-10, Extruded 7-7-10

Table J.41: Tensile Results for BA2Q1L set 1: Injection Molded 7-26-10, Extruded 7-7-10

Sample	Specimen	Tensile Ultimate Stress (MPa)	Tensile Strain at Ultimate Stress (%)	Tensile Fracture Stress (MPa)	Tensile Strain at Fracture Stress (%)	Tensile Modulus (MPa)
BA2Q1L Set 1	43	60.482	4.04	60.482	4.04	2563.2
	7	54.482	2.98	54.482	2.98	2608.2
	11	58.562	3.43	58.562	3.43	2807.2
	4	55.442	2.89	55.442	2.89	2766.5
	15	54.362	2.89	54.362	2.89	2670
Average		56.67	3.25	56.67	3.25	2683.02
Standard Deviation		2.73	0.50	2.73	0.50	103.09
Number		5	5	5	5	5

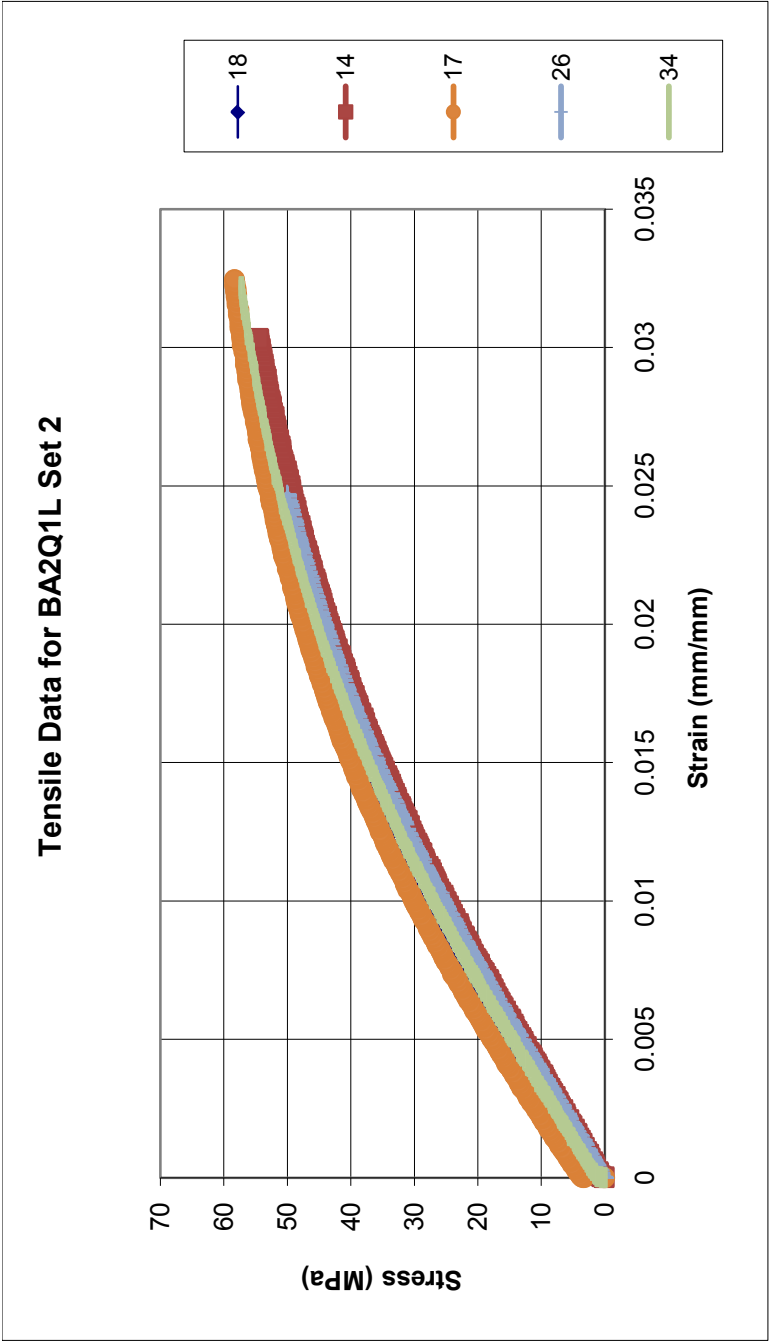


Figure J.42: Tensile Results for BA2Q1L set 2: Injection Molded 7-26-10, Extruded 7-7-10

Table J.42: Tensile Results for BA2Q1L set 2: Injection Molded 7-26-10, Extruded 7-7-10

Sample	Specimen	Tensile Ultimate Stress (MPa)	Tensile Strain at Ultimate Stress (%)	Tensile Fracture Stress (MPa)	Tensile Strain at Fracture Stress (%)	Tensile Modulus (MPa)
BA2Q1L Set 2	18	53.642	2.58	53.642	2.58	2774.9
	14	57.962	3.56	57.962	3.56	2512.4
	17	58.322	3.22	58.322	3.22	2793.2
	26	50.042	2.47	50.042	2.47	2599.9
	34	57.242	3.21	57.242	3.21	2646.9
Average		55.44	3.01	55.44	3.01	2665.46
Standard Deviation		3.55	0.46	3.55	0.46	118.71
Number		5	5	5	5	5

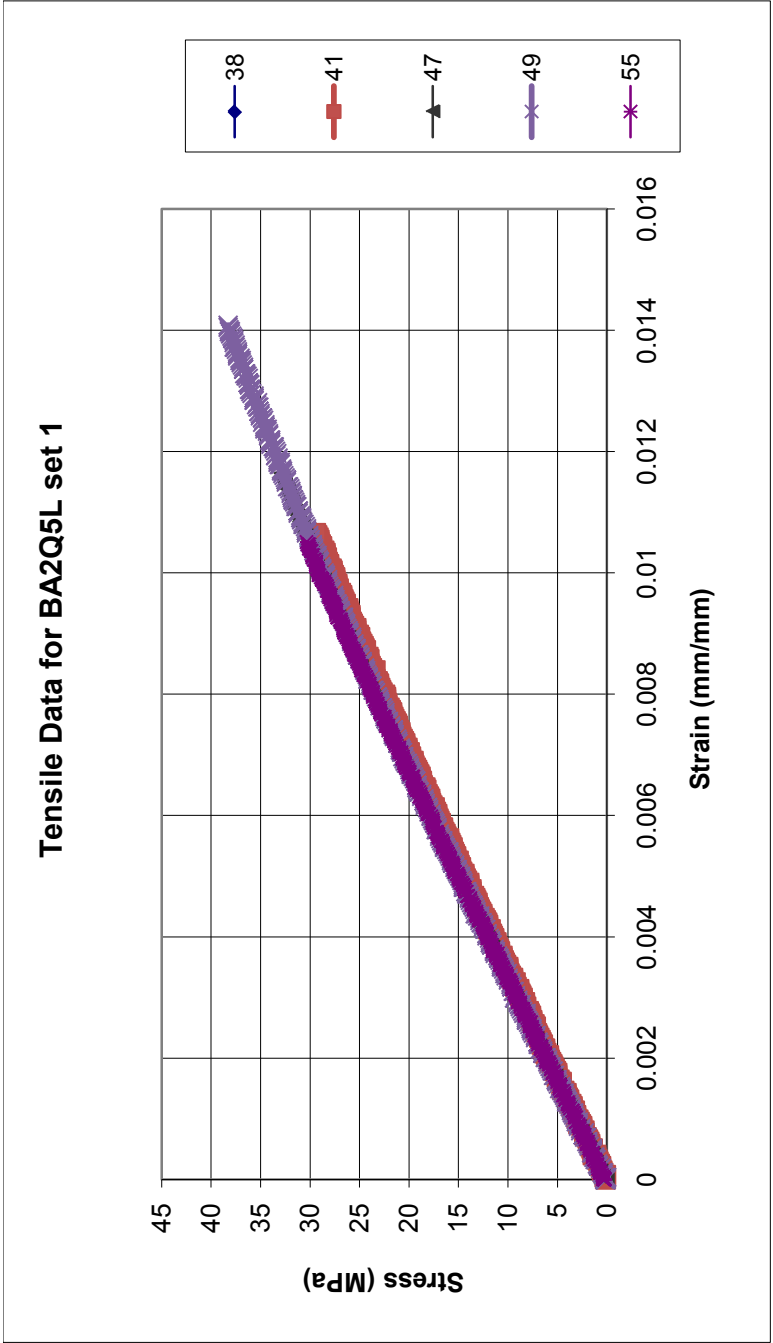


Figure J.43: Tensile Results for BA2Q5L set 1: Injection Molded 8-25-10, Extruded 7-7-10

Table J.43: Tensile Results for BA2Q5L set 1: Injection Molded 8-25-10, Extruded 7-7-10

Sample	Specimen	Tensile Ultimate Stress (MPa)	Tensile Strain at Ultimate Stress (%)	Tensile Fracture Stress (MPa)	Tensile Strain at Fracture Stress (%)	Tensile Modulus (MPa)
BA2Q5L Set 1	38	30.363	1.05	30.363	1.05	2966
	41	33.003	1.22	33.003	1.22	2863
	47	33.003	1.16	33.003	1.16	2992.2
	49	38.283	1.41	38.283	1.41	2955.1
	55	30.363	1.05	30.363	1.05	2950.3
Average		33.00	1.18	33.00	1.18	2945.32
Standard Deviation		3.23	0.15	3.23	0.15	48.79
Number		5	5	5	5	5

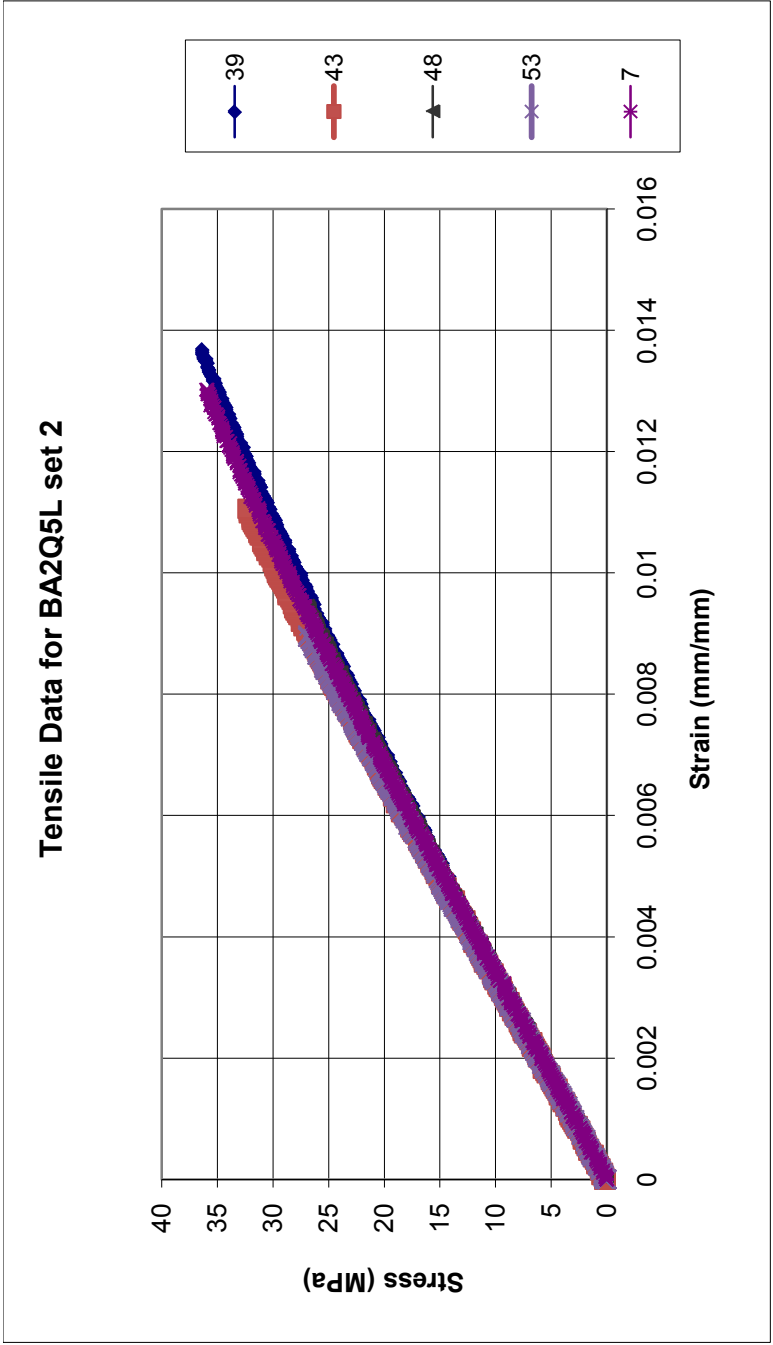


Figure J.44: Tensile Results for BA2Q5L set 2: Injection Molded 8-25-10, Extruded 7-7-10

Table J.44: Tensile Results for BA2Q5L set 2: Injection Molded 8-25-10, Extruded 7-7-10

Sample	Specimen	Tensile Ultimate Stress (MPa)	Tensile Strain at Ultimate Stress (%)	Tensile Fracture Stress (MPa)	Tensile Strain at Fracture Stress (%)	Tensile Modulus (MPa)
BA2Q5L Set 2	39	36.363	1.36	36.363	1.36	2838.1
	43	36.243	1.26	36.243	1.26	3000.7
	48	26.882	0.93	26.882	0.93	2956.6
	53	26.882	0.89	26.882	0.89	3037.3
	7	36.003	1.30	36.003	1.30	2946.9
Average		32.47	1.15	32.47	1.15	2955.92
Standard Deviation		5.11	0.22	5.11	0.22	75.15
Number		5	5	5	5	5

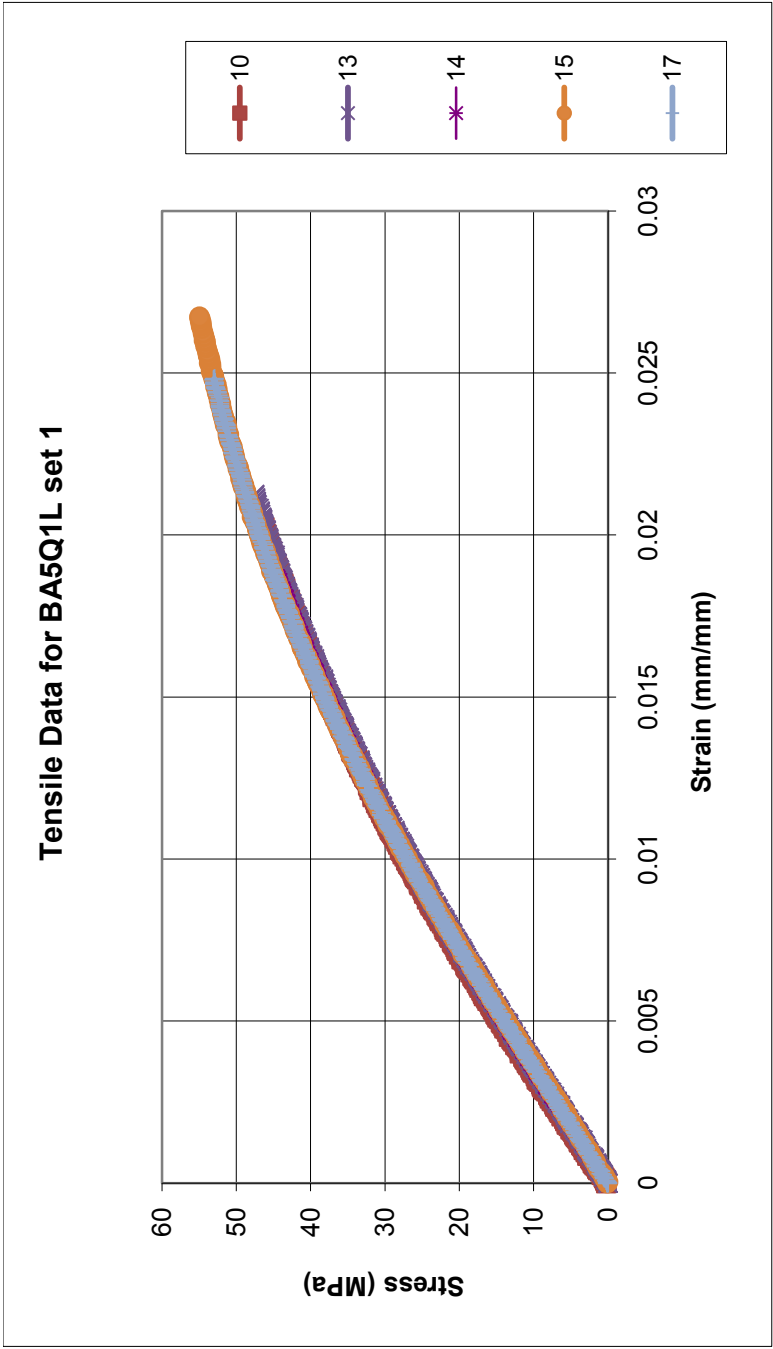


Figure J.45: Tensile Results for BA5Q1L set 1: Injection Molded 8-6-10, Extruded 7-7-10

Table J.45: Tensile Results for BA5Q1L set 1: Injection Molded 8-6-10, Extruded 7-7-10

Sample	Specimen	Tensile Ultimate Stress (MPa)	Tensile Strain at Ultimate Stress (%)	Tensile Fracture Stress (MPa)	Tensile Strain at Fracture Stress (%)	Tensile Modulus (MPa)
BA5Q1L Set 1	10	50.644	2.36	50.644	2.36	2748.5
	13	47.644	2.12	47.644	2.12	2720.2
	14	44.404	1.87	44.404	1.87	2733.7
	15	54.965	2.67	54.965	2.67	2745.2
	17	53.044	2.48	53.044	2.48	2737.5
Average		50.14	2.30	50.14	2.30	2737.02
Standard Deviation		4.22	0.31	4.22	0.31	11.10
Number		5	5	5	5	5

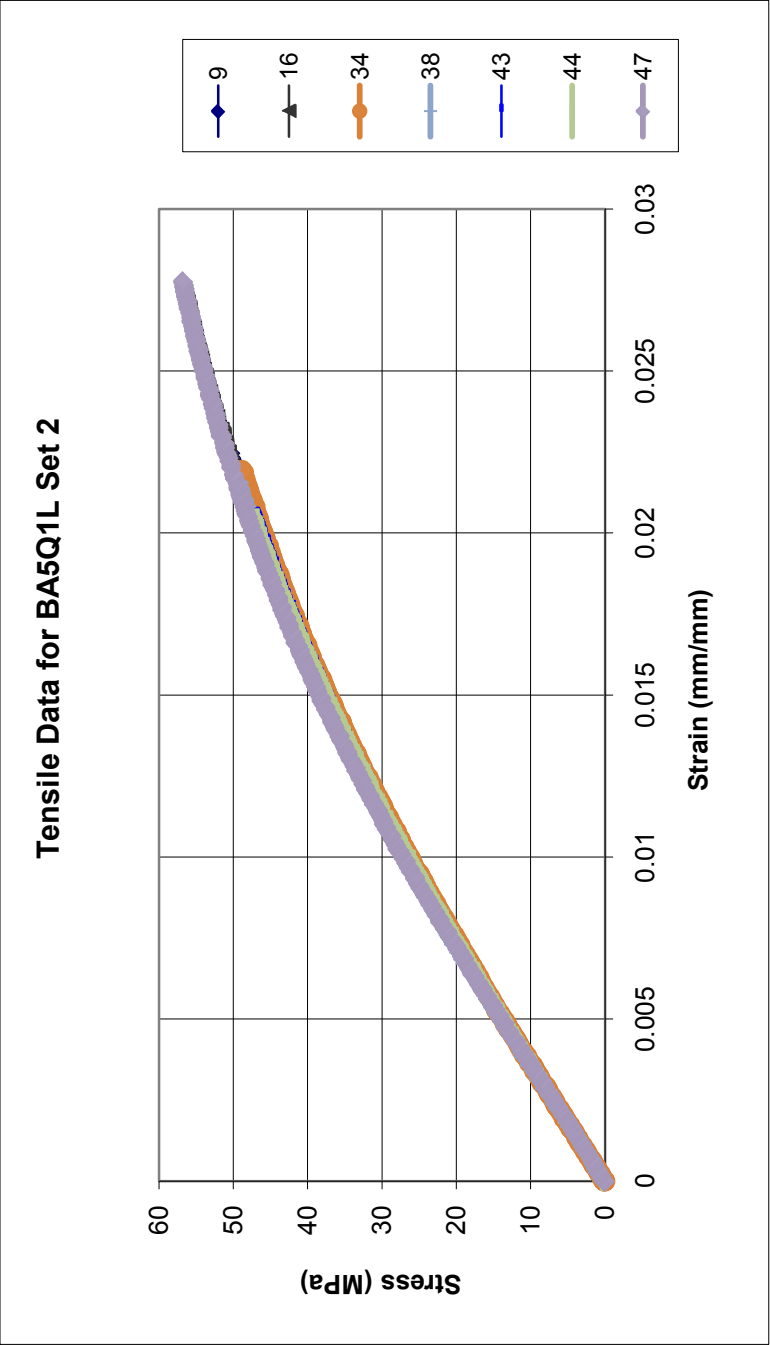


Figure J.46: Tensile Results for BA5Q1L set 2: Injection Molded 8-25-10, Extruded 7-7-10

Table J.46: Tensile Results for BA5Q1L set 2: Injection Molded 8-25-10, Extruded 7-7-10

Sample	Specimen	Tensile Ultimate Stress (MPa)	Tensile Strain at Ultimate Stress (%)	Tensile Fracture Stress (MPa)	Tensile Strain at Fracture Stress (%)	Tensile Modulus (MPa)
BA5Q1L Set 2	9	50.284	2.25	50.284	2.25	2756
	16	56.405	2.74	56.405	2.74	2713.4
	34	48.964	2.20	48.964	2.20	2688.1
	38	49.564	2.16	49.564	2.16	2783.2
	43	47.164	2.09	47.164	2.09	2700.8
	44	46.924	2.04	46.924	2.04	2672
	47	56.885	2.78	56.885	2.78	2782.7
Average		50.88	2.32	50.88	2.32	2728.03
Standard Deviation		4.12	0.31	4.12	0.31	45.65
Number		7	7	7	7	7

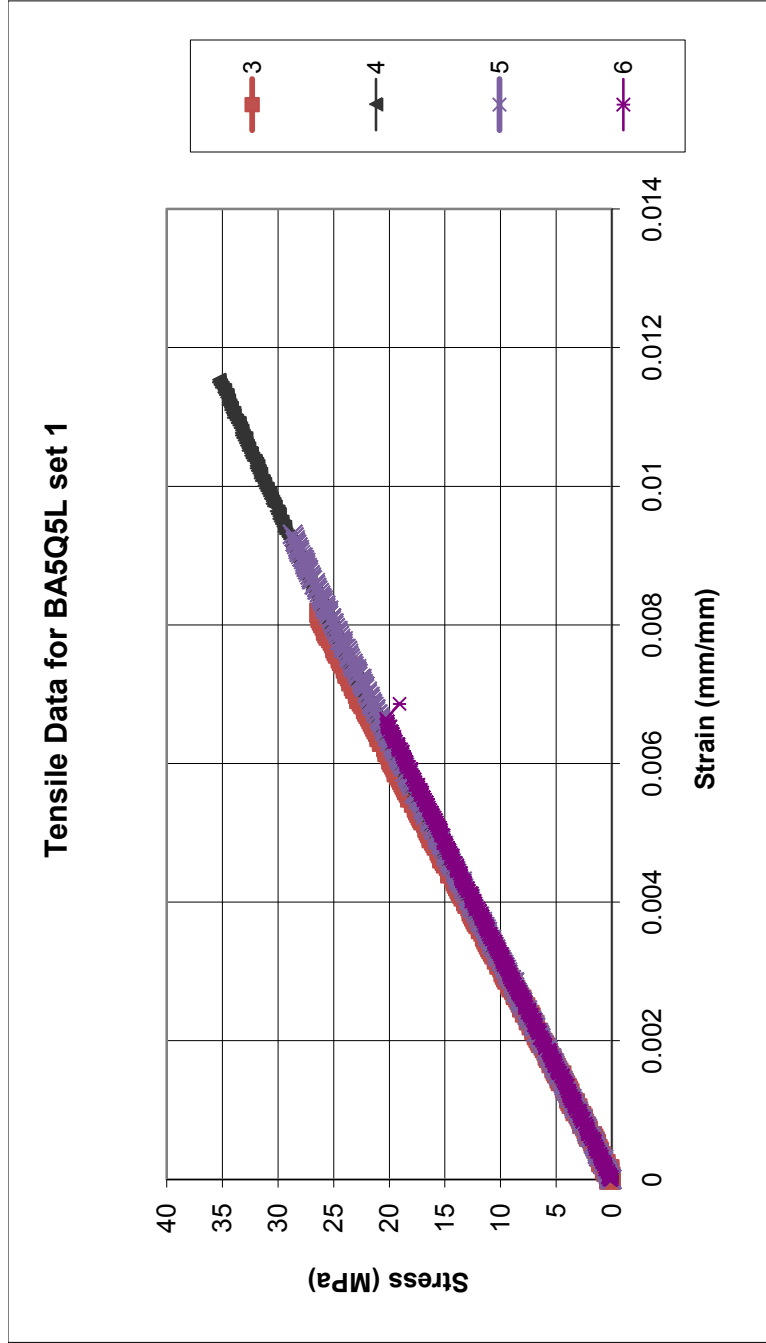


Figure J.47: Tensile Results for BA5Q5L set 1: Injection Molded 8-25-10, Extruded 7-7-10

Table J.47: Tensile Results for BA5Q5L set 1: Injection Molded 8-25-10, Extruded 7-7-10

Sample	Specimen	Tensile Ultimate Stress (MPa)	Tensile Strain at Ultimate Stress (%)	Tensile Fracture Stress (MPa)	Tensile Strain at Fracture Stress (%)	Tensile Modulus (MPa)
BA5Q5L Set 1	3	29.762	0.93	29.762	0.93	3267.9
	4	35.283	1.15	35.283	1.15	3216
	5	28.682	0.93	28.682	0.93	3162.2
	6	20.282	0.66	20.282	0.66	3097.5
Average		28.50	0.92	28.50	0.92	3185.90
Standard Deviation		6.20	0.20	6.20	0.20	73.04
Number		4	4	4	4	4

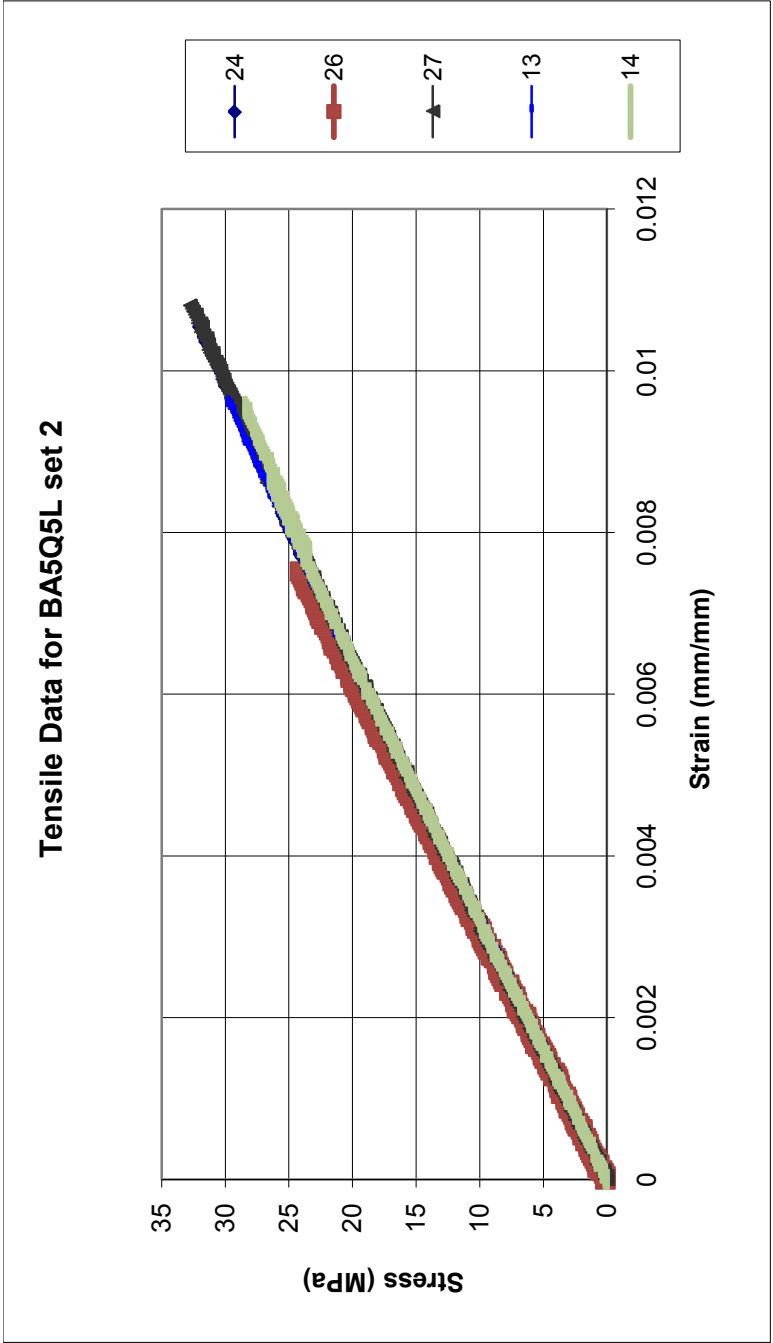


Figure J.48: Tensile Results for BA5Q5L set 2: Injection Molded 8-25-10, Extruded 7-7-10

Table J.48: Tensile Results for BA5Q5L set 2: Injection Molded 8-25-10, Extruded 7-7-10

Sample	Specimen	Tensile Ultimate Stress (MPa)	Tensile Strain at Ultimate Stress (%)	Tensile Fracture Stress (MPa)	Tensile Strain at Fracture Stress (%)	Tensile Modulus (MPa)
BA5Q5L Set 2	24	32.043	1.05	32.043	1.05	3138.7
	26	27.122	0.85	27.122	0.85	3242.6
	27	32.763	1.08	32.763	1.08	3133.3
	13	30.243	0.97	30.243	0.97	3137.4
	14	28.442	0.95	28.442	0.95	3123.5
Average		30.12	0.98	30.12	0.98	3155.10
Standard Deviation		2.37	0.09	2.37	0.09	49.28
Number		5	5	5	5	5

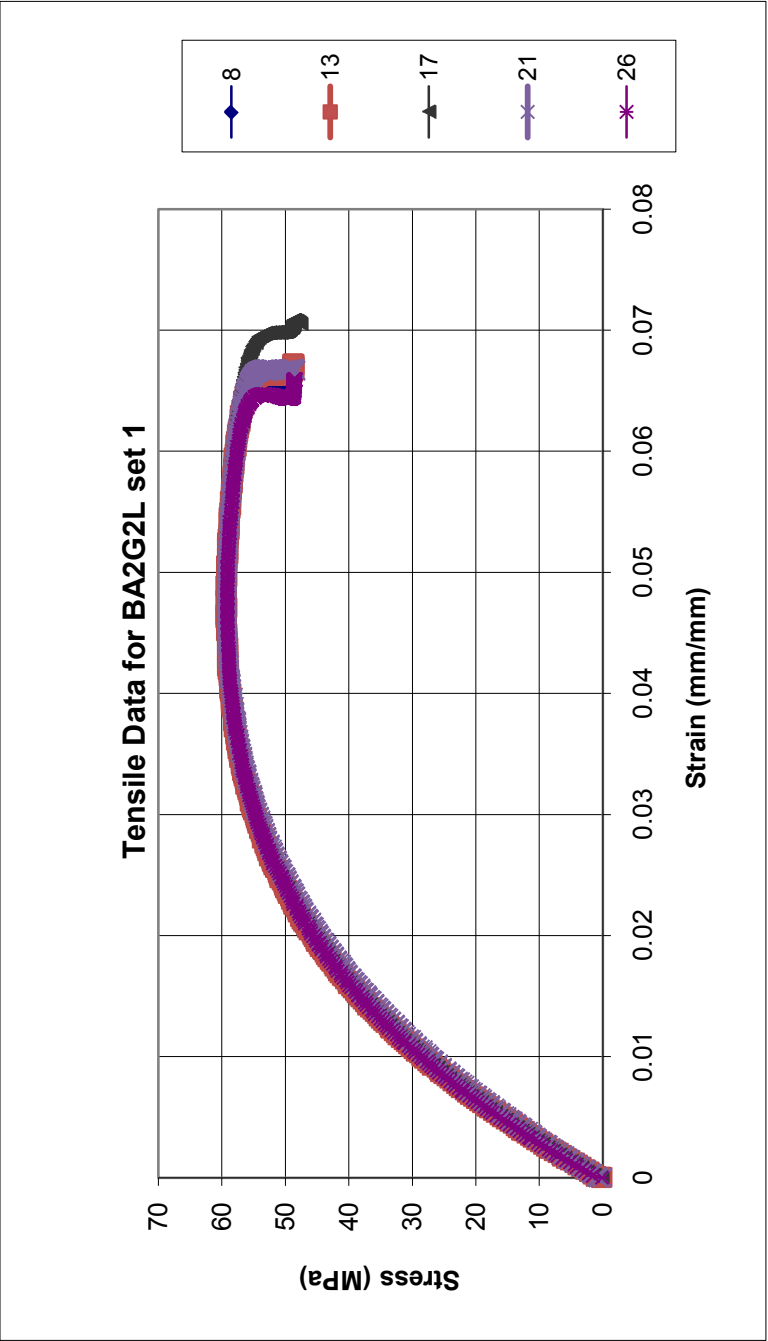


Figure J.49: Tensile Results for BA2G2L set 1: Injection Molded 8-18-10, Extruded 7-6-10

Table J.49: Tensile Results for BA2G2L set 1: Injection Molded 8-18-10, Extruded 7-6-10

Sample	Specimen	Tensile Ultimate Stress (MPa)	Tensile Strain at Ultimate Stress (%)	Tensile Fracture Stress (MPa)	Tensile Strain at Fracture Stress (%)	Tensile Modulus (MPa)
BA2G2L Set 1	8	59.400	4.86	48.480	6.60	2664.2
	13	59.400	4.62	48.480	6.79	2892
	17	59.400	4.61	47.640	7.06	2845.8
	21	59.280	4.56	48.360	6.67	2721
	26	59.160	4.53	48.360	6.59	2855.7
Average		59.33	4.64	48.26	6.74	2795.74
Standard Deviation		0.11	0.13	0.35	0.19	97.80
Number		5	5	5	5	5

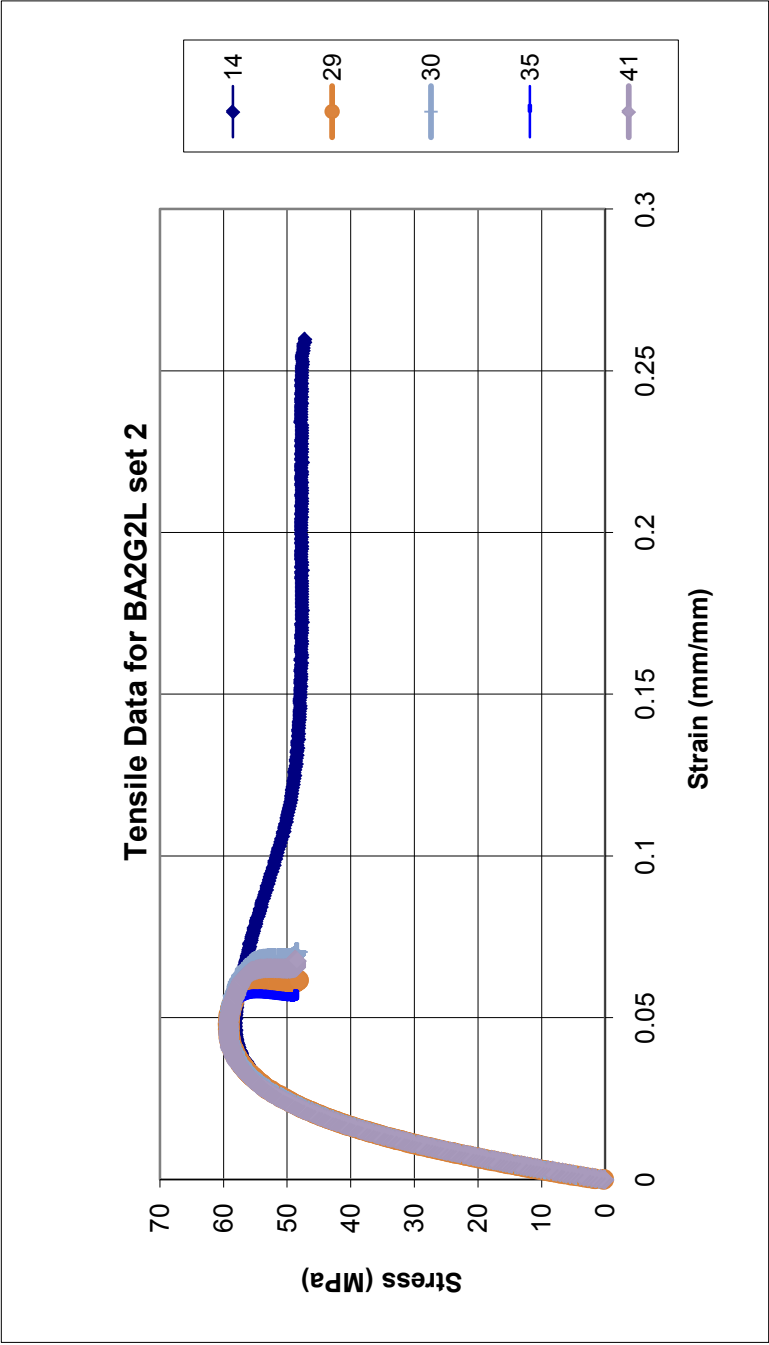


Figure J.50: Tensile Results for BA2G2L set 2: Injection Molded 8-18-10, Extruded 7-6-10

Table J.50: Tensile Results for BA2G2L set 2: Injection Molded 8-18-10, Extruded 7-6-10

Sample	Specimen	Tensile Ultimate Stress (MPa)	Tensile Strain at Ultimate Stress (%)	Tensile Fracture Stress (MPa)	Tensile Strain at Fracture Stress (%)	Tensile Modulus (MPa)
BA2G2L Set 2	14	58.205	4.67	47.164	25.90	2688.1
	29	59.280	4.64	48.360	6.16	2733.3
	30	59.280	4.61	48.360	7.03	2737
	35	59.160	4.17	48.480	5.64	2876.6
	41	59.280	4.47	48.600	6.77	2800.7
Average		59.04	4.51	48.19	10.30	2767.14
Standard Deviation		0.47	0.21	0.58	8.74	73.16
Number		5	5	5	5	5

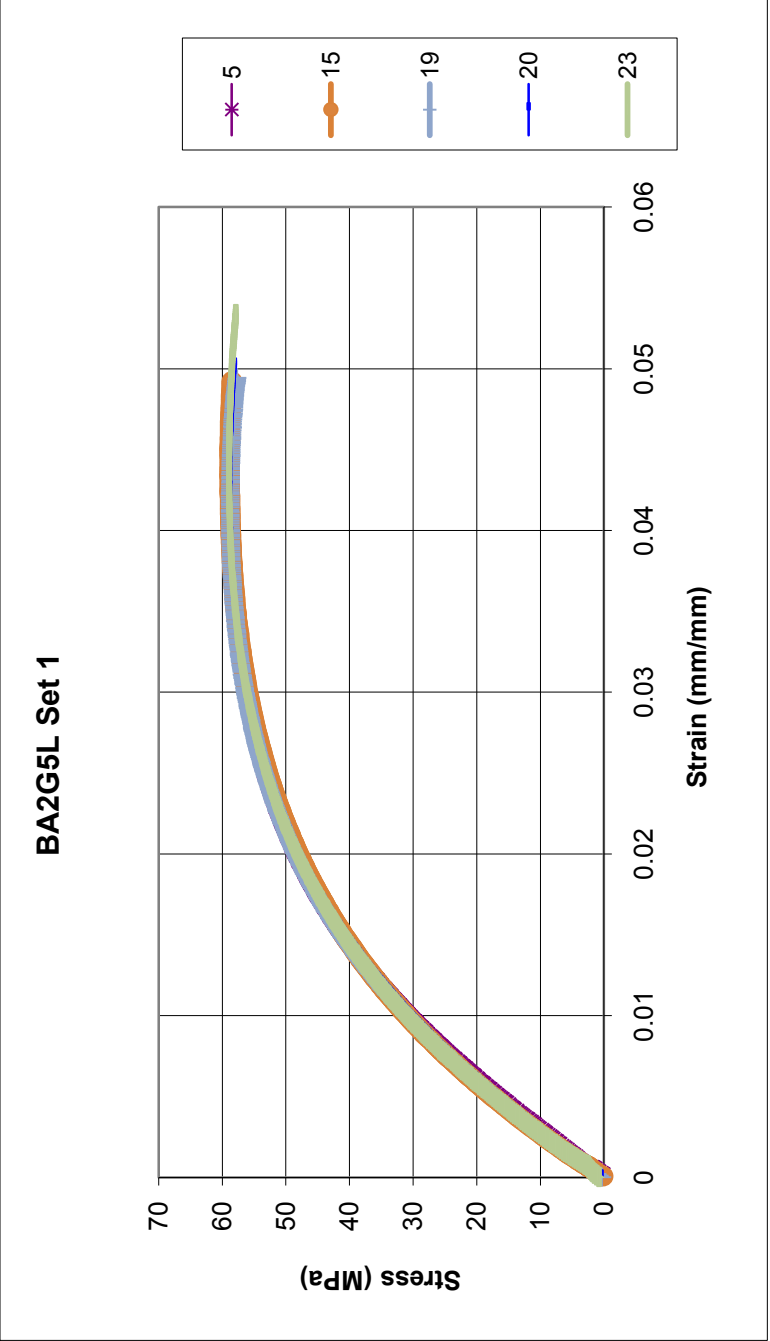


Figure J.51: Tensile Results for BA2G5L set1: Injection Molded 8-18-10, Extruded 7-6-10

Table J.51: Tensile Results for BA2G5L set 1: Injection Molded 8-18-10, Extruded 7-6-10

Sample	Specimen	Tensile Ultimate Stress (MPa)	Tensile Strain at Ultimate Stress (%)	Tensile Fracture Stress (MPa)	Tensile Strain at Fracture Stress (%)	Tensile Modulus (MPa)
BA2G5L Set 1	5	58.736	3.94	58.736	3.94	3211.1
	15	58.881	4.33	58.529	4.91	3335.3
	19	58.772	4.13	57.715	4.94	3325.3
	20	58.825	4.31	57.757	5.10	3236.7
	23	58.938	4.31	57.886	5.32	3302.9
Average		58.83	4.20	58.12	4.84	3282.26
Standard Deviation		0.08	0.17	0.47	0.53	55.30
Number		5	5	5	5	5

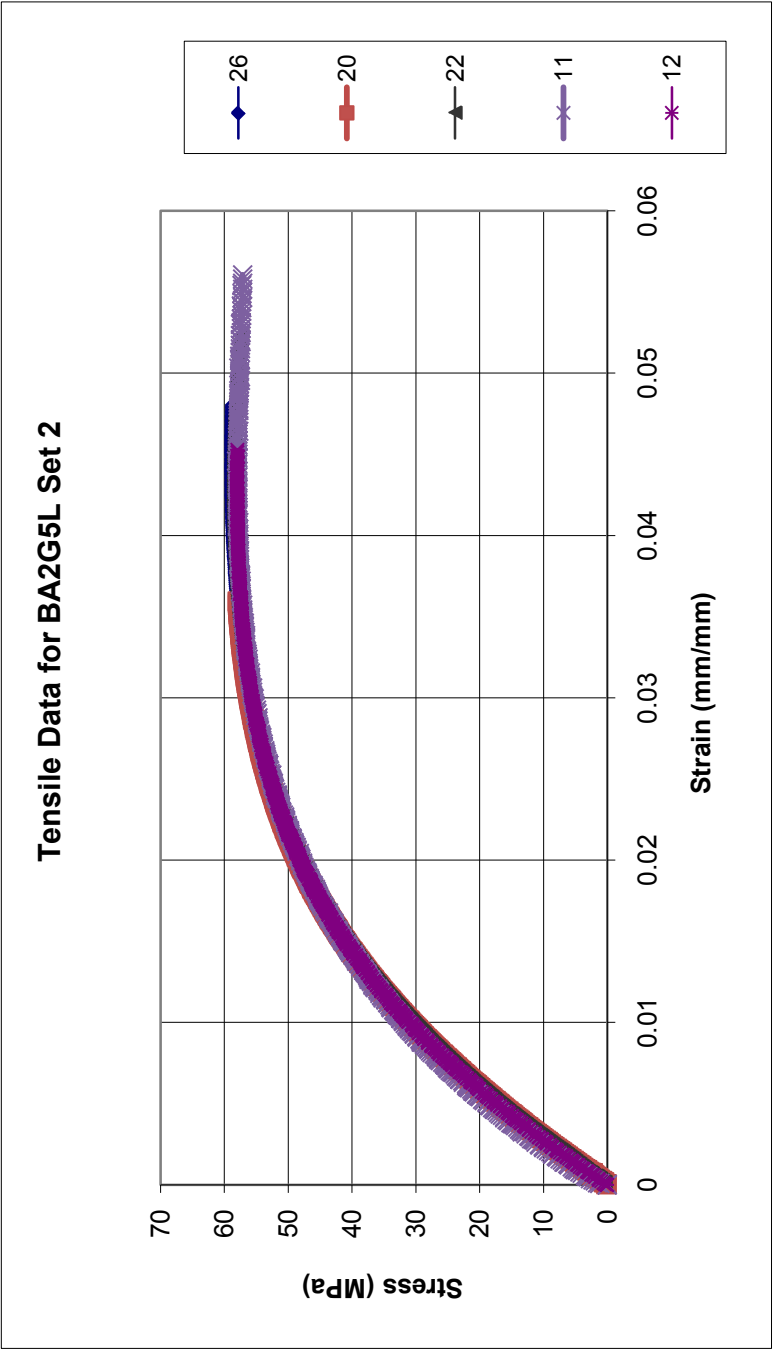


Figure J.52: Tensile Results for BA2G5L set 2: Injection Molded 8-18-10, Extruded 7-6-10

Table J.52: Tensile Results for BA2G5L set 2: Injection Molded 8-18-10, Extruded 7-6-10

Sample	Specimen	Tensile Ultimate Stress (MPa)	Tensile Strain at Ultimate Stress (%)	Tensile Fracture Stress (MPa)	Tensile Strain at Fracture Stress (%)	Tensile Modulus (MPa)
BA2G5L Set 2	26	58.918	4.56	58.811	4.78	3207.1
	20	58.364	4.18	58.307	4.34	3286.1
	22	58.556	4.27	57.312	5.23	3239.9
	11	58.085	4.46	57.125	5.52	3295.3
	12	58.085	4.10	57.965	4.45	3252.7
Average		58.40	4.31	57.90	4.86	3256.22
Standard Deviation		0.35	0.19	0.70	0.50	35.75
Number		5	5	5	5	5

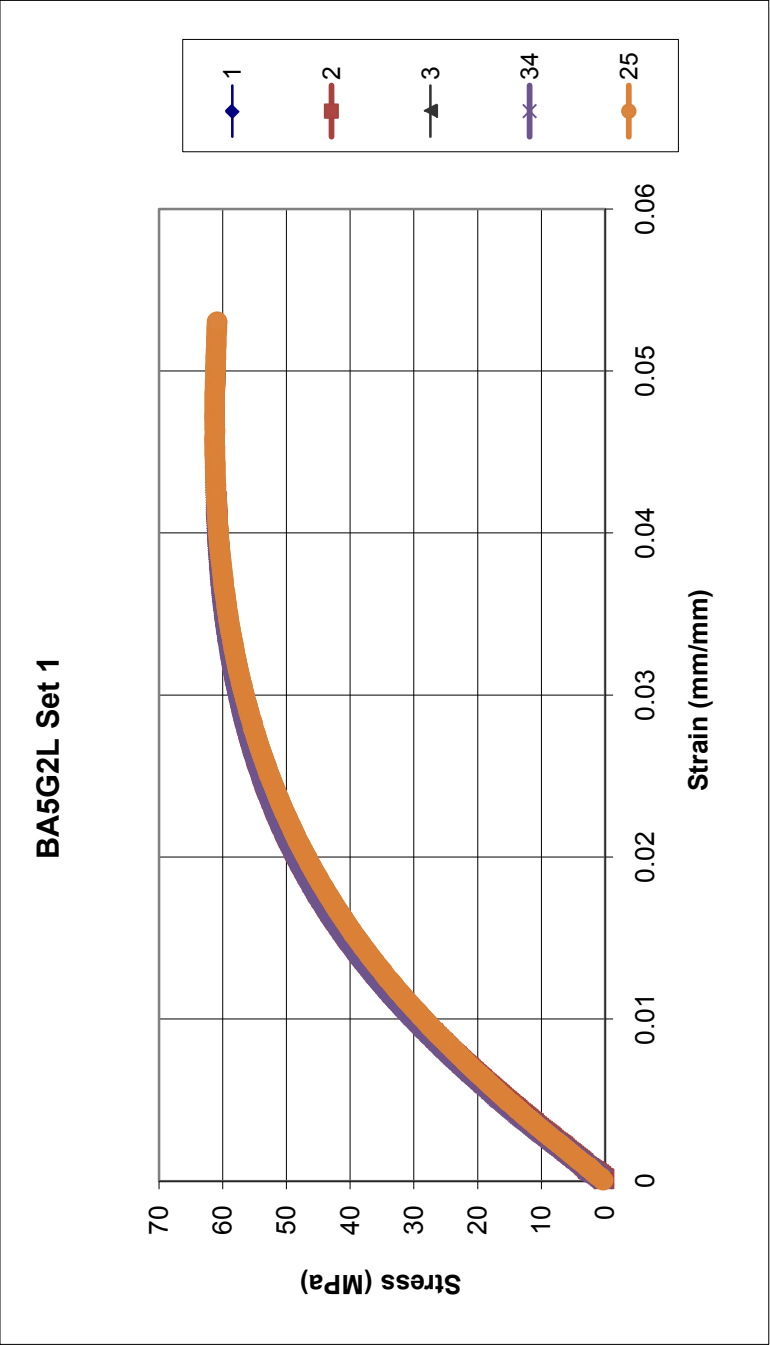


Figure J.53: Tensile Results for BA5G2L set 1: Injection Molded 8-18-10, Extruded 7-6-10

Table J.53: Tensile Results for BA5G2L set 1: Injection Molded 8-18-10, Extruded 7-6-10

Sample	Specimen	Tensile Ultimate Stress (MPa)	Tensile Strain at Ultimate Stress (%)	Tensile Fracture Stress (MPa)	Tensile Strain at Fracture Stress (%)	Tensile Modulus (MPa)
BA5G2L Set 1	1	61.268	4.54	61.065	4.93	3102.1
	2	61.160	4.58	60.666	5.25	3048
	3	61.069	4.48	60.807	4.97	3058.8
	34	61.261	4.52	61.183	4.72	3084.8
	25	61.279	4.57	60.886	5.28	2949.2
Average		61.21	4.54	60.92	5.03	3048.58
Standard Deviation		0.09	0.04	0.21	0.23	59.49
Number		5	5	5	5	5

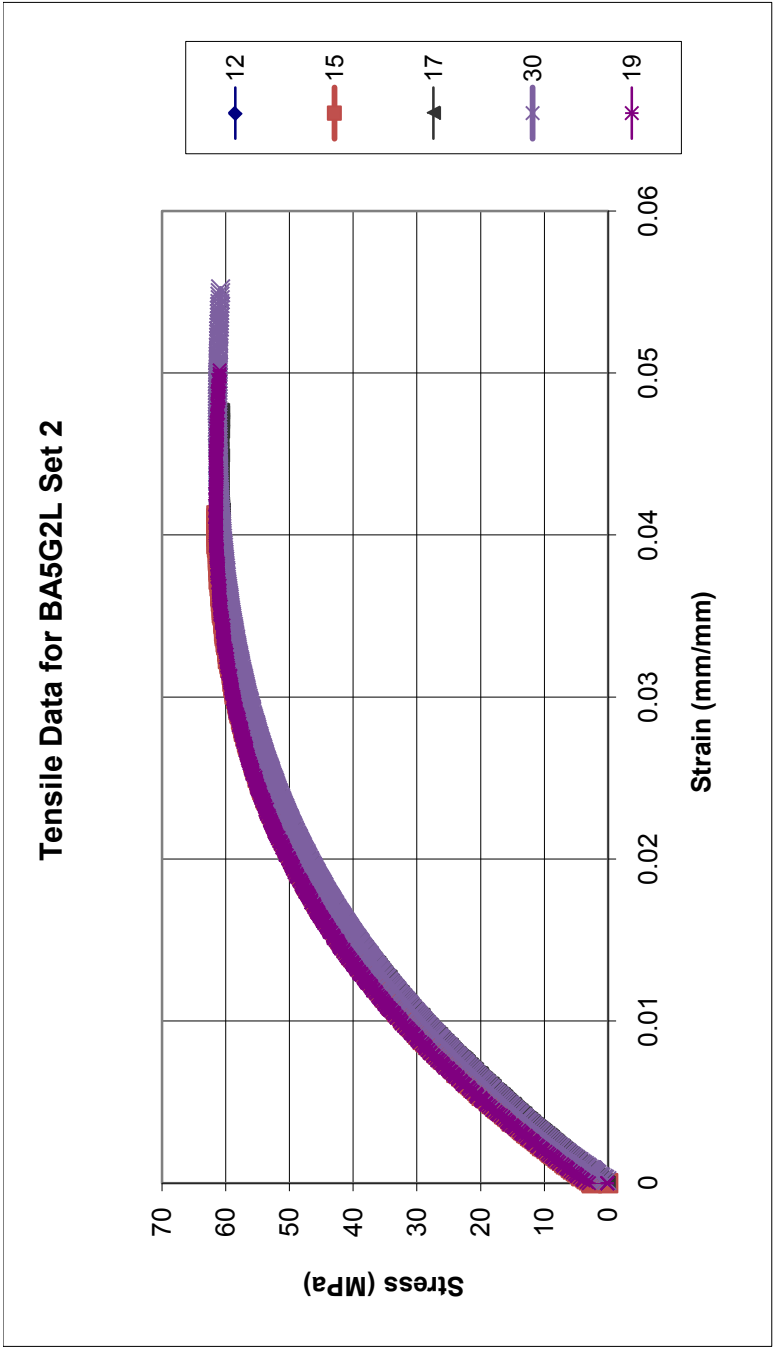


Figure J.54: Tensile Results for BA5G2L set 2: Injection Molded 8-18-10, Extruded 7-6-10

Table J.54: Tensile Results for BA5G2L set 2: Injection Molded 8-18-10, Extruded 7-6-10

Sample	Specimen	Tensile Ultimate Stress (MPa)	Tensile Strain at Ultimate Stress (%)	Tensile Fracture Stress (MPa)	Tensile Strain at Fracture Stress (%)	Tensile Modulus (MPa)
BA5G2L Set 2	12	61.560	4.05	61.320	4.54	3023.2
	15	61.680	4.36	61.080	4.99	3066.2
	17	60.845	4.51	60.605	4.73	2916.8
	30	61.293	4.80	60.826	5.50	3042.4
	19	61.680	4.11	60.960	4.95	3125.7
Average		61.41	4.37	60.96	4.94	3034.86
Standard Deviation		0.35	0.31	0.27	0.36	76.43
Number		5	5	5	5	5

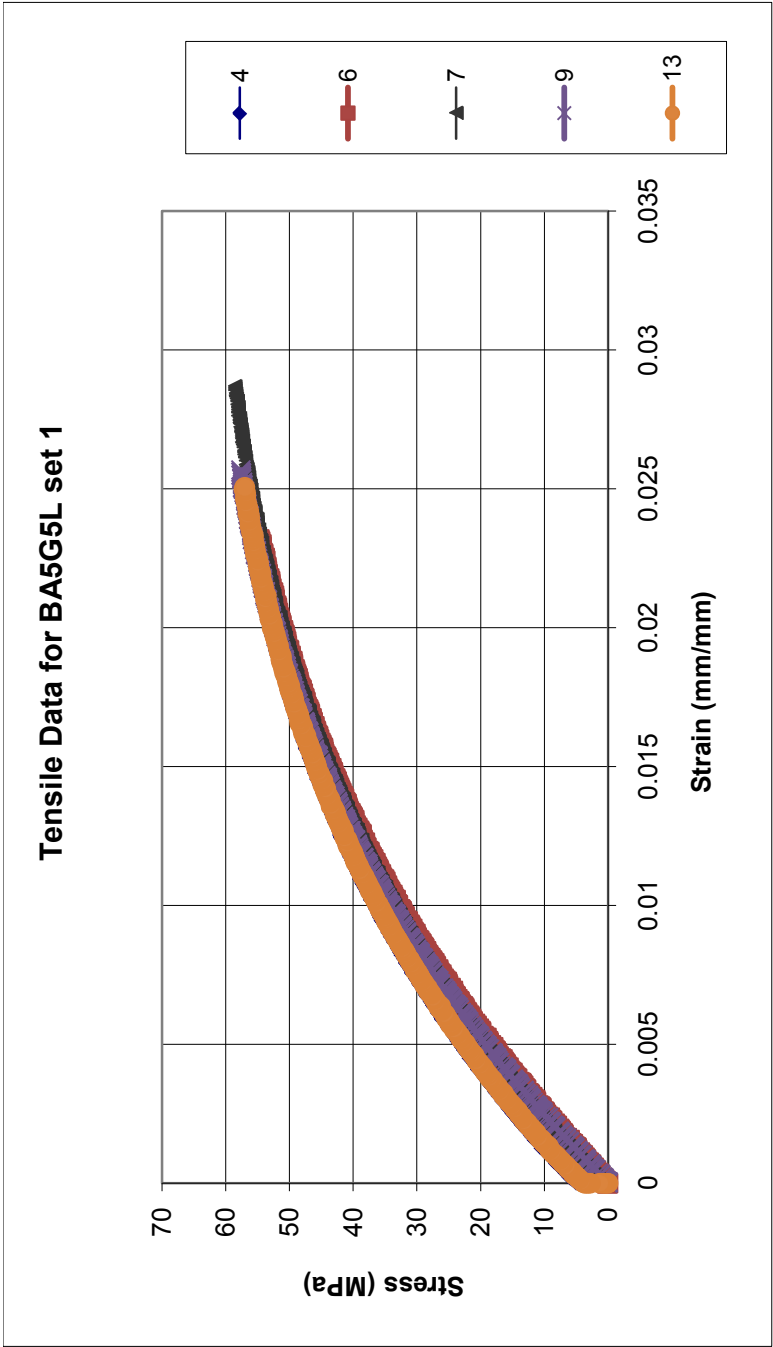


Figure J.55: Tensile Results for BA5G5L set 1: Injection Molded 8-6-10, Extruded 7-6-10

Table J.55: Tensile Results for BA5G5L set 1: Injection Molded 8-6-10, Extruded 7-6-10

Sample	Specimen	Tensile Ultimate Stress (MPa)	Tensile Strain at Ultimate Stress (%)	Tensile Fracture Stress (MPa)	Tensile Strain at Fracture Stress (%)	Tensile Modulus (MPa)
BA5G5L Set 1	4	57.125	2.45	57.125	2.45	3749.8
	6	57.845	2.73	57.845	2.73	3659.7
	7	58.685	2.87	58.685	2.87	3684.7
	9	57.605	2.55	57.605	2.55	3854.6
	13	57.125	2.50	57.125	2.50	3773.4
Average		57.68	2.62	57.68	2.62	3744.44
Standard Deviation		0.64	0.18	0.64	0.18	77.06
Number		5	5	5	5	5

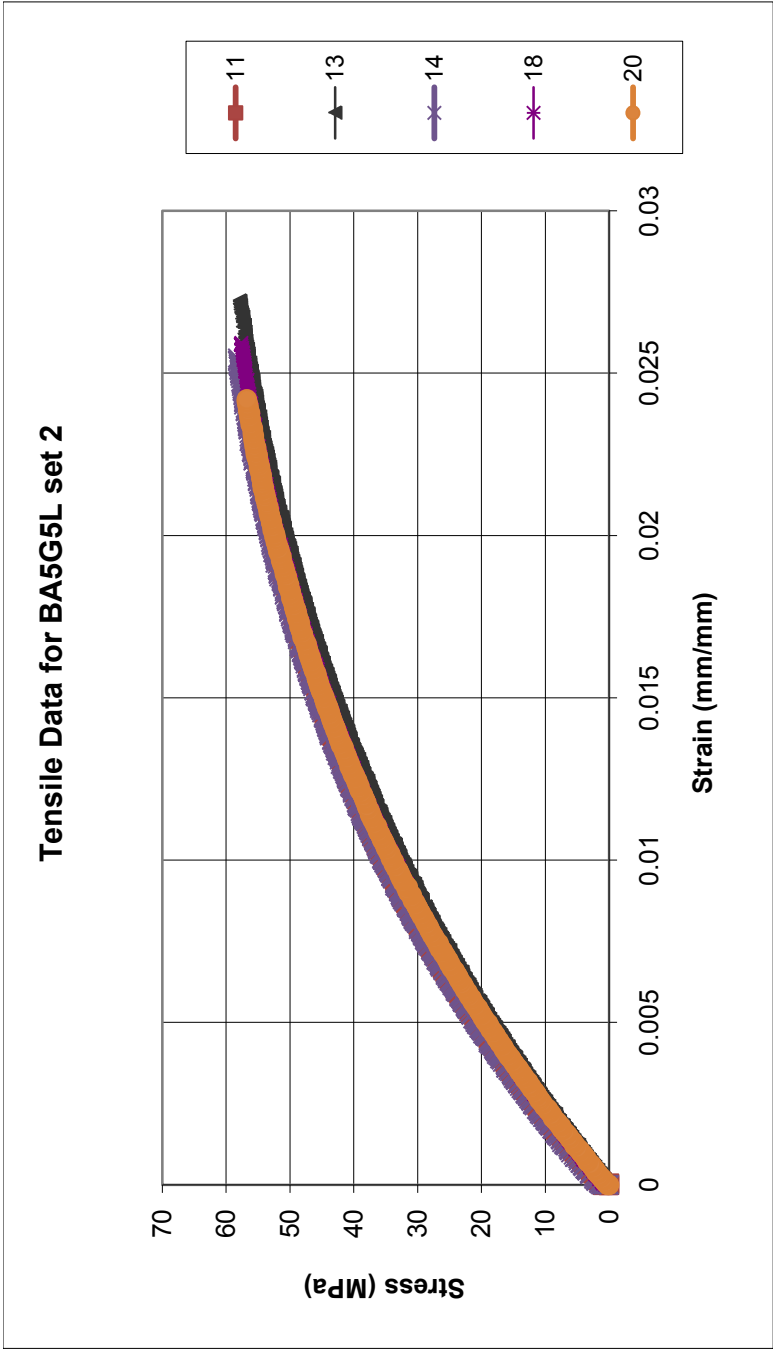


Figure J.56: Tensile Results for BA5G5L set 2: Injection Molded 8-6-10, Extruded 7-6-10

Table J.56: Tensile Results for BA5G5L set 2: Injection Molded 8-6-10, Extruded 7-6-10

Sample	Specimen	Tensile Ultimate Stress (MPa)	Tensile Strain at Ultimate Stress (%)	Tensile Fracture Stress (MPa)	Tensile Strain at Fracture Stress (%)	Tensile Modulus (MPa)
BA5G5L Set 2	11	58.320	2.61	58.200	2.59	3932.8
	13	57.840	2.71	57.840	2.71	3605.1
	14	58.200	2.54	58.200	2.54	3890.3
	18	57.720	2.59	57.720	2.59	3685
	20	56.760	2.41	56.760	2.41	3767.8
Average		57.77	2.57	57.74	2.57	3776.20
Standard Deviation		0.62	0.11	0.59	0.11	137.12
Number		5	5	5	5	5

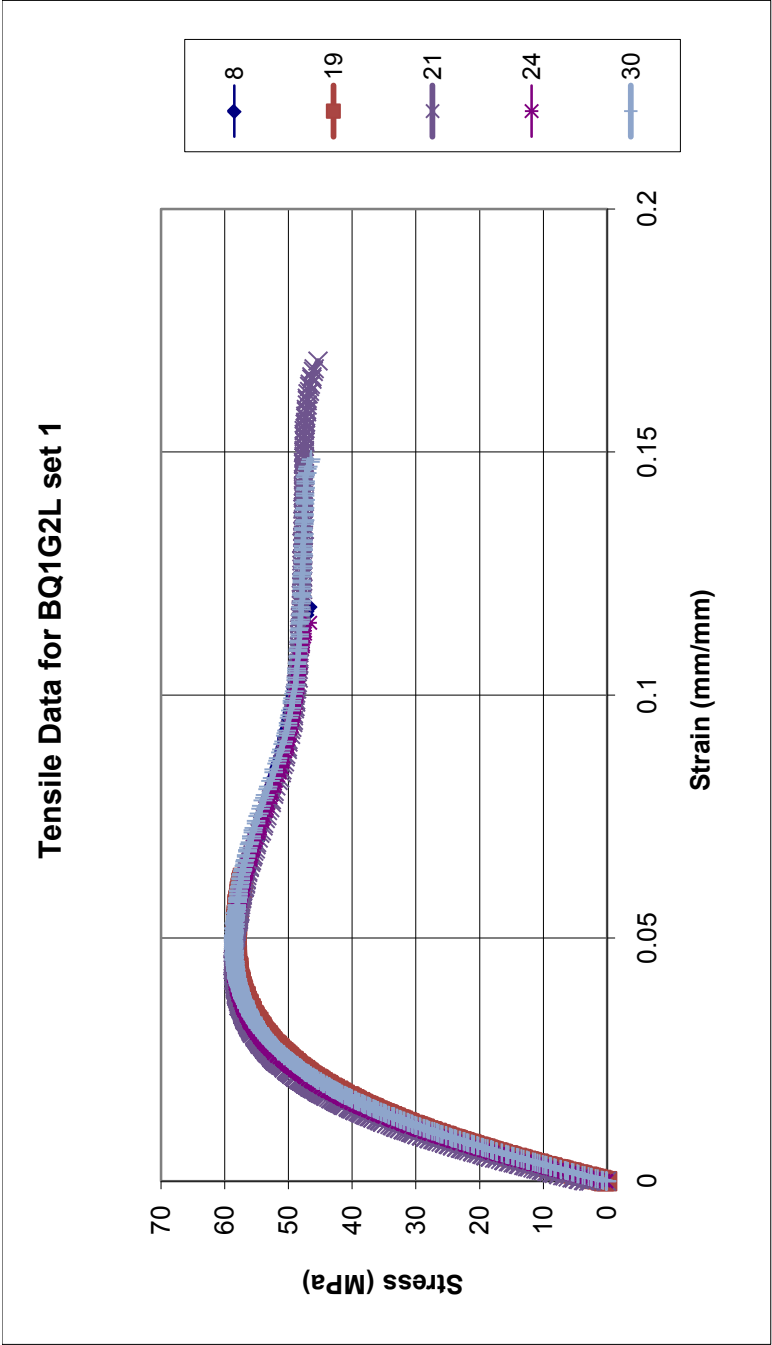


Figure J.57: Tensile Results for BQ1G2L set 1: Injection Molded 8-18-10, Extruded 7-1-10

Table J.57: Tensile Results for BQ1G2L set 1: Injection Molded 8-18-10, Extruded 7-1-10

Sample	Specimen	Tensile Ultimate Stress (MPa)	Tensile Strain at Ultimate Stress (%)	Tensile Fracture Stress (MPa)	Tensile Strain at Fracture Stress (%)	Tensile Modulus (MPa)
BQ1G2L Set 1	8	58.085	4.82	47.044	11.66	2716.8
	19	58.325	4.69	52.804	8.44	2717.8
	21	58.680	4.35	45.960	16.71	2870.8
	24	58.560	4.22	47.400	11.26	2833.5
	30	58.680	4.78	46.560	14.80	2706.9
Average		58.47	4.57	47.95	12.57	2769.16
Standard Deviation		0.26	0.27	2.77	3.23	77.02
Number		5	5	5	5	5

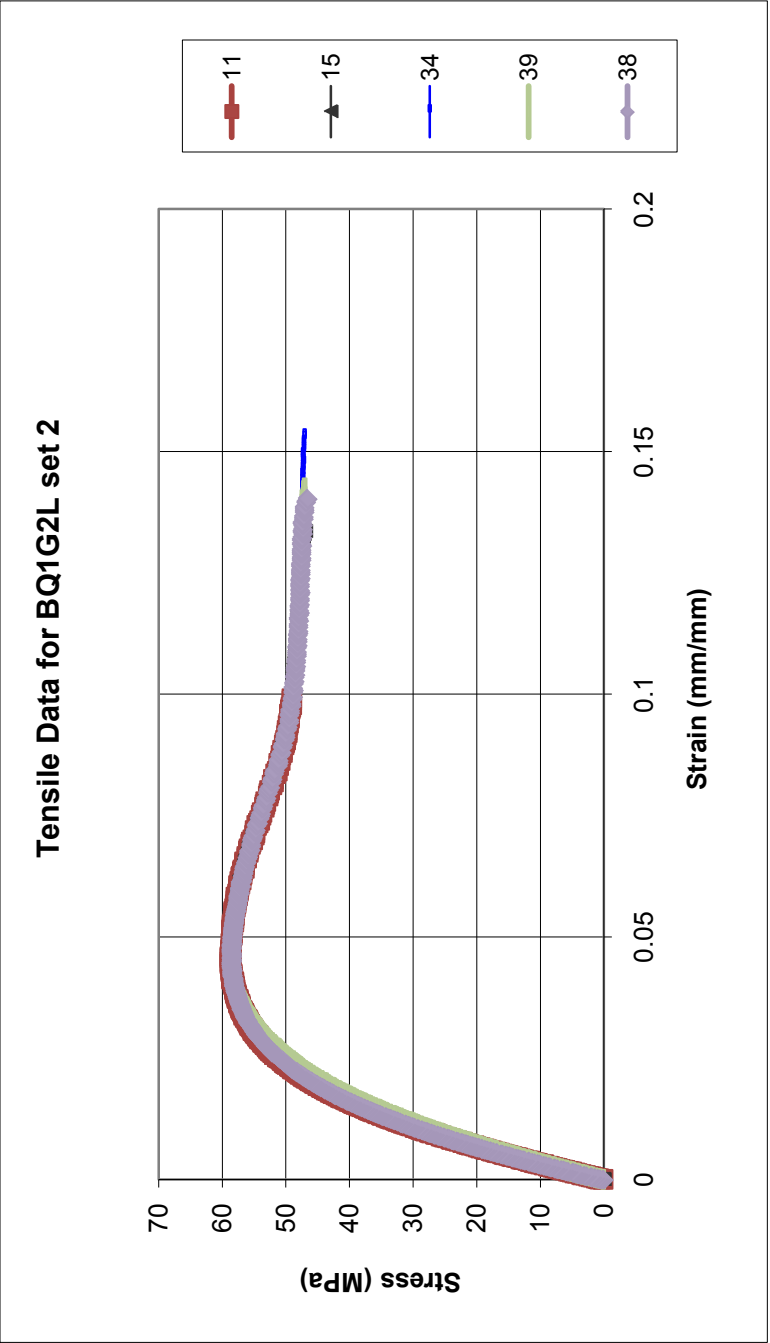


Figure J.58: Tensile Results for BQ1G2L set 2: Injection Molded 8-18-10, Extruded 7-1-10

Table J.58: Tensile Results for BQ1G2L set 2: Injection Molded 8-18-10, Extruded 7-1-10

Sample	Specimen	Tensile Ultimate Stress (MPa)	Tensile Strain at Ultimate Stress (%)	Tensile Fracture Stress (MPa)	Tensile Strain at Fracture Stress (%)	Tensile Modulus (MPa)
BQ1G2L Set 2	11	58.800	4.44	45.960	13.62	2831.4
	15	58.800	4.41	47.160	13.30	2859.2
	34	58.560	4.66	46.440	15.86	2708.3
	39	58.440	4.54	47.160	14.15	2670.4
	38	58.560	4.37	46.800	13.97	2847.1
Average		58.63	4.48	46.70	14.18	2783.28
Standard Deviation		0.16	0.11	0.51	0.99	87.34
Number		5	5	5	5	5

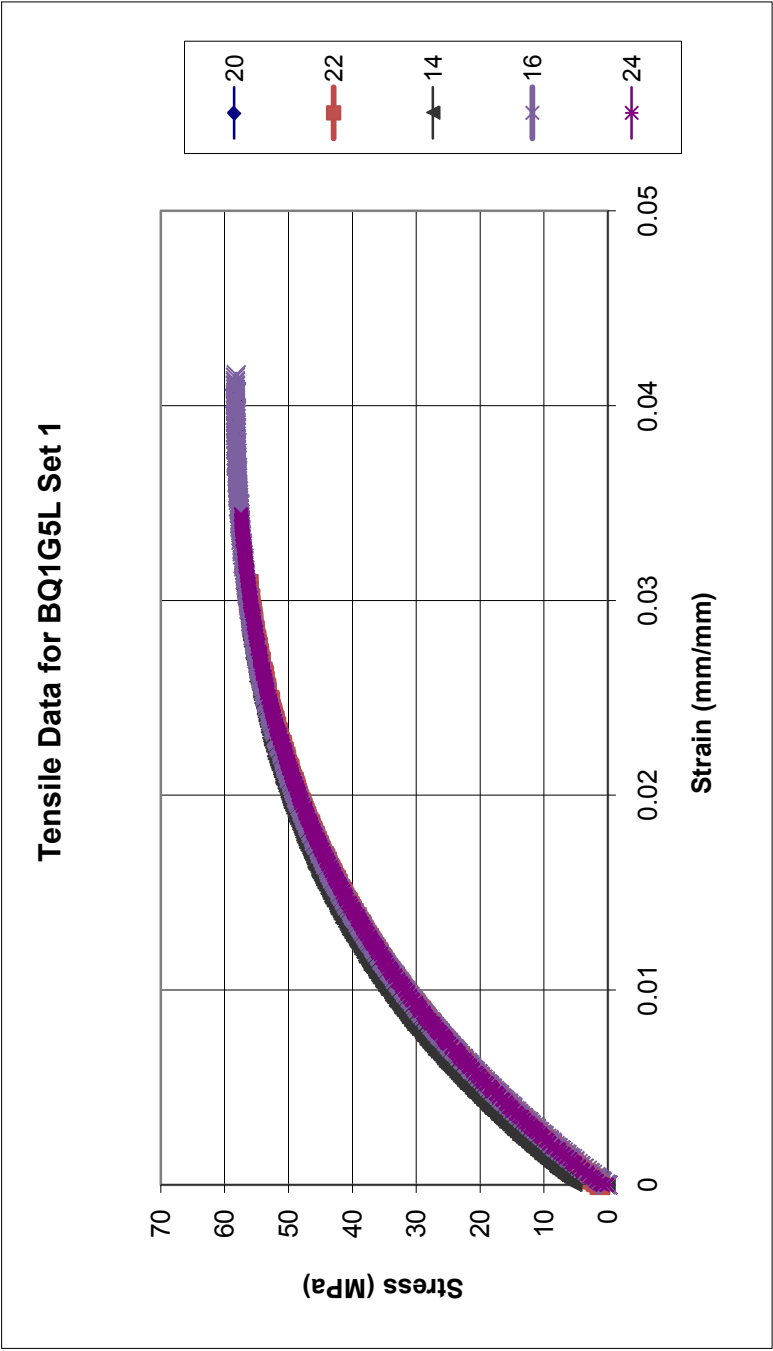


Figure J.59: Tensile Results for BQ1G5L set 1: Injection Molded 8-18-10, Extruded 7-1-10

Table J.59: Tensile Results for BQ1G5L set 1: Injection Molded 8-18-10, Extruded 7-1-10

Sample	Specimen	Tensile Ultimate Stress (MPa)	Tensile Strain at Ultimate Stress (%)	Tensile Fracture Stress (MPa)	Tensile Strain at Fracture Stress (%)	Tensile Modulus (MPa)
BQ1G5L Set 1	20	58.200	3.95	58.200	4.03	3356
	22	57.960	3.63	57.960	3.63	3445.8
	14	58.200	3.67	58.200	3.67	3438.2
	16	58.440	4.04	58.320	4.10	3541
	24	57.480	3.44	57.480	3.44	3451.9
Average		58.06	3.74	58.03	3.77	3446.58
Standard Deviation		0.36	0.24	0.34	0.28	65.61
Number		5	5	5	5	5

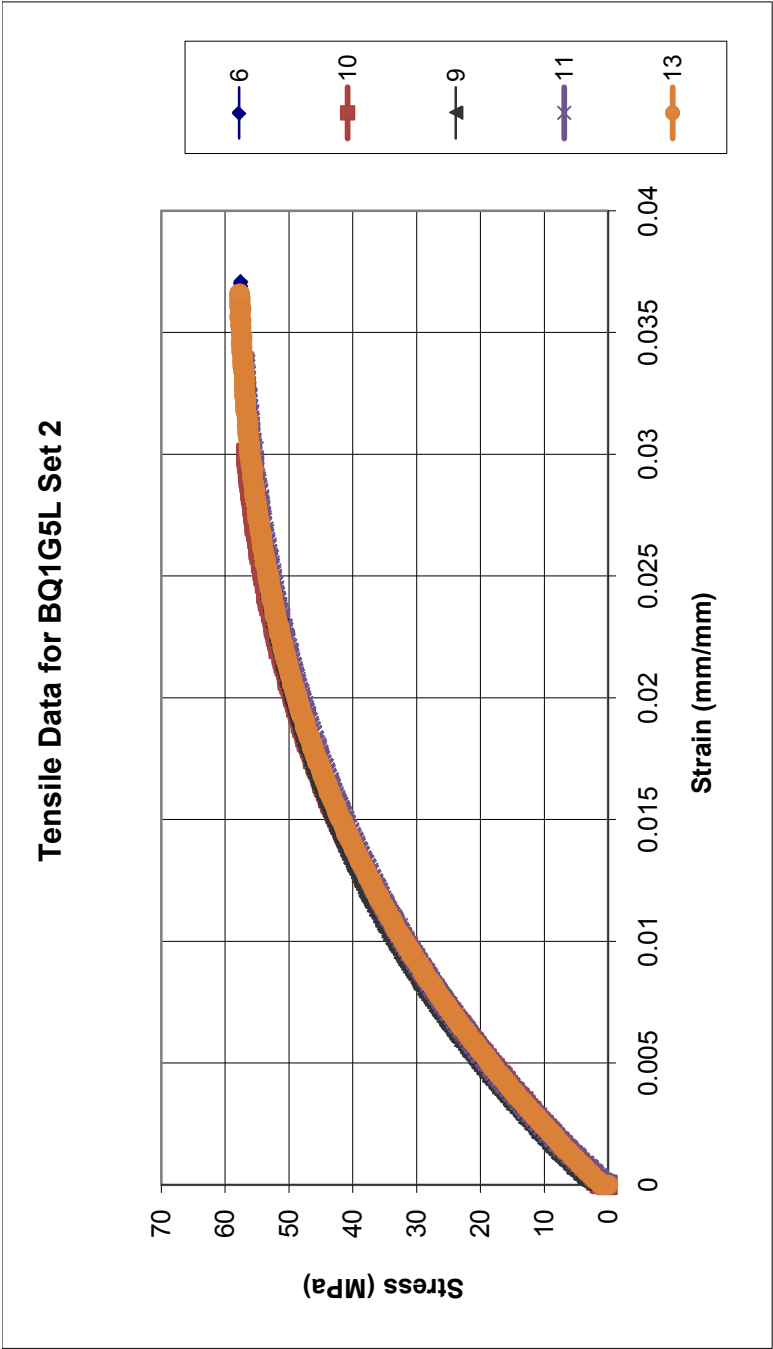


Figure J.60: Tensile Results for BQ1G5L set 2: Injection Molded 8-6-10, Extruded 7-1-10

Table J.60: Tensile Results for BQ1G5L set 2: Injection Molded 8-6-10, Extruded 7-1-10

Sample	Specimen	Tensile Ultimate Stress (MPa)	Tensile Strain at Ultimate Stress (%)	Tensile Fracture Stress (MPa)	Tensile Strain at Fracture Stress (%)	Tensile Modulus (MPa)
BQ1G5L Set 2	6	57.616	3.70	57.616	3.70	3315.8
	10	58.200	3.56	58.200	3.56	3462.2
	9	57.497	3.39	57.497	3.41	3502.7
	11	57.018	3.38	57.018	3.38	3570.9
	13	57.736	3.56	57.736	3.61	3440
Average		57.61	3.52	57.61	3.53	3458.32
Standard Deviation		0.43	0.13	0.43	0.13	93.95
Number		5	5	5	5	5

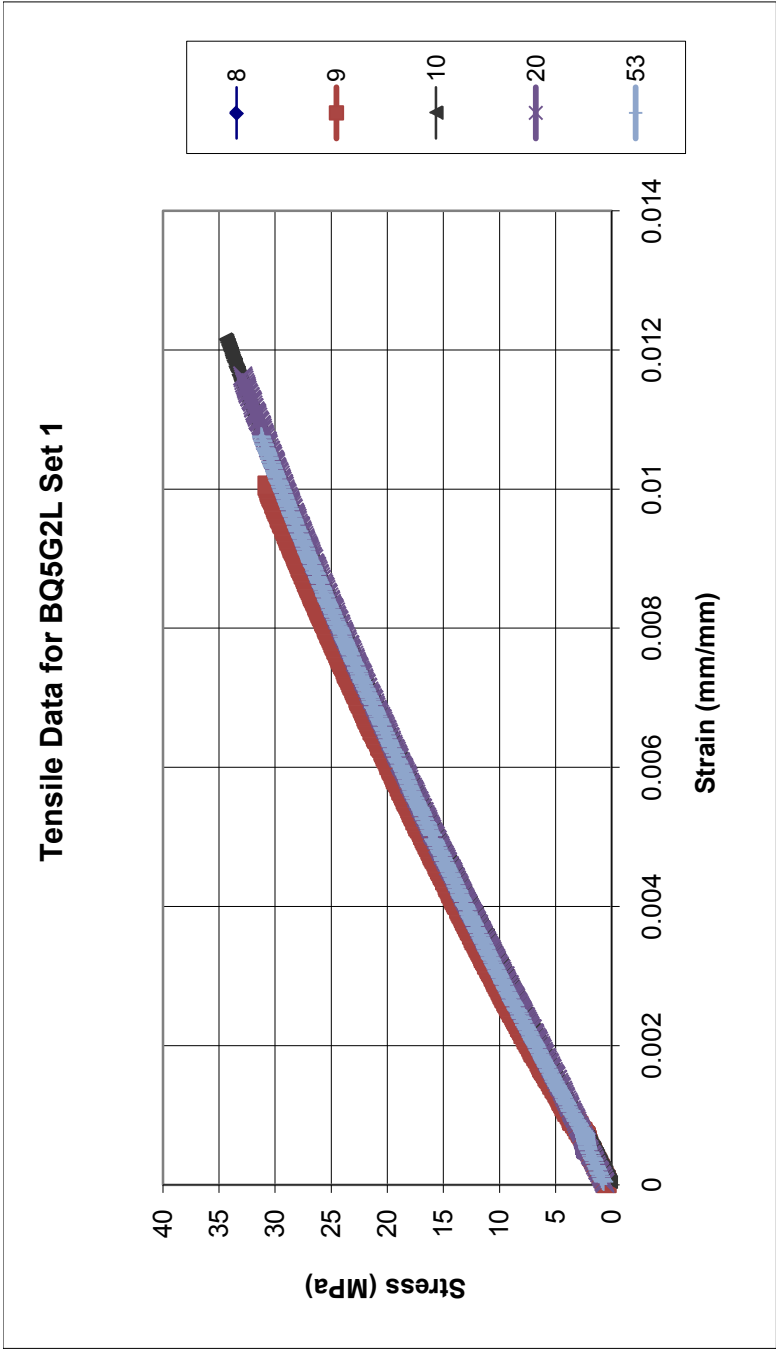


Figure J.61: Tensile Results for BQ5G2L set 1: Injection Molded 9-9-10, Extruded 7-1-10

Table J.61: Tensile Results for BQ5G2L set 1: Injection Molded 9-9-10, Extruded 7-1-10

Sample	Specimen	Tensile Ultimate Stress (MPa)	Tensile Strain at Ultimate Stress (%)	Tensile Fracture Stress (MPa)	Tensile Strain at Fracture Stress (%)	Tensile Modulus (MPa)
BQ5G2L Set 1	8	38.486	1.33	38.486	1.33	3176.3
	9	34.517	1.17	34.517	1.17	3177.5
	10	34.436	1.22	34.436	1.22	2996.7
	20	32.971	1.17	32.971	1.17	2974.7
	53	31.295	1.08	31.295	1.08	3019.9
Average		34.34	1.19	34.34	1.19	3069.02
Standard Deviation		2.66	0.09	2.66	0.09	99.77
Number		5	5	5	5	5

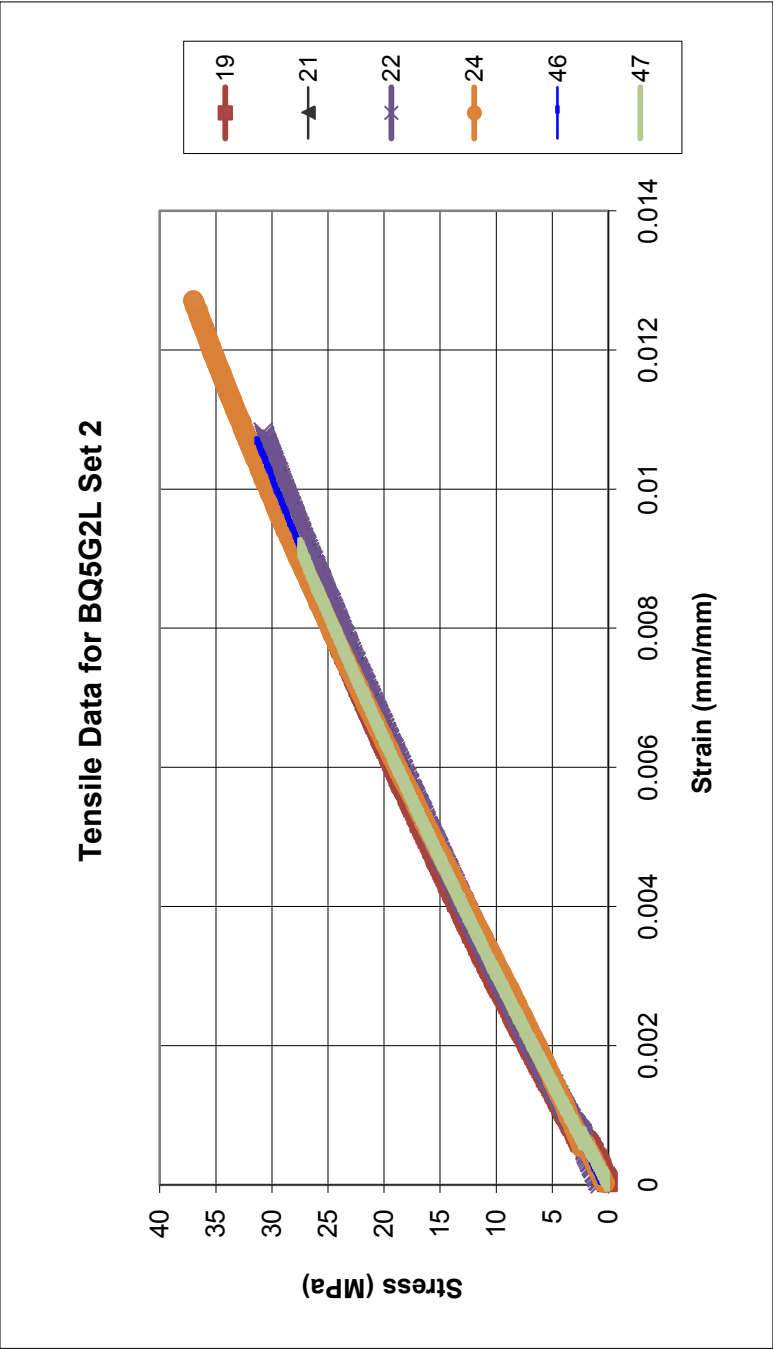


Figure J.62: Tensile Results for BQ5G2L set 2: Injection Molded 9-9-10, Extruded 7-1-10

Table J.62: Tensile Results for BQ5G2L set 2: Injection Molded 9-9-10, Extruded 7-1-10

Sample	Specimen	Tensile Ultimate Stress (MPa)	Tensile Strain at Ultimate Stress (%)	Tensile Fracture Stress (MPa)	Tensile Strain at Fracture Stress (%)	Tensile Modulus (MPa)
BQ5G2L Set 2	19	34.430	1.22	34.430	1.22	3051.2
	21	30.092	1.05	30.092	1.05	2965.5
	22	30.868	1.09	30.868	1.09	2942.2
	24	37.064	1.27	37.064	1.27	3051
	46	31.884	1.09	31.884	1.09	3049.4
	47	27.519	0.92	27.519	0.92	3050.6
Average		31.98	1.11	31.98	1.11	3018.32
Standard Deviation		3.36	0.13	3.36	0.13	50.48
Number		6	6	6	6	6

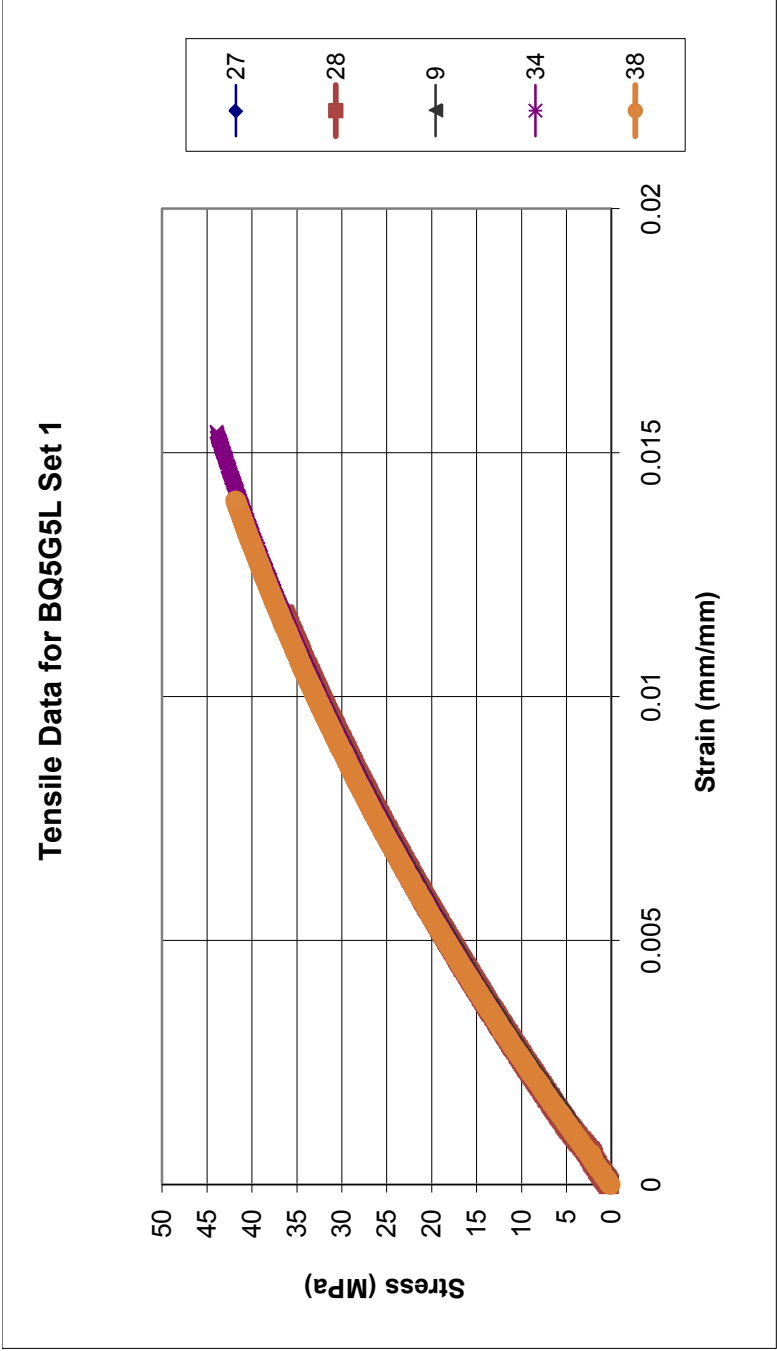


Figure J.63: Tensile Results for BQ5G5L set 1: Injection Molded 9-9-10, Extruded 7-1-10

Table J.63: Tensile Results for BQ5G5L set 1: Injection Molded 9-9-10, Extruded 7-1-10

Sample	Specimen	Tensile Ultimate Stress (MPa)	Tensile Strain at Ultimate Stress (%)	Tensile Fracture Stress (MPa)	Tensile Strain at Fracture Stress (%)	Tensile Modulus (MPa)
BQ5G5L Set 1	27	37.985	1.24	37.985	1.24	3460
	28	40.758	1.37	40.758	1.37	3487.4
	9	38.968	1.28	38.968	1.28	3446.6
	34	44.011	1.55	44.011	1.55	3501.1
	38	41.951	1.41	41.951	1.41	3556.5
Average		40.73	1.37	40.73	1.37	3490.32
Standard Deviation		2.39	0.12	2.39	0.12	42.82
Number		5	5	5	5	5

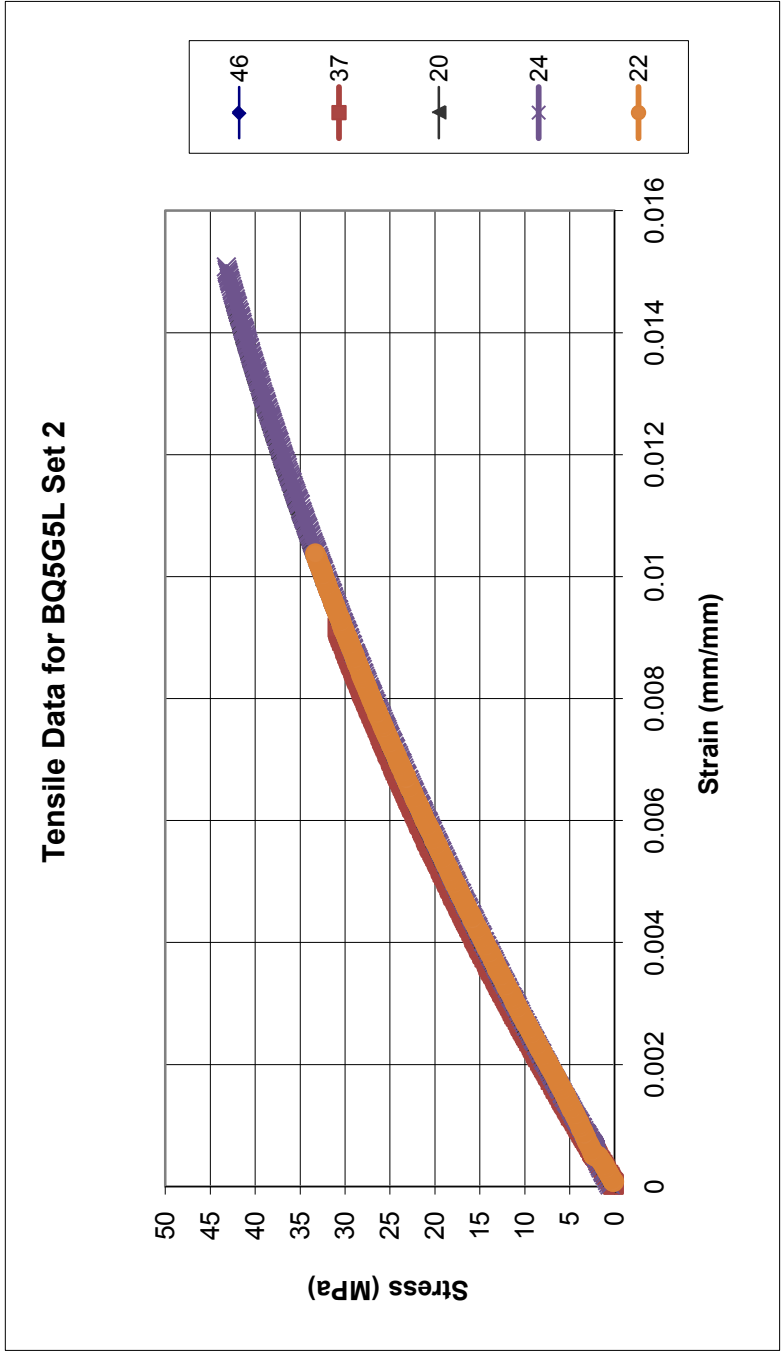


Figure J.64: Tensile Results for BQ5G5L set 2: Injection Molded 9-9-10, Extruded 7-1-10

Table J.64: Tensile Results for BQ5G5L set 2: Injection Molded 9-9-10, Extruded 7-1-10

Sample	Specimen	Tensile Ultimate Stress (MPa)	Tensile Strain at Ultimate Stress (%)	Tensile Fracture Stress (MPa)	Tensile Strain at Fracture Stress (%)	Tensile Modulus (MPa)
BQ5G5L Set 2	46	41.620	1.41	41.620	1.41	3436.1
	37	34.892	1.08	34.892	1.08	3584.8
	20	42.691	1.45	42.691	1.45	3533.6
	24	43.287	1.51	43.287	1.51	3415.9
	22	33.418	1.04	33.418	1.04	3437.4
Average		39.18	1.30	39.18	1.30	3481.56
Standard Deviation		4.66	0.22	4.66	0.22	73.65
Number		5	5	5	5	5

Appendix K: Mechanical Flexural Property Results

Appendix K.1: Polycarbonate with Carbon Nanotubes

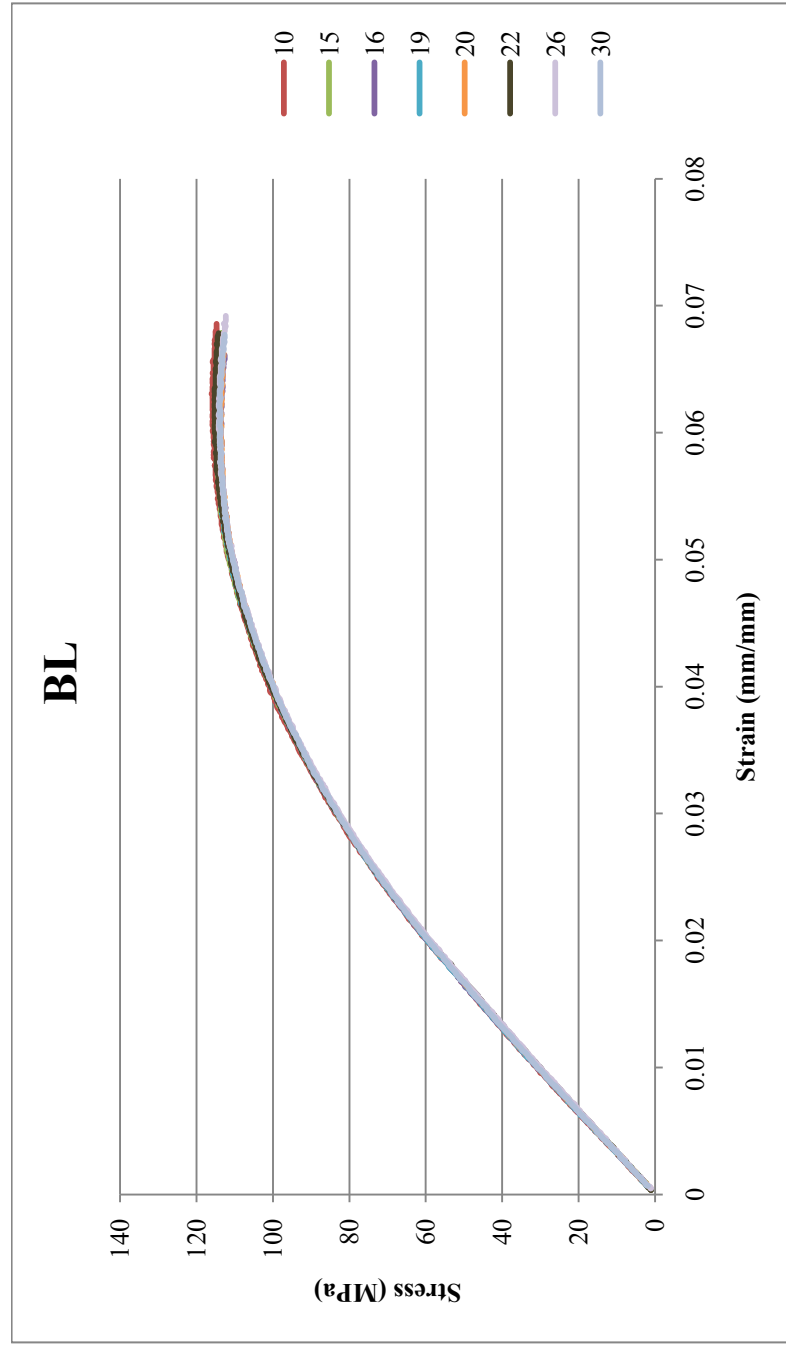


Figure K.1: Flexural Results for BL Lexan HF1130-111: Injection molded 5-26-09

Table K.1: Flexural Results for BL Lexan HF1130-111: Injection molded 5-26-09

Sample	Specimen	Flexural Maximum Stress (MPa)	Strain at Maximum Flexural Stress (%)	0.1% Offset Yield Flexural Stress (MPa)	Strain at 0.1% Yield Flexural Stress (%)	Flexural Modulus (MPa)
BL	10	116.024	6.31	67.066	2.28	3071.378
	15	114.971	5.97	67.856	2.33	3038.066
	16	113.655	5.76	66.540	2.26	3071.126
	19	114.708	5.84	66.014	2.25	3073.793
	20	113.655	5.84	65.224	2.23	3050.455
	22	115.234	5.93	68.909	2.39	3019.038
	26	114.181	6.03	66.803	2.32	3008.009
	30	113.918	5.90	67.330	2.30	3051.73
Average		114.54	5.95	66.97	2.30	3047.95
Standard Deviation		0.84	0.17	1.12	0.05	24.79
Number		8	8	8	8	8

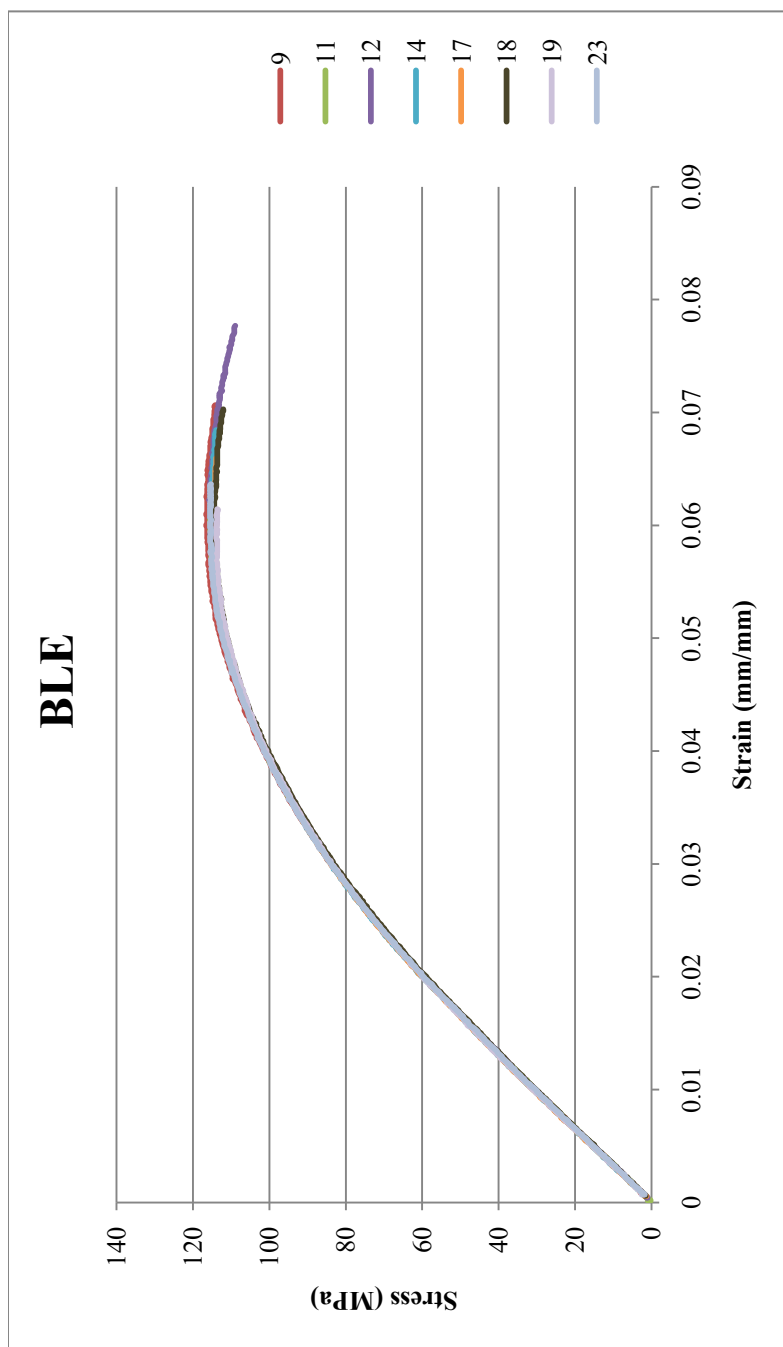


Figure K.2: Flexural Results for BL E Extruded Lexan HF1130-111: Injection molded 5-26-09

Table K.2: Flexural Results for BLE Extruded Lexan HF1130-111: Injection molded 5-26-09

Sample	Specimen	Flexural Maximum Stress (MPa)	Strain at Maximum Flexural Stress (%)	0.1% Offset Yield Flexural Stress (MPa)	Strain at 0.1% Yield Flexural Stress (%)	Flexural Modulus (MPa)
BLE	9	116.550	5.99	67.330	2.30	3051.45
	11	115.497	5.92	67.330	2.31	3042.797
	12	115.761	6.22	69.962	2.41	3028.889
	14	115.234	5.81	67.856	2.30	3087.017
	17	114.708	5.79	64.961	2.19	3101.713
	18	114.445	5.99	65.750	2.26	3038.727
	19	113.918	5.68	63.381	2.14	3103.995
	23	115.497	5.76	67.066	2.29	3065.028
Average		115.20	5.89	66.70	2.28	3064.95
Standard Deviation		0.83	0.17	1.99	0.08	29.34
Number		8	8	8	8	8

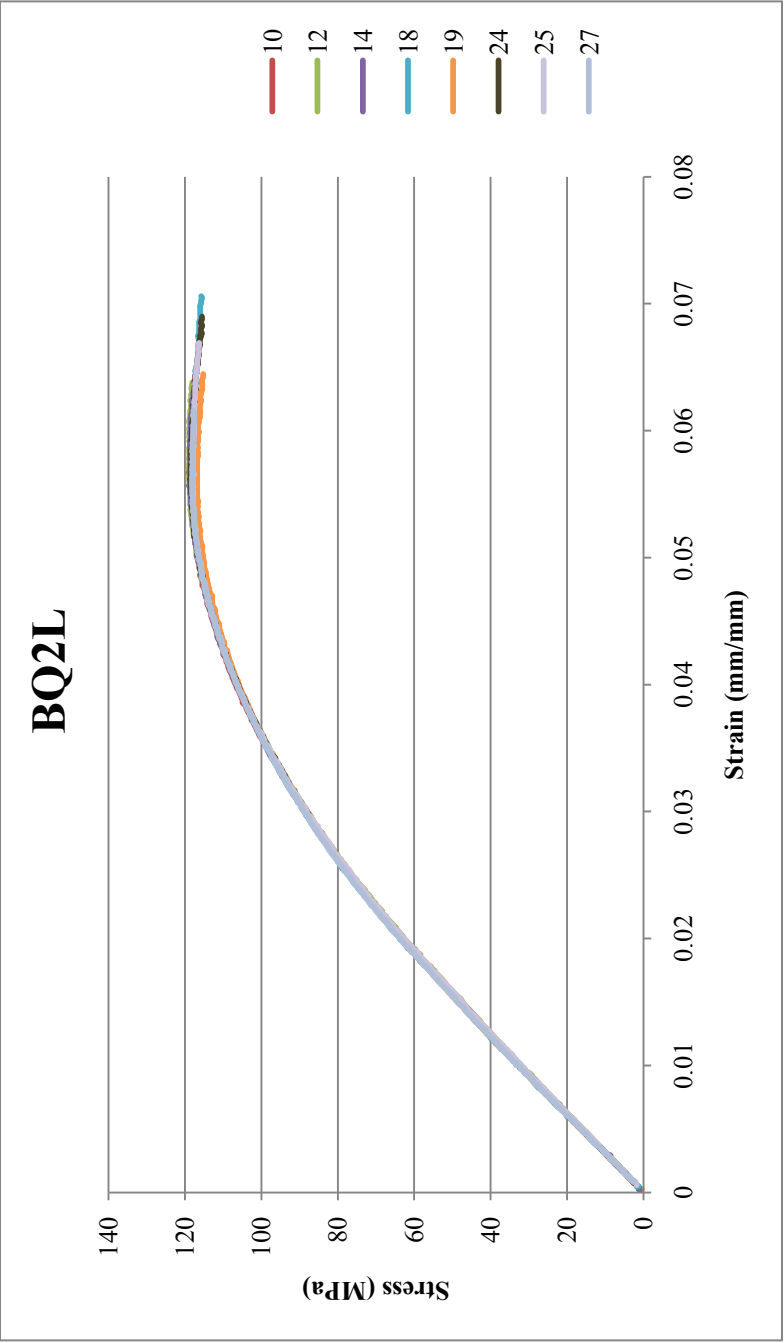


Figure K.3: Flexural Results for BQ2L: 2 wt% fibrils (carbon nanotubes) in Lexan HF1130-111: Injection Molded 5-26-09

Table K.3: Flexural Results for BQ2L: 2 wt% fibrils (carbon nanotubes) in Lexan HF1130-111: Injection Molded 5-26-09

Sample	Specimen	Flexural Maximum Stress (MPa)	Strain at Maximum Flexural Stress (%)	0.1% Offset Yield Flexural Stress (MPa)	Strain at 0.1% Yield Flexural Stress (%)	Flexural Modulus (MPa)
BQ2L	10	118.393	5.45	71.278	2.29	3244.467
	12	119.182	5.69	70.225	2.28	3211.139
	14	118.919	5.56	73.647	2.39	3218.775
	18	117.866	5.76	71.541	2.29	3273.498
	19	117.077	5.51	69.435	2.21	3287.379
	24	118.656	5.62	71.541	2.30	3240.23
	25	118.130	5.43	72.594	2.35	3206.544
	27	118.130	5.45	70.225	2.23	3294.604
Average		118.29	5.56	71.31	2.29	3247.08
Standard Deviation		0.66	0.12	1.37	0.06	34.58
Number		8	8	8	8	8

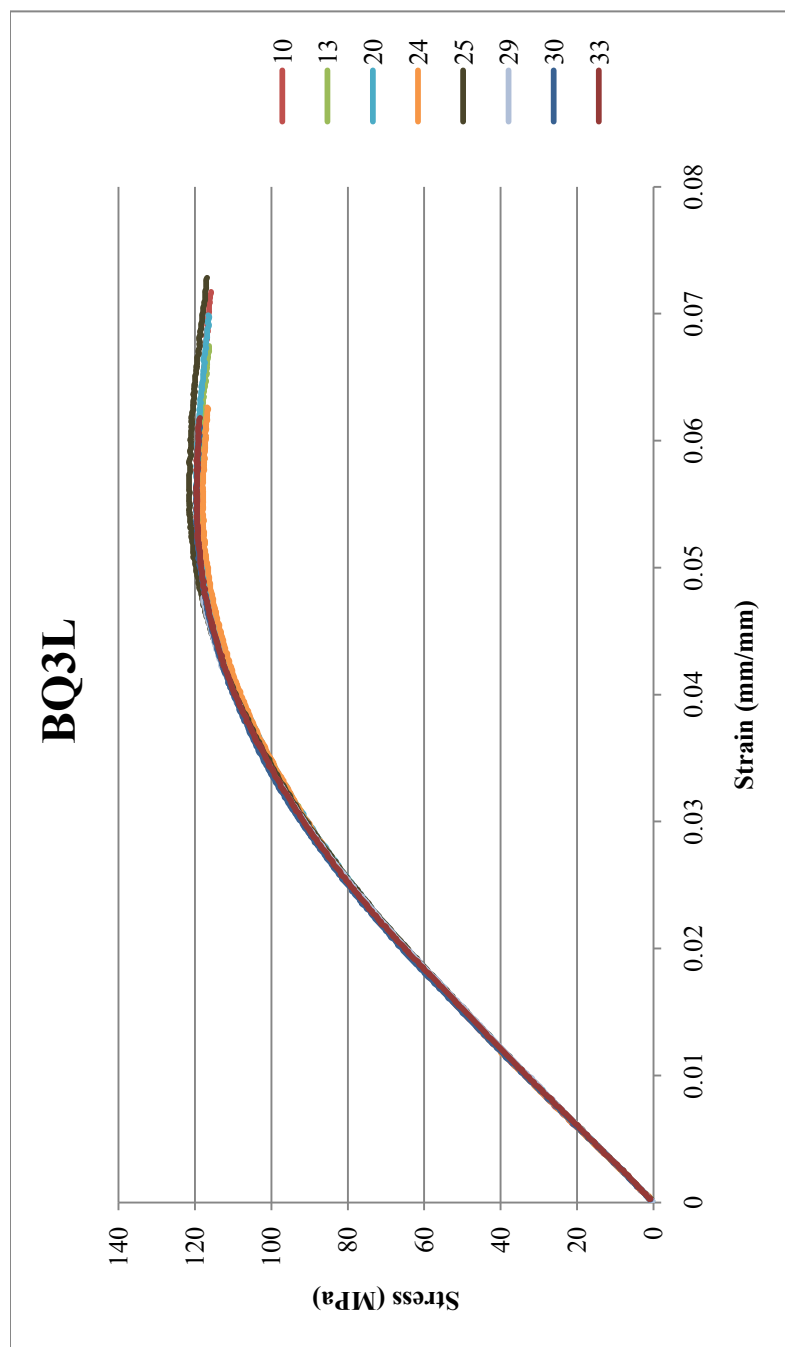


Figure K.4: Flexural Results for BQ3L: 3 wt% fibrils (carbon nanotubes) in Lexan HF1130-111: Injection Molded 5-26-09

Table K.4: Flexural Results for BQ3L: 3 wt% fibrils (carbon nanotubes) in Lexan HF1130-111: Injection Molded 5-26-09

Sample	Specimen	Flexural Maximum Stress (MPa)	Strain at Maximum Flexural Stress (%)	0.1% Offset Yield Flexural Stress (MPa)	Strain at 0.1% Yield Flexural Stress (%)	Flexural Modulus (MPa)
BQ3L	10	119.182	5.70	73.910	2.30	3357.749
	13	119.446	5.43	72.857	2.27	3343.724
	20	119.709	5.42	75.489	2.39	3296.908
	24	118.130	5.34	69.435	2.15	3382.485
	25	121.551	5.42	76.016	2.40	3299.1
	29	118.393	4.81	78.385	2.47	3297.611
	30	119.709	5.35	76.279	2.35	3371.614
	33	119.709	5.40	77.068	2.41	3328.135
Average		119.48	5.36	74.93	2.34	3334.67
Standard Deviation		1.04	0.25	2.81	0.10	34.59
Number		8	8	8	8	8

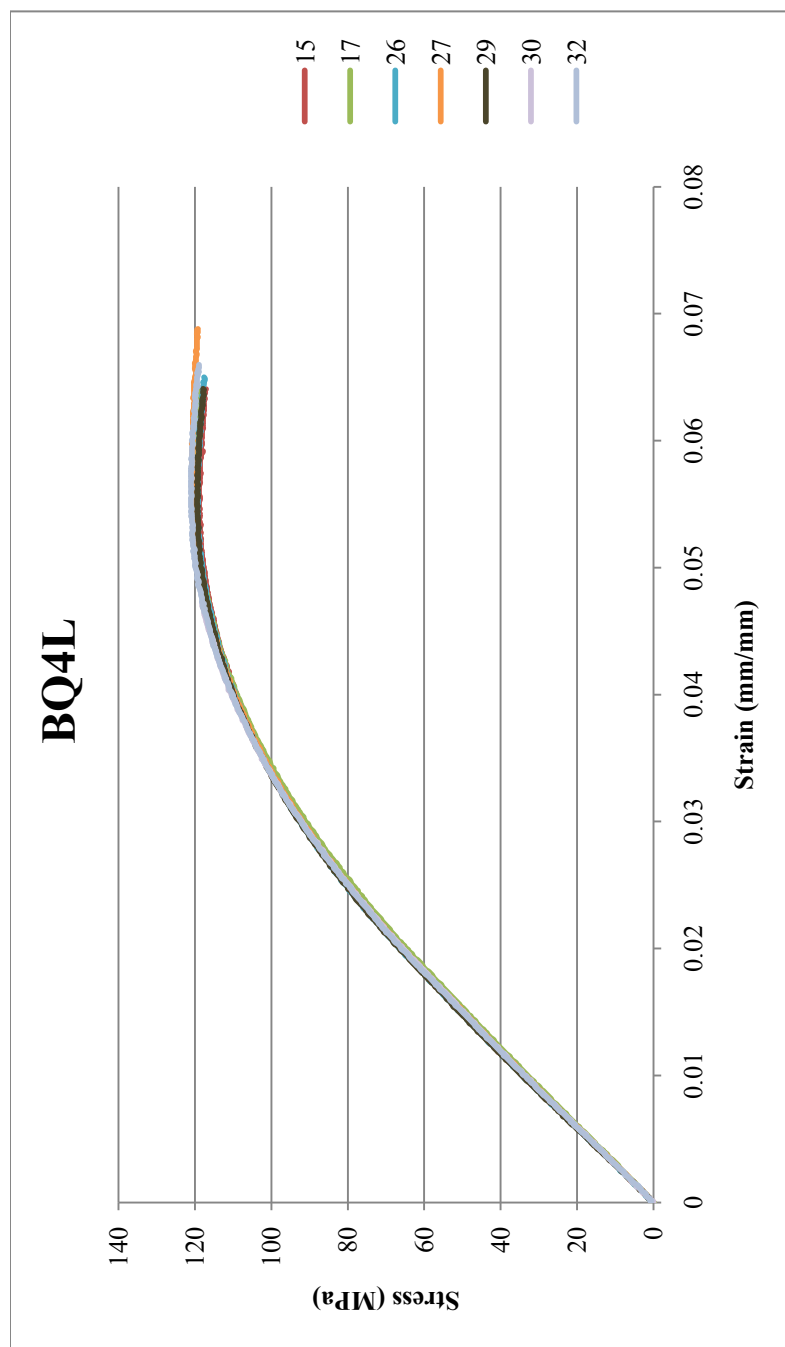


Figure K.5: Flexural Results for BQ4L: 4 wt% fibrils (carbon nanotubes) in Lexan HF1130-111: Injection Molded 5-26-09

Table K.5: Flexural Results for BQ4L: 4 wt% fibrils (carbon nanotubes) in Lexan HF1130-111: Injection Molded 5-26-09

Sample	Specimen	Flexural Maximum Stress (MPa)	Strain at Maximum Flexural Stress (%)	0.1% Offset Yield Flexural Stress (MPa)	Strain at 0.1% Yield Flexural Stress (%)	Flexural Modulus (MPa)
BQ4L	15	119.182	5.47	71.541	2.19	3424.149
	17	120.235	5.51	76.279	2.40	3303.134
	26	119.446	5.41	76.016	2.32	3419.142
	27	120.762	5.60	76.805	2.39	3360.076
	29	119.446	5.33	72.594	2.21	3439.223
	30	118.130	4.70	75.752	2.35	3364.975
	32	121.025	5.41	74.700	2.31	3376.263
Average		119.75	5.35	74.81	2.31	3383.85
Standard Deviation		1.00	0.30	2.00	0.08	47.31
Number		7	7	7	7	7

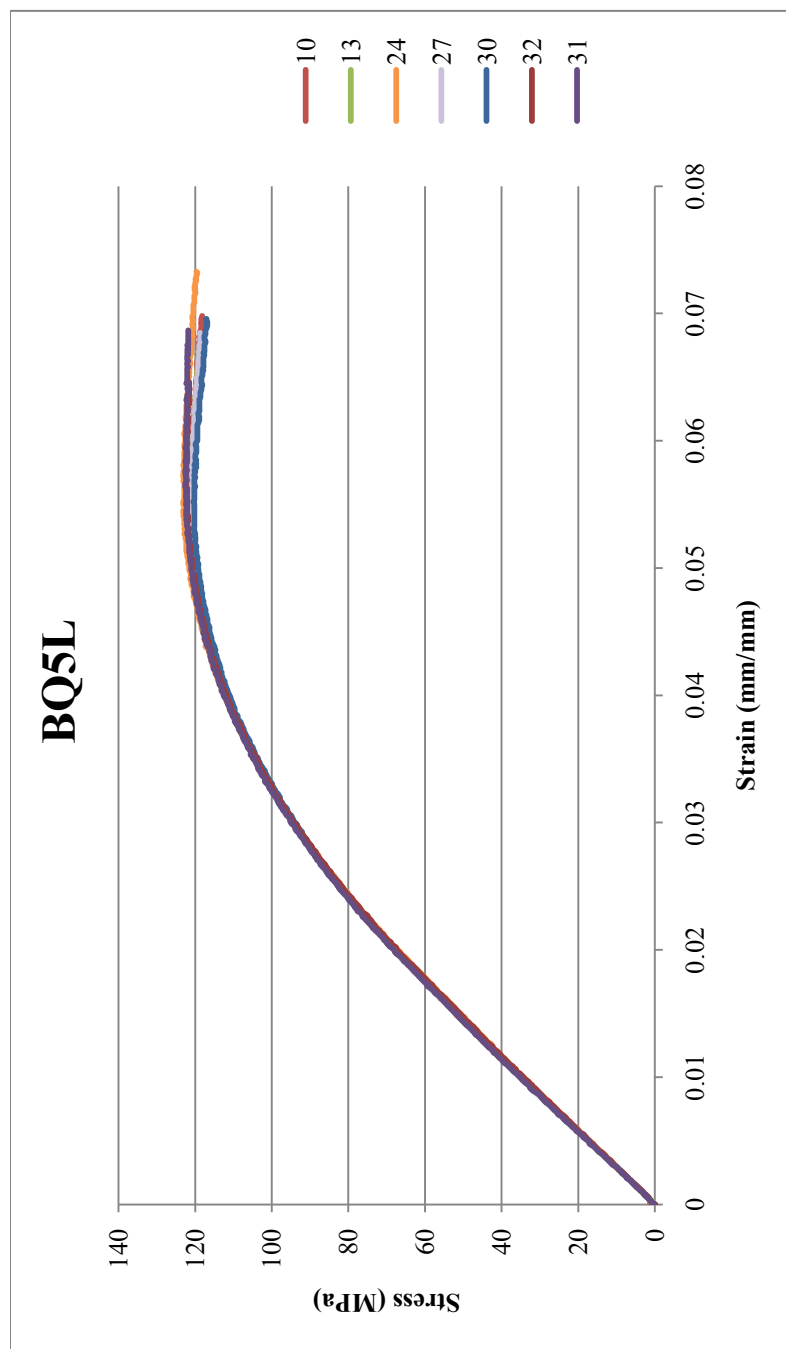


Figure K.6: Flexural Results for BQ5L: 5 wt% fibrils (carbon nanotubes) in Lexan HF1130-111: Injection Molded 5-26-09

Table K.6: Flexural Results for BQ5L: 5 wt% fibrils (carbon nanotubes) in Lexan HF1130-111: Injection Molded 5-26-09

Sample	Specimen	Flexural Maximum Stress (MPa)	Strain at Maximum Flexural Stress (%)	0.1% Offset Yield Flexural Stress (MPa)	Strain at 0.1% Yield Flexural Stress (%)	Flexural Modulus (MPa)
BQ5L	10	121.551	5.28	75.489	2.25	3507.968
	13	121.551	5.42	73.910	2.20	3503.291
	24	123.131	5.41	80.227	2.44	3433.488
	27	121.288	5.33	74.173	2.20	3516.607
	30	120.498	5.31	75.752	2.27	3491.565
	32	122.341	5.50	77.068	2.33	3444.253
	31	122.604	5.64	76.542	2.28	3521.49
Average		121.85	5.41	76.17	2.28	3488.38
Standard Deviation		0.89	0.13	2.13	0.08	35.28
Number		7	7	7	7	7

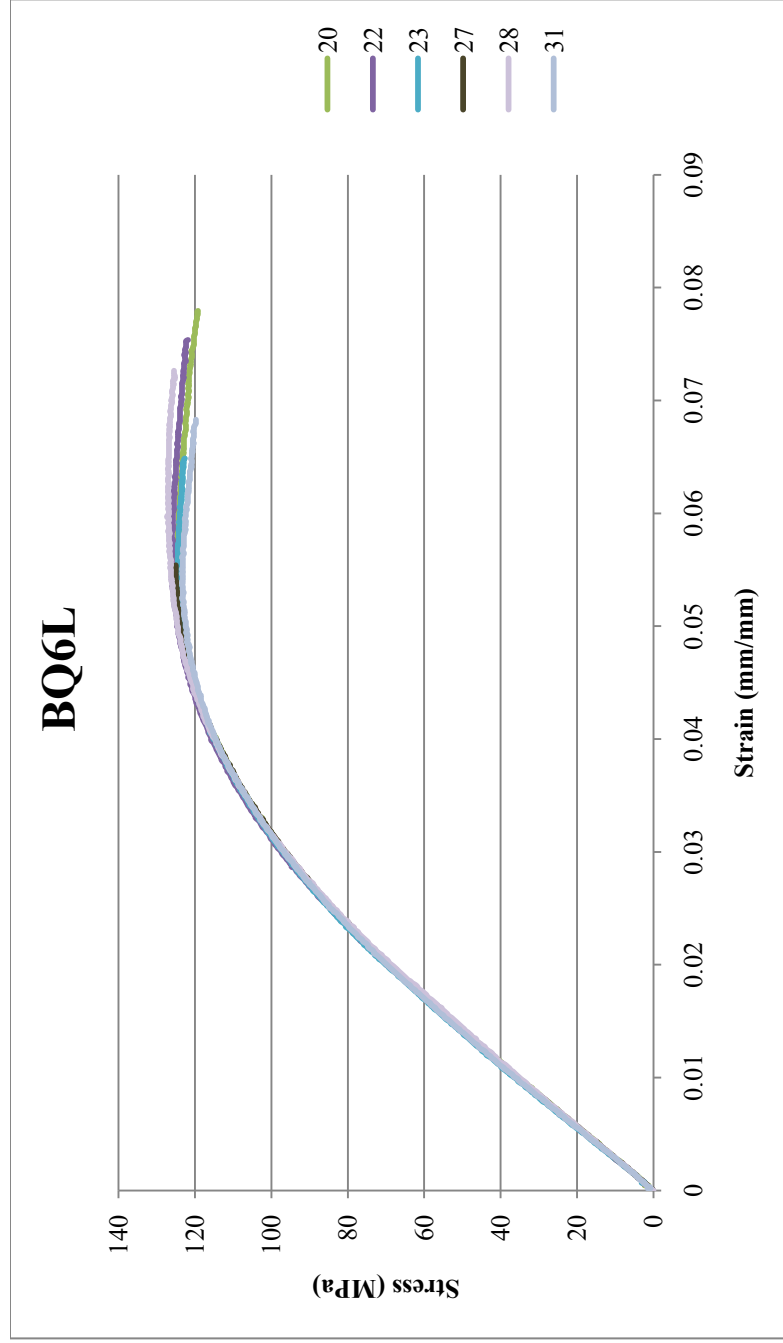


Figure K.7: Flexural Results for BQ6L: 6 wt% fibrils (carbon nanotubes) in Lexan HF1130-111: Injection Molded 5-26-09

Table K.7: Flexural Results for BQ6L: 6 wt% fibrils (carbon nanotubes) in Lexan HF1130-111: Injection Molded 5-26-09

Sample	Specimen	Flexural Maximum Stress (MPa)	Strain at Maximum Flexural Stress (%)	0.1% Offset Yield Flexural Stress (MPa)	Strain at 0.1% Yield Flexural Stress (%)	Flexural Modulus (MPa)
BQ6L	20	124.710	5.41	81.280	2.41	3519.643
	22	126.289	5.68	79.701	2.32	3582.885
	23	124.447	5.28	75.489	2.18	3636.655
	27	125.236	5.48	77.858	2.29	3543.642
	28	127.342	5.97	82.596	2.47	3491.347
	31	123.394	5.25	74.963	2.18	3606.274
Average		125.24	5.51	78.65	2.31	3563.41
Standard Deviation		1.40	0.27	3.09	0.12	54.92
Number		6	6	6	6	6

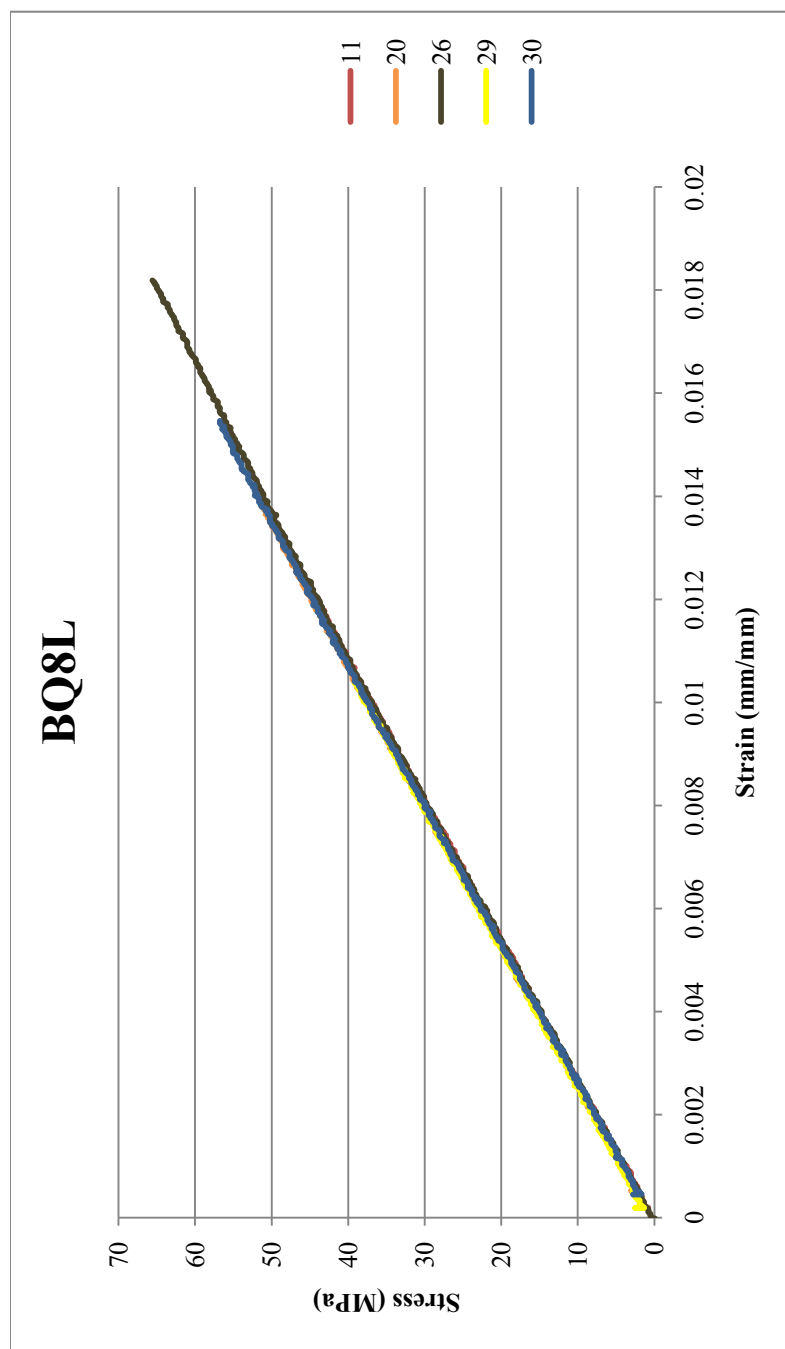


Figure K.8: Flexural Results for BQ8L: 8 wt% fibrils (carbon nanotubes) in Lexan HF1130-111: Injection Molded 5-26-09

Table K.8: Flexural Results for BQ8L: 8 wt% fibrils (carbon nanotubes) in Lexan HF1130-111: Injection Molded 5-26-09

Sample	Specimen	Flexural Maximum Stress (MPa)	Strain at Maximum Flexural Stress (%)	0.1% Offset Yield Flexural Stress (MPa)	Strain at 0.1% Yield Flexural Stress (%)	Flexural Modulus (MPa)
BQ8L	11	45.961	1.24	45.961	1.24	3697.514
	20	51.358	1.39	51.358	1.39	3608.162
	26	65.561	1.82	65.561	1.82	3600.813
	29	39.144	1.04	39.144	1.04	3609.802
	30	56.755	1.54	56.755	1.54	3663.339
Average		51.76	1.41	51.76	1.41	3635.93
Standard Deviation		10.10	0.30	10.10	0.30	42.52
Number		5	5	5	5	5

Appendix K.2: Polycarbonate with Carbon Black

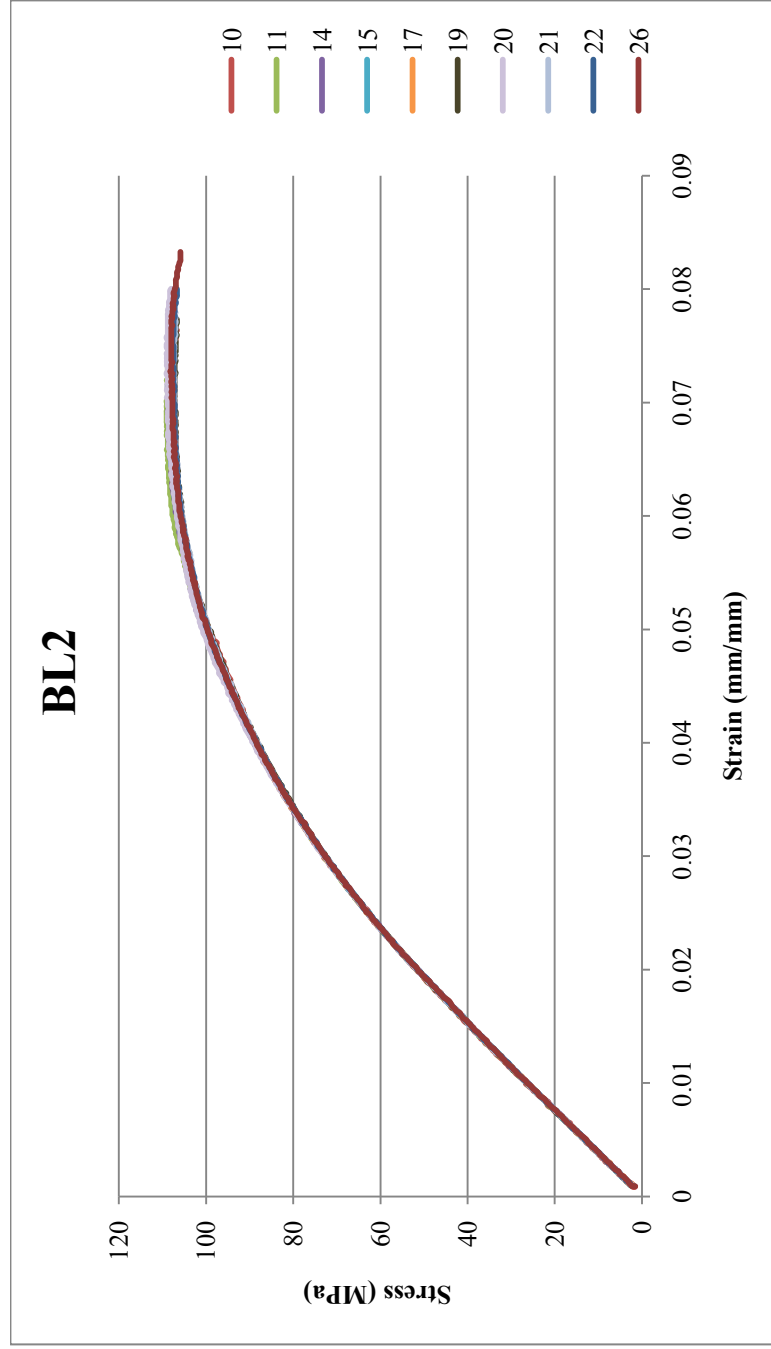


Figure K.9: Flexural Results for BL2 Lexan HF1130-111: Injection molded 12-4-09

Table K.9: Flexural Results for BL2 Lexan HF1130-111: Injection molded 12-4-09

Sample	Specimen	Flexural Maximum Stress (MPa)	Strain at Maximum Flexural Stress (%)	0.1% Offset Yield Flexural Stress (MPa)	Strain at 0.1% Yield Flexural Stress (%)	Flexural Modulus (MPa)
BL2 flex	10	108.253	6.49	59.095	2.33	2655.248
	11	109.038	6.58	60.925	2.41	2640.883
	14	108.776	6.92	60.141	2.39	2627.202
	15	108.776	7.14	62.233	2.48	2619.815
	17	108.515	7.07	60.925	2.41	2628.742
	19	107.469	7.04	60.402	2.39	2632.355
	20	109.038	7.04	61.710	2.45	2623.727
	21	107.469	6.93	60.664	2.40	2632.756
	22	107.730	7.19	60.925	2.42	2625.721
	26	108.253	7.27	63.279	2.51	2620.019
Average		108.33	6.97	61.03	2.42	2630.65
Standard Deviation		0.60	0.25	1.16	0.05	10.73
Number		10	10	10	10	10

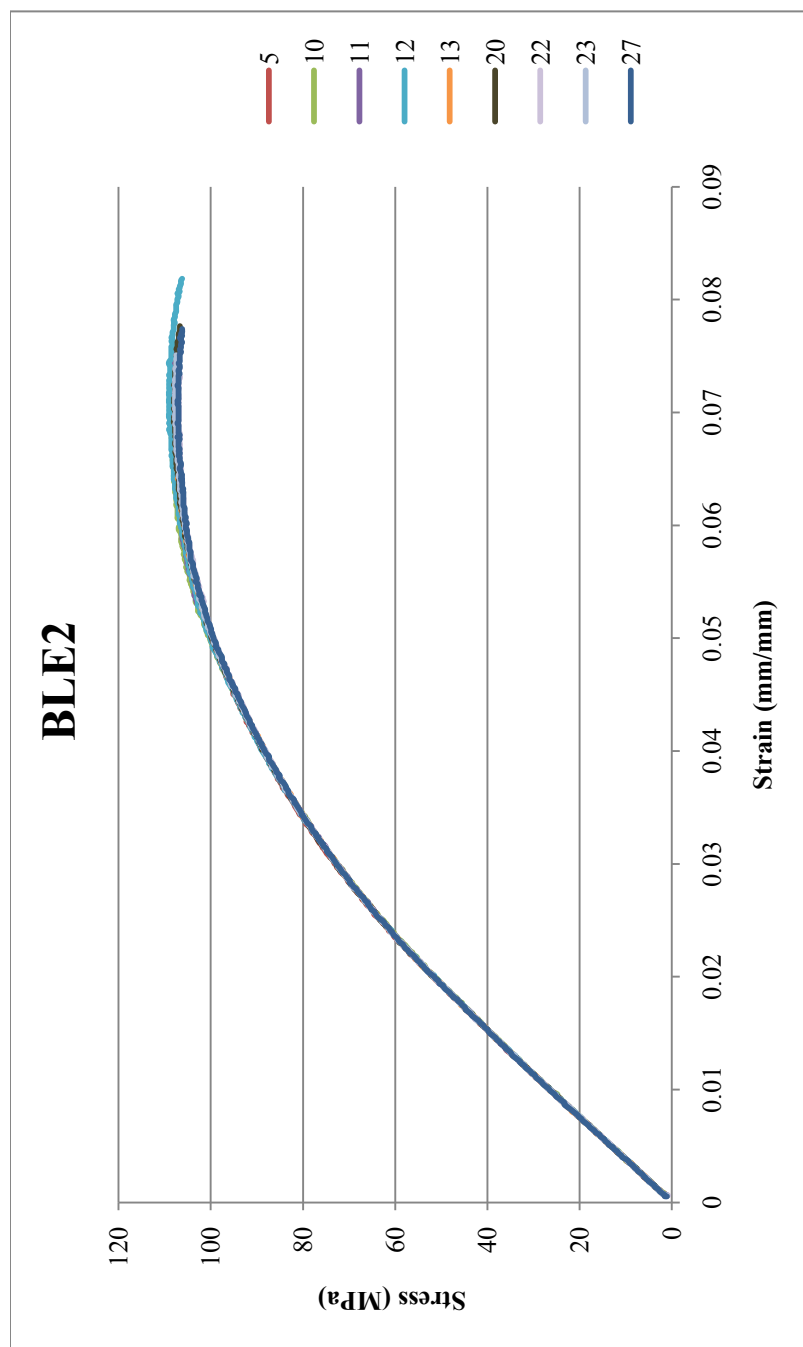


Figure K.10: Flexural Results for BLE2 Extruded Lexan HF1130-111: Extruded 11-5-09, Injection molded 12-4-09

Table K.10: Flexural Results for BLE2 Extruded Lexan HF1130-111: Extruded 11-5-09, Injection molded 12-4-09

Sample	Specimen	Flexural Maximum Stress (MPa)	Strain at Maximum Flexural Stress (%)	0.1% Offset Yield Flexural Stress (MPa)	Strain at 0.1% Yield Flexural Stress (%)	Flexural Modulus (MPa)
BLE2 flex	5	107.992	6.81	61.448	2.41	2648.651
	10	108.515	6.77	60.141	2.37	2639.176
	11	108.515	7.16	59.618	2.34	2650.438
	12	109.038	6.85	63.017	2.49	2630.894
	13	107.730	7.09	61.448	2.43	2644.902
	20	107.992	6.91	61.448	2.43	2639.212
	22	107.207	6.91	60.141	2.37	2652.044
	23	107.730	6.89	61.448	2.43	2642.159
Average	27	107.207	6.78	60.664	2.40	2642.043
		107.99	6.91	61.04	2.41	2643.28
	Standard Deviation	0.61	0.14	1.02	0.04	6.61
	Number	9	9	9	9	9

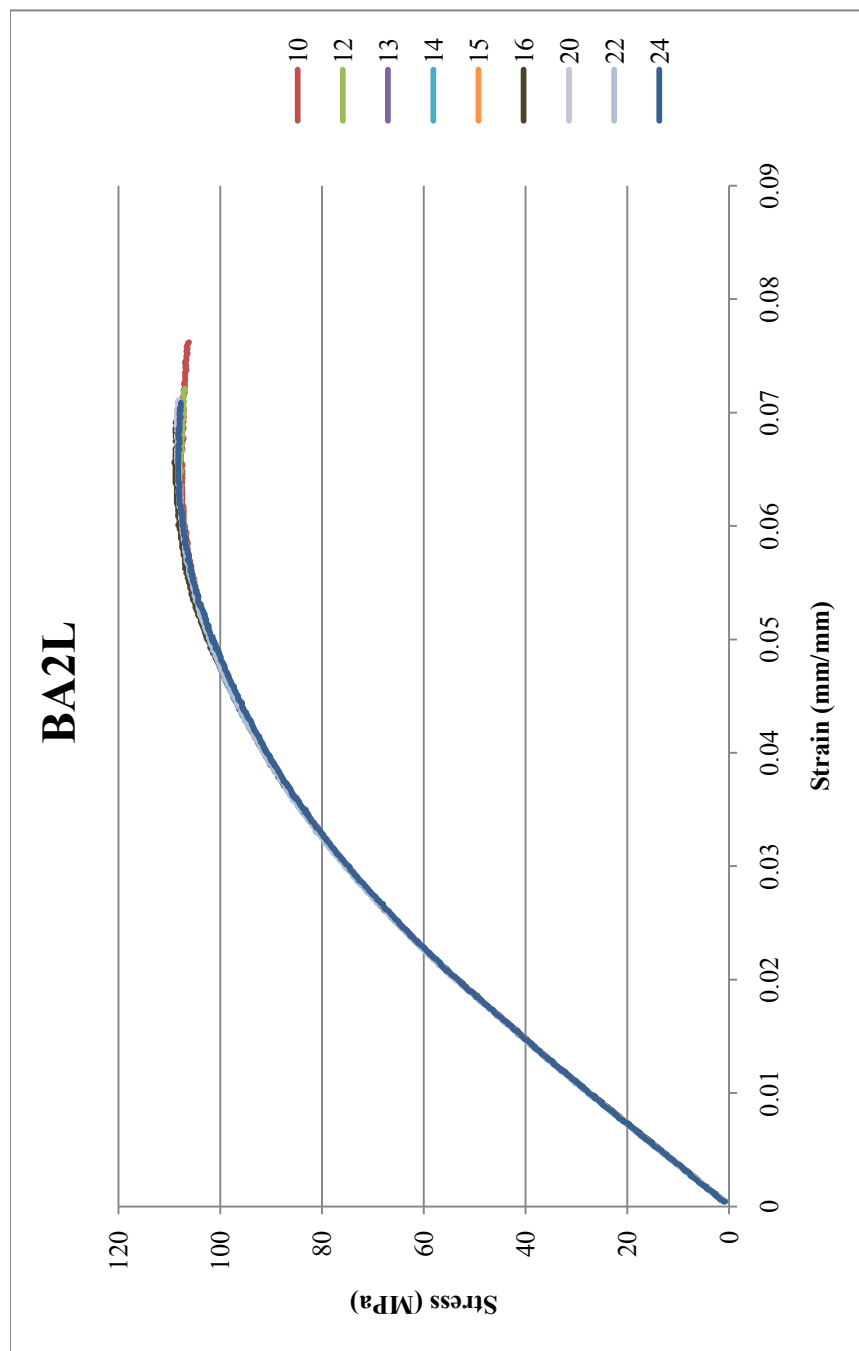


Figure K.11: Flexural Results for BA2L: 2 wt% Ketjenblack EC-600 JD (carbon black) in Lexan HF1130-111: Injection Molded 12-4-09

Table K.11: Flexural Results for BA2L: 2 wt% Ketjenblack EC-600 JD (carbon black) in Lexan HF1130-111: Injection Molded 12-4-09

Sample	Specimen	Flexural Maximum Stress (MPa)	Strain at Maximum Flexural Stress (%)	0.1% Offset Yield Flexural Stress (MPa)	Strain at 0.1% Yield Flexural Stress (%)	Flexural Modulus (MPa)
BA2L flex	10	107.730	6.22	61.187	2.33	2745.371
	12	108.253	6.30	60.925	2.32	2753.09
	13	108.515	6.32	59.618	2.25	2756.442
	14	108.515	6.45	61.448	2.33	2755.814
	15	108.776	6.61	61.448	2.34	2746.597
	16	109.038	6.56	60.402	2.29	2746.044
	20	108.515	6.56	61.448	2.34	2749.72
	22	108.515	6.60	60.925	2.30	2766.27
	24	108.253	6.29	60.141	2.29	2747.217
Average		108.46	6.43	60.84	2.31	2751.84
Standard Deviation		0.36	0.15	0.65	0.03	6.85
Number		9	9	9	9	9

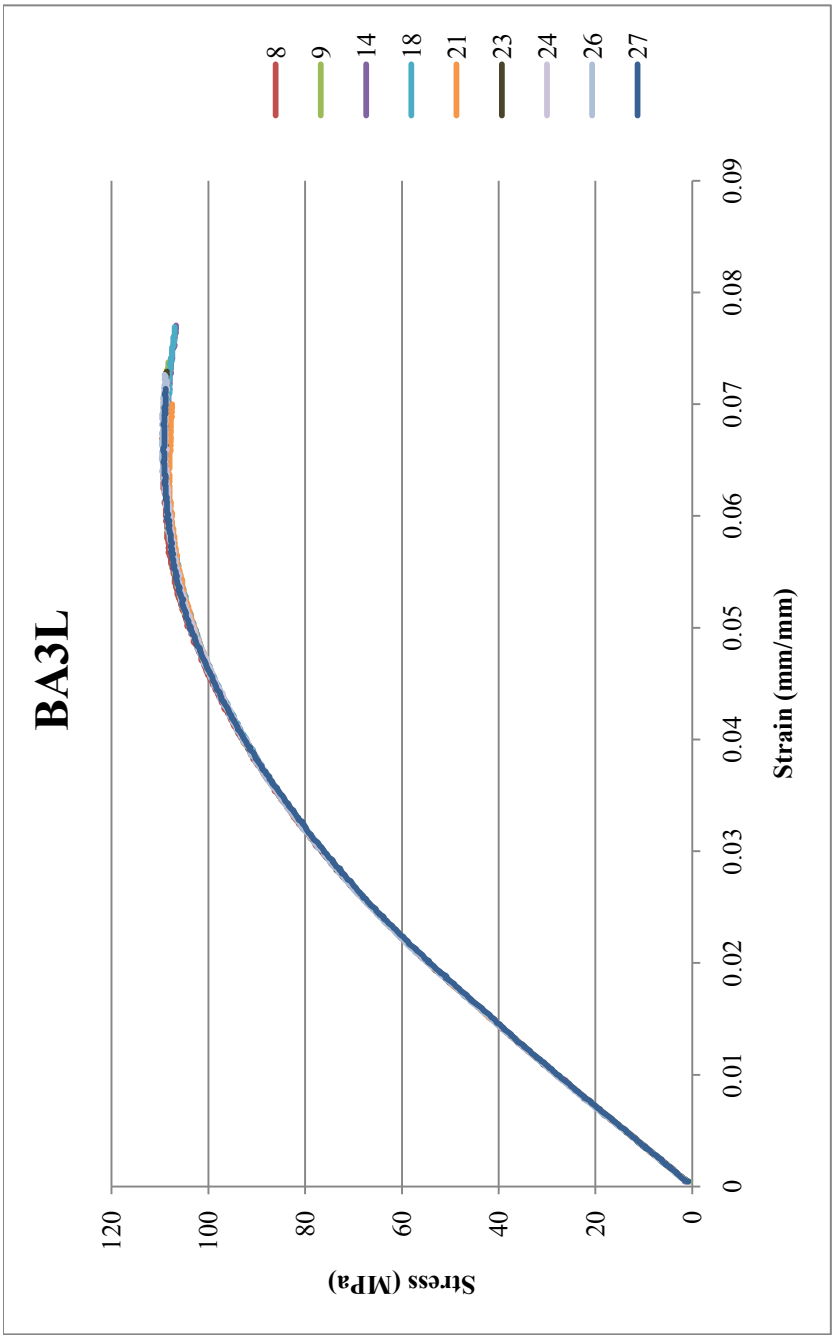


Figure K. 12: Flexural Results for BA3L: 3 wt% Ketjenblack EC-600 JD (carbon black) in Lexan HF1130-111: Injection Molded 12-4-09

Table K.12: Flexural Results for BA3L: 3 wt% Ketjenblack EC-600 JD (carbon black) in Lexan HF1130-111: Injection Molded 12-4-09

Sample	Specimen	Flexural Maximum Stress (MPa)	Strain at Maximum Flexural Stress (%)	0.1% Offset Yield Flexural Stress (MPa)	Strain at 0.1% Yield Flexural Stress (%)	Flexural Modulus (MPa)
BA3L flex	8	109.561	6.52	61.187	2.28	2806.364
	9	109.038	6.38	61.448	2.28	2792.583
	14	108.776	6.24	63.540	2.38	2787.539
	18	108.776	6.38	63.279	2.38	2785.102
	21	108.253	6.29	60.925	2.26	2805.693
	23	109.038	6.31	61.710	2.31	2794.348
	24	109.038	6.52	60.925	2.27	2792.583
	26	109.561	6.40	63.802	2.38	2801.883
	27	109.299	6.48	61.187	2.30	2781.893
Average		109.04	6.39	62.00	2.32	2794.22
Standard Deviation		0.41	0.10	1.19	0.05	8.82
Number		9	9	9	9	9

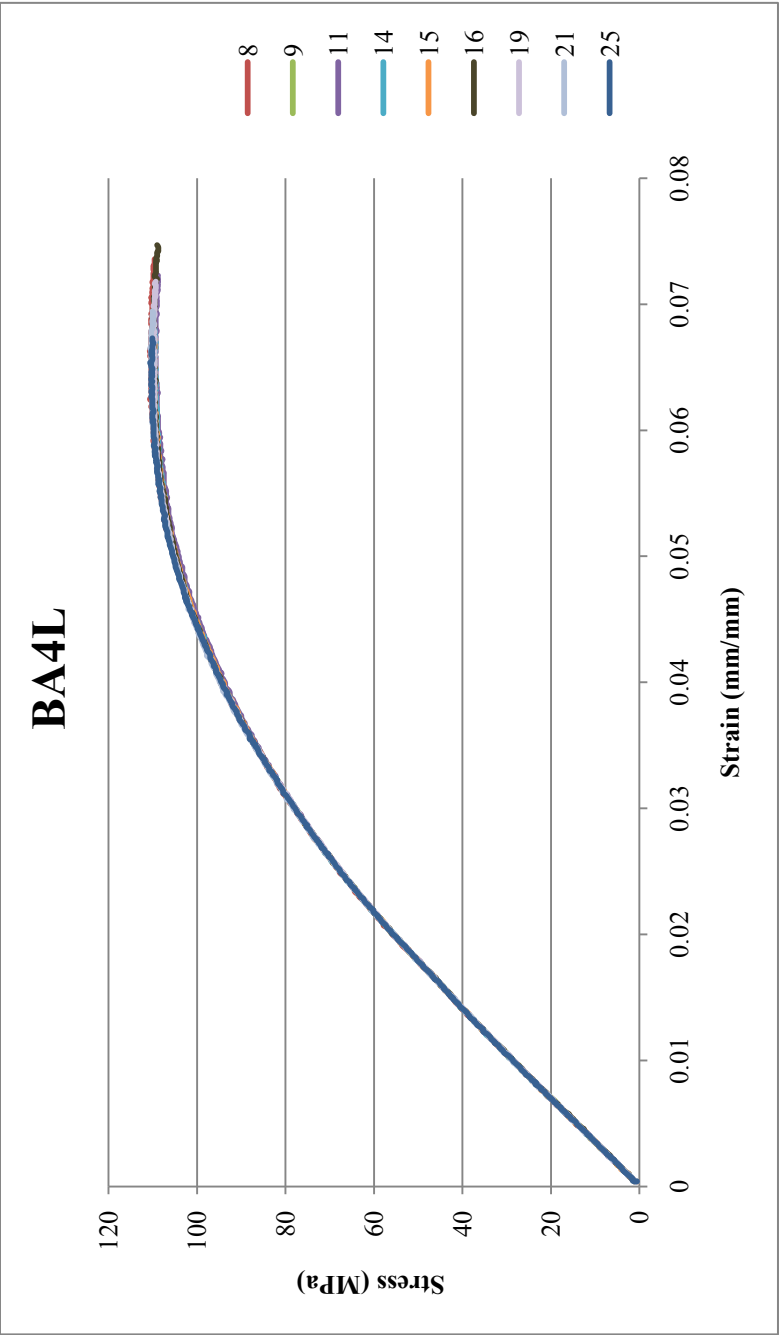


Figure K.13: Flexural Results for BA4L: 4 wt% Ketjenblack EC-600 JD (carbon black) in Lexan HF1130-111: Injection Molded
12-4-09

Table K.13: Flexural Results for BA4L: 4 wt% Ketjenblack EC-600 JD (carbon black) in Lexan HF1130-111: Injection Molded 12-4-09

Sample	Specimen	Flexural Maximum Stress (MPa)	Strain at Maximum Flexural Stress (%)	0.1% Offset Yield Flexural Stress (MPa)	Strain at 0.1% Yield Flexural Stress (%)	Flexural Modulus (MPa)
BA4L flex	8	110.607	6.24	64.324	2.34	2861.79
	9	110.084	6.40	62.494	2.29	2855.929
	11	109.561	6.60	63.540	2.33	2854.188
	14	109.822	6.51	63.017	2.30	2866.962
	15	109.822	6.17	61.971	2.27	2865.834
	16	110.084	6.60	63.017	2.31	2850.835
	19	109.822	6.07	63.017	2.30	2850.15
	21	110.607	6.65	63.017	2.30	2866.407
	25	110.607	6.53	62.233	2.27	2869.101
Average		110.11	6.42	62.96	2.30	2860.13
Standard Deviation		0.40	0.21	0.70	0.02	7.42
Number		9	9	9	9	9

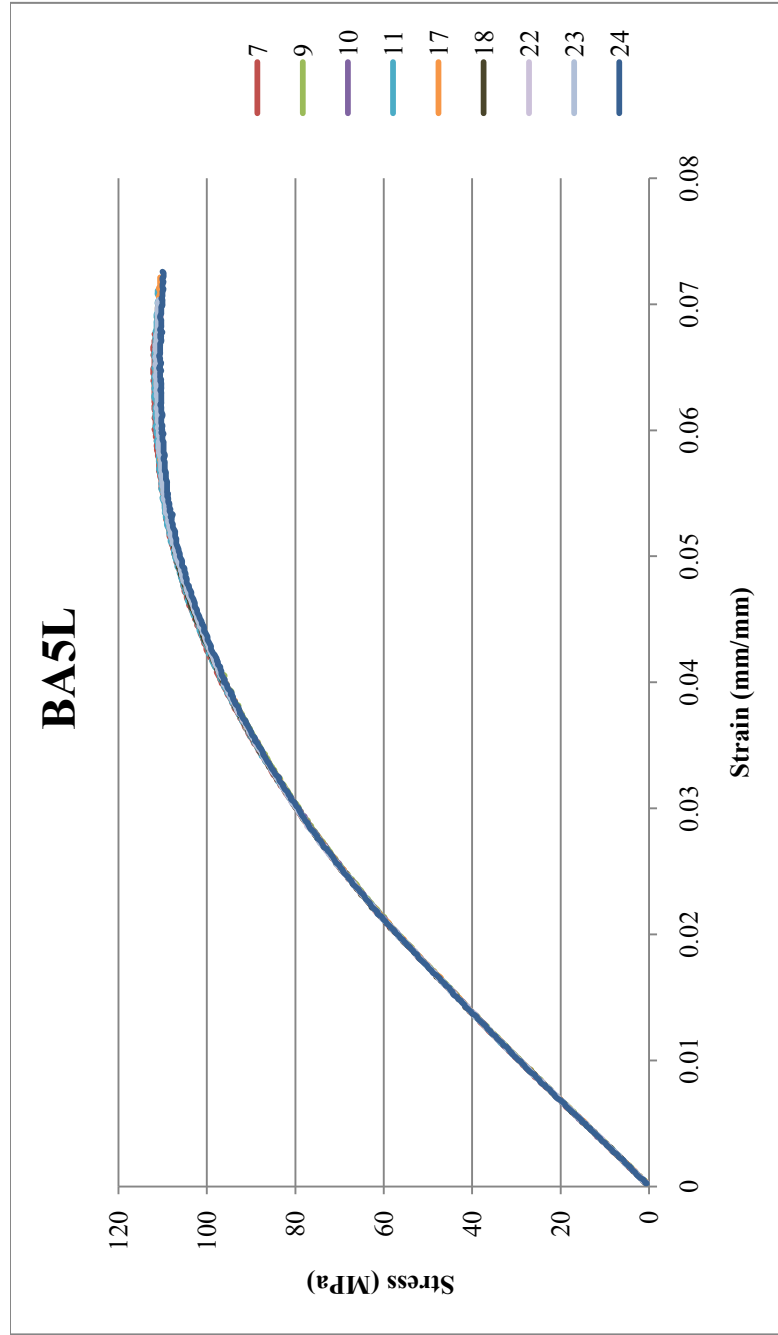


Figure K.14: Flexural Results for BA5L: 5 wt% Ketjenblack EC-600 JD (carbon black) in Lexan HF1130-111: Injection Molded
12-4-09

Table K.14: Flexural Results for BA5L: 5 wt% Ketjenblack EC-600 JD (carbon black) in Lexan HF1130-111: Injection Molded 12-4-09

Sample	Specimen	Flexural Maximum Stress (MPa)	Strain at Maximum Flexural Stress (%)	0.1% Offset Yield Flexural Stress (MPa)	Strain at 0.1% Yield Flexural Stress (%)	Flexural Modulus (MPa)
BA5L flex	7	112.176	6.39	63.279	2.25	2944.51
	9	111.391	6.28	62.756	2.24	2922.352
	10	111.391	6.30	64.324	2.30	2921.402
	11	111.914	6.26	63.540	2.26	2933.081
	17	111.391	6.36	64.324	2.30	2926.09
	18	111.130	6.48	65.109	2.31	2927.51
	22	111.391	6.58	63.540	2.26	2929.747
	23	111.653	6.43	64.586	2.31	2927.171
	24	110.868	6.49	64.324	2.30	2928.254
Average		111.48	6.40	63.98	2.28	2928.90
Standard Deviation		0.39	0.11	0.74	0.03	6.84
Number		9	9	9	9	9

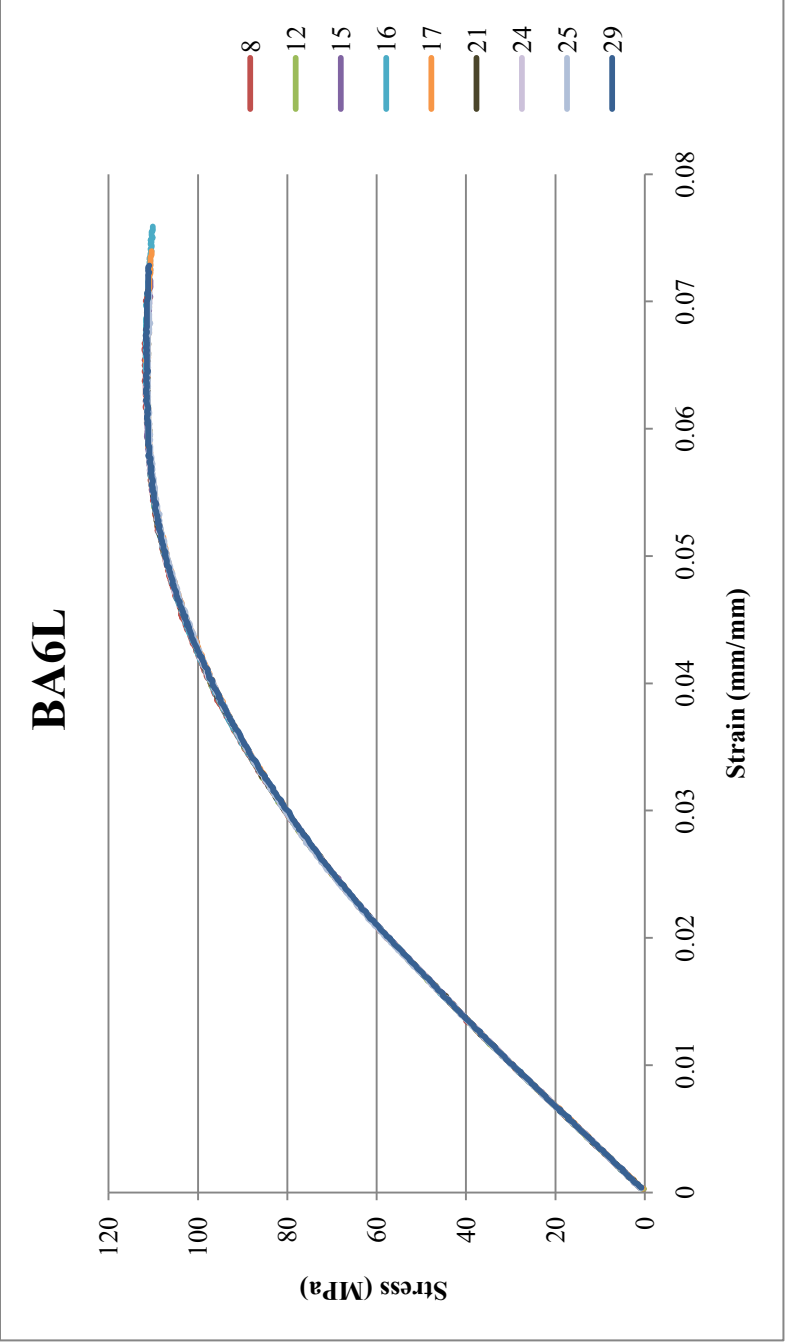


Figure K.15: Flexural Results for BA6L: 6 wt% Ketjenblack EC-600 JD (carbon black) in Lexan HF1130-111: Injection Molded
12-4-09

Table K.15: Flexural Results for BA6L: 6 wt% Ketjenblack EC-600 JD (carbon black) in Lexan HF1130-111: Injection Molded 12-4-09

Sample	Specimen	Flexural Maximum Stress (MPa)	Strain at Maximum Flexural Stress (%)	0.1% Offset Yield Flexural Stress (MPa)	Strain at 0.1% Yield Flexural Stress (%)	Flexural Modulus (MPa)
BA6L flex	8	111.914	6.38	64.586	2.28	2968.619
	12	111.653	6.45	63.802	2.25	2971.318
	15	111.653	6.22	63.540	2.25	2954.12
	16	111.653	6.36	66.155	2.35	2947.392
	17	111.653	6.53	64.063	2.27	2955.382
	21	111.391	6.18	64.586	2.29	2956.458
	24	111.653	6.21	62.756	2.21	2960.333
	25	111.391	6.31	66.155	2.34	2961.585
	29	111.653	6.22	63.540	2.24	2952.14
Average		111.62	6.32	64.35	2.27	2958.59
Standard Deviation		0.16	0.12	1.17	0.04	7.72
Number		9	9	9	9	9

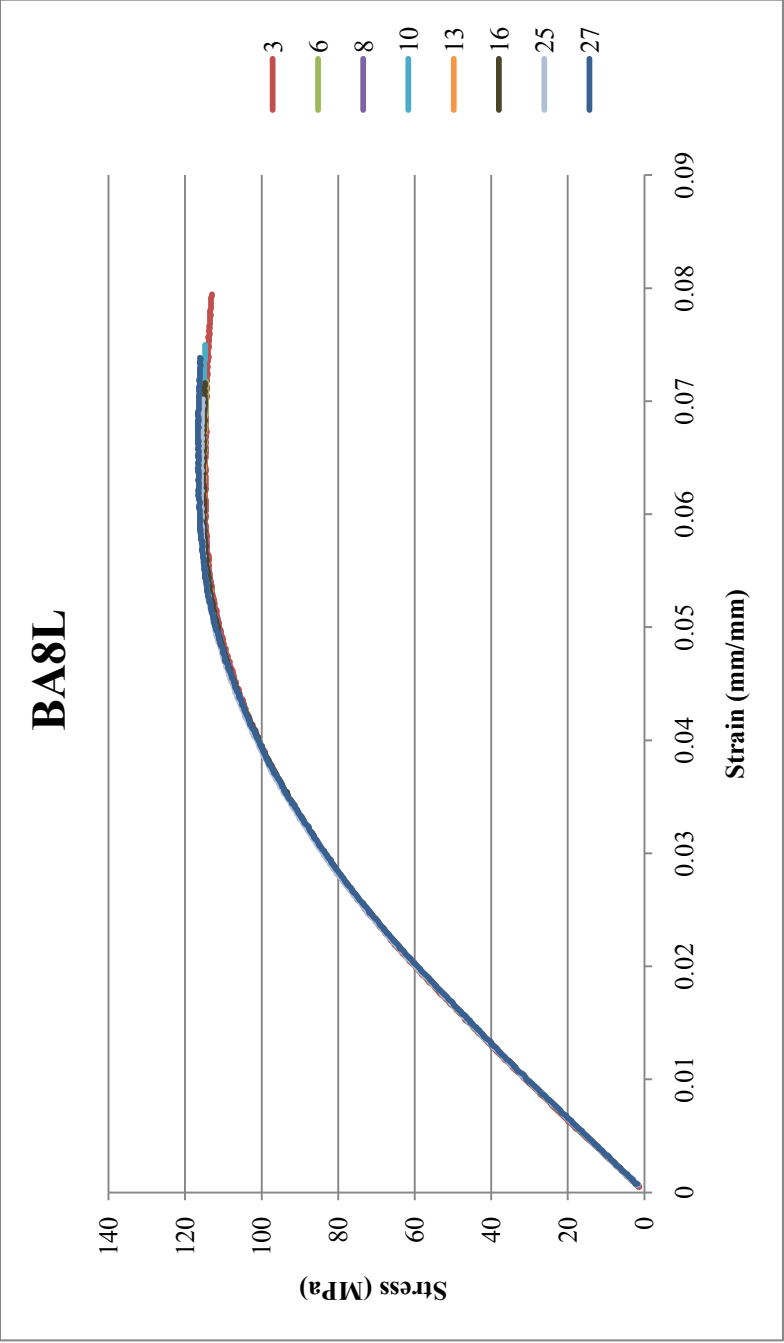


Figure K.16: Flexural Results for BA8L: 8 wt% Ketjenblack EC-600 JD (carbon black) in Lexan HF1130-111: Injection Molded
12-4-09

Table K.16: Flexural Results for BA8L: 8 wt% Ketjenblack EC-600 JD (carbon black) in Lexan HF1130-111: Injection Molded 12-4-09

Sample	Specimen	Flexural Maximum Stress (MPa)	Strain at Maximum Flexural Stress (%)	0.1% Offset Yield Flexural Stress (MPa)	Strain at 0.1% Yield Flexural Stress (%)	Flexural Modulus (MPa)
BA8L	3	115.037	6.71	69.545	2.38	3072.389
	6	115.298	5.95	66.146	2.24	3077.17
	8	115.298	6.05	66.930	2.28	3073.475
	10	115.559	6.07	69.545	2.37	3060.332
	13	115.559	6.04	68.499	2.34	3059.978
	16	115.298	5.93	67.453	2.30	3061.017
	25	116.082	6.23	67.192	2.27	3077.36
	27	116.605	6.17	68.238	2.34	3050.178
Average		115.59	6.14	67.94	2.31	3066.49
Standard Deviation		0.51	0.25	1.23	0.05	9.94
Number		8	8	8	8	8

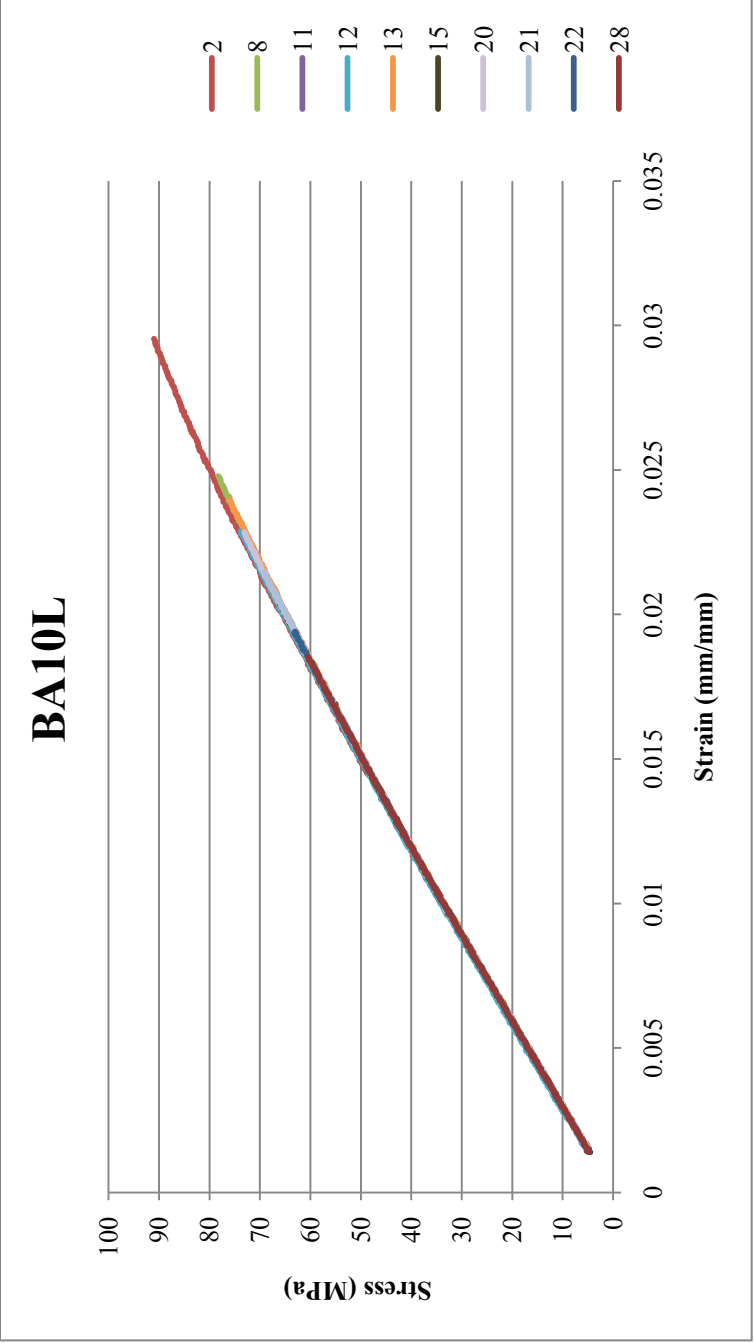


Figure K.17: Flexural Results for BA10L: 10 wt% Ketjenblack EC-600 JD (carbon black) in Lexan HF1130-111: Injection Molded 12-4-09

Table K.17: Flexural Results for BA10L: 10 wt% Ketjenblack EC-600 JD (carbon black) in Lexan HF1130-111: Injection Molded 12-4-09: All samples fractured

Sample	Specimen	Flexural Maximum and Failure Stress (MPa)	Strain at Maximum Flexural Stress (%)	0.1% Offset Yield Flexural Stress (MPa)	Strain at 0.1% Yield Flexural Stress (%)	Flexural Modulus (MPa)
BA10L	2	91.010	2.95	69.258	2.11	3424.154
	8	78.259	2.48	71.258	2.22	3352.066
	11	67.507	2.07	-	-	3374.207
	12	74.008	2.29	64.007	1.95	3453.608
	13	76.008	2.40	66.507	2.06	3372.518
	15	66.757	2.06	-	-	3369.506
	20	73.008	2.28	70.508	2.19	3368.49
	21	69.758	2.17	-	-	3352.455
	22	63.257	1.94	-	-	3377.217
	28	60.507	1.85	-	-	3342.409
Average		72.01	2.25	68.31	2.11	3378.66
Standard Deviation		8.71	0.32	3.01	0.11	34.39
Number		10	10	5	5	10

Appendix K.3: Polycarbonate with Graphite Nanoparticles

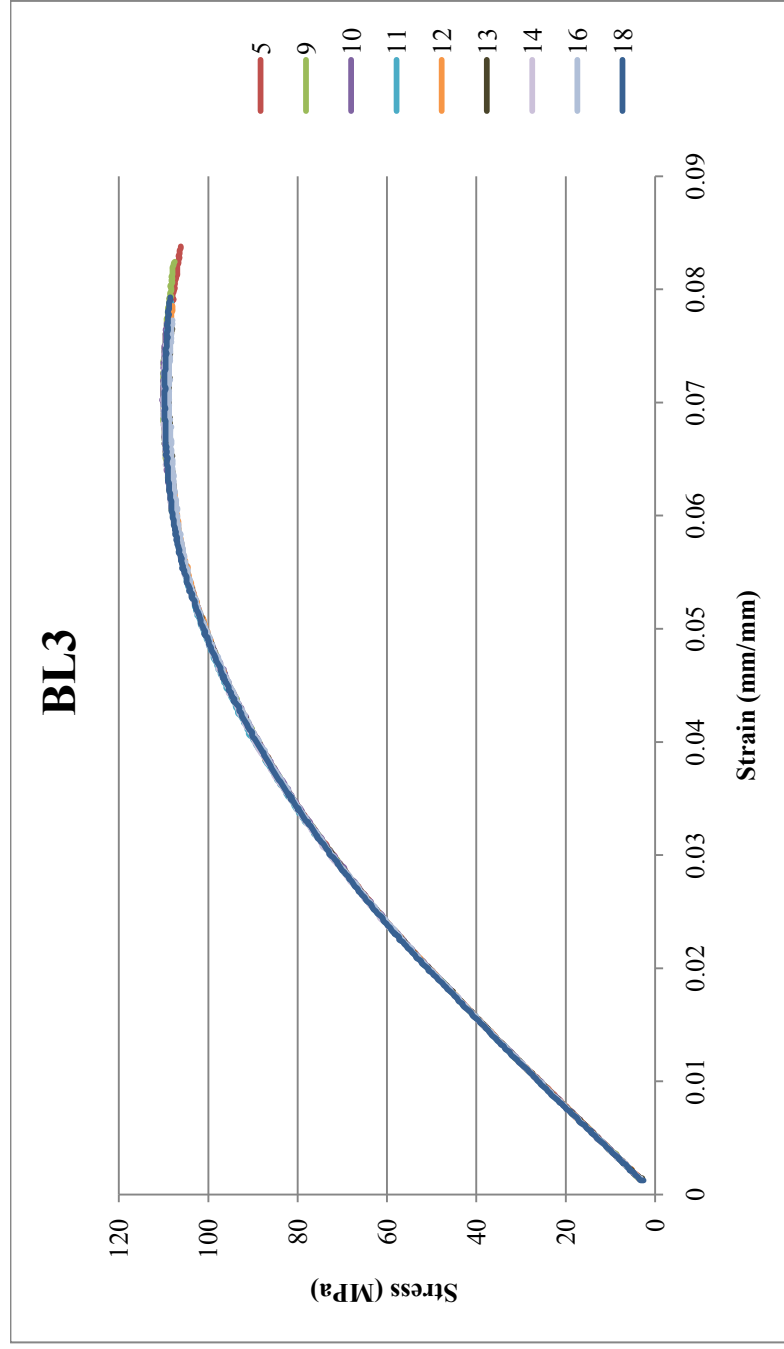


Figure K.18: Flexural Results for BL3 Lexan HF1130-111: Injection molded 6-3-10

Table K.18: Flexural Results for BL3 Lexan HF1130-111: Injection molded 6-3-10

Sample	Specimen	Flexural Maximum Stress (MPa)	Strain at Maximum Flexural Stress (%)	0.1% Offset Yield Flexural Stress (MPa)	Strain at 0.1% Offset Yield Flexural Stress (%)	Flexural Modulus (MPa)
BL3	5	109.827	6.94	63.804	2.57	2572.14
	9	110.088	6.83	64.327	2.61	2571.31
	10	110.349	7.02	63.542	2.57	2569.86
	11	109.827	6.87	64.850	2.62	2573.86
	12	109.304	6.86	63.804	2.58	2571.91
	13	109.042	6.91	64.327	2.60	2572.87
	14	110.088	6.80	65.111	2.62	2585.11
	16	109.042	7.00	64.588	2.62	2571.79
	18	109.827	6.85	64.850	2.61	2587.60
Average		109.71	6.90	64.36	2.60	2575.16
Standard Deviation		0.47	0.08	0.55	0.02	6.47
Number		9	9	9	9	9

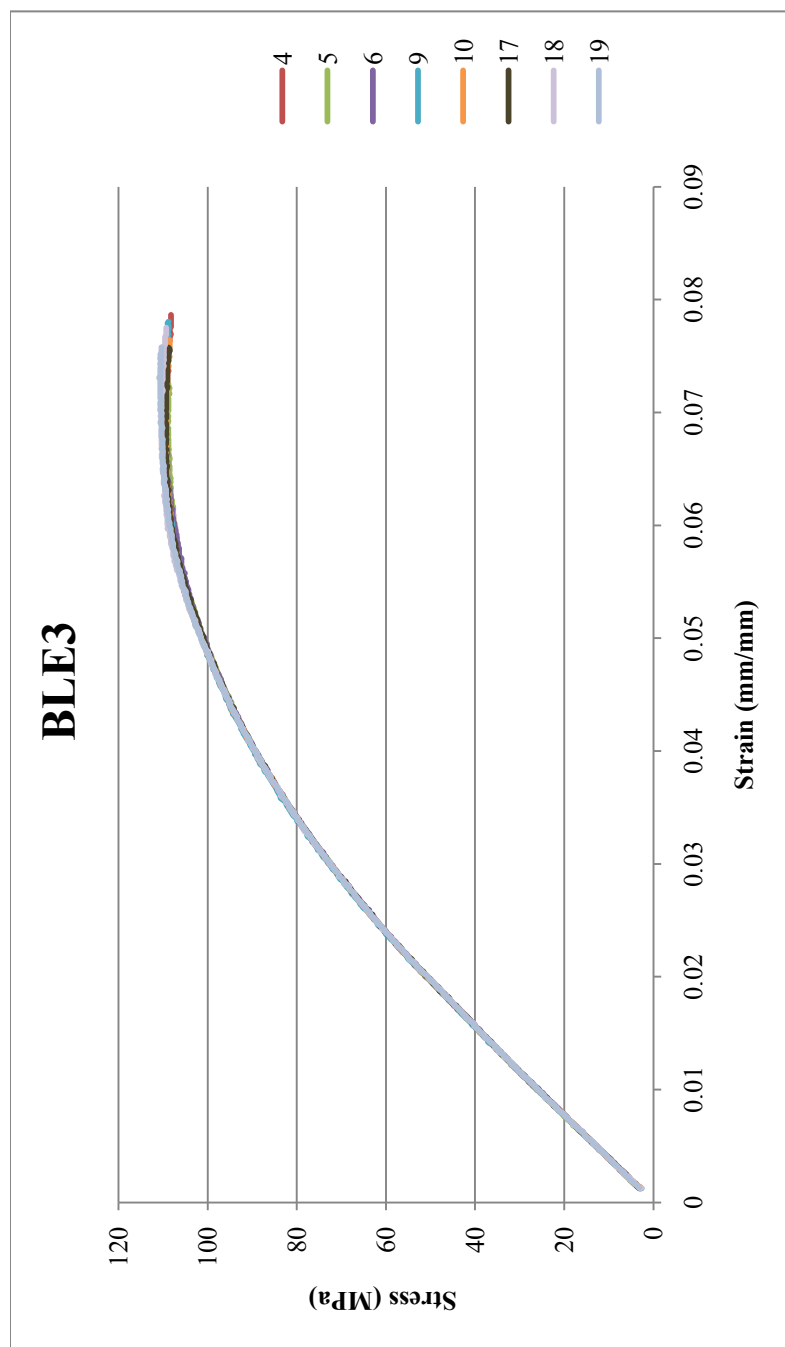


Figure K.19: Flexural Results for BLE3 Extruded Lexan HF1130-111: Extruded 5-26-10, Injection molded 6-3-10

Table K.19: Flexural Results for BLE3 Extruded Lexan HF1130-111: Extruded 5-26-10, Injection molded 6-3-10

Sample	Specimen	Flexural Maximum Stress (MPa)	Strain at Maximum Flexural Stress (%)	0.1% Offset Yield Flexural Stress (MPa)	Strain at 0.1% Offset Yield Stress (%)	Flexural Modulus (MPa)
BLE3	4	109.304	6.69	63.542	2.56	2583.88
	5	109.042	6.78	61.712	2.47	2600.86
	6	109.827	7.02	63.542	2.56	2579.64
	9	110.088	7.06	63.019	2.53	2596.16
	10	109.565	6.63	64.065	2.58	2583.73
	17	109.565	6.63	63.019	2.53	2585.18
	18	110.611	6.97	63.542	2.56	2585.10
	19	110.872	7.31	63.542	2.56	2579.28
Average		109.86	6.89	63.25	2.54	2586.73
Standard Deviation		0.63	0.24	0.70	0.03	7.71
Number		8	8	8	8	8

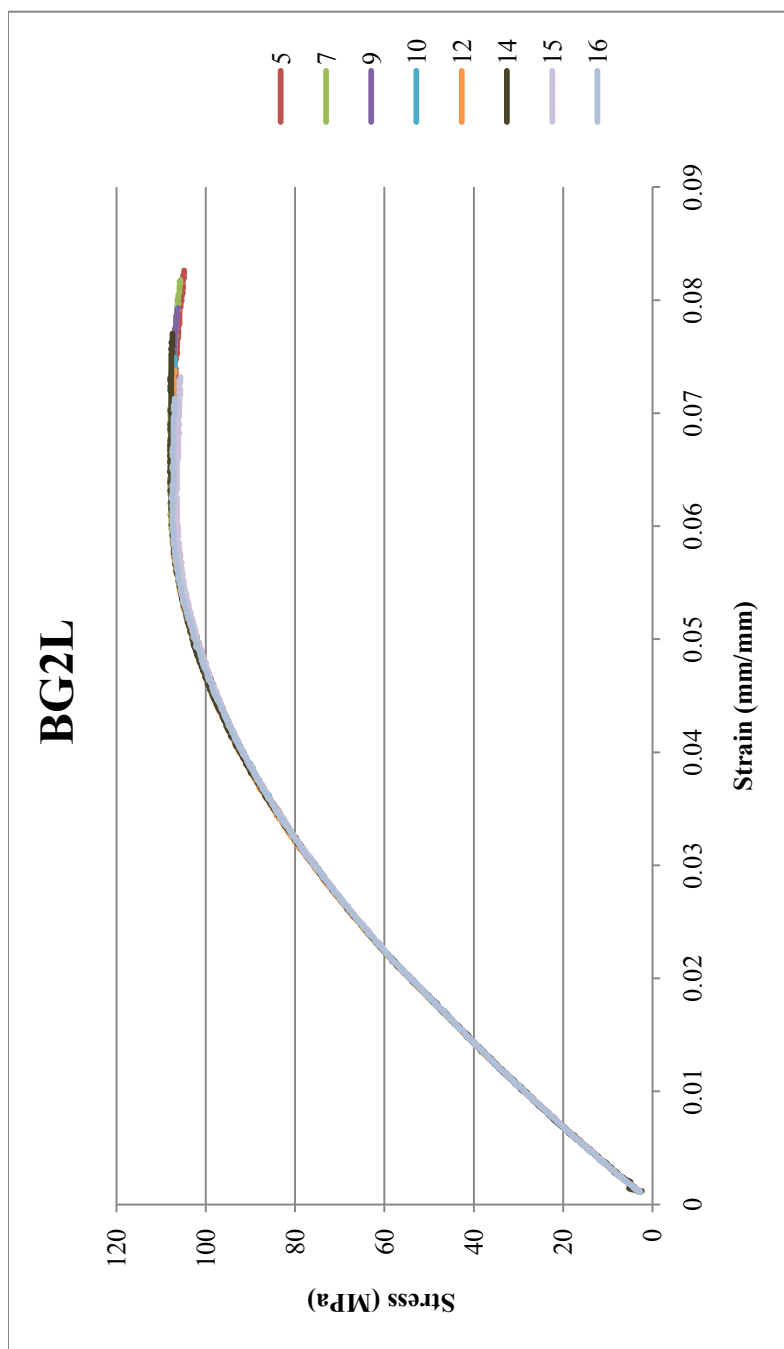


Figure K.20: Flexural Results for BG2L: 2 wt% xGnP in Lexan HF1130-111: Injection Molded 6-3-10

Table K.20: Flexural Results for BG2L: 2 wt% xGnP in Lexan HF1130-111: Injection Molded 6-3-10

Sample	Specimen	Flexural Maximum Stress (MPa)	Strain at Maximum Flexural Stress (%)	0.1% Offset Yield Flexural Stress (MPa)	Strain at 0.1% Offset Yield Stress (%)	Flexural Modulus (MPa)
BG2L	5	107.212	6.15	66.419	2.53	2758.37
	7	107.996	6.10	65.634	2.50	2771.22
	9	107.996	6.39	65.634	2.50	2772.72
	10	107.212	6.20	63.281	2.38	2778.43
	12	107.996	6.38	62.497	2.36	2795.41
	14	107.996	6.32	64.588	2.46	2766.49
	15	106.689	6.27	62.497	2.37	2786.08
	16	107.735	6.25	62.235	2.35	2793.18
Average		107.60	6.26	64.10	2.43	2777.74
Standard Deviation		0.50	0.10	1.67	0.07	13.04
Number		8	8	8	8	8

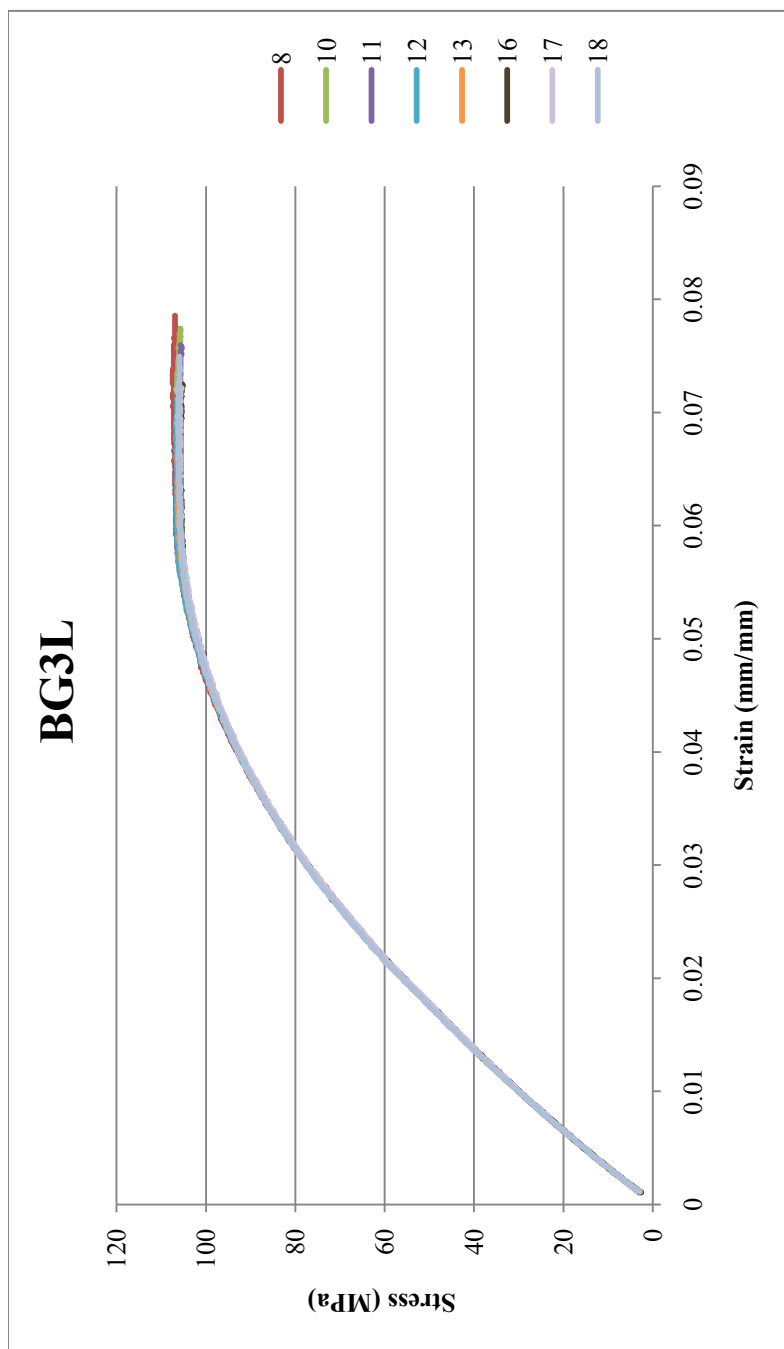


Figure K.21: Flexural Results for BG3L: 3 wt% xGnP in Lexan HF1130-111: Injection Molded 6-3-10

Table K.21: Flexural Results for BG3L: 3 wt% xGnP in Lexan HF1130-111: Injection Molded 6-3-10

Sample	Specimen	Flexural Maximum Stress (MPa)	Strain at Maximum Flexural Stress (%)	0.1% Offset Yield Flexural Stress (MPa)	Strain at 0.1% Offset Yield Stress (%)	Flexural Modulus (MPa)
BG3L	8	107.473	7.06	65.896	2.42	2877.12
	10	106.689	6.79	64.588	2.38	2870.84
	11	106.689	5.92	64.588	2.37	2864.85
	12	106.689	6.00	62.497	2.27	2902.99
	13	106.427	6.17	62.497	2.28	2898.97
	16	105.904	6.44	62.235	2.27	2899.53
	17	105.904	6.22	61.712	2.26	2882.22
	18	106.427	6.91	63.019	2.28	2907.71
Average		106.53	6.44	63.38	2.32	2888.03
Standard Deviation		0.50	0.43	1.47	0.06	16.25
Number		8	8	8	8	8

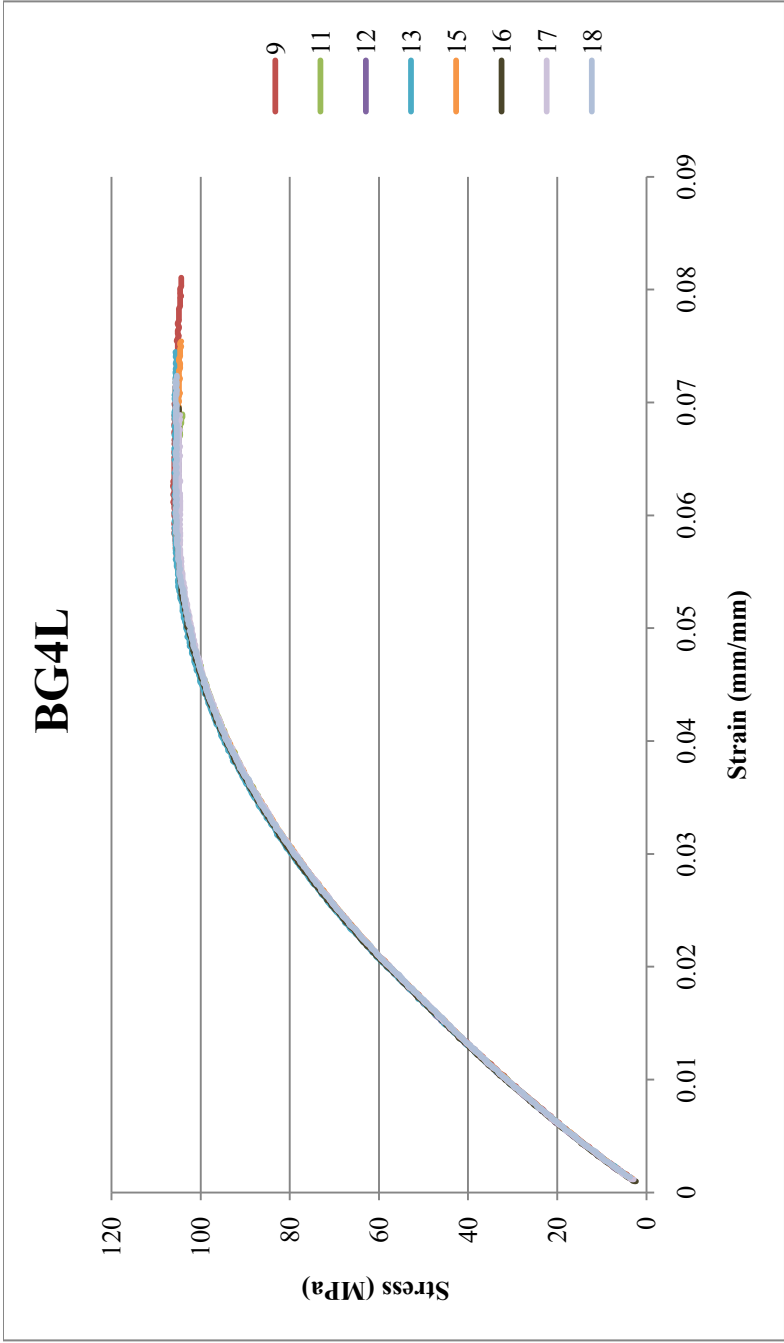


Figure K.22: Flexural Results for BG4L: 4 wt% xGnP (carbon black) in Lexan HF1130-111: Injection Molded 6-3-10

Table K.22: Flexural Results for BG4L: 4 wt% xGnP (carbon black) in Lexan HF1130-111: Injection Molded 6-3-10

Sample	Specimen	Flexural Maximum Stress (MPa)	Strain at Maximum Flexural Stress (%)	0.1% Offset Yield Flexural Stress (MPa)	Strain at 0.1% Offset Yield Stress (%)	Flexural Modulus (MPa)
BG4L	9	106.166	6.12	67.203	2.41	2950.56
	11	105.381	6.02	62.758	2.20	3015.07
	12	105.643	5.78	62.758	2.19	3044.76
	13	105.904	5.84	65.373	2.30	3019.46
	15	105.381	5.82	64.588	2.30	2983.22
	16	105.381	5.83	61.451	2.13	3051.33
	17	105.120	5.93	61.974	2.18	3023.43
	18	105.643	5.85	64.850	2.31	2980.53
Average		105.58	5.90	63.87	2.25	3008.55
Standard Deviation		0.34	0.12	1.96	0.09	34.46
Number		8	8	8	8	8

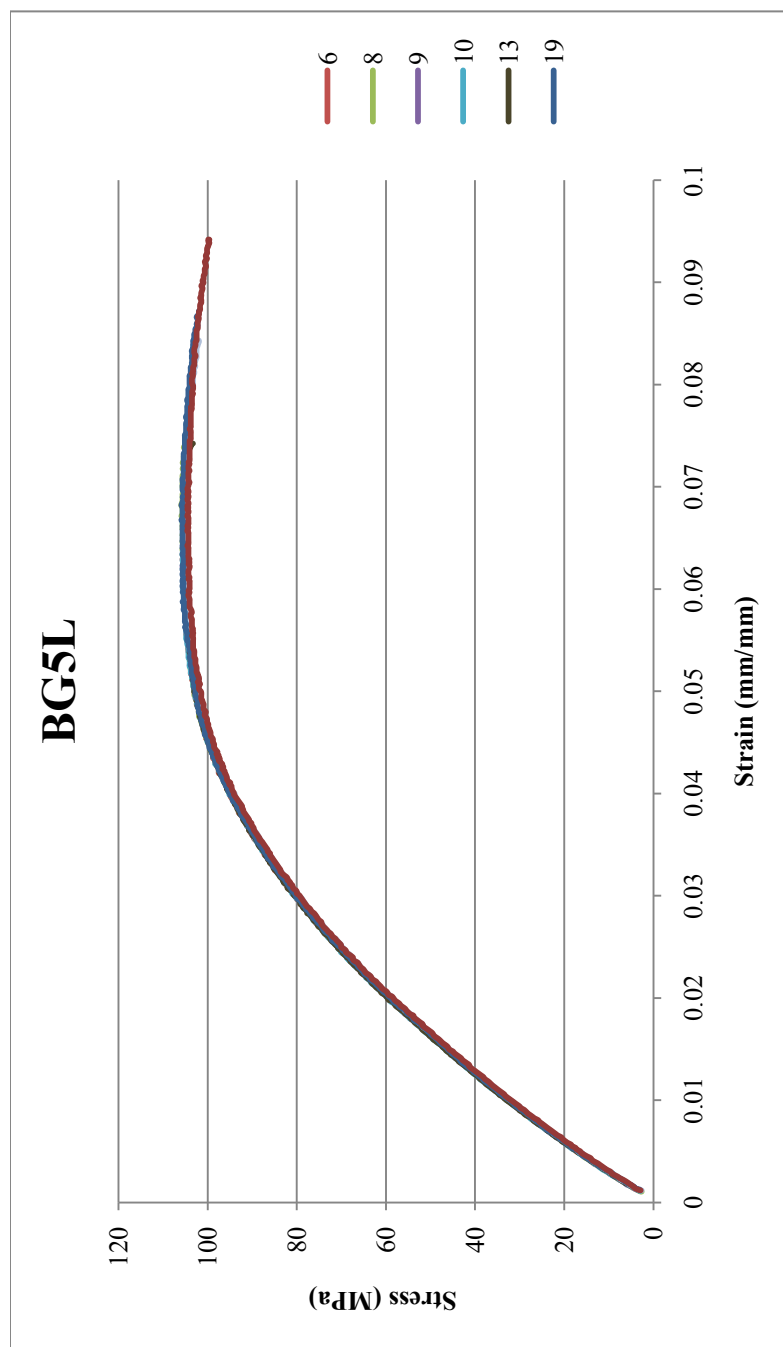


Figure K.23: Flexural Results for BG5L: 5 wt% xGnP in Lexan HF1130-111: Injection Molded 6-3-10

Table K.23: Flexural Results for BG5L: 5 wt% xGnP in Lexan HF1130-111: Injection Molded 6-3-10

Sample	Specimen	Flexural Maximum Stress (MPa)	Strain at Maximum Flexural Stress (%)	0.1% Offset Yield Flexural Stress (MPa)	Strain at 0.1% Offset Yield Stress (%)	Flexural Modulus (MPa)
BG5L	6	105.64	6.28	62.76	2.15	3116.11
	8	105.90	6.72	65.63	2.27	3083.28
	9	105.64	6.21	64.33	2.21	3110.66
	10	105.64	6.00	63.80	2.18	3126.92
	13	105.38	6.38	65.63	2.25	3099.02
	19	105.90	6.67	71.13	2.53	2995.01
Average		105.69	6.38	65.55	2.26	3088.50
Standard Deviation		0.20	0.28	2.95	0.14	48.18
Number		6	6	6	6	6

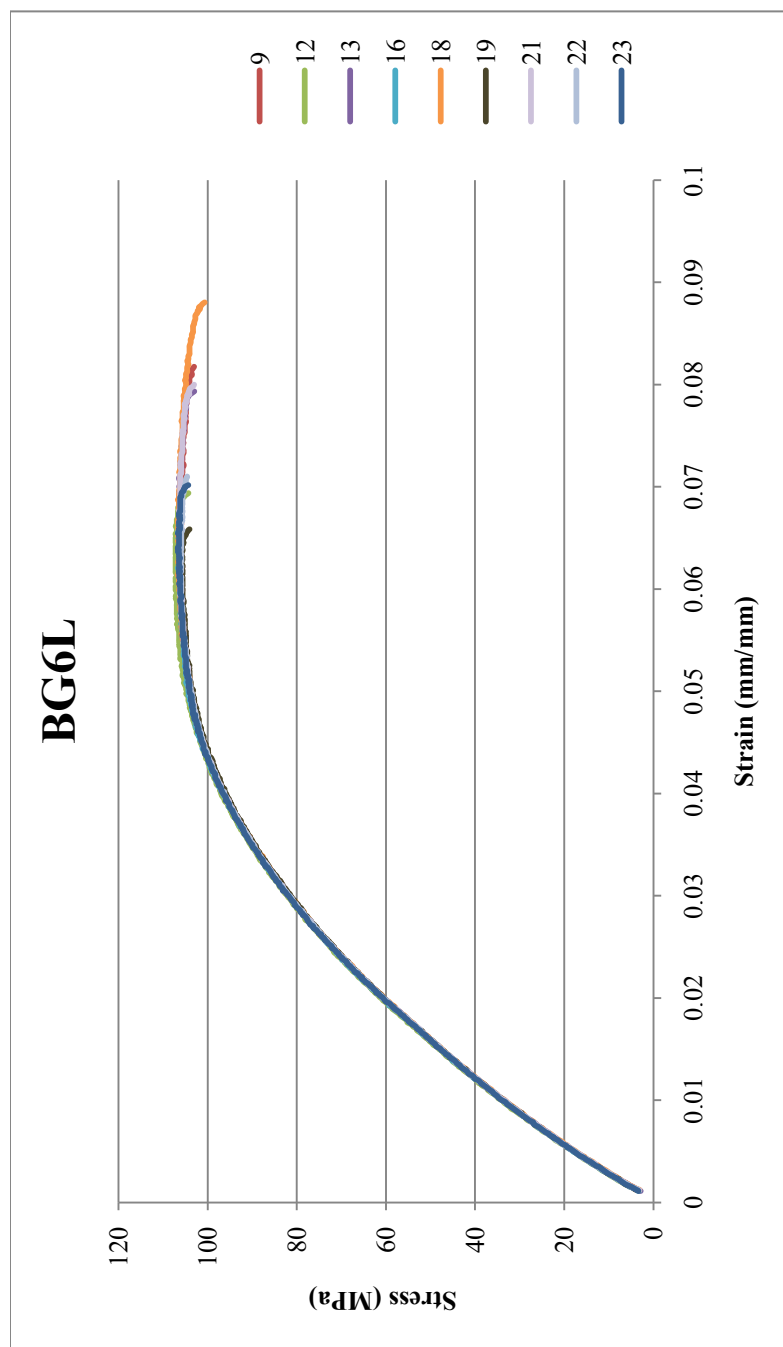


Figure K.24: Flexural Results for BG6L: 6 wt% xGnP in Lexan HF1130-111: Injection Molded 6-8-10

Table K.24: Flexural Results for BG6L: 6 wt% xGnP in Lexan HF1130-111: Injection Molded 6-8-10: All samples fractured.

Sample	Specimen	Flexural Maximum Stress (MPa)	Strain at Maximum Flexural Stress (%)	0.1% Offset Yield Flexural Stress (MPa)	Strain at 0.1% Offset Yield Stress (%)	Flexural Modulus (MPa)
BG6L	9	106.166	6.01	69.034	2.34	3127.06
	12	107.212	5.91	63.804	2.12	3229.40
	13	106.427	6.17	68.511	2.33	3133.54
	16	106.689	6.20	63.804	2.13	3210.12
	18	106.689	6.13	72.172	2.51	3063.64
	19	105.904	6.01	61.189	2.03	3224.89
	21	106.427	6.36	69.557	2.38	3119.85
	22	106.166	5.88	65.634	2.21	3179.73
	23	106.689	6.37	64.850	2.17	3205.42
Average		106.49	6.12	66.51	2.25	3165.96
Standard Deviation		0.39	0.18	3.50	0.15	57.40
Number		9	9	9	9	9

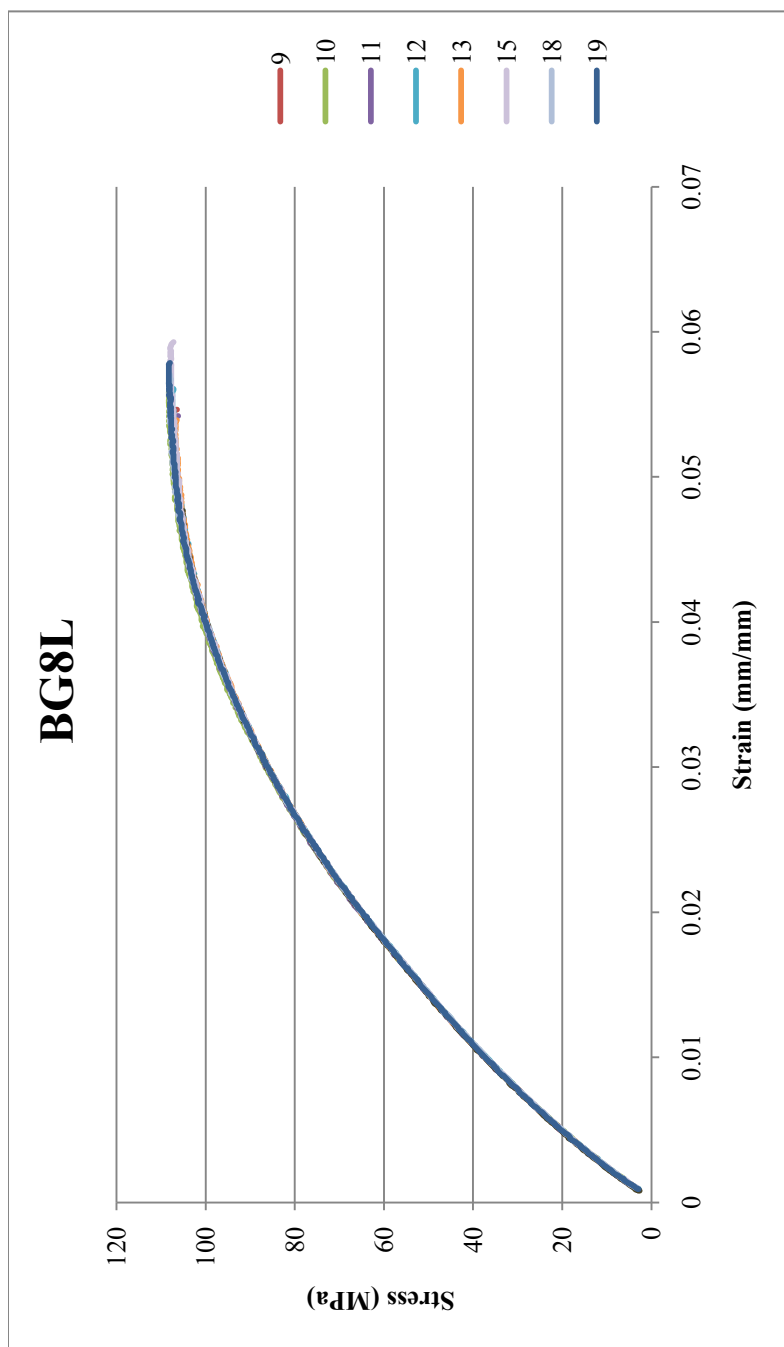


Figure K.25: Flexural Results for BG8L: 8 wt% xGnP in Lexan HF1130-111: Injection Molded 6-8-10

Table K.25: Flexural Results for BG8L: 8 wt% xGnP in Lexan HF1130-111: Injection Molded 6-8-10 : All samples fractured. Flexural Maximum and Fracture Stress and Strain are identical.

Sample	Specimen	Flexural Maximum Stress (MPa)	Strain at Maximum Flexural Stress (%)	0.1% Offset Yield Flexural Stress (MPa)	Strain at 0.1% Offset Yield Stress (%)	Flexural Modulus (MPa)
BG8L	9	107.735	5.43	57.79	1.72	3648.97
	10	108.258	5.35	58.05	1.72	3650.88
	11	107.473	5.34	56.22	1.66	3672.46
	12	107.473	5.43	58.57	1.76	3609.54
	13	106.950	5.27	57.01	1.69	3663.18
	15	107.996	5.79	60.14	1.82	3581.77
	18	108.258	5.57	58.31	1.75	3606.65
	19	108.258	5.56	58.05	1.74	3624.92
Average		107.80	5.47	58.02	1.73	3632.30
Standard Deviation		0.48	0.16	1.15	0.05	31.56
Number		8	8	8	8	8

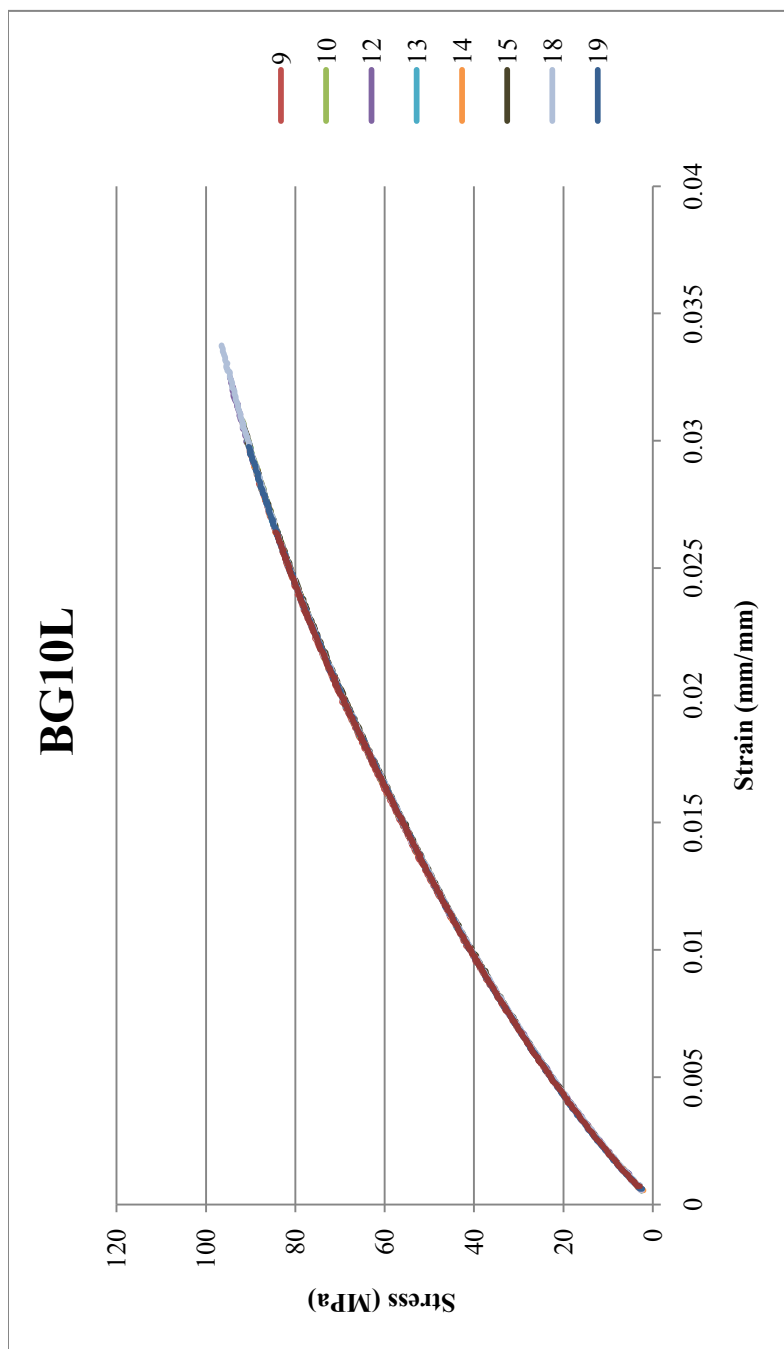


Figure K.26: Flexural Results for BG10L: 10 wt% xGnP in Lexan HF1130-111: Injection Molded 6-8-10

Table K.26: Flexural Results for BG10L: 10 wt% xGnP in Lexan HF1130-111: Injection Molded 6-8-10: All samples fractured. Flexural Maximum and Fracture Stress and Strain are identical.

Sample	Specimen	Flexural Maximum Stress (MPa)	Strain at Maximum Flexural Stress (%)	0.1% Offset Yield Flexural Stress (MPa)	Strain at 0.1% Offset Yield Stress (%)	Flexural Modulus (MPa)
BG10L	9	90.74	2.99	44.19	1.10	4491.00
	10	91.78	3.07	45.76	1.15	4422.88
	12	94.66	3.25	47.07	1.19	4357.27
	13	91.00	3.01	45.24	1.14	4416.82
	14	89.69	2.94	43.67	1.09	4451.86
	15	91.78	3.06	44.98	1.14	4408.67
	18	96.75	3.40	47.59	1.23	4300.31
	19	90.48	2.98	44.98	1.13	4444.52
	Average	92.11	3.09	45.43	1.15	4411.67
Standard Deviation		2.39	0.16	1.34	0.05	59.17
Number		8	8	8	8	8

Appendix K.4: Polycarbonate with Multiple Fillers

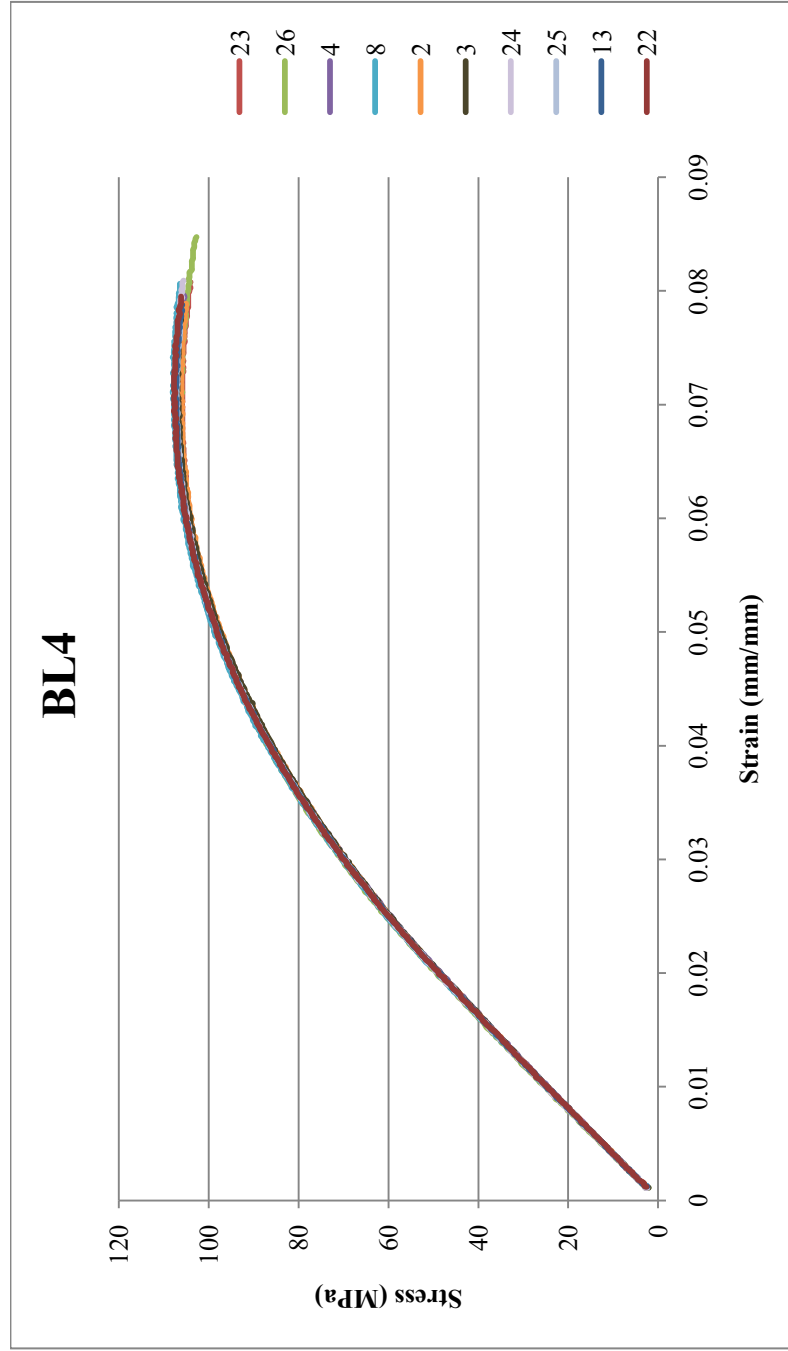


Figure K.27: Flexural Results for BL4 Lexan HF1130-111: Injection molded 7-26-10

Table K.27: Flexural Results for BL4 Lexan HF1130-111: Injection molded 7-26-10

Sample	Specimen	Flexural Maximum Stress (MPa)	Strain at Maximum Flexural Stress (%)	0.1% Offset Yield Flexural Stress (MPa)	Strain at 0.1% Offset Yield Stress (%)	Flexural Modulus (MPa)
BL4	23	106.127	7.00	64.565	2.70	2481.643
	26	106.388	6.83	64.042	2.66	2499.111
	4	106.911	6.93	61.690	2.61	2455.365
	8	107.957	7.05	62.997	2.63	2489.633
	2	106.388	7.05	62.735	2.64	2468.955
	3	107.173	7.10	62.212	2.61	2460.936
	24	107.695	7.09	62.735	2.63	2481.948
	25	107.173	6.84	62.735	2.62	2472.648
	13	107.434	6.99	61.167	2.56	2479.475
	22	107.695	6.94	63.258	2.65	2473.262
Average		107.09	6.98	62.81	2.63	2476.30
Standard Deviation		0.63	0.10	1.01	0.04	12.99
Number		10	10	10	10	10

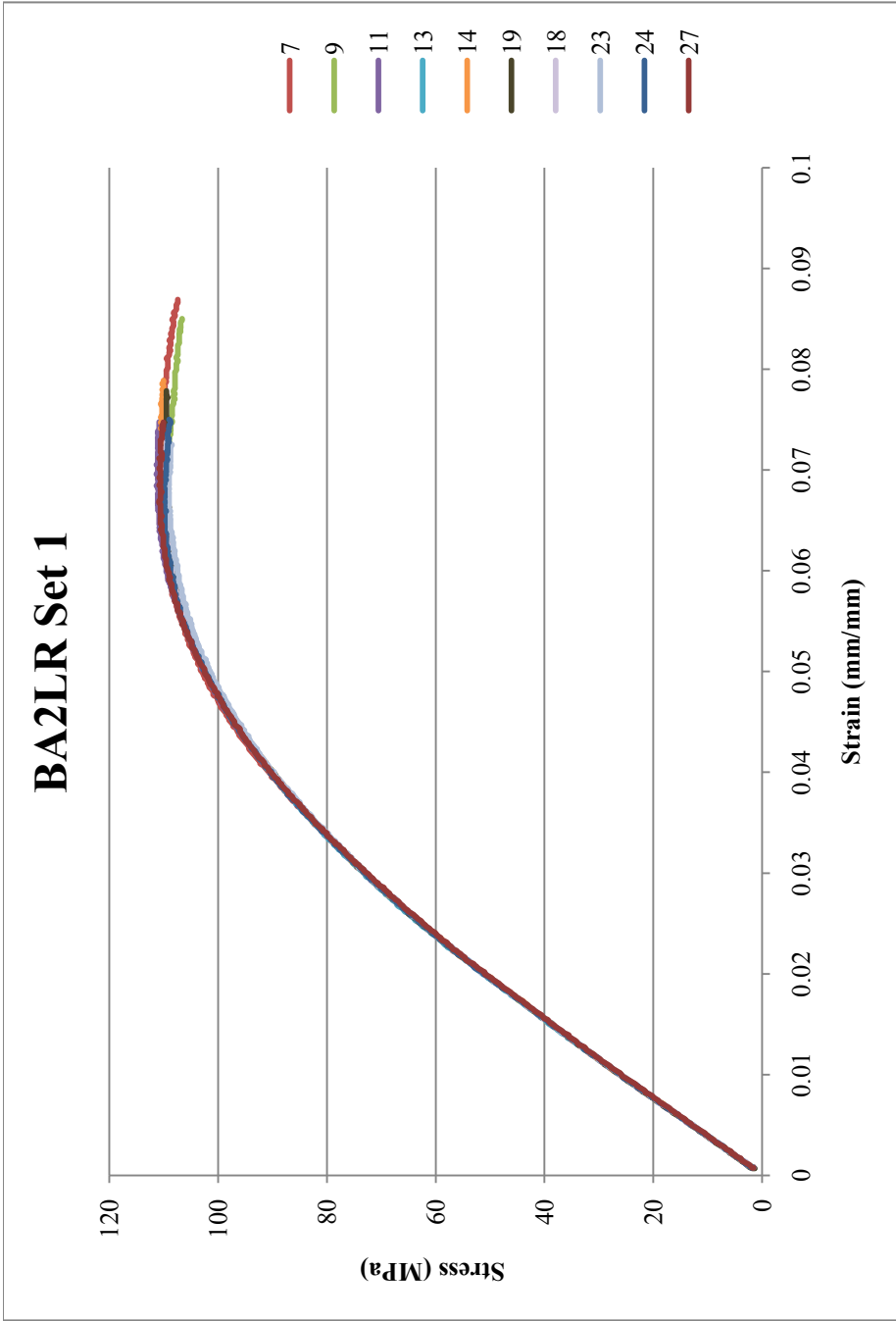


Figure K.28: Flexural Results for BA2LR Set 1: Extruded 7-8-10, Injection molded 7-26-10

Table K.28: Flexural Results for BA2LR Set 1: Extruded 7-8-10, Injection molded 7-26-10

Sample	Specimen	Flexural Maximum Stress (MPa)	Strain at Maximum Flexural Stress (%)	0.1% Offset Yield Flexural Stress (MPa)	Strain at 0.1% Offset Yield Stress (%)	Flexural Modulus (MPa)
BA2LR Set 1	7	110.571	7.07	66.133	2.66	2588.567
	9	109.787	6.52	65.872	2.65	2587.231
	11	111.355	6.84	62.997	2.52	2601.716
	13	110.048	6.72	61.167	2.43	2623.201
	14	110.571	7.42	63.519	2.54	2596.057
	19	109.787	6.91	65.088	2.60	2593.262
	18	110.048	6.50	61.428	2.45	2609.161
	23	109.264	6.79	61.690	2.47	2599.059
	24	110.048	6.42	63.519	2.54	2599.586
	27	110.832	6.68	61.951	2.49	2593.141
Average		110.23	6.79	63.34	2.54	2599.10
Standard Deviation		0.60	0.30	1.84	0.08	10.65
Number		10	10	10	10	10

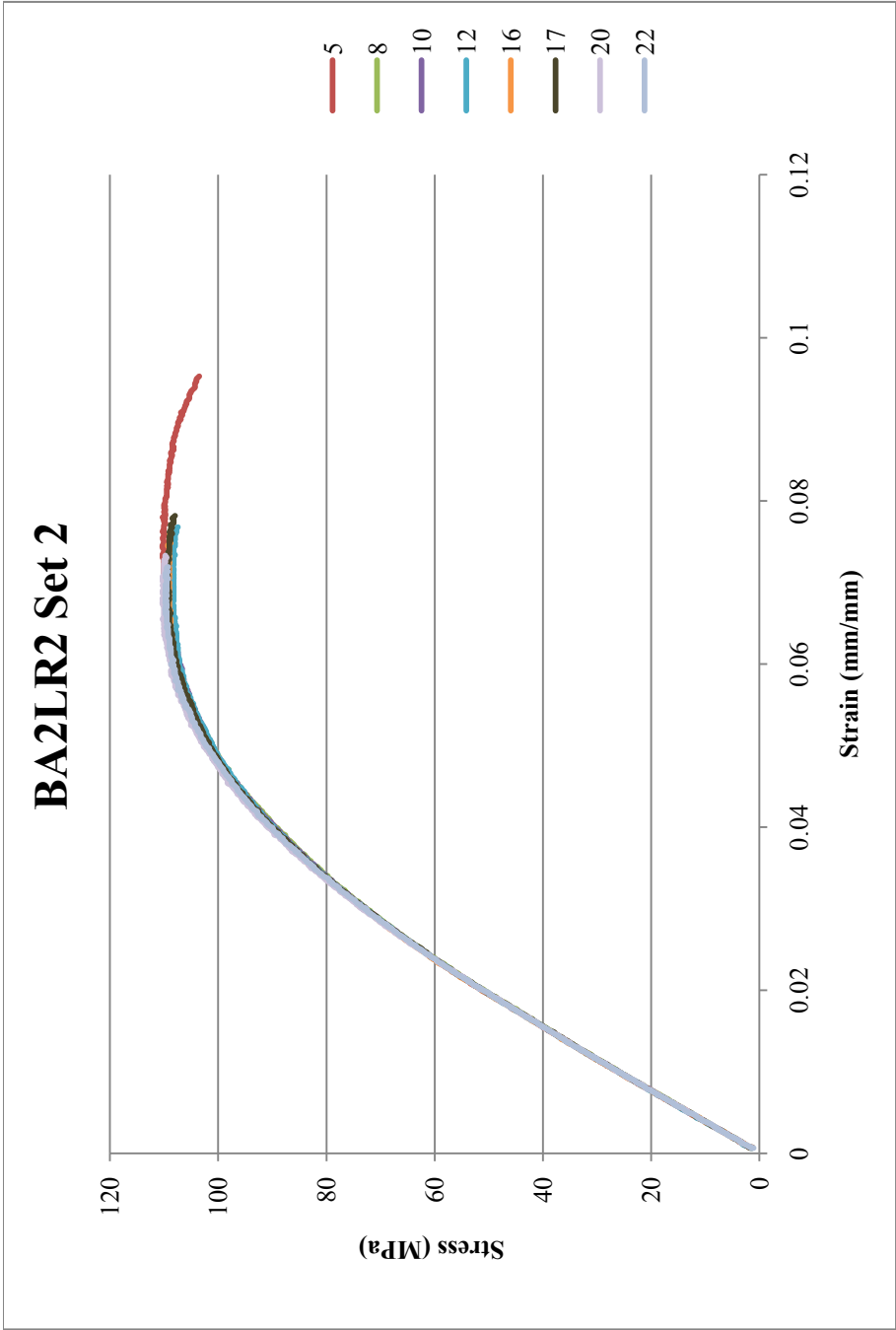


Figure K.29: Flexural Results for BA2LR Set 2: Extruded 7-8-10, Injection molded 7-26-10

Table K.29: Flexural Results for BA2LR Set 2: Extruded 7-8-10, Injection molded 7-26-10

Sample	Specimen	Flexural Maximum Stress (MPa)	Strain at Maximum Flexural Stress (%)	0.1% Offset Yield Flexural Stress (MPa)	Strain at 0.1% Offset Yield Stress (%)	Flexural Modulus (MPa)
BA2LR Set 2	5	110.309	7.31	67.702	2.74	2572.956
	8	109.002	6.87	61.690	2.46	2602.819
	10	108.741	6.70	60.905	2.43	2613.906
	12	108.480	6.74	63.258	2.54	2596.037
	16	109.525	7.22	61.690	2.46	2611.446
	17	109.525	6.90	62.474	2.51	2588.68
	20	110.309	6.55	63.519	2.53	2607.046
	22	109.787	6.62	62.212	2.48	2613.177
Average		109.46	6.86	62.93	2.52	2600.76
Standard Deviation		0.68	0.27	2.11	0.10	14.27
Number		8	8	8	8	8

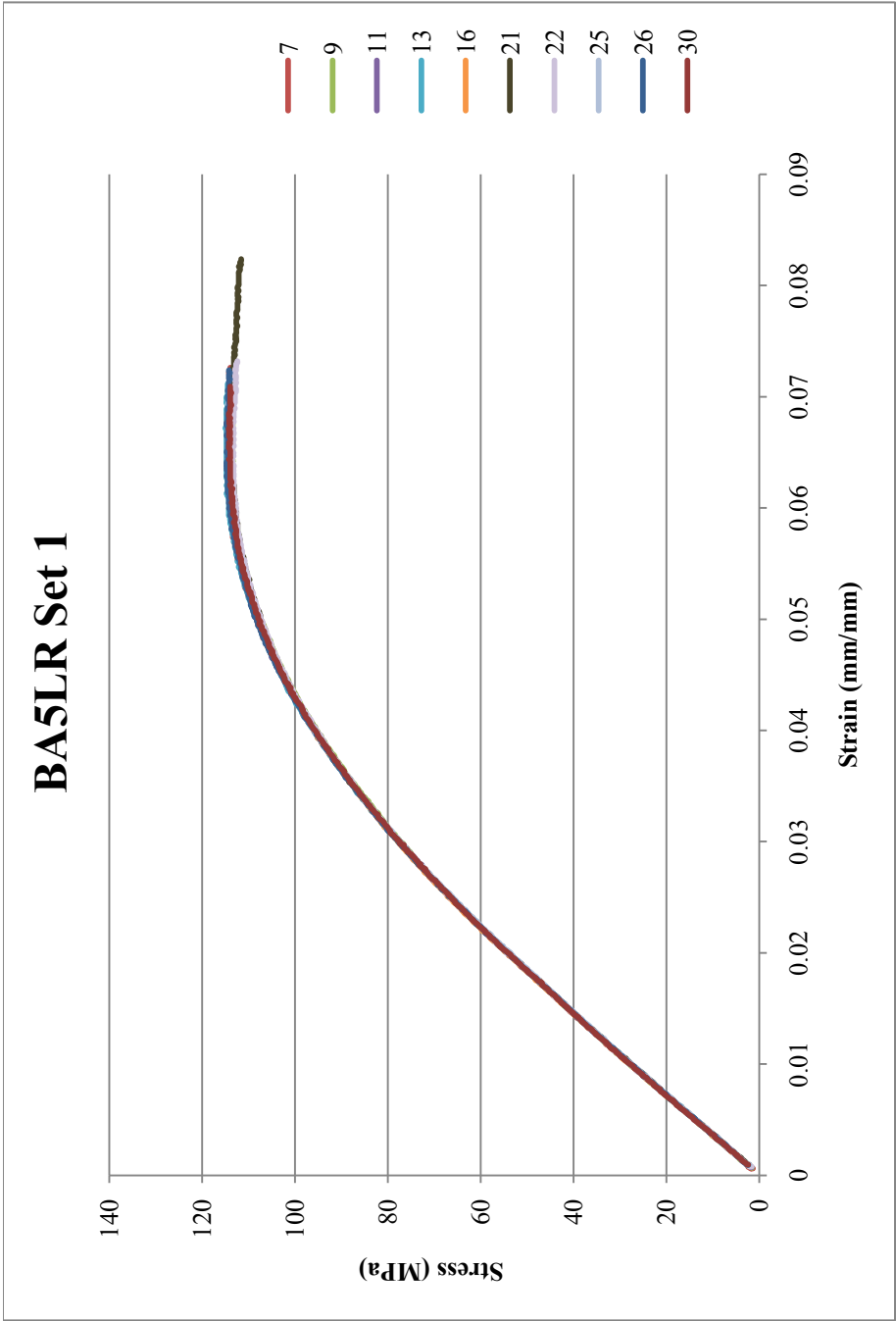


Figure K.30: Flexural Results for BA5LR Set 1: Extruded 7-8-10, Injection molded 7-26-10

Table K.30: Flexural Results for BA5LR Set 1: Extruded 7-8-10, Injection molded 7-26-10

Sample	Specimen	Flexural Maximum Stress (MPa)	Strain at Maximum Flexural Stress (%)	0.1% Offset Yield Flexural Stress (MPa)	Strain at 0.1% Offset Yield Stress (%)	Flexural Modulus (MPa)
BA5LR Set 1	7	114.753	6.67	65.349	2.45	2777.471
	9	113.708	6.18	64.304	2.41	2783.47
	11	114.230	6.53	66.133	2.49	2770.951
	13	115.015	6.72	65.088	2.44	2765.151
	16	114.230	6.32	67.179	2.51	2778.918
	21	113.969	6.56	69.009	2.62	2741.875
	22	113.708	6.43	66.656	2.51	2771.976
	25	114.492	6.43	66.133	2.50	2753.285
	26	114.753	6.29	67.179	2.53	2763.739
	30	114.230	6.44	66.395	2.50	2773.688
Average		114.31	6.46	66.34	2.50	2768.05
Standard Deviation		0.45	0.17	1.31	0.06	12.61
Number		10	10	10	10	10

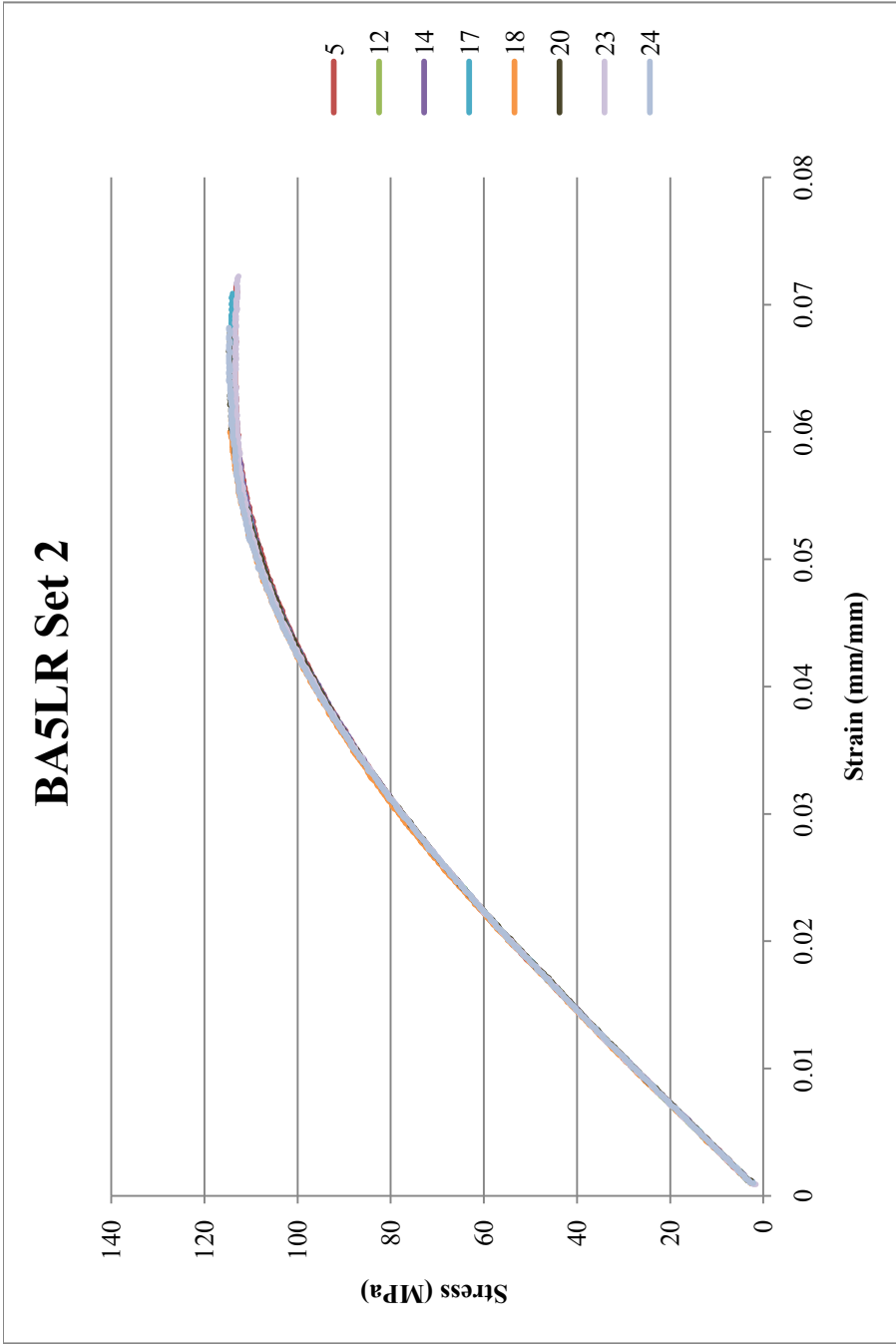


Figure K.31: Flexural Results for BA5LR Set 2: Extruded 7-8-10, Injection molded 7-26-10

Table K.31: Flexural Results for BA5LR Set 2: Extruded 7-8-10, Injection molded 7-26-10

Sample	Specimen	Flexural Maximum Stress (MPa)	Strain at Maximum Flexural Stress (%)	0.1% Offset Yield Flexural Stress (MPa)	Strain at 0.1% Offset Yield Stress (%)	Flexural Modulus (MPa)
BA5LR Set 2	5	113.708	6.55	65.088	2.44	2774.413
	12	114.492	6.42	65.611	2.47	2772.262
	14	113.969	6.40	65.611	2.47	2768.479
	17	114.492	6.40	66.133	2.49	2766.344
	18	114.492	6.00	65.611	2.45	2793.075
	20	114.753	6.63	65.349	2.45	2761.554
	23	113.446	6.23	65.088	2.45	2768.931
	24	114.753	6.40	64.304	2.42	2770.756
Average		114.26	6.38	65.35	2.46	2771.98
Standard Deviation		0.49	0.19	0.54	0.02	9.37
Number		8	8	8	8	8

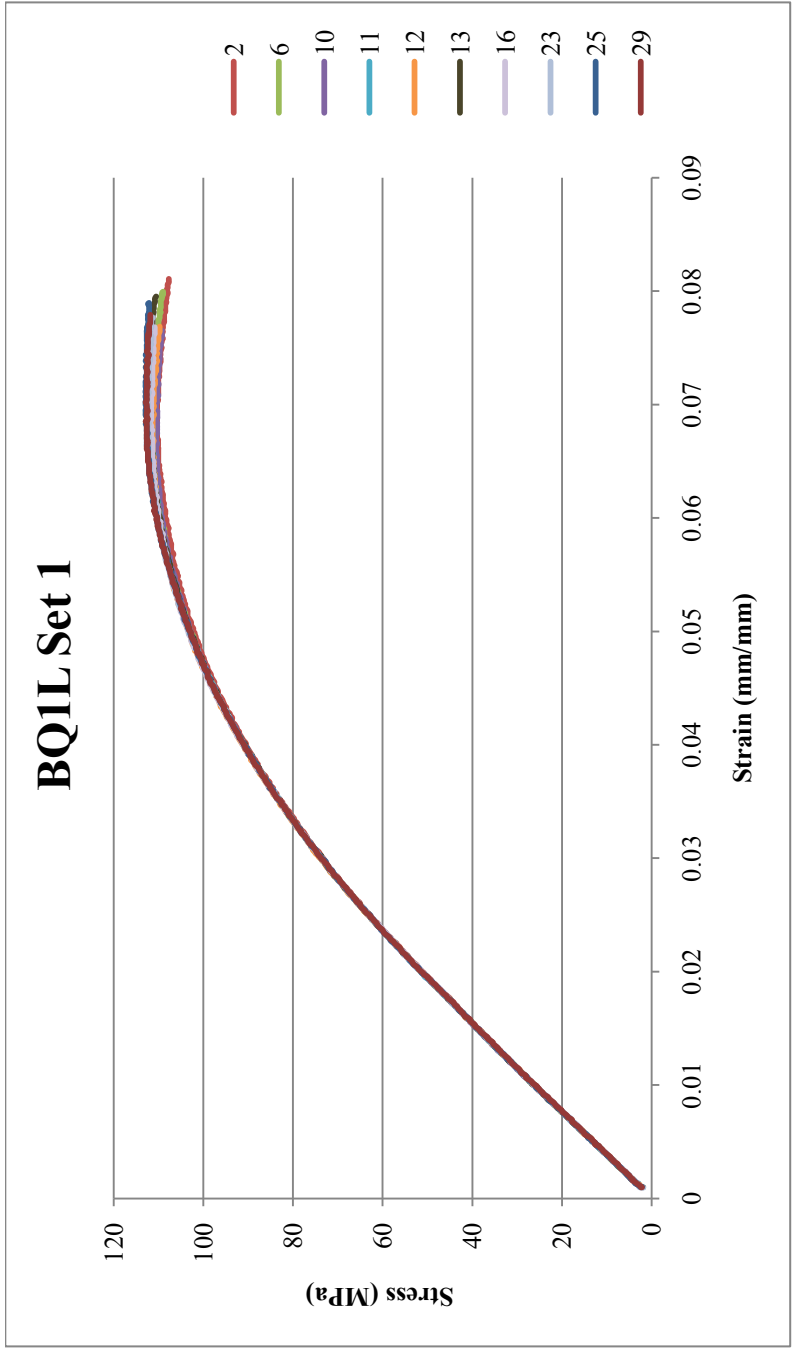


Figure K.32: Flexural Results for BQ1L Set 1: Extruded 6-30-10, Injection molded 7-26-10

Table K.32: Flexural Results for BQ1L Set 1: Extruded 6-30-10, Injection molded 7-26-10

Sample	Specimen	Flexural Maximum Stress (MPa)	Strain at Maximum Flexural Stress (%)	0.1% Offset Yield Flexural Stress (MPa)	Strain at 0.1% Offset Yield Stress (%)	Flexural Modulus (MPa)
BQ1L Set 1	2	110.309	6.64	67.179	2.70	2590.038
	6	111.355	6.82	66.395	2.64	2602.911
	10	110.571	6.52	65.349	2.60	2620.335
	11	111.616	6.60	65.088	2.59	2610.464
	12	111.355	6.44	67.963	2.71	2609.605
	13	112.139	6.84	65.872	2.63	2606.727
	16	111.878	6.83	65.872	2.62	2603.939
	23	112.662	7.03	65.088	2.59	2612.629
	25	112.923	6.83	66.918	2.67	2601.91
	29	112.923	6.85	65.088	2.59	2604.629
Average		111.77	6.74	66.08	2.63	2606.32
Standard Deviation		0.92	0.18	1.01	0.05	7.95
Number		10	10	10	10	10

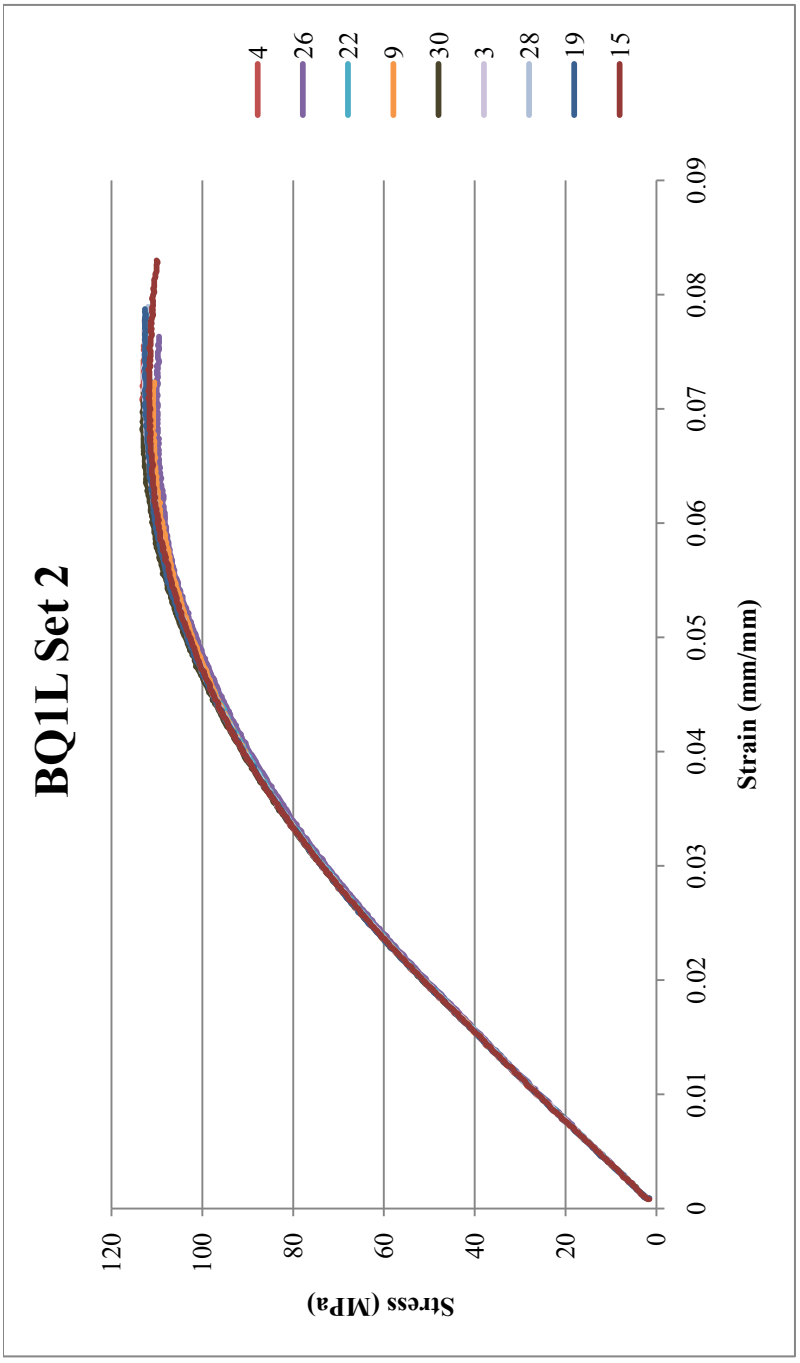


Figure K.33: Flexural Results for BQ1L Set 2: Extruded 6-30-10, Injection molded 7-26-10

Table K.33: Flexural Results for BQ1L Set 2: Extruded 6-30-10, Injection molded 7-26-10

Sample	Specimen	Flexural Maximum Stress (MPa)	Strain at Maximum Flexural Stress (%)	0.1% Offset Yield Flexural Stress (MPa)	Strain at 0.1% Offset Yield Stress (%)	Flexural Modulus (MPa)
BQ1L Set 2	4	113.185	7.07	66.656	2.65	2619.822
	26	110.048	6.75	63.519	2.55	2577.003
	22	111.878	6.79	64.826	2.58	2601.329
	9	111.094	6.81	64.042	2.54	2616.902
	30	113.185	6.81	64.565	2.55	2624.161
	3	112.923	7.16	67.179	2.69	2599.188
	28	112.401	7.13	66.656	2.67	2599.725
	19	112.662	6.95	67.702	2.70	2607.865
	15	111.878	7.09	66.656	2.67	2598.096
Average		112.14	6.95	65.76	2.62	2604.90
Standard Deviation		1.05	0.17	1.52	0.06	14.33
Number		9	9	9	9	9

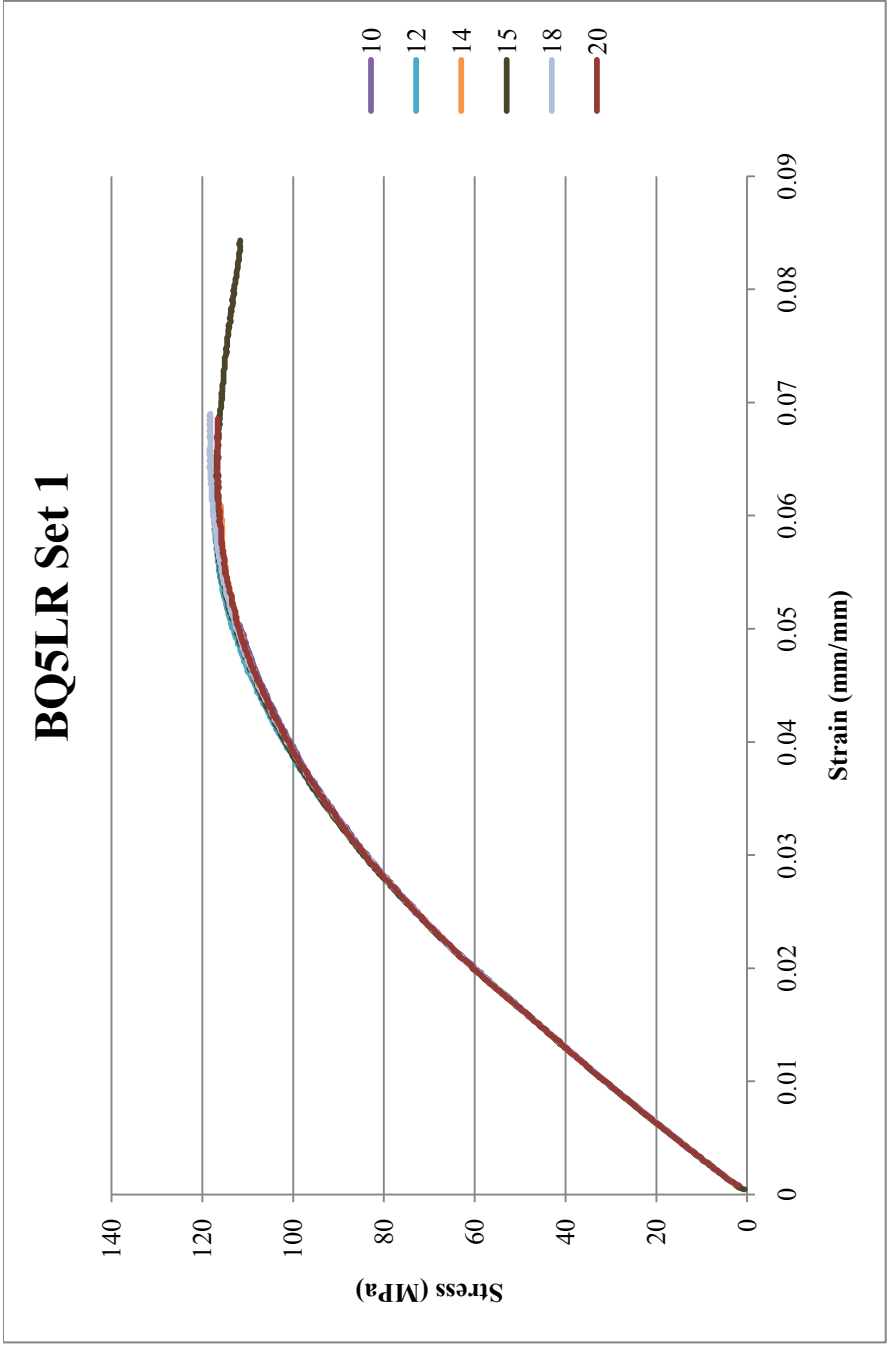


Figure K.34: Flexural Results for BQ5LR Set 1: Extruded 6-30-10, Injection molded 8-25-10

Table K.34: Flexural Results for BQ5LR Set 1: Extruded 6-30-10, Injection molded 8-25-10

Sample	Specimen	Flexural Maximum Stress (MPa)	Strain at Maximum Flexural Stress (%)	0.1% Offset Yield Flexural Stress (MPa)	Strain at 0.1% Offset Yield Stress (%)	Flexural Modulus (MPa)
BQ5LR Set 1	10	116.082	6.15	69.283	2.36	3087.401
	12	117.390	5.88	67.715	2.27	3117.72
	14	116.082	6.02	68.238	2.29	3115.734
	15	117.390	6.06	73.205	2.49	3055.19
	18	118.435	6.42	69.806	2.38	3079.072
	20	116.867	6.40	71.113	2.42	3080.515
Average		117.04	6.15	69.89	2.37	3089.27
Standard Deviation		0.90	0.22	2.02	0.08	23.90
Number		6	6	6	6	6

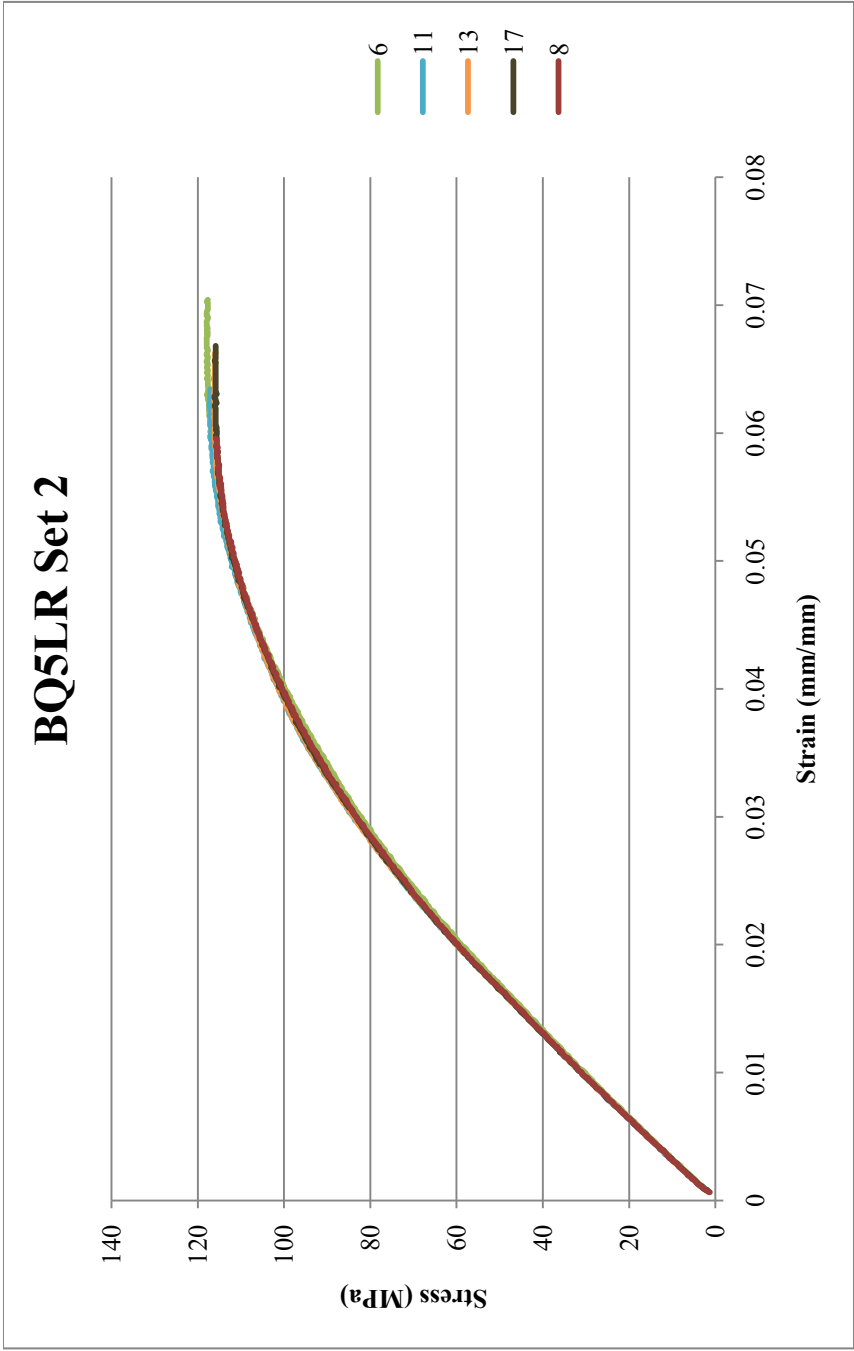


Figure K.35: Flexural Results for BQ5LR Set 2: Extruded 6-30-10, Injection molded 8-25-10

Table K.35: Flexural Results for BQ5LR Set 2: Extruded 6-30-10, Injection molded 8-25-10

Sample	Specimen	Flexural Maximum Stress (MPa)	Strain at Maximum Flexural Stress (%)	0.1% Offset Yield Flexural Stress (MPa)	Strain at 0.1% Offset Yield Stress (%)	Flexural Modulus (MPa)
BQ5LR Set 2	6	117.912	6.30	68.760	2.39	3008.726
	11	117.390	6.22	69.806	2.38	3082.546
	13	116.344	6.12	68.760	2.33	3074.826
	17	116.082	6.21	67.715	2.31	3082.512
	8	115.821	5.89	65.623	2.23	3088.146
Average		116.71	6.15	68.13	2.33	3067.35
Standard Deviation		0.90	0.16	1.59	0.06	33.11
Number		5	5	5	5	5

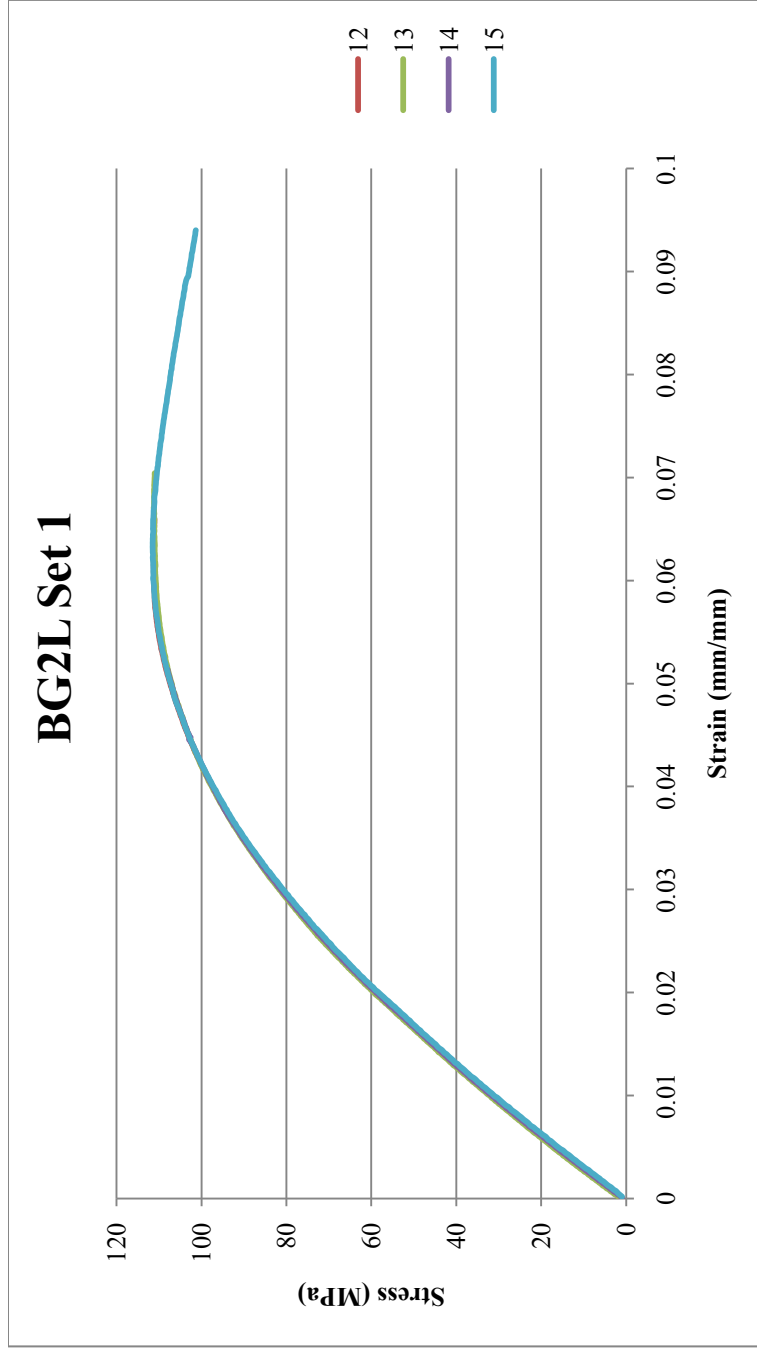


Figure K.36: Flexural Results for BG2L Set 1: Extruded May 2010, Injection molded 9-9-10

Table K.36: Flexural Results for BG2L Set 1: Extruded May 2010, Injection molded 9-9-10

Sample	Specimen	Flexural Maximum Stress (MPa)	Strain at Maximum Flexural Stress (%)	0.1% Offset Yield Flexural Stress (MPa)	Strain at 0.1% Offset Yield Stress (%)	Flexural Modulus (MPa)
BG2L Set 1	12	111.249	6.15	66.964	2.34	3036.253
	13	111.243	6.71	74.151	2.63	3016.902
	14	111.263	6.54	67.899	2.37	3044.353
	15	111.496	6.33	74.522	2.70	2924.432
Average		111.31	6.43	70.88	2.51	3005.48
Standard Deviation		0.12	0.24	4.01	0.18	55.25
Number		4	4	4	4	4

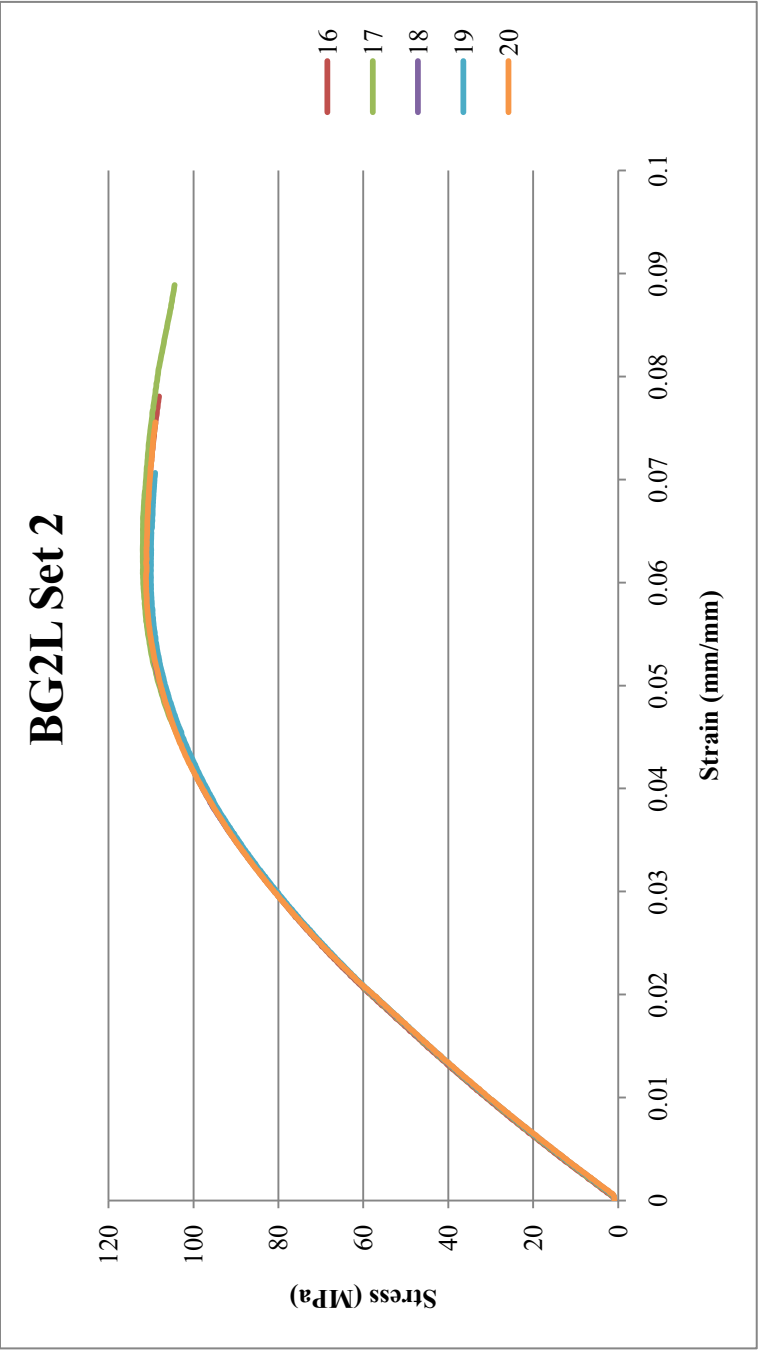


Figure K.37: Flexural Results for BG2L Set 2: Extruded May 2010, Injection molded 9-9-10

Table K.37: Flexural Results for BG2L Set 2: Extruded May 2010, Injection molded 9-9-10

Sample	Specimen	Flexural Maximum Stress (MPa)	Strain at Maximum Flexural Stress (%)	0.1% Offset Yield Flexural Stress (MPa)	Strain at 0.1% Offset Yield Stress (%)	Flexural Modulus (MPa)
BG2L Set 2	16	111.054	6.29	68.317	2.41	2996.273
	17	111.949	6.32	71.417	2.55	2946.639
	18	111.605	6.48	61.391	2.14	3029.994
	19	110.053	6.09	61.877	2.16	3013.806
	20	111.183	6.04	63.190	2.21	3002.097
Average		111.17	6.24	65.24	2.29	2997.76
Standard Deviation		0.72	0.18	4.41	0.18	31.35
Number		5	5	5	5	5

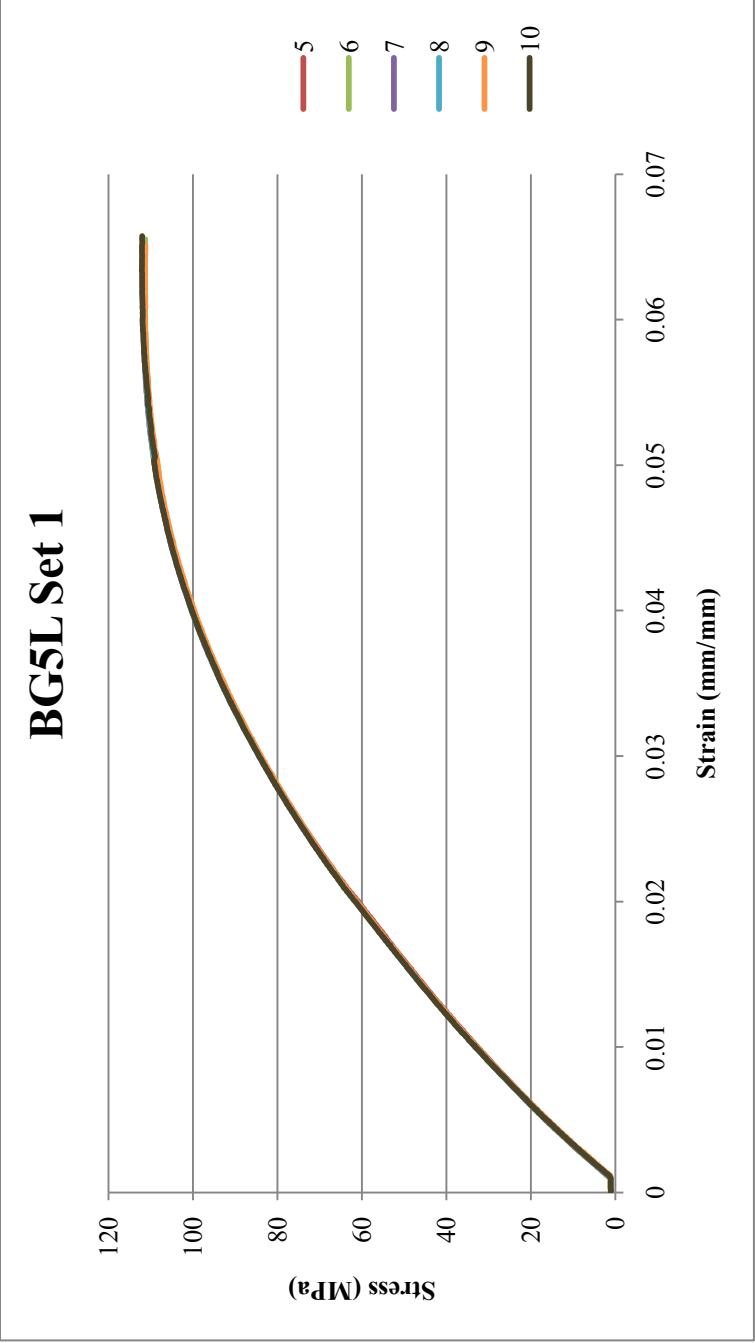


Figure K.38: Flexural Results for BG5L Set 1: Extruded May 2010, Injection molded 9-9-10

Table K.38: Flexural Results for BG5L Set 1: Extruded May 2010, Injection molded 9-9-10

Sample	Specimen	Peak Flexural Stress (MPa)	Strain at Peak Flexural Stress (%)	0.1% Offset Flexural Yield Stress (MPa)	Strain at 0.1% Offset Flexural Yield Stress (%)	Flexural Modulus (MPa)
BG5L Set 1	5	111.753	6.18	45.424	1.43	3353.643
	6	111.472	6.14	48.227	1.51	3371.202
	7	111.386	6.15	46.855	1.46	3380.372
	8	111.793	6.28	44.921	1.40	3389.24
	9	111.422	6.38	41.742	1.30	3391.939
	10	112.147	6.34	44.290	1.37	3403.081
Average		111.66	6.25	45.24	1.41	3381.58
Standard Deviation		0.29	0.10	2.23	0.08	17.42
Number		6	6	6	6	6

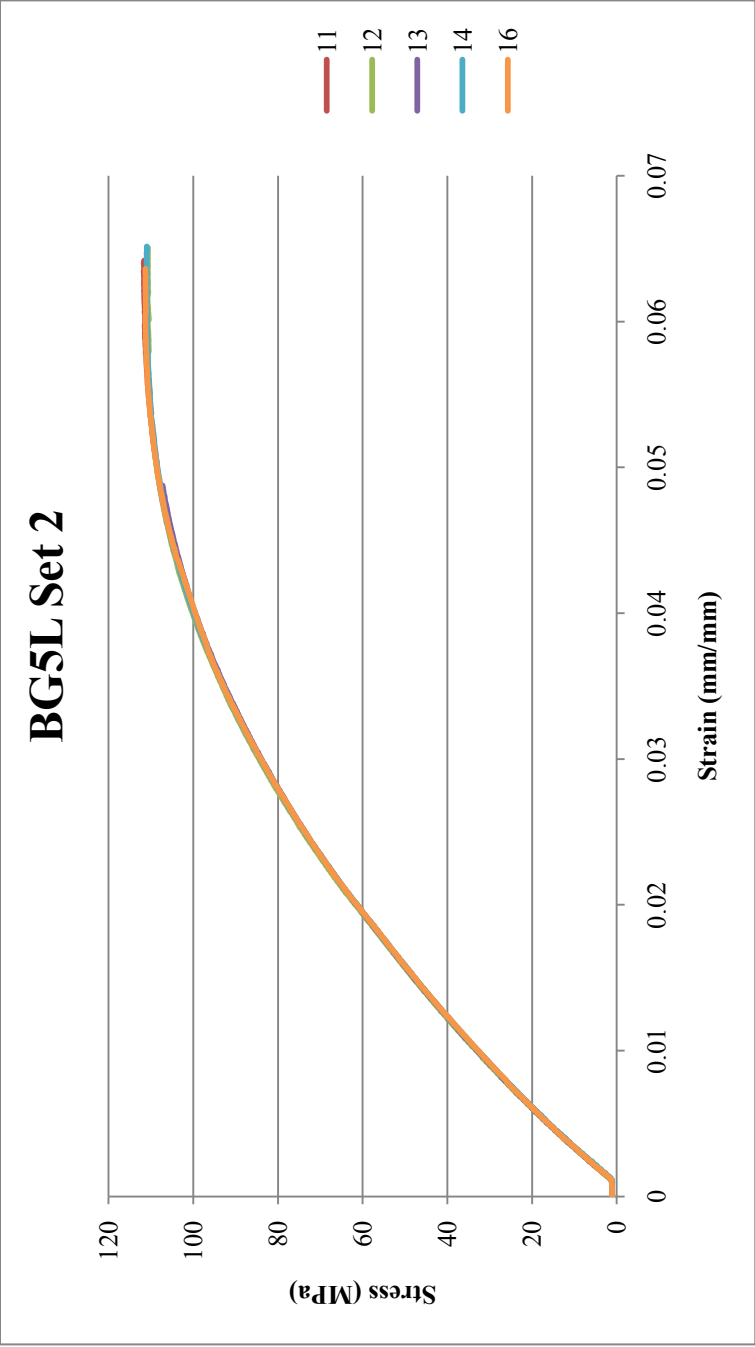


Figure K.39: Flexural Results for BG5L Set 2: Extruded May 2010, Injection molded 9-9-10

Table K.39: Flexural Results for BG5L Set 2: Extruded May 2010, Injection molded 9-9-10

Sample	Specimen	Flexural Maximum Stress (MPa)	Strain at Maximum Flexural Stress (%)	0.1% Offset Yield Flexural Stress (MPa)	Strain at 0.1% Offset Yield Stress (%)	Flexural Modulus (MPa)
BG5L Set 2	11	111.664	6.40	42.585	1.32	3398.224
	12	110.847	6.16	44.310	1.37	3412.624
	13	110.235	5.90	43.052	1.33	3406.092
	14	110.996	6.31	41.708	1.29	3395.99
	16	111.292	6.01	42.368	1.31	3393.483
Average		111.01	6.16	42.80	1.33	3401.28
Standard Deviation		0.53	0.20	0.97	0.03	7.90
Number		5	5	5	5	5

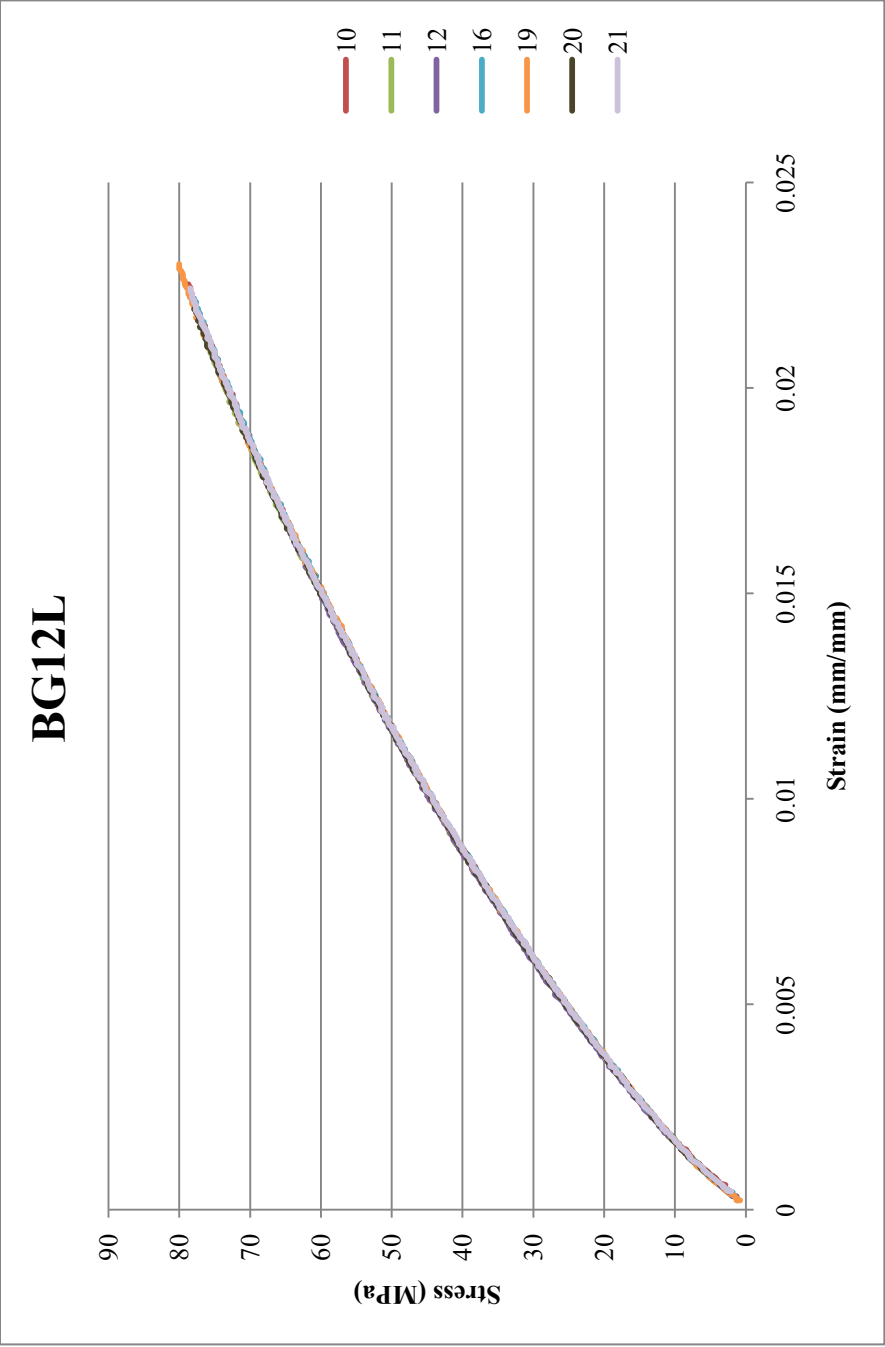


Figure K.40: Flexural Results for BG12L: Extruded 7-8-10, Injection molded 8-18-10

Table K.40: Flexural Results for BG12L: Extruded 7-8-10, Injection molded 8-18-10

Sample	Specimen	Flexural Maximum Stress (MPa)	Strain at Maximum Flexural Stress (%)	0.1% Offset Yield Flexural Stress (MPa)	Strain at 0.1% Offset Yield Stress (%)	Flexural Modulus (MPa)
BG12L	10	78.695	2.25	43.400	0.97	5084.46
	11	76.342	2.12	41.047	0.89	5227.677
	12	77.650	2.17	41.309	0.90	5257.131
	16	78.173	2.23	43.139	0.96	5105.195
	19	80.003	2.29	41.831	0.93	5151.527
	20	77.911	2.19	42.093	0.93	5150.972
	21	78.434	2.23	42.616	0.95	5107.685
Average		78.17	2.21	42.20	0.93	5154.95
Standard Deviation		1.11	0.06	0.89	0.03	65.11
Number		7	7	7	7	7

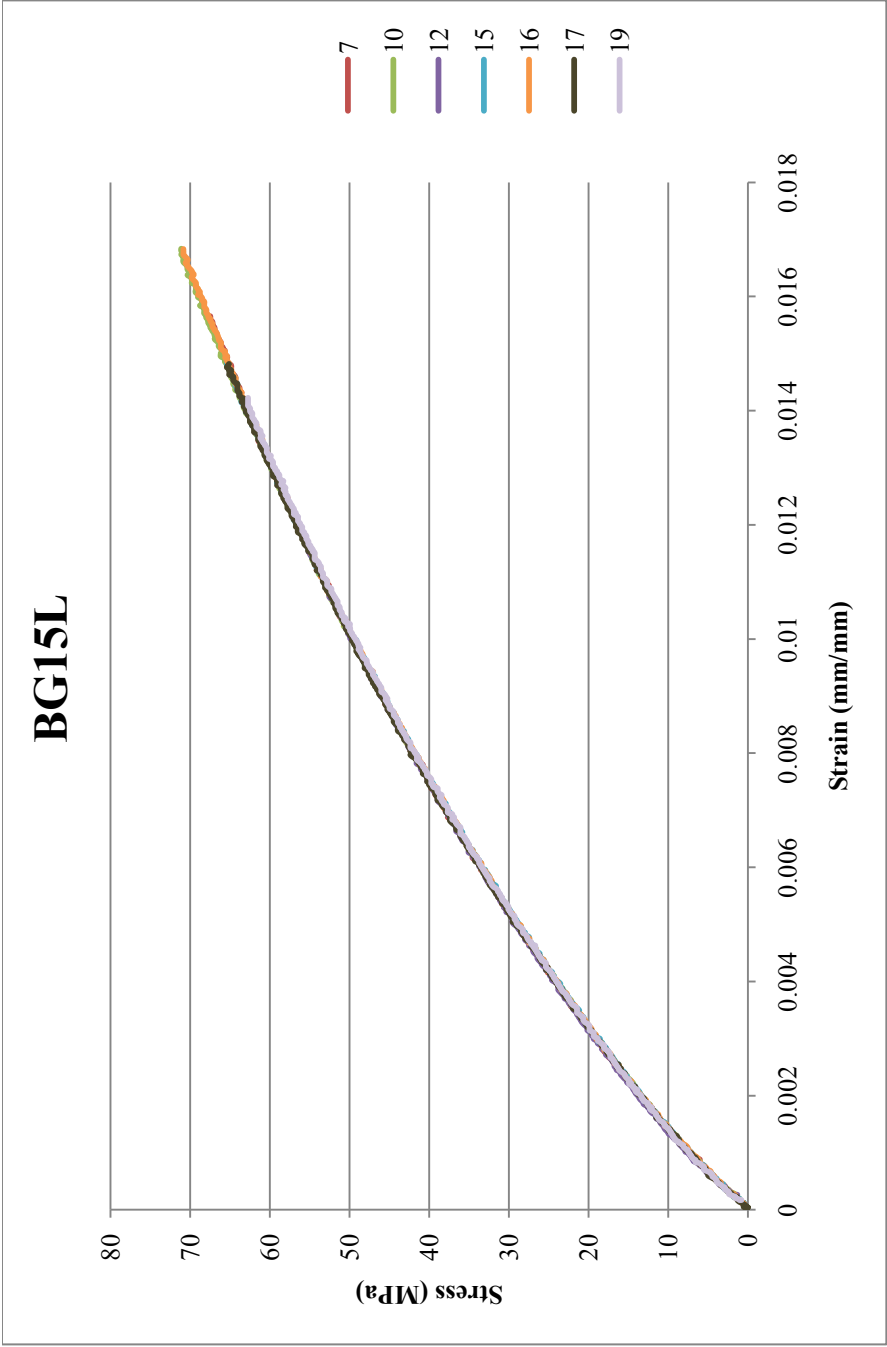


Figure K.41: Flexural Results for BG15L: Extruded 7-8-10, Injection molded 8-18-10

Table K.41: Flexural Results for BG15L: Extruded 7-8-10, Injection molded 8-18-10

Sample	Specimen	Flexural Maximum Stress (MPa)	Strain at Maximum Flexural Stress (%)	0.1% Offset Yield Flexural Stress (MPa)	Strain at 0.1% Offset Yield Stress (%)	Flexural Modulus (MPa)
BG15L	7	67.453	1.56	38.694	0.72	6351.954
	10	71.113	1.67	39.478	0.74	6248.301
	12	68.499	1.59	38.694	0.71	6357.393
	15	65.623	1.49	37.125	0.68	6413.688
	16	70.852	1.67	38.171	0.70	6323.503
	17	65.362	1.48	37.387	0.68	6474.131
	19	62.747	1.41	36.080	0.66	6450.099
Average		67.38	1.55	37.95	0.70	6374.15
Standard Deviation		3.05	0.10	1.15	0.03	78.00
Number		7	7	7	7	7

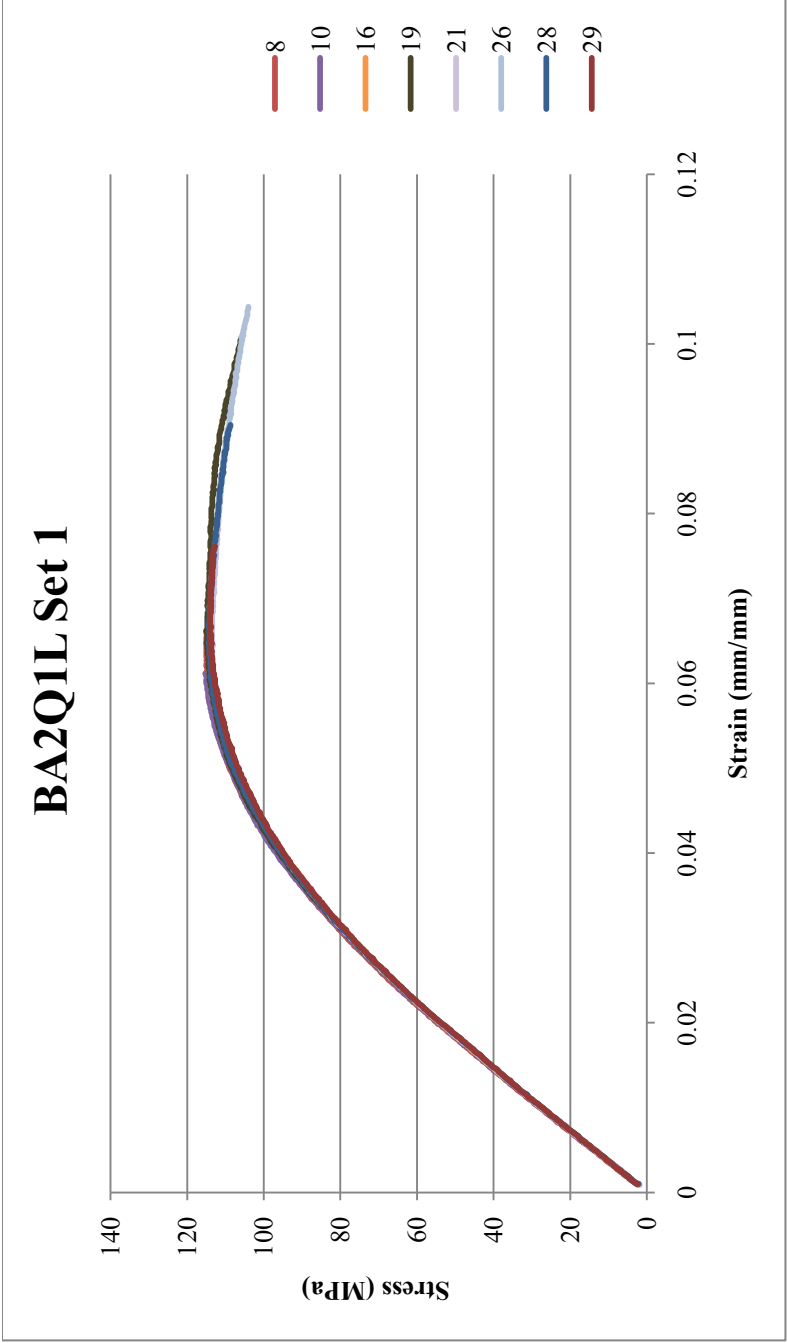


Figure K.42: Flexural Results for BA2Q1L Set 1: Extruded 7-7-10, Injection molded 7-26-10

Table K.42: Flexural Results for BA2Q1L Set 1: Extruded 7-7-10, Injection molded 7-26-10

Sample	Specimen	Flexural Maximum Stress (MPa)	Strain at Maximum Flexural Stress (%)	0.1% Offset Yield Flexural Stress (MPa)	Strain at 0.1% Offset Yield Stress (%)	Flexural Modulus (MPa)
BA2Q1L Set 1	8	115.015	6.13	67.702	2.52	2792.334
	10	115.276	6.12	65.088	2.43	2789.055
	16	114.492	6.32	65.611	2.48	2756.743
	19	115.015	6.48	74.498	2.87	2702.418
	21	113.708	6.42	70.838	2.70	2726.403
	26	114.230	6.90	73.714	2.84	2702.795
	28	114.492	6.47	72.930	2.80	2709.812
	29	113.969	6.49	67.963	2.59	2727.275
Average		114.52	6.41	69.79	2.65	2738.35
Standard Deviation		0.55	0.25	3.70	0.17	36.76
Number		8	8	8	8	8

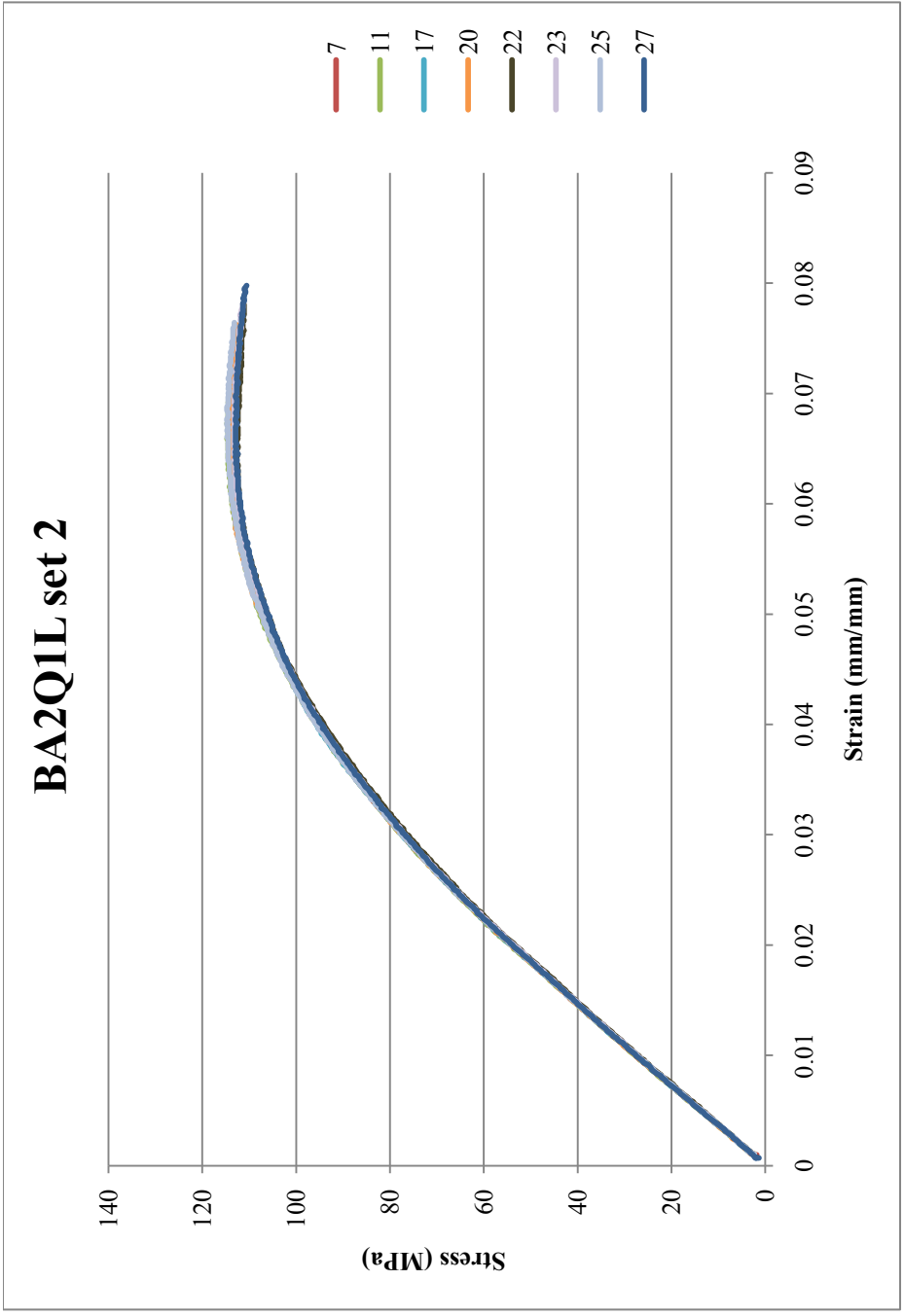


Figure K.43: Flexural Results for BA2Q1L Set 2: Extruded 7-7-10, Injection molded 7-26-10

Table K.43: Flexural Results for BA2Q1L Set 2: Extruded 7-7-10, Injection molded 7-26-10

Sample	Specimen	Flexural Maximum Stress (MPa)	Strain at Maximum Flexural Stress (%)	0.1% Offset Yield Flexural Stress (MPa)	Strain at 0.1% Offset Yield Stress (%)	Flexural Modulus (MPa)
BA2Q1L Set 2	7	114.230	6.70	67.702	2.56	2751.548
	11	114.753	6.59	68.486	2.58	2761.431
	17	114.230	6.37	68.486	2.59	2755.464
	20	114.230	6.56	68.747	2.61	2749.277
	22	112.662	6.23	65.872	2.50	2717.093
	23	113.185	6.39	67.963	2.58	2726.394
	25	114.753	6.60	67.963	2.57	2751.823
	27	112.923	6.37	69.009	2.63	2734.869
Average		113.87	6.48	68.03	2.58	2743.49
Standard Deviation		0.83	0.16	0.98	0.04	15.57
Number		8	8	8	8	8

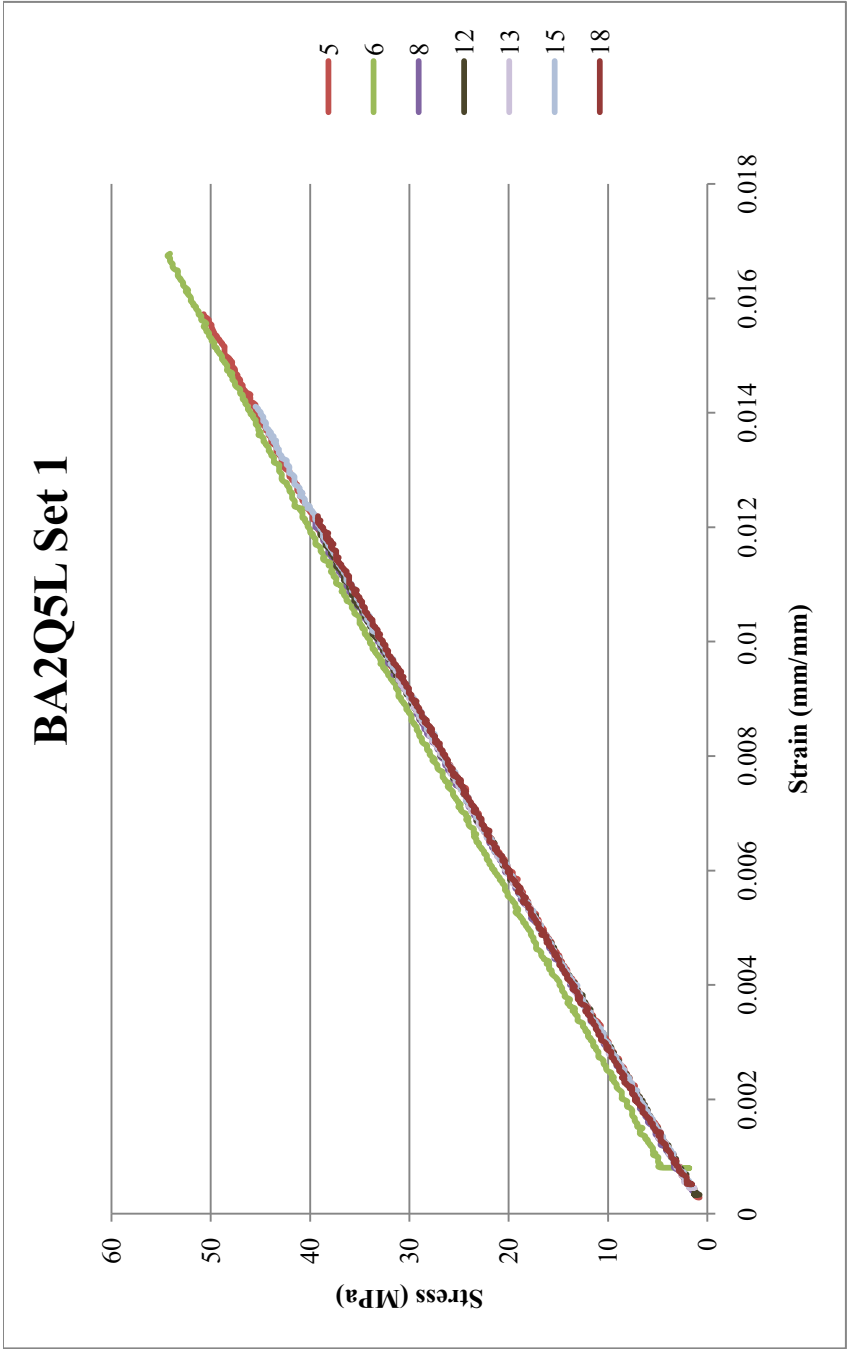


Figure K.44: Flexural Results for BA2Q5L Set 1: Extruded 7-7-10, Injection molded 8-25-10

Table K.44: Flexural Results for BA2Q5L Set 1: Extruded 7-7-10, Injection molded 8-25-10

Sample	Specimen	Flexural Maximum Stress (MPa)	Strain at Maximum Flexural Stress (%)	0.1% Offset Yield Flexural Stress (MPa)	Strain at 0.1% Offset Yield Stress (%)	Flexural Modulus (MPa)
BA2Q5L Set 1	5	50.982	1.57	broke	before yield	3319.465
	6	54.381	1.67	49.675	1.51	3576.554
	8	50.982	1.58	broke	before yield	3408.769
	12	38.956	1.19	broke	before yield	3364.725
	13	31.896	0.96	broke	before yield	3325.727
	15	45.753	1.42	broke	before yield	3390.39
	18	39.217	1.21	37.910	1.16	3559.711
Average		44.60	1.37	43.79	1.34	3420.76
Standard Deviation		8.17	0.26	8.32	0.25	105.73
Number		7	7	2	2	7

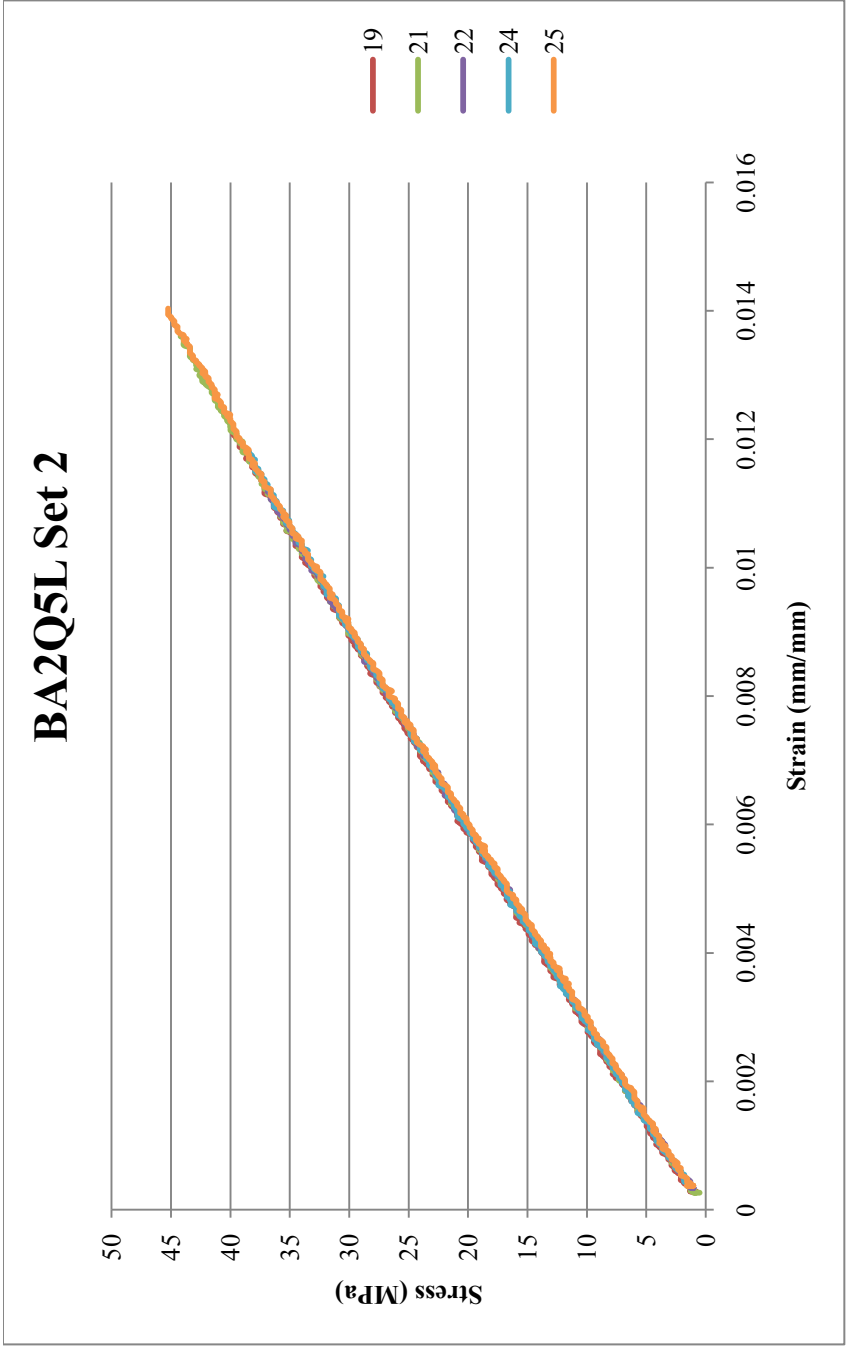


Figure K.45: Flexural Results for BA2Q5L Set 2: Extruded 7-7-10, Injection molded 8-25-10

Table K.45: Flexural Results for BA2Q5L Set 2: Extruded 7-7-10, Injection molded 8-25-10

Sample	Specimen	Flexural Maximum Stress (MPa)	Strain at Maximum Flexural Stress (%)	0.1% Offset Yield Flexural Stress (MPa)	Strain at 0.1% Offset Yield Stress (%)	Flexural Modulus (MPa)
BA2Q5L Set 2	19	39.740	1.21	broke	before yield	3501.765
	21	44.184	1.36	broke	before yield	3484.021
	22	47.583	1.47	broke	before yield	3404.005
	24	38.694	1.18	broke	before yield	3477.451
	25	45.230	1.39	broke	before yield	3351.098
Average		43.09	1.32			3443.67
Standard Deviation		3.76	0.12			63.81
Number		5	5			5

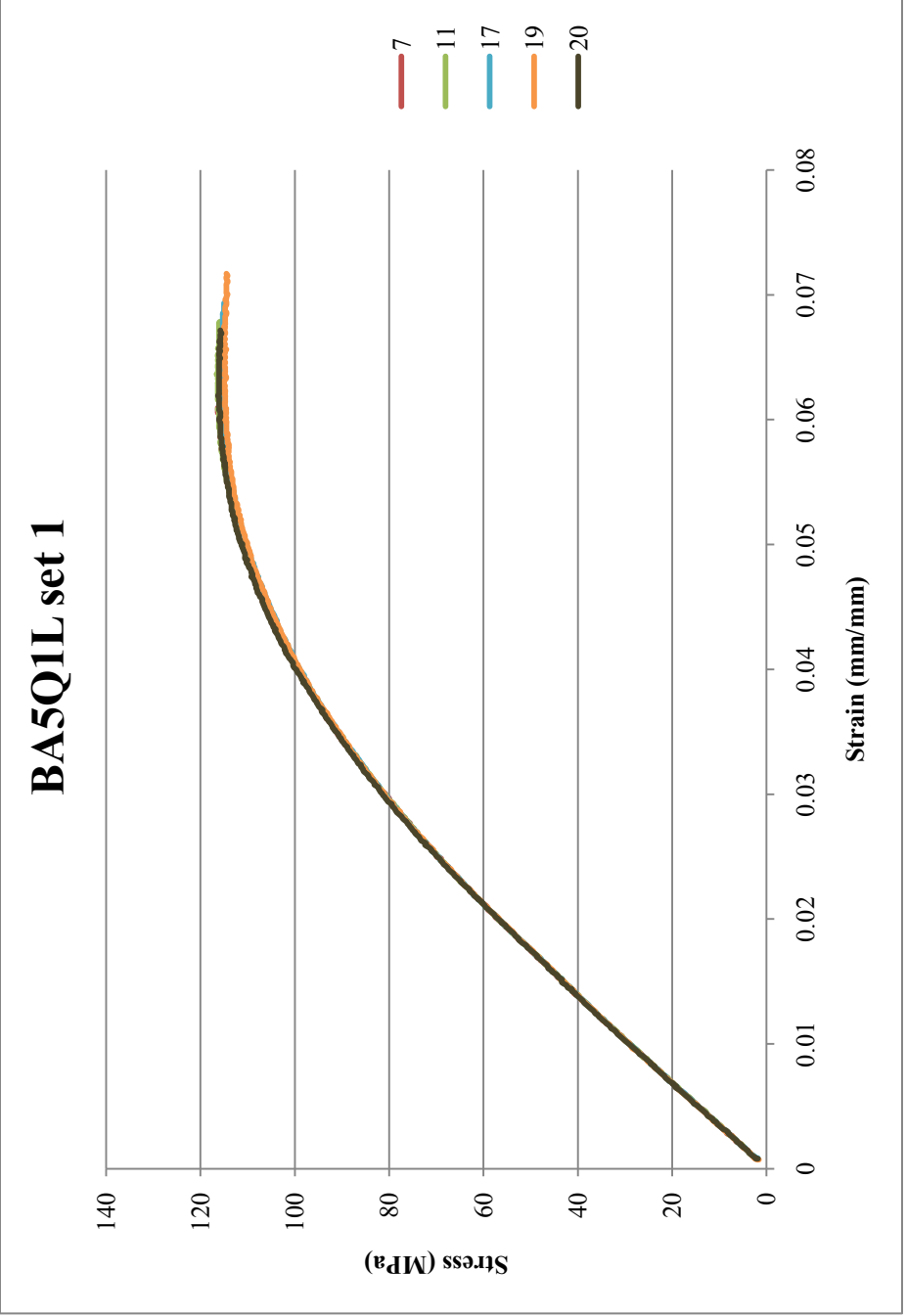


Figure K.46: Flexural Results for BA5Q1L Set 1: Extruded 7-7-10, Injection molded 7-26-10

Table K.46: Flexural Results for BA5Q1L Set 1: Extruded 7-7-10, Injection molded 7-26-10

Sample	Specimen	Flexural Maximum Stress (MPa)	Strain at Maximum Flexural Stress (%)	0.1% Offset Yield Flexural Stress (MPa)	Strain at 0.1% Offset Yield Stress (%)	Flexural Modulus (MPa)
BA5Q1L Set 1	7	116.321	6.05	65.349	2.33	2923.944
	11	116.583	6.37	68.225	2.45	2905.596
	17	115.537	6.11	69.270	2.47	2907.451
	19	115.015	6.00	70.316	2.53	2899.733
	20	116.321	6.19	67.702	2.41	2925.276
Average		115.96	6.14	68.17	2.44	2912.40
Standard Deviation		0.66	0.14	1.87	0.08	11.51
Number		5	5	5	5	5

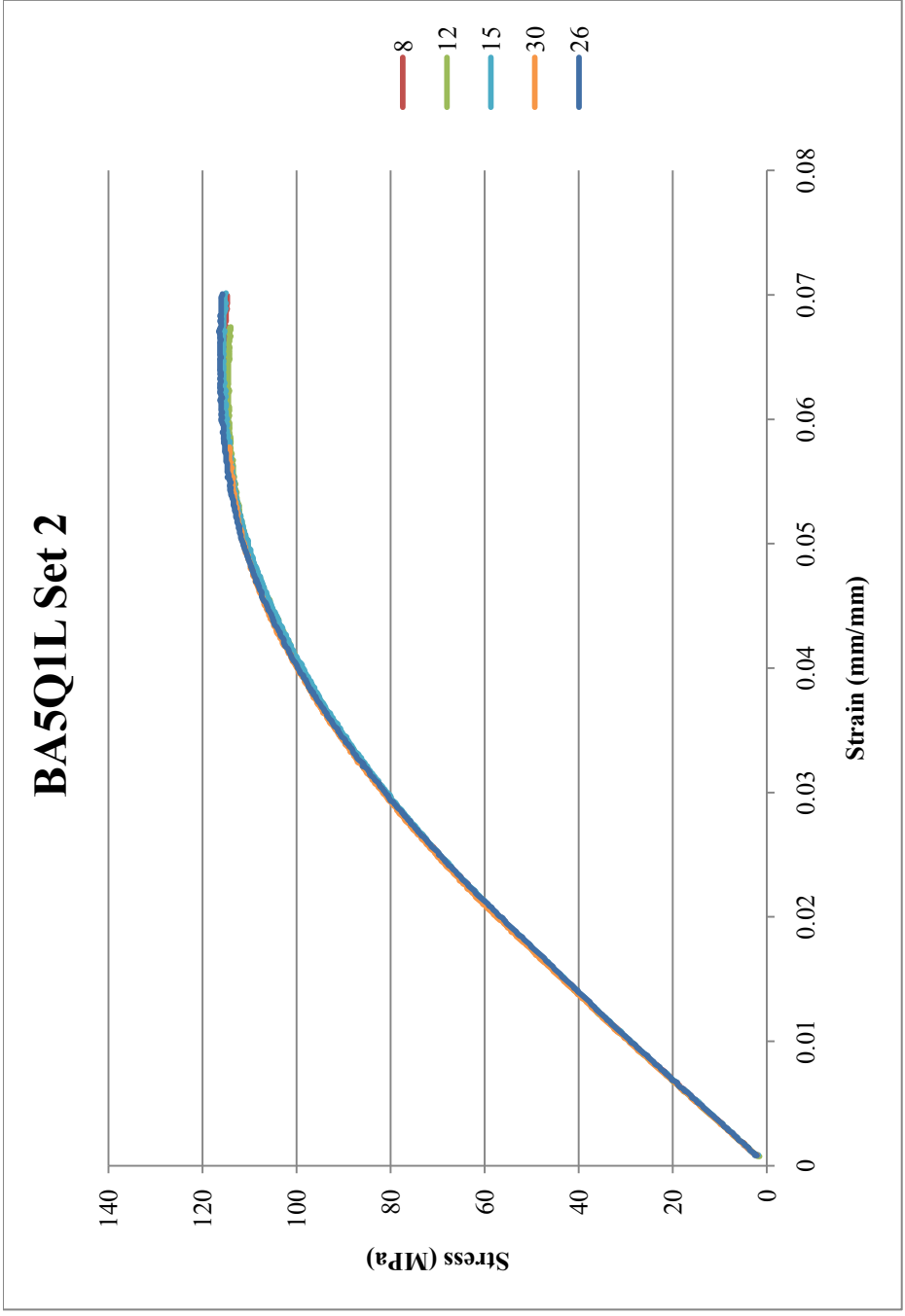


Figure K.47: Flexural Results for BA5Q1L Set 2: Extruded 7-7-10, Injection molded 7-26-10

Table K.47: Flexural Results for BA5Q1L Set 2: Extruded 7-7-10, Injection molded 7-26-10

Sample	Specimen	Flexural Maximum Stress (MPa)	Strain at Maximum Flexural Stress (%)	0.1% Offset Yield Flexural Stress (MPa)	Strain at 0.1% Offset Yield Stress (%)	Flexural Modulus (MPa)
BA5Q1L Set 2	8	115.276	6.17	70.054	2.51	2902.423
	12	114.753	6.27	66.918	2.38	2927.347
	15	115.799	6.38	69.532	2.49	2896.441
	30	114.492	5.73	65.611	2.31	2962.145
	26	116.583	6.71	69.793	2.50	2892.648
Average		115.38	6.25	68.38	2.44	2916.20
Standard Deviation		0.84	0.35	2.00	0.09	29.03
Number		5	5	5	5	5

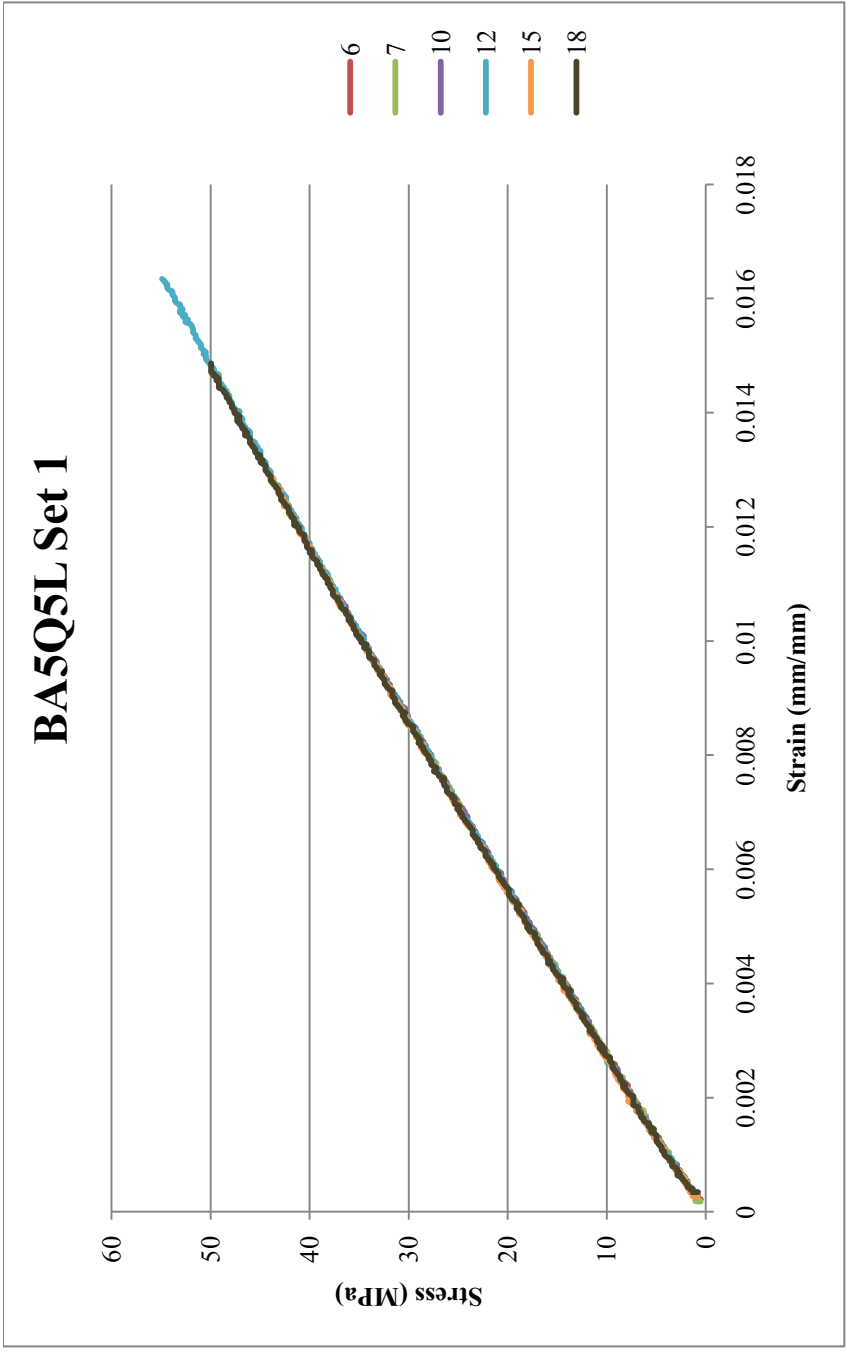


Figure K.48: Flexural Results for BA5Q5L Set 1: Extruded 7-7-10, Injection molded 8-25-10

Table K.48: Flexural Results for BA5Q5L Set 1: Extruded 7-7-10, Injection molded 8-25-10

Sample	Specimen	Flexural Maximum Stress (MPa)	Strain at Maximum Flexural Stress (%)	0.1% Offset Yield Flexural Stress (MPa)	Strain at 0.1% Offset Yield Stress (%)	Flexural Modulus (MPa)
BA5Q5L Set 1	6	49.413	1.46	broke	before yield	3622.435
	7	32.158	0.92	broke	before yield	3716.426
	10	47.845	1.41	47.583	1.41	3637.939
	12	54.904	1.63	48.106	1.42	3645.834
	15	44.184	1.29	41.047	1.19	3775.921
	18	50.459	1.49	broke	before yield	3618.609
Average		46.49	1.37	45.58	1.34	3669.53
Standard Deviation		7.84	0.25	3.93	0.13	63.07
Number		6	6	3	3	6

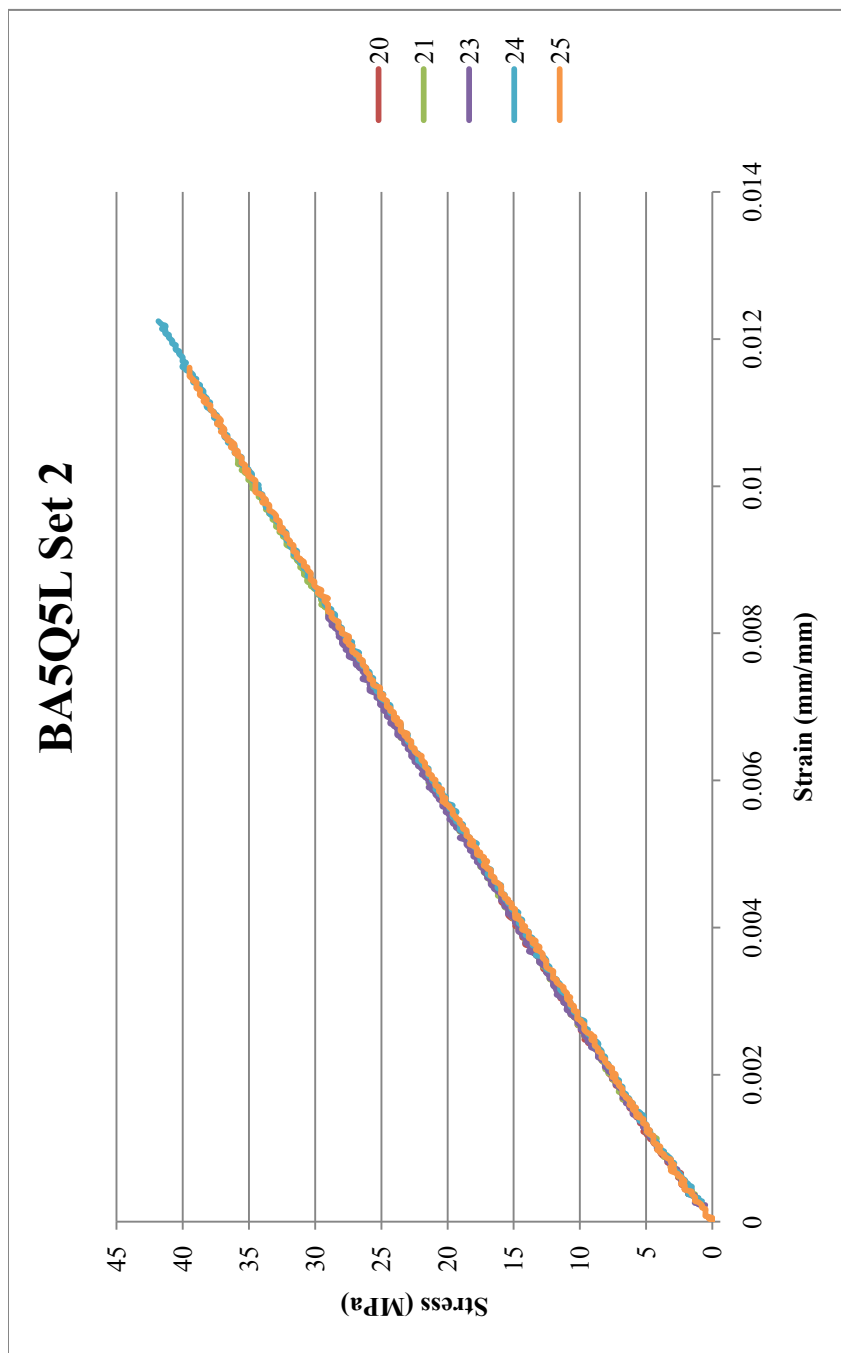


Figure K.49: Flexural Results for BA5Q5L Set 2: Extruded 7-7-10, Injection molded 8-25-10

Table K.49: Flexural Results for BA5Q5L Set 2: Extruded 7-7-10, Injection molded 8-25-10

Sample	Specimen	Flexural Maximum Stress (MPa)	Strain at Maximum Flexural Stress (%)	0.1% Offset Yield Flexural Stress (MPa)	Strain at 0.1% Offset Yield Stress (%)	Flexural Modulus (MPa)
BA5Q5L Set 2	20	39.478	1.14	broke	before yield	3779.575
	21	36.080	1.05	broke	before yield	3805.667
	23	37.910	1.09	broke	before yield	3837.001
	24	41.831	1.22	broke	before yield	3650.807
	25	39.478	1.15	37.125	1.07	3789.404
Average		38.96	1.13	37.13	1.07	3772.49
Standard Deviation		2.13	0.07	N/A	N/A	71.42
Number		5	5	1	1	5

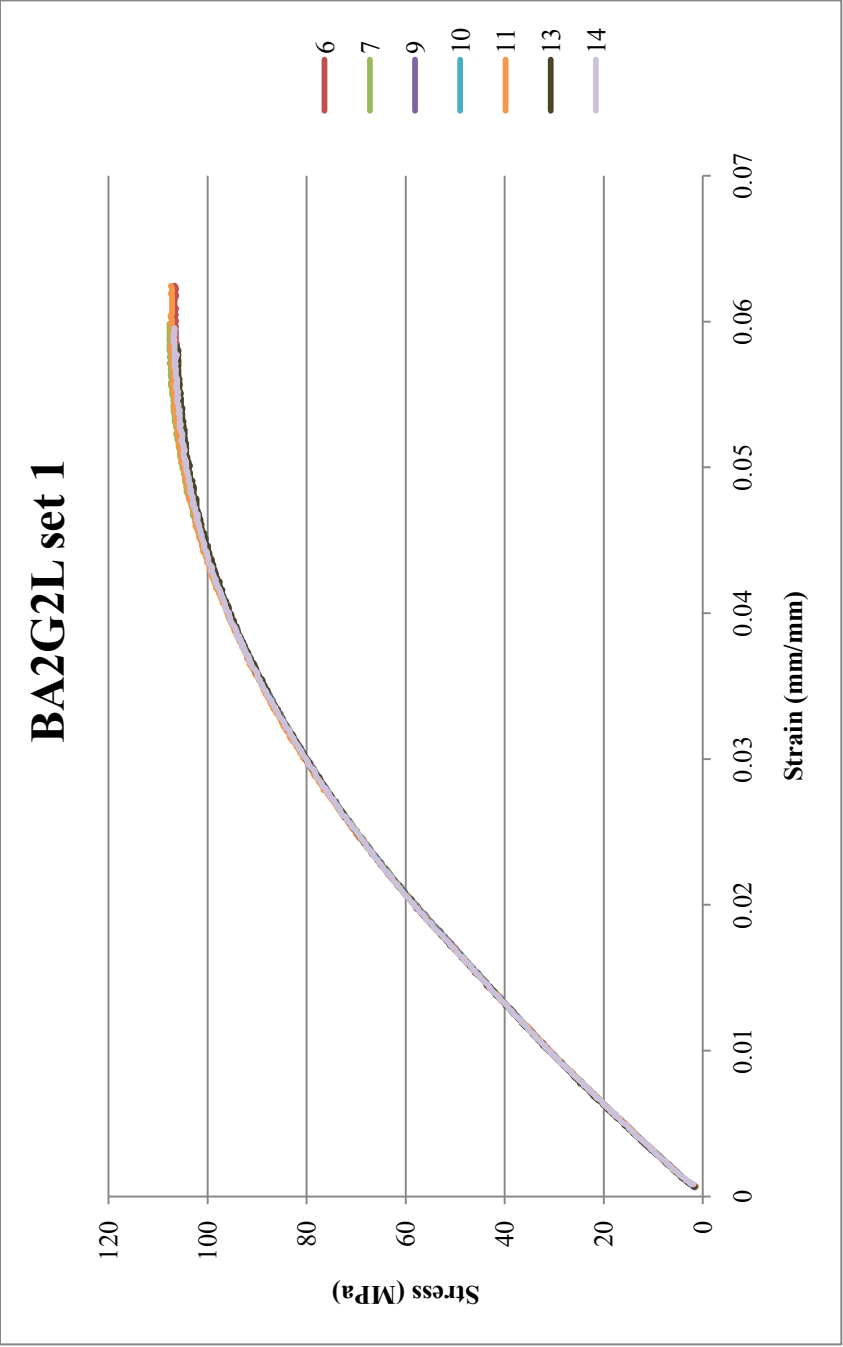


Figure K.50: Flexural Results for BA2G2L Set 1: Extruded 7-6-10, Injection molded 8-18-10

Table K.50: Flexural Results for BA2G2L Set 1: Extruded 7-6-10, Injection molded 8-18-10

Sample	Specimen	Flexural Maximum Stress (MPa)	Strain at Maximum Flexural Stress (%)	0.1% Offset Yield Flexural Stress (MPa)	Strain at 0.1% Offset Yield Stress (%)	Flexural Modulus (MPa)
BA2G2L Set 1	6	106.670	5.94	60.917	2.11	3051.827
	7	107.716	5.71	59.348	2.06	3059.38
	9	107.455	5.68	58.825	2.04	3064.789
	10	106.932	5.80	57.780	1.98	3082.62
	11	107.455	5.79	61.701	2.14	3048.346
	13	106.147	5.68	58.825	2.02	3075.767
	14	106.932	5.86	60.656	2.09	3066.904
Average		107.04	5.78	59.72	2.06	3064.23
Standard Deviation		0.54	0.10	1.40	0.06	12.30
Number		7	7	7	7	7

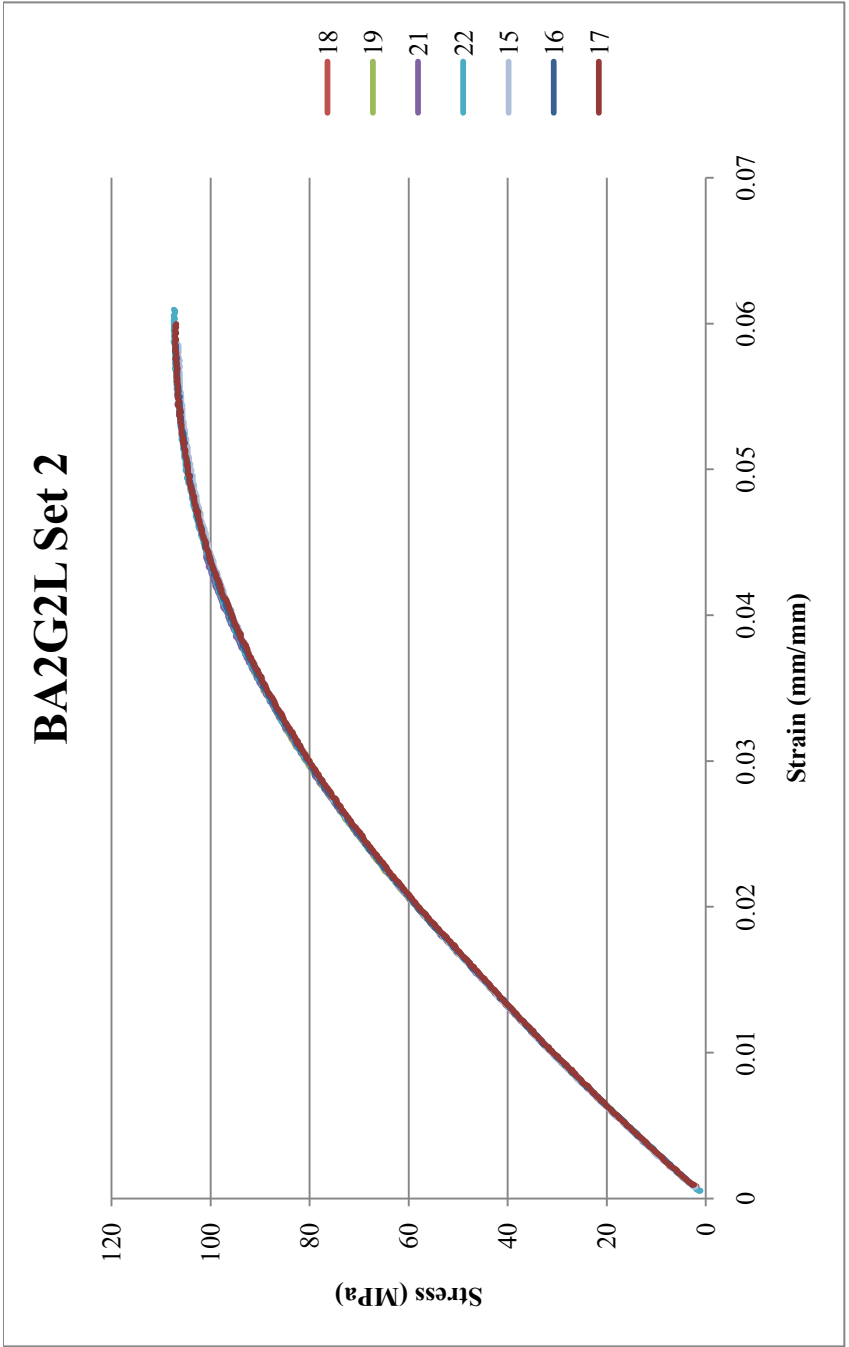


Figure K.51: Flexural Results for BA2G2L Set 2: Extruded 7-6-10, Injection molded 8-18-10

Table K.51: Flexural Results for BA2G2L Set 2: Extruded 7-6-10, Injection molded 8-18-10

Sample	Specimen	Flexural Maximum Stress (MPa)	Strain at Maximum Flexural Stress (%)	0.1% Offset Yield Flexural Stress (MPa)	Strain at 0.1% Offset Yield Stress (%)	Flexural Modulus (MPa)
BA2G2L Set 2	18	106.932	5.70	58.564	2.01	3087.336
	19	106.932	5.71	60.133	2.06	3075.641
	21	106.932	5.63	58.564	2.01	3080.115
	22	107.455	5.87	58.303	2.00	3068.908
	15	106.670	5.79	59.610	2.05	3073.868
	16	107.193	5.81	59.610	2.06	3063.524
	17	107.193	5.76	59.871	2.08	3040.988
Average		107.04	5.75	59.24	2.04	3070.05
Standard Deviation		0.26	0.08	0.74	0.03	14.91
Number		7	7	7	7	7

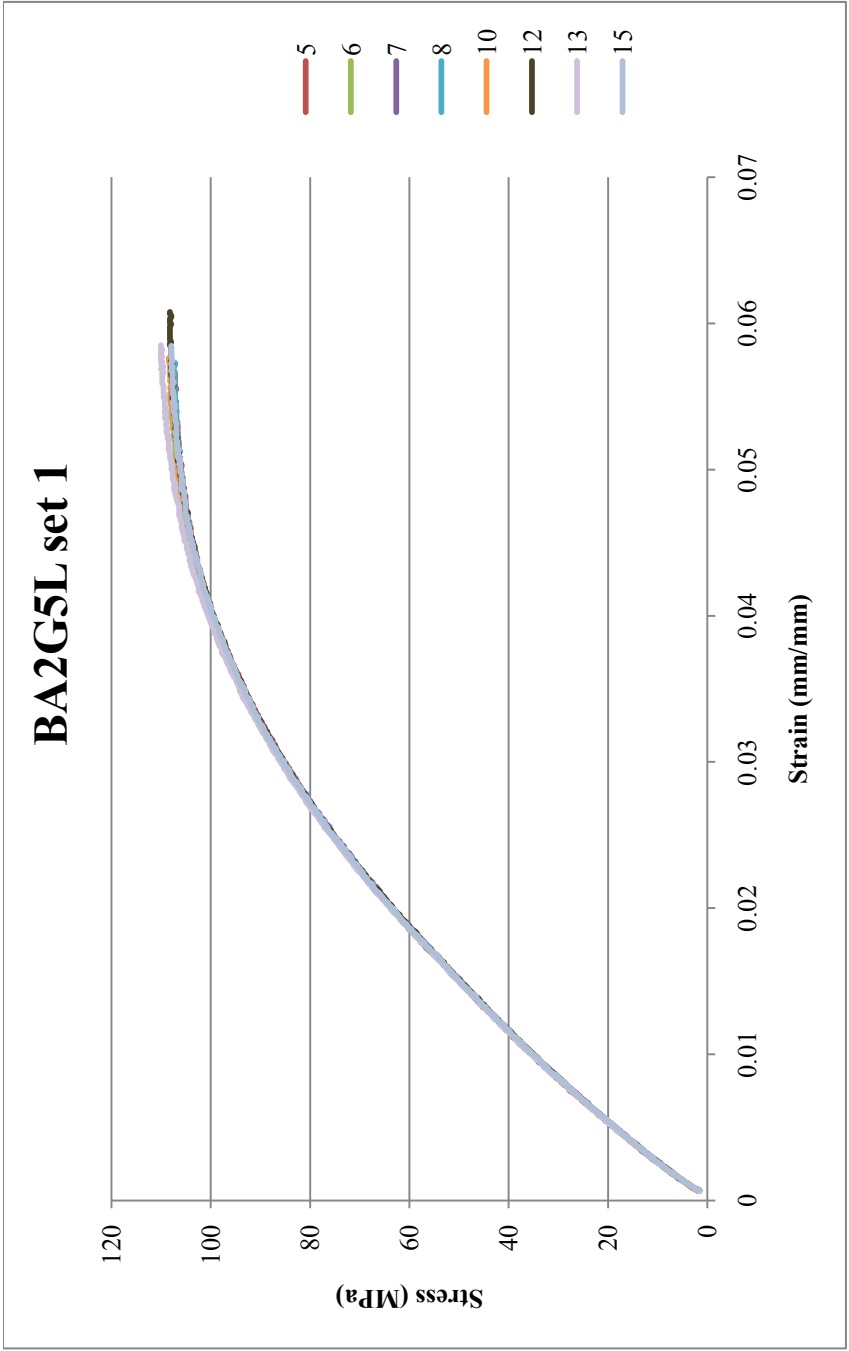


Figure K.52: Flexural Results for BA2G5L Set 1: Extruded 7-6-10, Injection molded 8-18-10

Table K.52: Flexural Results for BA2G5L Set 1: Extruded 7-6-10, Injection molded 8-18-10

Sample	Specimen	Flexural Maximum Stress (MPa)	Strain at Maximum Flexural Stress (%)	0.1% Offset Yield Flexural Stress (MPa)	Strain at 0.1% Offset Yield Stress (%)	Flexural Modulus (MPa)
BA2G5L Set 1	5	107.455	5.57	58.825	1.81	3480.354
	6	108.239	5.50	58.041	1.80	3479.991
	7	108.762	5.65	59.610	1.85	3442.347
	8	107.455	5.48	59.348	1.84	3460.829
	10	108.500	5.74	59.610	1.84	3455.128
	12	108.239	5.85	60.656	1.90	3424.118
	13	110.069	5.69	59.087	1.83	3481.738
	15	107.977	5.68	61.440	1.92	3439.465
Average		108.34	5.65	59.58	1.85	3458.00
Standard Deviation		0.84	0.12	1.06	0.04	21.71
Number		8	8	8	8	8

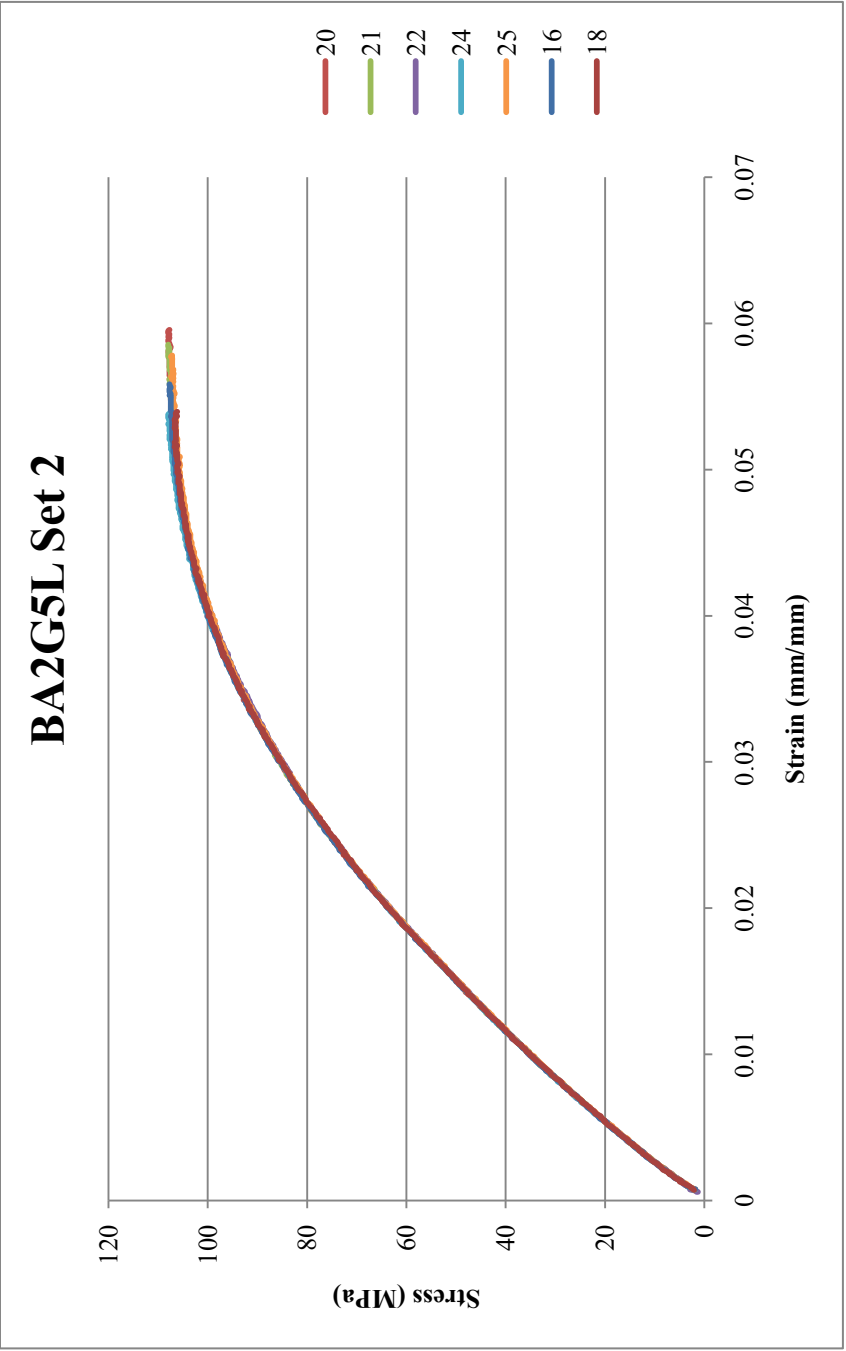


Figure K.53: Flexural Results for BA2G5L Set 2: Extruded 7-6-10, Injection molded 8-18-10

Table K.53: Flexural Results for BA2G5L Set 2: Extruded 7-6-10, Injection molded 8-18-10

Sample	Specimen	Flexural Maximum Stress (MPa)	Strain at Maximum Flexural Stress (%)	0.1% Offset Yield Flexural Stress (MPa)	Strain at 0.1% Offset Yield Stress (%)	Flexural Modulus (MPa)
BA2G5L Set 2	20	107.977	5.81	61.179	1.91	3439.658
	21	107.977	5.77	60.656	1.88	3439.18
	22	107.455	5.55	57.518	1.78	3468.38
	24	107.977	5.31	58.041	1.79	3480.871
	25	107.455	5.63	59.871	1.86	3428.712
	16	107.716	5.51	59.348	1.84	3459.066
	18	106.670	5.16	58.303	1.81	3471.164
Average		107.60	5.53	59.27	1.84	3455.29
Standard Deviation		0.47	0.24	1.38	0.05	19.59
Number		7	7	7	7	7

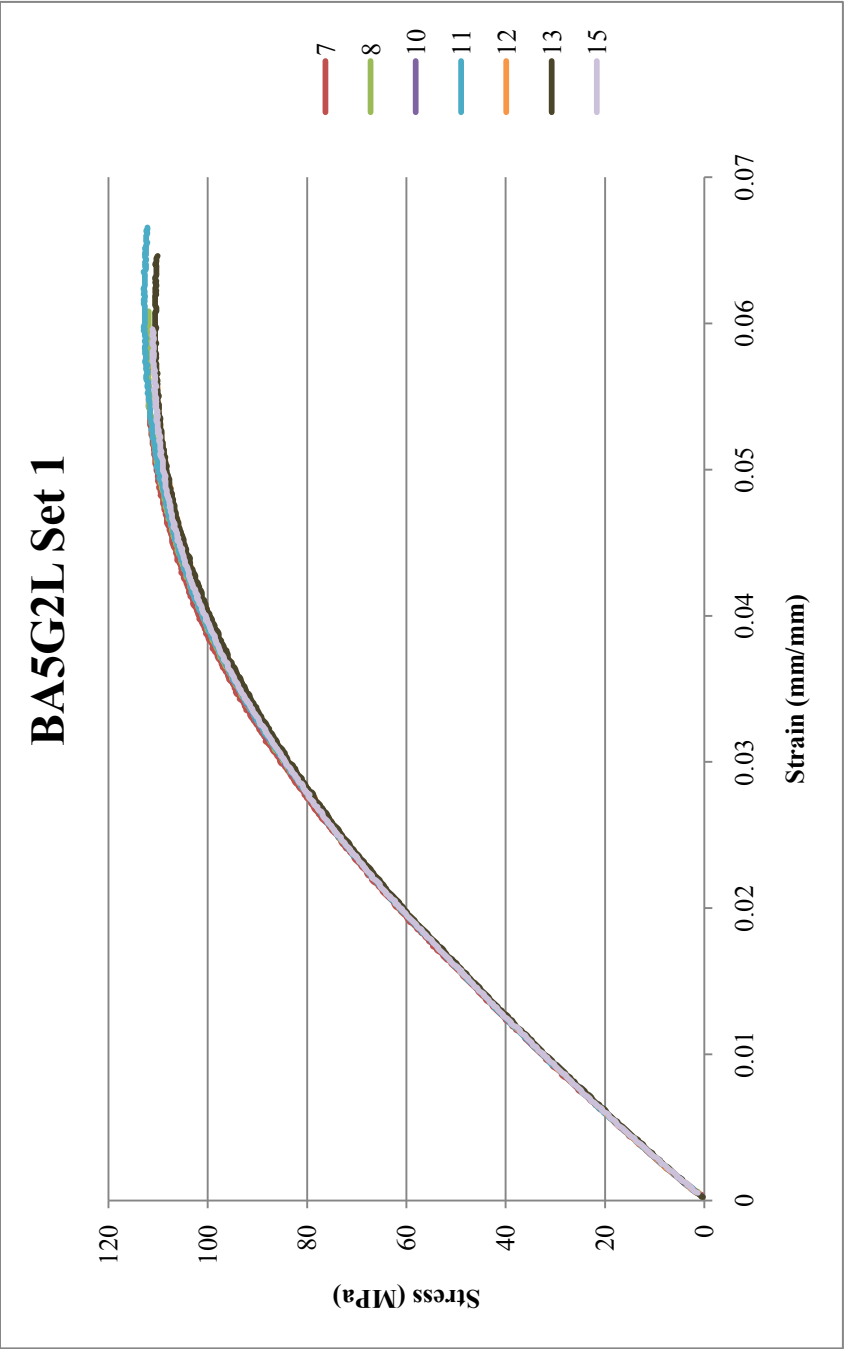


Figure K.54: Flexural Results for BA5G2L Set 1: Extruded 7-6-10, Injection molded 8-18-10

Table K.54: Flexural Results for BA5G2L Set 1: Extruded 7-6-10, Injection molded 8-18-10

Sample	Specimen	Flexural Maximum Stress (MPa)	Strain at Maximum Flexural Stress (%)	0.1% Offset Yield Flexural Stress (MPa)	Strain at 0.1% Offset Yield Stress (%)	Flexural Modulus (MPa)
BA5G2L Set 1	7	112.422	5.72	62.486	2.03	3248.139
	8	112.161	5.64	64.316	2.12	3204.799
	10	111.638	5.91	63.532	2.08	3225.649
	11	112.945	5.95	64.839	2.14	3203.676
	12	110.853	5.72	61.963	2.04	3210.512
	13	110.592	5.67	64.054	2.12	3174.592
	15	111.115	5.74	64.054	2.10	3221.379
Average		111.68	5.76	63.61	2.09	3212.68
Standard Deviation		0.87	0.12	1.03	0.04	22.73
Number		7	7	7	7	7

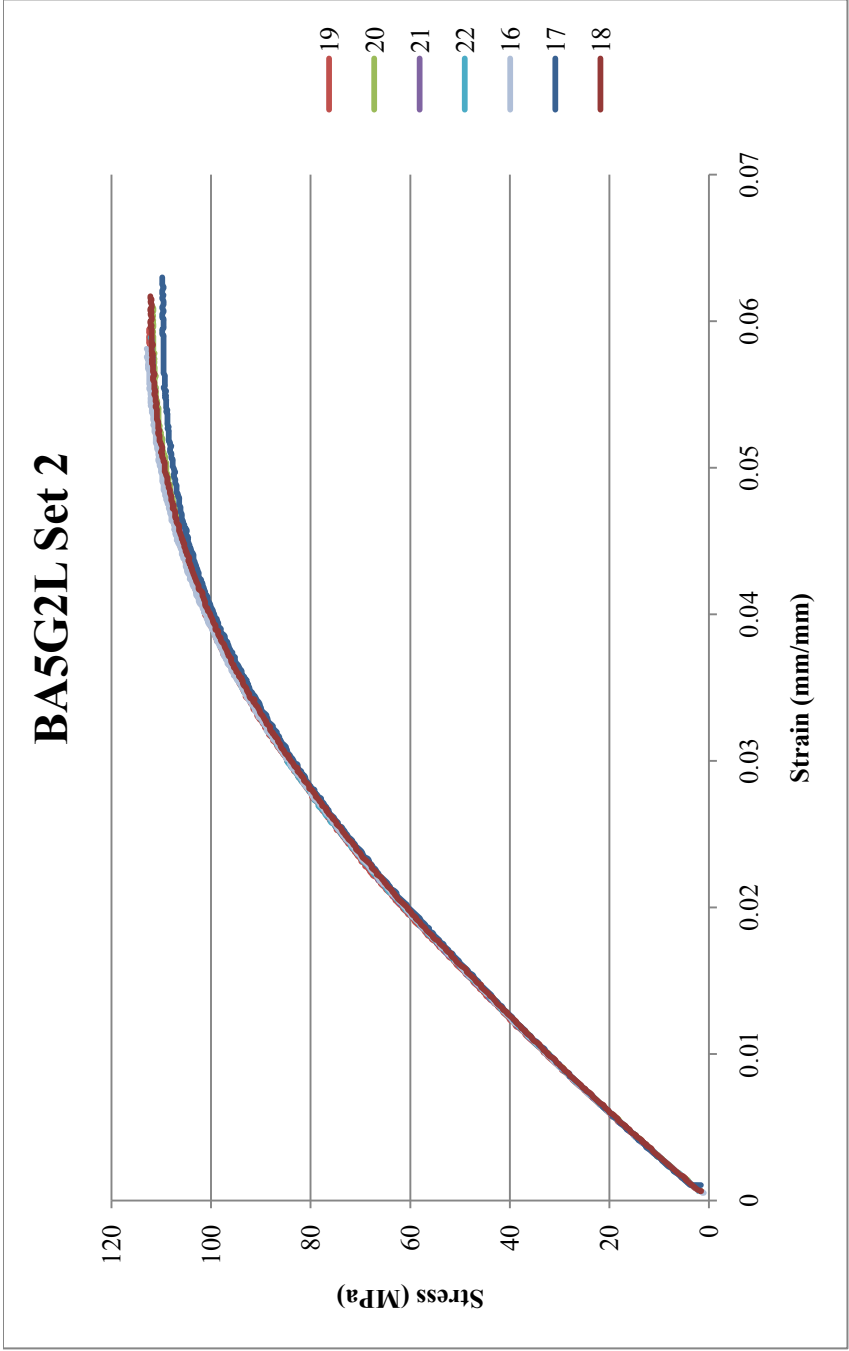


Figure K.55: Flexural Results for BA5G2L Set 2: Extruded 7-6-10, Injection molded 8-18-10

Table K.55: Flexural Results for BA5G2L Set 2: Extruded 7-6-10, Injection molded 8-18-10

Sample	Specimen	Flexural Maximum Stress (MPa)	Strain at Maximum Flexural Stress (%)	0.1% Offset Yield Flexural Stress (MPa)	Strain at 0.1% Offset Yield Stress (%)	Flexural Modulus (MPa)
BA5G2L Set 2	19	112.422	5.76	62.747	2.04	3253.148
	20	111.899	5.91	63.532	2.10	3205.48
	21	110.330	5.88	63.270	2.07	3218.23
	22	112.161	5.89	61.701	2.03	3226.128
	16	113.206	5.87	60.656	1.98	3232.669
	17	109.808	5.91	64.577	2.17	3162.33
	18	112.161	5.96	63.270	2.10	3192.821
Average		111.71	5.88	62.82	2.07	3212.97
Standard Deviation		1.20	0.06	1.29	0.06	29.52
Number		7	7	7	7	7

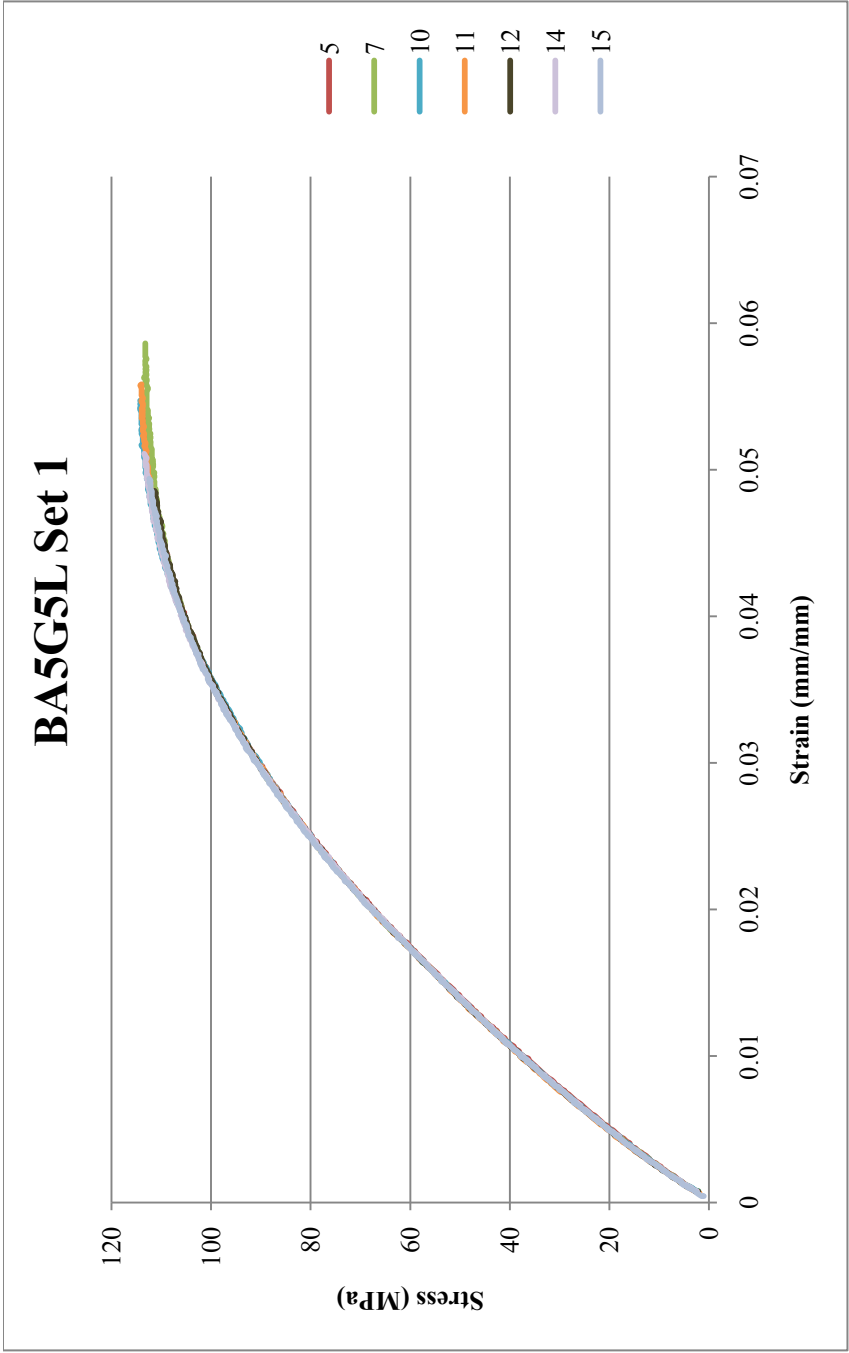


Figure K.56: Flexural Results for BA5G5L Set 1: Extruded 7-6-10, Injection molded 8-18-10

Table K.56: Flexural Results for BA5G5L Set 1: Extruded 7-6-10, Injection molded 8-18-10

Sample	Specimen	Flexural Maximum Stress (MPa)	Strain at Maximum Flexural Stress (%)	0.1% Offset Yield Flexural Stress (MPa)	Strain at 0.1% Offset Yield Stress (%)	Flexural Modulus (MPa)
BA5G5L Set 1	5	112.945	5.25	60.394	1.75	3695.401
	7	113.468	5.63	65.100	1.90	3668.459
	10	114.252	5.41	61.963	1.81	3697.984
	11	114.252	5.58	61.440	1.79	3719.224
	12	111.376	4.82	58.303	1.67	3768.599
	14	113.468	5.11	59.348	1.71	3735.174
	15	112.945	4.98	56.734	1.62	3784.178
Average		113.24	5.25	60.47	1.75	3724.15
Standard Deviation		0.98	0.30	2.72	0.09	41.51
Number		7	7	7	7	7

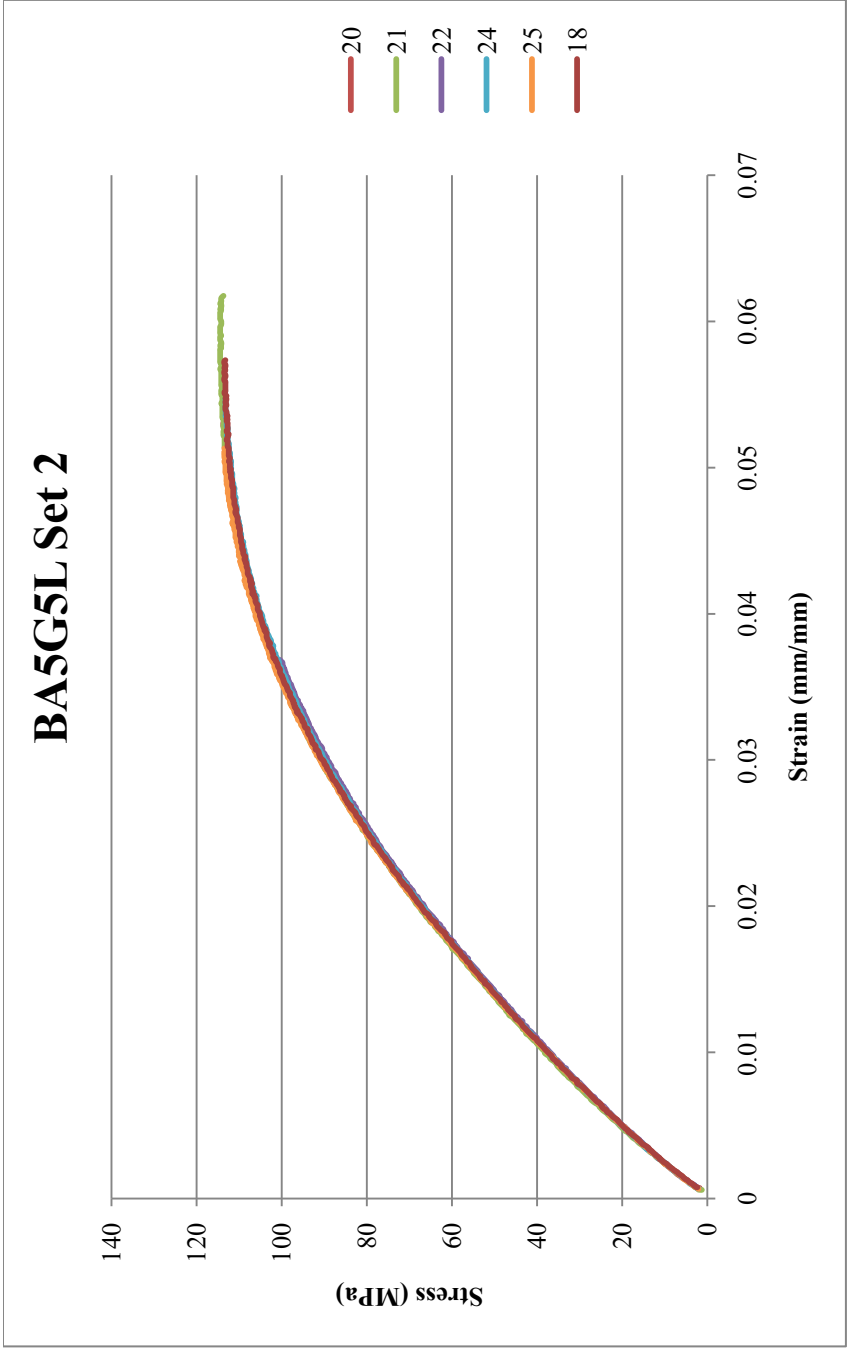


Figure K.57: Flexural Results for BA5G5L Set 2: Extruded 7-6-10, Injection molded 8-18-10

Table K.57: Flexural Results for BA5G5L Set 2: Extruded 7-6-10, Injection molded 8-18-10

Sample	Specimen	Flexural Maximum Stress (MPa)	Strain at Maximum Flexural Stress (%)	0.1% Offset Yield Flexural Stress (MPa)	Strain at 0.1% Offset Yield Stress (%)	Flexural Modulus (MPa)
BA5G5L Set 2	20	113.729	5.28	60.917	1.76	3721.508
	21	114.514	5.67	65.362	1.91	3701.6
	22	110.592	4.82	56.995	1.66	3709.359
	24	113.206	5.35	60.917	1.79	3685.603
	25	113.468	5.04	58.825	1.70	3737.826
	18	113.468	5.51	61.440	1.80	3672.141
Average		113.16	5.28	60.74	1.77	3704.67
Standard Deviation		1.34	0.31	2.81	0.09	23.82
Number		6	6	6	6	6

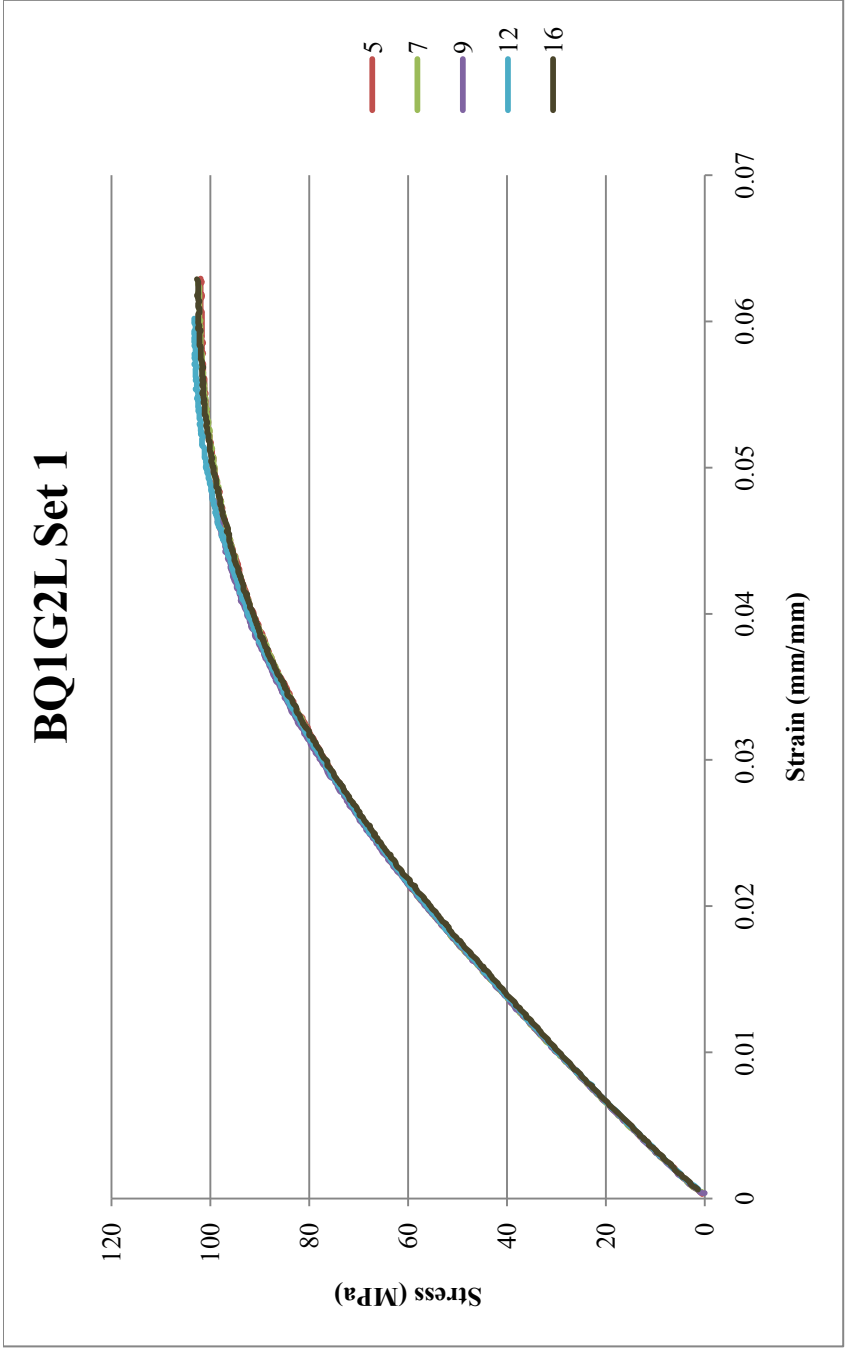


Figure K.58: Flexural Results for BQ1G2L Set 1: Extruded 7-1-10, Injection molded 8-18-10

Table K.58: Flexural Results for BQ1G2L Set 1: Extruded 7-1-10, Injection molded 8-18-10

Sample	Specimen	Flexural Maximum Stress (MPa)	Strain at Maximum Flexural Stress (%)	0.1% Offset Yield Flexural Stress (MPa)	Strain at 0.1% Offset Yield Stress (%)	Flexural Modulus (MPa)
BQ1G2L Set 1	5	101.964	5.80	59.610	2.13	2949.731
	7	102.487	6.20	59.087	2.12	2952.104
	9	103.271	6.09	60.394	2.17	2944.536
	12	103.271	5.71	58.303	2.09	2944.094
	16	102.749	6.18	59.610	2.16	2900.201
Average		102.75	5.99	59.40	2.13	2938.13
Standard Deviation		0.55	0.23	0.77	0.03	21.48
Number		5	5	5	5	5

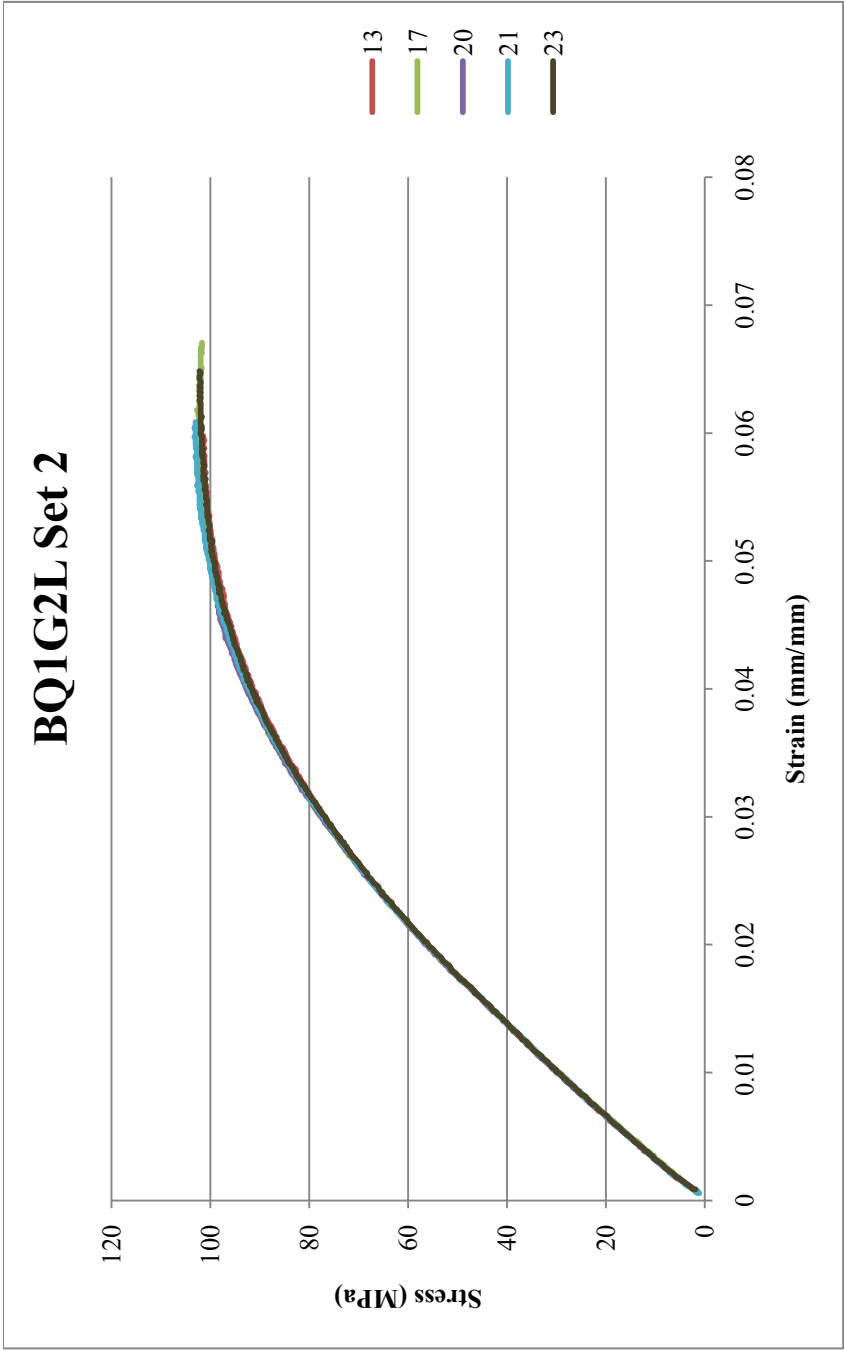


Figure K.59: Flexural Results for BQ1G2L Set 2: Extruded 7-1-10, Injection molded 8-18-10

Table K.59: Flexural Results for BQ1G2L Set 2: Extruded 7-1-10, Injection molded 8-18-10

Sample	Specimen	Flexural Maximum Stress (MPa)	Strain at Maximum Flexural Stress (%)	0.1% Offset Yield Flexural Stress (MPa)	Strain at 0.1% Offset Yield Stress (%)	Flexural Modulus (MPa)
BQ1G2L Set 2	13	101.441	5.72	59.610	2.14	2944.453
	17	102.749	6.08	63.532	2.32	2899.912
	20	103.010	5.85	60.133	2.16	2939.711
	21	103.271	5.97	59.871	2.15	2934.223
	23	102.226	6.25	60.133	2.17	2909.876
Average		102.54	5.97	60.66	2.19	2925.63
Standard Deviation		0.73	0.21	1.62	0.07	19.60
Number		5	5	5	5	5

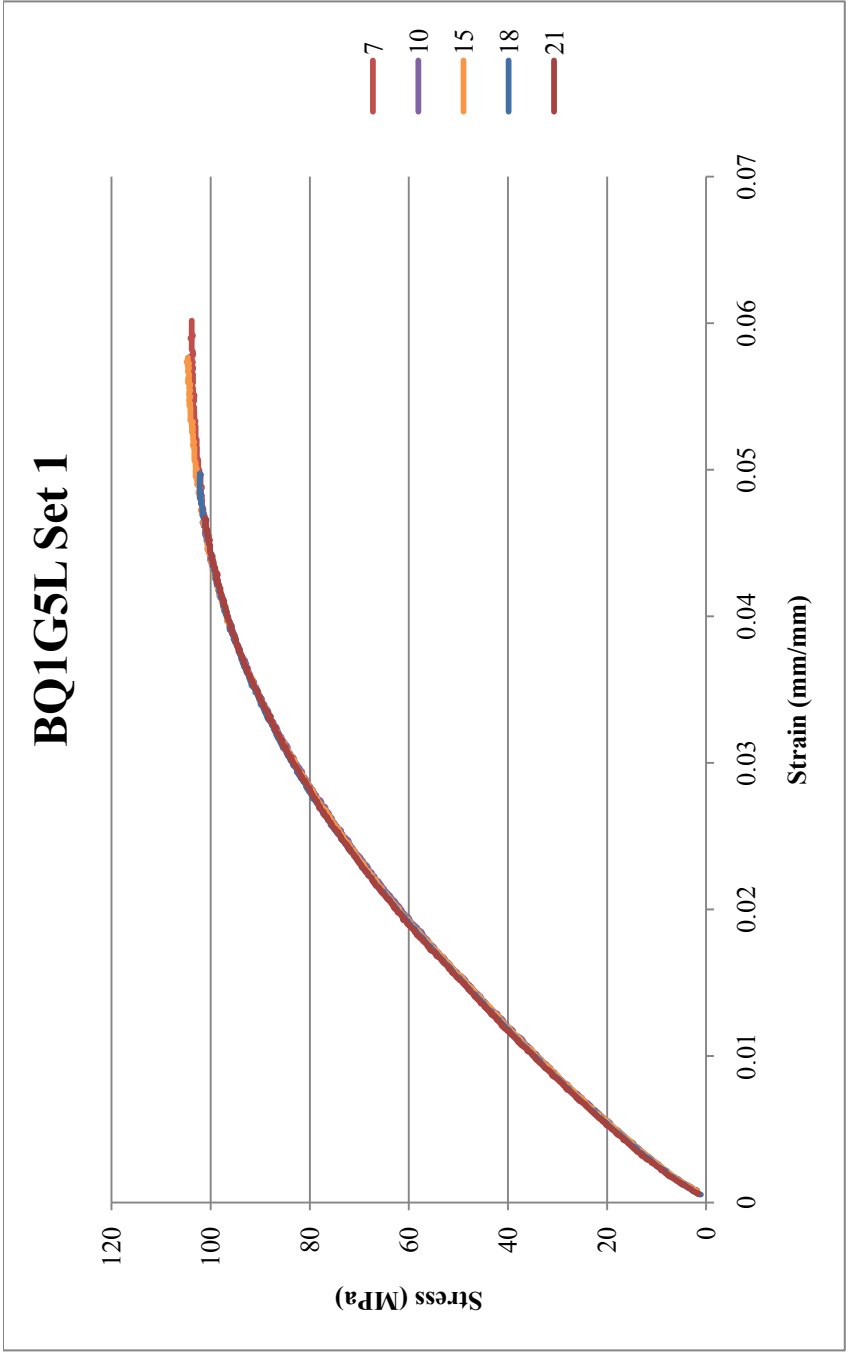


Figure K.60: Flexural Results for BQ1G5L Set 1: Extruded 7-1-10, Injection molded 8-18-10

Table K.60: Flexural Results for BQ1G5L Set 1: Extruded 7-1-10, Injection molded 8-18-10

Sample	Specimen	Flexural Maximum Stress (MPa)	Strain at Maximum Flexural Stress (%)	0.1% Offset Yield Flexural Stress (MPa)	Strain at 0.1% Offset Yield Stress (%)	Flexural Modulus (MPa)
BQ1G5L Set 1	7	104.056	5.77	61.701	1.97	3357.782
	10	104.840	5.67	61.440	1.98	3310.82
	15	104.840	5.73	60.133	1.93	3348.498
	18	102.226	4.81	53.597	1.66	3473.936
	21	101.180	4.61	54.642	1.70	3499.547
Average		103.43	5.32	58.30	1.85	3398.12
Standard Deviation		1.65	0.56	3.88	0.16	83.29
Number		5	5	5	5	5

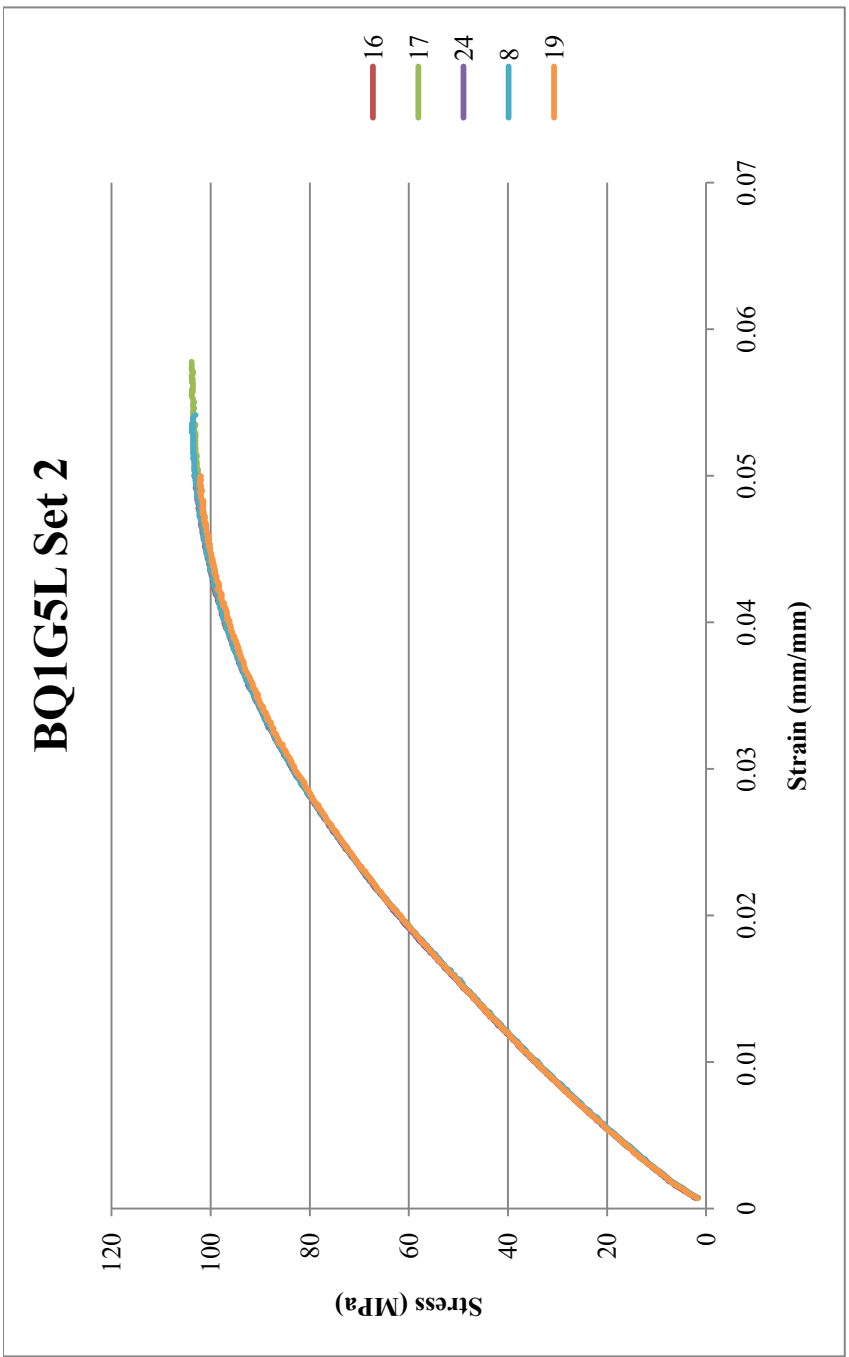


Figure K.61: Flexural Results for BQ1G5L Set 2: Extruded 7-1-10, Injection molded 8-18-10

Table K.61: Flexural Results for BQ1G5L Set 2: Extruded 7-1-10, Injection molded 8-18-10

Sample	Specimen	Flexural Maximum Stress (MPa)	Strain at Maximum Flexural Stress (%)	0.1% Offset Yield Flexural Stress (MPa)	Strain at 0.1% Offset Yield Stress (%)	Flexural Modulus (MPa)
BQ1G5L Set 2	16	103.271	4.99	53.597	1.68	3428.902
	17	103.794	5.54	60.133	1.92	3357.938
	24	102.226	4.60	52.812	1.64	3461.481
	8	103.794	5.30	58.564	1.88	3356.485
	19	102.226	4.89	54.904	1.73	3425.412
Average		103.06	5.06	56.00	1.77	3406.04
Standard Deviation		0.79	0.37	3.19	0.12	46.75
Number		5	5	5	5	5

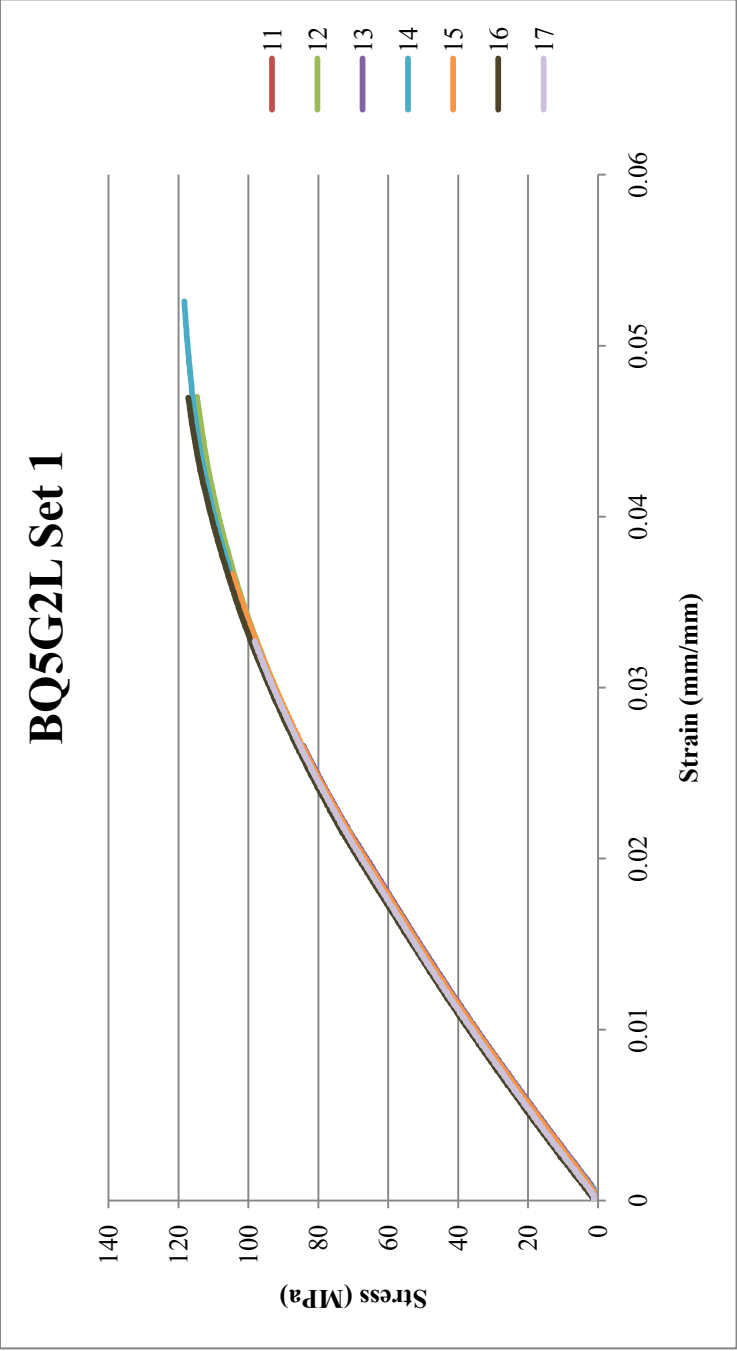


Figure K.62: Flexural Results for BQ5G2L Set 1: Extruded 7-1-10, Injection molded 9-9-10

Table K.62: Flexural Results for BQ5G2L Set 1: Extruded 7-1-10, Injection molded 9-9-10

Sample	Specimen	Flexural Maximum Stress (MPa)	Strain at Maximum Flexural Stress (%)	0.1% Offset Yield Flexural Stress (MPa)	Strain at 0.1% Offset Yield Stress (%)	Flexural Modulus (MPa)
BQ5G2L Set 1	11	112.861	4.33	58.488	1.72	3624.022
	12	114.723	4.72	60.625	1.79	3601.406
	13	101.923	3.52	58.222	1.74	3517.689
	14	118.456	5.30	58.027	1.71	3577.845
	15	104.850	3.69	61.345	1.83	3540.676
	16	117.194	4.70	72.486	2.13	3628.466
	17	98.416	3.28	59.718	1.74	3656.164
Average		109.77	4.22	61.27	1.81	3592.32
Standard Deviation		7.95	0.74	5.10	0.15	49.86
Number		7	7	7	7	7

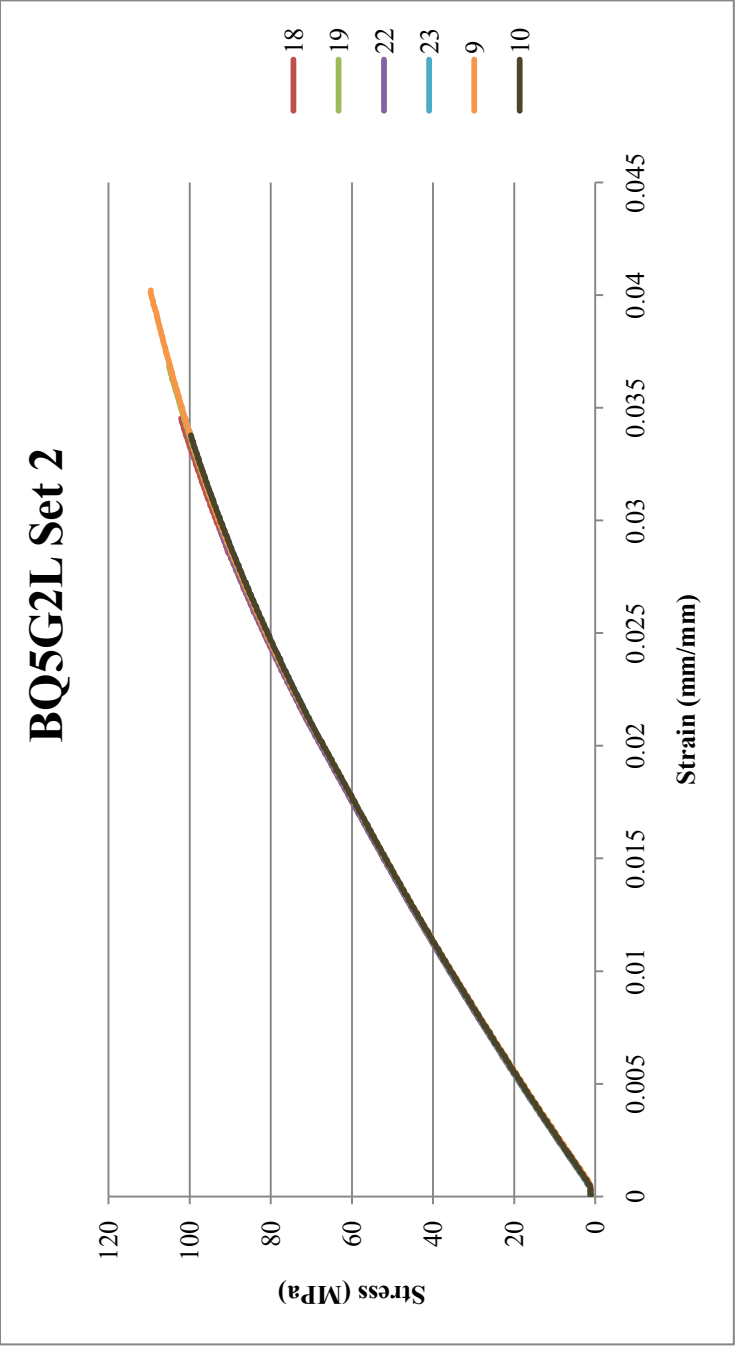


Figure K.63: Flexural Results for BQ5G2L Set 2: Extruded 7-1-10, Injection molded 9-9-10

Table K.63: Flexural Results for BQ5G2L Set 2: Extruded 7-1-10, Injection molded 9-9-10

Sample	Specimen	Flexural Maximum Stress (MPa)	Strain at Maximum Flexural Stress (%)	0.1% Offset Yield Flexural Stress (MPa)	Strain at 0.1% Offset Yield Stress (%)	Flexural Modulus (MPa)
BQ5G2L Set 2	18	102.302	3.46	57.189	1.66	3668.427
	19	105.296	3.70	60.051	1.76	3629.039
	22	108.543	3.90	59.462	1.74	3646.985
	23	101.282	3.47	60.183	1.78	3601.039
	9	109.722	4.03	57.116	1.68	3618.263
	10	99.830	3.39	56.800	1.67	3626.998
Average		104.50	3.66	58.47	1.71	3631.79
Standard Deviation		4.03	0.26	1.59	0.05	23.38
Number		6	6	6	6	6

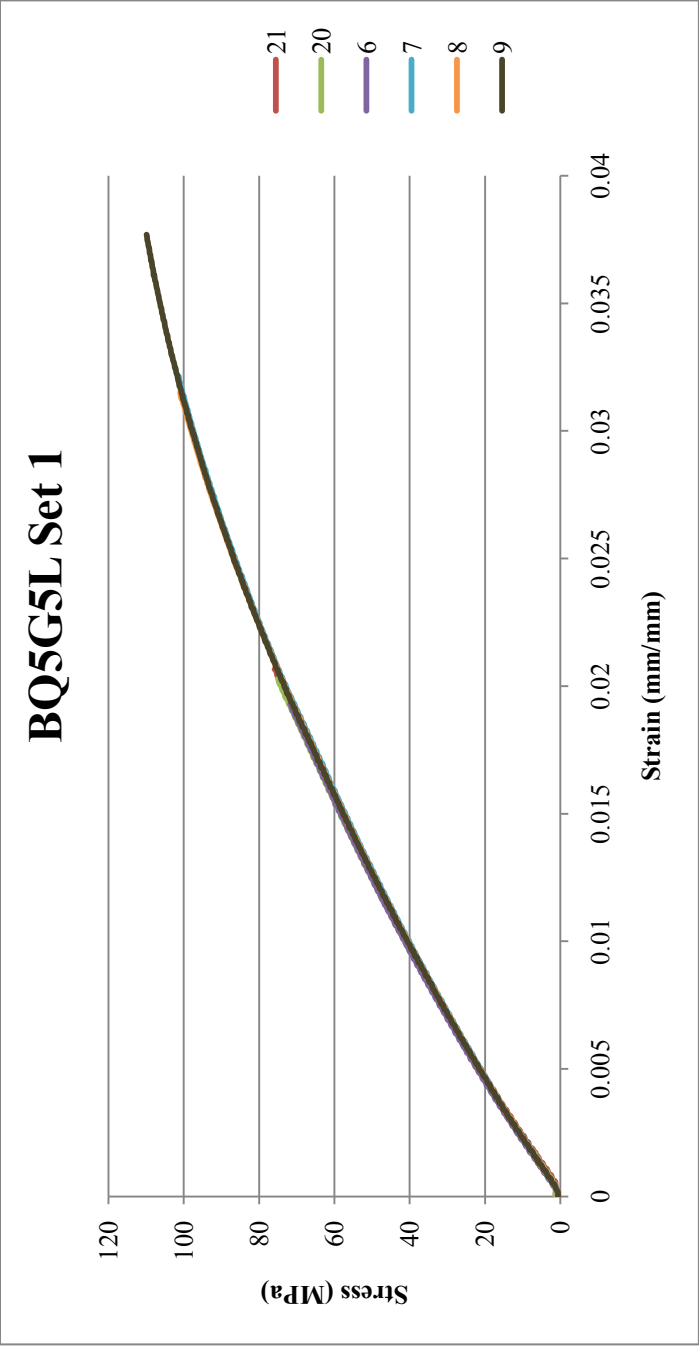


Figure K.64: Flexural Results for BQ5G5L Set 1: Extruded 7-1-10, Injection molded 9-9-10

Table K.64: Flexural Results for BQ5G5L Set 1: Extruded 7-1-10, Injection molded 9-9-10

Sample	Specimen	Flexural Maximum Stress (MPa)	Strain at Maximum Flexural Stress (%)	0.1% Offset Yield Flexural Stress (MPa)	Strain at 0.1% Offset Yield Stress (%)	Flexural Modulus (MPa)
BQ5G5L Set 1	21	76.119	2.08	47.775	1.19	4335.05
	20	75.324	2.03	52.259	1.31	4322.166
	6	88.674	2.56	46.814	1.15	4466.359
	7	101.749	3.24	51.232	1.32	4233.275
	8	101.191	3.16	49.840	1.27	4279.579
	9	109.943	3.77	52.636	1.35	4234.548
Average		92.17	2.81	50.09	1.26	4311.83
Standard Deviation		14.44	0.70	2.39	0.08	86.84
Number		6	6	6	6	6

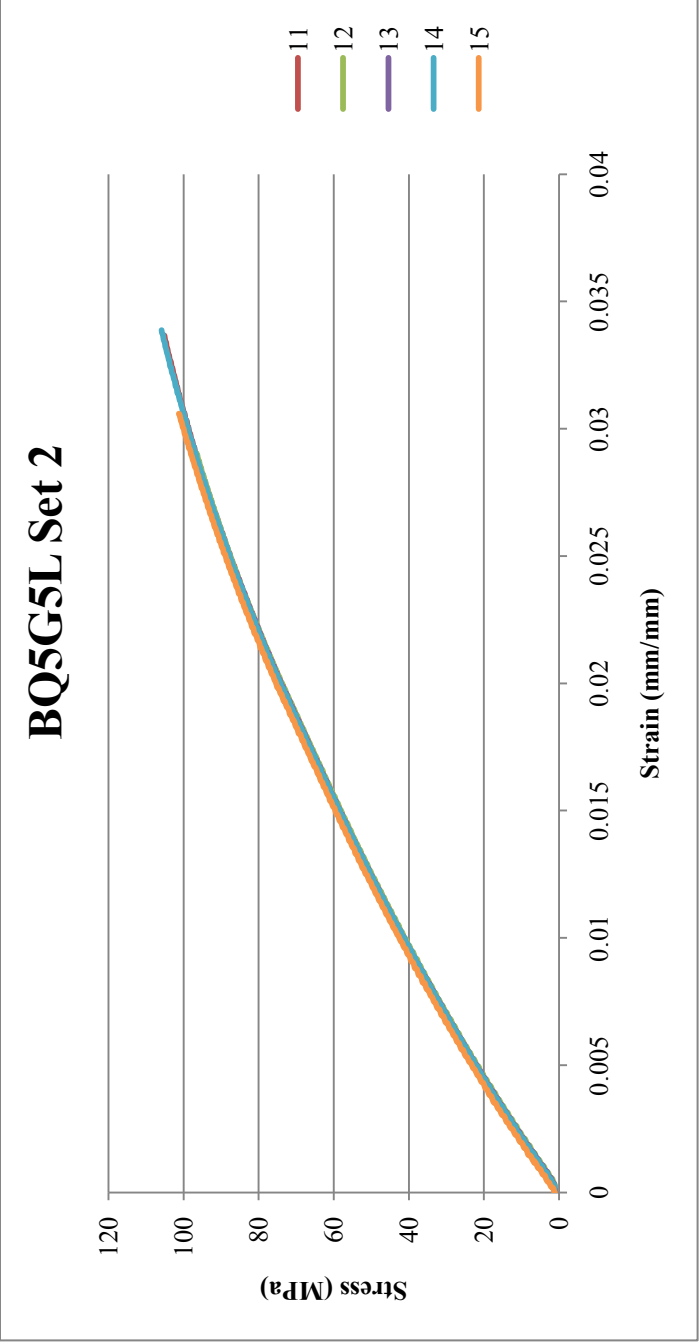


Figure K.65: Flexural Results for BQ5G5L Set 2: Extruded 7-1-10, Injection molded 9-9-10

Table K.65: Flexural Results for BQ5G5L Set 2: Extruded 7-1-10, Injection molded 9-9-10

Sample	Specimen	Flexural Maximum Stress (MPa)	Strain at Maximum Flexural Stress (%)	0.1% Offset Yield Flexural Stress (MPa)	Strain at 0.1% Offset Yield Stress (%)	Flexural Modulus (MPa)
BQ5G5L Set 2	11	105.322	3.37	53.405	1.35	4315.425
	12	96.871	2.92	48.911	1.22	4371.987
	13	103.166	3.23	51.479	1.29	4370.382
	14	106.215	3.41	54.069	1.37	4325.743
	15	101.536	3.08	56.960	1.42	4435.063
Average		102.62	3.20	52.96	1.33	4363.72
Standard Deviation		3.70	0.20	3.00	0.08	47.37
Number		5	5	5	5	5

Appendix L: Small Amplitude Oscillatory Shear Rheology Results

Appendix L.1: Polycarbonate with Carbon Nanotubes

Table L.1: SAOS Results for BL: Lexan HF1130-111 at various temperatures
Formulation: BL

Temperature °C	Frequency (rad/s)	Complex Viscosity (Pa·s)
210	1.00E-01	5.15E+03
	2.15E-01	5.08E+03
	4.64E-01	5.03E+03
	1.00E+00	4.98E+03
	2.15E+00	4.89E+03
	4.64E+00	4.69E+03
	1.00E+01	4.25E+03
	2.15E+01	3.71E+03
	4.64E+01	2.98E+03
	1.00E+02	2.19E+03
270	1.00E-01	3.66E+02
	2.15E-01	3.20E+02
	4.64E-01	2.84E+02
	1.00E+00	2.68E+02
	2.15E+00	2.62E+02
	4.64E+00	2.61E+02
	1.00E+01	2.59E+02
	2.15E+01	2.57E+02
	4.64E+01	2.52E+02
	1.00E+02	2.36E+02
230	1.00E-01	1.52E+03
	2.15E-01	1.45E+03
	4.64E-01	1.43E+03
	1.00E+00	1.43E+03
	2.15E+00	1.42E+03
	4.64E+00	1.41E+03
	1.00E+01	1.37E+03
	2.15E+01	1.30E+03
	4.64E+01	1.17E+03
	1.00E+02	9.87E+02

Table L.2: SAOS Results for BQ2L: 2 wt% Hyperion Fibrils (CNT) in Lexan HF1130-111 at various temperatures

Formulation: BQ2L

Temperature °C	Frequency (rad/s)	Complex Viscosity (Pa·s)
210	1.00E-01	1.99E+04
	2.15E-01	1.18E+04
	4.64E-01	7.56E+03
	1.00E+00	5.29E+03
	2.15E+00	3.96E+03
	4.64E+00	3.13E+03
	1.00E+01	2.71E+03
	2.15E+01	2.25E+03
	4.64E+01	1.80E+03
	1.00E+02	1.37E+03
270	1.00E-01	1.80E+04
	2.15E-01	8.83E+03
	4.64E-01	4.32E+03
	1.00E+00	2.15E+03
	2.15E+00	1.12E+03
	4.64E+00	6.20E+02
	1.00E+01	3.86E+02
	2.15E+01	2.63E+02
	4.64E+01	1.93E+02
	1.00E+02	1.46E+02
250	1.00E-01	1.28E+04
	2.15E-01	6.59E+03
	4.64E-01	3.43E+03
	1.00E+00	1.87E+03
	2.15E+00	1.11E+03
	4.64E+00	7.13E+02
	1.00E+01	5.20E+02
	2.15E+01	4.02E+02
	4.64E+01	3.22E+02
	1.00E+02	2.61E+02

Table L.2: SAOS Results for BQ2L: 2 wt% Hyperion Fibrils (CNT) in Lexan HF1130-111 at various temperatures continued

Formulation: BQ2L

Temperature °C	Frequency (rad/s)	Complex Viscosity (Pa·s)
310	1.00E-01	4.26E+04
	2.15E-01	2.11E+04
	4.64E-01	1.02E+04
	1.00E+00	4.94E+03
	2.15E+00	2.40E+03
	4.64E+00	1.18E+03
	1.00E+01	5.96E+02
	2.15E+01	3.14E+02
	4.64E+01	1.76E+02
	1.00E+02	1.04E+02

Table L.3: SAOS Results for BQ3L: 3 wt% Hyperion Fibrils (CNT) in Lexan HF1130-111 at various temperatures

Formulation: BQ3L

Temperature °C	Frequency (rad/s)	Complex Viscosity (Pa·s)
210	1.00E-01	2.00E+05
	2.15E-01	1.03E+05
	4.64E-01	7.86E+04
	1.00E+00	3.07E+04
	2.15E+00	1.85E+04
	4.64E+00	1.19E+04
	1.00E+01	8.88E+03
	2.15E+01	6.07E+03
	4.64E+01	4.52E+03
	1.00E+02	3.26E+03
270	1.00E-01	1.47E+05
	2.15E-01	7.19E+04
	4.64E-01	3.50E+04
	1.00E+00	1.72E+04
	2.15E+00	8.48E+03
	4.64E+00	4.37E+03
	1.00E+01	2.24E+03
	2.15E+01	1.29E+03
	4.64E+01	7.93E+02
	1.00E+02	5.26E+02
290	1.00E-01	1.16E+05
	2.15E-01	5.64E+04
	4.64E-01	2.75E+04
	1.00E+00	1.35E+04
	2.15E+00	6.76E+03
	4.64E+00	3.42E+03
	1.00E+01	1.67E+03
	2.15E+01	9.09E+02
	4.64E+01	4.99E+02
	1.00E+02	2.96E+02

Table L.3: SAOS Results for BQ3L: 3 wt% Hyperion Fibrils (CNT) in Lexan HF1130-111 at various temperatures continued

Formulation: BQ3L

Temperature °C	Frequency (rad/s)	Complex Viscosity (Pa·s)
310	1.00E-01	1.20E+05
	2.15E-01	5.86E+04
	4.64E-01	2.84E+04
	1.00E+00	1.38E+04
	2.15E+00	6.83E+03
	4.64E+00	3.41E+03
	1.00E+01	1.65E+03
	2.15E+01	8.74E+02
	4.64E+01	4.59E+02
	1.00E+02	2.57E+02
330	1.00E-01	1.14E+05
	2.15E-01	5.65E+04
	4.64E-01	2.77E+04
	1.00E+00	1.35E+04
	2.15E+00	6.66E+03
	4.64E+00	3.33E+03
	1.00E+01	1.63E+03
	2.15E+01	8.64E+02
	4.64E+01	4.46E+02
	1.00E+02	2.39E+02
350	1.00E-01	1.06E+05
	2.15E-01	5.40E+04
	4.64E-01	2.76E+04
	1.00E+00	1.37E+04
	2.15E+00	6.78E+03
	4.64E+00	3.39E+03
	1.00E+01	1.65E+03
	2.15E+01	8.65E+02
	4.64E+01	4.49E+02
	1.00E+02	2.36E+02

Table L.4: SAOS Results for BQ4L: 4 wt% Hyperion Fibrils (CNT) in Lexan HF1130-111 at various temperatures
Formulation: BQ4L

Temperature °C	Frequency (rad/s)	Complex Viscosity (Pa·s)
210	1.00E-01	4.65E+05
	2.15E-01	2.39E+05
	4.64E-01	1.80E+05
	1.00E+00	6.59E+04
	2.15E+00	3.71E+04
	4.64E+00	1.95E+04
	1.00E+01	1.59E+04
	2.15E+01	9.12E+03
	4.64E+01	6.01E+03
	1.00E+02	4.14E+03
230	1.00E-01	3.94E+05
	2.15E-01	1.96E+05
	4.64E-01	9.70E+04
	1.00E+00	4.92E+04
	2.15E+00	2.53E+04
	4.64E+00	1.37E+04
	1.00E+01	7.75E+03
	2.15E+01	4.66E+03
	4.64E+01	3.01E+03
	1.00E+02	2.04E+03
270	1.00E-01	3.14E+05
	2.15E-01	1.57E+05
	4.64E-01	7.65E+04
	1.00E+00	3.76E+04
	2.15E+00	1.86E+04
	4.64E+00	9.15E+03
	1.00E+01	4.42E+03
	2.15E+01	2.46E+03
	4.64E+01	1.38E+03
	1.00E+02	8.30E+02

Table L.4: SAOS Results for BQ4L: 4 wt% Hyperion Fibrils (CNT) in Lexan HF1130-111 at various temperatures continued

Formulation: BQ4L

Temperature °C	Frequency (rad/s)	Complex Viscosity (Pa·s)
290	1.00E-01	2.85E+05
	2.15E-01	1.39E+05
	4.64E-01	6.76E+04
	1.00E+00	3.30E+04
	2.15E+00	1.58E+04
	4.64E+00	7.89E+03
	1.00E+01	3.66E+03
	2.15E+01	1.94E+03
	4.64E+01	1.01E+03
	1.00E+02	5.61E+02
310	1.00E-01	3.38E+05
	2.15E-01	1.64E+05
	4.64E-01	7.88E+04
	1.00E+00	3.81E+04
	2.15E+00	1.81E+04
	4.64E+00	8.38E+03
	1.00E+01	4.07E+03
	2.15E+01	2.06E+03
	4.64E+01	1.03E+03
	1.00E+02	5.35E+02

Table L.5: SAOS Results for BQ5L: 5 wt% Hyperion Fibrils (CNT) in Lexan HF1130-111 at various temperatures
Formulation: BQ5L

Temperature °C	Frequency (rad/s)	Complex Viscosity (Pa·s)
210	1.00E-01	7.26E+05
	2.15E-01	3.70E+05
	4.64E-01	2.73E+05
	1.00E+00	1.02E+05
	2.15E+00	5.52E+04
	4.64E+00	2.90E+04
	1.00E+01	1.76E+04
	2.15E+01	1.09E+04
	4.64E+01	6.84E+03
	1.00E+02	4.57E+03
270	1.00E-01	5.91E+05
	2.15E-01	3.04E+05
	4.64E-01	1.49E+05
	1.00E+00	7.50E+04
	2.15E+00	3.59E+04
	4.64E+00	1.68E+04
	1.00E+01	8.43E+03
	2.15E+01	4.39E+03
	4.64E+01	2.32E+03
	1.00E+02	1.30E+03
290	1.00E-01	5.41E+05
	2.15E-01	2.66E+05
	4.64E-01	1.28E+05
	1.00E+00	6.31E+04
	2.15E+00	3.05E+04
	4.64E+00	1.34E+04
	1.00E+01	7.01E+03
	2.15E+01	3.49E+03
	4.64E+01	1.77E+03
	1.00E+02	9.39E+02

Table L.5: SAOS Results for BQ5L: 5 wt% Hyperion Fibrils (CNT) in Lexan HF1130-111 at various temperatures continued

Formulation: BQ5L

Temperature °C	Frequency (rad/s)	Complex Viscosity (Pa·s)
310	1.00E-01	5.99E+05
	2.15E-01	2.94E+05
	4.64E-01	1.42E+05
	1.00E+00	6.94E+04
	2.15E+00	3.37E+04
	4.64E+00	1.44E+04
	1.00E+01	7.47E+03
	2.15E+01	3.67E+03
	4.64E+01	1.81E+03
	1.00E+02	9.19E+02
330	1.00E-01	4.89E+05
	2.15E-01	2.43E+05
	4.64E-01	1.18E+05
	1.00E+00	5.74E+04
	2.15E+00	2.82E+04
	4.64E+00	1.25E+04
	1.00E+01	6.14E+03
	2.15E+01	2.97E+03
	4.64E+01	1.45E+03
	1.00E+02	7.19E+02
350	1.00E-01	5.49E+05
	2.15E-01	2.75E+05
	4.64E-01	1.35E+05
	1.00E+00	6.66E+04
	2.15E+00	3.17E+04
	4.64E+00	1.40E+04
	1.00E+01	7.34E+03
	2.15E+01	3.52E+03
	4.64E+01	1.67E+03
	1.00E+02	8.21E+02

Table L.6: SAOS Results for BQ6L: 6 wt% Hyperion Fibrils (CNT) in Lexan HF1130-111 at various temperatures
Formulation: BQ6L

Temperature °C	Frequency (rad/s)	Complex Viscosity (Pa·s)
210	1.00E-01	1.24E+06
	2.15E-01	6.17E+05
	4.64E-01	4.62E+05
	1.00E+00	1.58E+05
	2.15E+00	9.83E+04
	4.64E+00	3.44E+04
	1.00E+01	2.47E+04
	2.15E+01	1.35E+04
	4.64E+01	8.18E+03
	1.00E+02	5.05E+03
270	1.00E-01	8.67E+05
	2.15E-01	4.27E+05
	4.64E-01	2.08E+05
	1.00E+00	1.02E+05
	2.15E+00	4.94E+04
	4.64E+00	2.26E+04
	1.00E+01	1.15E+04
	2.15E+01	5.82E+03
	4.64E+01	2.98E+03
	1.00E+02	1.60E+03
290	1.00E-01	6.40E+05
	2.15E-01	3.16E+05
	4.64E-01	1.53E+05
	1.00E+00	7.61E+04
	2.15E+00	3.69E+04
	4.64E+00	1.58E+04
	1.00E+01	8.47E+03
	2.15E+01	4.15E+03
	4.64E+01	2.04E+03
	1.00E+02	1.06E+03

Table L.6: SAOS Results for BQ6L: 6 wt% Hyperion Fibrils (CNT) in Lexan HF1130-111 at various temperatures continued

Formulation: BQ6L

Temperature °C	Frequency (rad/s)	Complex Viscosity (Pa·s)
310	1.00E-01	7.32E+05
	2.15E-01	3.57E+05
	4.64E-01	1.73E+05
	1.00E+00	8.51E+04
	2.15E+00	4.09E+04
	4.64E+00	1.71E+04
	1.00E+01	9.12E+03
	2.15E+01	4.42E+03
	4.64E+01	2.14E+03
	1.00E+02	1.08E+03

Table L.7: SAOS Results for BQ8L: 8 wt% Hyperion Fibrils (CNT) in Lexan HF1130-111 at various temperatures
Formulation: BQ8L

Temperature °C	Frequency (rad/s)	Complex Viscosity (Pa·s)
210	1.00E-01	3.08E+06
	2.15E-01	1.53E+06
	4.64E-01	1.13E+06
	1.00E+00	4.03E+05
	2.15E+00	2.92E+05
	4.64E+00	7.69E+04
	1.00E+01	5.49E+04
	2.15E+01	2.79E+04
	4.64E+01	1.59E+04
	1.00E+02	9.39E+03
270	1.00E-01	2.04E+06
	2.15E-01	1.02E+06
	4.64E-01	5.26E+05
	1.00E+00	2.59E+05
	2.15E+00	1.21E+05
	4.64E+00	5.31E+04
	1.00E+01	2.69E+04
	2.15E+01	1.35E+04
	4.64E+01	6.80E+03
	1.00E+02	3.64E+03
290	1.00E-01	1.85E+06
	2.15E-01	9.14E+05
	4.64E-01	4.66E+05
	1.00E+00	2.33E+05
	2.15E+00	1.19E+05
	4.64E+00	4.05E+04
	1.00E+01	2.18E+04
	2.15E+01	1.12E+04
	4.64E+01	5.31E+03
	1.00E+02	2.64E+03

Table L.7: SAOS Results for BQ8L: 8 wt% Hyperion Fibrils (CNT) in Lexan HF1130-111 at various temperatures continued

Formulation: BQ8L

Temperature °C	Frequency (rad/s)	Complex Viscosity (Pa·s)
310	1.00E-01	1.78E+06
	2.15E-01	8.72E+05
	4.64E-01	4.42E+05
	1.00E+00	2.29E+05
	2.15E+00	1.11E+05
	4.64E+00	3.90E+04
	1.00E+01	2.13E+04
	2.15E+01	1.08E+04
	4.64E+01	5.15E+03
	1.00E+02	2.58E+03
330	1.00E-01	1.65E+06
	2.15E-01	8.06E+05
	4.64E-01	4.13E+05
	1.00E+00	2.18E+05
	2.15E+00	1.03E+05
	4.64E+00	3.72E+04
	1.00E+01	2.01E+04
	2.15E+01	1.03E+04
	4.64E+01	5.04E+03
	1.00E+02	2.57E+03
350	1.00E-01	1.61E+06
	2.15E-01	7.86E+05
	4.64E-01	4.29E+05
	1.00E+00	2.24E+05
	2.15E+00	1.09E+05
	4.64E+00	3.88E+04
	1.00E+01	2.09E+04
	2.15E+01	1.05E+04
	4.64E+01	4.99E+03
	1.00E+02	2.55E+03

Appendix F.2: Polycarbonate with Carbon Black

Table L.8: SAOS Results for BA2L: 2 wt% Carbon Black (CB) in Lexan HF1130-111 at various temperatures

Formulation BA2L

Temperature °C	Frequency (rad/s)	Complex Viscosity (Pa·s)
250	1.00E-01	3.08E+03
	2.15E-01	2.23E+03
	4.64E-01	1.63E+03
	1.00E+00	1.26E+03
	2.15E+00	1.02E+03
	4.64E+00	8.59E+02
	1.00E+01	7.44E+02
	2.15E+01	6.59E+02
	4.64E+01	5.84E+02
	1.00E+02	5.09E+02
270	1.00E-01	3.74E+03
	2.15E-01	2.26E+03
	4.64E-01	1.43E+03
	1.00E+00	9.71E+02
	2.15E+00	7.05E+02
	4.64E+00	5.47E+02
	1.00E+01	4.46E+02
	2.15E+01	3.78E+02
	4.64E+01	3.29E+02
	1.00E+02	2.84E+02
290	1.00E-01	4.57E+03
	2.15E-01	2.49E+03
	4.64E-01	1.41E+03
	1.00E+00	8.51E+02
	2.15E+00	5.51E+02
	4.64E+00	3.83E+02
	1.00E+01	2.85E+02
	2.15E+01	2.25E+02
	4.64E+01	1.86E+02
	1.00E+02	1.55E+02

Table L.8: SAOS Results for BA2L: 2 wt% Carbon Black (CB) in Lexan HF1130-111 at various temperatures continued

Formulation BA2L

Temperature °C	Frequency (rad/s)	Complex Viscosity (Pa·s)
310	1.00E-01	5.83E+03
	2.15E-01	3.03E+03
	4.64E-01	1.57E+03
	1.00E+00	8.57E+02
	2.15E+00	4.95E+02
	4.64E+00	3.08E+02
	1.00E+01	2.05E+02
	2.15E+01	1.47E+02
	4.64E+01	1.12E+02
	1.00E+02	8.67E+01
330	1.00E-01	7.30E+03
	2.15E-01	3.68E+03
	4.64E-01	1.82E+03
	1.00E+00	9.43E+02
	2.15E+00	5.05E+02
	4.64E+00	2.89E+02
	1.00E+01	1.79E+02
	2.15E+01	1.20E+02
	4.64E+01	8.70E+01
	1.00E+02	6.41E+01

Table L.9: SAOS Results for BA3L: 3 wt% Carbon Black (CB) in Lexan HF1130-111 at various temperatures
Formulation BA3L

Temperature °C	Frequency (rad/s)	Complex Viscosity (Pa·s)
250	1.00E-01	3.91E+04
	2.15E-01	1.96E+04
	4.64E-01	1.02E+04
	1.00E+00	5.57E+03
	2.15E+00	3.29E+03
	4.64E+00	2.11E+03
	1.00E+01	1.47E+03
	2.15E+01	1.09E+03
	4.64E+01	8.47E+02
	1.00E+02	6.69E+02
270	1.00E-01	3.78E+04
	2.15E-01	1.85E+04
	4.64E-01	9.17E+03
	1.00E+00	4.70E+03
	2.15E+00	2.55E+03
	4.64E+00	1.49E+03
	1.00E+01	9.49E+02
	2.15E+01	6.58E+02
	4.64E+01	4.87E+02
	1.00E+02	3.74E+02
290	1.00E-01	3.86E+04
	2.15E-01	1.88E+04
	4.64E-01	9.13E+03
	1.00E+00	4.52E+03
	2.15E+00	2.32E+03
	4.64E+00	1.27E+03
	1.00E+01	7.46E+02
	2.15E+01	4.80E+02
	4.64E+01	3.35E+02
	1.00E+02	2.46E+02

Table L.9: SAOS Results for BA3L: 3 wt% Carbon Black (CB) in Lexan HF1130-111 at various temperatures continued

Formulation BA3L

Temperature °C	Frequency (rad/s)	Complex Viscosity (Pa·s)
310	1.00E-01	4.10E+04
	2.15E-01	1.99E+04
	4.64E-01	9.65E+03
	1.00E+00	4.70E+03
	2.15E+00	2.33E+03
	4.64E+00	1.20E+03
	1.00E+01	6.62E+02
	2.15E+01	3.96E+02
	4.64E+01	2.58E+02
	1.00E+02	1.79E+02
330	1.00E-01	4.40E+04
	2.15E-01	2.15E+04
	4.64E-01	1.04E+04
	1.00E+00	5.08E+03
	2.15E+00	2.48E+03
	4.64E+00	1.24E+03
	1.00E+01	6.47E+02
	2.15E+01	3.62E+02
	4.64E+01	2.20E+02
	1.00E+02	1.43E+02

Table L.10: SAOS Results for BA4L: 4 wt% Carbon Black (CB) in Lexan HF1130-111 at various temperatures

Formulation BA4L

Temperature °C	Frequency (rad/s)	Complex Viscosity (Pa·s)
250	1.00E-01	9.68E+04
	2.15E-01	4.79E+04
	4.64E-01	2.42E+04
	1.00E+00	1.29E+04
	2.15E+00	7.34E+03
	4.64E+00	4.52E+03
	1.00E+01	3.01E+03
	2.15E+01	2.20E+03
	4.64E+01	1.66E+03
	1.00E+02	1.25E+03
270	1.00E-01	9.16E+04
	2.15E-01	4.45E+04
	4.64E-01	2.19E+04
	1.00E+00	1.10E+04
	2.15E+00	5.80E+03
	4.64E+00	3.26E+03
	1.00E+01	2.01E+03
	2.15E+01	1.36E+03
	4.64E+01	9.82E+02
	1.00E+02	7.32E+02
290	1.00E-01	9.18E+04
	2.15E-01	4.43E+04
	4.64E-01	2.14E+04
	1.00E+00	1.05E+04
	2.15E+00	5.26E+03
	4.64E+00	2.76E+03
	1.00E+01	1.57E+03
	2.15E+01	9.80E+02
	4.64E+01	6.62E+02
	1.00E+02	4.75E+02

Table L.10: SAOS Results for BA4L: 4 wt% Carbon Black (CB) in Lexan HF1130-111 at various temperatures continued

Formulation BA4L

Temperature °C	Frequency (rad/s)	Complex Viscosity (Pa·s)
310	1.00E-01	9.46E+04
	2.15E-01	4.56E+04
	4.64E-01	2.19E+04
	1.00E+00	1.05E+04
	2.15E+00	5.15E+03
	4.64E+00	2.59E+03
	1.00E+01	1.37E+03
	2.15E+01	7.91E+02
	4.64E+01	4.99E+02
	1.00E+02	3.40E+02
330	1.00E-01	9.81E+04
	2.15E-01	4.71E+04
	4.64E-01	2.26E+04
	1.00E+00	1.08E+04
	2.15E+00	5.21E+03
	4.64E+00	2.53E+03
	1.00E+01	1.29E+03
	2.15E+01	6.99E+02
	4.64E+01	4.11E+02
	1.00E+02	2.63E+02

Table L.11: SAOS Results for BA5L: 5 wt% Carbon Black (CB) in Lexan HF1130-111 at various temperatures
Formulation BA5L

Temperature °C	Frequency (rad/s)	Complex Viscosity (Pa·s)
250	1.00E-01	1.69E+05
	2.15E-01	8.44E+04
	4.64E-01	4.23E+04
	1.00E+00	2.19E+04
	2.15E+00	1.20E+04
	4.64E+00	6.95E+03
	1.00E+01	4.31E+03
	2.15E+01	3.04E+03
	4.64E+01	2.18E+03
	1.00E+02	1.59E+03
270	1.00E-01	1.77E+05
	2.15E-01	8.68E+04
	4.64E-01	4.23E+04
	1.00E+00	2.09E+04
	2.15E+00	1.06E+04
	4.64E+00	5.61E+03
	1.00E+01	3.17E+03
	2.15E+01	2.04E+03
	4.64E+01	1.37E+03
	1.00E+02	9.68E+02
290	1.00E-01	1.85E+05
	2.15E-01	8.95E+04
	4.64E-01	4.31E+04
	1.00E+00	2.09E+04
	2.15E+00	1.03E+04
	4.64E+00	5.11E+03
	1.00E+01	2.69E+03
	2.15E+01	1.59E+03
	4.64E+01	9.97E+02
	1.00E+02	6.70E+02

Table L.11: SAOS Results for BA5L: 5 wt% Carbon Black (CB) in Lexan HF1130-111 at various temperatures continued

Formulation BA5L

Temperature °C	Frequency (rad/s)	Complex Viscosity (Pa·s)
310	1.00E-01	1.93E+05
	2.15E-01	9.35E+04
	4.64E-01	4.48E+04
	1.00E+00	2.15E+04
	2.15E+00	1.03E+04
	4.64E+00	5.03E+03
	1.00E+01	2.51E+03
	2.15E+01	1.38E+03
	4.64E+01	8.01E+02
	1.00E+02	5.03E+02
330	1.00E-01	2.01E+05
	2.15E-01	9.72E+04
	4.64E-01	4.65E+04
	1.00E+00	2.22E+04
	2.15E+00	1.06E+04
	4.64E+00	5.02E+03
	1.00E+01	2.45E+03
	2.15E+01	1.29E+03
	4.64E+01	6.99E+02
	1.00E+02	4.08E+02

Table L.12: SAOS Results for BA6L: 6 wt% Carbon Black (CB) in Lexan HF1130-111 at various temperatures
Formulation BA6L

Temperature °C	Frequency (rad/s)	Complex Viscosity (Pa·s)
250	1.00E-01	3.62E+05
	2.15E-01	1.75E+05
	4.64E-01	8.45E+04
	1.00E+00	4.16E+04
	2.15E+00	2.09E+04
	4.64E+00	1.05E+04
	1.00E+01	5.82E+03
	2.15E+01	3.54E+03
	4.64E+01	2.29E+03
	1.00E+02	1.55E+03
270	1.00E-01	3.45E+05
	2.15E-01	1.67E+05
	4.64E-01	8.03E+04
	1.00E+00	3.89E+04
	2.15E+00	1.86E+04
	4.64E+00	9.13E+03
	1.00E+01	4.67E+03
	2.15E+01	2.65E+03
	4.64E+01	1.58E+03
	1.00E+02	1.01E+03
290	1.00E-01	3.44E+05
	2.15E-01	1.67E+05
	4.64E-01	7.99E+04
	1.00E+00	3.85E+04
	2.15E+00	1.85E+04
	4.64E+00	8.86E+03
	1.00E+01	4.33E+03
	2.15E+01	2.29E+03
	4.64E+01	1.28E+03
	1.00E+02	7.65E+02

Table L.12: SAOS Results for BA6L: 6 wt% Carbon Black (CB) in Lexan HF1130-111 at various temperatures continued

Formulation BA6L

Temperature °C	Frequency (rad/s)	Complex Viscosity (Pa·s)
310	1.00E-01	3.50E+05
	2.15E-01	1.69E+05
	4.64E-01	8.07E+04
	1.00E+00	3.89E+04
	2.15E+00	1.86E+04
	4.64E+00	8.56E+03
	1.00E+01	4.15E+03
	2.15E+01	2.15E+03
	4.64E+01	1.12E+03
	1.00E+02	6.30E+02
330	1.00E-01	3.51E+05
	2.15E-01	1.72E+05
	4.64E-01	8.24E+04
	1.00E+00	3.96E+04
	2.15E+00	1.89E+04
	4.64E+00	8.75E+03
	1.00E+01	4.16E+03
	2.15E+01	2.10E+03
	4.64E+01	1.06E+03
	1.00E+02	5.61E+02

Table L.13: SAOS Results for BA8L: 8 wt% Carbon Black (CB) in Lexan HF1130-111 at various temperatures

Formulation BA8L

Temperature °C	Frequency (rad/s)	Complex Viscosity (Pa·s)
250	1.00E-01	1.12E+06
	2.15E-01	5.49E+05
	4.64E-01	2.68E+05
	1.00E+00	1.29E+05
	2.15E+00	6.40E+04
	4.64E+00	2.92E+04
	1.00E+01	1.66E+04
	2.15E+01	8.64E+03
	4.64E+01	5.06E+03
	1.00E+02	3.04E+03
270	1.00E-01	1.08E+06
	2.15E-01	5.22E+05
	4.64E-01	2.55E+05
	1.00E+00	1.22E+05
	2.15E+00	6.05E+04
	4.64E+00	2.64E+04
	1.00E+01	1.40E+04
	2.15E+01	7.05E+03
	4.64E+01	3.83E+03
	1.00E+02	2.19E+03
290	1.00E-01	1.06E+06
	2.15E-01	5.13E+05
	4.64E-01	2.49E+05
	1.00E+00	1.21E+05
	2.15E+00	5.85E+04
	4.64E+00	2.54E+04
	1.00E+01	1.31E+04
	2.15E+01	6.45E+03
	4.64E+01	3.33E+03
	1.00E+02	1.81E+03

Table L.13: SAOS Results for BA8L: 8 wt% Carbon Black (CB) in Lexan HF1130-111 at various temperatures continued

Formulation BA8L

Temperature °C	Frequency (rad/s)	Complex Viscosity (Pa·s)
310	1.00E-01	1.05E+06
	2.15E-01	5.09E+05
	4.64E-01	2.46E+05
	1.00E+00	1.17E+05
	2.15E+00	5.74E+04
	4.64E+00	2.46E+04
	1.00E+01	1.26E+04
	2.15E+01	6.13E+03
	4.64E+01	3.07E+03
	1.00E+02	1.61E+03
330	1.00E-01	1.02E+06
	2.15E-01	4.98E+05
	4.64E-01	2.39E+05
	1.00E+00	1.16E+05
	2.15E+00	5.39E+04
	4.64E+00	2.42E+04
	1.00E+01	1.23E+04
	2.15E+01	5.94E+03
	4.64E+01	2.91E+03
	1.00E+02	1.48E+03

Appendix L.3: Polycarbonate with Graphene Nanoplatelets

Table L.14: SAOS Results for BG2L: 2 wt% Graphene Nanoplatelets (GNP) in Lexan HF1130-111 at various temperatures

Formulation BG2L

Temperature °C	Frequency (rad/s)	Complex Viscosity (Pa·s)
250	1.00E-01	8.41E+02
	2.15E-01	7.25E+02
	4.64E-01	6.53E+02
	1.00E+00	6.22E+02
	2.15E+00	6.10E+02
	4.64E+00	5.97E+02
	1.00E+01	5.86E+02
	2.15E+01	5.71E+02
	4.64E+01	5.41E+02
	1.00E+02	4.87E+02
270	1.00E-01	4.04E+02
	2.15E-01	3.36E+02
	4.64E-01	2.79E+02
	1.00E+00	2.38E+02
	2.15E+00	2.16E+02
	4.64E+00	2.07E+02
	1.00E+01	2.03E+02
	2.15E+01	1.98E+02
	4.64E+01	1.92E+02
	1.00E+02	1.80E+02
290	1.00E-01	2.68E+02
	2.15E-01	2.22E+02
	4.64E-01	1.83E+02
	1.00E+00	1.51E+02
	2.15E+00	1.30E+02
	4.64E+00	1.20E+02
	1.00E+01	1.15E+02
	2.15E+01	1.11E+02
	4.64E+01	1.07E+02
	1.00E+02	9.89E+01

Table L.14: SAOS Results for BG2L: 2 wt% Graphene Nanoplatelets (GNP) in Lexan HF1130-111 at various temperatures continued

Formulation BG2L

Temperature °C	Frequency (rad/s)	Complex Viscosity (Pa·s)
310	1.00E-01	2.00E+02
	2.15E-01	1.61E+02
	4.64E-01	1.28E+02
	1.00E+00	1.03E+02
	2.15E+00	8.36E+01
	4.64E+00	7.31E+01
	1.00E+01	6.78E+01
	2.15E+01	6.44E+01
	4.64E+01	6.12E+01
	1.00E+02	5.42E+01
330	1.00E-01	2.54E+02
	2.15E-01	1.52E+02
	4.64E-01	1.07E+02
	1.00E+00	8.10E+01
	2.15E+00	6.51E+01
	4.64E+00	5.55E+01
	1.00E+01	4.92E+01
	2.15E+01	4.54E+01
	4.64E+01	4.21E+01
	1.00E+02	3.52E+01

Table L.15: SAOS Results for BG3L: 3 wt% Graphene Nanoplatelets (GNP) in Lexan HF1130-111 at various temperatures

Formulation BG3L

Temperature °C	Frequency (rad/s)	Complex Viscosity (Pa·s)
250	1.00E-01	1.38E+03
	2.15E-01	1.13E+03
	4.64E-01	1.00E+03
	1.00E+00	9.30E+02
	2.15E+00	8.77E+02
	4.64E+00	8.47E+02
	1.00E+01	8.10E+02
	2.15E+01	7.71E+02
	4.64E+01	7.22E+02
	1.00E+02	6.48E+02
270	1.00E-01	8.58E+02
	2.15E-01	6.79E+02
	4.64E-01	5.67E+02
	1.00E+00	4.96E+02
	2.15E+00	4.55E+02
	4.64E+00	4.26E+02
	1.00E+01	4.08E+02
	2.15E+01	3.87E+02
	4.64E+01	3.69E+02
	1.00E+02	3.41E+02
290	1.00E-01	6.61E+02
	2.15E-01	4.99E+02
	4.64E-01	3.88E+02
	1.00E+00	3.17E+02
	2.15E+00	2.75E+02
	4.64E+00	2.50E+02
	1.00E+01	2.33E+02
	2.15E+01	2.18E+02
	4.64E+01	2.04E+02
	1.00E+02	1.88E+02

Table L.15: SAOS Results for BG3L: 3 wt% Graphene Nanoplatelets (GNP) in Lexan HF1130-111 at various temperatures continued

Formulation BG3L

Temperature °C	Frequency (rad/s)	Complex Viscosity (Pa·s)
310	1.00E-01	8.49E+02
	2.15E-01	5.42E+02
	4.64E-01	3.70E+02
	1.00E+00	2.68E+02
	2.15E+00	2.10E+02
	4.64E+00	1.74E+02
	1.00E+01	1.52E+02
	2.15E+01	1.37E+02
	4.64E+01	1.24E+02
	1.00E+02	1.12E+02
330	1.00E-01	1.55E+03
	2.15E-01	8.66E+02
	4.64E-01	5.00E+02
	1.00E+00	3.05E+02
	2.15E+00	2.01E+02
	4.64E+00	1.44E+02
	1.00E+01	1.11E+02
	2.15E+01	9.20E+01
	4.64E+01	7.83E+01
	1.00E+02	6.64E+01

Table L.16: SAOS Results for BG4L: 4 wt% Graphene Nanoplatelets (GNP) in Lexan HF1130-111 at various temperatures

Formulation BG4L

Temperature °C	Frequency (rad/s)	Complex Viscosity (Pa·s)
250	1.00E-01	1.77E+03
	2.15E-01	1.29E+03
	4.64E-01	9.76E+02
	1.00E+00	7.94E+02
	2.15E+00	6.79E+02
	4.64E+00	6.00E+02
	1.00E+01	5.48E+02
	2.15E+01	5.13E+02
	4.64E+01	4.75E+02
	1.00E+02	4.30E+02
270	1.00E-01	2.11E+03
	2.15E-01	1.33E+03
	4.64E-01	8.97E+02
	1.00E+00	6.54E+02
	2.15E+00	5.12E+02
	4.64E+00	4.21E+02
	1.00E+01	3.61E+02
	2.15E+01	3.26E+02
	4.64E+01	2.93E+02
	1.00E+02	2.62E+02
290	1.00E-01	3.52E+03
	2.15E-01	1.97E+03
	4.64E-01	1.13E+03
	1.00E+00	7.02E+02
	2.15E+00	4.72E+02
	4.64E+00	3.42E+02
	1.00E+01	2.66E+02
	2.15E+01	2.22E+02
	4.64E+01	1.88E+02
	1.00E+02	1.61E+02

Table L.16: SAOS Results for BG4L: 4 wt% Graphene Nanoplatelets (GNP) in Lexan HF1130-111 at various temperatures continued

Formulation BG4L

Temperature °C	Frequency (rad/s)	Complex Viscosity (Pa·s)
310	1.00E-01	6.49E+03
	2.15E-01	3.37E+03
	4.64E-01	1.73E+03
	1.00E+00	9.28E+02
	2.15E+00	5.34E+02
	4.64E+00	3.32E+02
	1.00E+01	2.28E+02
	2.15E+01	1.68E+02
	4.64E+01	1.31E+02
	1.00E+02	1.04E+02
330	1.00E-01	8.68E+03
	2.15E-01	4.40E+03
	4.64E-01	2.15E+03
	1.00E+00	1.07E+03
	2.15E+00	5.58E+02
	4.64E+00	3.09E+02
	1.00E+01	1.86E+02
	2.15E+01	1.21E+02
	4.64E+01	8.48E+01
	1.00E+02	6.05E+01

Table L.17: SAOS Results for BG5L: 5 wt% Graphene Nanoplatelets (GNP) in Lexan HF1130-111 at various temperatures

Formulation BG5L

Temperature °C	Frequency (rad/s)	Complex Viscosity (Pa·s)
250	1.00E-01	5.09E+03
	2.15E-01	3.66E+03
	4.64E-01	2.82E+03
	1.00E+00	2.28E+03
	2.15E+00	1.92E+03
	4.64E+00	1.65E+03
	1.00E+01	1.49E+03
	2.15E+01	1.35E+03
	4.64E+01	1.20E+03
	1.00E+02	1.05E+03
270	1.00E-01	3.90E+03
	2.15E-01	2.58E+03
	4.64E-01	1.81E+03
	1.00E+00	1.36E+03
	2.15E+00	1.09E+03
	4.64E+00	8.98E+02
	1.00E+01	7.89E+02
	2.15E+01	7.02E+02
	4.64E+01	6.28E+02
	1.00E+02	5.57E+02
290	1.00E-01	6.08E+03
	2.15E-01	3.47E+03
	4.64E-01	2.07E+03
	1.00E+00	1.32E+03
	2.15E+00	9.12E+02
	4.64E+00	6.70E+02
	1.00E+01	5.32E+02
	2.15E+01	4.42E+02
	4.64E+01	3.76E+02
	1.00E+02	3.24E+02

Table L.17: SAOS Results for BG5L: 5 wt% Graphene Nanoplatelets (GNP) in Lexan HF1130-111 at various temperatures continued

Formulation BG5L

Temperature °C	Frequency (rad/s)	Complex Viscosity (Pa·s)
310	1.00E-01	1.26E+04
	2.15E-01	6.57E+03
	4.64E-01	3.43E+03
	1.00E+00	1.87E+03
	2.15E+00	1.09E+03
	4.64E+00	6.81E+02
	1.00E+01	4.69E+02
	2.15E+01	3.43E+02
	4.64E+01	2.65E+02
	1.00E+02	2.12E+02
330	1.00E-01	1.79E+04
	2.15E-01	9.10E+03
	4.64E-01	4.50E+03
	1.00E+00	2.27E+03
	2.15E+00	1.19E+03
	4.64E+00	6.70E+02
	1.00E+01	4.06E+02
	2.15E+01	2.66E+02
	4.64E+01	1.86E+02
	1.00E+02	1.37E+02

Table L.18: SAOS Results for BG6L: 6 wt% Graphene Nanoplatelets (GNP) in Lexan HF1130-111 at various temperatures

Formulation BG6L

Temperature °C	Frequency (rad/s)	Complex Viscosity (Pa·s)
250	1.00E-01	5.48E+03
	2.15E-01	3.96E+03
	4.64E-01	3.02E+03
	1.00E+00	2.42E+03
	2.15E+00	2.02E+03
	4.64E+00	1.72E+03
	1.00E+01	1.58E+03
	2.15E+01	1.42E+03
	4.64E+01	1.26E+03
	1.00E+02	1.09E+03
270	1.00E-01	7.03E+03
	2.15E-01	4.31E+03
	4.64E-01	2.78E+03
	1.00E+00	1.93E+03
	2.15E+00	1.42E+03
	4.64E+00	1.11E+03
	1.00E+01	9.29E+02
	2.15E+01	7.92E+02
	4.64E+01	6.82E+02
	1.00E+02	5.91E+02
290	1.00E-01	1.38E+04
	2.15E-01	7.38E+03
	4.64E-01	4.01E+03
	1.00E+00	2.32E+03
	2.15E+00	1.43E+03
	4.64E+00	9.52E+02
	1.00E+01	6.97E+02
	2.15E+01	5.34E+02
	4.64E+01	4.27E+02
	1.00E+02	3.52E+02

Table L.18: SAOS Results for BG6L: 6 wt% Graphene Nanoplatelets (GNP) in Lexan HF1130-111 at various temperatures continued

Formulation BG6L

Temperature °C	Frequency (rad/s)	Complex Viscosity (Pa·s)
310	1.00E-01	2.41E+04
	2.15E-01	1.24E+04
	4.64E-01	6.17E+03
	1.00E+00	3.17E+03
	2.15E+00	1.71E+03
	4.64E+00	9.92E+02
	1.00E+01	6.25E+02
	2.15E+01	4.22E+02
	4.64E+01	3.02E+02
	1.00E+02	2.29E+02
330	1.00E-01	2.89E+04
	2.15E-01	1.42E+04
	4.64E-01	6.84E+03
	1.00E+00	3.36E+03
	2.15E+00	1.71E+03
	4.64E+00	9.11E+02
	1.00E+01	5.21E+02
	2.15E+01	3.20E+02
	4.64E+01	2.10E+02
	1.00E+02	1.47E+02

Table L.19: SAOS Results for BG8L: 8 wt% Graphene Nanoplatelets (GNP) in Lexan HF1130-111 at various temperatures

Formulation BG8L

Temperature °C	Frequency (rad/s)	Complex Viscosity (Pa·s)
250	1.00E-01	2.41E+04
	2.15E-01	1.30E+04
	4.64E-01	6.71E+03
	1.00E+00	3.64E+03
	2.15E+00	2.08E+03
	4.64E+00	1.29E+03
	1.00E+01	8.89E+02
	2.15E+01	6.50E+02
	4.64E+01	4.97E+02
	1.00E+02	3.98E+02
270	1.00E-01	3.40E+04
	2.15E-01	1.65E+04
	4.64E-01	8.13E+03
	1.00E+00	4.15E+03
	2.15E+00	2.23E+03
	4.64E+00	1.28E+03
	1.00E+01	8.02E+02
	2.15E+01	5.40E+02
	4.64E+01	3.85E+02
	1.00E+02	2.93E+02
290	1.00E-01	4.04E+04
	2.15E-01	1.94E+04
	4.64E-01	9.23E+03
	1.00E+00	4.52E+03
	2.15E+00	2.29E+03
	4.64E+00	1.23E+03
	1.00E+01	7.08E+02
	2.15E+01	4.40E+02
	4.64E+01	2.93E+02
	1.00E+02	2.10E+02

Table L.19: SAOS Results for BG8L: 8 wt% Graphene Nanoplatelets (GNP) in Lexan HF1130-111 at various temperatures continued

Formulation BG8L

Temperature °C	Frequency (rad/s)	Complex Viscosity (Pa·s)
310	1.00E-01	4.66E+04
	2.15E-01	2.27E+04
	4.64E-01	1.09E+04
	1.00E+00	5.20E+03
	2.15E+00	2.54E+03
	4.64E+00	1.29E+03
	1.00E+01	6.86E+02
	2.15E+01	3.91E+02
	4.64E+01	2.38E+02
	1.00E+02	1.57E+02
330	1.00E-01	5.11E+04
	2.15E-01	2.47E+04
	4.64E-01	1.17E+04
	1.00E+00	5.58E+03
	2.15E+00	2.68E+03
	4.64E+00	1.31E+03
	1.00E+01	6.71E+02
	2.15E+01	3.59E+02
	4.64E+01	2.04E+02
	1.00E+02	1.24E+02

Table L.20: SAOS Results for BG10L: 10 wt% Graphene Nanoplatelets (GNP) in Lexan HF1130-111 at various temperatures

Formulation BG10L

Temperature °C	Frequency (rad/s)	Complex Viscosity (Pa·s)
250	1.00E-01	7.58E+04
	2.15E-01	4.13E+04
	4.64E-01	2.27E+04
	1.00E+00	1.30E+04
	2.15E+00	7.82E+03
	4.64E+00	5.42E+03
	1.00E+01	3.75E+03
	2.15E+01	2.75E+03
	4.64E+01	2.09E+03
	1.00E+02	1.59E+03
270	1.00E-01	8.94E+04
	2.15E-01	4.63E+04
	4.64E-01	2.38E+04
	1.00E+00	1.27E+04
	2.15E+00	7.13E+03
	4.64E+00	4.35E+03
	1.00E+01	2.68E+03
	2.15E+01	1.85E+03
	4.64E+01	1.31E+03
	1.00E+02	9.69E+02
290	1.00E-01	1.09E+05
	2.15E-01	5.62E+04
	4.64E-01	2.78E+04
	1.00E+00	1.41E+04
	2.15E+00	7.53E+03
	4.64E+00	4.14E+03
	1.00E+01	2.34E+03
	2.15E+01	1.47E+03
	4.64E+01	9.54E+02
	1.00E+02	6.51E+02

Table L.20: SAOS Results for BG10L: 10 wt% Graphene Nanoplatelets (GNP) in Lexan HF1130-111 at various temperatures continued

Formulation BG10L

Temperature °C	Frequency (rad/s)	Complex Viscosity (Pa·s)
310	1.00E-01	1.31E+05
	2.15E-01	6.64E+04
	4.64E-01	3.28E+04
	1.00E+00	1.62E+04
	2.15E+00	8.20E+03
	4.64E+00	4.23E+03
	1.00E+01	2.24E+03
	2.15E+01	1.31E+03
	4.64E+01	7.95E+02
	1.00E+02	5.15E+02
330	1.00E-01	1.44E+05
	2.15E-01	7.35E+04
	4.64E-01	3.64E+04
	1.00E+00	1.78E+04
	2.15E+00	8.71E+03
	4.64E+00	4.39E+03
	1.00E+01	2.21E+03
	2.15E+01	1.21E+03
	4.64E+01	6.90E+02
	1.00E+02	4.11E+02

Table L.21: SAOS Results for BG12L: 12 wt% Graphene Nanoplatelets (GNP) in Lexan HF1130-111 at various temperatures

Formulation BG12L

Temperature °C	Frequency (rad/s)	Complex Viscosity (Pa·s)
250	1.00E-01	5.06E+05
	2.15E-01	2.51E+05
	4.64E-01	1.25E+05
	1.00E+00	6.54E+04
	2.15E+00	3.47E+04
	4.64E+00	1.78E+04
	1.00E+01	1.05E+04
	2.15E+01	6.07E+03
	4.64E+01	3.77E+03
	1.00E+02	2.44E+03
270	1.00E-01	4.00E+05
	2.15E-01	1.98E+05
	4.64E-01	9.84E+04
	1.00E+00	4.96E+04
	2.15E+00	2.49E+04
	4.64E+00	1.35E+04
	1.00E+01	7.23E+03
	2.15E+01	4.04E+03
	4.64E+01	2.40E+03
	1.00E+02	1.52E+03
290	1.00E-01	3.62E+05
	2.15E-01	1.79E+05
	4.64E-01	8.78E+04
	1.00E+00	4.34E+04
	2.15E+00	2.14E+04
	4.64E+00	1.12E+04
	1.00E+01	5.76E+03
	2.15E+01	3.15E+03
	4.64E+01	1.80E+03
	1.00E+02	1.08E+03

Table L.21: SAOS Results for BG12L: 12 wt% Graphene Nanoplatelets (GNP) in Lexan HF1130-111 at various temperatures continued

Formulation BG12L

Temperature °C	Frequency (rad/s)	Complex Viscosity (Pa·s)
310	1.00E-01	3.42E+05
	2.15E-01	1.73E+05
	4.64E-01	8.52E+04
	1.00E+00	4.19E+04
	2.15E+00	2.06E+04
	4.64E+00	1.02E+04
	1.00E+01	5.17E+03
	2.15E+01	2.76E+03
	4.64E+01	1.51E+03
	1.00E+02	8.67E+02
330	1.00E-01	2.91E+05
	2.15E-01	1.50E+05
	4.64E-01	7.61E+04
	1.00E+00	3.73E+04
	2.15E+00	1.87E+04
	4.64E+00	9.59E+03
	1.00E+01	4.73E+03
	2.15E+01	2.43E+03
	4.64E+01	1.30E+03
	1.00E+02	7.26E+02

Table L.22: SAOS Results for BG15L: 15 wt% Graphene Nanoplatelets (GNP) in Lexan HF1130-111 at various temperatures

Formulation BG15L

Temperature °C	Frequency (rad/s)	Complex Viscosity (Pa·s)
250	1.00E-01	8.37E+05
	2.15E-01	4.29E+05
	4.64E-01	2.31E+05
	1.00E+00	1.22E+05
	2.15E+00	6.52E+04
	4.64E+00	3.25E+04
	1.00E+01	1.83E+04
	2.15E+01	1.02E+04
	4.64E+01	5.89E+03
	1.00E+02	3.65E+03
270	1.00E-01	5.78E+05
	2.15E-01	3.15E+05
	4.64E-01	1.70E+05
	1.00E+00	9.20E+04
	2.15E+00	4.84E+04
	4.64E+00	2.32E+04
	1.00E+01	1.32E+04
	2.15E+01	7.01E+03
	4.64E+01	3.97E+03
	1.00E+02	2.39E+03
290	1.00E-01	5.61E+05
	2.15E-01	3.11E+05
	4.64E-01	1.62E+05
	1.00E+00	8.49E+04
	2.15E+00	4.20E+04
	4.64E+00	2.02E+04
	1.00E+01	1.13E+04
	2.15E+01	5.84E+03
	4.64E+01	3.17E+03
	1.00E+02	1.82E+03

Table L.22: SAOS Results for BG15L: 15 wt% Graphene Nanoplatelets (GNP) in Lexan HF1130-111 at various temperatures continued

Formulation BG15L

Temperature °C	Frequency (rad/s)	Complex Viscosity (Pa·s)
310	1.00E-01	5.71E+05
	2.15E-01	3.07E+05
	4.64E-01	1.57E+05
	1.00E+00	8.25E+04
	2.15E+00	4.16E+04
	4.64E+00	2.03E+04
	1.00E+01	1.08E+04
	2.15E+01	5.40E+03
	4.64E+01	2.85E+03
	1.00E+02	1.58E+03
330	1.00E-01	5.37E+05
	2.15E-01	2.88E+05
	4.64E-01	1.50E+05
	1.00E+00	7.78E+04
	2.15E+00	4.00E+04
	4.64E+00	1.85E+04
	1.00E+01	9.82E+03
	2.15E+01	4.96E+03
	4.64E+01	2.59E+03
	1.00E+02	1.37E+03

Appendix M: Capillary Rheology Results

Appendix M.1: Polycarbonate with Carbon Nanotubes

Table M.1: Capillary Rheometer Results at 270°C

Formulation	CNT Wt%	Viscosity (Pa s) at Apparent Shear Rate (1/s) at 270°C				
		100	200	500	1000	2000
BL	0	597.4 ± 4.8 n=5	549.1 ± 4.7 n=5	461.1 ± 0.8 n=5	358.5 ± 1.2 n=5	244.7 ± 2.1 n=5
BQ2L	2	444.1 ± 4.2 n=4	353.7 ± 5.9 n=4	280.9 ± 2.4 n=4	230.1 ± 0.9 n=4	177.0 ± 0.4 n=4
BQ3L	3	349.7 ± 7.1 n=5	296.5 ± 5.4 n=5	244.9 ± 3.4 n=5	205.1 ± 2.8 n=5	163.5 ± 1.8 n=5
BQ4L	4	349.0 ± 2.9 n=5	286.4 ± 3.4 n=5	230.5 ± 2.7 n=5	193.9 ± 1.8 n=4	151.5 ± 2.9 n=5
BQ5L	5	377.0 ± 8.5 n=5	301.7 ± 7.9 n=5	237.2 ± 6.4 n=5	195.3 ± 4.5 n=5	152.1 ± 3.0 n=5
BQ6L	6	391.8 ± 4.2 n=5	298.2 ± 2.1 n=5	221.9 ± 1.3 n=5	181.3 ± 0.9 n=5	141.9 ± 1.3 n=5
BQ8L	8	472.0 ± 6.5 n=5	337.1 ± 4.6 n=5	233.6 ± 3.1 n=5	183.5 ± 1.9 n=5	142.4 ± 1.4 n=5

Table M.2: Capillary Rheometer Results at 300°C

Formulation	CNT Wt%	Viscosity (Pa s) at Apparent Shear Rate (1/s) at 300°C					
		50	100	200	500	1000	2000
BL	0	235.9 ± 6.2 n=3	203.9 ± 5.8 n=2	188.2 ± 3.5 n=4	163.4 ± 7.0 n=4	141.0 ± 8.2 n=5	118.9 ± 9.7 n=5
BQ2L	2	194.5 ± 6.5 n=3	142.3 ± 6.0 n=3	116.0 ± 1.1 n=3	92.5 ± 1.2 n=3	81.6 ± 0.3 n=2	69.8 ± 0.6 n=2
BQ3L	3	179.8 ± 2.2 n=3	140.3 ± 2.3 n=3	112.9 ± 1.4 n=3	88.9 ± 1.3 n=3	75.0 ± 0.1 n=3	63.3 ± 1.7 n=2
BQ4L	4	167.5 ± 2.1 n=3	117.9 ± 1.8 n=3	86.4 ± 1.2 n=3	62.2 ± 1.2 n=3	50.6 ± 1.3 n=3	42.4 ± 3.0 n=2
BQ5L	5	192.5 n=1	144.5 ± 1.4 n=3	101.6 ± 0.5 n=3	69.4 ± 0.4 n=3	54.5 ± 0.5 n=3	44.1 ± 0.7 n=3
BQ6L	6	301.5 ± 2.7 n=2	203.2 ± 1.4 n=2	140.7 ± 1.1 n=2	91.4 ± 4.1 n=3	74.1 ± 3.1 n=3	61.7 ± 2.5 n=3
BQ8L	8	302.5 ± 7.8 n=3	192.5 ± 2.4 n=3	125.8 ± 2.5 n=3	78.1 ± 1.8 n=3	57.3 ± 0.4 n=3	44.3 ± 0.3 n=3

Table M.3: Capillary Rheometer Results at 320°C

Formulation	CNT Wt%	Viscosity (Pa s) at Apparent Shear Rate (1/s) at 320°C					
		50	100	200	500	1000	2000
BQ2L	2	109.3 ± 1.0 n=2	80.8 ± 2.0 n=3	66.0 ± 1.7 n=3	52.1 ± 2.8 n=6	46.9 ± 2.2 n=7	42.0 ± 1.5 n=5
BQ3L	3	132.4 ± 2.4 n=4	94.0 ± 1.4 n=4	70.2 ± 1.7 n=5	53.0 ± 1.6 n=5	45.2 ± 1.1 n=5	40.2 ± 1.0 n=5
BQ4L	4	154.2 ± 2.8 n=3	107.0 ± 3.5 n=4	77.0 ± 1.9 n=4	53.5 ± 0.4 n=3	45.0 ± 1.9 n=4	38.0 ± 1.2 n=4
BQ5L	5	177.1 ± 10.2 n=7	124.9 ± 7.8 n=7	92.1 ± 5.9 n=8	61.9 ± 3.8 n=8	48.5 ± 3.1 n=7	38.8 ± 2.6 n=7
BQ6L	6	191.8 ± 1.8 n=2	132.4 ± 1.8 n=2	89.8 ± 0.2 n=2	55.6 ± 0.8 n=3	40.5 ± 0.1 n=2	30.7 ± 0.5 n=2
BQ8L	8	323.7 ± 12.8 n=2	217.1 ± 16.2 n=4	148.7 ± 9.8 n=4	83.2 ± 3.8 n=4	55.2 ± 1.8 n=4	37.5 ± 1.0 n=5

Appendix M.2: Polycarbonate with Carbon Black

Table M.4: Capillary Rheometer Results at 270°C

Formulation	CB Wt%	Viscosity (Pa s) at Apparent Shear Rate (1/s) at 270°C					
		50	100	200	500	1000	2000
BA2L	2	851.2 ± 0.0 n=2	778.8 ± 8.0 n=5	709.7 ± 6.0 n=5	588.9 ± 3.2 n=5	447.2 ± 1.4 n=5	295.0 ± 1.4 n=4
	3	1041.1 ± 18.7 n=4	939.5 ± 10.1 n=5	841.7 ± 4.7 n=5	682.6 ± 1.0 n=5	503.2 ± 1.4 n=5	323.4 ± 2.2 n=3
BA4L	4	1218.2 ± 10.4 n=4	1085.6 ± 2.3 n=5	955.9 ± 5.3 n=5	761.6 ± 4.1 n=5	550.4 ± 1.2 n=5	347.5 ± 6.4 n=2
	5	1434.4 ± 10.7 n=3	1256.9 ± 4.6 n=7	1099.3 ± 6.7 n=7	843.1 ± 16.0 n=7	597.6 ± 7.9 n=7	Not Run
BA6L	6	1710.4 ± 17.8 n=4	1401.2 ± 27.5 n=6	1145.2 ± 16.2 n=6	828.1 ± 7.2 n=6	580.0 ± 3.2 n=6	367.5 ± 0.5 n=3
	8	2488.3 ± 34.9 n=4	1936.0 ± 34.4 n=6	1511.9 ± 24.9 n=6	1022.4 ± 15.0 n=6	681.4 ± 7.5 n=6	416.7 ± 1.6 n=3

Table M.5: Capillary Rheometer Results at 300°C

Formulation	CB Wt%	Viscosity (Pa s) at Apparent Shear Rate (1/s) at 300°C					
		50	100	200	500	1000	2000
BA2L	2	Not Run	293.5 ± 0.0 n=4	271.2 ± 2.4 n=5	243.9 ± 2.0 n=5	214.0 ± 1.6 n=5	171.1 ± 1.8 n=5
BA3L	3	403.0 ± 6.4 n=3	355.3 ± 2.4 n=5	324.2 ± 2.2 n=5	286.7 ± 1.9 n=5	248.3 ± 1.1 n=5	195.2 ± 0.6 n=5
BA4L	4	482.6 ± 10.4 n=4	417.3 ± 7.0 n=5	372.4 ± 3.5 n=5	321.1 ± 2.0 n=5	274.2 ± 1.4 n=5	212.3 ± 0.9 n=5
BA5L	5	588.2 ± 9.7 n=7	495.9 ± 6.5 n=7	435.6 ± 4.8 n=7	369.4 ± 2.6 n=7	309.4 ± 2.2 n=7	233.0 ± 1.7 n=7
BA6L	6	744.1 ± 13.8 n=5	609.4 ± 6.8 n=5	520.1 ± 3.2 n=5	429.9 ± 2.6 n=5	353.5 ± 1.4 n=5	260.1 ± 1.8 n=5
BA8L	8	1143.0 ± 29.2 n=2	903.1 ± 12.8 n=3	707.8 ± 39.7 n=7	559.5 ± 22.2 n=7	437.0 ± 13.5 n=7	306.1 ± 14.8 n=2

Appendix M.3: Polycarbonate with Graphene Nanoplatelets

Table M.6: Capillary Rheometer Results at 270°C

Formulation	GNP Wt%	Viscosity (Pa·s) at Apparent Shear Rate (1/s) at 270°C				
		50	100	200	500	1000
BG2L	2	710.4 ± 24.6 n=7	669.1 ± 14.6 n=8	608.4 ± 11.4 n=8	498.8 ± 7.6 n=8	381.8 ± 5.0 n=8
						258.7 ± 1.9 n=6
BG3L	3	771.4 ± 8.9 n=7	701.7 ± 6.5 n=7	627.0 ± 12.2 n=8	503.2 ± 7.2 n=8	383.3 ± 3.6 n=8
						259.6 ± 2.4 n=4
BG4L	4	883.0 ± 7.6 n=2	778.3 ± 7.2 n=4	677.6 ± 0.0 n=4	520.1 ± 3.3 n=4	387.6 ± 2.8 n=4
						259.5 ± 0.6 n=3
BG5L	5	938.4 n=1	816.0 ± 19.1 n=8	697.4 ± 15.8 n=8	523.6 ± 11.2 n=8	391.1 ± 6.5 n=5
						259.6 ± 3.8 n=3
BG6L	6	990.1 ± 27.5 n=8	841.5 ± 15.2 n=8	713.2 ± 14.4 n=7	527.4 ± 9.8 n=8	389.4 ± 6.8 n=8
						260.1 ± 3.2 n=5
BG8L	8	1091.4 ± 11.8 n=5	916.2 ± 13.1 n=5	748.5 ± 10.4 n=5	538.1 ± 6.8 n=5	393.6 ± 4.6 n=5
						262.0 ± 1.1 n=2
BG10L	10	1096.8 ± 34.3 n=5	883.7 ± 23.9 n=5	707.3 ± 21.2 n=5	510.3 ± 15.1 n=5	381.2 ± 10.2 n=5
						259.7 ± 2.2 n=2
BG12L	12	1200.5 ± 25.0 n=4	994.9 ± 32.9 n=7	793.2 ± 25.5 n=9	566.8 ± 19.8 n=9	415.4 ± 2.4 n=5
						Not Run
BG15L	15	1285.5 ± 26.9 n=6	1029.6 ± 42.0 n=11	834.8 ± 32.4 n=15	606.2 ± 15.6 n=13	Not Run
						Not Run

Table M.7: Capillary Rheometer Results at 300°C

Formulation	GNP Wt%	Viscosity (Pa·s) at Apparent Shear Rate (1/s) at 300°C					
		50	100	200	500	1000	2000
BG2L	2	239.9 ± 9.3 n=7	227.7 ± 1.3 n=8	213.5 ± 1.3 n=9	201.8 ± 6.3 n=18	183.1 ± 2.1 n=10	149.2 ± 1.4 n=10
BG3L	3	254.0 ± 18.2 n=6	242.2 ± 4.6 n=6	222.3 ± 5.4 n=6	205.7 ± 6.6 n=14	183.3 ± 1.5 n=10	147.1 ± 1.3 n=9
BG4L	4	271.1 ± 6.5 n=6	251.8 ± 5.7 n=6	234.6 ± 6.0 n=6	219.4 ± 7.5 n=13	184.0 ± 2.4 n=10	138.7 ± 1.4 n=10
BG5L	5	336.5 ± 10.5 n=8	294.0 ± 6.0 n=8	262.1 ± 4.3 n=9	225.8 ± 7.9 n=18	190.3 ± 2.1 n=10	142.0 ± 1.1 n=10
BG6L	6	348.6 ± 7.2 n=8	304.0 ± 7.1 n=9	268.6 ± 7.8 n=9	234.1 ± 7.1 n=13	189.6 ± 3.2 n=10	138.2 ± 2.1 n=9
BG8L	8	373.1 ± 20.4 n=12	314.2 ± 20.4 n=12	304.0 ± 11.3 n=9	244.4 ± 4.0 n=6	187.2 ± 2.2 n=6	132.8 ± 1.6 n=6
BG10L	10	379.4 ± 11.6 n=12	320.2 ± 9.6 n=12	330.2 ± 10.2 n=10	246.8 ± 5.5 n=10	186.6 ± 3.0 n=10	131.4 ± 2.1 n=7
BG12L	12	379.4 ± 11.6 n=12	320.2 ± 9.6 n=12	330.2 ± 10.2 n=10	246.8 ± 5.5 n=10	186.6 ± 3.0 n=10	131.4 ± 2.1 n=7
BG15L	15	571.5 ± 20.2 n=7	444.2 ± 11.8 n=7	352.9 ± 10.6 n=7	245.5 ± 19.1 n=12	199.5 ± 3.3 n=4	N/A

Appendix M.4: Polycarbonate with Multiple Fillers

Table M.8: Capillary Rheometer Results at 270°C

Formulation	Viscosity (Pa·s) at Apparent Shear Rate (1/s) at 270°C					
	50	100	200	500	1000	2000
BQ1L	451.1 ± 6.1 n=5	422.7 ± 5.2 n=4	397.0 ± 5.8 n=4	348.0 ± 4.5 n=4	291.3 ± 4.0 n=4	214.0 ± 1.8 n=4
BA2Q1L	564.4 ± 11.3 n=6	491.4 ± 6.5 n=6	444.4 ± 6.8 n=6	384.5 ± 4.4 n=6	318.1 ± 2.4 n=6	232.4 ± 1.3 n=4
BA2Q5L	601.4 ± 0.0 n=4	426.2 ± 4.2 n=5	325.6 ± 3.3 n=4	248.9 ± 1.9 n=4	209.1 ± 2.3 n=4	166.8 ± 1.1 n=4
BA5Q1L	878.4 ± 6.1 n=4	712.9 ± 2.9 n=5	612.2 ± 6.1 n=5	508.1 ± 5.9 n=5	407.7 ± 4.0 n=6	283.9 ± 1.5 n=3
BA5Q5L	1143.4 ± 12.2 n=4	787.2 ± 12.6 n=4	593.2 ± 5.4 n=4	432.8 ± 4.8 n=5	346.3 ± 2.2 n=5	251.3 ± 2.5 n=4
BA2G2L	974.6 ± 17.9 n=5	860.6 ± 5.9 n=5	762.0 ± 3.2 n=5	604.1 ± 1.9 n=5	449.7 ± 2.0 n=9	293.8 ± 0.8 n=6
BA2G5L	1219.4 ± 18.3 n=6	1034.4 ± 8.9 n=6	868.7 ± 7.0 n=6	635.3 ± 3.3 n=6	455.9 ± 2.5 n=8	293.5 ± 1.4 n=5
BA5G2L	1524.4 ± 26.7 n=5	1282.5 ± 6.9 n=5	1083.5 ± 11.1 n=5	804.6 ± 6.1 n=5	561.4 ± 4.6 n=5	348.6 ± 2.4 n=5
BA5G5L	1939.1 ± 8.3 n=5	1554.3 ± 2.5 n=5	1225.7 ± 3.6 n=5	837.2 ± 2.0 n=5	563.6 ± 0.9 n=5	343.0 ± 0.4 n=5

Table M.8: Capillary Rheometer Results at 270°C continued

Formulation	Viscosity (Pa·s) at Apparent Shear Rate (1/s) at 270°C					
	50	100	200	500	1000	2000
BQ1G2L	608.7 ± 6.3 n=4	539.6 ± 8.0 n=4	489.2 ± 3.3 n=4	406.3 ± 3.5 n=4	325.2 ± 3.8 n=3	230.1 ± 2.1 n=3
BQ1G5L	820.2 ± 19.3 n=4	696.6 ± 8.7 n=4	591.4 ± 4.1 n=5	453.2 ± 1.6 n=4	344.8 ± 2.4 n=4	236.8 ± 1.3 n=4
BQ5G2L	621.0 ± 10.0 n=4	449.6 ± 11.2 n=4	349.9 ± 10.2 n=4	267.6 ± 6.1 n=4	218.6 ± 2.1 n=5	166.2 ± 1.9 n=5
BQ5G5L	688.2 ± 11.3 n=3	514.5 ± 8.1 n=3	416.4 ± 6.7 n=3	338.8 ± 5.5 n=3	288.1 ± 5.3 n=3	236.2 ± 4.3 n=3